



Universiteit  
Leiden  
The Netherlands

## **Zebrafish as research model to study Gaucher disease: Insights into molecular mechanisms**

Lelieveld, L.T.

### **Citation**

Lelieveld, L. T. (2020, October 20). *Zebrafish as research model to study Gaucher disease: Insights into molecular mechanisms*. Retrieved from <https://hdl.handle.net/1887/137851>

Version: Publisher's Version

License: [Licence agreement concerning inclusion of doctoral thesis in the Institutional Repository of the University of Leiden](#)

Downloaded from: <https://hdl.handle.net/1887/137851>

**Note:** To cite this publication please use the final published version (if applicable).

Cover Page



Universiteit Leiden



The handle <http://hdl.handle.net/1887/137851> holds various files of this Leiden University dissertation.

**Author:** Lelieveld, L.T.

**Title:** Zebrafish as research model to study Gaucher disease: Insights into molecular mechanisms

**Issue date:** 2020-10-20



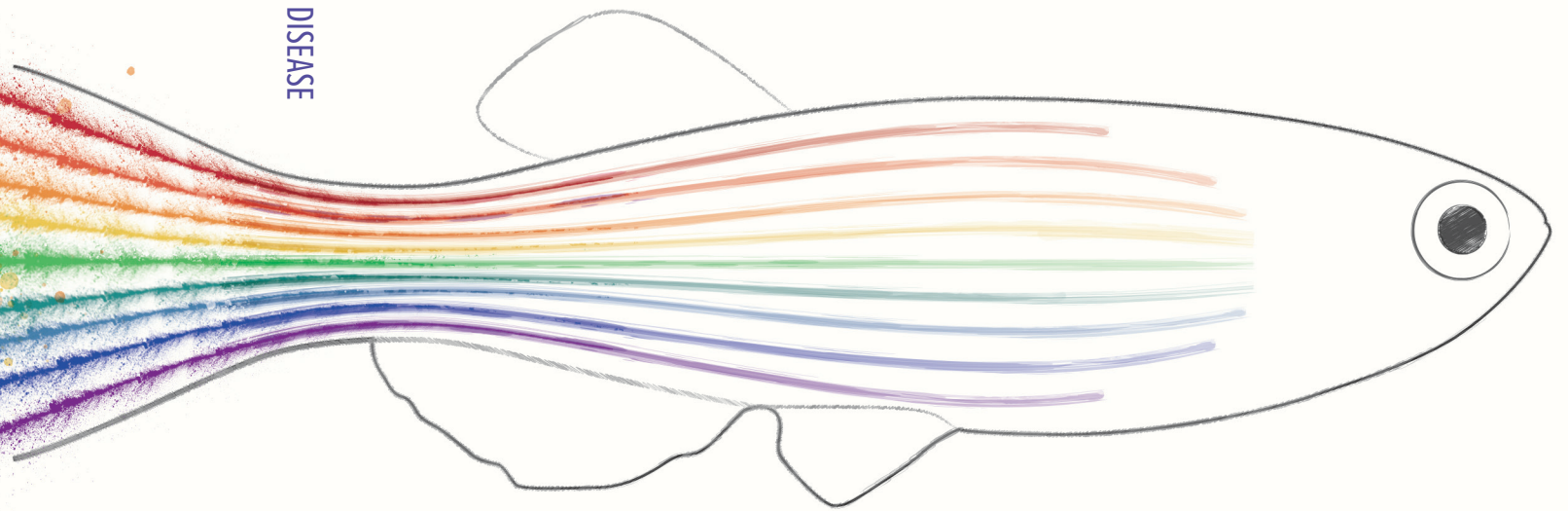
# ZEBRAFISH AS RESEARCH MODEL TO STUDY GAUCHER DISEASE

INSIGHTS INTO MOLECULAR MECHANISMS

LINDSEY T. LELIEVELD

ZEBRAFISH AS RESEARCH MODEL TO STUDY GAUCHER DISEASE

LINDSEY T. LELIEVELD



## Promotiecommissie

Promotor:	Prof. dr. J.M.F.G. Aerts	Leiden University
Copromotor:	dr. R.G. Boot	Leiden University
Overige leden:	Prof. dr. M. van der Stelt	Leiden University
	Prof. dr. J. Brouwer	Leiden University
	Prof. dr. A.H. Meijer	Leiden University
	Prof. dr. M. Horowitz	Tel Aviv University
	Prof. dr. L. Ramakrishnan	University of Cambridge

ISBN: 978-94-6421-015-6  
Printed by: Ipskamp printing  
Cover design: Harald Pieper - In Zicht Grafisch Ontwerp

All rights reserved. No part of this thesis may be reproduced in any matter or by any means without permission from the author.

**Zebrafish as research model to study Gaucher disease.  
Insights into molecular mechanisms**

Proefschrift

ter verkrijging van  
de graad van Doctor aan de Universiteit Leiden,  
op gezag van Rector Magnificus prof.mr. C.J.J.M. Stolker,  
volgens besluit van het College voor Promoties  
te verdedigen op dinsdag 20 oktober 2020  
klokke 11:15 uur

door

Lindsey Theresia Lelieveld

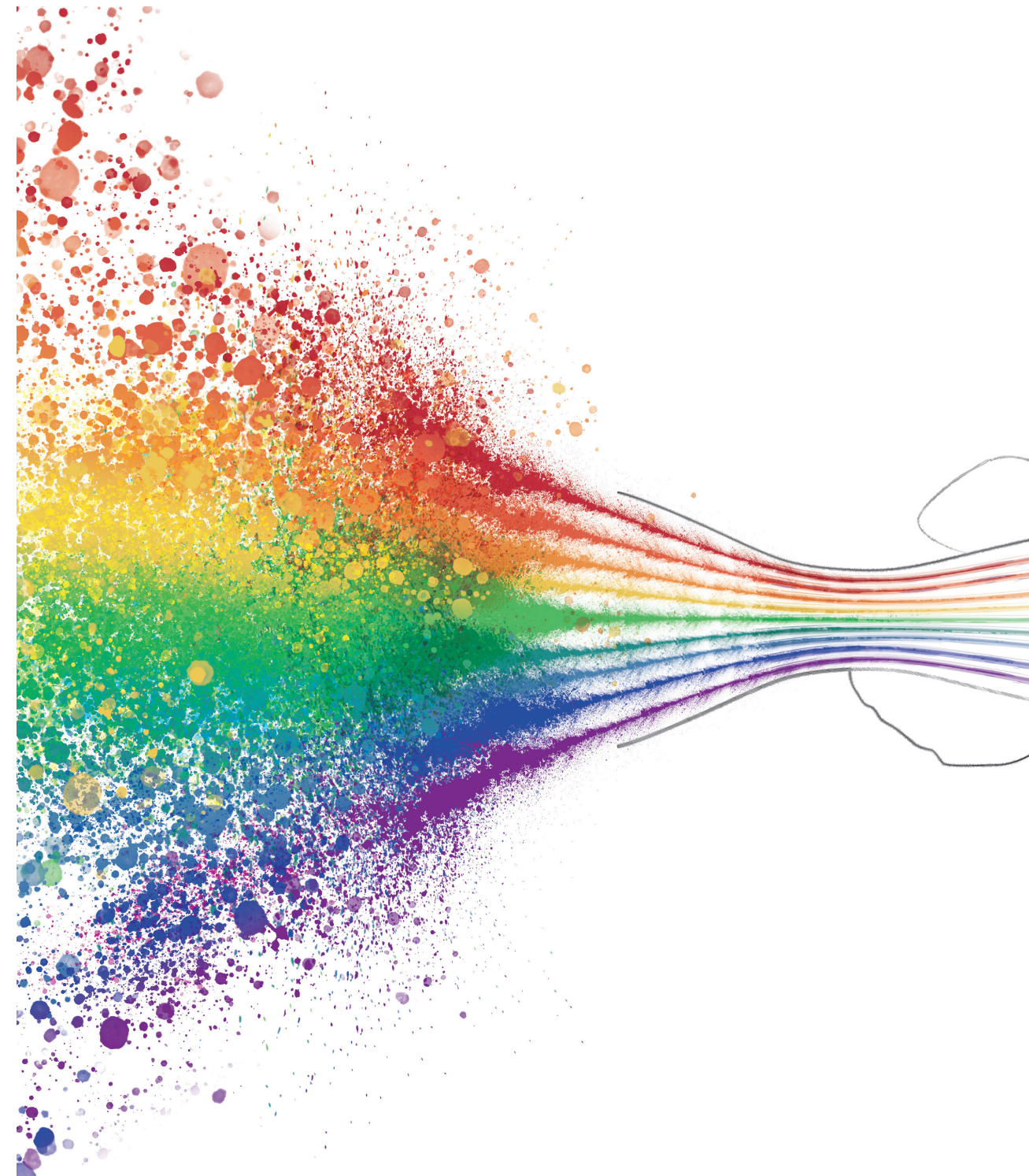
geboren te Monster

op 28 juli 1990



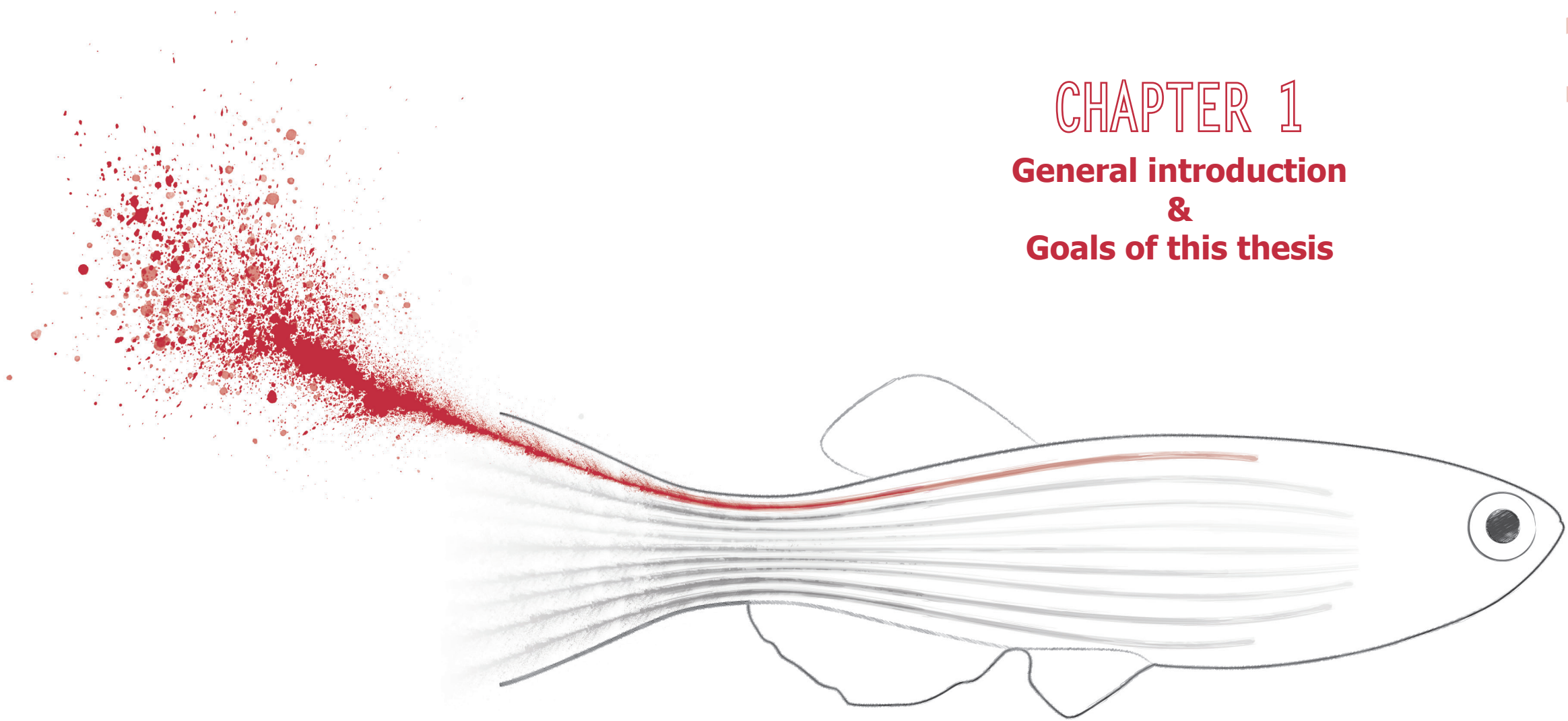
## Table of contents

	<b>Chapter 1</b>
General introduction and goals of this thesis	● 6-37
	<b>Chapter 2</b>
Biochemical evaluation and comparison of GCase enzymes of different species	● 38-63
	<b>Chapter 3</b>
Pharmacological modulation of glycosidases in zebrafish	● 64-85
	<b>Chapter 4</b>
CRISPR/Cas9 mediated genome editing in zebrafish	● 68-115
	<b>Chapter 5</b>
Role of Gba1 & Gba2 in aberrant glycosphingolipid metabolism of zebrafish larvae	● 116-145
	<b>Chapter 6</b>
The detrimental role of excessive GlcSph during GCase deficiency in zebrafish	● 146-173
	<b>Chapter 7</b>
Progression of pathology in zebrafish with GCase deficiency	● 174-203
	<b>Chapter 8</b>
α-Galactosidases in zebrafish	● 204-229
	<b>Chapter 9</b>
Discussion and future prospect	● 230-249
Summary, Samenvatting, Publications, About the author	● 250-263
Dankwoord	



# CHAPTER 1

## General introduction & Goals of this thesis



## Glycosphingolipids

In the nineteenth century, the chemist Johannes Ludwig Thudichum had a large impact on neurochemistry by extracting, purifying and elucidating many substances from the brain which he named cerebrosides, sphingosine and sphingomyelin<sup>1</sup>. These lipids are classified as sphingolipids and chemically defined by a long-chain aliphatic amino alcohol, also called sphingoid base, to which an amide-linked fatty acid is attached, thereby forming ceramide<sup>2-4</sup>. In mammals, the most abundant sphingoid base is sphingosine containing 18 carbons and one double bond (d18:1). In contrast, the length of the sphingoid base in glycosphingolipids of *Drosophila melanogaster* is shorter, with mainly C14 and C16 chains<sup>5,6</sup>. The attached fatty acid in glycosphingolipids shows considerable variation in structure<sup>3</sup>.

### GSL biosynthesis

Sphingolipids are generated via *de novo* synthesis or a salvage pathway (**Figure 1A**)<sup>3</sup>. *De novo* synthesis of sphingolipids starts in the endoplasmic reticulum (ER) with condensation of the amino acid L-serine and an acyl-CoA thioester into a 3-ketosphinganine. In mammals this reaction is mediated by serine palmitoyltransferase (SPT) which prefers a palmitoyl-CoA (C16:0 palmitate), thereby generating mainly sphingolipids with a d18:1 sphingoid base. 3-Ketosphinganine is reduced to sphinganine by 3-ketosphinganine reductase, followed by acylation mediated by a member of the ceramide synthase (CerS) family. The formed dihydroceramide is subsequently desaturated by a desaturase, forming ceramide<sup>3</sup>. DES1 generates the 4,5-trans double bond of ceramide while DES2 adds a hydroxyl group forming the t18:0 backbone of phytoceramide. Catabolism of ceramide by neutral and acid ceramidase enzymes results in sphingosine that, via the so-called 'salvage pathway', can be reacylated by one of the CerS enzymes.

Six CerS isoforms have been detected in mammals and the fatty acid composition of sphingolipids originates from the expression level, tissue distribution and acyl-CoA substrate selectivity of the different CerS enzymes<sup>3</sup>. CerS1 is structurally and functionally different from the other CerS isoforms with a high expression in brain and a preference for stearoyl-CoA generating C18-dihydroceramide<sup>7</sup>. Both CerS2 and CerS3 prefer longer chain acyl-CoAs, between C20 and C26. CerS2 is highly expressed with a broad tissue distribution, but detected higher in kidney and liver<sup>8</sup>. Whereas CerS1 is highly expressed in neurons of the mouse brain, CerS2 expression is high in oligodendrocytes and Schwann cells. Moreover, the transient increase in CerS2 mRNA during the period of active myelination suggests a role for longer fatty acids in myelin sphingolipids<sup>9</sup>. CerS3 expression seems restricted to epidermal keratinocytes and male germ cells and generates abundant epidermal ceramide species such as ceramides with very long fatty acids (C26-C36), 2-hydroxy- and  $\omega$ -hydroxy fatty acids, the latter which are precursors of esterified glucosylceramide and ceramide lipids<sup>10-12</sup>. CerS4 is expressed ubiquitously at low levels and generates ceramides with C18-22 fatty acids<sup>3</sup>. CerS5 and CerS6 both make ceramides with C16 fatty acid, while CerS6 also utilizes myristoyl-CoA to make C14-dihydroceramide<sup>7</sup>. The majority of the membrane sphingolipids are composed of saturated fatty acids<sup>3</sup>.

The produced ceramide species are subsequently transported to different parts of the ER or Golgi complex, where they are modified into more complex sphingolipids (**Figure 1A**).

Intracellular transport of ceramide is often mediated by CERT in a non-vesicular manner<sup>13</sup>. The major plasma membrane component, sphingomyelin, is generated by a transfer from the phosphocholine headgroup of phosphorylcholine to the 1-hydroxyl position of ceramide by either SMS1, located in Golgi membranes, or SMS2, present in plasma membranes<sup>3</sup>.

Another group of more complex sphingolipids are the glycosphingolipids (GSLs), whereby the C1 hydroxyl of ceramide is modified by one or a chain of glycan moieties<sup>2</sup>. Two simple glycosphingolipids are the starting point of more complex GSLs: galactosylceramide (GalCer) and glucosylceramide (GlcCer). In general, the first sugar attached to ceramide is either a glucose- or galactose moiety and attached via a  $\beta$ -linkage, although  $\alpha$ -linked GalCer has been found in bacteria and a marine sponge<sup>14-16</sup>. The ER localized ceramide galactosyltransferase (CGT) transfers a galactosyl moiety to the 1-hydroxyl position of ceramide, generating a  $\beta$ -linked GalCer, an important lipid in the brain as major constituent of myelin<sup>17</sup>. The formation of GlcCer is mediated by UDP-GlcCer glucosyltransferase (UGCG), also called glucosylceramide synthase (GCS) located on the cytosolic leaflet of the ER or early cis-Golgi membranes<sup>3</sup>. Newly formed GlcCer can be metabolized by the non-lysosomal membrane-associated glucosylceramidase GBA2<sup>18-20</sup>, but most of it is relocated to the luminal leaflet of trans-Golgi membranes. Here,  $\beta$ 4-galactosyltransferase (B4GALT5) mediates the transfer of a  $\beta$ -linked galactose to GlcCer generating lactosylceramide (LacCer), a Gal $\beta$ (1,4)Glc $\beta$ (1)-Cer. LacCer is an important intermediate as starting point for more complex GSL lipids by addition of various sugars, including glucose, galactose, mannose, xylose, fucose, glucuronic acid, N-acetyl glucosamine and N-acetyl galactosamine. The complex GSLs are classified as members of globo-, isoglobo-, lacto-, neolacto- and ganglio-families and only a limited number of glycosyltransferases are required to obtain a large variety of root-structured GSLs by addition of different  $\alpha$ - or  $\beta$ -linked glycan moieties to the 3-O- or 4-O position (**Figure 1A**)<sup>3,21</sup>.

### GSL function

The eukaryotic plasma membrane is formed of a bilayer of amphiphilic phospholipids, sphingolipids and sterols. In the plasma membrane, sphingolipids and sterols are thought to organize in transient semi-ordered lipid microdomains, called lipid rafts<sup>22-25</sup>.

In particular, cholesterol and sphingomyelin are very abundant among the plasma membrane lipids (30-40 mol% and 10-20 mol% respectively), while GSLs are typically present at low levels however depending on the cell type<sup>22,26</sup>. Most of the sphingolipids are present in the outer leaflet of the plasma membrane bilayer, thereby having their hydrophilic head group facing the extracellular environment. The different head groups of sphingolipids and GSLs offer a variety of chemical surface characteristics. Sphingolipids and GSLs in lipid rafts are suggested to play a role in a variety of important biological functions, ranging from signal transduction, apoptosis, cell adhesion, synaptic transmission, organization of the cytoskeleton and protein sorting to the cellular entry of viruses, bacteria and toxins<sup>22,27-30</sup>.

The synthesis of distinct GSLs is cell-type specific and different tissues can have different compositions of specific surface GSLs. For example, gangliosides are present in the plasma membrane of neuronal cells, while galactosylceramide, together with cholesterol, is a major lipid constituent in the myelin sheaths surrounding axons<sup>31,32</sup>. Myelin is formed by



specific glia cells, either oligodendrocytes in the central nervous system or Schwann cells in the peripheral nervous system. A change in lipid composition of myelin could contribute to myelin destabilization and breakdown<sup>32</sup>. Another distinct feature is the role of sphingolipids and GSLs in the skin of terrestrial animals. The specific ceramide species with very long fatty acids (C26-C36), 2-hydroxy-,  $\omega$ -hydroxy fatty acids and esterified GlcCer and ceramide lipids are of importance for the organization of the corneocytes in the stratum corneum, in order to prevent trans-epidermal water loss and thereby lethal dehydration<sup>12,33,34</sup>. Ceramide species with very long fatty acids are also important for male fertility in sperm cell maturation<sup>10</sup>.

Sphingolipids and GSLs might also have intracellular biological functions, as not all sphingolipids are associated with the plasma membrane<sup>35,36</sup>. Specific types of sphingolipids and GSLs are involved in different biological processes. Sphingolipids such as sphingosine and ceramide are thought to be involved in the eukaryotic stress response, mediating differentiation, cell cycle arrest, apoptosis and senescence, whereas sphingosine-1-phosphate, as ligand for G-protein coupled receptors, appears to promote proliferation and survival<sup>30,37-41</sup>.

### GSL catabolism

Catabolism of glycosphingolipids predominantly takes place in endosomes and lysosomes (**Figure 1B**). GSLs end up in endosomal-lysosomal compartments via various ways, including receptor-mediated endocytosis or internalization of cellular membranes through intraluminal vesicles, also called multivesicular bodies<sup>2,26</sup>. Macrophages are specialized in the phagocytosis of larger cellular debris, dying or dead cells and pathogens. The resulting phagosome is fused with lysosomes which contains the necessary enzymes to break down its content. Generally (glyco)sphingolipid breakdown is achieved by hydrolysis of the complex sphingolipid to separate components via lysosomal enzymes with acidic pH optima, however hydrolytic enzymes are also reported at other locations in the cell with other pH optima<sup>2</sup>. The stepwise removal of the terminal glycan moieties of the GSLs occurs sequentially by specific glycosidases<sup>42,43</sup>. For example, sialidase enzymes mediate removal of terminal sialic acid residues,  $\beta$ -hexosaminidase enzymes of N-acetyl-Glc or -Gal moieties,  $\alpha$ -galactosidase removes terminal  $\alpha$ -Gal moieties,  $\beta$ -galactosidase of terminal  $\beta$ -Gal moieties, glucocerebrosidase mediates hydrolysis of GlcCer and acid sphingomyelinase mediates removal of the phosphocholine head group of sphingomyelin. The biosynthetic enzymes in the ER and Golgi are generally membrane-bound, while the catabolic glycosidases in the lysosomes are not bound to membranes. In contrast, the sphingolipids and GSLs destined for hydrolysis are typically embedded in the lysosomal membrane. Several glycosidases therefore require the assistance of membrane-perturbing and lipid-binding proteins in order to efficiently interact with their target substrate lipid in the membrane.

Four sphingolipid activator proteins (saposins, Sap A-D) are known and originate from a single encoded prosaposin polypeptide sequence. The best studied Sap variant is Sap C which is essential for glucocerebrosidase (lysosomal acid  $\beta$ -glucosidase; GCase) to hydrolyse GlcCer located in the lysosomal membrane<sup>26,44,45</sup>.



The final step in GSL catabolism is the cleavage of ceramide into sphingosine and a free fatty acid. This step is performed in the lysosome by acid ceramidase but could also be performed in other parts of the cell by one of the neutral ceramidases<sup>2,46</sup>.

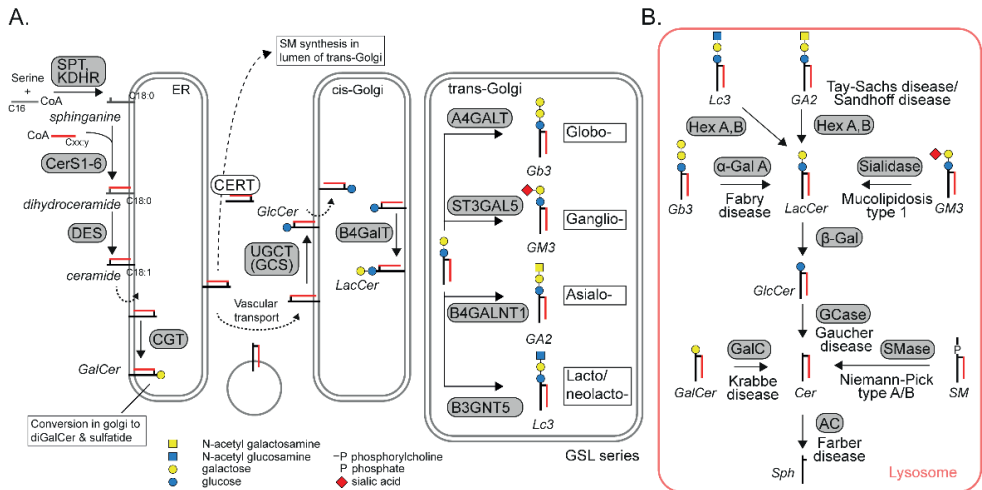


**Figure 1 | Glycosphingolipid metabolism**

Schematic representation of (glyco)sphingolipid biosynthesis and catabolism. Enzymes are depicted in grey. **(A)** (Glyco)sphingolipids (given in *italics*) are synthesized in ER and Golgi compartments. Root-structured GSLs are grouped in families (globo-, ganglio-, asialo and lacto/neolacto- series). The first GSL of the series is depicted and others are generated by sequential addition of different glycan moieties. **(B)** Catabolism of GSLs occurs in lysosomes through the sequential action of lysosomal glycosidases. A defect in one of the lysosomal glycosidases results in accumulation of GSLs and clinical symptoms specific for that lysosomal storage disorder.

## Lysosomal storage disorders

Inherited lysosomal storage disorders (LSDs) are a group of orphan diseases characterized by impaired lysosomal catabolism or lysosomal dysfunction. More than 70 LSDs occur, summarized by Platt et al., and affect collectively about 1 in 5000 live births<sup>43</sup>. The majority of the LSDs is due to mutations in genes encoding specific lysosomal glycosidases, however LSDs can also occur when related lysosomal activator proteins, lysosomal transporters or integral membrane proteins are not functioning properly<sup>21,43,47</sup>. The so-called (glyco) sphingolipidoses are those LSDs that are characterized by accumulation of (glyco) sphingolipid. Despite the similarity in the chemical nature of the storage material, the (glyco)sphingolipidoses are clinically quite distinct and with each of these diseases there is variability among patients in severity, nature of symptoms and age of onset. The primary defect and prominent clinical features of a number of relevant LSDs are summarized in **Table 1**, including selected murine and zebrafish models.

Three LSDs and their compromised lysosomal hydrolyses receive particular attention in this thesis and therefore warrant more detailed introduction. These LSDs are Gaucher disease (GD) caused by deficiency of lysosomal acid  $\beta$ -glucosidase, Fabry disease caused by deficiency of lysosomal  $\alpha$ -galactosidase A and Farber disease caused by deficiency of acid ceramidase.

**Gaucher disease** – A relatively common lysosomal storage disorder is Gaucher disease (GD), with a frequency of approximately 1 in 40.000 live births in the general population and 1 in 450 in the Ashkenazi Jewish population<sup>43</sup>. GD is caused by a defect in lysosomal acid  $\beta$ -glucosidase (glucocerebrosidase, GCase; EC 3.2.1.45) and leads to lysosomal accumulation of GlcCer, particularly in lysosomes of tissue macrophages that transform into Gaucher cells<sup>48-50</sup>. GCase is encoded by the *GBA* gene, located in man on locus 1q21, and several hundred mutations in this gene have meanwhile been associated with GD. GCase (Glycosyl Hydrolase (GH) family 30) is a 497 amino acid glycoprotein with four N-linked glycans and a retaining  $\beta$ -glucosidase with a characteristic  $(\alpha/\beta)_8$  TIM barrel catalytic domain<sup>51,52</sup>. In this domain, Glu 340 acts as catalytic nucleophile and Glu 235 as acid/base residue<sup>53</sup>. Cyclophellitol and its synthetic derivative conduritol B-epoxide (CBE) are potent suicide inhibitors of GCase that bind covalently and irreversibly to the nucleophile Glu 340 of GCase. Recently, superior inhibitors for GCase have been designed with a bulky hydrophobic substituent at C8 of the cyclophellitol<sup>54</sup>. These cyclophellitol derivatives inactivate GCase with even higher affinity and specificity than CBE and cyclophellitol, the latter inhibitors have shown to react with GBA2 and/or acid  $\alpha$ -glucosidase<sup>55</sup>. Selective activity-based probes (ABPs) have been designed by attaching a reporter group (biotin or BODIPY) to the C8 of cyclophellitol, enabling visualization and identification of active GCase<sup>56</sup>. Next, cyclophellitol aziridine ABPs with attached reporter groups have also been developed that target multiple retaining  $\beta$ -glucosidases including GCase, the cytosol faced membrane-associated protein GBA2 and the cytosolic GBA3<sup>57</sup>.

GCase is transported to lysosomes independent of the mannose-6-phosphate receptor pathway unlike other lysosomal hydrolyses<sup>58</sup>. Instead, lysosomal integral membrane

protein 2 (LIMP2) binds newly formed GCase in the ER and transports it to lysosomes<sup>59-61</sup>. Mutations in the *SCARB2* gene, encoding LIMP2, cause action myoclonus-renal failure syndrome (AMRF)<sup>62,63</sup>. Interestingly, AMRF patients do not develop lipid-laden macrophages, indicating that the residual activity of GCase in these cell, acquired by re-uptake of faulty secreted enzyme, is sufficient<sup>64</sup>. The activator lipid-binding protein saposin C (Sap C) is required for optimal intralysosomal functioning of GCase as is illustrated by the finding that defective Sap C causes symptoms similar to GD<sup>44,65</sup>.

GD is clinically remarkable heterogeneous<sup>48</sup>. Patients with considerable residual GCase activity develop only visceral symptoms, including hepatosplenomegaly, thrombocytopenia, abnormalities in coagulation, anaemia due to reduced erythrocyte populations and skeletal manifestations such as bone pain and bone fractures<sup>66-68</sup>. This non-neuronopathic type 1 GD variant differs from the acute and subacute neuronopathic GD variants type 2 and type 3. The very low residual GCase activity in types 2 and 3 GD patients causes a more severe visceral pathology with additional neurological manifestations, like epilepsy, apraxia and scoliosis<sup>48,69</sup>. Subcategories are distinguished for the heterogeneous neuronopathic GD variants and it has been proposed to consider the disorder as continuum of disease manifestations, each variable among individual patients<sup>70</sup>. An almost complete deficiency of GCase causes a unique phenotype, the collodion baby with a disturbed skin permeability barrier incompatible with terrestrial life<sup>33,71</sup>. The same lethal impairment is observed in mice with a complete genetic knockout of GCase<sup>72</sup>. GCase has an essential role in the stratum corneum where it converts extruded GlcCer lipids into ceramide which are required for formation of optimal lipid lamellae<sup>33,73</sup>.

The molecular basis for the marked phenotypic heterogeneity among GD patients is still not fully known. It is apparent that some of the several hundred *GBA* mutations are associated with a milder course of disease. For example, patients with the common amino acid substitution N370S in GCase typically display no neuropathology<sup>74</sup>. The amino acid substitution D409H in GCase is associated with cardiac symptoms involving the aortic and mitral valve<sup>75,76</sup>. On the other hand, within one *GBA* genotype, variation in severity of disease is encountered. Most strikingly, monozygotic GD twins have been reported with discordance in phenotype<sup>77,78</sup>. Modifier genes, epigenetics and external factors have been proposed to contribute to variability of disease manifestations<sup>79,80</sup>. Polymorphisms in the genes encoding LIMP2, GCS and Sap C have been put forward as GD modifiers<sup>81-83</sup>. Another candidate modifier, based on a GWAS study in patients homozygous for N370S mutation, is the ER transmembrane protein CLN8<sup>84</sup>. CLN8 has recently been shown to be involved in the transport of newly formed lysosomal enzymes between ER and Golgi apparatus<sup>85</sup>.

Mice have been used to study more closely the pathology associated with GCase deficiency. However, complete GCase deficiency in mice is lethal due to the altered permeability barrier function, as described for man<sup>33,72</sup>. Amino acid substitutions known to cause GD types 1 and 2 in man are introduced in the mouse genome, but these mice do not always show disease manifestations as observed in patients<sup>86</sup>. No phenotype or GlcCer accumulation has been observed in mice with the amino acid substitutions V394L, D409H and D409V, while mice with the common amino acid substitutions N370S, leading to type 1 GD, or L444P, causing a neuronopathic form of GD, die soon after birth<sup>87,88</sup>.

In addition to the mice with point mutations, conditional knockouts have been generated with GCase deficiency restricted to specific cell lineages, such as the hematopoietic and mesenchymal cell lineage (*Mx1-Cre-loxP*<sup>89</sup>), the neuron stem cell lineages (*Nestin-flox/flox*<sup>90</sup>) or GCase deficiency in all tissues except skin (*K14-Inl/Inl*<sup>90</sup>). Defective GCase in the hematopoietic cell lineage is sufficient to induce formation of Gaucher cells, hepatosplenomegaly and haematological symptoms<sup>91</sup>, however for skeletal deterioration a combined GCase deficiency in hematopoietic and mesenchymal cell lineages is needed<sup>89</sup>. Studies with mice developing neuropathology, either by genetically induced deficiency in neuronal cells or the overall inactivation of GCase with the suicide inhibitor CBE, have revealed that activated microglia and neuroinflammation are associated with damaged brain areas<sup>90,92</sup>. Activated microglia has been proposed by some researchers as key mediator of GD neuropathology, however whether the inflammation precedes neuron death or is concomitant with it remains unclear<sup>93-95</sup>.

No strict correlation of GCase activity levels, as measured *in vitro*, with neuropathology has been observed and intriguingly neither with GlcCer levels or those of its metabolite glucosylsphingosine (see below)<sup>95</sup>. Thus, beyond the primary defective GCase other factors might influence GD neuropathology. A considered candidate in this respect is the enzyme GBA2 that is abundant in Purkinje neuronal cell bodies and dendrites. Prominent ABP labelling of GBA2, confirmed by antibody staining, is seen in the cerebellar cortex and thalamus which coincides closer with areas involved in neuropathology than the distribution of GCase<sup>96,97</sup>. Intriguingly, carriers of mutations in the *GBA* gene have an increased risk of developing Parkinson's disease or Lewy body disorders<sup>98,99</sup>. Active GCase molecules were detected in regions involved in motor functioning, which are areas susceptible to develop Lewy Bodies<sup>96</sup>. The 20-fold increased incidence of  $\alpha$ -synucleinopathies in carriers of GD remains yet unexplained and is worldwide investigated.

It has become recognized that metabolic adaptation occur during GCase deficiency<sup>100</sup>. Firstly, in plasma and spleen of GD patients increases of the ganglioside GM3 have been noted, possibly due to increased shuttling of newly formed GlcCer to gangliosides and/ or impaired recycling of gangliosides<sup>101</sup>. The elevated concentrations of GM3 in GD patients are accompanied by insulin insensitivity, however without overt hyperglycemia<sup>102</sup>. Secondly, the  $\beta$ -glucosidases GCase and GBA2 can act as transglucosylase and form glucosylated cholesterol (GlcChol) from GlcCer and a cholesterol acceptor<sup>103-105</sup>. It has been suggested that GCase is typically involved in hydrolysis of lysosomal GlcChol, while the membrane-associated GBA2 generates GlcChol. Increased GlcChol levels were detected in plasma and spleen of GD patients and GD mouse models, while reduced GlcChol levels in plasma and liver of GBA2 deficient mice were observed<sup>103</sup>. It is conceivable that also other metabolites are glucosylated by GBA2 using GlcCer as sugar donor, which are accumulated during GCase deficiency. The possible role of excessive glucosylated metabolites in the complex GD pathology is yet unknown. Finally, accumulating GlcCer in lysosomes is converted to its sphingoid base glucosylsphingosine (GlcSph) by lysosomal acid ceramidase (ACase)<sup>106</sup>. Toxicity of excessive GlcSph in GD patients is considered in various GD disease manifestations. The lipid has been implicated in osteopenia, the common reduced bone mineral density in GD patients, through impairing osteoblasts<sup>107</sup>.

In addition, GlcSph is found to promote  $\alpha$ -synuclein aggregation, a hallmark of Parkinson disease<sup>108</sup>. It has been proposed that antigenicity of GlcCer, and possibly GlcSph, underlies the common gammopathies in GD patients that can evolve into multiple myeloma<sup>109</sup>. In addition, GlcSph has been proposed to activate the complement cascade activation and associated local tissue inflammation<sup>110,111</sup>. GlcSph is also hypothesized to diminish the cerebral microvascular density in GD mice<sup>112</sup>. In line with signs and symptoms of GD, it has been earlier hypothesized that high concentrations of GlcSph promote lysis of red blood cells, impair cell fission during cytokinesis leading to multi-nucleated cells, damage specific neurons, interfere with growth and activate pro-inflammatory phospholipase A2<sup>49</sup>.

The lipid-laden Gaucher cells are viable, alternatively activated macrophages that release specific proteins, leading to elevated plasma levels in symptomatic GD patients<sup>113</sup>. Such proteins, used as biomarkers of Gaucher cells, include the chitinase, chitotriosidase<sup>114,115</sup>, the chemokine CCL18/PARC (Chemokine (C-C motif) ligand 18; Pulmonary and activation-regulated chemokine)<sup>116</sup> and a soluble fragment of glycoprotein nonmetastatic melanoma protein B (gpNMB)<sup>117,118</sup>. Levels of these proteins as well as GlcSph levels in plasma are employed as biomarkers to assist diagnosis of GD patients and monitor treatment<sup>116,119,120</sup>.

Since Gaucher cells play a prominent role in many of the visceral symptoms of type 1 GD patients, rational therapies have been designed aiming to prevent and/or correct the lipid-laden macrophages. The first effective treatment of type 1 GD has been enzyme replacement therapy (ERT) which is aimed to supplement the GCase-lacking macrophages by repeated intravenous enzyme infusion<sup>121</sup>. The infused recombinant GCase is modified with mannose-terminal N-glycans to ensure targeting to macrophages. ERT results in prominent reduction of excessive liver and spleen volumes and correction of haematological symptoms<sup>122</sup>. However, at present, ERT does not prevent neurological symptoms due to the inability of the enzyme to pass the blood brain barrier<sup>123</sup>. An alternative treatment is substrate reduction therapy (SRT), which is aimed to balance synthesis of GlcCer with the reduced GCase activity of GD patients<sup>124,125</sup>. Miglustat and Eliglustat are two approved oral inhibitors of GCS which have been used in the clinic for years to treat type 1 GD patients without major adverse effects<sup>126-129</sup>. Brain-permeable inhibitors of GCS are presently tested<sup>130</sup>. Other types of brain-permeable small compounds are also actively studied, including chemical chaperones for improved folding of mutant GCase in the ER also called pharmacological chaperone therapy (PCT). Ongoing studies with Ambroxol, a weak inhibitor of GCase, have revealed impressive reductions in spleen and liver volumes in treated type 1 GD patients as well as neurological improvements in type 3 GD patients<sup>131,132</sup>. Another approach investigated is enzyme enhancement therapy with small compounds (EET). An example is arimoclomol, a heat shock protein amplifier found to improve refolding, maturation and lysosomal activity of GCase in GD fibroblasts and neuronal cells<sup>133</sup>.

**Fabry disease** – In 1898, two dermatologists, Johannes Fabry and William Anderson, independently published case reports of patients with characteristic skin lesions called angiokeratoma corporis diffusum<sup>134</sup>. It was soon realized that such individuals represent a distinct disease entity, now named Anderson-Fabry disease (AFD) or Fabry disease (FD). Presently, FD is thought to be the most common glycosphingolipidosis among Caucasians with a birth prevalence of at least 1 in 4000 in European populations<sup>135</sup>. FD is an X-linked disorder in man caused by deficiency of the lysosomal enzyme  $\alpha$ -galactosidase A ( $\alpha$ -GAL A; EC 3.2.1.22) encoded by the *GLA* gene (human locus Xq22)<sup>134</sup>. The gene encodes a 429 amino acid precursor that is processed to a 398 amino acid glycoprotein functioning as a homodimer<sup>134</sup>. The N-linked glycans of  $\alpha$ -Gal A acquire mannose-6-phosphate moieties and are sorted to lysosomes through interaction with mannose-6-phosphate receptors. The enzyme  $\alpha$ -GAL A is a retaining  $\alpha$ -galactosidase belonging to the GH 27 family, with a catalytic  $(\alpha/\beta)_8$  TIM barrel domain and Asp 170 acting as nucleophile and Asp 231 as acid/base<sup>136</sup>. A highly homologous  $\alpha$ -N-acetylgalactosaminidase ( $\alpha$ -NAGAL; EC 3.2.1.49) is encoded in mammals by the *NAGA* gene (human locus 22q13) due to an ancient gene duplication. The  $\alpha$ -NAGAL enzyme hydrolyses terminal  $\alpha$ -N-acetylgalactosyl moieties but shows minor  $\alpha$ -galactosidase activity *in vitro*, while  $\alpha$ -GAL A can only accommodate and hydrolyse  $\alpha$ -galactose configured lipids<sup>137,138</sup>. Substitution of two specific amino acids of the  $\alpha$ -NAGAL protein into the respective residue of  $\alpha$ -GAL A, Ser 188 into glutamic acid (Glu) and Ala 191 into leucine (Leu), renders an enzyme ( $\alpha$ -NAGAL<sup>EL</sup>) with improved activity towards the primary substrate of  $\alpha$ -GAL A, the glycosphingolipid globotriaosylceramide (Gb3)<sup>137,138</sup>. ABPs consisting of an  $\alpha$ -galactosyl configured cyclophellitol aziridine, have been designed allowing labelling of  $\alpha$ -GAL A and  $\alpha$ -NAGAL enzymes from human, mouse and plant material<sup>139,140</sup>.

In FD, glycosphingolipids accumulate with terminal  $\alpha$ -galactosyl moieties in endothelial, perithelial and smooth muscle cells of the vascular system, as well as renal epithelial cells and cells of the autonomic nervous system<sup>134</sup>. No plasma protein biomarkers of storage cells have yet been identified for FD, contrary to GD<sup>49</sup>. The most prominent storage lipid is Gb3, also named ceramidetrihexoside (CTH), with lesser amounts of galabiosylceramide (Gb2) and blood group B, B1 and P1 antigens<sup>141-144</sup>. Characteristic disease manifestations of FD in males range from skin lesions, corneal opacity, neuropathic pain (acroparasthesias), heat intolerance, inability to sweat and micro-albuminuria, while later in life progressive kidney disease, cardiac symptoms and cerebrovascular disease (stroke) may develop<sup>134</sup>. Intriguingly, many female heterozygotes display attenuated forms of FD, although with a later onset than displayed in affected hemizygous males<sup>145</sup>. The severity of manifestations has been suggested to depend on the degree of inactivation of the normal X-chromosome. A variation of 25-75% in enzyme levels has been observed with random skewing of X-inactivation<sup>145</sup>. Two atypical FD phenotypes are discerned: a cardiac and a renal variant with symptoms restricted to a single organ<sup>146,147</sup>. The N215S  $\alpha$ -GAL A substitution appears associated with the cardiac phenotype<sup>148</sup>. However, among the more than 300 reported mutations in the *GLA* gene, a large number is of unknown significance, being either disease-causing or a polymorphism<sup>149</sup>. Again, modifiers might play a role in FD manifestation. For example two polymorphisms in the *NOS3* gene, encoding eNOS, seem to influence cardiomyopathy<sup>150</sup>.

Interestingly, GD and FD differ in severity of disease manifestation in relation to residual enzyme capacity. For example, almost complete GCase deficiency results in the collodion baby and marked reduction of the activity leads to acute neuronopathic GD type 2, while  $\alpha$ -GAL A deficient FD males manifest symptoms surprisingly late in life. The correlation between Gb3-laden cells and clinical symptoms in FD patients is poor<sup>49</sup>. Therefore, it is not surprising that the present ERT treatments for FD did not prevent disease progression, despite the observed clearance of vascular endothelial Gb3 deposits<sup>151,152</sup>. The poor response of male classic FD patients can be partly ascribed to generation of neutralizing antibodies against the therapeutic enzyme<sup>153-155</sup>.

The striking discrepancies between lipid storage cells, plasma Gb3 levels and clinical symptoms as well as the disappointing outcome of ERT, prompted a search for missing pathogenic factors in FD pathology. It was discovered that in FD the lipid Gb3 is deacylated by acid ceramidase to water-soluble globotriaosylsphingosine (lysoGb3), as also observed for GlcCer in GD<sup>106,156</sup>. LysoGb3 levels are generally over hundred-fold elevated in plasma of classic male FD patients. Classic FD females often show normal plasma Gb3 levels and hardly any endothelial Gb3 deposits, while abnormal high plasma lysoGb3 is detected, thereby assisting diagnosis<sup>156,157</sup>. Chronically elevated plasma lysoGb3 is thought to be toxic. Exposure of cultured smooth muscle cells (SMCs) to lysoGb3 at concentrations encountered in classic FD males promotes their proliferation and might contribute to the increased vessel wall thickness in FD patients and associated vasculopathy<sup>158</sup>. More recently, inhibition of eNOS by lysoGb3 at concentrations as occur in plasma of GD patients has been observed, rendering an explanation for the abnormalities in FD patients in nitrogen oxide, vital for normal vasculature biology<sup>159</sup>. In addition, excessive lysoGb3 is proposed to promote fibrosis and toxic effects towards podocytes and nociceptive neurons have been documented<sup>160-162</sup>. These findings might offer an explanation for the peripheral pain and renal complications in FD patients.

**Farber disease** – Lipogranulomatosis, also known as ceramidosis or Farber disease, is due to deficiency of the lysosomal acid ceramidase (AC; N-acylsphingosine deacylase; EC 3.5.1.23)<sup>46</sup>. The human *ASAHL1* gene is located on the short arm of chromosome 8 (8p21.3-p.22). AC is synthesized as 50 kDa that, via autoproteolysis in endosomes and lysosomes, matures into 13 and 40 kDa  $\alpha$ - and  $\beta$ -subunits, respectively<sup>163,164</sup>. The  $\beta$ -subunit has 5 N-linked oligosaccharide chains but the  $\alpha$ -subunit is not glycosylated<sup>165</sup>. In AC, the nucleophilic thiol of Cys143 is exposed at the N-terminus of the  $\beta$ -subunit after the autoproteolytic cleavage of the precursor protein<sup>163</sup>. Recently, crystal structures of the proenzyme and autocleaved forms of mammalian AC enzymes were described<sup>164,166</sup>. These findings suggested a conformational change of AC upon autocleavage uncovering a narrow hydrophobic channel leading to the active site. This is thought to constrain the orientation of the ceramide lipid due to the location of the catalytic cysteine and oxyanion hole. Interestingly, it was found that head groups of larger sphingolipids cannot be fitted in the catalytic pocket in a similar manner as ceramide<sup>164</sup>. Based on the non-specific AC inhibitor Carmofur as scaffold, ABPs labelling the enzyme were designed<sup>167</sup>. Recently superior and specific ABPs reacting with AC have been designed and characterized<sup>168</sup>.



Farber published the first case report in 1952 of a lipid metabolic disorder with lipogranulomas<sup>169</sup>. Farber disease results in tissue accumulation of ceramide and is typically characterized by the manifestation of subcutaneous skin nodules which progresses to joint stiffness and immobilization<sup>170</sup>. Severe cases develop neurological symptoms such as paralysis of the arms and legs (quadriplegia), seizures, loss of speech and involuntary muscle jerks (myoclonus)<sup>171,172</sup>. The involvement of neuronal dysfunction depends on the residual lysosomal ceramide turnover<sup>170</sup>. Farber disease patients without neurological involvement can be treated with allogeneic hematopoietic stem cell transplantation<sup>170</sup>. Of note, spinal muscular atrophy with myoclonic epilepsy (SMA-PME; OMIM #159950) is also caused by mutations in the *ASAH1* gene<sup>173-175</sup>.

**Glycosphingoid bases in glycosphingolipidoses** – In recent years it has become apparent that the lysosomal AC plays a key role in several glycosphingolipidoses by mediating the deacylation of the primary accumulating GSL in the lysosome, thereby generating the respective glycosphingoid base<sup>21,106</sup>. This phenomenon is documented for Gaucher disease with GlcSph, Fabry disease with lysoGb3, but also Krabbe disease with galactosylsphingosine (GalSph) and GM2 gangliosidosis ( $\beta$ -hexosaminidase deficiency)<sup>157,176,177</sup>. Likewise, acid ceramidase seems responsible for deacylation of sphingomyelin to lysoSM in Niemann-Pick disease type A/B (acid sphingomyelinase deficiency) and Niemann-Pick disease type C<sup>178</sup>. The availability of (isotope-encoded) standards of the various sphingoid bases allows multiplex assays for various glycosphingolipidoses<sup>179</sup>. The marked increase of glycosphingoid bases assists diagnostics, monitoring disease progression and corrections by therapy. The presumed toxicity of GlcSph and lysoGb3 in GD and FD has been addressed above. A recently published double genetic mouse model of Krabbe disease and AC deficiency showed a less progressive phenotype compared to the Krabbe mouse model alone, with an increased life span, improved motor activity and only minor neuroinflammation, and suggests an acute toxicity of GalSph<sup>180</sup>. AC is envisioned as novel target for glycosphingoid base reduction therapy. However, the window for such type of intervention might be very small, due to ceramide accumulation and the induction of Farber-like symptoms by AC inhibition. The popular AC inhibitor Carmofur is notoriously aspecific, however more specific inhibitors of AC have been designed in recent years<sup>168</sup>. In conclusion, it is still unknown to which extent clinical symptoms of glycosphingolipidoses can be attributed to 'toxic' glycosphingoid bases, a possibility that deserves extensive investigation.



**Table 1 | List of sphingolipidoses**

Overview of various human sphingolipidoses with the defective protein, human gene name and accumulating material as well as reported mouse models and zebrafish models.

Disorder	Defective protein	Gene	Accumulating material	Mouse model	Zebrafish model
<b>Gaucher disease</b>	Glucocerebrosidase; GCase	<i>GBA</i>	GlcCer, GlcSph, LacCer, GlcChol	Mice KO: not viable <i>Mx1-Cre-LoxP</i> : white blood cell lineage, GD type 1 <sup>89</sup> Nestin-flox/flox: neuronal stem cell lineage, GD type 2 <sup>90</sup> K14-Inl/Inl: <i>GBA</i> KO in all tissues except skin, GD type 2 <sup>90</sup>	<i>gba</i> : Complete KO <sup>181,182</sup> Zf GCase studied in <b>Ch. 2 &amp; 3</b> Mutants studied in <b>Ch. 5-7</b>
<b>Fabry disease</b>	α-galactosidase A; α-Gal A	<i>GLA</i>	Gb3, lyso-Gb3, diGalCer, blood group B antigens	Mouse KO; only minor cardiorenal phenotype <sup>183-185</sup> Rat KO; cardiorenal phenotype and pain <sup>186-188</sup>	Not reported Zf α-Gal A studied in <b>Ch. 8</b>
<b>Krabbe disease</b>	Galactocerebrosidase	<i>GALC</i>	GalCer, GalSph	Naturally occurring Twitcher KO mouse <sup>189</sup> GALC/ACase: improved phenotype <sup>180</sup>	<i>galca/galc</i> : morphant <sup>190</sup>
<b>Schindler disease</b>	α-N-acetyl-galactosaminidase; α-NAGAL	<i>NAGA</i>	Sialylated or asialo glycopeptides and GSLs	-	Not reported
<b>Farber disease</b>	Acid ceramidase; AC	<i>ASAH</i>	Ceramide	Mouse KO <sup>191</sup>	<i>asah1b</i> : morphant <sup>174</sup> <i>asah1a/asah1b</i> : KO, <b>Ch. 6</b>
<b>Tay-Sachs disease</b>	Hexosaminidase A	<i>HEXA</i>	GM2 ganglioside, GSLs and oligosaccharides	Reviewed in <sup>192</sup> Mouse KO: limited clinical signs	
<b>Sandhoff disease</b>	Hexosaminidase B	<i>HEXB</i>	GM2 ganglioside, GA2 glycolipid and oligosaccharides	Reviewed in <sup>192</sup> Mouse KO: <sup>193</sup>	<i>Hexb</i> KO <sup>194</sup>
<b>Niemann-Pick disease type A &amp; B</b>	Acid sphingomyelinase; aSMase	<i>SMPD1</i>	SM, lyso-SM, lyso-509	aSMase mouse KO: <sup>195</sup>	Not reported
<b>Niemann-Pick disease type C</b>	NPC intracellular cholesterol transporter 1 and -2	<i>NPC1</i> <i>NPC2</i>	Cholesterol, sphingolipids, lyso-SM, lyso-509, GlcChol	Naturally occurring mouse model. <sup>97,196</sup>	<i>Npc1</i> : KO <sup>197</sup> Mutant made in <b>Ch. 4</b>

## Zebrafish as vertebrate model organism in research

Zebrafish (*Danio rerio*) are common domesticated freshwater fish, but have emerged over the past decades into a popular vertebrate model organism for research, including vertebrate genetics, development, toxicology and human diseases<sup>198</sup>.

The zebrafish is a teleost fish that is part of the Cyprinidae family, which also includes carps. They naturally occur in still waters in South Asia, however different environments have been reported including temperature ranges from 24-38 °C with no reported heat stress response<sup>199</sup>. Laboratory zebrafish are maintained according to standardized protocols, such as a fixed temperature of 28 °C, a controlled circadian rhythm, optimized water quality and feeding, in order to improve the health of the zebrafish and the amount and quality of the offspring. Breeding occurs at the onset of light: courtship by the fish is followed by egg-laying and sperm release, resulting in external fertilization. Embryonic development of zebrafish off-spring is fast at 28 °C with most major organ systems developed around 36 hours post-fertilization (hpf)<sup>200</sup>. The first cell cycles are rapid and rely on the maternally provided mRNA. The tenth cell cycle initiates the mid-blastula transition, when the cells of the embryo start transcribing and translating their own genome. A chorion protects the developing embryo from external factors and the fish hatches typically between 2 to 3 days post-fertilization (dpf). The swim bladder inflates around 3 to 4 dpf, which initiates upright swimming and feeding behaviour<sup>200</sup>. Larvae of 4 to 5 dpf have a functional digestive system, including intestine, liver, gallbladder and pancreas as well as intestinal microbiota, required to digest external food. The latter process is essential since the nutrients from the maternally deposited yolk are exhausted around 5 dpf<sup>200</sup>. Zebrafish typically become sexually mature around 10-12 weeks post-fertilization (wpf), with growth and sexual maturation depending on temperature, density and individual differences<sup>198</sup>. Zebrafish can live up to 3-4 years, however they start showing signs of aging around 2 years including a redundancy in the amount and the quality of the off-spring<sup>201</sup>.

The cost-effective maintenance, fertility, *ex vivo* fertilization and rapid development are attractive features of zebrafish for use as vertebrate animal model. Moreover, the embryonic and larval zebrafish off-spring offers additional advantages such as ex-uterine development, transparency, small size and ease of genetic manipulation with techniques such as CRISPR/Cas9. Additionally, the zebrafish genome has been sequenced and more than 26,000 protein-coding genes are annotated. There is a high conservation of genes between humans and zebrafish with 70% of the human genes having at least one orthologue in the zebrafish genome. This percentage is even higher for genes implicated in human disorders, with approximately 82% of the human genes having at least one orthologue in the zebrafish genome<sup>202</sup>. However the evolutionary divergence between man and fish ( $\pm$  450 million years) is larger than between man and rodents ( $\pm$  40 million years)<sup>203</sup>. Moreover, the teleost genome has undergone an additional genome duplication, which means that a variety of genes have two copies in the zebrafish<sup>204,205</sup>. It is not always known whether one gene copy is redundant, degenerated as pseudo-gene, or both gene copies are functional and have undergone neofunctionalization, acquiring novel functional properties, or subfunctionalization in which the ancestral function is divided and each

paralog independently performs its respective function.

In the vertebrate fish, organs and tissues are present with analogous functions to those of mammals, including brain, heart, liver, kidney, pancreas, intestinal tract and spleen. Lacking are the typical mammalian organs such as lung, skin with a stratum corneum and mammary gland. Anatomical and physiological similarities and differences have been reviewed by Lieschke and Currie<sup>206</sup>. For the study of lysosomal disorders certain organ systems are noteworthy. Firstly, the liver contains hepatocytes, endothelial cells and bile duct epithelial cells, but Kupffer cells, specialized macrophages in the mammalian liver, seem absent in fish<sup>207</sup>. Since zebrafish lack bone marrow, the kidney interstitium acts as main site for haematopoiesis, consisting of the same cell types such as erythrocytes (but nucleated), neutrophils, eosinophils, lymphocytes and macrophages<sup>206,208</sup>. Finally, the basic structure of the central nervous system in the zebrafish brain is similar to mammals, although distinct brain areas, such as the telencephalon and tectum, display more pronounced differences<sup>206,209</sup>. In contrast to mammals, zebrafish lack a distinct neocortex and neuronal populations in the midbrain are absent<sup>210</sup>. Dopaminergic neurons in the posterior tuberculum have been suggested as functional homolog of the mammalian cluster in the substantia nigra, while the fish optic tectum is suggested to perform vision-related functions performed by the neocortex of mammals<sup>211</sup>.

## Zebrafish models of lysosomal storage disorders

Various inherited and acquired human disorders are studied in zebrafish larvae or adults, ranging from cancer, inflammation, haematological, neurological and lysosomal disorders. Genetic disorders can be generated using injection of antisense morpholino oligonucleotides, resulting in a transient knockdown, also called 'morphants'<sup>212</sup>. The antisense morpholino, injected in fertilized eggs, targets both maternal and zygotic transcripts, however off-target effects are problematic and the induced phenotype is transient and can only be studied for a limited period of time<sup>212</sup>. A stable knockout is rapidly becoming the standard, assisted by the development of convenient gene-editing techniques such as CRISPR/Cas9 technology, that also allow examination of mutant adult zebrafish. Obviously, generating a stable knockout line is more labour intensive and requires more time. Published morphant and stable knockout models in zebrafish of lysosomal sphingolipid storage disorders are discussed below and summarized in **Table 1**.

**Gaucher disease: *gba*** – Three zebrafish models of GD were generated by means of a complete knockout of *gba*<sup>181,213,214</sup>. The fish are viable in contrast to complete GCase deficient mice and humans, which die immediately after birth due to trans-epidermal water loss<sup>33</sup>. Marked accumulation of GlcSph and GlcCer develops soon in zebrafish larvae (5 dpf) as well as microglial activation<sup>181,214</sup>. Around 8 wpf the phenotype worsens with an apparent curved back and reduced motor activity at 12 wpf. Infiltration of Gaucher-like cells occurs in brain and liver, with extensive microglia invasion and autophagy in the brain. Dopaminergic neuronal cell count is reduced in the caudal hypothalamus and posterior tuberculum in the presence of ubiquitin-positive, intra-neuronal inclusions in the larger hindbrain neurons<sup>181</sup>.

## Chapter 1

In another study it was noted that GCase deficiency in zebrafish is associated with defective canonical Wnt signalling, a reduction in bone mineralization and impaired osteoblast differentiation<sup>213</sup>. Chapters 5, 6 and 7 of this thesis describe *gba* knockout zebrafish as larvae and adults, recapitulating findings observed in the earlier generated models.

**Non-lysosomal GBA2** – The non-lysosomal  $\beta$ -glucosidase, GBA2, has so far been limited studied in zebrafish. An antisense morpholino knockdown of *gba2* was found to develop abnormal motor behaviour and impaired axonal outgrowths<sup>215</sup>. In chapters 5 and 7, own findings with *gba2* knockout zebrafish are described for larvae and adult fish, as well as concomitant knockouts of *gba* and *gba2*.

**Acid ceramidase deficiency: *asah1b*** – Zebrafish possess two acid ceramidase genes: *asah1a* and *asah1b* (Chapter 6 of this thesis). Previous research using transient *asah1b* morphant showed reduction of axonal outgrowths accompanied by cellular death in the spinal cord<sup>174</sup>.

**Krabbe disease: *galc*** – The zebrafish genome encodes two orthologues of human galactocerebrosidase (GALC). Both *Galca* and *Galcb* have high amino acid similarity to the human protein (both 61% identity) with a fully conserved active site with topologically conserved positions of residues required for substrate specificity<sup>190</sup>. A transient knockdown of both zebrafish *galc* co-orthologues, using morpholinos, was found to develop a neurological phenotype<sup>190</sup>. Of note, *galca/galcb* double morphants had partial Galc activity and no elevated GalSph levels were detected.

**Tay-Sachs/Sandhoff disease: *hexb*** – The dimeric  $\beta$ -hexosaminidase enzyme mediates hydrolysis of terminal  $\beta$ -N-acetylgalactosamine or  $\beta$ -N-acetylglucosamine residues of glycolipids and oligosaccharides<sup>216</sup>. Mutations in the gene encoding subunit HEXB leads to the lysosomal disorder Sandhoff disease, while a defect in HEXA leads to Tay-Sachs which has clinically identical symptoms as Sandhoff disease<sup>216,217</sup>. Patients and mouse models accumulate the ganglioside GM2 or oligosaccharides with terminal  $\beta$ -N-acetylglucosamine moieties. This metabolite accumulation is accompanied by severe neuropathology with neuronal loss and infiltration of microglia<sup>216-218</sup>. A single *hexb* gene is present in the zebrafish genome and the encoding Hexb protein shares high amino acid identity with the human orthologue (approximately 64%)<sup>194</sup>. *hexb* deficient 5 dpf larvae show abnormal lysosomes in microglia and radial glia, accompanied by reduced locomotor activity. Adult *hexb*<sup>-/-</sup> zebrafish accumulate oligosaccharides in the brain, but no neurological symptoms were observed<sup>194</sup>.

**Fabry disease: *gla*** – Although the zebrafish genome contains an orthologue of  $\alpha$ -GAL A, no transient knockdown or stable knockout of *gla* have been generated to study FD in the fish. A plausible explanation for this is the lack of globosides in fish due to the absence of the enzyme generating Gb3, Gb3 synthase also called A4GALT, which is the subject of investigations described in chapter 7.

**Niemann-Pick type C** – Low-density lipoprotein particles (LDL) end up in lysosomes following endocytosis where cholesterol esters are processed by the lysosomal acid lipase to cholesterol. Next, free cholesterol binds to NPC2, a small soluble glycoprotein that transfers it to the large, transmembrane protein NPC1, which mediates export from the lysosome<sup>219</sup>. Niemann-Pick disease type C (NPC) is caused by mutations in the genes encoding NPC1, encompassing approximately 95% of the clinical cases, or encoding NPC2. The impaired efflux of cholesterol from lysosome causes secondary deficiencies in activities of acid sphingomyelinase and GCase in lysosomes. As a result, cholesterol, sphingomyelin and GlcCer accumulate in liver, spleen and brain of NPC patients<sup>97</sup>. The clinical presentation of NPC is heterogeneous and includes visceral symptoms and progressive neurodegeneration with an onset in infancy or childhood, although lethal, prenatal onset has been described in severe NPC cases<sup>43,220</sup>.

Zebrafish *Npc1* shows 60% of identity with the polypeptide sequence of human NPC1 and shares the NPC-like region (NPCL) as well as the SSD motif crucial for correct functioning of NPC1<sup>221</sup>. *Npc1* knockouts have been generated. The mutant fish are significantly smaller than *npc1*<sup>+/+</sup> siblings and die sooner<sup>197,222</sup>. Mutants show an early-onset liver defect, with large vacuole-like structures and accumulation of unesterified cholesterol. Later in life, *npc1* mutant fish present hepatosplenomegaly, a severe liver defect and develop disorganized swimming suggesting a CNS defect<sup>197,222</sup>. The abnormal phenotype starts with an impaired ability to maintain an upright position during swimming, which progresses rapidly into rapid spinning and tumbling movements<sup>197</sup>. Neurological abnormalities are observed, including axonal spheroids in the hindbrain and disorganized Purkinje neurons in the cerebellum, corresponding to findings in patients and mammalian models<sup>196,223,224</sup>.

## Tools to study zebrafish

Several standard histopathological, biochemical and analytical techniques can be used to study zebrafish (**Table 2** and **Figure 2**). Additional techniques exploit the beneficial features of zebrafish such as extra-uterine development and transparency. In the past years, numerous zebrafish lines have been generated expressing fluorescent reporters that either mark specific cell-types, sub-cellular compartments or under regulation of an inducible promoter<sup>225,226</sup>. These lines are also summarized on [zfin.org](http://zfin.org)<sup>227</sup>. Generation of a knockout in zebrafish using CRISPR/Cas9 or overexpression of a given gene is experimentally straightforward and can be achieved in a matter of months. The small size of larvae make them fit in 96-well plates, allowing easy administration of small molecules by addition to the swimming water, often in combination with phenotypic high-throughput screenings<sup>228</sup>.

For the investigation of lysosomal glycosidases, several tools are available. Enzyme activities can be evaluated by studying the activity towards commercial fluorogenic substrates, such as 4-methylumbelliferone (4MU)-sugars, or nitrobenzoxadiazole (NBD)-labelled lipids. A novel tool-box comprise cyclophellitol activity-based probes (ABPs) that label specific retaining glycosidases<sup>229</sup>. As discussed above, the first ABP was developed for GCase<sup>56</sup>. This approach has been extended to other glycosidases with tuning of the configuration of the broad-spectrum aziridine-cyclophellitol scaffold to match the configuration of the target lysosomal retaining glycosidase (**Table 2**). The mechanism-based binding of the ABP allows profiling of glycosidases from man to plant and bacterial origin<sup>57,140</sup>. ABPs are particularly useful for zebrafish materials as limited zebrafish specific antibodies are available and antibodies reacting with protein from man or mouse origin generally do not cross-react. Of note, activity-based and affinity-based probes are also available for other enzyme classes including kinases<sup>230</sup>, serine hydrolases<sup>231,232</sup> and cathepsins<sup>233</sup>. In principle, ABPs could be employed to visualize active enzymes in transparent zebrafish larvae. However, further optimization of probes and methodology is however still required to reach better window between enzyme labelling and non-specific labelling stemming from unreacted probe.

Cyclophellitol analogues can also be employed to specifically inactivate glycosidases of interest. It has been recently demonstrated that GCase in zebrafish can be inactivated on demand by exposure of the animals to ME656, a cyclophellitol with a bulky hydrophobic group at C8<sup>54</sup>. Pharmacological inactivation of GCase or other glycosidases nicely complements the study of genetic knockouts of these glycosidases<sup>214</sup>.

Finally, ultrasensitive LC-MS/MS techniques are available to quantitatively measure glycosphingolipid abnormalities<sup>103,179</sup>. These protocols are exploited, optimized and broadened in this thesis in order to measure a broad range of sphingolipids and GSL in the limited zebrafish material. In particular, the impressive sensitivity of GSL detection enabled monitoring of individual zebrafish larvae<sup>214</sup>.

Table 2 | Toolbox

Overview of genetic-, biochemical-, pathological- and *in vivo* tools used to study zebrafish larvae or adults.

Type of tool			Chapter
Genetic-	Genome-editing	CRISPR/Cas9 and Tol2 transposase	Chapter 4
	Transgenic zebrafish	Expression of reporter tag using (sub)cellular promoter	
Biochemical-	Fluorogenic substrates		Chapter 2, 3, 8
	Activity-based probes	Cyclophellitol-configured molecule modified with a reporter tag	Chapter 3, 5
			Chapter 3, 5
			Chapter 3
			Chapter 3
			Chapter 8
			Chapter 8
			Chapter 3
			Chapter 3
	Mass spectrometry	Quantitative detection of sphingolipids and GSLs (LC-MS/MS)	Chapter 2-8
	Protein expression	Immunoblotting using antibodies	Chapter 6 & 7
Pathological-	RNA expression	RT-qPCR using specific primers, RNA sequencing	Chapter 6 & 7
	Histology	Standard stains for microscopic anatomy For example: haematoxylin & eosin	Chapter 6 & 7
	Immunohistochemistry	Visualize (sub)cellular localization of target protein	-
	In situ hybridization	Visualize (sub)cellular localization of target mRNA	-
In vivo-	Transgenic lines	See above	-
	Life stains	Visualize specific cells or compartments <i>in vivo</i> and in real-time. For example: lysotracker to visualize lysosomes	-
	Phenotype	Morphology & behavioural studies	Chapter 6, 7
	Drug administration	Emerge ZF in swimming water with small molecule	Chapter 3, 5

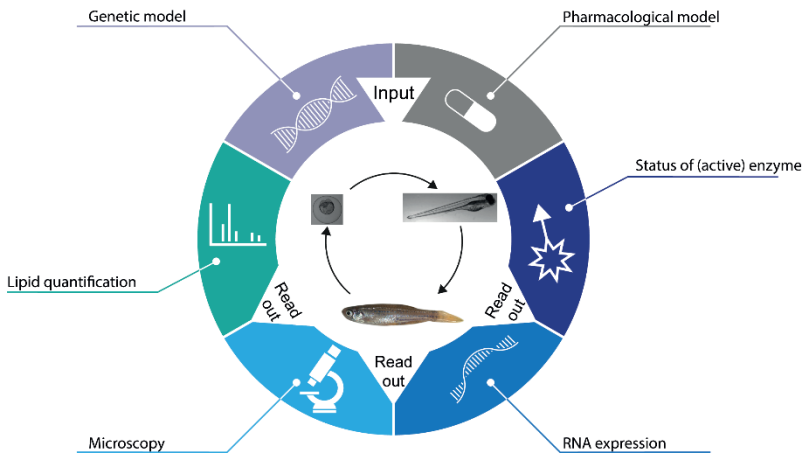


Figure 2 | Zebrafish as research model for glycosphingolipidoses

## Goals of the thesis investigations

The primary goal of this thesis has been to use zebrafish as vertebrate animal model for the investigation of lysosomal storage disorders, in particular Gaucher disease (GD). Several biochemical and genetic techniques have been used and optimized in order to study the catalytic features of zebrafish glucocerebrosidase (GCase) and to investigate the consequences of its defect in zebrafish larvae and adults. In addition, the impact of two other enzymes, non-lysosomal GBA2 and lysosomal acid ceramidase, on GCase-deficient zebrafish received attention.

In **chapter 2**, GCase enzymes from different species (man, zebrafish, frog and turtle) are compared in enzymatic features by means of biochemical assays and *in silico* structure analysis using homology modelling of human GCase. Subtle differences were noted among the different GCase enzymes. Zebrafish and frog GCase required no additives for *in vitro* hydrolysis contrary to the human enzyme, while the fish enzyme was not able to perform transglucosylation in contrast to frog and human enzyme. Over-expression of the GCase enzymes from the different species corrected increased GlcCer and GlcSph levels in human GCase deficient cells.

**Chapter 3** reports on the pharmacological inactivation of GCase in zebrafish and compares conduritol B epoxide, cyclophellitol and newly synthesized cyclophellitol derivatives in selectivity towards GCase and other retaining glycosidases. Adult zebrafish allowed the assessment of brain permeability of the new superior GCase inhibitors.

In **chapter 4** a detailed protocol for the generation of knockouts in zebrafish by CRISPR/Cas9 technology is described, including notes and considerations. The chapter also includes information on the genomic location and obtained mutations in the genes of *gba1*, *gba2*, *gpnmb*, *asah1a*, *asah1b*, *npc1* and *cln8*. Finally, proof-of-concept is provided for the introduction of exogenous target DNA sequences in the zebrafish genome using the Tol2 transposase technique.

**Chapter 5** evaluates the metabolism of glucosylceramide (GlcCer) in zebrafish larvae (up to 5 days post-fertilization, 5dpf) that are single or double knockouts of *gba1* and *gba2*. Adaptations in lipid metabolism as the result of enzyme deficiencies were monitored by LC-MS/MS methods. Recapitulating GD, *gba1* knockout larvae massively generate glucosylsphingosine (GlcSph). In addition, the feasibility of pharmacological modulation of GlcCer metabolism in individual 5 dpf larvae is reported.

In **chapter 6** the detrimental role of excessive GlcSph in GD pathology is evaluated. A specific acid ceramidase (*Asah1b*) is reported which is responsible for conversion of GlcCer to GlcSph. The other acid ceramidase (*Asah1a*) is not able to generate GlcSph, however its presence prohibits ceramide accumulation. Comparing *gba1* knockout zebrafish with excessive GlcSph to *gba1:asah1b* knockout zebrafish without GlcSph, rendered new insight in the toxicity of the sphingoid base and the role of storage cells, neuroinflammation and neurodegeneration in the pathophysiology of GD.



**Chapter 7** reports an overview and comparison of biochemical and pathological findings of adult zebrafish with a knockout of *gba1*, *gba2* and *asah1b* and combinations thereof. In addition mutant zebrafish at different developmental stages are examined with emphases on morphology and accompanying lipid-, protein and RNA abnormalities. The investigation sheds further light on the effects of non-functional Gba2 or acid ceramidase during GCase deficiency in zebrafish.

**Chapter 8** concerns the potential use of zebrafish to study a different lysosomal storage disorder, Fabry disease. The presence of  $\alpha$ -Gal A and  $\alpha$ -Nagal enzymes in zebrafish cells, larvae and organs is described.

**Chapter 9** discusses the obtained results of the undertaken investigations and describes future prospects of research. Opportunities are described including established and novel techniques to address other common clinical manifestations of GD patients and study their underlying molecular mechanisms. In addition, anatomical and physiological similarities and differences of the zebrafish compared to mammals are discussed in order to put the use of the zebrafish GD model in perspective.

## References

1. Thudichum J.L.W. (1884) A treatise on the chemical constitution of the brain, (London: Bailliere Tindall and Cox).
2. Wennekens T., van den Berg R.J., Boot R.G., van der Marel G.A., Overkleeft H.S. and Aerts J.M. (2009) Glycosphingolipids--nature, function, and pharmacological modulation. *Angewandte Chemie* **48**, 8848-8869.
3. Merrill A.H., Jr. (2011) Sphingolipid and glycosphingolipid metabolic pathways in the era of sphingolipidomics. *Chem Rev* **111**, 6387-6422.
4. Carter H.E., Glick F.J., Norris W.P. and Phillips G.E. (1947) Biochemistry of the Sphingolipides .3. Structure of Sphingosine. *J Biol Chem* **170**, 285-294.
5. Kraut R. (2011) Roles of sphingolipids in Drosophila development and disease. *J Neurochem* **116**, 764-778.
6. Cabasso O., Paul S., Dorot O., Maor G., Krivoruk O., Pasmanik-Chor M.,... and Horowitz M. (2019) Drosophila melanogaster Mutated in its GBA1b Ortholog Recapitulates Neuronopathic Gaucher Disease. *J Clin Med* **8**.
7. Levy M. and Futerman A.H. (2010) Mammalian ceramide synthases. *IUBMB Life* **62**, 347-356.
8. Laviad E.L., Albee L., Pankova-Kholmyansky I., Epstein S., Park H., Merrill A.H., Jr. and Futerman A.H. (2008) Characterization of ceramide synthase 2: tissue distribution, substrate specificity, and inhibition by sphingosine 1-phosphate. *J Biol Chem* **283**, 5677-5684.
9. Becker I., Wang-Eckhardt L., Yaghootfam A., Gieselmann V. and Eckhardt M. (2008) Differential expression of (dihydro)ceramide synthases in mouse brain: oligodendrocyte-specific expression of CerS2/Lass2. *Histochem Cell Biol* **129**, 233-241.
10. Sandhoff R. (2010) Very long chain sphingolipids: tissue expression, function and synthesis. *FEBS Lett* **584**, 1907-1913.
11. Mizutani Y., Kihara A., Chiba H., Tojo H. and Igarashi Y. (2008) 2-Hydroxy-ceramide synthesis by ceramide synthase family: enzymatic basis for the preference of FA chain length. *J Lipid Res* **49**, 2356-2364.
12. Rabionet M., Gorgas K. and Sandhoff R. (2014) Ceramide synthesis in the epidermis. *Biochimica et biophysica acta* **1841**, 422-434.
13. Hanada K., Kumagai K., Yasuda S., Miura Y., Kawano M., Fukasawa M. and Nishijima M. (2003) Molecular machinery for non-vesicular trafficking of ceramide. *Nature* **426**, 803-809.
14. Wieland Brown L.C., Penaranda C., Kashyap P.C., Williams B.B., Clardy J., Kronenberg M.,... and Fischbach M.A. (2013) Production of alpha-galactosylceramide by a prominent member of the human gut microbiota. *Plos Biol* **11**, e1001610.
15. Natori T., Koezuka Y. and Higa T. (1993) Agelasphins, Novel Alpha-Galactosylceramides from the Marine Sponge Agelas-Mauritianus. *Tetrahedron Lett* **34**, 5591-5592.
16. von Gerichten J., Schlosser K., Lamprecht D., Morace I., Eckhardt M., Wachten D.,... and Sandhoff R. (2017) Diastereomer-specific quantification of bioactive hexosylceramides from bacteria and mammals. *J Lipid Res* **58**, 1247-1258.
17. Sprong H., Kruitthof B., Leijendekker R., Slot J.W., van Meer G. and van der Sluijs P. (1998) UDP-galactose:ceramide galactosyltransferase is a class I integral membrane protein of the endoplasmic reticulum. *J Biol Chem* **273**, 25880-25888.
18. van Weely S., Brandsma M., Strijland A., Tager J.M. and Aerts J.M. (1993) Demonstration of the existence of a second, non-lysosomal glucocerebrosidase that is not deficient in Gaucher disease. *Biochimica et biophysica acta* **1181**, 55-62.
19. Yildiz Y., Matern H., Thompson B., Allegood J.C., Warren R.L., Ramirez D.M.,... and Russell D.W. (2006) Mutation of beta-glucosidase 2 causes glycolipid storage disease and impaired male fertility. *The Journal of clinical investigation* **116**, 2985-2994.
20. Boot R.G., Verhoek M., Donker-Koopman W., Strijland A., van Marle J., Overkleeft H.S.,... and Aerts J.M. (2007) Identification of the non-lysosomal glucosylceramidase as beta-glucosidase 2. *J Biol Chem* **282**, 1305-1312.
21. Aerts J., Kuo C.L., Lelieveld L.T., Boer D.E.C., van der Lienden M.J.C., Overkleeft H.S. and Artola M. (2019) Glycosphingolipids and lysosomal storage disorders as illustrated by gaucher disease. *Current opinion in chemical biology* **53**, 204-215.
22. Munro S. (2003) Lipid rafts: elusive or illusive? *Cell* **115**, 377-388.
23. Mukherjee S. and Maxfield F.R. (2004) Membrane domains. *Annu Rev Cell Dev Biol* **20**, 839-866.
24. Sonnino S. and Prinetti A. (2013) Membrane domains and the "lipid raft" concept. *Curr Med Chem* **20**, 4-21.
25. Lingwood D. and Simons K. (2010) Lipid rafts as a membrane-organizing principle. *Science* **327**, 46-50.
26. Kolter T. and Sandhoff K. (2010) Lysosomal degradation of membrane lipids. *FEBS Lett* **584**, 1700-1712.
27. Aerts J., Artola M., van Eijk M., Ferraz M.J. and Boot R.G. (2019) Glycosphingolipids and Infection. Potential New Therapeutic Avenues. *Front Cell Dev Biol* **7**, 324.
28. Langeveld M. and Aerts J.M. (2009) Glycosphingolipids and insulin resistance. *Prog Lipid Res* **48**, 196-205.

29. Nakayama H., Nagafuku M., Suzuki A., Iwabuchi K. and Inokuchi J.I. (2018) The regulatory roles of glycosphingolipid-enriched lipid rafts in immune systems. *FEBS Lett* **592**, 3921-3942.
30. Garcia-Ruiz C., Morales A. and Fernandez-Checa J.C. (2015) Glycosphingolipids and cell death: one aim, many ways. *Apoptosis* **20**, 607-620.
31. Yu R.K., Tsai Y.T., Ariga T. and Yanagisawa M. (2011) Structures, biosynthesis, and functions of gangliosides--an overview. *J Oleo Sci* **60**, 537-544.
32. Schmitt S., Castelvetti L.C. and Simons M. (2015) Metabolism and functions of lipids in myelin. *Biochimica et biophysica acta* **1851**, 999-1005.
33. Holleran W.M., Ginns E.I., Menon G.K., Grundmann J.U., Fartasch M., McKinney C.E.,... and Sidransky E. (1994) Consequences of beta-glucocerebrosidase deficiency in epidermis. Ultrastructure and permeability barrier alterations in Gaucher disease. *The Journal of clinical investigation* **93**, 1756-1764.
34. Doering T., Holleran W.M., Potratz A., Vielhaber G., Elias P.M., Suzuki K. and Sandhoff K. (1999) Sphingolipid activator proteins are required for epidermal permeability barrier formation. *J Biol Chem* **274**, 11038-11045.
35. Gillard B.K., Thurmon L.T. and Marcus D.M. (1993) Variable subcellular localization of glycosphingolipids. *Glycobiology* **3**, 57-67.
36. Contreras F.X., Ernst A.M., Haberkant P., Bjorkholm P., Lindahl E., Gonen B.,... and Brugger B. (2012) Molecular recognition of a single sphingolipid species by a protein's transmembrane domain. *Nature* **481**, 525-529.
37. Taha T.A., Mullen T.D. and Obeid L.M. (2006) A house divided: ceramide, sphingosine, and sphingosine-1-phosphate in programmed cell death. *Biochimica et biophysica acta* **1758**, 2027-2036.
38. Spiegel S. and Milstien S. (2003) Sphingosine-1-phosphate: an enigmatic signalling lipid. *Nat Rev Mol Cell Biol* **4**, 397-407.
39. Rohrbach T., Maceyka M. and Spiegel S. (2017) Sphingosine kinase and sphingosine-1-phosphate in liver pathobiology. *Crit Rev Biochem Mol Biol* **52**, 543-553.
40. Maceyka M., Harikumar K.B., Milstien S. and Spiegel S. (2012) Sphingosine-1-phosphate signaling and its role in disease. *Trends Cell Biol* **22**, 50-60.
41. Coant N., Sakamoto W., Mao C. and Hannun Y.A. (2017) Ceramidases, roles in sphingolipid metabolism and in health and disease. *Adv Biol Regul* **63**, 122-131.
42. Breiden B. and Sandhoff K. (2018) Ganglioside Metabolism and Its Inherited Diseases. *Methods Mol Biol* **1804**, 97-141.
43. Platt F.M., d'Azzo A., Davidson B.L., Neufeld E.F. and Tift C.J. (2018) Lysosomal storage diseases. *Nat Rev Dis Primers* **4**, 27.
44. Tytki-Szymanska A., Czartoryska B., Vanier M.T., Poorthuis B.J., Groener J.A., Lugowska A.,... and Jurkiewicz E. (2007) Non-neuronopathic Gaucher disease due to saposin C deficiency. *Clin Genet* **72**, 538-542.
45. Tytki-Szymanska A., Groener J.E., Kaminski M.L., Lugowska A., Jurkiewicz E. and Czartoryska B. (2011) Gaucher disease due to saposin C deficiency, previously described as non-neuronopathic form--no positive effects after 2-years of miglustat therapy. *Mol Genet Metab* **104**, 627-630.
46. Park J.H. and Schuchman E.H. (2006) Acid ceramidase and human disease. *Biochimica et biophysica acta* **1758**, 2133-2138.
47. Ballabio A. and Gieselmann V. (2009) Lysosomal disorders: from storage to cellular damage. *Biochimica et biophysica acta* **1793**, 684-696.
48. Beutler E. and Grabowski G.A. (2001) Gaucher disease. In *The Metabolic and Molecular Bases of Inherited disease*, Volume III, 8th Edition, C.R. Scriver, A.L. Beaudet, W.S. Sly and D. Valle, eds. (New York: McGraw-Hill), pp. 3635-3668.
49. Ferraz M.J., Kallemeijn W.W., Mirzaian M., Herrera Moro D., Marques A., Wisse P.,... and Aerts J.M. (2014) Gaucher disease and Fabry disease: new markers and insights in pathophysiology for two distinct glycosphingolipidoses. *Biochimica et biophysica acta* **1841**, 811-825.
50. Brady R.O., Kanfer J.N., Bradley R.M. and Shapiro D. (1966) Demonstration of a deficiency of glucocerebrosidase-cleaving enzyme in Gaucher's disease. *The Journal of clinical investigation* **45**, 1112-1115.
51. Dvir H., Harel M., McCarthy A.A., Toker L., Silman I., Futerman A.H. and Sussman J.L. (2003) X-ray structure of human acid-beta-glucosidase, the defective enzyme in Gaucher disease. *EMBO Rep* **4**, 704-709.
52. Brumshtein B., Greenblatt H.M., Butters T.D., Shaaltiel Y., Aviezer D., Silman I.,... and Sussman J.L. (2007) Crystal structures of complexes of N-butyl- and N-nonyl-deoxynojirimycin bound to acid beta-glucosidase: insights into the mechanism of chemical chaperone action in Gaucher disease. *J Biol Chem* **282**, 29052-29058.
53. Kallemeijn W.W., Witte M.D., Voorn-Brouwer T.M., Walvoort M.T., Li K.Y., Codee J.D.,... and Aerts J.M. (2014) A sensitive gel-based method combining distinct cyclophellitol-based probes for the identification of acid/base residues in human retaining beta-glucosidases. *J Biol Chem* **289**, 35351-35362.
54. Artola M., Kuo C.L., Lelieveld L.T., Rowland R.J., van der Marel G.A., Codee J.D.C.,... and Overkleeft H.S. (2019) Functionalized Cyclophellitols Are Selective Glucocerebrosidase Inhibitors and Induce a Bona Fide

- Neuropathic Gaucher Model in Zebrafish. *Journal of the American Chemical Society* **141**, 4214-4218.
55. Kuo C.L., Kallemeijn W.W., Lelieveld L.T., Mirzaian M., Zoutendijk I., Vardi A.,... and Artola M. (2019) In vivo inactivation of glycosidases by conduritol B epoxide and cyclophellitol as revealed by activity-based protein profiling. *FEBS J* **286**, 584-600.
  56. Witte M.D., Kallemeijn W.W., Aten J., Li K.Y., Strijland A., Donker-Koopman W.E.,... and Aerts J.M. (2010) Ultrasensitive in situ visualization of active glucocerebrosidase molecules. *Nature chemical biology* **6**, 907-913.
  57. Kallemeijn W.W., Li K.Y., Witte M.D., Marques A.R., Aten J., Scheij S.,... and Overkleeft H.S. (2012) Novel activity-based probes for broad-spectrum profiling of retaining beta-exoglucosidases in situ and in vivo. *Angewandte Chemie* **51**, 12529-12533.
  58. Aerts J.M., Schram A.W., Strijland A., van Weely S., Jonsson L.M., Tager J.M.,... and Murray G.J. (1988) Glucocerebrosidase, a lysosomal enzyme that does not undergo oligosaccharide phosphorylation. *Biochimica et biophysica acta* **964**, 303-308.
  59. Rijnboutt S., Aerts H.M., Geuze H.J., Tager J.M. and Strous G.J. (1991) Mannose 6-phosphate-independent membrane association of cathepsin D, glucocerebrosidase, and sphingolipid-activating protein in HepG2 cells. *J Biol Chem* **266**, 4862-4868.
  60. Reczek D., Schwake M., Schroder J., Hughes H., Blanz J., Jin X.,... and Saftig P. (2007) LIMP-2 is a receptor for lysosomal mannose-6-phosphate-independent targeting of beta-glucocerebrosidase. *Cell* **131**, 770-783.
  61. Saftig P. and Klumperman J. (2009) Lysosome biogenesis and lysosomal membrane proteins: trafficking meets function. *Nat Rev Mol Cell Biol* **10**, 623-635.
  62. Berkovic S.F., Dibbens L.M., Oshlack A., Silver J.D., Katerelos M., Vears D.F.,... and Bahlo M. (2008) Array-based gene discovery with three unrelated subjects shows SCARB2/LIMP-2 deficiency causes myoclonus epilepsy and glomerulosclerosis. *Am J Hum Genet* **82**, 673-684.
  63. Dibbens L.M., Michelucci R., Gambardella A., Andermann F., Rubboli G., Bayly M.A.,... and Berkovic S.F. (2009) SCARB2 mutations in progressive myoclonus epilepsy (PME) without renal failure. *Ann Neurol* **66**, 532-536.
  64. Gaspar P., Kallemeijn W.W., Strijland A., Scheij S., Van Eijk M., Aten J.,... and Aerts J.M. (2014) Action myoclonus-renal failure syndrome: diagnostic applications of activity-based probes and lipid analysis. *J Lipid Res* **55**, 138-145.
  65. Vaccaro A.M., Motta M., Tatti M., Scarpa S., Masuelli L., Bhat M.,... and Salvio R. (2010) Saposin C mutations in Gaucher disease patients resulting in lysosomal lipid accumulation, saposin C deficiency, but normal prosaposin processing and sorting. *Human molecular genetics* **19**, 2987-2997.
  66. Hollak C.E., Levi M., Berends F., Aerts J.M. and van Oers M.H. (1997) Coagulation abnormalities in type 1 Gaucher disease are due to low-grade activation and can be partly restored by enzyme supplementation therapy. *Br J Haematol* **96**, 470-476.
  67. Wenstrup R.J., Roca-Espiau M., Weinreb N.J. and Bembi B. (2002) Skeletal aspects of Gaucher disease: a review. *Br J Radiol* **75 Suppl 1**, A2-12.
  68. Stirnemann J., Belmatoug N., Camou F., Serratrice C., Froissart R., Caillaud C.,... and Berger M.G. (2017) A Review of Gaucher Disease Pathophysiology, Clinical Presentation and Treatments. *Int J Mol Sci* **18**.
  69. Wong K., Sidransky E., Verma A., Mixon T., Sandberg G.D., Wakefield L.K.,... and Schiffmann R. (2004) Neuropathology provides clues to the pathophysiology of Gaucher disease. *Mol Genet Metab* **82**, 192-207.
  70. Sidransky E. (2004) Gaucher disease: complexity in a "simple" disorder. *Mol Genet Metab* **83**, 6-15.
  71. Stone D.L., Carey W.F., Christodoulou J., Sillence D., Nelson P., Callahan M.,... and Sidransky E. (2000) Type 2 Gaucher disease: the collodion baby phenotype revisited. *Arch Dis Child Fetal Neonatal Ed* **82**, F163-166.
  72. Sidransky E., Sherer D.M. and Ginns E.I. (1992) Gaucher disease in the neonate: a distinct Gaucher phenotype is analogous to a mouse model created by targeted disruption of the glucocerebrosidase gene. *Pediatr Res* **32**, 494-498.
  73. van Smeden J., Dijkhoff I.M., Helder R.W.J., Al-Khakany H., Boer D.E.C., Schreuder A.,... and Bouwstra J.A. (2017) In situ visualization of glucocerebrosidase in human skin tissue: zymography versus activity-based probe labeling. *J Lipid Res* **58**, 2299-2309.
  74. Boot R.G., Hollak C.E., Verhoek M., Sloof P., Poorthuis B.J., Kleijer W.J.,... and van Weely S. (1997) Glucocerebrosidase genotype of Gaucher patients in The Netherlands: limitations in prognostic value. *Hum Mutat* **10**, 348-358.
  75. Abrahamov A., Elstein D., Gross-Tsur V., Farber B., Glaser Y., Hadas-Halpern I.,... and Zimran A. (1995) Gaucher's disease variant characterised by progressive calcification of heart valves and unique genotype. *Lancet* **346**, 1000-1003.
  76. Chabas A., Cormand B., Grinberg D., Burguera J.M., Balcells S., Merino J.L.,... and Vilageliu L. (1995) Unusual expression of Gaucher's disease: cardiovascular calcifications in three sibs homozygous for the D409H mutation. *J Med Genet* **32**, 740-742.

77. Biegstraaten M., van Schaik I.N., Aerts J.M., Langeveld M., Mannens M.M., Bour L.J.,... and Hollak C.E. (2011) A monozygotic twin pair with highly discordant Gaucher phenotypes. *Blood Cells Mol Dis* **46**, 39-41.
78. Lachmann R.H., Grant I.R., Halsall D. and Cox T.M. (2004) Twin pairs showing discordance of phenotype in adult Gaucher's disease. *QJM* **97**, 199-204.
79. Goker-Alpan O., Hruska K.S., Orvisky E., Kishnani P.S., Stubblefield B.K., Schiffmann R. and Sidransky E. (2005) Divergent phenotypes in Gaucher disease implicate the role of modifiers. *J Med Genet* **42**, e37.
80. Lo S.M., Choi M., Liu J., Jain D., Boot R.G., Kallemijn W.W.,... and Mistry P.K. (2012) Phenotype diversity in type 1 Gaucher disease: discovering the genetic basis of Gaucher disease/hematologic malignancy phenotype by individual genome analysis. *Blood* **119**, 4731-4740.
81. Velayati A., DePaolo J., Gupta N., Choi J.H., Moaven N., Westbroek W.,... and Sidransky E. (2011) A mutation in SCARB2 is a modifier in Gaucher disease. *Hum Mutat* **32**, 1232-1238.
82. Alfonso P., Navascues J., Navarro S., Medina P., Bolado-Carrancio A., Andreu V.,... and Giraldo P. (2013) Characterization of variants in the glucosylceramide synthase gene and their association with type 1 Gaucher disease severity. *Hum Mutat* **34**, 1396-1403.
83. Siebert M., Westbroek W., Chen Y.C., Moaven N., Li Y., Velayati A.,... and Sidransky E. (2014) Identification of miRNAs that modulate glucocerebrosidase activity in Gaucher disease cells. *RNA Biol* **11**, 1291-1300.
84. Zhang C.K., Stein P.B., Liu J., Wang Z., Yang R., Cho J.H.,... and Mistry P.K. (2012) Genome-wide association study of N370S homozygous Gaucher disease reveals the candidacy of CLN8 gene as a genetic modifier contributing to extreme phenotypic variation. *Am J Hematol* **87**, 377-383.
85. di Ronza A., Bajaj L., Sharma J., Sanagasetti D., Lotfi P., Adamski C.J.,... and Sardiello M. (2018) CLN8 is an endoplasmic reticulum cargo receptor that regulates lysosome biogenesis. *Nat Cell Biol* **20**, 1370-1377.
86. Farfel-Becker T., Vitner E.B. and Futerman A.H. (2011) Animal models for Gaucher disease research. *Dis Model Mech* **4**, 746-752.
87. Xu Y.H., Quinn B., Witte D. and Grabowski G.A. (2003) Viable mouse models of acid beta-glucosidase deficiency: the defect in Gaucher disease. *Am J Pathol* **163**, 2093-2101.
88. Liu Y., Suzuki K., Reed J.D., Grinberg A., Westphal H., Hoffmann A.,... and Proia R.L. (1998) Mice with type 2 and 3 Gaucher disease point mutations generated by a single insertion mutagenesis procedure. *Proc Natl Acad Sci U S A* **95**, 2503-2508.
89. Mistry P.K., Liu J., Yang M., Nottoli T., McGrath J., Jain D.,... and Zaidi M. (2010) Glucocerebrosidase gene-deficient mouse recapitulates Gaucher disease displaying cellular and molecular dysregulation beyond the macrophage. *Proc Natl Acad Sci U S A* **107**, 19473-19478.
90. Enquist I.B., Lo Bianco C., Ooka A., Nilsson E., Mansson J.E., Ehinger M.,... and Karlsson S. (2007) Murine models of acute neuronopathic Gaucher disease. *Proc Natl Acad Sci U S A* **104**, 17483-17488.
91. Dahl M., Doyle A., Olsson K., Mansson J.E., Marques A.R.A., Mirzaian M.,... and Karlsson S. (2015) Lentiviral gene therapy using cellular promoters cures type 1 Gaucher disease in mice. *Mol Ther* **23**, 835-844.
92. Vardi A., Zigdon H., Meshcheriakova A., Klein A.D., Yaacobi C., Eilam R.,... and Futerman A.H. (2016) Delineating pathological pathways in a chemically induced mouse model of Gaucher disease. *J Pathol* **239**, 496-509.
93. Farfel-Becker T., Vitner E.B., Pressey S.N., Eilam R., Cooper J.D. and Futerman A.H. (2011) Spatial and temporal correlation between neuron loss and neuroinflammation in a mouse model of neuronopathic Gaucher disease. *Human molecular genetics* **20**, 1375-1386.
94. Vitner E.B., Farfel-Becker T., Eilam R., Biton I. and Futerman A.H. (2012) Contribution of brain inflammation to neuronal cell death in neuronopathic forms of Gaucher's disease. *Brain* **135**, 1724-1735.
95. Farfel-Becker T., Vitner E.B., Kelly S.L., Bame J.R., Duan J., Shinder V.,... and Futerman A.H. (2014) Neuronal accumulation of glucosylceramide in a mouse model of neuronopathic Gaucher disease leads to neurodegeneration. *Human molecular genetics* **23**, 843-854.
96. Herrera Moro Chao D., Kallemijn W.W., Marques A.R., Orre M., Ottenhoff R., van Roomen C.,... and Aerts J.M. (2015) Visualization of Active Glucocerebrosidase in Rodent Brain with High Spatial Resolution following In Situ Labeling with Fluorescent Activity Based Probes. *PLoS one* **10**, e0138107.
97. Marques A.R., Aten J., Ottenhoff R., van Roomen C.P., Herrera Moro D., Claessen N.,... and Aerts J.M. (2015) Reducing GBA2 Activity Ameliorates Neuropathology in Niemann-Pick Type C Mice. *PLoS one* **10**, e0135889.
98. Tsuang D., Leverenz J.B., Lopez O.L., Hamilton R.L., Bennett D.A., Schneider J.A.,... and Zabetian C.P. (2012) GBA mutations increase risk for Lewy body disease with and without Alzheimer disease pathology. *Neurology* **79**, 1944-1950.
99. Sidransky E., Nalls M.A., Aasly J.O., Aharon-Peretz J., Annesi G., Barbosa E.R.,... and Ziegler S.G. (2009) Multicenter analysis of glucocerebrosidase mutations in Parkinson's disease. *N Engl J Med* **361**, 1651-1661.
100. Aerts J.M., Ferraz M.J., Mirzaian M., Gaspar P., Oussoren S.V., Wisse P.,... and Marques A.R.A. (2017) Lysosomal Storage Diseases. For Better or Worse: Adapting to Defective Lysosomal Glycosphingolipid Breakdown. *In eLS*. (John Wiley & Sons, Ltd), pp. 1-13.

## Chapter 1

101. Ghauharali-van der Vlugt K., Langeveld M., Poppema A., Kuiper S., Hollak C.E., Aerts J.M. and Groener J.E. (2008) Prominent increase in plasma ganglioside GM3 is associated with clinical manifestations of type I Gaucher disease. *Clin Chim Acta* **389**, 109-113.
102. Langeveld M., Ghauharali K.J., Sauerwein H.P., Ackermans M.T., Groener J.E., Hollak C.E.,... and Serlie M.J. (2008) Type I Gaucher disease, a glycosphingolipid storage disorder, is associated with insulin resistance. *J Clin Endocrinol Metab* **93**, 845-851.
103. Marques A.R., Mirzaian M., Akiyama H., Wisse P., Ferraz M.J., Gaspar P.,... and Aerts J.M. (2016) Glucosylated cholesterol in mammalian cells and tissues: formation and degradation by multiple cellular beta-glucosidases. *J Lipid Res* **57**, 451-463.
104. Akiyama H. and Hirabayashi Y. (2017) A novel function for glucocerebrosidase as a regulator of sterylglucoside metabolism. *Biochim Biophys Acta Gen Subj* **1861**, 2507-2514.
105. Akiyama H., Kobayashi S., Hirabayashi Y. and Murakami-Murofushi K. (2013) Cholesterol glucosylation is catalyzed by transglucosylation reaction of beta-glucosidase 1. *Biochem Biophys Res Commun* **441**, 838-843.
106. Ferraz M.J., Marques A.R., Appelman M.D., Verhoek M., Strijland A., Mirzaian M.,... and Aerts J.M. (2016) Lysosomal glycosphingolipid catabolism by acid ceramidase: formation of glycosphingoid bases during deficiency of glycosidases. *FEBS Lett* **590**, 716-725.
107. Reed M.C., Schiffer C., Heales S., Mehta A.B. and Hughes D.A. (2018) Impact of sphingolipids on osteoblast and osteoclast activity in Gaucher disease. *Mol Genet Metab* **124**, 278-286.
108. Taguchi Y.V., Liu J., Ruan J., Pacheco J., Zhang X., Abbasi J.,... and Chandra S.S. (2017) Glucosylsphingosine Promotes alpha-Synuclein Pathology in Mutant GBA-Associated Parkinson's Disease. *J Neurosci* **37**, 9617-9631.
109. Nair S., Branagan A.R., Liu J., Boddupalli C.S., Mistry P.K. and Dhodapkar M.V. (2016) Clonal Immunoglobulin against Lysolipids in the Origin of Myeloma. *N Engl J Med* **374**, 555-561.
110. Pandey M.K., Burrow T.A., Rani R., Martin L.J., Witte D., Setchell K.D.,... and Grabowski G.A. (2017) Complement drives glucosylceramide accumulation and tissue inflammation in Gaucher disease. *Nature* **543**, 108-112.
111. Pandey M.K., Grabowski G.A. and Kohl J. (2018) An unexpected player in Gaucher disease: The multiple roles of complement in disease development. *Semin Immunol* **37**, 30-42.
112. Smith N.J., Fuller M., Saville J.T. and Cox T.M. (2018) Reduced cerebral vascularization in experimental neuronopathic Gaucher disease. *J Pathol* **244**, 120-128.
113. Boven L.A., van Meurs M., Boot R.G., Mehta A., Boon L., Aerts J.M. and Laman J.D. (2004) Gaucher cells demonstrate a distinct macrophage phenotype and resemble alternatively activated macrophages. *Am J Clin Pathol* **122**, 359-369.
114. Hollak C.E., van Weely S., van Oers M.H. and Aerts J.M. (1994) Marked elevation of plasma chitotriosidase activity. A novel hallmark of Gaucher disease. *The Journal of clinical investigation* **93**, 1288-1292.
115. Boot R.G., Renkema G.H., Strijland A., van Zonneveld A.J. and Aerts J.M. (1995) Cloning of a cDNA encoding chitotriosidase, a human chitinase produced by macrophages. *J Biol Chem* **270**, 26252-26256.
116. Deegan P.B., Moran M.T., McFarlane I., Schofield J.P., Boot R.G., Aerts J.M. and Cox T.M. (2005) Clinical evaluation of chemokine and enzymatic biomarkers of Gaucher disease. *Blood Cells Mol Dis* **35**, 259-267.
117. Kramer G., Wegdam W., Donker-Koopman W., Ottenhoff R., Gaspar P., Verhoek M.,... and van Eijk M. (2016) Elevation of glycoprotein nonmetastatic melanoma protein B in type 1 Gaucher disease patients and mouse models. *FEBS Open Bio* **6**, 902-913.
118. Murugesan V., Liu J., Yang R., Lin H., Lischuk A., Pastores G.,... and Mistry P.K. (2018) Validating glycoprotein non-metastatic melanoma B (gpNMB, osteoactivin), a new biomarker of Gaucher disease. *Blood Cells Mol Dis* **68**, 47-53.
119. Dekker N., van Dussen L., Hollak C.E., Overkleeft H., Scheij S., Ghauharali K.,... and Aerts J.M. (2011) Elevated plasma glucosylsphingosine in Gaucher disease: relation to phenotype, storage cell markers, and therapeutic response. *Blood* **118**, e118-127.
120. van Dussen L., Hendriks E.J., Groener J.E., Boot R.G., Hollak C.E. and Aerts J.M. (2014) Value of plasma chitotriosidase to assess non-neuronopathic Gaucher disease severity and progression in the era of enzyme replacement therapy. *J Inher Metab Dis* **37**, 991-1001.
121. Brady R.O. (2003) Enzyme replacement therapy: conception, chaos and culmination. *Philos Trans R Soc Lond B Biol Sci* **358**, 915-919.
122. Barton N.W., Furbish F.S., Murray G.J., Garfield M. and Brady R.O. (1990) Therapeutic response to intravenous infusions of glucocerebrosidase in a patient with Gaucher disease. *Proc Natl Acad Sci U S A* **87**, 1913-1916.
123. Sechi A., Deroma L., Dardis A., Ciana G., Bertin N., Concolino D.,... and Bembi B. (2014) Long term effects of enzyme replacement therapy in an Italian cohort of type 3 Gaucher patients. *Mol Genet Metab* **113**, 213-218.



124. Aerts J.M., Hollak C.E., Boot R.G., Groener J.E. and Maas M. (2006) Substrate reduction therapy of glycosphingolipid storage disorders. *J Inher Metab Dis* **29**, 449-456.
125. Platt F.M., Jeyakumar M., Andersson U., Priestman D.A., Dwek R.A., Butters T.D.,... and Zimran A. (2001) Inhibition of substrate synthesis as a strategy for glycolipid lysosomal storage disease therapy. *J Inher Metab Dis* **24**, 275-290.
126. Giraldo P., Andrade-Campos M., Alfonso P., Irun P., Atutxa K., Acedo A.,... and Pocovi M. (2018) Twelve years of experience with miglustat in the treatment of type 1 Gaucher disease: The Spanish ZAGAL project. *Blood Cells Mol Dis* **68**, 173-179.
127. Cox T.M., Drelichman G., Cravo R., Balwani M., Burrow T.A., Martins A.M.,... and Peterschmitt M.J. (2017) Eliglustat maintains long-term clinical stability in patients with Gaucher disease type 1 stabilized on enzyme therapy. *Blood* **129**, 2375-2383.
128. Peterschmitt M.J., Freisens S., Underhill L.H., Foster M.C., Lewis G. and Gaemers S.J.M. (2019) Long-term adverse event profile from four completed trials of oral eliglustat in adults with Gaucher disease type 1. *Orphanet J Rare Dis* **14**, 128.
129. Lukina E., Watman N., Dragosky M., Lau H., Avila Arreguin E., Rosenbaum H.,... and Peterschmitt M.J. (2019) Outcomes after 8 years of eliglustat therapy for Gaucher disease type 1: Final results from the Phase 2 trial. *Am J Hematol* **94**, 29-38.
130. Shayman J.A. and Larsen S.D. (2014) The development and use of small molecule inhibitors of glycosphingolipid metabolism for lysosomal storage diseases. *J Lipid Res* **55**, 1215-1225.
131. Maegawa G.H., Tropak M.B., Buttner J.D., Rigat B.A., Fuller M., Pandit D.,... and Mahuran D.J. (2009) Identification and characterization of ambroxol as an enzyme enhancement agent for Gaucher disease. *J Biol Chem* **284**, 23502-23516.
132. Narita A., Shirai K., Itamura S., Matsuda A., Ishihara A., Matsushita K.,... and Suzuki Y. (2016) Ambroxol chaperone therapy for neuronopathic Gaucher disease: A pilot study. *Ann Clin Transl Neurol* **3**, 200-215.
133. Fog C.K., Zago P., Malini E., Solanko L.M., Peruzzo P., Bornaes C.,... and Kirkegaard T. (2018) The heat shock protein amplifier arimoclochol improves refolding, maturation and lysosomal activity of glucocerebrosidase. *EBioMedicine* **38**, 142-153.
134. Desnick R.J., Ioannou Y. and Eng C.M. (2001)  $\alpha$ -Galactosidase A deficiency: Fabry disease. In *The metabolic and Molecular Bases of Inherited Disease*, C.R. Scriver, A.L. Beaudet, W.S. Sly and D. Valle, eds. (New York: McGraw-Hill), pp. 3733-3744.
135. Spada M., Pagliardini S., Yasuda M., Tükel T., Thiagarajan G., Sakuraba H.,... and Desnick R.J. (2006) High incidence of later-onset fabry disease revealed by newborn screening. *Am J Hum Genet* **79**, 31-40.
136. Garman S.C. and Garboczi D.N. (2004) The molecular defect leading to Fabry disease: structure of human alpha-galactosidase. *J Mol Biol* **337**, 319-335.
137. Tajima Y., Kawashima I., Tsukimura T., Sugawara K., Kuroda M., Suzuki T.,... and Sakuraba H. (2009) Use of a modified alpha-N-acetylgalactosaminidase in the development of enzyme replacement therapy for Fabry disease. *Am J Hum Genet* **85**, 569-580.
138. Kytidou K., Beenakker T.J.M., Westerhof L.B., Hokke C.H., Moolenaar G.F., Goosen N.,... and Aerts J. (2017) Human Alpha Galactosidases Transiently Produced in Nicotiana benthamiana Leaves: New Insights in Substrate Specificities with Relevance for Fabry Disease. *Front Plant Sci* **8**, 1026.
139. Willems L.I., Beenakker T.J., Murray B., Scheij S., Kallemeijn W.W., Boot R.G.,... and Overkleeft H.S. (2014) Potent and selective activity-based probes for GH27 human retaining alpha-galactosidases. *Journal of the American Chemical Society* **136**, 11622-11625.
140. Kytidou K., Beekwilder J., Artola M., van Meel E., Wilbers R.H.P., Moolenaar G.F.,... and Aerts J. (2018) Nicotiana benthamiana alpha-galactosidase A1.1 can functionally complement human alpha-galactosidase A deficiency associated with Fabry disease. *J Biol Chem* **293**, 10042-10058.
141. Sweeley C.C. and Klionsky B. (1963) Fabry's Disease: Classification as a Sphingolipidosis and Partial Characterization of a Novel Glycolipid. *J Biol Chem* **238**, 3148-3150.
142. Rybova J., Kuchar L., Hulkova H., Asfaw B., Dobrovolny R., Sikora J.,... and Ledvinova J. (2018) Specific storage of glycoconjugates with terminal alpha-galactosyl moieties in the exocrine pancreas of Fabry disease patients with blood group B. *Glycobiology* **28**, 382-391.
143. Kuchar L., Faltyskova H., Krasny L., Dobrovolny R., Hulkova H., Ledvinova J.,... and Havlicek V. (2015) Fabry disease: renal sphingolipid distribution in the alpha-Gal A knockout mouse model by mass spectrometric and immunohistochemical imaging. *Anal Bioanal Chem* **407**, 2283-2291.
144. Asfaw B., Ledvinova J., Dobrovolny R., Bakker H.D., Desnick R.J., van Diggelen O.P.,... and Schindler D. (2002) Defects in degradation of blood group A and B glycosphingolipids in Schindler and Fabry diseases. *J Lipid Res* **43**, 1096-1104.

145. Deegan P.B., Bahner F., Barba M., Hughes D.A. and Beck M. (2006) Fabry disease in females: clinical characteristics and effects of enzyme replacement therapy. In *Fabry Disease: Perspectives from 5 Years of FOS*, A. Mehta, M. Beck and G. Sunder-Plassmann, eds. (Oxford).
146. Lin H.Y., Chong K.W., Hsu J.H., Yu H.C., Shih C.C., Huang C.H.,... and Niu D.M. (2009) High incidence of the cardiac variant of Fabry disease revealed by newborn screening in the Taiwan Chinese population. *Circ Cardiovasc Genet* **2**, 450-456.
147. Schiffmann R. (2009) Fabry disease. *Pharmacol Ther* **122**, 65-77.
148. Eng C.M., Resnick-Silverman L.A., Niehaus D.J., Astrin K.H. and Desnick R.J. (1993) Nature and frequency of mutations in the alpha-galactosidase A gene that cause Fabry disease. *Am J Hum Genet* **53**, 1186-1197.
149. Smid B.E., Hollak C.E., Poorthuis B.J., van den Bergh Weerman M.A., Florquin S., Kok W.E.,... and Linthorst G.E. (2015) Diagnostic dilemmas in Fabry disease: a case series study on GLA mutations of unknown clinical significance. *Clin Genet* **88**, 161-166.
150. Rohard I., Schaefer E., Kampmann C., Beck M. and Gal A. (2008) Association between polymorphisms of endothelial nitric oxide synthase gene (NOS3) and left posterior wall thickness (LPWT) of the heart in Fabry disease. *J Inherit Metab Dis* **31 Suppl 2**, S349-356.
151. Rombach S.M., Hollak C.E., Linthorst G.E. and Dijkgraaf M.G. (2013) Cost-effectiveness of enzyme replacement therapy for Fabry disease. *Orphanet J Rare Dis* **8**, 29.
152. Rombach S.M., Smid B.E., Bouwman M.G., Linthorst G.E., Dijkgraaf M.G. and Hollak C.E. (2013) Long term enzyme replacement therapy for Fabry disease: effectiveness on kidney, heart and brain. *Orphanet J Rare Dis* **8**, 47.
153. Linthorst G.E., Hollak C.E., Donker-Koopman W.E., Strijland A. and Aerts J.M. (2004) Enzyme therapy for Fabry disease: neutralizing antibodies toward agalsidase alpha and beta. *Kidney Int* **66**, 1589-1595.
154. Lenders M., Neusser L.P., Rudnicki M., Nordbeck P., Canaan-Kuhl S., Nowak A.,... and Brand E. (2018) Dose-Dependent Effect of Enzyme Replacement Therapy on Neutralizing Antidrug Antibody Titers and Clinical Outcome in Patients with Fabry Disease. *J Am Soc Nephrol* **29**, 2879-2889.
155. Arends M., Biegstraaten M., Hughes D.A., Mehta A., Elliott P.M., Oder D.,... and Hollak C.E.M. (2017) Retrospective study of long-term outcomes of enzyme replacement therapy in Fabry disease: Analysis of prognostic factors. *PLoS one* **12**, e0182379.
156. Aerts J.M., Groener J.E., Kuiper S., Donker-Koopman W.E., Strijland A., Ottenhoff R.,... and Poorthuis B.J. (2008) Elevated globotriaosylsphingosine is a hallmark of Fabry disease. *Proc Natl Acad Sci U S A* **105**, 2812-2817.
157. Gold H., Mirzaian M., Dekker N., Joao Ferraz M., Lugtenburg J., Codee J.D.,... and Poorthuis B.J. (2013) Quantification of globotriaosylsphingosine in plasma and urine of fabry patients by stable isotope ultraperformance liquid chromatography-tandem mass spectrometry. *Clin Chem* **59**, 547-556.
158. Rombach S.M., van den Bogaard B., de Groot E., Groener J.E., Poorthuis B.J., Linthorst G.E.,... and Aerts J.M. (2012) Vascular aspects of Fabry disease in relation to clinical manifestations and elevations in plasma globotriaosylsphingosine. *Hypertension* **60**, 998-1005.
159. Kaissarian N., Kang J., Shu L., Ferraz M.J., Aerts J.M. and Shayman J.A. (2018) Dissociation of globotriaosylceramide and impaired endothelial function in alpha-galactosidase-A deficient EA.hy926 cells. *Mol Genet Metab* **125**, 338-344.
160. Weidemann F., Sanchez-Nino M.D., Politei J., Oliveira J.P., Wanner C., Warnock D.G. and Ortiz A. (2013) Fibrosis: a key feature of Fabry disease with potential therapeutic implications. *Orphanet J Rare Dis* **8**, 116.
161. Choi L., Vernon J., Kopach O., Minett M.S., Mills K., Clayton P.T.,... and Wood J.N. (2015) The Fabry disease-associated lipid Lyso-Gb3 enhances voltage-gated calcium currents in sensory neurons and causes pain. *Neurosci Lett* **594**, 163-168.
162. Sanchez-Nino M.D., Carpio D., Sanz A.B., Ruiz-Ortega M., Mezzano S. and Ortiz A. (2015) Lyso-Gb3 activates Notch1 in human podocytes. *Human molecular genetics* **24**, 5720-5732.
163. Shtraizent N., Eliyahu E., Park J.H., He X., Shalgi R. and Schuchman E.H. (2008) Autoproteolytic cleavage and activation of human acid ceramidase. *J Biol Chem* **283**, 11253-11259.
164. Gebai A., Gorelik A., Li Z., Illes K. and Nagar B. (2018) Structural basis for the activation of acid ceramidase. *Nature communications* **9**, 1621.
165. Ferlinz K., Kopal G., Bernardo K., Linke T., Bar J., Breiden B.,... and Sandhoff K. (2001) Human acid ceramidase: processing, glycosylation, and lysosomal targeting. *J Biol Chem* **276**, 35352-35360.
166. Dementiev A., Joachimiak A., Nguyen H., Gorelik A., Illes K., Shabani S.,... and Doan N. (2019) Molecular Mechanism of Inhibition of Acid Ceramidase by Carmofur. *Journal of medicinal chemistry* **62**, 987-992.
167. Ouairy C.M., Ferraz M.J., Boot R.G., Baggelaar M.P., van der Stelt M., Appelman M.,... and Overkleeft H.S. (2015) Development of an acid ceramidase activity-based probe. *Chemical communications* **51**, 6161-6163.
168. Ordóñez Y.F., Abad J.L., Aseeri M., Casas J., García V., Casasampere M.,... and Fabrias G. (2019) Activity-Based Imaging of Acid Ceramidase in Living Cells. *Journal of the American Chemical Society* **141**, 7736-7742.



169. Farber S. (1952) A lipid metabolic disorder: disseminated lipogranulomatosis; a syndrome with similarity to, and important difference from, Niemann-Pick and Hand-Schuller-Christian disease. *AMA Am J Dis Child* **84**, 499-500.
170. Ehler K., Frosch M., Fehse N., Zander A., Roth J. and Vormoor J. (2007) Farber disease: clinical presentation, pathogenesis and a new approach to treatment. *Pediatr Rheumatol Online J* **5**, 15.
171. Tanaka T., Takahashi K., Hakozaaki H., Kimoto H. and Suzuki Y. (1979) Farber's disease (disseminated lipogranulomatosis)--a pathological, histochemical and ultrastructural study. *Acta Pathol Jpn* **29**, 135-155.
172. Bonafe L., Kariminejad A., Li J., Royer-Bertrand B., Garcia V., Mahdavi S.,... and Superti-Furga A. (2016) Brief Report: Peripheral Osteolysis in Adults Linked to ASAH1 (Acid Ceramidase) Mutations: A New Presentation of Farber's Disease. *Arthritis Rheumatol* **68**, 2323-2327.
173. Gan J.J., Garcia V., Tian J., Tagliati M., Parisi J.E., Chung J.M.,... and Pierson T.M. (2015) Acid ceramidase deficiency associated with spinal muscular atrophy with progressive myoclonic epilepsy. *Neuromuscul Disord* **25**, 959-963.
174. Zhou J., Tawk M., Tiziano F.D., Veillet J., Bayes M., Nolent F.,... and Melki J. (2012) Spinal muscular atrophy associated with progressive myoclonic epilepsy is caused by mutations in ASAH1. *Am J Hum Genet* **91**, 5-14.
175. Schuchman E.H. (2016) Acid ceramidase and the treatment of ceramide diseases: The expanding role of enzyme replacement therapy. *Biochimica et biophysica acta* **1862**, 1459-1471.
176. Ferraz M.J., Marques A.R., Gaspar P., Mirzaian M., van Roomen C., Ottenhoff R.,... and Aerts J.M. (2016) Lyso-glycosphingolipid abnormalities in different murine models of lysosomal storage disorders. *Mol Genet Metab* **117**, 186-193.
177. Marshall J., Nietupski J.B., Park H., Cao J., Bangari D.S., Silvescu C.,... and Cheng S.H. (2019) Substrate Reduction Therapy for Sandhoff Disease through Inhibition of Glucosylceramide Synthase Activity. *Mol Ther* **27**, 1495-1506.
178. Kuchar L., Sikora J., Gulinello M.E., Poupetova H., Lugowska A., Malinova V.,... and Ledvinova J. (2017) Quantitation of plasmatic lysosphingomyelin and lysosphingomyelin-509 for differential screening of Niemann-Pick A/B and C diseases. *Anal Biochem* **525**, 73-77.
179. Mirzaian M., Wisse P., Ferraz M.J., Marques A.R.A., Gaspar P., Oussoren S.V.,... and Aerts J.M. (2017) Simultaneous quantitation of sphingoid bases by UPLC-ESI-MS/MS with identical (13)C-encoded internal standards. *Clin Chim Acta* **466**, 178-184.
180. Li Y., Xu Y., Benitez B.A., Nagree M.S., Dearborn J.T., Jiang X.,... and Sands M.S. (2019) Genetic ablation of acid ceramidase in Krabbe disease confirms the psychosine hypothesis and identifies a new therapeutic target. *Proc Natl Acad Sci U S A* **116**, 20097-20103.
181. Keatinge M., Bui H., Menke A., Chen Y.C., Sokol A.M., Bai Q.,... and Bandmann O. (2015) Glucocerebrosidase 1 deficient Danio rerio mirror key pathological aspects of human Gaucher disease and provide evidence of early microglial activation preceding alpha-synuclein-independent neuronal cell death. *Human molecular genetics* **24**, 6640-6652.
182. Watson L., Keatinge M., Gegg M., Bai Q., Sandulescu M.C., Vardi A.,... and Bandmann O. (2019) Ablation of the pro-inflammatory master regulator miR-155 does not mitigate neuroinflammation or neurodegeneration in a vertebrate model of Gaucher's disease. *Neurobiol Dis* **127**, 563-569.
183. Ohshima T., Murray G.J., Swaim W.D., Longenecker G., Quirk J.M., Cardarelli C.O.,... and Kulkarni A.B. (1997) alpha-Galactosidase A deficient mice: a model of Fabry disease. *Proc Natl Acad Sci U S A* **94**, 2540-2544.
184. Nguyen Dinh Cat A., Escoubet B., Agrapart V., Griol-Charhbil V., Schoeb T., Feng W.,... and Jaisser F. (2012) Cardiomyopathy and response to enzyme replacement therapy in a male mouse model for Fabry disease. *PLoS one* **7**, e33743.
185. Rodrigues L.G., Ferraz M.J., Rodrigues D., Pais-Vieira M., Lima D., Brady R.O.,... and Sa-Miranda M.C. (2009) Neurophysiological, behavioral and morphological abnormalities in the Fabry knockout mice. *Neurobiol Dis* **33**, 48-56.
186. Miller J.J., Aoki K., Mascari C.A., Beltrame A.K., Sokumbi O., North P.E.,... and Dahms N.M. (2019) alpha-Galactosidase A-deficient rats accumulate glycosphingolipids and develop cardiorenal phenotypes of Fabry disease. *FASEB J* **33**, 418-429.
187. Miller J.J., Aoki K., Moehring F., Murphy C.A., O'Hara C.L., Tiemeyer M.,... and Dahms N.M. (2018) Neuropathic pain in a Fabry disease rat model. *JCI Insight* **3**.
188. Miller J.J., Aoki K., Reid C.A., Tiemeyer M., Dahms N.M. and Kassem I.S. (2019) Rats deficient in alpha-galactosidase A develop ocular manifestations of Fabry disease. *Sci Rep* **9**, 9392.
189. Kobayashi T., Yamanaka T., Jacobs J.M., Teixeira F. and Suzuki K. (1980) The Twitcher mouse: an enzymatically authentic model of human globoid cell leukodystrophy (Krabbe disease). *Brain Res* **202**, 479-483.
190. Zizioli D., Guarienti M., Tobia C., Gariano G., Borsani G., Bresciani R.,... and Presta M. (2014) Molecular cloning and knockdown of galactocerebrosidase in zebrafish: new insights into the pathogenesis of Krabbe's

- disease. *Biochimica et biophysica acta* **1842**, 665-675.
191. Alayoubi A.M., Wang J.C., Au B.C., Carpentier S., Garcia V., Dworski S.,... and Medin J.A. (2013) Systemic ceramide accumulation leads to severe and varied pathological consequences. *EMBO Mol Med* **5**, 827-842.
  192. Lawson C.A. and Martin D.R. (2016) Animal models of GM2 gangliosidosis: utility and limitations. *Appl Clin Genet* **9**, 111-120.
  193. Sango K., Yamanaka S., Hoffmann A., Okuda Y., Grinberg A., Westphal H.,... and Proia R.L. (1995) Mouse models of Tay-Sachs and Sandhoff diseases differ in neurologic phenotype and ganglioside metabolism. *Nat Genet* **11**, 170-176.
  194. Kuil L.E., Lopez Marti A., Carreras Mascaro A., van den Bosch J.C., van den Berg P., van der Linde H.C.,... and van Ham T.J. (2019) Hexb enzyme deficiency leads to lysosomal abnormalities in radial glia and microglia in zebrafish brain development. *Glia* **67**, 1705-1718.
  195. Horinouchi K., Erlich S., Perl D.P., Ferlinz K., Bisgaier C.L., Sandhoff K.,... and Schuchman E.H. (1995) Acid sphingomyelinase deficient mice: a model of types A and B Niemann-Pick disease. *Nat Genet* **10**, 288-293.
  196. Loftus S.K., Morris J.A., Carstea E.D., Gu J.Z., Cummings C., Brown A.,... and Pavan W.J. (1997) Murine model of Niemann-Pick C disease: mutation in a cholesterol homeostasis gene. *Science* **277**, 232-235.
  197. Tseng W.C., Loeb H.E., Pei W., Tsai-Morris C.H., Xu L., Cluzeau C.V.,... and Porter F.D. (2018) Modeling Niemann-Pick disease type C1 in zebrafish: a robust platform for in vivo screening of candidate therapeutic compounds. *Dis Model Mech* **11**.
  198. Meyers J.R. (2018) Zebrafish: Development of a Vertebrate Model Organism. *Current Protocols Essential Laboratory Techniques* **16**, e19.
  199. Engeszer R.E., Patterson L.B., Rao A.A. and Parichy D.M. (2007) Zebrafish in the wild: a review of natural history and new notes from the field. *Zebrafish* **4**, 21-40.
  200. Kimmel C.B., Ballard W.W., Kimmel S.R., Ullmann B. and Schilling T.F. (1995) Stages of embryonic development of the zebrafish. *Developmental dynamics : an official publication of the American Association of Anatomists* **203**, 253-310.
  201. Gerhard G.S., Kauffman E.J., Wang X., Stewart R., Moore J.L., Kasales C.J.,... and Cheng K.C. (2002) Life spans and senescent phenotypes in two strains of Zebrafish (*Danio rerio*). *Exp Gerontol* **37**, 1055-1068.
  202. Howe K., Clark M.D., Torroja C.F., Torrance J., Berthelot C., Muffato M.,... and Stemple D.L. (2013) The zebrafish reference genome sequence and its relationship to the human genome. *Nature* **496**, 498-503.
  203. Kumar S. and Hedges S.B. (1998) A molecular timescale for vertebrate evolution. *Nature* **392**, 917-920.
  204. Meyer A. and Schartl M. (1999) Gene and genome duplications in vertebrates: the one-to-four (-to-eight in fish) rule and the evolution of novel gene functions. *Curr Opin Cell Biol* **11**, 699-704.
  205. Meyer A. and Van de Peer Y. (2005) From 2R to 3R: evidence for a fish-specific genome duplication (FSGD). *Bioessays* **27**, 937-945.
  206. Lieschke G.J. and Currie P.D. (2007) Animal models of human disease: zebrafish swim into view. *Nat Rev Genet* **8**, 353-367.
  207. Menke A.L., Spitsbergen J.M., Wolterbeek A.P. and Woutersen R.A. (2011) Normal anatomy and histology of the adult zebrafish. *Toxicol Pathol* **39**, 759-775.
  208. Jagannathan-Bogdan M. and Zon L.I. (2013) Hematopoiesis. *Development* **140**, 2463-2467.
  209. Panula P., Chen Y.C., Priyadarshini M., Kudo H., Semenova S., Sundvik M. and Sallinen V. (2010) The comparative neuroanatomy and neurochemistry of zebrafish CNS systems of relevance to human neuropsychiatric diseases. *Neurobiol Dis* **40**, 46-57.
  210. Rink E. and Wullmann M.F. (2001) The teleostean (zebrafish) dopaminergic system ascending to the subpallium (striatum) is located in the basal diencephalon (posterior tuberculum). *Brain Res* **889**, 316-330.
  211. Friedrich R.W., Jacobson G.A. and Zhu P. (2010) Circuit neuroscience in zebrafish. *Curr Biol* **20**, R371-381.
  212. Eisen J.S. and Smith J.C. (2008) Controlling morpholino experiments: don't stop making antisense. *Development* **135**, 1735-1743.
  213. Zancan I., Bellesso S., Costa R., Salvalaio M., Stroppiano M., Hammond C.,... and Moro E. (2015) Glucocerebrosidase deficiency in zebrafish affects primary bone ossification through increased oxidative stress and reduced Wnt/beta-catenin signaling. *Human molecular genetics* **24**, 1280-1294.
  214. Lelieveld L.T., Mirzaian M., Kuo C.L., Artola M., Ferraz M.J., Peter R.E.A.,... and Aerts J. (2019) Role of beta-glucosidase 2 in aberrant glycosphingolipid metabolism: model of glucocerebrosidase deficiency in zebrafish. *J Lipid Res* **60**, 1851-1867.
  215. Martin E., Schule R., Smets K., Rastetter A., Boukhris A., Loureiro J.L.,... and Stevanin G. (2013) Loss of function of glucocerebrosidase GBA2 is responsible for motor neuron defects in hereditary spastic paraplegia. *Am J Hum Genet* **92**, 238-244.
  216. Gravel R.A., Kaback M.M., Proia R.L., Sandhoff K., Suzuki K. and Suzuki K. (2001) The G<sub>M2</sub> Gangliosidoses. In *The Metabolic & Molecular Bases of Inherited Disease*, Volume 3, C.R. Scriver, A.L. Beaudet, W.S. Sly and D. Valle, eds. (McGraw-Hill ), pp. 3827-3876.

217. Suzuki K. and Chen G.C. (1967) Brain ceramide hexosides in Tay-Sachs disease and generalized gangliosidosis (GM1-gangliosidosis). *J Lipid Res* **8**, 105-113.
218. Jeyakumar M., Thomas R., Elliot-Smith E., Smith D.A., van der Spoel A.C., d'Azzo A.,... and Platt F.M. (2003) Central nervous system inflammation is a hallmark of pathogenesis in mouse models of GM1 and GM2 gangliosidosis. *Brain* **126**, 974-987.
219. Pfeffer S.R. (2019) NPC intracellular cholesterol transporter 1 (NPC1)-mediated cholesterol export from lysosomes. *J Biol Chem* **294**, 1706-1709.
220. Gumus E., Haliloglu G., Karhan A.N., Demir H., Gurakan F., Topcu M. and Yuce A. (2017) Niemann-Pick disease type C in the newborn period: a single-center experience. *Eur J Pediatr* **176**, 1669-1676.
221. Schwend T., Loucks E.J., Snyder D. and Ahlgren S.C. (2011) Requirement of Npc1 and availability of cholesterol for early embryonic cell movements in zebrafish. *J Lipid Res* **52**, 1328-1344.
222. Lin Y., Cai X., Wang G., Ouyang G. and Cao H. (2018) Model construction of Niemann-Pick type C disease in zebrafish. *Biol Chem* **399**, 903-910.
223. Sarna J.R., Larouche M., Marzban H., Sillitoe R.V., Rancourt D.E. and Hawkes R. (2003) Patterned Purkinje cell degeneration in mouse models of Niemann-Pick type C disease. *J Comp Neurol* **456**, 279-291.
224. Paul C.A., Boegle A.K. and Maue R.A. (2004) Before the loss: neuronal dysfunction in Niemann-Pick Type C disease. *Biochimica et biophysica acta* **1685**, 63-76.
225. Felker A. and Mosimann C. (2016) Contemporary zebrafish transgenesis with Tol2 and application for Cre/lox recombination experiments. *Methods Cell Biol* **135**, 219-244.
226. Udvadia A.J. and Linney E. (2003) Windows into development: historic, current, and future perspectives on transgenic zebrafish. *Dev Biol* **256**, 1-17.
227. Howe D.G., Bradford Y.M., Conlin T., Eagle A.E., Fashena D., Frazer K.,... and Westerfield M. (2013) ZFIN, the Zebrafish Model Organism Database: increased support for mutants and transgenics. *Nucleic acids research* **41**, D854-860.
228. Zon L.I. and Peterson R.T. (2005) In vivo drug discovery in the zebrafish. *Nature reviews. Drug discovery* **4**, 35-44.
229. Kuo C.L., van Meel E., Kytidou K., Kallemeijn W.W., Witte M., Overkleeft H.S.,... and Aerts J.M. (2018) Activity-Based Probes for Glycosidases: Profiling and Other Applications. *Methods Enzymol* **598**, 217-235.
230. Zhao Q., Ouyang X., Wan X., Gajiwala K.S., Kath J.C., Jones L.H.,... and Taunton J. (2017) Broad-Spectrum Kinase Profiling in Live Cells with Lysine-Targeted Sulfonyl Fluoride Probes. *Journal of the American Chemical Society* **139**, 680-685.
231. Baggelaar M.P., Janssen F.J., van Esbroeck A.C., den Dulk H., Allara M., Hoogendoorn S.,... and van der Stelt M. (2013) Development of an activity-based probe and in silico design reveal highly selective inhibitors for diacylglycerol lipase- $\alpha$  in brain. *Angewandte Chemie* **52**, 12081-12085.
232. Simon G.M. and Cravatt B.F. (2010) Activity-based proteomics of enzyme superfamilies: serine hydrolases as a case study. *J Biol Chem* **285**, 11051-11055.
233. Paulick M.G. and Bogoy M. (2011) Development of activity-based probes for cathepsin X. *ACS Chem Biol* **6**, 563-572.
234. Jiang J., Kuo C.L., Wu L., Franke C., Kallemeijn W.W., Florea B.I.,... and Aerts J.M. (2016) Detection of Active Mammalian GH31  $\alpha$ -Glucosidases in Health and Disease Using In-Class, Broad-Spectrum Activity-Based Probes. *ACS Cent Sci* **2**, 351-358.
235. Marques A.R., Willems L.I., Herrera Moro D., Florea B.I., Scheij S., Ottenhoff R.,... and Aerts J.M. (2017) A Specific Activity-Based Probe to Monitor Family GH59 Galactosylceramidase, the Enzyme Deficient in Krabbe Disease. *Chembiochem* **18**, 402-412.
236. Jiang J., Kallemeijn W.W., Wright D.W., van den Nieuwendijk A., Rohde V.C., Folch E.C.,... and Overkleeft H.S. (2015) In vitro and in vivo comparative and competitive activity-based protein profiling of GH29  $\alpha$ -l-fucosidases. *Chem Sci* **6**, 2782-false.
237. Wu L., Jiang J., Jin Y., Kallemeijn W.W., Kuo C.L., Artola M.,... and Davies G.J. (2017) Activity-based probes for functional interrogation of retaining beta-glucuronidases. *Nature chemical biology* **13**, 867-873.
238. Artola M., Kuo C.L., McMahon S.A., Oehler V., Hansen T., van der Lienden M.,... and Aerts J. (2018) New Irreversible  $\alpha$ -l-Iduronidase Inhibitors and Activity-Based Probes. *Chemistry* **24**, 19081-19088.

## CHAPTER 2

### Biochemical evaluation and comparison of GCase enzymes of different species

2



## Abstract

The glycosphingolipid glucosylceramide (GlcCer) is degraded in the lysosome by the acid  $\beta$ -glucosidase glucocerebrosidase (GCase, official gene name *GBA*). A defect in GCase leads to the common lysosomal storage disorder Gaucher disease (GD). A complete deficiency of GCase in man and mouse is lethal due to trans-epidermal water loss, but fortuitously a complete *gba* knockout zebrafish is viable. In this chapter, a combination of biochemical assays and molecular modelling is used to study and compare features of GCase enzymes of different species, including man, zebrafish, frog and turtle. All GCase enzymes showed hydrolysis of the artificial substrate 4-methylumbelliferyl  $\beta$ -glucoside at an acidic pH optimum. Human GCase required either saposin C or sodium taurocholate at pH 5.2 for optimal activity, while zebrafish and frog GCase showed high hydrolysis rates at pH 4 without additives. Increased levels of endogenous GlcCer and the deacylated sphingoid base, glucosylsphingosine (GlcSph), in the *GBA*-depleted cells were corrected by expression of any of the GCase enzymes. Zebrafish GCase was remarkably active at low temperature (10 °C) when compared to the enzyme from other species. In sharp contrast to human and frog GCase, the zebrafish enzyme was unable to perform an *in vitro* transglucosylation reaction with cholesterol as acceptor. Zebrafish GCase showed slight glucose transfer to acceptor lipids composed of hydrophobic alkyl tails, such as ceramide, hypothesizing that cholesterol might not fit the catalytic pocket of zebrafish GCase. *In silico* comparisons of modelled structures of the various GCase enzymes, based on the established 3D-structure of the human enzyme, revealed divergent residues in the flexible loops of GCase. Attention was drawn to three residues with hydrophobic chains positioned close to the catalytic pocket of zebrafish GCase. However, zebrafish GCase with substitutions of these amino acids did not show improvement in transglucosylation. To further test the hypothesis it should be considered to swap entire loops among enzymes of different species.

## Introduction

Lysosomal deficiency of the enzyme acid  $\beta$ -glucosidase (glucocerebrosidase, GCase, EC 3.2.1.45, family GH 30) hydrolysing glucosylceramide (GlcCer) constitutes the molecular basis of the lysosomal storage disorder Gaucher disease (GD)<sup>1</sup>. Newly synthesized GCase is translocated to the lumen of the endoplasmic reticulum (ER), where the N-terminal signal peptide is removed, four N-linked glycans are attached to asparagine residues and folding of the protein occurs<sup>2,3</sup>. Correctly folded protein becomes rapidly membrane-associated through binding to the lysosomal integral membrane protein 2 (LIMP2)<sup>4-7</sup>. In the Golgi apparatus the N-glycans of GCase are predominantly modified to complex-type structures and no mannose-6-phosphate moieties are generated<sup>8</sup>. Instead LIMP2 mediates transport of the GCase-LIMP2 complex to the lysosome<sup>4-7</sup>. The activator lipid-binding protein saposin C is required for optimal intralysosomal activity of GCase as is illustrated by findings that defects in saposin C causes symptoms similar to GD<sup>9-11</sup>.

The structure of human GCase, as resolved by crystallography, shows three domains (**Figure 1A and B**)<sup>12</sup>. Domain I (residues 1-27 and 383-414; pink) consists of a 3-stranded antiparallel  $\beta$ -sheet followed by a loop, domain II (residues 30-75 and 431-497; green) of an 8-stranded  $\beta$ -barrel, resembling an immunoglobulin fold, and domain III (residues 76-381 and 416-430, blue) consists of the catalytic ( $\beta/\alpha$ )<sub>8</sub> triosephosphate isomerase (TIM) barrel, a domain conserved among glycosidases<sup>12,13</sup>. The catalytic residues are located in the TIM barrel with Glu 340 functioning as nucleophile and Glu 235 as acid/base. For a recent review see also Ben Bdira *et al.*<sup>14</sup>.

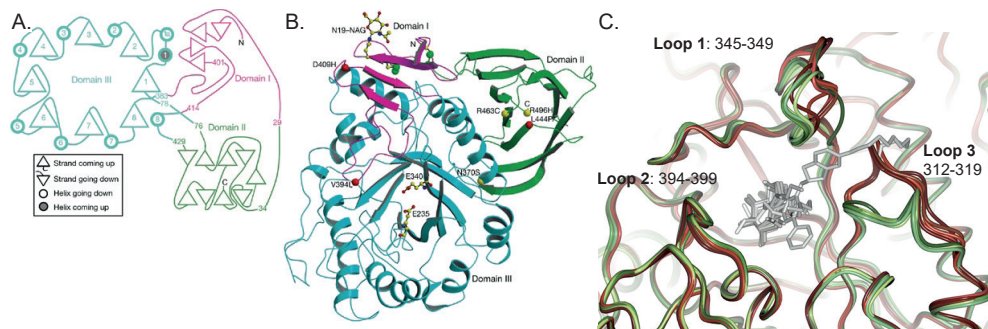


**Figure 1 | Structural arrangement of human GCase**

Two-dimensional topology (**A**) and 3D structure (**B**) of human GCase. Domain I is shown in pink, domain II in green and domain III in blue, with the numbers of  $\alpha$ -helices and  $\beta$ -strands of domain III numbered according to the position in the sequence. Figure (A) and (B) are used from Dvir *et al.*<sup>12</sup>. (**C**) Conformational changes of loops 1, 2 and 3 from the inactive (red) to the active, ligand associated conformation (green), with modelled ligands in the active site (grey). Reported structures without ligand: PDB codes 1OGS, 2J25, 3GXD, 3GXI and 3GXM, and ligand associated: PDB codes 2XWE, 2V3D, 2V3E, 2NSK, 3GXF, 5LVX, 2VTO, 2WCG, 2XWD, 3RIK and 3RIL1OGS, 2J25, 3GXD, 3GXI and 3GXM.



## Chapter 2

Like other retaining glycosidases, GCCase employs a Koshland double-displacement mechanism with Glu 340 performing a nucleophilic attack at the anomeric C1 carbon of the  $\beta$ -D-glucose moiety of GlcCer and Glu 235 protonating the oxygen of the glycosidic bond<sup>15</sup>. The aglycon is released and a covalent enzyme-glucose intermediate is formed. Insights into the reaction mechanism and covalent intermediate have been used to design covalent inhibitors for GCCase inactivation and activity-based probes to visualize active GCCase<sup>16,17</sup>. Next, Glu 235 activates a water molecule that acts as nucleophile and the glucose is released from the enzyme. In this second step, another suitable hydroxyl-containing molecule could serve as acceptor in a so-called transglucosylation reaction<sup>18</sup>. An established acceptor in the transreaction is cholesterol<sup>18-20</sup>.

Three loops surround the catalytic active site: loop 1 (residues 345-349), loop 2 (residues 394-399) and loop 3 (residues 312-319), with amino acid numbering of human GCCase based on the mature protein following the numbering described in previously published reports<sup>13,21</sup>. Crystallography and modelling studies point to a high flexibility of the three loops, adopting different conformations (**Figure 1C**)<sup>13,22</sup>. In the structure of the inactive enzyme the catalytic pocket seems small and suboptimal for substrate binding<sup>13,22</sup>. Loop 3 appears to change from an extended loop in the inactive enzyme conformation into a helical structure in the active GCCase structure (**Figure 1C**)<sup>22-24</sup>. As a result, several residues change their hydrogen bonding interactions and together these conformational changes induce opening of the active site, which becomes wider and shallower. The structural changes are reviewed and visualized in detail in 2011 by Lieberman *et al.*<sup>23</sup>.

The outer layer of the human skin, the stratum corneum, contains a large amount of active GCCase molecules<sup>25</sup>. Complete absence of GCCase is incompatible with terrestrial life in man and mice<sup>26-28</sup>, while a complete GCCase-deficient zebrafish is viable (chapter 6 and 7<sup>29,30</sup>). Therefore, the catalytic features of human and zebrafish GCCase were studied and compared, as well as features of GCCase enzymes from the amphibian *Xenopus laevis* (African clawed frog), and the reptile *Chrysemys picta belii* (western painted turtle, a freshwater turtle). These species were chosen in view of evolutionary aspects of the transition to terrestrial life and accompanying changes in skin composition. The outcome of the investigation is reported and discussed in this chapter.



## Results

### GCase of all tested species is catalytically active, although at different conditions

In order to allow a direct comparison of the GCase enzymes, CRISPR/Cas9 technology was used to generate human HEK293T cells lacking endogenous GCase activity. The various GCase enzymes were expressed under a CMV promoter in these *GBA* knockout (KO) HEK293T cells cultured at 37 °C. The comparison of the catalytic features of the different GCase enzymes was started by evaluating the enzymatic activity towards the artificial 4-methylumbelliferyl  $\beta$ -glucoside (4MU- $\beta$ -Glc) substrate. All GCase enzymes were able to hydrolyse the substrate albeit at different conditions. Human GCase showed optimal hydrolysis at an acidic pH of 5.2 and required the additives Triton-X100 (Tx) and sodium taurocholate (Tc) for optimal hydrolysis, as described before<sup>31</sup> (Figure 2A, pink circles; closed and open for additives and no additives respectively). Activation of human GCase could also be obtained by addition of recombinant saposin C (SapC) and the negatively charged lipid phosphatidylserine (PS) (Supplementary Figure 1A). Turtle GCase also showed optimal hydrolysis around pH 5.2 and Tx/Tc slightly increased hydrolysis (Figure 2A, orange circles and inset). Both zebrafish and frog GCase did not require Tx/Tc and showed the highest hydrolytic activity around pH 4 (Figure 2A, blue and green circles for zebrafish and frog respectively). The  $K_m$  and  $V_{max}$  values for the 4MU- $\beta$ -Glc substrate were determined for the different GCase enzymes. A high  $V_{max}$  of zebrafish and frog GCase was observed, while the low  $K_m$  of human GCase indicates a high affinity for 4MU- $\beta$ -Glc as substrate.

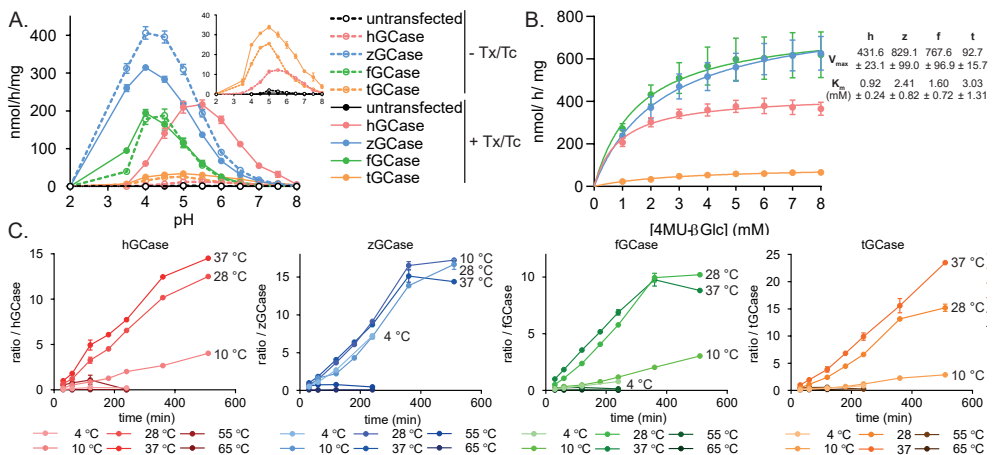


**Figure 2 | Enzymatic activity of GCase enzymes towards 4MU- $\beta$ -Glc**

(A) Hydrolytic activity of untransfected cells (black) or cells over-expressing human (h, pink), zebrafish (z, blue), frog (f, green) and turtle (t, orange) GCase towards 4MU- $\beta$ -Glc at different pH values without additives (open circles) or with additives (Triton-X100 (Tx) and Sodium Taurocholate (Tc); closed circles), incubated for 30 min at 37 °C. (B) Homogenate is incubated with different concentrations 4MU- $\beta$ -Glc for 30 min at 37°C.  $V_{max}$  and  $K_m$  values are calculated using a Michaelis-Menten non-linear fit. (C) Activity of human GCase enzymes at different time points incubated at a range of temperatures. Activity is calculated as ratio compared to the activity at 30 min at 37 °C of that specific species. Activity is measured from 3 independent homogenate preparations for (A) and (B) and 2 independent homogenate preparations for (C). Data is depicted as mean  $\pm$  SEM.

Next, hydrolysis was evaluated at different temperatures in time. The data is depicted as ratio compared to hydrolytic activity of the specific GCase at 37 °C and 30 min (**Figure 2C**). Zebrafish GCase showed relatively high activity over a broad temperature range from 4 °C to 37 °C, while the other enzymes showed 3-4 fold lower activity at 10 °C compared to 28 and 37 °C. The broad range of optimal temperatures for the zebrafish aligns with the poikilothermous nature of these animals, with their body temperature depending on the surrounding water.

A high potency of the GCase specific inhibitor, ME656<sup>32</sup>, was observed for human and zebrafish GCase, with comparable IC<sub>50</sub> values of 40 and 100 nM for human and zebrafish respectively (**Supplementary Figure 1B**).

### Detection of active GCase using specific activity-based probe

The specific fluorescent activity-based probe for GCase was used to label all active enzyme. As expected, no band of approximately 50-60 kDa was observed in untransfected *GBA* KO cell homogenate. For human GCase, a broader band was observed around 55 kDa, corresponding to the differently glycosylated forms of GCase as described before (**Figure 3A**, top panel)<sup>16</sup>. ABP-labelled zebrafish, frog and turtle GCase was visualized around 55-60 kDa. An ABP-enzyme complex with lower molecular weight was apparent for all three GCase enzymes, which is likely a degradation product.

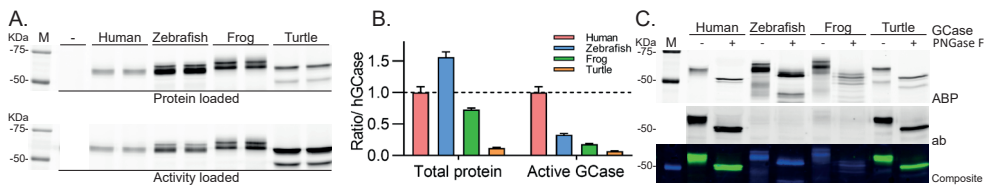


**Figure 3 | Visualization of active GCase and total GCase**

**(A)** Labeling of active GCase using a GCase specific ABP. Homogenates of untransfected cells (-) or cells over-expressing the different GCase enzymes were used and either loaded with similar amount of total protein (top panel) or similar activity towards 4MU- $\beta$ -Glc (bottom panel). Two independent homogenate preparations were used. **(B)** Activity was calculated with respect to total protein levels (left) or the intensity of the GCase-ABP complex (right) quantified from (A) and depicted as ratio compared to hGCase. **(C)** Homogenate was labeled and subsequently deglycosylated using PNGase F (top panel; ABP). A commercial GCase specific primary antibody was used to visualize all GCase, both active and inactive (middle panel; ab). The composite figure (bottom panel) shows active GCase-ABP complex in blue and total GCase detected using anti-GCase in green.

Detection of zebrafish and frog GCase with ABP was good, however it was observed that the ratio of activity per unit of ABP-complex was lower compared to human GCase (**Figure 3A** and **B**). In contrast, expression and detection of turtle GCase was relatively low which corresponds to the observed low activity (**Figure 3A** and **B**).

Deglycosylation of the GCase enzymes by PNGase F removes all N-linked glycans and revealed a ABP-complex at a lower molecular weight of 50 kDa for all GCase enzymes (**Figure 3C**). The breakdown products described above were also apparent after deglycosylation. A commercially available antibody binding GCase could only visualize human and turtle GCase, while the ABP did not show species specificity (**Figure 3C**). The C-terminal part of human GCase was used to generate the commercial antibody (amino acids 478-497; underlined in **Figure 7**), a part of the protein with quite some variation between the different species.

### Zebrafish GCase hardly shows transfer of glucose to a cholesterol acceptor

First, the optimal conditions for transglucosylation activity were determined for the different GCase enzymes. Cholesterol is a very apolar lipid, practically insoluble in water and aqueous solutions of bile salts or detergents are known to help solubilize cholesterol. Human GCase requires additives not only for optimal hydrolysis but also to perform optimal transglucosylation at pH 5.2 (**Figure 4A-C** and **Supplementary Figure 2**). Zebrafish GCase did not show significant GlcChol formation at the optimal conditions for hydrolysis (**Figure 4A-C**, -Tx/Tc). Addition of sodium taurocholate improved the amount of formed GlcChol, although decreased the hydrolytic activity compared to the condition without additives. The most interesting differences were found for frog GCase. This enzyme showed high enzymatic activity in the absence of additives, however no GlcChol was formed (**Figure 4A-C**). In the presence of Triton-X100, the hydrolytic activity remained similar and the amount of formed GlcChol is much higher compared to the condition without additives (**Figure 4A-C**). In contrast, addition of sodium taurocholate lowered both the amount of formed GlcChol and enzymatic activity towards 4MU- $\beta$ -Glc. Similar findings for transglucosylation were found using the fluorescently labelled NBD-cholesterol as acceptor (**Supplementary Figure 3**). It is apparent from the investigation that addition of Triton-X100 and sodium taurocholate should be optimized for every GCase enzyme and experimental setting.

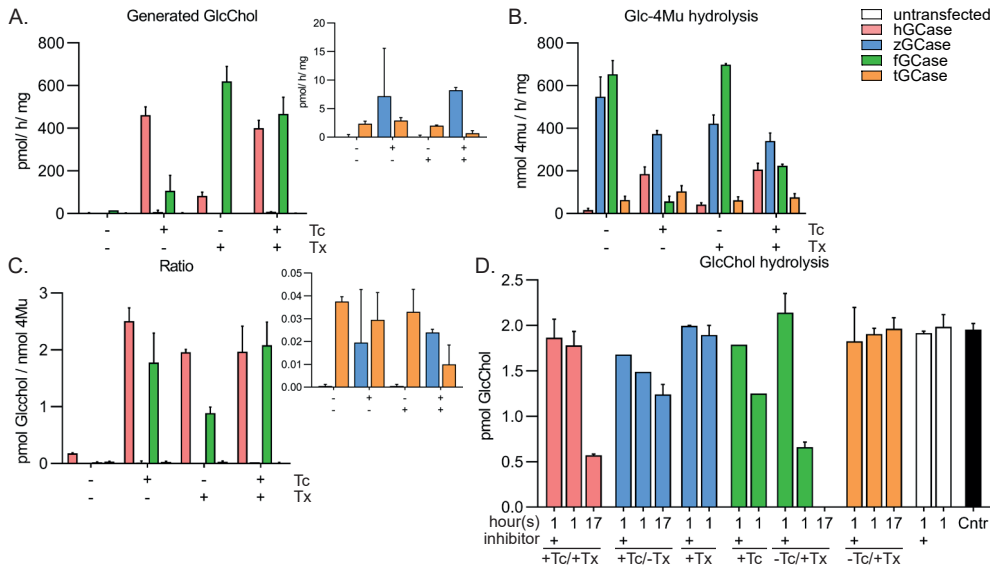


**Figure 4 | In vitro generation and hydrolysis of GlcChol**

(A-C) Homogenate ( $\pm 40 \mu\text{g}$  total protein) was incubated with 4MU- $\beta$ -Glc as glucose donor and cholesterol as acceptor with different buffer conditions: without additives (-Tc/-Tx), with sodium taurocholate (+Tc/-Tx), with Triton-X100 (-Tc/+Tx) or with both additives (+Tc/+Tx). Formed GlcChol was measured using LC-MS/MS methods (A), while the hydrolytic activity was measured by 4MU detection (B). The ratio was calculated of pmol GlcChol formed for 1 nmol of hydrolysed 4MU- $\beta$ -Glc (C). (D) Homogenate ( $\pm 40 \mu\text{g}$ ) was pre-treated with vehicle or a GCase inhibitor for 30 min at 37 °C and subsequently incubated with 2 pmol GlcChol for 1 or 17 hours at 37 °C in the presence of Tx and/or Tc. For Ctr, lysis buffer was incubated with 2 pmol for 1 hour at 37 °C. Activity is measured from 2 independent homogenate preparations and data is depicted as mean  $\pm$  SD.

Next, the ability to hydrolyse the formed GlcChol was evaluated (**Figure 4D**). GCase enzymes were incubated with a fixed amount of GlcChol for 1 hour or overnight ( $\pm 17$  hours). To account for other enzymes and the different conditions, GCase homogenate was pre-blocked with a GCase inhibitor before addition of GlcChol. Both mock and turtle GCase did not show a significant decrease in GlcChol. Human GCase and zebrafish GCase did not show significant decrease in GlcChol after 1 hour of incubation, however both enzymes were able to hydrolyse part of the added GlcChol after overnight incubation. In contrast, frog GCase was able to hydrolyse most of the added GlcChol within 1 hour of incubation and no GlcChol was present after 17 hours of incubation.

Cholesterol, consisting of four hydrocarbon rings, is a bulky sterol, which might influence the positioning of the acceptor within the active site of the enzyme. Other NBD-lipids were tested as acceptor: sphingosine (Sph) and ceramide (Cer). Both human and frog GCase showed product formation when Sph and Cer were used (**Figure 5**). Turtle GCase, expressed at low amounts, did not show prominent GlcChol formation measured using the LC/MS-MS method and no NBD-GlcChol product could be detected using HPTLC as well. However, prominent NBD-Glc-product was visualized when Sph and Cer were used as acceptor. Zebrafish GCase did not show product formation when Chol was used as acceptor. When Cer was used as acceptor lipid, minor product formation was observed.

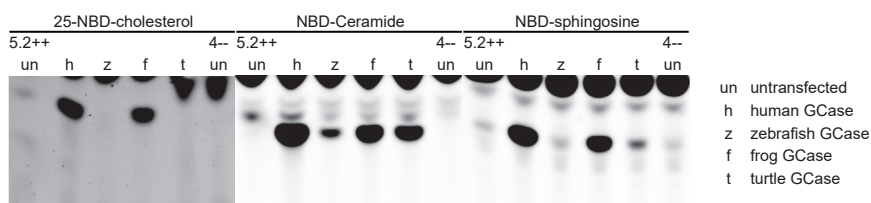


**Figure 5 | In-vitro transglucosylation using different NBD-conjugated acceptor lipids**

Homogenate ( $\pm 40 \mu\text{g}$ ) of untransfected cells (un) or cells over-expressing human- (h), zebrafish- (z), frog- (f) or turtle- (t) GCase was incubated with donor (4MU- $\beta$ -Glc) and different NBD-lipids for 1 hour at  $37^\circ\text{C}$  with the optimal buffer conditions for every GCase enzyme. Lipids were separated on HPTLC silica gel plates using chloroform/ methanol (85:15, v/v) and visualized using fluorescent scanning of the plate.

Taken together, LC-MS/MS and HPTLC experiments indicate that human and frog are able to perform *in vitro* transglucosylation using multiple different types of acceptor lipids. Zebrafish GCase, on the other hand, is only able to use ceramide and possibly sphingosine. These findings lead to the hypothesis that a more flexible acceptor could be able to enter the active site of zebrafish GCase while a rigid, bulky acceptor lipid cannot.

### GCase of all species is able to correct cellular glycosphingolipid abnormalities

The *GBA* KO HEK 293T cells show accumulation of the primary substrate GlcCer and the de-acylated sphingoid base, GlcSph (**Figure 6**; untransfected cells; white bar). These lipid abnormalities were corrected by the stable over-expression of either human, zebrafish, frog and turtle GCase (**Figure 6**). An increase in GlcSph was again observed when the cells were incubated with the GCase specific inhibitor ME656, indicating that the decrease of GlcSph can be attributed to the respective GCase. These findings confirm that the different GCase enzymes are both active and functional in their physiological environment, even though the *in vitro* activity of for example turtle GCase is much lower.

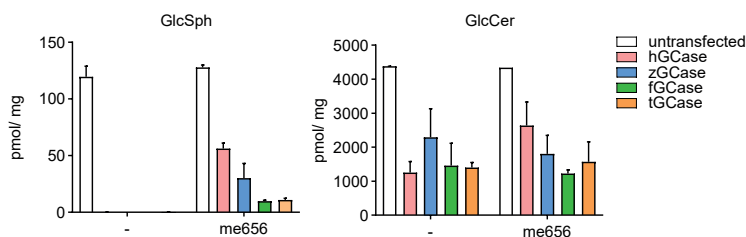


**Figure 6 | Endogenous glycosphingolipid levels of cells expressing GCase enzymes of different species**

*GBA* KO HEK273T cells over-expressing human-, zebrafish-, frog- or turtle GCase and *GBA* KO HEK293T control cells were incubated with vehicle (0.1% (v/v) DMSO) or a GCase inhibitor (100 nM me656, 0.1% (v/v) DMSO) for 36 hours. GlcSph and GlcCer levels were measured and calculated in pmol/mg total protein. Two independent cell experiments were performed and data is depicted as mean  $\pm$  SD.

### Alignment and homology models indicate differences in GCase enzymes

The observed differences in enzymatic activity and transglucosylation might be related to structural differences between the GCase enzymes of different species. Two approaches were used to compare the amino acid sequences of the different GCase enzymes. First, the mature amino acid sequences of human, zebrafish, frog and turtle GCase were aligned using Clustal Omega and important residues highlighted (**Figure 7**). In addition, simple homology models were generated of the zebrafish, frog and turtle structures with SwissModel, based on the established 3D-structure of the human enzyme (PDB code 2XWE), in order to evaluate the position of aberrant residues (**Figure 8**). Conserved and aberrant residues located in the catalytic pocket and the three flexible loops are summarized in **Table 1**.

In the alignment of the primary sequences, the nucleophilic and acid/base glutamic acid residues are conserved (**Figure 7**; Nucleophile (N) and Acid/Base (a/b), arrows) as well as the four cysteine residues forming disulfide bridges are conserved in all species (**Figure 7**, orange). The four N-glycosylation sites with reported glycans in human GCase<sup>2,3</sup> are not all conserved in the different GCase of other species (**Figure 7**; Asn 19, Asn 59, Asn 146 and Asn 270, dark green). *In silico* prediction of N-glycosylation sites showed only 3 predicted sites for zebrafish, 4 sites for frog and 3 sites for turtle GCase (**Figure 7**, dark and light green). Results of the PNGase F treatment (**Figure 3C**) only indicated that GCase of zebrafish, frog and turtle indeed have N-linked glycans, although it is not known how many they have. Properly folded GCase is recognized by LIMP2 and transported as LIMP2-GCase complex to the lysosome. Helix 1a and 1b (residues Thr 86- Leu 96 and Pro 99 – Ser 110) and helix 2 (Pro 150 – Arg 168) of GCase were found important for LIMP2 binding (underlined in **Figure 7**)<sup>5</sup>. These helix motifs displayed hydrophobic patches interacting with LIMP2 (yellow highlight in **Figure 7**). These hydrophobic patches of human GCase are conserved in the amino acid sequences of the other GCase enzymes. This could explain the functional lysosomal localisation of the different enzymes in the human *GBA*-KO cells which would imply interaction of the non-mammalian GCase with human LIMP2.

## Chapter 2

Several residues of prevalent GD mutations are conserved not only in mammals, but also in the GCase sequences studied in this chapter (**Figure 7**, red)<sup>33</sup>. The residues leading to D409H, R463C and R496H are conserved in zebrafish, frog and turtle GCase. The polar uncharged Asn 370, leading to the prevalent N370S mutations is present in turtle GCase, however a negatively charged Asp residue is present at this position in zebrafish and frog GCase. The human Leu 444, leading to the L444P mutation, is present in the zebrafish and frog protein sequence, while another hydrophobic residue, Met, is present at this position in the turtle GCase sequence.

**Table 1** | Divergent residues in zebrafish, frog and turtle GCase compared to human GCase are depicted in orange and bold. Data was obtained from the alignment of the mature amino acid sequence using Clustal Omega and the generated homology models, based on the reported 3D-structure of human GCase.

	Human	Zebrafish	Frog	Turtle	
Loop 3	W312	W314	W313	W312	
"	Y313	Y314	Y314	Y313	
"	L314	F316	L315	L314	
"	D315	D317	D316	D315	
"	F316	R318	A317	F316	
"	L317	L319	I318	I317	
"	A318	V320	V319	A318	
"	P319	P321	P320	P319	
	C342	C344	C343	C342	
	V343	A345	T344	T343	
	G344	G346	G345	G344	
Loop 1	S345	W347	F346	S345	
"	K346	S348	T347	H346	
"	F347	P349	P349	F347	
"	W348	V350	W349	W348	
"	E349	D351	N350	E349	
	Q350	R352	K351	R350	
Loop 2	V394	V396	V395	V394	
"	R395	K397	E396	Q395	
"	N396	N398	N397	N396	
"	F397	F399	N398	L397	
"	V398	V400	V399	V398	
"	D399	D401	D400	D399	
Acid/base	E235	E237	E236	E235	
Nucleophile	E340	E342	E341	E340	
	N370	D372	D371	N370	N370S mutation
	D409	D411	D410	D409	D409H mutation
	L444	L446	L446	M447	L444P mutation
	R463	R465	R465	R466	R463C mutation
	R496	R498	R498	R499	R496H mutation

### *In silico* comparisons of modelled GCase structures

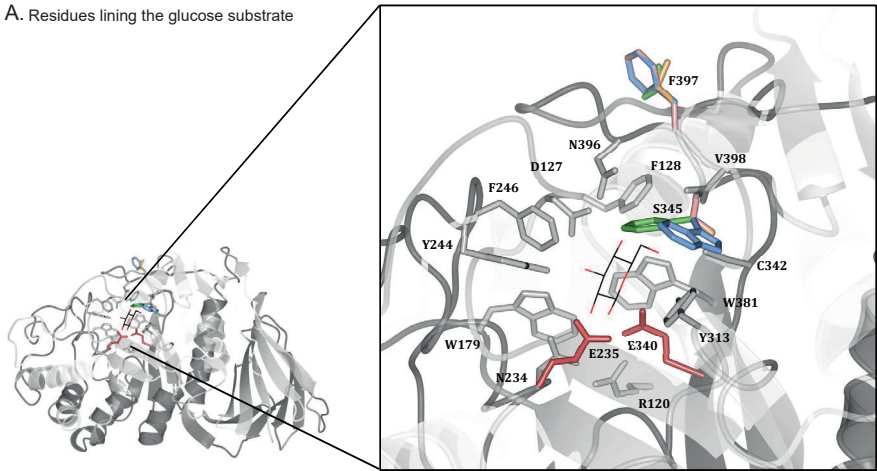
Besides the nucleophile and acid/base glutamic acid residues, several residues line the catalytic pocket of human GCase, which were apparent in established 3D-structures<sup>22,23,34,35</sup>. Most of these residues are conserved in the zebrafish, frog and turtle GCase as shown by the homology model (**Figure 8A**), including Arg 120, Asp 127, Phe 128, Trp 179, Asn 234, Tyr 244, Phe 246, Tyr 313, Cys 342, Ser 345, Trp 381, Asn 396, Phe 397, and Val 398 of human GCase. Two exceptions were observed: the polar side chain of Ser 345 is replaced by a hydrophobic side chain in the zebrafish and frog (Trp and Phe respectively), while the hydrophobic side chain of Phe 397 is present in the zebrafish but is replaced by the hydrophobic, small side chain of Leu in turtle and the polar side chain of Asn in frog (**Figure 8A** and **Table 1**).





Chapter 2

A. Residues lining the glucose substrate



B.

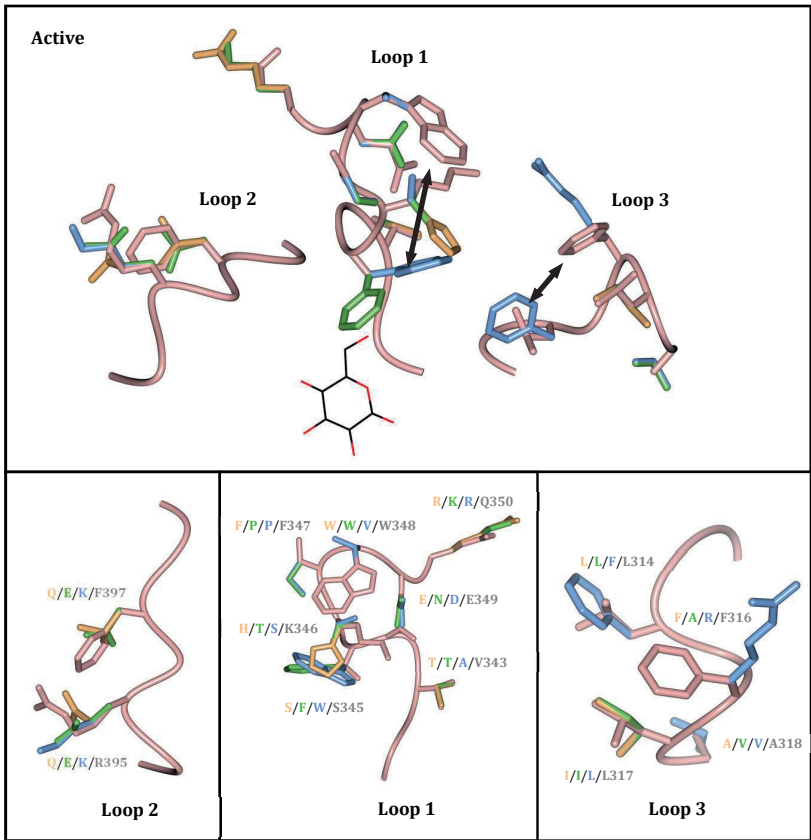


**Figure 8 | *In silico* comparison of homology GCCase models**

Homology models were generated of the zebrafish, frog and turtle structures with Swissmodel, based on the reported 3D-structure of human GCCase (PDB code 2XWE<sup>36</sup>). **(A)** Glucose-lining residues. Similar residues with respect to the human structure are depicted in grey, the nucleophilic Glu 340 and acid/base Glu 235 in red, while aberrant residues are visualized with the respective color for human (pink), zebrafish (blue), frog (green) or turtle (orange) residues. **(B)** Loops 1, 2 and 3 in the active conformation of human GCCase with residues of human (pink/grey), zebrafish (blue), frog (green) and turtle (orange) GCCase. Divergent residues at the modelled position are given in the respective color in the lower panel.

### Mutagenesis of selected amino acids in zebrafish GCase does not changes its features

Established 3D-structures of GCase revealed different conformations of loops 1, 2 and 3 in the inactive- versus the active, ligand associated human GCase structures. Interactions of specific residues in these loops are thought to facilitate the closed conformation of the inactive, unbound structure, while conformational changes of the loops is suggested to open the active site<sup>13,23</sup>. Several residues are different in the modelled loops 1, 2 and 3 of the zebrafish, frog and turtle structures (**Figure 8B**). The most intriguing differences are between the human and zebrafish sequences. In the homology model, Trp 348 of loop 1 in human GCase is replaced in the zebrafish sequence by a Val, while a Trp with bulky side chain of zebrafish GCase substitutes human Ser 345. In loop 3, Phe 316 in human GCase is replaced in zebrafish by an Arg residue, while Leu 314 is replaced by a Phe residue. These *in silico* models suggest that the hydrophobic side chains of Trp and Phe are present in the zebrafish structure, albeit positioned closer to the catalytic pocket (depicted in **Figure 8B** by the arrows).

It was hypothesized that these substitutions might impair entrance of the bulky sterol acceptor. In order to test this hypothesis, three different mutations of the zebrafish GCase were generated and evaluated: 1) F316L, 2) W347S, and 3) a double mutation of F316L + R318F. GCase enzymes with these mutations were transiently expressed in the *GBA* KO cells and the catalytic features were determined in a pilot experiment. No change in pH optimum of the hydrolysis reaction was observed nor an improvement in GlcChol formation. A decrease in activity of the W347S zebrafish GCase was observed, however transient transfection was only performed once and this effect might be due to biological variation. Taken together, these single- and double amino acid substitutions did not validate the hypothesis of improved access of cholesterol in the zebrafish enzyme. To test further this hypothesis, future endeavours could focus on swapping the entire candidate loop 1 or 3 among the different species.

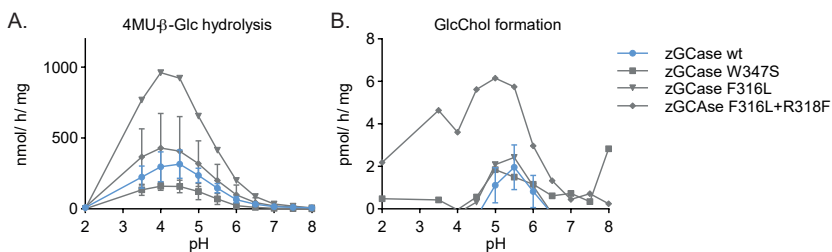


**Figure 9 | Enzymatic activity and GlcChol formation of zebrafish GCase variants**

**(A)** Hydrolytic activity of zebrafish GCase WT and GCase variants (W347S, F316L and F316L+R318F) towards 4MU-β-Glc at different pH values without additives incubated for 30 min at 37 °C. **(B)** Homogenates ( $\pm 40 \mu\text{g}$  total protein) were incubated with 4MU-β-Glc as glucose donor and cholesterol as acceptor at different pH with 0.1% (w/v) BSA and 0.1% (v/v) Triton-X100. Formed GlcChol was measured using LC-MS/MS methods. Data is depicted from a single pilot experiment (no error bars) or biological duplicate with mean  $\pm$  SEM.

## Discussion

Zebrafish are an emerging and attractive research model to evaluate the potency and selectivity of small molecules and to study genetic disorders such as the lysosomal storage disease GD. The aim of present study was to evaluate whether the highly homologous zebrafish GCase enzyme has similar features to its human counterpart. In parallel, GCase enzymes of an amphibian (*Xenopus laevis*, frog) and reptile (*Chrysemys picta bellii*, turtle) were studied. The zebrafish, frog and turtle GCase enzymes were highly homologous to the human counterpart, with an amino acid identity of 57.8 % for zebrafish, 63.5 % for frog and 64.6 % for turtle GCase. In particular residues lining the catalytic pocket showed high conservation among the different GCase sequences.

The coding sequences of the different GCase enzymes were cloned into a mammalian expression vector and stably expressed in *GBA* KO human embryonic kidney (HEK293T) cells, generated by means of CRISPR/Cas9. ABP-labelling revealed GCase-labelled proteins at comparable molecular weight as well as the presence of N-linked glycans in all enzymes. The enzymatic features of zebrafish, frog and turtle GCase were quite comparable to the human GCase. All four enzymes were active *in vitro* towards the artificial substrate 4MU- $\beta$ -Glc at an acid pH optimum and were able to correct endogenous accumulated GlcCer and GlcSph in the *GBA* KO HEK293T cells. These findings implied that newly synthesized GCase enzymes of zebrafish, frog and turtle are able to interact *in situ* with the endogenous human LIMP2 protein. In similar manner, it can be argued that the non-mammalian GCase enzymes are able to interact *in situ* with human Saposin C. However, caution is warranted since over-expression of GCase as such might be sufficient to correct the increased GlcCer and GlcSph lipids.

Of note, comparable enzymatic features were noted when the non-lysosomal  $\beta$ -glucosidase Gba2 of the zebrafish was compared to its human counterpart<sup>37</sup>. In addition, *in vivo* treatment of developing zebrafish larvae with inhibitors of GCase, Gba2 or glucosylceramide synthase (GCS) showed aberrant glycosphingolipid levels similar to treatments of mammalian systems as discussed in chapter 5<sup>32,38-40</sup>. Altogether these data suggest that GlcCer metabolism as well as enzymes responsible for synthesis and catabolism are similar in zebrafish as compared to mammals.

Although all GCase enzymes were found to be active, several differences were also observed. **Table 2** summarizes the most relevant observations in this respect. First, it became apparent that human GCase requires additives, either Triton-X100 and sodium taurocholate or recombinant Saposin C with phosphatidylserine, for maximal activity. Both zebrafish and frog GCase require no additives for maximal enzymatic activity towards 4MU- $\beta$ -Glc and show a lower pH optimum of pH 4. A striking difference between zebrafish GCase and the other studied GCases is the high activity of the former enzyme at low temperature. Sharply contrasting with human GCase, zebrafish enzyme was at 4 and 10 °C as active as at 28 and 37 °C.

Another major difference between zebrafish and human GCase is the inability of the former to catalyse a transglucosylation reaction *in vitro* using cholesterol as acceptor. Frog GCase is able to efficiently transfer the glucose from a glucose donor to a cholesterol

acceptor, as human GCase<sup>18</sup>. GlcChol formation by frog GCase was low in the absence of additives. Transglucosylation activity increased when Triton-X100 was added, but prohibited by sodium taurocholate, sharply contrasting human GCase<sup>31</sup>. It is of interest to stress that zebrafish GCase showed *in vitro* transglucosylation activity when a more flexible NBD-lipid like ceramide was used as acceptor.

**Table 2 |** Overview of the findings regarding *in vitro* hydrolysis and transglucosylation as well as *in situ* correction. 0 = no stimulation, ND = not determined, NR = not reproducible, SA/ABP = specific activity / ABP-complex.

Enzyme	Tc/Tx	Hydrolysis				Transglucosylation		GlcChol hydrolysis	<i>In situ</i> GlcCer/GlcSph correction
	stimulation	SapC simulation	pH optimum	SA/ABP	10/37 °C	Ability?	Additives?		
Human	++	++	5.2	++	--	yes	Tx/Tc	++	Yes
Turtle	(+)	ND	5.2	--	--	NR	NR	NR	Yes
Frog	0	ND	4.0	-	--	yes	Tx	+++	Yes
Zebrafish	0	0	4.0	-	++	no	(Tc)	+	Yes

The combined findings raised the possibility that zebrafish GCase is in a more active fold permanently, independent of temperature and additives, as compared to human GCase. This more 'rigid' conformation of zebrafish GCase may as downside limit the enzyme's ability to transfer glucose to structurally rigid acceptors like cholesterol. Of note, zebrafish GCase shows hydrolytic activity towards GlcChol that is formed in cells by the non-lysosomal GBA2 (see Chapters 5 and 7).

It was hypothesized that specific side chains of the zebrafish GCase might impair entrance of a bulky acceptor, like cholesterol, for the transglucosylation reaction. *In silico* comparison of the modelled structures revealed that most of the glucose-lining residues of the catalytic pocket were conserved among the three GCase enzymes compared to human GCase, while aberrant residues were apparent in flexible loops 1, 2 and 3. In particular, substitutions of human Leu 314 and Phe 316 of loop 3 and Ser 345 of loop 1 were noticed in the zebrafish GCase enzyme and it appeared that the hydrophobic side chains were positioned closer to the catalytic pocket of the zebrafish enzyme. Interestingly, a recent patent filed by Amicus describes a mutated human GCase with the double amino acid substitution F316A and L317F located in loop 3, showing increased catalytic activity and a doubled half-life at pH 7.5 compared to WT human GCase<sup>41</sup>. It was considered that specific side-chain conformations could form a more ordered region near the catalytic pocket and might be less prone to unfolding at neutral pH. Human Phe 316 is among one of the contrasting residues in the zebrafish and frog GCase enzymes. In addition, it has been found that the structural stability of recombinant GCase improves at acidic pH, showing an increased half-life, higher melting temperature and lower sensitivity to tryptic digestion<sup>42</sup>. Binding of (semi-)covalent inhibitors increased the structural stability even further. Therefore, it might be informative to study the structural stability of the GCase enzymes of different species in order to evaluate the structural compactness and susceptibility for proteolytic cleavage of the different enzymes.

A detailed comparison of human and zebrafish GCase, with parallel comparisons of frog and turtle GCase, was chosen in view of evolutionary aspects and accompanying changes in skin composition associated with the transition to terrestrial life. GCase sequences of several other non-mammalian species are known and alignment in combination with simple

modelling indicates that a lower number of divergent residues are present in loops 1, 2 and 3 of reptiles and birds compared to the fish and amphibian species (**Supplementary Table 1**: python, goose, crocodile, dolphin and mouse GCCase). Loop 3 is entirely conserved in reptiles, birds and mammals, but not in zebrafish and frog. This loop 3 shows the largest conformational change based on the established 3D-structures of human GCCase<sup>22-24</sup>. Studying the *in vitro* hydrolysis, transglucosylation and stability of these additional GCCase enzymes could provide more information on the impact of divergent residues in the GCCase enzymes. Of note, efforts have been made to express the GCCase enzyme of the python, exactly as performed for the other GCCase enzymes. Surprisingly, no enzymatic activity and no ABP-labelled band could be found for python GCCase (data not shown). A possible explanation for the complete absence of expression in case of python and low expression of turtle GCCase might be the utilized endogenous signal peptide of the respective GCCase. In future experiments the predicted signal peptide sequence could be replaced by the human signal peptide sequence in order to evaluate the influence of the endogenous signal peptide and possibly improve expression.

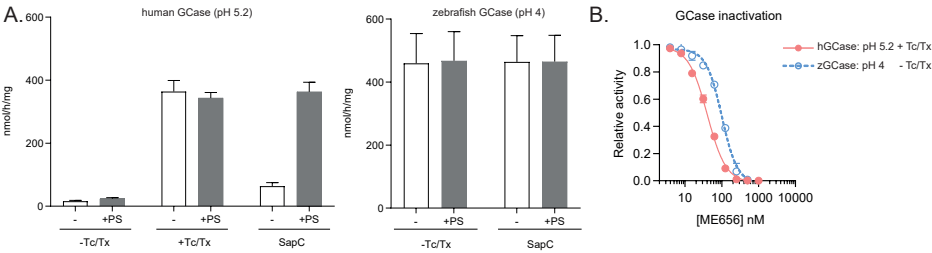
As final part of this study, site-directed mutagenesis of the zebrafish GCCase enzyme was performed to test the hypothesis of impaired access of cholesterol by the residues with hydrophobic side chains. The zebrafish GCCase variants with rationalized single- and double amino acid substitutions did not impact the pH optimum or GlcChol formation. Swapping the entire candidate loop 1 or 3 among the different species might be a more productive approach for evaluating the influence of these loops on GlcChol formation. In addition, crystallization of the zebrafish GCCase enzyme could be very informative, as present *in silico* comparisons are limited by the simple molecular modelling of divergent residues. Crystallization and subsequent comparison of the zebrafish GCCase structures with human counterparts could reveal real differences in the 3D-structure of GCCase.

In conclusion, the zebrafish GCCase enzyme shows comparable hydrolytic activity to human GCCase, but markedly differs in ability to transglucosylate and the influence of temperature on enzymatic activity. The molecular basis for these difference warrants further investigation by detailed studies of the structures of the GCases.

## Acknowledgments

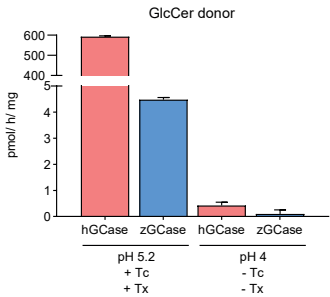
Daniel van Geest is kindly acknowledged for his extensive contribution to this study by performing part of the enzymatic assay as well as generation of the zebrafish GCCase variants and subsequent pilot experiments. Marc Hazeu is acknowledged for the expression and purification of recombinant human saposin C.

Supplementary information



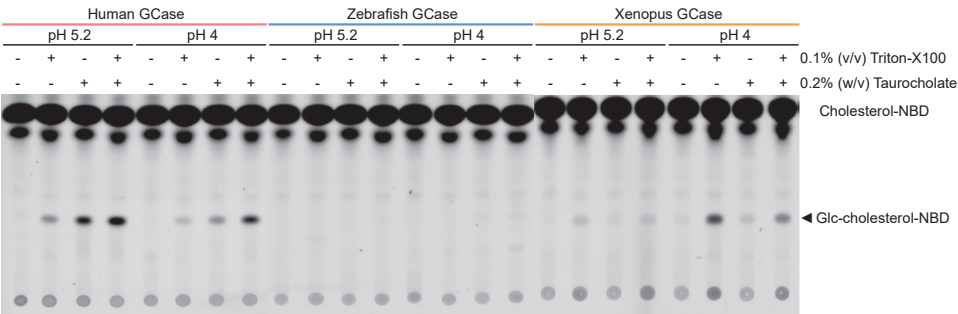
Supplementary Figure 1

(A) Enzymatic activity towards 4MU- $\beta$ -Glc in the presence of the additives Triton-X100 (Tx) and sodium taurocholate (Tc) or Saposin C with or without addition of phosphatidylserine (PS) of human GCase at pH 5.2 (left) or zebrafish GCase at pH 4 (right). (B)  $IC_{50}$  curves of the inactivation of human (pink) or zebrafish (blue) GCase by the GCase specific inhibitor, ME656. Activity is measured from 3 independent homogenate preparations for (A) and in technical duplicate for (B). Data is depicted as mean  $\pm$  SD.



Supplementary Figure 2 | Transglucosylation with GlcCer as donor

Cell homogenate ( $\pm$  40  $\mu$ g) expressing human or zebrafish GCase was incubated with GlcCer d18:1/18:1 as glucose donor and cholesterol as acceptor in buffer of pH 4 without additives (-Tc/-Tx) or buffer of pH 5.2 with Triton-X100 and sodium taurocholate (+Tc/+Tx) for 5 hours at 37  $^{\circ}$ C. Formed GlcChol was measured using LC-MS/MS techniques in technical duplicate.



Supplementary Figure 3 | Effect of Triton-X100 and Sodium Taurocholate on transglucosylation with NBD-Chol

Cell homogenate ( $\pm$  40  $\mu$ g) expressing human, zebrafish or frog GCase was incubated with 4MU- $\beta$ -Glc as glucose donor and NBD-cholesterol as acceptor in McIlvaine buffer of pH 4 or pH 5.2 supplement with Triton-X100 and/or Sodium Taurocholate and incubated for 1 h at 37  $^{\circ}$ C. Formed NBD-GlcChol was detected using fluorescent scanning of the separated lipids on a HPTLC plate using  $CHCl_3$ /MeOH (80:20) as eluents.

## Chapter 2

**Supplementary Table 1** | Comparison of residue substitutions of human, zebrafish, frog, turtle GCase and GCase enzymes of additional species: python, goose, saltwater crocodile, freshwater crocodile, dolphin and mouse GCase. Data was obtained from the alignment of the mature amino acid sequence using Clustal Omega and the generated homology models, based on the reported 3D-structure of human GCase. Different residues compared to the human enzyme are depicted in orange and bold.

	Human	Zebrafish	Frog	Turtle	Python	Goose	Crocodile (salt)	Crocodile (fresh)	Dolphin	Mouse
Loop 3	W312	W314	W313	W312	W312	W312	W312	W312	W312	W311
"	Y313	Y314	Y314	Y313	Y313	Y313	Y313	Y313	Y313	Y312
"	L314	<b>F316</b>	L315	L314	L314	L314	L314	L314	L314	<b>M313</b>
"	D315	D317	D316	D315	D315	D315	D315	D315	D315	D314
"	F316	<b>R318</b>	<b>A317</b>	F316	F316	F316	F316	F316	F316	F315
"	L317	L319	<b>I318</b>	<b>I317</b>	L317	<b>I317</b>	L317	L317	L317	L316
"	A318	<b>V320</b>	<b>V319</b>	A318	A318	<b>G318</b>	A318	A318	A318	A317
"	P319	P321	P320	P319	P319	P319	P319	P319	P319	P318
	C342	C344	C343	C342	<b>S342</b>	C342	<b>S345</b>	C342	C342	C341
	V343	<b>A345</b>	<b>T344</b>	<b>T343</b>	<b>T343</b>	<b>I343</b>	<b>A346</b>	V343	V343	V342
	G344	G346	G345	G344	G344	G344	G347	G344	G344	G343
Loop 1	S345	<b>W347</b>	<b>F346</b>	S345	S345	<b>A345</b>	S348	S345	S345	S344
"	K346	<b>S348</b>	<b>T347</b>	<b>H346</b>	<b>Y346</b>	<b>H346</b>	<b>Y349</b>	K346	K346	K345
"	F347	<b>P349</b>	<b>P349</b>	F347	F347	F347	F350	F347	F347	F346
"	W348	<b>V350</b>	W349	W348	W348	W348	W351	W348	W348	W347
"	E349	<b>D351</b>	<b>N350</b>	E349	E349	E349	E352	E349	E349	E348
	Q350	<b>R352</b>	<b>K351</b>	<b>R350</b>	<b>P350</b>	<b>R350</b>	<b>P353</b>	Q350	Q350	Q349
Loop 2	V394	V396	V395	V394	<b>S394</b>	V394	<b>S397</b>	V394	V394	V393
"	R395	<b>K397</b>	<b>E396</b>	<b>Q395</b>	<b>K395</b>	<b>K395</b>	<b>K398</b>	<b>K395</b>	R395	R394
"	N396	N398	N397	N396	N396	N396	N399	N396	N396	N395
"	F397	F399	<b>N398</b>	<b>L397</b>	<b>Y397</b>	<b>Y397</b>	<b>Y400</b>	F397	F397	F396
"	V398	V400	V399	V398	V398	V398	V401	V398	V398	V397
"	D399	D401	D400	D399	D399	D399	D402	D399	D399	D398
Acid/base	E235	E237	E236	E235	E235	E235	E238	E235	E235	E234
Nucleophile	E340	E342	E341	E340	E340	E340	E343	E340	E340	E339



## Experimental procedures

**Chemicals and reagents** - The GCase specific inhibitor (ME656), ABP (ME569) and  $^{13}\text{C}_6$ -GlcChol internal standard were synthesized as described earlier<sup>16,18,32</sup>. Chemicals were obtained from Sigma-Aldrich (St. Louis, MO, USA) if not otherwise indicated. Primers (**Supplementary Table 2**) were ordered from Integrated DNA technologies (IDT; Coralville, USA) without additional purification.

**Cloning of the coding sequence of *gba* from different species** - Design of cloning primers and plasmids containing the coding sequence of *gba* of different species were based on NCBI sequences NM\_000157.4 (human), XM\_682379.7 (zebrafish), XM\_018229065.1 (frog) and XM\_005280678.2 (turtle). The coding regions of human and zebrafish GCase were amplified using Phusion HighFidelity PCR mastermix (Thermo Fisher Scientific, Waltham, USA) using the primers given in **Supplementary Table 2**. Fragments of human and zebrafish *GBA* were cloned into the pDONR vector using GATEWAY™ recombination cloning technology (BP reaction, Thermo Fisher) according to the manufacturer's instruction and subsequently shuttled to a pDEST-zeo expression vector (derived by replacing the neomycin selection marker with a zeomycin selection marker) using the LR reaction.

Plasmids including the coding sequences of frog and turtle with flanking LR sequences and cloned into the pUC57-Kan vector backbone, were ordered from Baseclear (Leiden, the Netherlands). A LR reaction was performed shuttling the respective *gba* sequence to the pDEST-zeo expression vector. For CRISPR/Cas9 mediated *GBA* knockouts of HEK293T cells, sgRNA guides given in **Supplementary Table 2** were cloned into the BbsI restriction site of the px330-U6-chimeric\_BB-CB-hSpCas9 (Addgene plasmid #42230). All plasmids were isolated from transformed DH5α cells using a plasmid isolation kit (Qiaprep spin Miniprep kit; Qiagen, Hilden, Germany) and sequenced.

**Site-directed mutagenesis** – Point mutations were introduced in the zebrafish GCase pDONR vector using the QuickChange Lightning Site-Directed Mutagenesis Kit (Agilent, Santa Clara, USA) according to the suppliers protocol with the primers given in **Supplementary Table 2**. The double F316L+R318F mutation was generated by mutating the pDONR vector of the zebrafish GCase variant with the F316L mutation. The pDONR vectors were sequenced before shuttling the GCase encoding sequences to the pDEST-zeo expression vector.

**Supplementary Table 2** | List of oligonucleotide sequences.

Primer	Sequence (5' -3')	Purpose
Human <i>GBA</i> F	GGGGACAAGTTTGTACAAAAAGCAGGCTccACCACCATGGAGTTTTCAGTCCCTCC	Gateway cloning
Human <i>GBA</i> R	GGGGACCACTTTGTACAGAAAGCTGGGTTCATCACTGGCGACGCCACAGTA	Gateway cloning
Zebrafish <i>gba</i> F	GGGGACAAGTTTGTACAAAAAGCAGGCTACCACATGAGAGAAACGGCTCTTTTATTC	Gateway cloning
Zebrafish <i>gba</i> R	GGGGACCACTTTGTACAGAAAGCTGGGTcTTACTGTCTGTCCACAGTAGTG	Gateway cloning
Hu <i>GBA</i> sgRNA F	CACCGCGCTATGAGAGTACACGCAG	sgRNA for px330
Hu <i>GBA</i> sgRNA R	AAACCTGCGTGTACTCTCATAGCGC	sgRNA for px330
Zf GCase W347S F	gaggcatgcgctgggtCgagtcacagtggatcgt	Mutagenesis
Zf GCase W347S R	acgatccactggactcGacccagcgcatgcctc	Mutagenesis
Zf GCase F316L F	gcattggtgttcaactggatattGgatcgcttgtgcc	Mutagenesis
Zf GCase F316L R	ggcacaagggcgtacCaaataccagtgaaacaccaatgc	Mutagenesis
Zf GCase R318F F	attggtgttcaactggatattGgatTTccttgtgccgcctg	Mutagenesis
Zf GCase R318F R	caggcggcacaaaggAAatcCaaataccagtgaaacaccaat	Mutagenesis

**Cell culture and transfection** - HEK293T (CRL-3216) were purchased from ATCC (Manassas, VA, USA) and cultured at 37 °C and 5% CO<sub>2</sub> in DMEM medium, supplied with 10% (v/v) FCS, 0.1% (w/v) penicillin/streptomycin, and 1% (v/v) Glutamax. *GBA* KO cells were obtained by CRISPR/Cas9 technology by transfecting HEK293T cells seeded in 6-well plates with the px330-*GBA* plasmid in combination with Fugene 6 (Roche; Basel, Switzerland) in a ratio of Fugene:DNA of 3:1. After 72 hours, cells were diluted to approximately 0.5 cell/well, seeded in 96-well plates and individual clones were cultured over the next weeks. GCase activity was determined of the single cell clones, as described below, and only clones without residual activity were maintained. *GBA* KO clone 35 was verified using Sanger sequencing and used for experiments, subsequently called *GBA* KO cells. *GBA* KO cells were transfected using PEI and the pDEST-zeo-*gba* construct (PEI/DNA: 3/1 (w/w)). Cells expressing the

## Chapter 2

protein of interest were selected by sub-culturing the cells in medium supplemented with 200 µg/mL Zeomycin for at least 5 passages starting 24 hours after transfection. For transient expression, cells were transfected, as described above, for 72 hours before harvesting. Cells were harvested in PBS and washed twice with PBS. Cell pellets were stored at -80 °C until use.

**Homogenate preparation** - Cells were resuspended in 25mM potassium phosphate buffer supplemented with 0.1% (v/v) Triton-X100 and benzonase (25mM Kpi pH6.5, 0.1% Triton-X100 and 25U/mL benzonase) and lysed using sonication (20% amplitude, 3s on, 3s off for 4 cycles) while on ice. Protein concentration was determined (BCA kit; Pierce, Thermo Fisher) with BSA as standard.

### Enzyme activity assay

**General activity procedures** – Generally, assays were performed using homogenate in KPi lysis buffer (12.5 µL, ± 12.5 µg protein) by addition of Mcllvaine buffer (citric acid – Na<sub>2</sub>HPO<sub>4</sub>) of the appropriate pH (12.5 µL; 150mM Mcllvaine pH4 or pH5.2) before addition of 4-methylumbelliferyl β-glucoside mix. Assays were performed using 4MU-β-Glc mixes optimized for each protein; 100 µL of 3.75 mM 4MU-β-Glc substrate, 0.1% (w/v) BSA, 0.1% (v/v) Triton-X and 0.2% (w/v) Sodium Taurocholate at pH5.2 for human GCase (pH5.2++), 3.75 mM 4MU-β-Glc substrate and 0.1% (w/v) BSA at pH 4 for zebrafish and frog GCase (pH4--) and 3.75 mM 4MU-β-Glc substrate and 0.1% (w/v) BSA at pH 5.2 for turtle GCase (pH 5.2--). Incubation was performed for 30min at 37 °C and stopped by addition of glycine-NaOH STOP buffer (200 µL; 1 M Glycine-NaOH, pH 10.3) unless stated otherwise. All activity assays were measured using a LS-55 (PerkinElmer, Waltham, USA; λ<sub>ex</sub> of 366 nm, λ<sub>em</sub> of 445nm) and calculated using a standard of 1nmol 4MU. All activities were measured using three independent homogenates measured in technical duplicate unless indicated otherwise in the result section.

**pH curves** – pH curves were obtained by incubating homogenate (12.5 µL, ± 12.5 µg total protein) with Mcllvaine of the appropriate pH (62.5 µL; 300 mM Mcllvaine, pH 2-8) on ice for 5 minutes before addition of two-times concentrated Glc-4Mu substrate mix with additives (50 µL; 7.5 mM Glc-4Mu, 0.2% (w/v) BSA, 0.2% (v/v) Triton-X and 0.4% (w/v) Sodium Taurocholate in MilliQ) or without additives (50 µL; 7.5 mM GlcMu and 0.2% (w/v) BSA in MilliQ).

**Michaelis-Menten kinetics** – To homogenate (12.5 µL, ± 12.5 µg protein) was added Mcllvaine with the appropriate pH (12.5 µL, 150 mM Mcllvaine pH 4 or pH 5.2) and subsequently incubated with different substrate concentrations (100 µL; 0-10 mM Glc-4Mu +0.1% (w/v) BSA in either 150 mM Mcllvaine buffer pH 4 (pH4--), 150 mM Mcllvaine buffer pH 5.2 or 150 mM Mcllvaine buffer pH 5.2 + 0.1% (v/v) Triton-X + 0.2% (w/v) Sodium Taurocholate (pH5.2++)). K<sub>m</sub> and V<sub>max</sub> values were calculated using Graphpad Prism 8.0 (GraphPad Software, San Diego, USA).

**Temperature curve** – Homogenates were incubated with 4MU-β-Glc mixes in PCR tubes as described in the general assay procedures and incubated at different temperatures. At indicated time points, 5 µL of the sample was removed from the mixture, added to 200 µL STOP buffer and the fluorescence was measured and calculated in pmol/h/mg. The relative activity was calculated using the activity of the respective GCase at 30 min and 37 °C incubation.

**IC<sub>50</sub> curve** – For the covalent GCase specific inhibitor, human or zebrafish GCase expressing cell homogenate (12.5 µL, ± 12.5 µg protein) was pre-incubated with ME656 (2x concentrated in 300 mM Mcllvaine pH 4 or pH 5.2 with 1% (v/v) DMSO) for 30 min at 37 ° before addition of the respective 4MU-β-Glc mix, incubation and measurement in the general assay procedures. IC<sub>50</sub> curves were fitted using GraphPad Prism.

**Saposin C/phosphatidylserine activation** - Phosphatidylserine (PS, 10 mg/mL in chloroform/ methanol) was concentrated and resuspended in Mcllvaine buffer (2x concentrated 'PS mix'; 80 µg/mL PS, 300 mM Mcllvaine pH 4 or pH 5.2). Recombinant human Saposin C (900 µg/µL) was diluted in Mcllvaine buffer (50 µg/µL, 300 mM Mcllvaine buffer pH 4 or pH 5.2). To human or zebrafish GCase expressing cell homogenates (12.5 µL, 12.5 µg protein) was added Saposin C mix or Mcllvaine (12.5µL), 'PS mix' or Mcllvaine (50 µL) and 4MU-β-Glc mix (2x concentrated, 50 µL; 7.5 mM 4MU-β-Glc and 0.2% (w/v) BSA in MilliQ or 50 µL of 7.5 mM 4MU-β-Glc, 0.2% (w/v) BSA, 0.2% (v/v) Triton-X and 0.4% (w/v) Sodium Taurocholate in MilliQ). Assays were incubated and measured as described above.

### Activity-based probe (ABP) labelling

**General ABP labelling procedures** – Homogenates (10  $\mu$ L, 10  $\mu$ g total protein or protein amount to obtain equal activity towards 4MU- $\beta$ -Glc) was labelled with the cy5-modified cyclophellitol-epoxide ABP ME569 (200 nM ME569 in 10  $\mu$ L 300 mM Mcllvaine buffer pH 4 or 5.2, without additives or supplemented with 0.2% (v/v) Triton-X100 and 0.4% (w/v) Sodium Taurocholate for human GCase, 1% (v/v) DMSO; final concentration 100 nM ME569 and 0.5% (v/v) DMSO). Proteins were denatured with 5x Laemmli sample buffer (25% (v/v) 1.25 M Tris-HCL pH 6.8, 50% (v/v) 100% glycerol, 10% (w/v) sodium dodecyl sulfate (SDS), 8% (w/v) dithiothreitol (DTT) and 0.1% (w/v) bromophenol blue) and boiled for 5 min at 98 °C. ABP-labelled protein samples were separated by electrophoreses on 10% (w/v) SDS-PAGE gels, before scanning the fluorescence of the wet-slab gel with a Typhoon FLA 9500 (GE Healthcare, Chicaco, USA; cy5 ( $\lambda_{ex}$  of 635 nm,  $\lambda_{em}$  of 655-685 nm), 750 V, pixel size 100  $\mu$ M). Gels wer stained with Coomassie Brilliant Blue staining or transferred to a nitrocellulose membrane (BioRad, Hercules, USA).

**Deglycosylation using PNGase F** – Glycoproteins were deglycosylated using PNGase F (NEB, Ipswich, USA). Briefly, homogenate was labelled with ME569, as described above, in 2x volumes (40  $\mu$ L final volume). After incubation for 30 min at 37 °C, the mixture was denatured using Glycoprotein buffer (supplied) and boiled for 10 min at 98 °C. The sample was divided, NP-40 (supplied) and MQ was added to both samples NP-40 and one 20  $\mu$ L sample was incubated with PNGase F, while the other 20  $\mu$ L sample was incubated with MQ for 1 h at 37 °C. Laemmli sample buffer (5x) was added after incubation and the samples were separated on a 10% (w/v) SDS-PAGE gel and scanned as described.

**Immunoblot** – Proteins were transferred to a 0.2  $\mu$ m nitrocellulose membrane by Trans-Blot Turbo™ transfer system (Bio-Rad). Membrane was blocked with 5% (w/v) BSA in TBST for 1 h at rt and incubated overnight at 4 °C with primary antibody (anti-GCase, Sigma-Aldrich G4171; 1:1000). Membrane was washed three times with TBST and incubated with secondary antibody (goat anti-rabbit IgG (H+L)-HRP, Bio-Rad; 1:5000) for 1 h at 37 °C, washed twice with TBST and a final time with TBS before development using the Clarity Max ECL substrates (Bio-Rad) and detected by the ChemiDoc™ MP system (Bio-Rad).

### Transglucosylation and GlcChol hydrolysis

**General transglucosylation using LC-MS/MS measurement** – Generally, transglucosylation activity of was determined with 4MU- $\beta$ -Glc as donor and natural cholesterol as acceptor, as described with minor modifications<sup>18</sup>. Briefly, to GCase expressing cell homogenates (12.5  $\mu$ L,  $\pm$  40-50  $\mu$ g total protein) was added a mix of cholesterol acceptor and 4MU- $\beta$ -Glc donor in Mcllvaine buffer of the appropriate pH and supplemented with additives (100  $\mu$ L including 3.75 mM 4MU- $\beta$ -Glc, 0.1% (w/v) BSA and 25  $\mu$ M cholesterol with 1% ethanol in 150 mM Mcllvaine pH 4 or pH 5.2 supplemented with 0.1% (v/v) Triton-X100 and/or 0.2% (w/v) Sodium Taurocholate). After 1 h incubation at 37 °C with shaking, 5  $\mu$ L of the sample was transferred in duplicate to 200  $\mu$ L STOP buffer, 4MU was measured and enzymatic activity was calculated. The residual sample was snap-frozen in liquid nitrogen or <sup>13</sup>C<sub>6</sub>-GlcChol internal standard (20  $\mu$ L, 0.1 pmol/ $\mu$ L in methanol) was added to the 115  $\mu$ L of remaining sample, followed by methanol and chloroform (2:1 (v/v)) to precipitate the protein. After centrifugation, lipids of the supernatant were extracted using a Bligh-Dyer extraction (MeOH:CHCl<sub>3</sub>:H<sub>2</sub>O, 1:1:0.9) and measured using previously described methods<sup>18</sup>.

**GlcChol hydrolysis** – An appropriate volume of GlcChol (2 pmol per reaction) was concentrated and resuspended in ethanol to a concentration of 1.6 pmol/ $\mu$ L. A mixture of GlcChol in Mcllvaine of the appropriate pH was prepared with BSA (0.1 % (w/v)) and with the necessary additives for every GCase enzymes as described in the result section (0.1% (v/v) Triton-X100) and/ or 0.2% (w/v) Sodium Taurocholate). GCase expressing cell homogenates (12.5  $\mu$ L,  $\pm$  40-50  $\mu$ g total protein) were incubated with vehicle or the GCase specific inhibitor ME656 (12.5  $\mu$ L of 2 $\mu$ M ME656 in 300 mM Mcllvaine pH 4 or pH 5.2, 1% (v/v) DMSO) for 30 min at 37 °C before addition of the GlcChol mix (100  $\mu$ L; 1.25  $\mu$ L GlcChol (1.6 pmol/ $\mu$ L in ethanol) in 150 mM Mcllvaine pH 4 or pH 5.2, 0.1% (w/v) BSA, 0.1% (v/v) Triton-X100 and/or 0.2% (w/v) Sodium Taurocholate; final ethanol concentration of 1% (v/v)).

## Chapter 2

Samples were incubated for 1 h or overnight (17 hours) at 37 °C, stopped by addition of internal standard, methanol and chloroform and subsequently extracted using the Bligh-Dyer extraction and lipid measurements as described for the transglucosylation.

Transglucosylation with NBD-lipids and HPTLC – NBD modified lipids including N-[12-[(7-nitro-2-1,3-benzoxadiazol-4-yl)amino]dodecanoyl]-d-erythro-sphingosine (C12-NBD-Cer), N-[6-[(7-Nitro-2-1,3-benzoxadiazol-4-yl)amino]caproyl]-D-glucosyl- $\beta$ 1-1'-sphingosine (C6-NBD-Spho) and 25-[N-[(7-nitro-2-1,3-benzoxadiazol-4-yl)methyl]amino]-27-norcholesterol (NBD-Chol) were purchased from Sigma or Avanti Polar lipids (Alabaster, USA). To GCCase expressing cell homogenates (12.5  $\mu$ L,  $\pm$  40-50  $\mu$ g total protein) was added McIlvaine with the appropriate pH (12.5  $\mu$ L 150 mM McIlvaine pH 4 or pH 5.2) and a mixture of 4MU- $\beta$ -Glc as glucose donor and NBD-lipid as acceptor in McIlvaine buffer pH 4 or pH 5.2 with or without appropriate additives (100  $\mu$ L; 1.25  $\mu$ L NBD-lipid (in 100% ethanol; 1% final concentration) in 150 mM McIlvaine pH 4 or pH 5.2, 0.1% (w/v) BSA without additives or supplemented with 0.1% (v/v) Triton-X100 and/ or 0.2% (w/v) Sodium Taurocholate. Final concentration of the NBD-lipids: 20  $\mu$ M for NBD-Chol, 10  $\mu$ M for NBD-Cer and 10  $\mu$ M for NBD-Sph. Samples were incubated for 1 h at 37 °C and lipids were extracted using the Bligh- Dyer extraction as described above. Lipids were reconstituted in 20  $\mu$ L methanol and separated by thin layer chromatography on HPTLC silica gel 60 plates using CHCl<sub>3</sub>:MeOH (80:20, v/v) as eluent. The HPTLC plate with NBD-lipids was scanned using a Typhoon imaging system (cy2 settings ( $\lambda_{ex}$  of 488 nm,  $\lambda_{em}$  of 515-535 nm), 250 V, pixel size 100  $\mu$ M

Alignment and modelling – For alignment and modelling sequences of zebrafish (Uniprot code E7EZM1), frog (Uniprot code AOA1L8FDF0) and turtle (NCBI code XP\_005280735) GCCase were used. Signal peptides were predicted using SignalP5.0<sup>43</sup> and sequences without predicted signal peptides were aligned with Clustal Omega<sup>44</sup>. Zebrafish, frog and turtle structures were modelled with Swiss-Model<sup>45</sup> using the established 3D-structure of human GCCase associated with 5N,6S-(N'-(N-octyl)imino)-6-thionojirimycin (6S-NOI-NJ) in the catalytic pocket (PDB 2XWE<sup>36</sup>) as search model. Structures were superimposed and visualized with CCP4MG<sup>46</sup> with glucose docked at the 6S-NOI-NJ ligand position. For alignment of predicted GCCase sequences of additional species were used: python (*Python bivittatus*, NCBI code XP\_007435239), goose (*Anser cygnoides domesticus*, NCBI code XP\_013055943), saltwater crocodile (*Crocodylus porosus*, NCBI code XP\_019412408), freshwater crocodile (*Gavialis gangetus*, NCBI code XP\_019383528), dolphin (*tursiops truncatus*, NCBI code XP\_004315654) and mouse (*Mus musculus*, NCBI code NP\_032120)

## References

1. Brady R.O., Kanfer J.N., Bradley R.M. and Shapiro D. (1966) Demonstration of a deficiency of glucocerebrosidase-cleaving enzyme in Gaucher's disease. *The Journal of clinical investigation* **45**, 1112-1115.
2. Van Weely S., Aerts J.M., Van Leeuwen M.B., Heikoop J.C., Donker-Koopman W.E., Barranger J.A.,... and Schram A.W. (1990) Function of oligosaccharide modification in glucocerebrosidase, a membrane-associated lysosomal hydrolase. *Eur J Biochem* **191**, 669-677.
3. Berg-Fussman A., Grace M.E., Ioannou Y. and Grabowski G.A. (1993) Human acid beta-glucosidase. N-glycosylation site occupancy and the effect of glycosylation on enzymatic activity. *J Biol Chem* **268**, 14861-14866.
4. Reczek D., Schwake M., Schroder J., Hughes H., Blanz J., Jin X.,... and Saftig P. (2007) LIMP-2 is a receptor for lysosomal mannose-6-phosphate-independent targeting of beta-glucocerebrosidase. *Cell* **131**, 770-783.
5. Zunke F., Andresen L., Wesseler S., Groth J., Arnold P., Rothaug M.,... and Schwake M. (2016) Characterization of the complex formed by beta-glucocerebrosidase and the lysosomal integral membrane protein type-2. *Proc Natl Acad Sci U S A* **113**, 3791-3796.
6. Rijnboutt S., Aerts H.M., Geuze H.J., Tager J.M. and Strous G.J. (1991) Mannose 6-phosphate-independent membrane association of cathepsin D, glucocerebrosidase, and sphingolipid-activating protein in HepG2 cells. *J Biol Chem* **266**, 4862-4868.
7. Saftig P. and Klumperman J. (2009) Lysosome biogenesis and lysosomal membrane proteins: trafficking meets function. *Nat Rev Mol Cell Biol* **10**, 623-635.
8. Aerts J.M., Schram A.W., Strijland A., van Weely S., Jonsson L.M., Tager J.M.,... and Murray G.J. (1988) Glucocerebrosidase, a lysosomal enzyme that does not undergo oligosaccharide phosphorylation. *Biochimica et biophysica acta* **964**, 303-308.
9. Tytki-Szymanska A., Czartoryska B., Vanier M.T., Poorthuis B.J., Groener J.A., Lugowska A.,... and Jurkiewicz E. (2007) Non-neuronopathic Gaucher disease due to saposin C deficiency. *Clin Genet* **72**, 538-542.
10. Tytki-Szymanska A., Groener J.E., Kaminski M.L., Lugowska A., Jurkiewicz E. and Czartoryska B. (2011) Gaucher disease due to saposin C deficiency, previously described as non-neuronopathic form--no positive effects after 2-years of miglustat therapy. *Mol Genet Metab* **104**, 627-630.
11. Vaccaro A.M., Motta M., Tatti M., Scarpa S., Masuelli L., Bhat M.,... and Salvioli R. (2010) Saposin C mutations in Gaucher disease patients resulting in lysosomal lipid accumulation, saposin C deficiency, but normal prosaposin processing and sorting. *Human molecular genetics* **19**, 2987-2997.
12. Dvir H., Harel M., McCarthy A.A., Toker L., Silman I., Futerman A.H. and Sussman J.L. (2003) X-ray structure of human acid-beta-glucosidase, the defective enzyme in Gaucher disease. *EMBO Rep* **4**, 704-709.
13. Smith L., Mullin S. and Schapira A.H.V. (2017) Insights into the structural biology of Gaucher disease. *Exp Neurol* **298**, 180-190.
14. Ben Bdira F., Artola M., Overkleeft H.S., Ubbink M. and Aerts J. (2018) Distinguishing the differences in beta-glycosylceramidase folds, dynamics, and actions informs therapeutic uses. *J Lipid Res* **59**, 2262-2276.
15. Rye C.S. and Withers S.G. (2000) Glycosidase mechanisms. *Current opinion in chemical biology* **4**, 573-580.
16. Witte M.D., Kallemeijn W.W., Aten J., Li K.Y., Strijland A., Donker-Koopman W.E.,... and Aerts J.M. (2010) Ultrasensitive in situ visualization of active glucocerebrosidase molecules. *Nature chemical biology* **6**, 907-913.
17. Kallemeijn W.W., Li K.Y., Witte M.D., Marques A.R., Aten J., Scheij S.,... and Overkleeft H.S. (2012) Novel activity-based probes for broad-spectrum profiling of retaining beta-exoglucosidases in situ and in vivo. *Angewandte Chemie* **51**, 12529-12533.
18. Marques A.R., Mirzaian M., Akiyama H., Wisse P., Ferraz M.J., Gaspar P.,... and Aerts J.M. (2016) Glucosylated cholesterol in mammalian cells and tissues: formation and degradation by multiple cellular beta-glucosidases. *J Lipid Res* **57**, 451-463.
19. Akiyama H. and Hirabayashi Y. (2017) A novel function for glucocerebrosidase as a regulator of sterylglucoside metabolism. *Biochim Biophys Acta Gen Subj* **1861**, 2507-2514.
20. Akiyama H., Nakajima K., Itoh Y., Sayano T., Ohashi Y., Yamaguchi Y.,... and Hirabayashi Y. (2016) Aglycon diversity of brain sterylglucosides: structure determination of cholesteryl- and sitosterylglucoside. *J Lipid Res* **57**, 2061-2072.
21. Brumshtein B., Greenblatt H.M., Butters T.D., Shaaltiel Y., Aviezer D., Silman I.,... and Sussman J.L. (2007) Crystal structures of complexes of N-butyl- and N-nonyl-deoxynojirimycin bound to acid beta-glucosidase: insights into the mechanism of chemical chaperone action in Gaucher disease. *J Biol Chem* **282**, 29052-29058.
22. Lieberman R.L., D'Aquino J.A., Ringe D. and Petsko G.A. (2009) Effects of pH and iminosugar pharmacological chaperones on lysosomal glycosidase structure and stability. *Biochemistry* **48**, 4816-4827.
23. Lieberman R.L. (2011) A Guided Tour of the Structural Biology of Gaucher Disease: Acid-beta-Glucosidase and Saposin C. *Enzyme Res* **2011**, 973231.

24. Kacher Y., Brumshtein B., Boldin-Adamsky S., Tokar L., Shainskaya A., Silman I.,... and Futerman A.H. (2008) Acid beta-glucosidase: insights from structural analysis and relevance to Gaucher disease therapy. *Biol Chem* **389**, 1361-1369.
25. van Smeden J., Dijkhoff I.M., Helder R.W.J., Al-Khakany H., Boer D.E.C., Schreuder A.,... and Bouwstra J.A. (2017) In situ visualization of glucocerebrosidase in human skin tissue: zymography versus activity-based probe labeling. *J Lipid Res* **58**, 2299-2309.
26. Chan A., Holleran W.M., Ferguson T., Crumrine D., Goker-Alpan O., Schiffmann R.,... and Sidransky E. (2011) Skin ultrastructural findings in type 2 Gaucher disease: diagnostic implications. *Mol Genet Metab* **104**, 631-636.
27. Doering T., Holleran W.M., Potratz A., Vielhaber G., Elias P.M., Suzuki K. and Sandhoff K. (1999) Sphingolipid activator proteins are required for epidermal permeability barrier formation. *J Biol Chem* **274**, 11038-11045.
28. Holleran W.M., Ginns E.I., Menon G.K., Grundmann J.U., Fartasch M., McKinney C.E.,... and Sidransky E. (1994) Consequences of beta-glucocerebrosidase deficiency in epidermis. Ultrastructure and permeability barrier alterations in Gaucher disease. *The Journal of clinical investigation* **93**, 1756-1764.
29. Keatinge M., Bui H., Menke A., Chen Y.C., Sokol A.M., Bai Q.,... and Bandmann O. (2015) Glucocerebrosidase 1 deficient Danio rerio mirror key pathological aspects of human Gaucher disease and provide evidence of early microglial activation preceding alpha-synuclein-independent neuronal cell death. *Human molecular genetics* **24**, 6640-6652.
30. Zancan I., Bellesso S., Costa R., Salvalaio M., Stroppiano M., Hammond C.,... and Moro E. (2015) Glucocerebrosidase deficiency in zebrafish affects primary bone ossification through increased oxidative stress and reduced Wnt/beta-catenin signaling. *Human molecular genetics* **24**, 1280-1294.
31. Aerts J.M., Sa Miranda M.C., Brouwer-Kelder E.M., Van Weely S., Barranger J.A. and Tager J.M. (1990) Conditions affecting the activity of glucocerebrosidase purified from spleens of control subjects and patients with type 1 Gaucher disease. *Biochimica et biophysica acta* **1041**, 55-63.
32. Artola M., Kuo C.L., Lelieveld L.T., Rowland R.J., van der Marel G.A., Codee J.D.C.,... and Overkleeft H.S. (2019) Functionalized Cyclophellitols Are Selective Glucocerebrosidase Inhibitors and Induce a Bona Fide Neuropathic Gaucher Model in Zebrafish. *Journal of the American Chemical Society* **141**, 4214-4218.
33. Hruska K.S., LaMarca M.E., Scott C.R. and Sidransky E. (2008) Gaucher disease: mutation and polymorphism spectrum in the glucocerebrosidase gene (GBA). *Hum Mutat* **29**, 567-583.
34. Lieberman R.L., Wustman B.A., Huertas P., Powe A.C., Jr., Pine C.W., Khanna R.,... and Petsko G.A. (2007) Structure of acid beta-glucosidase with pharmacological chaperone provides insight into Gaucher disease. *Nature chemical biology* **3**, 101-107.
35. Martinez-Bailen M., Carmona A.T., Patterson-Orazem A.C., Lieberman R.L., Ide D., Kubo M.,... and Moreno-Vargas A.J. (2019) Exploring substituent diversity on pyrrolidine-aryltriazole iminosugars: Structural basis of beta-glucocerebrosidase inhibition. *Bioorg Chem* **86**, 652-664.
36. Brumshtein B., Aguilar-Moncayo M., Benito J.M., Garcia Fernandez J.M., Silman I., Shaaltiel Y.,... and Ortiz Mellet C. (2011) Cyclodextrin-mediated crystallization of acid beta-glucosidase in complex with amphiphilic bicyclic nojirimycin analogues. *Organic & biomolecular chemistry* **9**, 4160-4167.
37. Sultana S., Truong N.Y., Vieira D.B., Wigger J.G., Forrester A.M., Veinotte C.J.,... and van der Spoel A.C. (2016) Characterization of the Zebrafish Homolog of beta-Glucosidase 2: A Target of the Drug Miglustat. *Zebrafish* **13**, 177-187.
38. Kuo C.L., Kallemeyn W.W., Lelieveld L.T., Mirzaian M., Zoutendijk I., Vardi A.,... and Artola M. (2019) In vivo inactivation of glycosidases by conduritol B epoxide and cyclophellitol as revealed by activity-based protein profiling. *FEBS J* **286**, 584-600.
39. Lelieveld L.T., Mirzaian M., Kuo C.L., Artola M., Ferraz M.J., Peter R.E.A.,... and Aerts J. (2019) Role of beta-glucosidase 2 in aberrant glycosphingolipid metabolism: model of glucocerebrosidase deficiency in zebrafish. *J Lipid Res* **60**, 1851-1867.
40. Aerts J., Kuo C.L., Lelieveld L.T., Boer D.E.C., van der Lienden M.J.C., Overkleeft H.S. and Artola M. (2019) Glycosphingolipids and lysosomal storage disorders as illustrated by gaucher disease. *Current opinion in chemical biology* **53**, 204-215.
41. Do H.V. (2017) Variant, recombinant beta-glucocerebrosidase proteins with increased stability and increased retained catalytic activity **Volume US9254313B2**. (United States: Amicus Therapeutics Inc ).
42. Ben Bdira F., Kallemeyn W.W., Oussoren S.V., Scheij S., Bleijlevens B., Florea B.I.,... and Aerts J. (2017) Stabilization of Glucocerebrosidase by Active Site Occupancy. *ACS Chem Biol* **12**, 1830-1841.
43. Almagro Armenteros J.J., Tsirigos K.D., Sonderby C.K., Petersen T.N., Winther O., Brunak S.,... and Nielsen H. (2019) SignalP 5.0 improves signal peptide predictions using deep neural networks. *Nat Biotechnol* **37**, 420-423.
44. Madeira F., Park Y.M., Lee J., Buso N., Gur T., Madhusoodanan N.,... and Lopez R. (2019) The EMBL-EBI search and sequence analysis tools APIs in 2019. *Nucleic acids research* **47**, W636-W641.



45. Waterhouse A., Bertoni M., Bienert S., Studer G., Tauriello G., Gumienny R.,... and Schwede T. (2018) SWISS-MODEL: homology modelling of protein structures and complexes. *Nucleic acids research* **46**, W296-W303.
46. McNicholas S., Potterton E., Wilson K.S. and Noble M.E. (2011) Presenting your structures: the CCP4mg molecular-graphics software. *Acta Crystallogr D Biol Crystallogr* **67**, 386-394.



# CHAPTER 3

## Pharmacological modulation of glycosidases in zebrafish



Adapted from: FEBS J. 2019 Feb;286(3):584-600  
Kuo CL, Kallemeijn WW, Lelieveld LT, Mirzaian M, Zoutendijk I, Vardi A, Futerman AH, Meijer AH, Spalink HP, Overkleeft HS, Aerts JMFG and Artola M.  
● In vivo inactivation of glycosidases by conduritol B epoxide and cyclophellitol as revealed by activity-based protein profiling.

and from: JACS. 2019 Mar 13;141(10):4214-4218  
Artola M, Kuo CL, Lelieveld LT, Rowland RJ, van der Marel GA, Codée JDC, Boot RG, Davies GJ, Aerts JMFG and Overkleeft HS.  
● Functionalized Cyclophellitols Are Selective Glucocerebrosidase Inhibitors and Induce a Bona Fide Neuropathic Gaucher Model in Zebrafish.

## Abstract

**Z**ebrafish, and especially their developing off-spring, offer attractive features to study the molecular basis of genetic disorders as well as pharmacological intervention in a whole organism. Gaucher disease (GD) is a common lysosomal storage disorder, characterized by a defect in the enzyme glucocerebrosidase (GCase or GBA, official gene name: *GBA*) which hydrolyses the lipid glucosylceramide in lysosomes. Studying GD in an animal model has been hampered by the premature death of mammals with a complete genetic abrogation of GBA. Therefore, on-demand GBA deficiency has been induced chemically, by treatment of animals with the mechanism-based irreversible GBA inhibitors conduritol B epoxide (CBE) or cyclophellitol (CP). Zebrafish larvae are used in this chapter to study the *in vivo* target engagement of CBE and CP and compare the results to values obtained from cultured human cells. Only at significantly higher CBE concentrations, non-lysosomal glucosylceramidase (GBA2) and lysosomal  $\alpha$ -glucosidase were identified as major off-targets both in cells and zebrafish larvae. CP was found to inactivate GBA and GBA2 with equal affinity and is therefore not suitable to generate genuine GD-like models. New CP derivatives, functionalized with a bulky hydrophobic moiety at C8, were validated as potent and selective GBA inhibitors in cultured cells and developing zebrafish larvae. Moreover, these CP analogues selectively inhibit GBA in the brain of adult zebrafish. Overall, this chapter demonstrates the applicability of enzymatic assays and ABPs as tools to study zebrafish glycosidase enzymes as well as the attractive features of the zebrafish animal model for evaluating drug potency, specificity and biodistribution, in particular brain permeability.

## Introduction

The lysosomal enzyme glucocerebrosidase (GCase or GBA, EC 3.2.1.45) is a retaining  $\beta$ -glucosidase that degrades the glycosphingolipid, glucosylceramide (GlcCer). Inherited deficiency of GBA is the cause of autosomal recessive Gaucher disease (GD)<sup>1</sup>. Most GD patients display heterogeneous symptoms including spleen and liver enlargement, bone deterioration, anaemia, leukopenia, and thrombocytopenia, while some patients also develop fatal neurological symptoms<sup>2</sup>.

Research on GD has been hampered by the premature death of mice with a complete genetic abrogation of GBA. Therefore, on-demand GBA deficiency have been generated by treatment of animals with conduritol B epoxide (CBE **1**, **Figure 1A**)<sup>3-5</sup>. CBE is a cyclitol epoxide that covalently and irreversibly reacts with the catalytic nucleophile of GBA and thus inactivates the enzyme irreversibly (**Figure 1B**). The crystal structure of GBA with bound CBE confirmed the covalent linkage of the compound to the catalytic nucleophile Glu 340<sup>6,7</sup>. Building on the initial work by Kanfer and co-workers, a regimen using different doses of CBE has been established to generate a phenotypic copy of neuronopathic GD in mice<sup>4,6-8</sup>. This pharmacological model is widely used to study the nature of neuropathology resulting from GBA deficiency, including Parkinsonism<sup>9-11</sup>.

A major advantage of CBE's pharmacological use in cultured cells and mice is its tunability: the extent of GBA inactivation can be adjusted by variation of the inhibitor concentration and/or exposure time<sup>4</sup>. However, distinct treatment regimens across studies have been reported: exposure of cells ranging from 50  $\mu$ M to 100 mM CBE for 2 hours up to 60 days<sup>12-18</sup> and daily exposure of mice from 25 to 300 mg per kg body weight during 2 hours up to 36 days<sup>4</sup>. The use of a high CBE concentration raises concerns about specificity since the compound has been reported to inhibit other glycosidases than GBA at high concentrations. Examples are *in vitro* inhibition of retaining  $\alpha$ -glucosidases (EC 3.2.1.20)<sup>19-21</sup>, *in vitro*<sup>22</sup> and *in situ*<sup>23</sup> cell inhibition of the non-lysosomal glucosylceramidase (GBA2, EC 3.2.1.45), and inhibition of the lysosomal  $\beta$ -glucuronidase (GUSB, EC 3.2.1.31) in mice<sup>24</sup>. The reactivity of CBE towards both  $\beta$ - and  $\alpha$ -glucosidases can be explained by the C2-symmetry found in its structure<sup>25</sup> (**Figure 1A**), which allows reaction with the catalytic nucleophile of both classes of enzymes. Another structurally related cyclitol epoxide, cyclophellitol (CP **2**, **Figure 1A**), is a structurally closer  $\beta$ -glucose mimic and inhibits GBA with far higher affinity than CBE<sup>26,27</sup>. It exhibits selectivity over  $\alpha$ -glucosidases due to the C5-hydroxymethyl group<sup>26-28</sup>, and was also shown to induce Gaucher phenotypes in mice<sup>26</sup>. However, its reactivity *in vivo* towards GBA2 and other glycosidases is unknown. Recently, CP derivatives have been functionalized with a fluorescent substituent at C8 (**3a-e**, **Figure 1A**). The generated cyclophellitol-epoxide activity-based probe (ABP **3**) showed very potent and selective reactivity towards GBA and was used to visualize and monitor GBA activity *in vitro*, *in situ* and *in vivo*<sup>28,29</sup>.

Next, a configured cyclophellitol-aziridine tagged with a fluorophore was developed which enabled labelling of all retaining  $\beta$ -glucosidases (ABP **4**)<sup>30</sup>. To date, a library of ABPs is available labelling a range of retaining glycosidases (**Figure 1A**), including ABPs targeting  $\beta$ -glucuronidase (GUSB, ABP **5**)<sup>31</sup> and  $\alpha$ -glucosidase (GAA and GANAB, ABP **6**)<sup>32</sup> as well as ABPs functionalized with different fluorophores (**Figure 1C**). It has been previously established that the CP derivative, functionalized with a BODIPY group, does not penetrate the brain sufficiently<sup>29</sup>. Changing the fluorescent BODIPY substituent to a simple, hydrophobic moiety at C8 (inhibitors **3d** and **3e**, **Figure 1C**) is thought to preserve the high potency and selectivity of the inhibitor, while improving GBA inactivation in the brain. This would make them suitable for generating chemically-induced neuropathic Gaucher disease models.

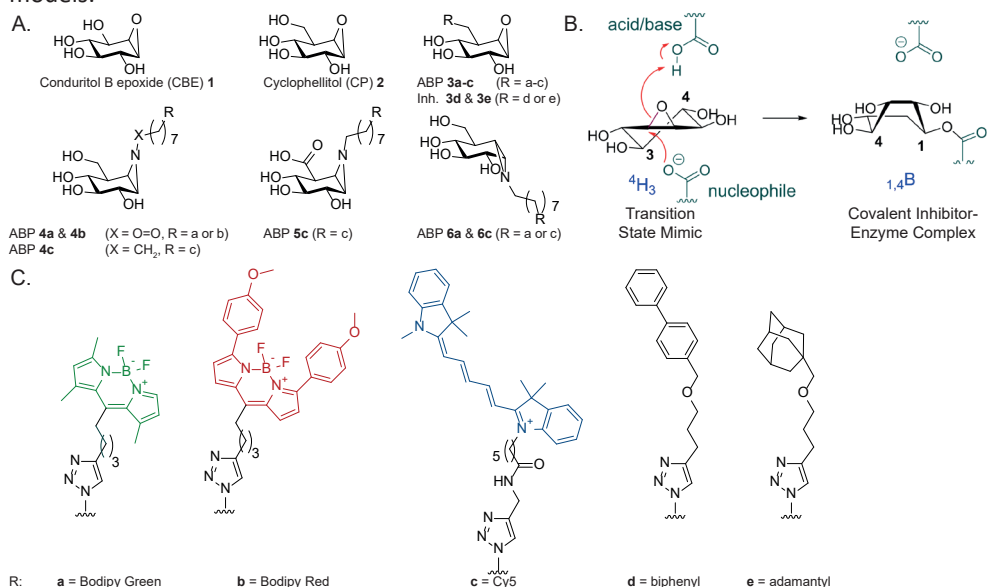


**Figure 1 | Overview of chemical structures used in this study**

**(A)** Top panel: Chemical structures of Conduritol B epoxide (CBE), cyclophellitol (CP), CP-configured ABPs (ABP **3a-c**) and CP-derived inhibitors (**3d,e**). Lower panel: ABP labelling GBA and GBA2 (ABP **4a-c**), GUSB (ABP **5c**) and GAA and GANAB (ABP **6a** and **6c**) **(B)** Reaction mechanism of CBE binding to  $\beta$ -glucosidase. **(C)** Chemical structures of R-groups in A: Bodipy Green (a), Bodipy Red (b), Cy5 (c), biphenyl (d) and adamantyl moiety (e).

This chapter describes a systematic study of the *in vitro* and *in vivo* potency and selectivity of CBE, CP and CP derivatives using cultured cells and developing zebrafish larvae. Both enzymatic assays, employing specific fluorogenic substrates, and competitive activity-based protein profiling (cABPP) using a library of ABPs (**Figure 1A**, ABPs **3-6**) are used. Finally, two CP derivatives, one with a BODIPY-substituent at C6 (compound **3a**) and the other with a hydrophobic group (compound **3e**), were administered to adult zebrafish to assess the penetration and target engagement of these inhibitors in the brain.

## Results

### A competitive ABPP method to determine GBA target engagement of CBE and CP

ABP **4c** was used in a competitive ABPP method to assess the irreversible occupancy of the catalytic nucleophile of GBA after pre-incubation with CBE **1** or CP **2**. As a validation, competition of ABP labelling by CBE and CP was compared to the loss of GBA activity measured using the artificial fluorogenic substrate, 4-methylumbelliferyl- $\beta$ -glucoside<sup>33</sup>. For this, recombinant human GBA (rGBA) was pre-incubated with CBE across a range of concentrations at 37 °C for 0, 30 and 180 minutes<sup>34</sup>. Subsequent labelling of GBA by ABP **4c** enabled quantification by SDS-PAGE and fluorescence scanning. IC<sub>50</sub> values (concentrations of inhibitor yielding a 50% reduction of ABP **4c** labelling) were determined and found to be 26.6  $\mu$ M at 30 min CBE preincubation, and 2.30  $\mu$ M at 180 min pre-incubation (**Figure 2A**). These values match the ones determined by measurement of residual enzymatic activity of the GBA assay (**Figure 2A**, lower right panel), validating the competitive ABPP methodology. Next, CP was comparably studied using rGBA and its IC<sub>50</sub> values determined by cABPP were 0.15  $\mu$ M at 30 min pre-incubation and 0.03  $\mu$ M at 180 min pre-incubation, comparable to values determined by enzymatic assay (**Figure 2B**).

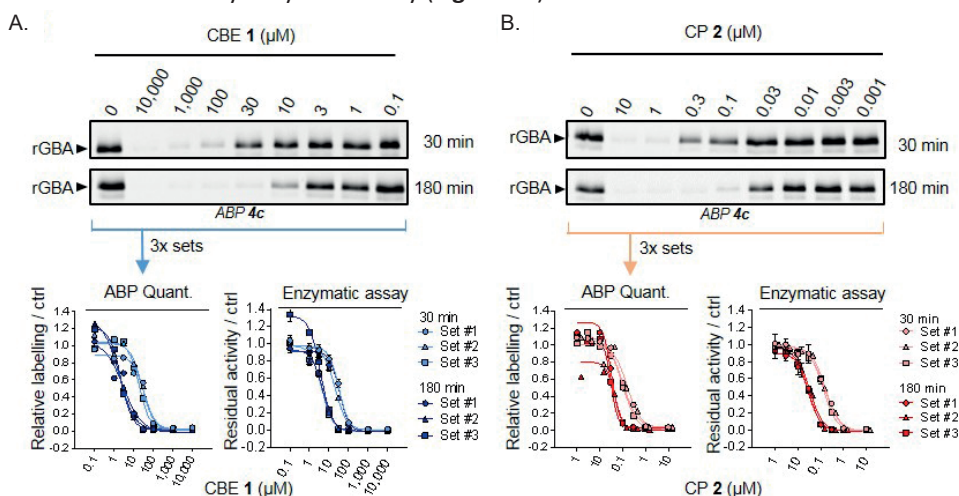


**Figure 2 | Effect of pre-incubation with CBE or CP on ABP labelling of recombinant GBA.**

(A) Representative gel images of rGBA pre-incubated with CBE (10,000–0.1  $\mu$ M) for 30 min or 180 min and fluorescently labelled with ABP **4c**. Fluorescent signals were quantified and normalized to the untreated sample (ctrl, 0  $\mu$ M CBE) (bottom left) and compared to the inhibition curves obtained with enzymatic assay (bottom right). (B) Same as A, with CP at 10–0.001  $\mu$ M. Error ranges in enzymatic assay =  $\pm$  SD, n = 3 (technical replicates).

### Selectivity of CBE and CP in cultured cells

Next, the targets of CBE and CP were evaluated in intact cultured human cells and zebrafish larvae. These biological materials contain besides GBA the candidate off-target glycosidases: GBA2,  $\alpha$ -glucosidases (GAA and GANAB), and lysosomal  $\beta$ -glucuronidase GUSB. For each of these enzymes ABPs have been designed, and enzymatic activity assays with fluorogenic substrates established<sup>30–32</sup>. Of note, ABP **4** allows simultaneous visualization of active GBA (58–66 kDa) and GBA2 (110 kDa) following SDS-PAGE analysis.



First, HEK293T cells overexpressing GBA2 were exposed to different concentrations of CBE (0.1  $\mu\text{M}$ –10 mM) or CP (0.001 – 10  $\mu\text{M}$ ) for 24 h. The residual amount of GBA, GBA2, GAA, GANAB and GUSB that can still be labelled with the appropriate ABPs (**Figure 1C**) was determined in the exposed cell lysates (**Figure 3A** and **D** for CBE and CP respectively).

For CBE, competitive ABPP showed that besides GBA, all other candidate off-target enzymes are inactivated but with marked lower affinity: GBA ( $\text{IC}_{50} = 0.59 \mu\text{M}$ ), GBA2 ( $\text{IC}_{50} = 315 \mu\text{M}$ ), GAA ( $\text{IC}_{50} = 249 \mu\text{M}$ ), GANAB ( $\text{IC}_{50} = 2900 \mu\text{M}$ ) and GUSB ( $\text{IC}_{50} = 857 \mu\text{M}$ ) (**Figure 3B**, **Supplementary Figure 1A** and **Supplementary Table 1**). Comparable results were obtained by determination of residual enzyme activities: GBA ( $\text{IC}_{50} = 0.33 \mu\text{M}$ ), GBA2 ( $\text{IC}_{50} = 272 \mu\text{M}$ ), GAA ( $\text{IC}_{50} = 309 \mu\text{M}$ ), GANAB ( $\text{IC}_{50} = 1580 \mu\text{M}$ ) and GUSB ( $\text{IC}_{50} = 607 \mu\text{M}$ ) (**Figure 3C** and **Supplementary Figure 1B**). CP is a much more potent inhibitor of GBA<sup>26</sup> and reported to inhibit poorly  $\alpha$ -glucosidases *in vitro*<sup>27</sup>. However, the *in vivo* reactivity of CP towards other glycosidases has not been thoroughly investigated. To compare the selectivity windows of CP to the ones of CBE, the concentration range of CP was chosen at 0.001–10  $\mu\text{M}$  for cultured cells. As determined by the competitive ABPP method, CP was found to inhibit GBA2 on a par with GBA in cells overexpressing GBA2 upon incubation with varying inhibitor concentrations (0.1–10  $\mu\text{M}$  CP) for 24 hours (**Figure 3D-F**).

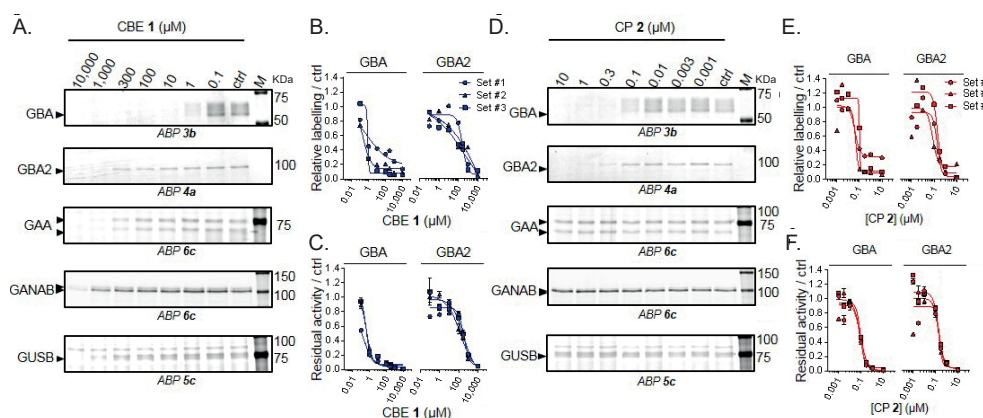


**Figure 3 | *In vivo* glycosidase targets of CBE and CP in cultured cells**

(A, D) Representative gel images (1 set from  $n = 3$  biological replicates) showing fluorescent ABP labelling of GBA, GBA2, GAA, GANAB, and GUSB in lysates of cells treated *in vivo* for 24 h with CBE (A) and CP (D) respectively. (B, E) Quantification of relative ABP labelling of GBA and GBA2 in lysates of cells treated *in vivo* for 24 h with CBE (B) and CP (E) respectively. (C, F) Residual activities of GBA and GBA2 in cell lysates treated *in vivo* with CBE (C) and CP (F). Error ranges =  $\pm$  SD,  $n = 3$  (technical replicates).

$\text{IC}_{50}$  values of CP for blocking ABP labelling were 0.063  $\mu\text{M}$  for GBA and 0.154  $\mu\text{M}$  for GBA2 (**Figure 3E** and **Supplementary Table 1**), which was comparable to results obtained by determination of residual enzymatic activities of GBA and GBA2 measured with the fluorogenic 4Mu substrate (**Figure 3F**). No reduction of ABP labelling of GAA, GANAB and GUSB was observed in lysates of cells incubated for 24 h up to 10  $\mu\text{M}$  of CP (**Figure 3D**). The apparent  $\text{IC}_{50}$  values of CP for the other glycosidase enzymes exceeded at least 10  $\mu\text{M}$  (**Supplementary Table 1** and ref.<sup>35</sup>).

***In vivo* targets of CBE and CP in zebrafish larvae**

Next, the *in vivo* target engagement of CBE and CP was studied in intact zebrafish larvae. Fertilized zebrafish eggs (0 days post-fertilization (dpf)) were exposed for five days to CBE (1  $\mu$ M–100 mM) or CP (0.001–100  $\mu$ M) supplemented to the egg water. The larvae were collected, lysed, and analysed by the competitive ABPP method. Exposure to 100 mM CBE was found to reduce ABP labelling of all five glycosidases (**Figure 4A** and **Supplementary Figure 2A**). The  $IC_{50}$  values determined by the competitive ABPP method were: GBA ( $IC_{50}$  = 44.1  $\mu$ M), GBA2 ( $IC_{50}$  = 890  $\mu$ M), GAA ( $IC_{50}$  = 9550  $\mu$ M), GANAB ( $IC_{50}$  = 4700  $\mu$ M) and GUSB ( $IC_{50}$  = 6470  $\mu$ M) (**Supplementary Figure 2A** and **Supplementary Table 1**). Thus, inactivation of GBA in zebrafish larvae takes place 20-fold more avidly than that of GBA2 and 100- to 200-fold more potently than that of GAA, GANAB and GUSB. Analysis of residual enzymatic activity of the various enzymes gave similar results (**Supplementary Figure 2B**). Analysis by enzymatic assay revealed that exposure of the animals to 10 mM CBE did not lead to significant inactivation of other glycosidases ( $\alpha$ - and  $\beta$ -mannosidase, *N*-acetyl  $\alpha$ -galactosidase,  $\beta$ -hexosaminidase,  $\alpha$ -fucosidase and  $\alpha$ -iduronidase) except for  $\beta$ -galactosidase ( $IC_{50}$  = 11.2 mM) and  $\alpha$ -galactosidase ( $IC_{50}$  = 22.5 mM) (**Supplementary Figure 2B**). Exposure of zebrafish to CP (5 days at 1–100  $\mu$ M) also comparably competed GBA and GBA2 labelling, but not that of GUSB, GAA and GANAB (**Figure 4B**). This finding was again supported by results obtained from measurement of residual enzymatic activities (**Supplementary Figure 2B**).

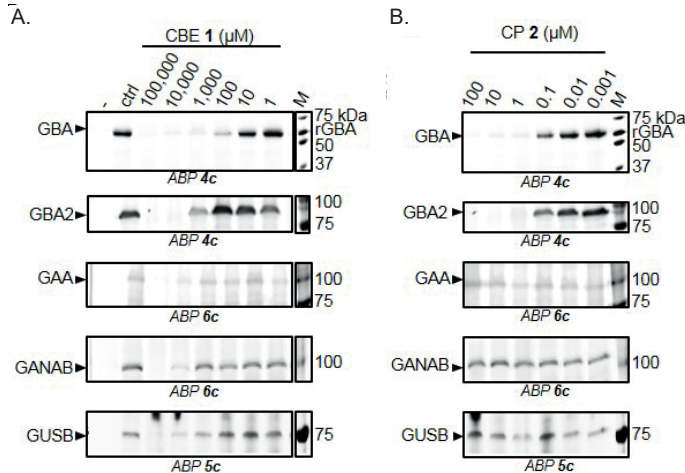


**Figure 4 | *In vivo* glycosidase targets of CBE and CP in developing zebrafish larvae**

Zebrafish embryos were incubated with (A) CBE 0.001–10 mM or (B) CP (0.001–100  $\mu$ M) from 8–120 hours before lysis and subjection to ABP labelling with appropriate ABPs.

### Potency and selectivity of functionalized cyclophellitol inhibitors

From the noted lack of selectivity of CP with respect to inactivation of GBA and GBA2, it is obvious that CP does not allow generation of specific GBA-deficiency in cell and animal models. Functionalized cyclophellitol compounds bearing a fluorescent moiety at C8 have been described as highly potent and selective inhibitors for GBA<sup>28</sup>. Cyclophellitols bearing a simple but bulky hydrophobic moiety at C8, either a biphenyl (compound **3d**) or adamantyl moiety (compound **3e**) were synthesized to generate superior potent and selective GBA inhibitors, with the potential ability to penetrate the brain.

First, the *in vitro* activity and selectivity of these two functionalized cyclophellitol compounds were evaluated towards GBA and the two major off-target glycosidases of CBE and CP: GBA2 and GAA. The inhibitors were preincubated with recombinant human GBA (rGBA, Cerezyme), human GBA2 (from lysates of GBA2 overexpressed cells) and recombinant human GAA (rGAA, Myozyme) for 3 h, followed by enzymatic measurements. Both compound **3d** and **3e** were nanomolar inhibitors of rGBA ( $IC_{50} = 1.0$  nM), which were 4000-fold more potent than CBE **1** (Table 1). In contrast to CBE and CP, both compound **3d** and **3e** were rather inactive toward GBA2 and GAA ( $IC_{50} > 100$   $\mu$ M), thus making them 4000 times and 200 times more selective than for example CBE **1** ( $IC_{50}$  ratio = 23.6 for GBA2/GBA and 444 for GAA/GBA, Table 1).

**Table 1** | Apparent  $IC_{50}$  values for *in vitro* inhibition of GBA, GBA2 and GAA in recombinant enzymes (rGBA and rGAA) or overexpressed cell lysates (GBA2) by compounds CBE 1, CP 2, ABP 3a, ABP 3c, 3d and 3e measured as residual glycosidase activity. Error ranges depict standard deviations from biological triplicates.

<i>In vitro</i>	CBE 1 (nM)	CP 2 (nM)	ABP 3a (nM)	ABP 3c (nM)	3d (nM)	3e (nM)
<b>rGBA</b>	4,280 ± 500	29.6 ± 2.40	1.20 ± 0.30	3.20 ± 0.17	1.06 ± 0.19	0.96 ± 0.17
<b>GBA2</b> (HEK293T lysates)	101,000 ± 20,100	29.7 ± 3.13	> 10 <sup>5</sup>	412,000 ± 10,100	> 10 <sup>5</sup>	> 10 <sup>5</sup>
<b>rGAA</b>	1,900,000 ± 192,000	> 10 <sup>5</sup>	> 10 <sup>5</sup>	> 10 <sup>5</sup>	> 10 <sup>5</sup>	> 10 <sup>5</sup>
<b>Ratio (<i>in vitro</i>)</b>						
GBA2/ GBA	24	1	> 10 <sup>5</sup>	> 10 <sup>4</sup>	> 10 <sup>5</sup>	> 10 <sup>5</sup>
GAA/ GBA	444	> 10 <sup>3</sup>	> 10 <sup>6</sup>	> 10 <sup>6</sup>	> 10 <sup>6</sup>	> 10 <sup>6</sup>

As for CBE **1** and CP **2**, the *in vivo* activity of compounds **3d** and **3e** was evaluated by addition of the compounds to the swimming water of developing zebrafish embryos. After 5 days of incubation at 28 °C, larvae were homogenized and enzyme selectivity was analysed by appropriate competitive ABP labelling. Quantification of ABP-labelled bands revealed that compounds **3d** and **3e** had *in vivo* apparent  $IC_{50}$  values towards GBA of 4-6 nM and that they were 5-70-fold more potent than ABP **3a** or **3c** and 7500-fold more potent than CBE **1** (Table 2). Potential off-target glycosidases such as GBA2, LPH, GAA, GANAB and GUSB were not identified with compounds **3d** and **3e**<sup>36</sup>.

**Table 2 |** Apparent  $IC_{50}$  values for *in vivo* inhibition in 5-day treated zebrafish embryos with compounds 1, 2, 3a, 3c, 3d and 3e as evaluated by quantification of residual labelling using appropriate ABPs. Error ranges depict standard deviations from n = 12-24 individuals.

<i>In vivo</i> <i>Danio rerio</i> larvae	CBE 1 (nM)	CP 2 (nM)	ABP 3a (nM)	ABP 3c (nM)	3d (nM)	3e (nM)
<b>GBA</b>	$4.41 \times 10^4$	83	$31.6 \pm 8.88$	$284 \pm 31.5$	$5.85 \pm 2.44$	$3.94 \pm 0.21$
<b>GBA2</b>	$8.90 \times 10^5$	59	$> 10^4$	$> 10^4$	$> 10^4$	$> 10^4$
<b>GAA</b>	$9.55 \times 10^6$	$> 10^5$	$> 10^4$	$> 10^4$	$> 10^4$	$> 10^4$
<b>Ratio (<i>in vivo</i>)</b>						
GBA2/ GBA	22	0.714	$> 316$	$> 35$	$> 1710$	$> 2540$
GAA/ GBA	233	$> 120$	$> 316$	$> 35$	$> 1710$	$> 2540$

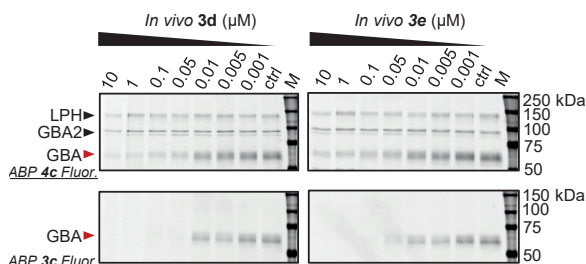


**Figure 5 |** *In vivo* glycosidase targets of compounds 3d and 3e in developing zebrafish larvae.

Zebrafish embryos were incubated with compound 3d and 3e (0.001-10  $\mu$ M) from 8-120 hours before lysis and subjection to ABP labelling with broad-spectrum retaining  $\beta$ -glucosidase ABP 4c, targeting GBA, GBA2 and LPH, and selective GBA ABP 3c as readout.

### Impact of inhibitors on glycosphingolipids accumulation in treated zebrafish larvae

Next the functional impact of the GBA inhibitors was evaluated by exposing embryos for 5 days to CBE, CP or the functionalized CP compounds. *In vivo* inactivation of GBA leads to compensatory formation of glucosylsphingosine (GlcSph) by acid ceramidase-mediated conversion of accumulating GlcCer in lysosomes and such accumulation of GlcSph is a biomarker of the inactivation of GBA<sup>33,37</sup>. The exposure of zebrafish larvae to CBE 1, CP 2 and functionalized cyclophellitol ABP 3a and compounds 3d and 3e led to pronounced accumulation of GlcSph. A 4-fold increase in the case of 1000  $\mu$ M CBE 1 and 6-fold increase at 10  $\mu$ M CP 2 was observed while ABP 3a and inhibitors 3d and 3e reached a 10-30-fold elevation in the level of GlcSph using only 0.1-10  $\mu$ M of inhibitor (Figure 6). Thus, the observed *in vivo* target engagement of GBA according to ABP detection was confirmed by the accumulation of GlcSph at comparable inhibitor concentrations. However, reaching similar GlcSph levels in the zebrafish with CBE 1 required 100-10000-fold higher concentration in contrast to compounds 3d and 3e, concentrations at which GBA2 and GAA may also be targeted (Figure 4 and Table 2).

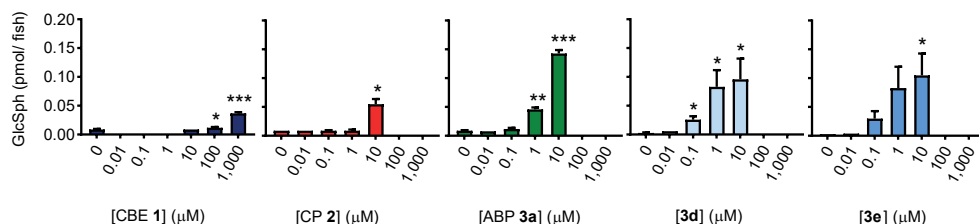


**Figure 6 |** Glucosylsphingosine levels in zebrafish embryos treated for 5 days with inhibitors CBE **1**, CP **2**, ABP **3a**, compounds **3d** or **3e**. Error ranges depict standard deviations from  $n = 3$  individuals. \*  $P < 0.5$ , \*\*\*  $P < 0.001$ .

### Brain permeability of functionalized cyclophellitol inhibitors

Finally, brain penetration of the new cyclophellitol inhibitors was evaluated, a crucial feature for their future application in the study of neuropathic Gaucher disease and Parkinson's disease. Adult zebrafish of 3 months' age were treated with DMSO, ABP **3a** or compound **3e** (1.6 nmol/fish, approximately 4 μmol/kg) administered via food intake, and after 16 h brains and other organs were isolated, homogenized, and analysed by ABP labelling using appropriate ABPs for GBA, GBA2, GAA, GANAB and GUSB. Labelling of brain homogenate of adult zebrafish with ABP **3c** resulted in considerable GBA labelling in control and ABP **3a** treated fish, but no labelling in brain homogenates from fish treated with compound **3e** (Figure 7A).

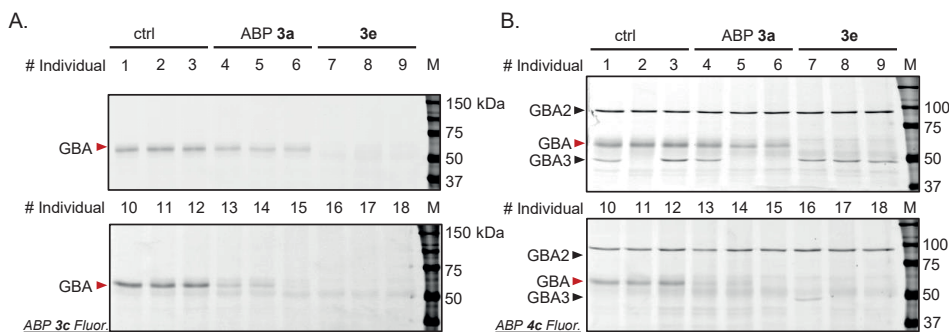


**Figure 7 |** In vivo targets of functionalized cyclophellitols in zebrafish adult brain

Adult zebrafish were treated with DMSO, ABP **3a** or compound **3e** and *in vivo* target engagement was visualized by labelling with (A) selective GBA ABP **3c** or (B) broad-spectrum retaining β-glucosidase ABP **4c** labelling GBA, GBA2 and GBA3.

Labelling by the broad-spectrum β-glucosidase ABP **4c** showed that GBA2 was not a target of compound **3e** (Figure 7B), nor was the lower running band (48 kDa), which we hypothesize to be the cytosolic β-glucosidase, GBA3. We noted that the expression level of this protein is likely variable among individual fish, as 4 out of 6 fishes in the control group lacked this band. ABP labelling of other glycosidase targets, such as GAA, GANAB and GUSB, were not affected either<sup>36</sup>. In the visceral organs (both liver and spleen), both ABP **3a** and compound **3e** selectively abrogated GBA while not affecting the labelling of other tested glycosidases (Supplementary Figure 3 and ref. 36).

## Discussion

Zebrafish offer attractive features for pharmacological screenings. Hundreds of fertilized eggs can be easily obtained and their ex-vivo, rapid embryogenesis and organ development as well as small size have enabled researchers to study the effects of various small molecules in a whole organism in a relatively high throughput manner<sup>38,39</sup>. Off-target effects can have detrimental consequences, not only in the process of drug discovery and development but also in fundamental research when pharmacological modulation is used to study the molecular basis of a human disorder in a model organism. On-demand GBA deficiency has been used to study GD in mouse models, however concerns about potential off-target effects have been raised when using high concentrations of the established GBA selective inhibitors CBE and CP. In the present study, developing zebrafish larvae were used to determine the *in vivo* potency of CBE and CP as well as in-house synthesized CP derivatives and to evaluate their dose-dependent target engagement.

First of all, it is noteworthy to mention that the same tools can be used for the study of glycosidases in zebrafish as for cellular and mouse samples. In chapter 2 it was shown that the catalytic features of zebrafish GBA could be studied using the artificial 4MU- $\beta$ -Glc substrate and this chapter revealed that it was possible to evaluate enzymatic activity of other glycosidases by use of their corresponding fluorogenic substrates. In addition, the library of fluorescent ABPs provide a complementary method for activity assessment and visualization of active retaining glycosidases. The ABPs bind in a mechanism-based manner and the required nucleophilic and acid base residues are generally conserved across species. Therefore ABPs have not only been found to react with retaining glycosidases of mammals, but also with those from zebrafish, plants, bacteria and fungi<sup>30,40-42</sup>. In contrast, none of the in-house available commercial glycosidase antibodies were found to react with the respective enzyme from zebrafish materials, including tested antibodies for GBA, GBA2,  $\alpha$ -galactosidase A and galactocerebrosidase (data not shown). Modification of the reporter tag of the ABP enables researchers to visualize active enzyme by means of a fluorescent tag in combination with in-gel fluorescence scanning or fluorescence microscopy<sup>28,29</sup>, while affinity tags allows the enrichment and identification of target enzymes by chemical proteomics approaches<sup>43</sup>. Zebrafish research could profit extensively from the use of ABPs. Mechanism-based ABPs, as well as affinity-based ones, have been developed for other enzyme classes including serine hydrolases<sup>44,45</sup>, kinases<sup>46</sup>, proteases<sup>47</sup> and subunits of the proteasome<sup>48</sup>.

Another advantage is that the ABP only reacts with an active enzyme, thereby enabling evaluation of selectivity and potency of small molecules by an approach called competitive activity-based protein profiling (cABPP). This approach was adopted in this study to verify the use of zebrafish larvae as whole organismal model to study target engagement of GBA inhibitors. The apparent  $IC_{50}$  values of zebrafish larvae were compared to those obtained in cultured cells, using both activity measurements with fluorogenic substrates as well as cABPP in parallel.



In general, inhibitors were approximately 5-fold more potent in cultured cells compared to developing zebrafish larvae (CBE: 0.6  $\mu\text{M}$  vs 44  $\mu\text{M}$  and CP: 15 nM vs 83 nM for cultured cells and zebrafish larvae respectively). The observed selectivity of CBE and CP was similar in cultured cells and developing zebrafish larvae. Non-lysosomal  $\beta$ -glucosidase GBA2 and the lysosomal  $\alpha$ -glucosidase GAA were determined as off-targets of CBE both in cultured cells overexpressing GBA2 and in developing zebrafish larvae upon incubation with high concentrations of CBE. A selective window for *in vivo* GBA inactivation was apparent of 0.6-315  $\mu\text{M}$  for cultured cells and 44-890  $\mu\text{M}$  for zebrafish larvae (**Figure 8**). Such selectivity has also been observed in brain of mice treated with a low and high concentrations of CBE<sup>35</sup>. CP showed potent GBA inactivation both in cultured cells and zebrafish larvae, however this compound also inactivated GBA2 with comparable potency. Therefore this inhibitor presents a small GBA selective window for cultured cells and none for zebrafish larvae (**Figure 8**).

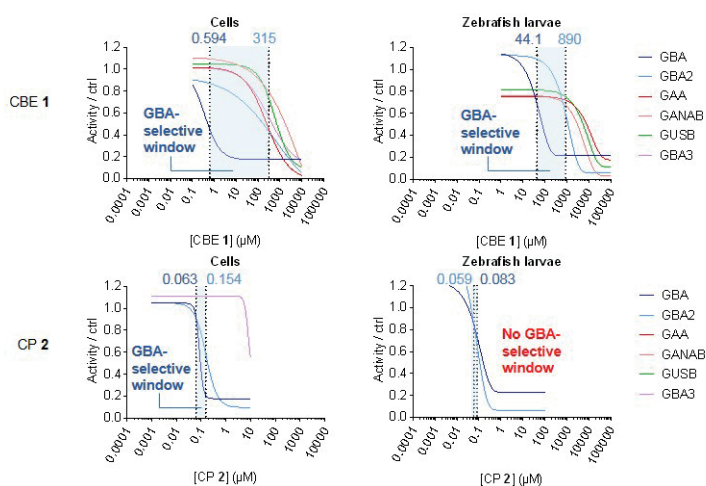


**Figure 8 | Window for selective GBA inhibition by CBE and CP in cultured cells and zebrafish larvae.**

Inhibition curves for CBE or CP towards GBA and other glycosidases were derived from the results of ABP detection (average of  $n = 3$  biological replicates). The GBA selective window is depicted as the blue area between the two dotted lines and defined as the concentration range for CBE or CP between its  $\text{IC}_{50}$  values towards GBA and the next major glycosidase target (in all cases, GBA2).

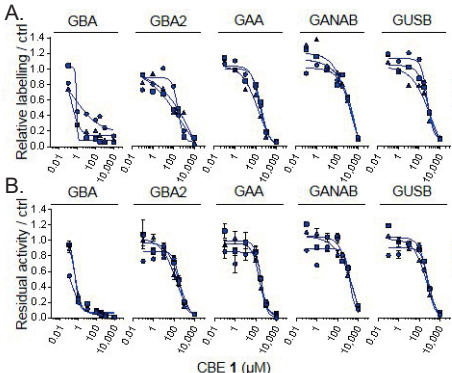
The CP derivatives, functionalized at C8 with a BODIPY (**3a**), biphenyl (**3d**) or adamantyl (**3e**), displayed both a very high potency and selectivity for GBA inactivation in developing zebrafish larvae. Apparent  $\text{IC}_{50}$  values of 4-31 nM were determined and no subsequent effect on *in vitro* ABP labelling of GBA2, LPH, GAA, ER  $\alpha$ -glucosidase GANAB or lysosomal  $\beta$ -glucuronidase (GUSB) even at high concentrations of inhibitor ( $>10 \mu\text{M}$ ). Overall, these results show comparable *in vivo* potency and selectivity in cultured cells and developing zebrafish larvae. A slightly higher potency was again observed using cultured cells, however this could be explained by the route of administration, possible storage of the small molecule in the lipid- and protein rich environment of the yolk (unpublished observations of Wouter Kallemeijn) as well as the complexity of the zebrafish embryo which includes different cell types.

Next, the physiological impact of GBA inactivation was studied by glycosphingolipid analysis. Inhibitor treated zebrafish revealed accumulation of GlcSph, a biochemical biomarker of *in vivo* inactivation of lysosomal GBA. Only a minor significant increase in GlcSph was observed when high concentrations of CBE (1000  $\mu$ M) and CP (10  $\mu$ M) were used, while the CP derivatives significantly increased GlcSph levels already at low concentrations (0.1-1  $\mu$ M). GlcSph levels are also highly elevated in human GD patients<sup>49</sup>, mouse GD models<sup>50</sup> and zebrafish genetic *gba* knockouts (Chapter 5<sup>51</sup>). In the latter study it became obvious that incubation with a relatively high concentration (10  $\mu$ M) of the CP derivative **3e** showed higher GlcSph levels as compared to the genetic *gba*<sup>-/-</sup> larvae. It became apparent that genetic *gba* KO larvae have maternally derived GBA enzyme in their early life, which was also inactivated by treatment with compound **3e**<sup>51</sup>. Due to the easy and throughput administration, compound **3e** is used extensively throughout this thesis to study GBA deficiency in a variety of genetic backgrounds. In addition, no genotyping of the off-spring is necessary, as for the genetic *gba* zebrafish in chapter 5, and all treated off-spring have a GBA deficiency. This could accelerate and simplify the process of sample preparation at 5 dpf.

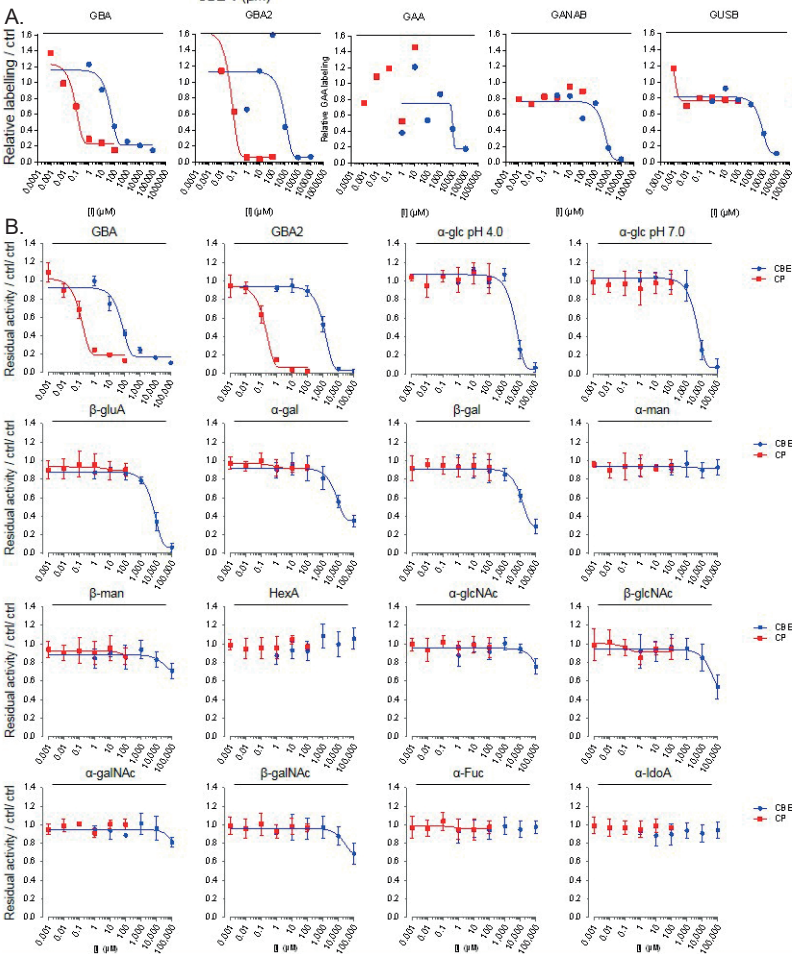
The use of the selective and potent BODIPY functionalized ABP **3a** has been hampered by its inability to inactivate GBA in the brain<sup>29</sup>. As final part of the present study, the newly synthesized CP derivatives were administered to adult zebrafish to evaluate their brain penetration. As expected, ABP **3a** showed inactivation of GBA activity in the spleen and liver but limited inactivation of GBA in the brain, as has already been observed in mice<sup>29,36</sup>. The limited penetration into the brain of the BODIPY ABP can be likely attributed to active removal via Pgp proteins<sup>52</sup>. Compound **3e**, on the other hand, showed complete inactivation of GBA in the liver, spleen and brain without inhibition of off-target proteins. Of note, the CP derivative modified with a Cy5 molecule at C8 (**3c**) was a very potent inhibitor of GBA *in vitro* and in developing zebrafish larvae, however no inactivation of GBA was neither found in brain, liver or spleen and accumulation in the gut was observed (unpublished data).

In conclusion, this study has shown that both zebrafish larvae and adult zebrafish are helpful models to evaluate the potency and target engagement of small molecule inhibitors of GBA. In addition, it has determined that compound **3e** is a superior GBA inhibitor enabling generation of a GBA deficiency, both on-demand in the brain and without any off-target effects, to assist research in the context of neuropathic GD and PD.

Supplementary information



**Supplementary Figure 1 |**  
(A) Quantification of relative ABP labelling of GBA, GBA2, GAA, GANAB and GUSB in lysates of cells treated *in vivo* for 24 h with CBE. (B) Residual activity of glycosidases in cell lysates treated *in vivo* with CBE. Error ranges =  $\pm$  SD, n = 3 (technical replicates).

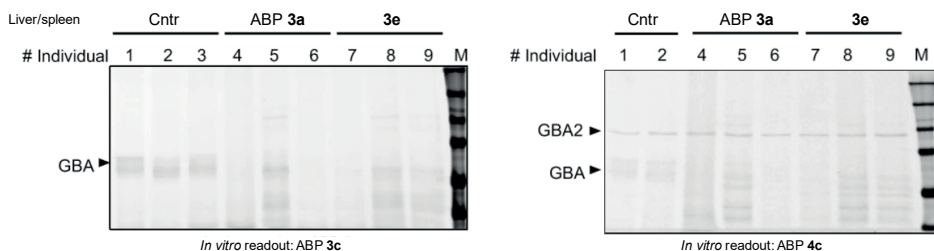


**Supplementary Figure 2 | In vivo incubation with CBE and CP in zebrafish larvae**  
(A) Quantification of gels from Figure 4. (B) Residual activity of glycosidases by enzymatic assay. Error range =  $\pm$  SD, n = 2 technical replicates

**Supplementary Table 1 | *In vivo* target engagement of CBE and CP in cultured cells and zebrafish larvae.**

Cultured cells were incubated for 24 hours and developing zebrafish for 5 days. Apparent  $IC_{50}$  values ( $\mu M$ ) were derived biological triplicate incubations as measured by quantification of *in vitro* ABP labelling on residual active enzymes. – indicates no inhibition at the tested concentrations. Error ranges =  $\pm$  SD, n = 3 biological replicates.

Enzyme	CBE 1 ( $\mu M$ )		CP 2 ( $\mu M$ )	
	Cultured cells	ZF larvae	Cultured cells	ZF larvae
GBA	$0.59 \pm 0.3$	44.1	$0.063 \pm 0.026$	0.083
GBA2	$315 \pm 63$	890	$0.154 \pm 0.07$	0.059
GAA	$249 \pm 84$	9550	–	–
GANAB	$2900 \pm 1120$	4700	–	–
GUSB	$857 \pm 341$	6470	–	–

**Supplementary Figure 3 | *In vivo* targets of ABP 3a and compound 3e in adult liver/spleen.**

DMSO (cntr) or compound soaked food was administered to adult zebrafish and *in vivo* target engagement was visualized by *in vitro* labelling of liver/spleen homogenates with selective GBA ABP 3c (left) or broad-spectrum retaining  $\beta$ -glucosidase ABP 4c labelling GBA, GBA2 and GBA3 (right).

## Experimental procedures

**General materials and methods** - Cyclophellitol (CP), the CP derivatives **3d** and **3e** and the ABPs **3a-c**, **4**, **5** and **6** were synthesized as described earlier<sup>28,30,32,36,53</sup>. Chemicals were obtained from Sigma-Aldrich (St. Louis, MO, USA) if not otherwise indicated. Conduritol B-epoxide (CBE) was purchased from Enzo Life Sciences (Farmingdale, NY, USA). Recombinant GBA (rGBA, imiglucerase) and recombinant human GAA (rGAA, alglucosidase alfa, Myozyme) were obtained from Sanofi Genzyme (Cambridge, MA, USA). HEK293T cells overexpressing human GBA2 were generated as previously described<sup>54</sup> and cultured in DMEM medium (Sigma-Aldrich) supplied with 10% (v/v) FCS, 0.1% (w/v) penicillin/streptomycin, and 1% (v/v) Glutamax, under 5% CO<sub>2</sub>.

**Zebrafish housing and embryo incubations** – Zebrafish were housed at the University of Leiden, the Netherlands, according to standard protocols (zfin.org). The breeding of fish lines was approved by the local animal welfare committee (Instantie voor dierwelzijn, IvD, Leiden). Adults, embryos and larvae were kept at a constant temperature of 28.5 °C. Embryos and larvae, before the free-feeding stage, not falling under animal experimentation law according to the EU animal protection Directive 2010/63/EU, were raised in egg water (60 µg L<sup>-1</sup> sea salt, Sera marin). Synchronized wild-type ABTL zebrafish embryos were acquired after mating of single male and female couples (both > 3 months old) and incubated with appropriate inhibitors as described below.

**Preparation of homogenates** - Homogenates of cells and zebrafish were prepared by lysis in potassium phosphate lysis buffer (25 mM KH<sub>2</sub>PO<sub>4</sub>-K<sub>2</sub>HPO<sub>4</sub>, pH 6.5, protease inhibitor cocktail (EDTA-free, Roche, Basel, Switzerland) and supplemented with 2.5 U/mL benzonase for HEK293T cell homogenates). Cell pellets from two 15-cm culture dishes were resuspended in 1200 µL lysis buffer, while 4µL lysis buffer was used to homogenize 1 zebrafish larvae. Homogenates were prepared by sonication with a Polytron PT 1300D sonicator (Kinematica, Luzern, Switzerland) on ice at 20% power for 3 times 3 s (zebrafish) or passed through a 30-gauge needle 10 times using a 1 mL syringe (HEK293T cells overexpressing GBA2). Protein concentration was measured using Pierce BCA assay kit (Thermo Fisher Scientific, Waltham, MA, USA).

**Enzymatic assays** - All assays were performed in 96-well plates at 37 °C for human and zebrafish materials. For measurements in rGBA or rGAA, 3.16 ng of rGBA enzyme or 2.1 ng rGAA enzyme, while for *in-vitro* measurements in GBA2-overexpressing cell lysates, 8 volumes of cell lysates (7µg total protein/ µL) was used and firstly pre-incubated with 1 volume of ABP **3a** (100 nM final concentration, 0.5% (v/v) DMSO) for 30 min at 37 °C to selectively inhibit GBA activity.

Samples were incubated with compounds (CBE **1**, CP **2**, ABP **3a**, ABP **3c**, **3d** or **3e**) in a final volume of 25 µL, at pH appropriate for each enzyme, while DMSO concentration was kept at 1% (v/v) in all assays during incubation with compounds. Assays were performed by incubating the samples with 100 µL 4MU- (4-methylumbelliferyl-) substrates diluted in McIlvaine buffer (150 mM citric acid—Na<sub>2</sub>HPO<sub>4</sub>, 0.1% (w/v) bovine serum albumin) for a period of 30 min to 2 h and performed in duplicate sets, with 3 replicates at each inhibitor concentration. After stopping the substrate reaction with 200 µL 1M NaOH-glycine (pH 10.3), 4MU-emitted fluorescence was measured with a fluorimeter LS55 (Perkin Elmer, Waltham, MA, USA) using λ<sub>ex</sub> 366 nm and λ<sub>em</sub> 445 nm<sup>28</sup>. Measured activities were subtracted with background values (from samples without enzyme), normalized with the average values from the control samples (no inhibitor), and curve-fitted to inhibitor concentrations using Prism 7.0 (Graphpad) by the [inhibitor] vs response— various slope (four parameters) method to obtain IC<sub>50</sub> values. The substrate mixtures used for each enzyme are listed as follows: GBA, 3.75 mM 4MU-β-D-glucopyranoside (Glycosynth, Warrington Cheshire, UK) at pH 5.2, supplemented with 0.2% (w/v) sodium taurocholate and 0.1% (v/v) Triton X-100, and 25 nM *N*-(5-adamantane-1-ylmethoxy-pentyl)-deoxynojirimycin (AMP-DNM), a GBA2-specific inhibitor<sup>55</sup>; GBA2, 3.75 mM 4MU-β-Dglucopyranoside at pH 5.8, with pre-incubation with 1 µM ABP **3a** for 30 min to specifically inhibit GBA activity; α-glucosidases, 3 mM 4MU-α-D-glucopyranoside at pH 4.0 (GAA) or at 7.0 (GANAB), GUSB, 2 mM

4MU- $\beta$ -D-glucuronide at pH 5.0;  $\alpha$ -galactosidases, 2 mM 4MU- $\alpha$ -D-galactopyranoside at pH 4.6;  $\beta$ -galactosidases, 1 mM 4MU $\beta$ -D-galactopyranoside at pH 4.3 with 0.2 M NaCl;  $\alpha$ -mannosidases, 10 mM 4MU- $\alpha$ -D-mannopyranoside at pH 4.0;  $\beta$ -mannosidases, 2 mM 4MU- $\beta$ -D-mannopyranoside (Glycosynth) at pH 4.2;  $\beta$ -hexosaminidase HexA, 5 mM 4MU- $\beta$ -D6-sulpho-2-acetamido-2-deoxy-glucopyranoside at pH 4.4;  $\beta$ -hexosaminidases HexA/B, 5 mM 4MU- $\beta$ -N-acetylglucosaminide at pH 4.5;  $\alpha$ -N-acetyl-galactosaminidase, 1 mM 4MU- $\alpha$ -N-acetyl-galactosaminide at pH 4.5;  $\alpha$ -L-fucosidase, 1 mM 4MU- $\alpha$ -L-fucopyranoside at pH 5.0,  $\alpha$ -L-iduronidase, 2 mM 4MU- $\alpha$ -L-iduronide (Glycosynth) at pH 4.0; GBA3, 3.75 mM 4MU- $\beta$ -D-glucopyranoside at pH 6.0.

**Fluorescent ABP labelling and detection** - Residual active, not irreversibly inhibited glycosidases were labelled with excess fluorescent ABPs in the optimum McIlvaine buffer, if not otherwise stated (see above). ABP labelling was performed at 37 °C for 30 min for all materials, in a total sample volume of 20–40  $\mu$ L and 0.5–1% DMSO concentration. GBA was labelled with 200 nM ABP **3b** (pH 5.2, 0.1% (v/v) Triton-100, 0.2% (w/v) sodium taurocholate), or labelled together with GBA2 using 200 nM  $\beta$ -aziridine ABP **4c** at pH 5.5. GBA2 was labelled with 200 nM  $\beta$ -aziridine ABP **4a**, **4b** or **4c**. The  $\alpha$ -glucosidases GAA and GANAB were first pre-incubated with 200 nM ABP **4a** for 30 min (pH 4.0 for GAA and pH 7.0 for GANAB), followed by labelling with 500 nM ABP **6a** or **6c** at pH 4.0 or 7.0. The  $\beta$ -glucuronidase GUSB was preincubated with 200 nM ABP **4a** for 30 min, followed by labelling with 200 nM  $\beta$ -aziridine ABP **5c**. After ABP incubation, proteins were denatured by boiling the samples with 5 $\times$  Laemmli buffer (50% (v/v) 1 M Tris-HCl, pH 6.8, 50% (v/v) 100% glycerol, 10% (w/v) DTT, 10% (w/v) SDS, 0.01% (w/v) bromophenol blue) for 5 min at 98 °C, and separated by electrophoresis on 7.5% or 10% (w/v) SDS-PAGE gels running continuously at 90 V<sup>28,30-32</sup>. Wet slab-gels were scanned on fluorescence using the Typhoon FLA 9500 (GE Healthcare) at  $\lambda_{\text{ex}}$  473 nm and  $\lambda_{\text{em}}$   $\geq$  510 nm for green fluorescent ABP **4a** and **6a**; at  $\lambda_{\text{ex}}$  532 nm and  $\lambda_{\text{em}}$   $\geq$  575 nm for ABP **3b** and **4b**; and at  $\lambda_{\text{ex}}$  635 nm and  $\lambda_{\text{em}}$   $\geq$  665 nm for ABP **4c**, **5c** and **6c**. ABP-emitted fluorescence was quantified using ImageQuant software (GE Healthcare, Chicago, IL, USA) and curve-fitted using Prism 7.0 (Graphpad). After fluorescence scanning, SDS-PAGE gels were stained for total protein with Coomassie G250 and scanned on a ChemiDoc MP imager (Bio-Rad).

***In vivo* effects of CBE and CP in intact cultured cells** - Confluent HEK293T stably expressing human GBA2 were cultured in 12-well plates in triplicates with(out) CBE (0.01–10,000  $\mu$ M) or CP (0.001–10  $\mu$ M) for 24 h at 37 °C. For lysis, cells were washed three times with PBS, subsequently lysed by scraping in potassium phosphate buffer (K<sub>2</sub>HPO<sub>4</sub>–KH<sub>2</sub>PO<sub>4</sub>, 25 mM, pH 6.5, supplemented with 0.1% (v/v) Triton X100 and protease inhibitor cocktail (Roche)), aliquoted, and stored at –80 °C. After determination of the protein concentration, lysates containing equal protein amount (5–20  $\mu$ g total protein per measurement) were adjusted to 12  $\mu$ L with potassium phosphate buffer and subjected to residual activity measurements using enzymatic assay (n = 3 technical replicates for each biological triplicate at each treatment condition) or ABP detection (n = 3 biological replicates) as described above.

***In vivo* effects of inhibitors in living zebrafish larvae** - For in vivo inhibitor treatment, a single fertilized embryo was seeded in each well of a 96-wells plate, and exposed to 200  $\mu$ L egg water supplemented with CBE (1–100,000  $\mu$ M), CP (0.001–100  $\mu$ M), ABP **3a** (0.001–10  $\mu$ M), ABP **5** (0.0001–10  $\mu$ M), inhibitor **3c** (0.001–10  $\mu$ M) or **3e** (0.001–10  $\mu$ M) with a final DMSO concentration of 0.5% (v/v) for 120 hours at 28.5 °C. Per condition, n = 24–48 embryos were used. At 120 hours (5 dpf), larvae were collected, rinsed three times with egg water, fully aspirated, snap-frozen in liquid nitrogen and stored at –80 °C until homogenization in 4  $\mu$ L potassium phosphate buffer per individual zebrafish as described above. Samples containing 20–45  $\mu$ g total protein were subjected to the enzymatic assay described in the previous section or diluted in 14  $\mu$ L lysis buffer, added with McIlvaine buffer at various pHs and subjected to ABP detection at a final volume of 32  $\mu$ L for 30 min at 37 °C using ABP methods described above.



## Chapter 3

*In vivo* activity of inhibitors in adult zebrafish - Surplus wild-type adult zebrafish of 3 months of age were administrated with a single dose of food grain mixed with DMSO, ABP **3a** or inhibitor **3e** (1.6 nmol/fish, approximately 4  $\mu$ mol/kg,  $n = 3$  for each treatment) in  $n = 2$  sets, according to project licence AVD1060020184725,1-04. An initial experiment was performed with 3 adult zebrafish and the effect was confirmed by additional 3 individuals per experimental condition. Zebrafish were sacrificed after 24 h using tricaine methane sulfate (MS222; 250 mg/L), organs were harvested, snap-frozen in liquid nitrogen and stored at  $-80^{\circ}\text{C}$  until use. Food grain consisted of Gemma micro mixed with Gemma diamond (Skretting, Stavanger, Norway). Lysis was performed with 50  $\mu$ L lysis buffer (without benzonase) per sample, and lysates containing 20–60  $\mu$ g total protein were analysed by ABP method for GBA, GBA2, GAA, GANAB, and GUSB.

Sphingolipid extraction and analysis by mass spectrometry in zebrafish larvae - Zebrafish embryos at 8 hpf were seeded in 12-well plates (15 fish/well, 3 mL egg water/well) and treated with CBE **1** (10–1,000  $\mu$ M), CP **2** (0.01–10  $\mu$ M), inhibitor **3d** (0.001–10  $\mu$ M) or **3e** (0.001–10  $\mu$ M) for 120 hours at  $28.5^{\circ}\text{C}$ . Thereafter, zebrafish larvae were washed three times with egg water, and collected in clean screw-cap Eppendorf tubes (three tubes of three larvae per inhibitor concentration). Lipids were extracted and measured according to methods described previously<sup>56</sup>. Briefly, after removing of the egg water, 20  $\mu$ L of 13C-GlcSph<sup>57</sup> from concentration 0.1 pmol/ $\mu$ L in MeOH, 480  $\mu$ L MeOH, and 250  $\mu$ L  $\text{CHCl}_3$  were added to the sample, stirred, incubated for 30 min at RT, sonicated (5 x 1 min in sonication water bath), and centrifuged for 10 min at 15,700 g. Supernatant was collected in a clean tube, 250  $\mu$ L  $\text{CHCl}_3$  and 450  $\mu$ L 100 mM formate buffer (pH 3.2) were added. The sample was stirred and centrifuged, the upper phase was transferred to a clean tube. The lower phase was extracted with 500  $\mu$ L MeOH and 450  $\mu$ L formate buffer. The upper phases were pooled and taken to dryness in a vacuum concentrator at  $45^{\circ}\text{C}$ . The residue was extracted with 700  $\mu$ L butanol and 700  $\mu$ L water, stirred and centrifuged. The upper phase (butanol phase) was dried and the residue was dissolved in 100  $\mu$ L MeOH. 10  $\mu$ L of this sample was injected to the LC-MS for lipid measurement with LC-MS/MS methods described previously<sup>56</sup>. Two-tailed unpaired t-test was performed in Prism 7.0 software (Graphpad) to derive statistical significance, where  $p < 0.05$  was considered significant.

## References

1. Brady R.O., Kanfer J.N., Bradley R.M. and Shapiro D. (1966) Demonstration of a deficiency of glucocerebrosidase-cleaving enzyme in Gaucher's disease. *The Journal of clinical investigation* **45**, 1112-1115.
2. Beutler E. and Grabowski G.A. (2001) Gaucher disease. In *The Metabolic and Molecular Bases of Inherited disease*, Volume III, 8th Edition, C.R. Scriver, A.L. Beaudet, W.S. Sly and D. Valle, eds. (New York: McGraw-Hill), pp. 3635-3668.
3. Legler G. (1966) [Studies on the action mechanism of glycoside splitting enzymes, I. Presentation and properties of specific inhibitors]. *Hoppe Seylers Z Physiol Chem* **345**, 197-214.
4. Vardi A., Zigdon H., Meshcheriakova A., Klein A.D., Yaacobi C., Eilam R.,... and Futerman A.H. (2016) Delineating pathological pathways in a chemically induced mouse model of Gaucher disease. *J Pathol* **239**, 496-509.
5. Legler G. (1990) Glycoside hydrolases: mechanistic information from studies with reversible and irreversible inhibitors. *Adv Carbohydr Chem Biochem* **48**, 319-384.
6. Kacher Y., Brumshtein B., Boldin-Adamsky S., Toker L., Shainskaya A., Silman I.,... and Futerman A.H. (2008) Acid beta-glucosidase: insights from structural analysis and relevance to Gaucher disease therapy. *Biol Chem* **389**, 1361-1369.
7. Premkumar L., Sawkar A.R., Boldin-Adamsky S., Toker L., Silman I., Kelly J.W.,... and Sussman J.L. (2005) X-ray structure of human acid-beta-glucosidase covalently bound to conduritol-B-epoxide. Implications for Gaucher disease. *J Biol Chem* **280**, 23815-23819.
8. Kanfer J.N., Legler G., Sullivan J., Raghavan S.S. and Mumford R.A. (1975) The Gaucher mouse. *Biochem Biophys Res Commun* **67**, 85-90.
9. Manning-Bog A.B., Schule B. and Langston J.W. (2009) Alpha-synuclein-glucocerebrosidase interactions in pharmacological Gaucher models: a biological link between Gaucher disease and parkinsonism. *Neurotoxicology* **30**, 1127-1132.
10. Xu Y.H., Sun Y., Ran H., Quinn B., Witte D. and Grabowski G.A. (2011) Accumulation and distribution of alpha-synuclein and ubiquitin in the CNS of Gaucher disease mouse models. *Mol Genet Metab* **102**, 436-447.
11. Rocha E.M., Smith G.A., Park E., Cao H., Graham A.R., Brown E.,... and Isacson O. (2015) Sustained Systemic Glucocerebrosidase Inhibition Induces Brain alpha-Synuclein Aggregation, Microglia and Complement C1q Activation in Mice. *Antioxid Redox Signal* **23**, 550-564.
12. Newburg D.S., Shea T.B., Yatziv S., Raghavan S.S. and McCluer R.H. (1988) Macrophages exposed in vitro to conduritol B epoxide resemble Gaucher cells. *Exp Mol Pathol* **48**, 317-323.
13. Newburg D.S., Yatziv S., McCluer R.H. and Raghavan S. (1986) beta-Glucosidase inhibition in murine peritoneal macrophages by conduritol-B-epoxide: an in vitro model of the Gaucher cell. *Biochimica et biophysica acta* **877**, 121-126.
14. Prenc E.M., Chaturvedi P. and Newburg D.S. (1996) In vitro accumulation of glucocerebrosidase in neuroblastoma cells: a model for study of Gaucher disease pathobiology. *J Neurosci Res* **43**, 365-371.
15. Bieberich E., Freischutz B., Suzuki M. and Yu R.K. (1999) Differential effects of glycolipid biosynthesis inhibitors on ceramide-induced cell death in neuroblastoma cells. *J Neurochem* **72**, 1040-1049.
16. Berger J., Lecourt S., Vanneaux V., Rapatel C., Boisgard S., Caillaud C.,... and Berger M.G. (2010) Glucocerebrosidase deficiency dramatically impairs human bone marrow haematopoiesis in an in vitro model of Gaucher disease. *Br J Haematol* **150**, 93-101.
17. Schueler U.H., Kolter T., Kaneski C.R., Zirzow G.C., Sandhoff K. and Brady R.O. (2004) Correlation between enzyme activity and substrate storage in a cell culture model system for Gaucher disease. *J Inherit Metab Dis* **27**, 649-658.
18. Lecourt S., Vanneaux V., Cras A., Freida D., Heraoui D., Herbi L.,... and Larghero J. (2012) Bone marrow microenvironment in an in vitro model of Gaucher disease: consequences of glucocerebrosidase deficiency. *Stem Cells Dev* **21**, 239-248.
19. Quaroni A., Gershon E. and Semenza G. (1974) Affinity labeling of the active sites in the sucrase-isomaltase complex from small intestine. *J Biol Chem* **249**, 6424-6433.
20. Yang S.J., Ge S.G., Zeng Y.C. and Zhang S.Z. (1985) Inactivation of alpha-glucosidase by the active-site-directed inhibitor, conduritol B epoxide. *Biochimica et biophysica acta* **828**, 236-240.
21. Hermans M.M., Kroos M.A., van Beeumen J., Oostra B.A. and Reuser A.J. (1991) Human lysosomal alpha-glucosidase. Characterization of the catalytic site. *J Biol Chem* **266**, 13507-13512.
22. van Weely S., Brandsma M., Strijland A., Tager J.M. and Aerts J.M. (1993) Demonstration of the existence of a second, non-lysosomal glucocerebrosidase that is not deficient in Gaucher disease. *Biochimica et biophysica acta* **1181**, 55-62.
23. Ridley C.M., Thur K.E., Shanahan J., Thillaiappan N.B., Shen A., Uhl K.,... and van der Spoel A.C. (2013) beta-Glucosidase 2 (GBA2) activity and imino sugar pharmacology. *J Biol Chem* **288**, 26052-26066.
24. Hara A. and Radin N.S. (1979) Enzymic effects of beta-glucosidase destruction in mice. Changes in

- glucuronidase levels. *Biochimica et biophysica acta* **582**, 423-433.
25. Braun H., Legler G., Deshusses J. and Semenza G. (1977) Stereospecific ring opening of condurititol-B-epoxide by an active site aspartate residue of sucrase-isomaltase. *Biochimica et biophysica acta* **483**, 135-140.
26. Atsumi S., Iinuma H., Nosaka C. and Umezawa K. (1990) Biological activities of cyclophellitol. *J Antibiot (Tokyo)* **43**, 1579-1585.
27. Withers S.G. and Umezawa K. (1991) Cyclophellitol: a naturally occurring mechanism-based inactivator of beta-glucosidases. *Biochem Biophys Res Commun* **177**, 532-537.
28. Witte M.D., Kallemeijn W.W., Aten J., Li K.Y., Strijland A., Donker-Koopman W.E.,... and Aerts J.M. (2010) Ultrasensitive in situ visualization of active glucocerebrosidase molecules. *Nature chemical biology* **6**, 907-913.
29. Herrera Moro Chao D., Kallemeijn W.W., Marques A.R., Orre M., Ottenhoff R., van Roomen C.,... and Aerts J.M. (2015) Visualization of Active Glucocerebrosidase in Rodent Brain with High Spatial Resolution following In Situ Labeling with Fluorescent Activity Based Probes. *PLoS one* **10**, e0138107.
30. Kallemeijn W.W., Li K.Y., Witte M.D., Marques A.R., Aten J., Scheij S.,... and Overkleeft H.S. (2012) Novel activity-based probes for broad-spectrum profiling of retaining beta-exoglucosidases in situ and in vivo. *Angewandte Chemie* **51**, 12529-12533.
31. Wu L., Jiang J., Jin Y., Kallemeijn W.W., Kuo C.L., Artola M.,... and Davies G.J. (2017) Activity-based probes for functional interrogation of retaining beta-glucuronidases. *Nature chemical biology* **13**, 867-873.
32. Jiang J., Kuo C.L., Wu L., Franke C., Kallemeijn W.W., Florea B.I.,... and Aerts J.M. (2016) Detection of Active Mammalian GH31 alpha-Glucosidases in Health and Disease Using In-Class, Broad-Spectrum Activity-Based Probes. *ACS Cent Sci* **2**, 351-358.
33. Dekker N., van Dussen L., Hollak C.E., Overkleeft H., Scheij S., Ghauharali K.,... and Aerts J.M. (2011) Elevated plasma glucosylsphingosine in Gaucher disease: relation to phenotype, storage cell markers, and therapeutic response. *Blood* **118**, e118-127.
34. Aerts J.M., Donker-Koopman W.E., van Laar C., Brul S., Murray G.J., Wenger D.A.,... and Schram A.W. (1987) Relationship between the two immunologically distinguishable forms of glucocerebrosidase in tissue extracts. *Eur J Biochem* **163**, 583-589.
35. Kuo C.L., Kallemeijn W.W., Lelieveld L.T., Mirzaian M., Zoutendijk I., Vardi A.,... and Artola M. (2019) In vivo inactivation of glycosidases by condurititol B epoxide and cyclophellitol as revealed by activity-based protein profiling. *FEBS J* **286**, 584-600.
36. Artola M., Kuo C.L., Lelieveld L.T., Rowland R.J., van der Marel G.A., Codee J.D.C.,... and Overkleeft H.S. (2019) Functionalized Cyclophellitols Are Selective Glucocerebrosidase Inhibitors and Induce a Bona Fide Neuropathic Gaucher Model in Zebrafish. *Journal of the American Chemical Society* **141**, 4214-4218.
37. Ferraz M.J., Marques A.R., Appelman M.D., Verhoek M., Strijland A., Mirzaian M.,... and Aerts J.M. (2016) Lysosomal glycosphingolipid catabolism by acid ceramidase: formation of glycosphingoid bases during deficiency of glycosidases. *FEBS Lett* **590**, 716-725.
38. MacRae C.A. and Peterson R.T. (2015) Zebrafish as tools for drug discovery. *Nature reviews. Drug discovery* **14**, 721-731.
39. Rennekamp A.J. and Peterson R.T. (2015) 15 years of zebrafish chemical screening. *Current opinion in chemical biology* **24**, 58-70.
40. Kytidou K., Beenakker T.J.M., Westerhof L.B., Hokke C.H., Moolenaar G.F., Goosen N.,... and Aerts J. (2017) Human Alpha Galactosidases Transiently Produced in *Nicotiana benthamiana* Leaves: New Insights in Substrate Specificities with Relevance for Fabry Disease. *Front Plant Sci* **8**, 1026.
41. Kuo C.L., van Meel E., Kytidou K., Kallemeijn W.W., Witte M., Overkleeft H.S.,... and Aerts J.M. (2018) Activity-Based Probes for Glycosidases: Profiling and Other Applications. *Methods Enzymol* **598**, 217-235.
42. Schroder S.P., de Boer C., McGregor N.G.S., Rowland R.J., Moroz O., Blagova E.,... and Overkleeft H.S. (2019) Dynamic and Functional Profiling of Xylan-Degrading Enzymes in *Aspergillus* Secretomes Using Activity-Based Probes. *ACS Cent Sci* **5**, 1067-1078.
43. van Rooden E.J., Florea B.I., Deng H., Baggelaar M.P., van Esbroeck A.C.M., Zhou J.,... and van der Stelt M. (2018) Mapping in vivo target interaction profiles of covalent inhibitors using chemical proteomics with label-free quantification. *Nat Protoc* **13**, 752-767.
44. Baggelaar M.P., Janssen F.J., van Esbroeck A.C., den Dulk H., Allara M., Hoogendoorn S.,... and van der Stelt M. (2013) Development of an activity-based probe and in silico design reveal highly selective inhibitors for diacylglycerol lipase- $\alpha$  in brain. *Angewandte Chemie* **52**, 12081-12085.
45. Liu Y., Patricelli M.P. and Cravatt B.F. (1999) Activity-based protein profiling: the serine hydrolases. *Proc Natl Acad Sci U S A* **96**, 14694-14699.
46. Zhao Q., Ouyang X., Wan X., Gajiwala K.S., Kath J.C., Jones L.H.,... and Taunton J. (2017) Broad-Spectrum Kinase Profiling in Live Cells with Lysine-Targeted Sulfonyl Fluoride Probes. *Journal of the American Chemical Society* **139**, 680-685.

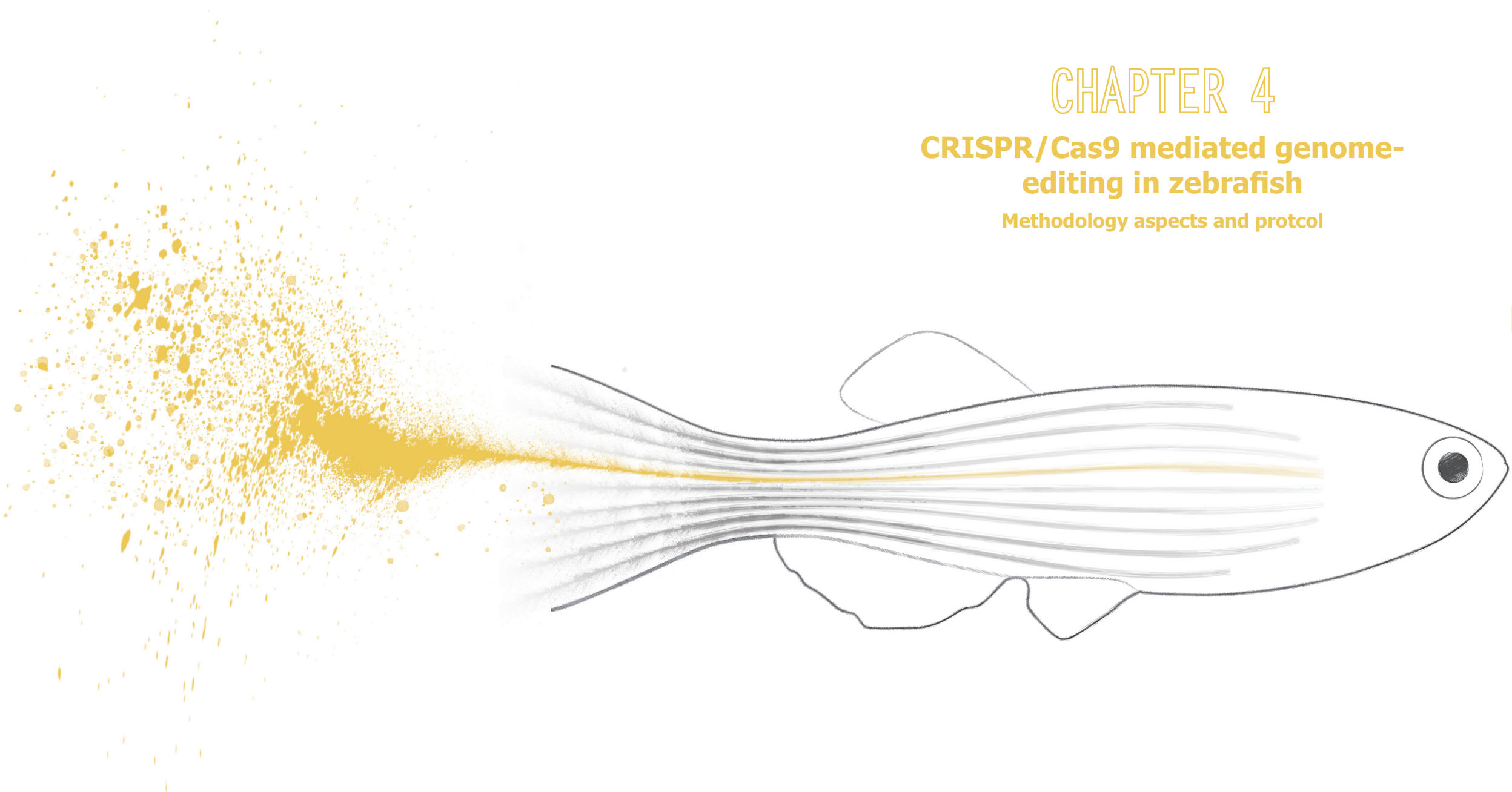
47. Sanman L.E. and Bogoy M. (2014) Activity-based profiling of proteases. *Annu Rev Biochem* **83**, 249-273.
48. Xin B.T., Espinal C., de Bruin G., Filippov D.V., van der Marel G.A., Florea B.I. and Overkleeft H.S. (2020) Two-Step Bioorthogonal Activity-Based Protein Profiling of Individual Human Proteasome Catalytic Sites. *ChemBiochem* **21**, 248-255.
49. Mirzaian M., Wisse P., Ferraz M.J., Gold H., Donker-Koopman W.E., Verhoek M.,... and Aerts J.M. (2015) Mass spectrometric quantification of glucosylsphingosine in plasma and urine of type 1 Gaucher patients using an isotope standard. *Blood Cells Mol Dis* **54**, 307-314.
50. Ferraz M.J., Marques A.R., Gaspar P., Mirzaian M., van Roomen C., Ottenhoff R.,... and Aerts J.M. (2016) Lyso-glycosphingolipid abnormalities in different murine models of lysosomal storage disorders. *Mol Genet Metab* **117**, 186-193.
51. Lelieveld L.T., Mirzaian M., Kuo C.L., Artola M., Ferraz M.J., Peter R.E.A.,... and Aerts J. (2019) Role of beta-glucosidase 2 in aberrant glycosphingolipid metabolism: model of glucocerebrosidase deficiency in zebrafish. *J Lipid Res* **60**, 1851-1867.
52. Fischer S., Kluver N., Burkhardt-Medicke K., Pietsch M., Schmidt A.M., Wellner P.,... and Luckenbach T. (2013) Abcb4 acts as multixenobiotic transporter and active barrier against chemical uptake in zebrafish (*Danio rerio*) embryos. *BMC Biol* **11**, 69.
53. Schroder S.P., van de Sande J.W., Kallemeijn W.W., Kuo C.L., Artola M., van Rooden E.J.,... and Overkleeft H.S. (2017) Towards broad spectrum activity-based glycosidase probes: synthesis and evaluation of deoxygenated cyclophellitol aziridines. *Chemical communications* **53**, 12528-12531.
54. Lahav D., Liu B., van den Berg R., van den Nieuwendijk A., Wennekes T., Ghisaidoobe A.T.,... and Overkleeft H.S. (2017) A Fluorescence Polarization Activity-Based Protein Profiling Assay in the Discovery of Potent, Selective Inhibitors for Human Nonlysosomal Glucosylceramidase. *Journal of the American Chemical Society* **139**, 14192-14197.
55. Overkleeft H.S., Renkema G.H., Neele J., Vianello P., Hung I.O., Strijland A.,... and Aerts J.M. (1998) Generation of specific deoxynojirimycin-type inhibitors of the non-lysosomal glucosylceramidase. *J Biol Chem* **273**, 26522-26527.
56. Mirzaian M., Wisse P., Ferraz M.J., Marques A.R.A., Gaspar P., Oussoren S.V.,... and Aerts J.M. (2017) Simultaneous quantitation of sphingoid bases by UPLC-ESI-MS/MS with identical (<sup>13</sup>C)-encoded internal standards. *Clin Chim Acta* **466**, 178-184.
57. Wisse P., Gold H., Mirzaian M., Ferraz M.J., Lutteke G., van den Berg R.J.B.H.N.,... and Overkleeft H.S. (2015) Synthesis of a Panel of Carbon-13-Labelled (Glyco)Sphingolipids. *Eur J Org Chem* **2015**, 2661-2677.

# CHAPTER 4

## CRISPR/Cas9 mediated genome- editing in zebrafish

Methodology aspects and protocol

4



## Abstract

The CRISPR/Cas9 system enables a relatively easy manner of specific genome-editing in cells and organisms. This chapter describes the genome-editing approaches underlying the zebrafish loss-of-function mutants characterized in subsequent experimental chapters. First of all, a detailed protocol for the generation of CRISPR/Cas9 modified zebrafish is provided, including notes and considerations. Next, the protocol is applied to generate zebrafish with a loss-of-function mutation in proteins involved in lysosomal storage disorders. For the target proteins *Gba1*, *Gba2*, *Gpnmb*, *Asah1a*, *Asah1b*, *Npc1* and *Cln8*, information on chromosome location and obtained mutant gene- and protein sequences of the zebrafish knockouts are provided. RNA expression and lipid analysis of mutant larvae of *Gpnmb*, *Npc1* and *Cln8* confirmed that functional gene knockout have been generated, while the impact of defective *Gba1*, *Gba2*, *Asah1a* and/or *Asah1b* is described in chapters 5, 6 and 7.

In addition, pilot experiments using the Tol2 transposase technique were undertaken to introduce an exogenous target DNA sequence in the zebrafish genome. The coding sequence of human *GBA* was introduced in the zebrafish *gba1*<sup>-/-</sup> genetic background. In addition, the coding sequence of zebrafish prosaposin was introduced harbouring a point mutation in the saposin C region thought to impair a disulfide bridge.

In conclusion, this chapter describes a relatively easy, straightforward and cheap method to generate genome-edited zebrafish using CRISPR/Cas9 and Tol2 transposase technology. It is advised to closely monitor the experimental steps to achieve high mutagenesis efficiencies with low mortality rates and off-target effects. This could reduce the number of required animals while maintaining a mixed genetic background.



## Introduction

In the twentieth century, knowledge on heredity increased with the rediscovery of Gregor Mendel's pea plant research, driving the elucidation of the structure of the double DNA helix and cracking the genetic code<sup>1</sup>. It became apparent that DNA, including smaller or bigger changes, is transmitted from parent to offspring and that these mutations can have detrimental effects on the health state of the offspring. For years, understanding the molecular mechanisms underlying human inherited disorders was limited by the inability to specifically change the endogenous genome of model organisms<sup>2,3</sup>. Early genome-editing endeavours were labour intensive and not specific. Mutagenesis induced by the chemical N-ethyl N-nitrosourea (ENU) required extensive screenings to determine a mutation in a target gene without off-target effects. The spontaneous homologous recombination technique, commonly used in mouse embryo-derived stem cells, was very inefficient and also showed a high frequency of undesired genome-editing events<sup>2,3</sup>.

A new era of specific genome-editing commenced when several new programmable nucleases were developed starting with Zinc finger-FokI nucleases (ZFNs), transcription activator-like effector nucleases (TALENs) and, more recently, CRISPR-associated (Cas) enzymes in combination with Clustered Regularly Interspaced Short Palindromic Repeats (CRISPR). The first two techniques utilize protein fusions composed of the DNA cleavage domain of FokI endonuclease with multiple modules of either Zinc fingers<sup>4</sup> or TALE proteins<sup>5</sup>. One particular module could recognize either a 3-bp DNA code (Zinc finger) or one single base (TALE protein), which required combinatorial assembly of multiple modules. Re-design and engineering of new sets of proteins for each target was one of the main limitations of both techniques. Therefore, adaptation of the CRISPR/Cas system has revolutionized the research community, enabling specific and facile genome editing for all researchers.

The CRISPR/Cas system has been adapted from an endogenous prokaryotic immune response. CRISPRs and Cas enzymes are used by prokaryotes as adaptive immune system to cleave invading foreign genetic elements<sup>6</sup>. Prokaryotic Cas enzymes are guided by short CRISPR RNAs (crRNA) which are transcribed from non-repeating spacer DNA sequences originating from viruses and other mobile genetic elements<sup>7</sup>. The spacer sequences acquired by the prokaryote are highly similar in regions called protospacer-adjacent motifs (PAMs) and critical for the CRISPR system<sup>8</sup>. An important step in the discovery and design of the genome-editing technique was the reprogramming of Cas9 from *Streptococcus thermophilus* and *S. pyogenes*<sup>9</sup>, which enabled targeting of an intended bacterial DNA sequence<sup>10,11</sup>. These findings were followed by the discovery that 'humanized' versions of *S. pyogenes* Cas9 system also worked in eukaryotic systems<sup>12-14</sup> and the technique expanded quickly to other cell types and whole organisms such as mice, drosophila and zebrafish<sup>15</sup>.

The two short RNAs were combined into a single guide RNA (sgRNA)<sup>12</sup>. The sgRNA is composed of a specific sequence of 20 nucleotides at the 5' end of the sgRNA, which binds specifically to the DNA target site by Watson-Crick base pairing, followed by a RNA sequence at the 3' end that forms the complex with the Cas9 endonuclease through RNA hairpins. The target DNA sequence requires the Cas9 specific PAM sequence of 'NGG', immediately adjacent to the 20 bp sequence complementary to the sgRNA, to guide and program the Cas9 protein–sgRNA complex<sup>12</sup>.

In general, off-target effects are one of the main problems of genome-editing tools. The 10-12 bp sequence adjacent to the PAM sequence is called the 'seed region' and requires perfect complementarity with the sgRNA. Mismatches in the 8 bp sequence distal to the PAM are tolerated<sup>10</sup> even though it does not necessarily lead to DNA cleavage *in vivo*, making off-target effects difficult to predict<sup>16,17</sup>. Therefore both on-target activity (efficiency) and off-target effects (specificity) of the system can be dependent on sgRNA sequence (including GC content, secondary structures and sequence length), cell type, Cas9 enzyme concentration and sgRNA/Cas9 delivery methods<sup>18</sup>.

Zebrafish are an attractive vertebrate model to study human diseases, with characteristics such as large progeny, fast embryonic development including functional liver, kidney and tissue barriers and a high occurrence (83%) of functional zebrafish orthologs of human disease-related genes<sup>19</sup>. Generation of a zebrafish knockout using CRISPR/Cas9 technology can be achieved with a relatively straightforward method, a high rate of success and generated in a matter of months instead of years. Therefore many zebrafish disease models have been successfully generated<sup>20</sup>.

This chapter provides a detailed workflow, including notes and considerations, for the generation and high-throughput screening of CRISPR/Cas9 mediated gene knockout zebrafish models. The protocol relies on non-homologous end-joining (NHEJ), the most dominant repair mechanism of vertebrates for repairing DNA double-strand breaks. Insertions and deletions (indels) are introduced due to end resection of the complementary strands and misaligned repair. Next, the protocol is used to establish zebrafish models of lysosomal storage disorders. Seven target genes are selected and obtained mutations described. In addition, preliminary biochemical data is described of mutant larvae which are not studied in detail in subsequent chapters. In addition, the Tol2 transposon approach is used to introduce two target sequence, human *GBA* and *prosaposin* with a point mutation, in the zebrafish genome.

## Workflow

The procedure is summarized in **Figure 1**. Part 1 requires approximately one week including target design, RNA synthesis and injection of the sgRNA/Cas9 mRNA mixture. Part 2 consists of screening the  $F_0$  and  $F_1$  adult zebrafish for desired modifications using the high resolution melt (HRM) analysis and Sanger sequencing. For the  $F_2$  generation, and subsequent generations, only a HRM analysis is required, accelerating screening of the fish. Several outbred crossings are preferred, before incrossing, to obtain a zebrafish line with a healthy genetic background. The whole procedure of obtaining a zebrafish line with a homozygous mutation comprises approximately 6-16 months: depending on the sexual maturation of the fish and the preference of crossing carrier zebrafish with wildtype (WT) zebrafish (outbred) to the  $F_3$  generation before crossing the carriers with each other (inbred).

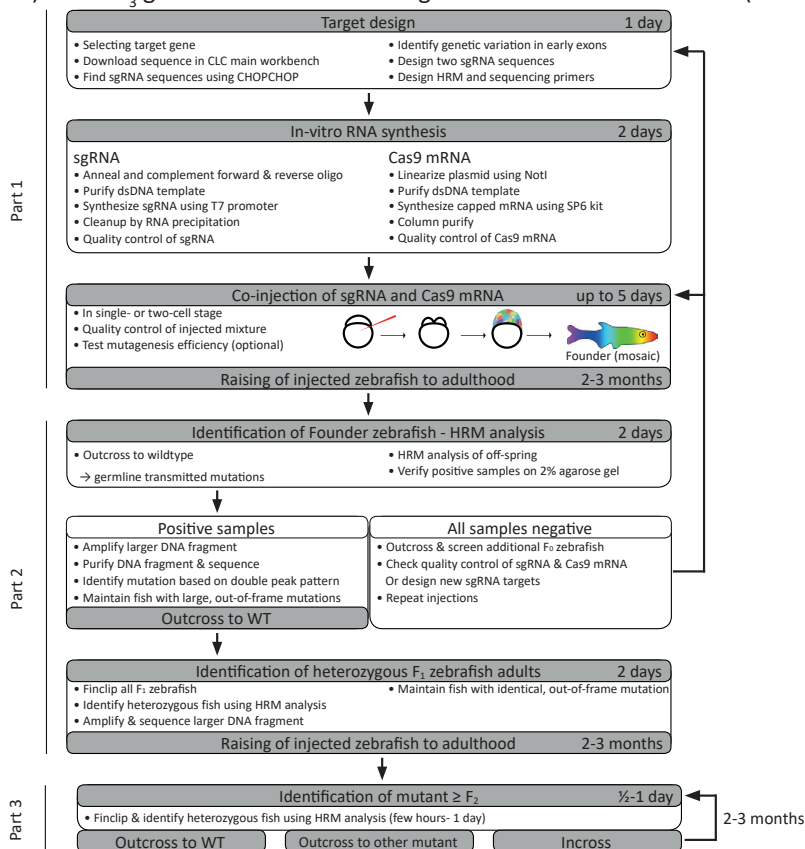


**Figure 1 | Protocol for generation of CRISPR/Cas9 mediated knockout zebrafish**

### **Part 1 | Target design, RNA preparation & injection**

#### **Genetic variation**

As starting point, Ensembl and NCBI databases are used to identify zebrafish orthologues of the target gene. Zebrafish underwent an additional whole-genome duplication and approximately 20% of human genes have co-orthologues in the zebrafish genome<sup>19,21,22</sup>. Therefore, a protein BLAST of the human protein of interest is performed to identify additional zebrafish co-orthologues of the human target. Sequences can be found and downloaded from the NCBI database using the program CLC main workbench, including whole chromosome, mRNA or protein sequences. The chromosome of interest is particularly useful because it includes chromosome positions and annotations such as coding sequences (CDS), exons, introns and non-coding sequences (example in **Figure 2A**). The obtained sequence does not include genetic variations, while genetic variation between different zebrafish lines and within a laboratory stock is large<sup>23</sup>. Therefore, genetic variations of the target region are manually annotated using the Ensembl Variation database before the design of sgRNA sequences and primers (**Figure 2A**). In specific cases, it is recommended to sequence the target region as we have noticed that various indels are not annotated in the variation database. Double peaks in the obtained sequence trace indicate heterozygous SNPs or indels and confirm amplification of both alleles.

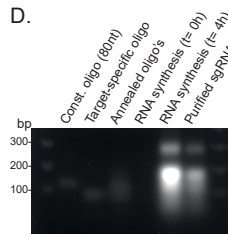
#### **SgRNA design**

Several CRISPR/Cas9 target design web tools are available and we use the CHOPCHOP web-tool<sup>24,25</sup>. It offers the option to enter via RefSeq, gene ID or fasta sequences as well as various options for target specific regions, PAM sequence, efficiency score, 5' requirements for sgRNA and self-complementarity. We use the gene ID, together with the newest available genome (DanRer11/GRCz11 in 2019) and 'NGG' as Cas9-specific PAM sequence. Our method requires the target sequences to start with 5' GG in order to have efficient *in vitro* RNA transcription due to promoter requirements of the utilized T7 RNA polymerase. Therefore, the option 'GN' or 'NG' is applied as 5' requirements as well as the option to check for self-complementarity when the leading nucleotides are replaced with 'GG'. All other settings of the web-tool are left on default.

Two target sequences are chosen with regard to certain guidelines: high efficiency, low number of off-targets, located in close proximity of each other, in the first few exons common to all known splice variants (exon 1-3) and preferably in the middle of the exon (**Figure 2B**). Two efficient target sequences in close proximity are ideal for screening since both targets can be screened using the same primer pair. Mutants with target sequences in the middle of the exon showed more straightforward prediction of the *in silico* mutation and a lower chance of exon-intron mutations.

#### **RNA preparation and microinjection**

A cloning- and PCR-free method is used to obtain the double strand template for RNA synthesis<sup>26</sup>. The target-specific oligo consists of a GCG clamp, the T7 promoter, the chosen target sgRNA sequence and a sequence complementary to the constant reverse oligo of 80-nt, that contains the Cas9 binding region (**Figure 2C**). Target- and constant reverse oligo are annealed, extended with DNA polymerase and purified double-strand DNA template

[illegible]

**(A)** Visualization of the *gba1* locus using CLC main workbench, with the genomic sequence (annotated as blue box), mRNA sequence (green box) and coding sequence (CDS, yellow box). Genetic variation is added manually (red triangles) as well as used primer sequences (green) and sgRNA target sequence (grey). **(B)** sgRNA of the zebrafish *gba1* gene determined by the CHOPCHOP web-tool. **(C)** Target-specific oligo (top sequence), with the T7 promoter underlined, target sequence in green and the constant reverse oligo (bottom) with the sequences complementary to each other in grey. **(D)** SG RNA generation on 1% agarose gel with from left to right: only constant oligo, only target-specific oligo, annealed oligos, RNA sample at  $t = 0$  h, RNA sample after 3 h of transcription without degradation of the dsDNA template and purified sgRNA running as two bands between 100 and 200 bp due to secondary structures. **(E)** Different sgRNA/Cas9 injection mixtures with comparable RNA concentrations measured by Nanodrop. **(F)** Microinjection of sgRNA/Cas9 with PhenolRed to visualize proper injection into the single-cell stage of the embryo.

93

Part 2 & 3 | Germline transmitted mutations & screening

High-resolution Melt (HRM) Analysis

Several methods are available to evaluate sgRNA mutagenic efficiency in injected zebrafish embryos and adult founder zebrafish, including T7 endonuclease I analysis, the Surveyor assay or fluorescence PCR<sup>27,28</sup>. We adapted a high-resolution melt (HRM) analysis method to evaluate mutations, using the specific melting characteristics of a particular DNA fragment<sup>29</sup>. A short fragment around the region of interest (100-150 bp) is amplified in the presence of a dsDNA-intercalating dye. After amplification, the PCR product is heated gradually from 55 °C to 95 °C. With increasing temperature, the strands of the dsDNA sequence are melted and the fluorescence decreases (**Figure 3A**). The specific combination of nucleotides in the DNA sequence results in a characteristic melting curve. NHEJ typically generates small indels which influences the melting curve, although differences between WT and mutant DNA are generally not large enough to analyse the obtained melting temperature. Therefore, fluorescent data of each sample is normalized using the start fluorescence at 55°C (**Figure 3B**) and the difference between the target sample and a reference sample (WT genomic DNA) is calculated and visualized as maximum or minimum (**Figure 3C and D** for *gba1*, and **3F** for *gba2*). The deletion or insertion is subsequently verified by loading the PCR amplicon on a 2-2.5% agarose gel (**Figure 3G** for *gba2*).

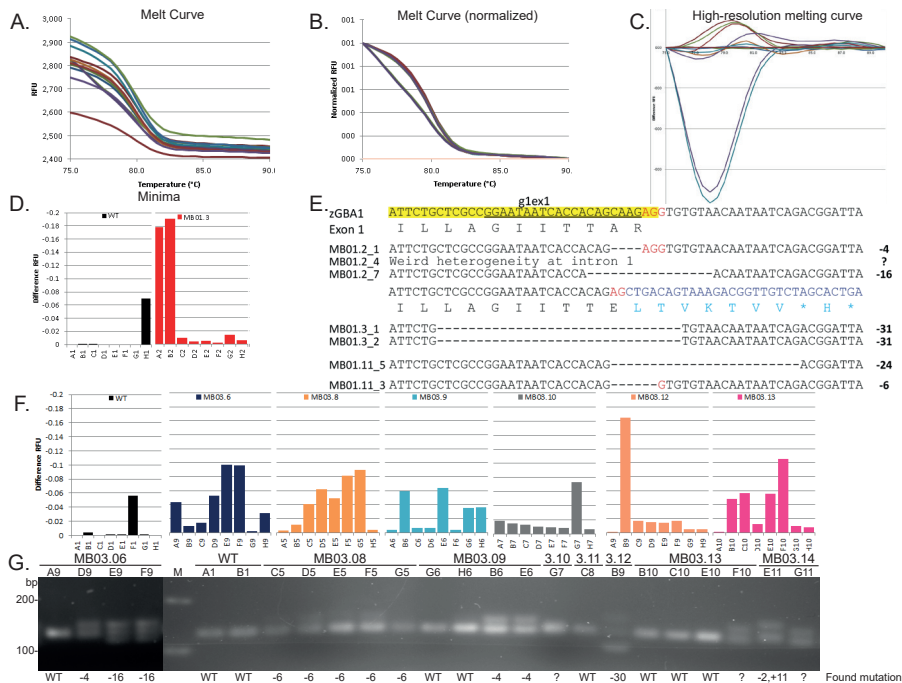


Figure 3 | Screening of founder fish by high-resolution melt (HRM) analysis

(A-E) Screening of offspring of founders injected with *gba* sgRNA (LL031). (A) The melting curve plotted as fluorescence (in RFU) against temperature. (B) Fluorescence is normalized using the fluorescence at 55 °C. (C) The difference between the target sample and reference sample is plotted against the temperature and (D) the minimum (or maximum) visualized as bar graph. (E) The mutation is verified and reconstituted using Sanger sequencing. (F,G) Screening of offspring of founders injected with *gba2* sgRNA (LL039) with mutations (minima) visualized in a bar graph (F) and verified on 2-2.5 % agarose gel and by Sanger sequencing (G).



Unlike other methods, the HRM assay only requires materials and equipment routinely used in laboratories performing RT-PCR analysis such as multiwell PCR plates, multichannel pipettes, a buffer with dsDNA-binding dye and a real-time PCR instrument. Moreover, a simple excel sheet is used to calculate the differences instead of the available but expensive HRM programs. The simplicity and pace of the method is advantageous because fish can be screened and put back in the aquarium in only a day, thereby reducing the stress of individual housing. A potential disadvantage of this method is that very large deletions might not be detected as these could remove the primer binding site(s) of the small amplicon, generally located 20-25 bp from the target sgRNA cut-site (**Figure 2A**).

### Evaluation of injected adult zebrafish (founders) and subsequent generations

Injection of embryos typically generates mosaic mutagenesis in the developing larvae; cells can have unmodified DNA or different mutations. At this stage, the HRM analysis can only be used to evaluate the mutagenic efficiency of the sgRNA. A visible difference and accompanying smeared band on agarose gel, indicates a highly efficient sgRNA as most of the cells of the developing embryo have a mutated target sequence. Subsequently, larvae of the same injected batch are raised to adulthood.

Adult founder fish are crossed with a genetically WT strain, albino for easy crossing. Individual embryos (n= 8) of each outcross are screened by HRM analysis and verified on gel to find founder fish with germ-line transmitted mutations (**Figure 3**). A larger fragment is amplified from positive samples to obtain information of the precise mutation using Sanger sequencing. A fragment of 300-700 bp is amplified with primers, located at a minimum of 50 bp from the target site for optimal sequencing results (**Figure 2A**). If primer design in the flanking introns is difficult, due to genetic variation, an exon in close proximity is used to amplify a larger but more specific fragment. With the determined mutation, the modified *in silico* mRNA sequence is evaluated for the prediction of an early stop codon in the protein sequence (**Figure 4**). We typically keep founder fish with large, out-of-frame mutations leading to an early stop codon and preferably easily detected with the HRM assay.

For the F<sub>1</sub> generation, one- to two suitable founder fish are crossed with WT (not of albino background) and raised. Genomic DNA of finclipped adults is used in an HRM assay followed by sequencing of the positive samples. Fish with different mutations are generally found, indicating that germ cells of the founder fish can have different mutations. Adult F<sub>1</sub> zebrafish with the same mutation are maintained, WT fish or fish with suboptimal mutations are discarded.

It is important to be aware of potential off-target effects that might occur. Our WT zebrafish are maintained as genetically heterogeneous outbred stocks and therefore we always cross several generations to WT (>F<sub>3</sub> generation, outbred) before generating a homozygous adult zebrafish line (inbred). This common approach results in a diverse genetic background and reduces the selection of fish that show undesired off-target modifications besides the desired genetic modification. Heterozygous adult fish can be crossed with each other and offspring used in pilot biochemical experiments to confirm generation of a functional KO. For experiments, we always use and compare genetically WT zebrafish larvae from crossings of mutant heterozygotes (inbred, ¼ ratio) and from crossings of WT stocks.

## Results and preliminary findings

The described CRISPR/Cas9 protocol was used successfully for generation of loss-of-function zebrafish mutants in order to study lysosomal storage disorders. To date, seven targets are selected: lysosomal  $\beta$ -glucosidase (glucocerebrosidase (GCase), gene name *gba1*) impaired in Gaucher disease (GD), the membrane associated  $\beta$ -glucosidase GBA2 (*gba2*), the Gaucher biomarker transmembrane glycoprotein NMB (*gpnmb*), both acid ceramidase co-orthologues (*asah1a* and *asah1b*), NPC intracellular cholesterol transporter 1 (*npc1*) defective in Niemann-Pick disease type C1<sup>30</sup> and CLN8 (*cln8*) which results in neuronal ceroid lipofuscinosis when defective<sup>31</sup> and is reported as genetic modifier in GD<sup>32</sup>. The genetic location of each target in the zebrafish genome is given in **Table 1**, as well as gene and protein annotations.

**Table 1 | Selected targets related to lysosomal storage disorders**

Information of protein and gene names, including representative RefSeq and Uniprot codes with genetic locations, transcript (in bp), number of amino acids (aa), predicted protein size (kDa) and amino acid identity compared to the human orthologue (in %). Some of the generated zebrafish are characterized in other chapters, while results of pilot experiments of other zebrafish lines are presented in this chapter.

Protein name	Gene	Chr	mRNA: refseq	bp	Uniprot	aa	kDa	Identity	
Glucosylceramidase	<i>gba</i>	16	XM_682379	4173	E7EZM1	518	58	58%	Ch. 5-7
Non-lysosomal glucosylceramidase	<i>gba2</i>	7	XM_005172332	3676	E7F65W0	851	96.5	66%	Ch. 5, 6
Glycoprotein nmb	<i>gpnmb</i> X1	19	XM_009294247	5185	E7F7J7	627	70	33%	Pilot exp.
N-acylsphingosine amidohydrolase	<i>asah1a</i>	14	NM_001006088	1578	Q5XJR7	390	44.6	61%	Ch. 6, 7
Acid ceramidase 1a									
Acid ceramidase 1b	<i>asah1b</i>	1	NM_200577	1717	Q6PH71	395	44.6	60%	Ch. 6, 7
CLN8, transmembrane ER and ERGIC protein	<i>cln8</i>	17	NM_001114588	1473	F1QYC0	289	33.8	61%	Pilot exp.
Niemann-Pick disease, type C1	<i>npc1</i> X2	2	XM_005163659	5059	F1QNG7	1276	143	69%	Pilot exp.

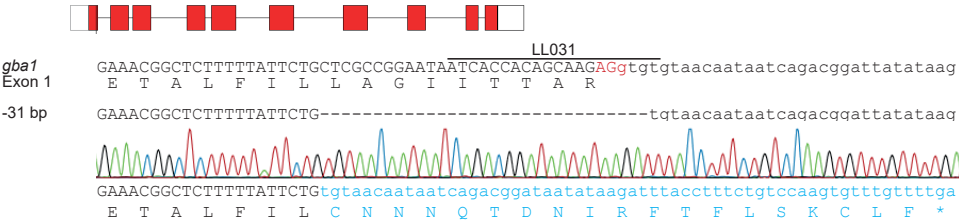
For every target, two sgRNA sequences were considered, given in **Supplementary Table 4**. Injection of sgRNA and Cas9 mRNA was performed as described above and multiple adult founder and F<sub>1</sub> zebrafish were screened until a suitable modification was found. To obtain the genetic zebrafish knockouts, more than 500 embryos were injected, approximately 130 founder F<sub>0</sub> fish were crossed and screened, while roughly 750 zebrafish of the F<sub>1</sub> generation were finclipped and screened. From the total screened founder fish, approximately 25% transmitted mutations to the offspring, although not all founder F<sub>0</sub> fish showed suitable modifications. Founder fish transmitting small (-1 bp, TMB010) or in-frame mutations (-6 bp, MB002) were discarded, while founder fish with large and frameshift germline transmitted mutations were selected (**Table 2**). F<sub>1</sub> zebrafish were finclipped, genotyped and selected based on the desired modifications (**Table 2**). Selected F<sub>1</sub> zebrafish were used for subsequent crossings generating both outbred, inbred and double mutant zebrafish lines (**Supplementary Table 1**).

Schematic representations of the target locus, location of the sgRNA, target sequence and obtained mutation with sequence trace of the verified genetic KO zebrafish are given in **Figure 4**.

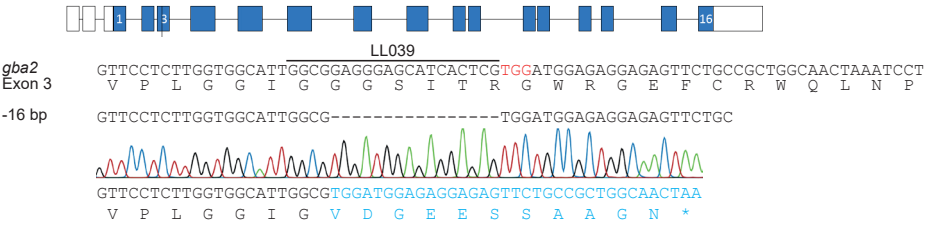


Chapter 4

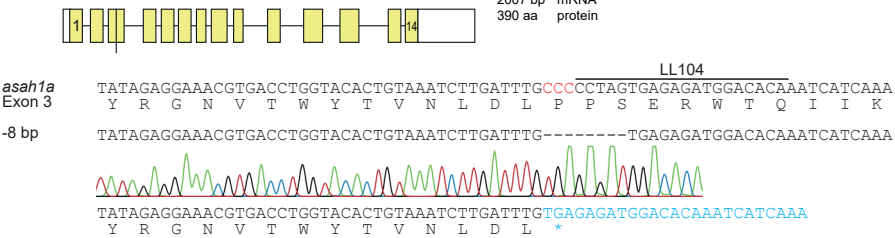
A. *Gba* (Chr16: 14,326,461-14,341,192)



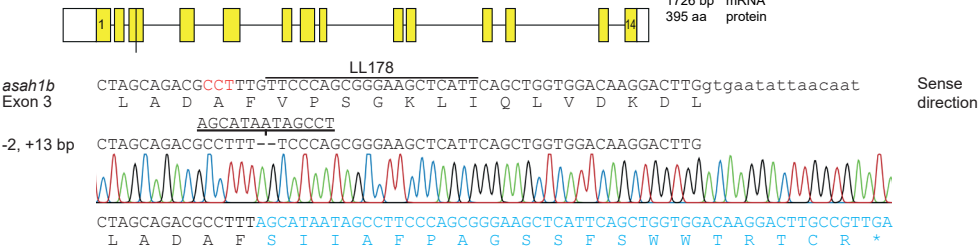
B. *Gba2* (Chr7: 24,374,029-24,402,239)



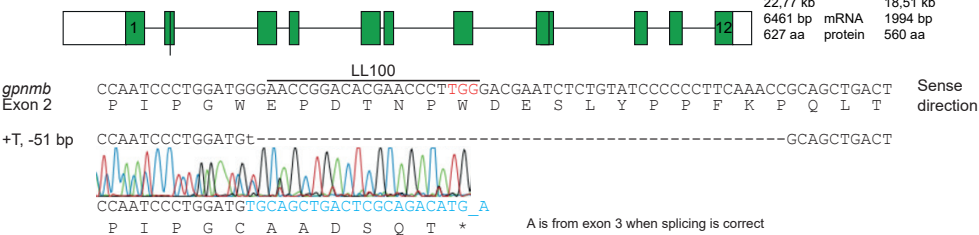
C.



D.



E.



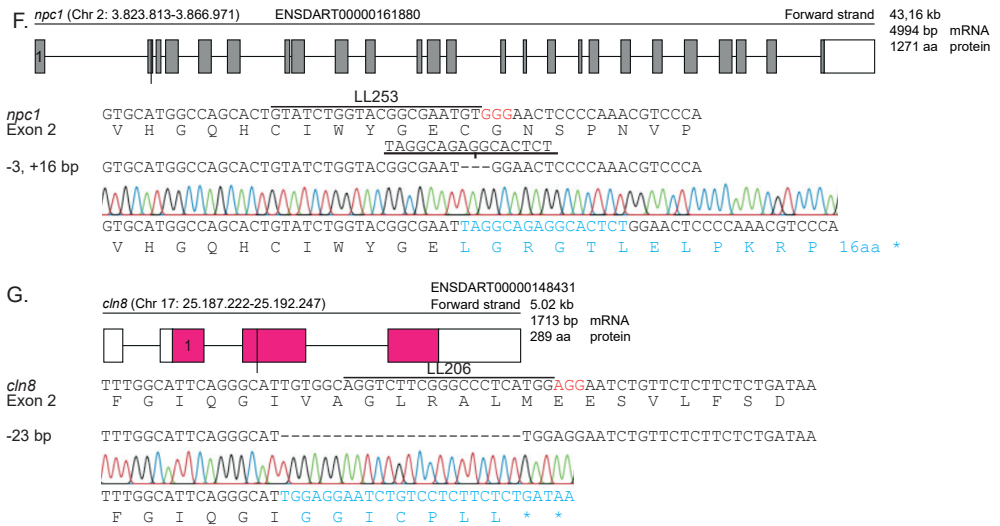


**Figure 4 | Schematic representation of the obtained CRISPR/Cas9 mediated genetic modifications.**

(A) *gba1* (B) *gba2* (C) *asah1a* (D) *asah1b* (E) *gpnmb* (F) *npc1* and (G) *cln8*. Top panel: schematic representation of the respective gene with the location and sequence of the sgRNA target given in Supplementary Table 1. Middle panel: DNA sequence of the WT target sequence, with the exon sequence in uppercase and intron sequence in lowercase, the sgRNA sequence lined above, PAM site in red and the protein sequence shown below. Lower panel: the mutation as obtained from the sequence trace and the predicted translated protein sequence. Of note, the sequence trace of a heterozygous *gpnmb* sample is displayed.

On average, ten fish are screened to obtain a suitable mutation. The number of screened fish necessary appeared to be dependent on the location of the sgRNA, the quality of the injected sgRNA and the internal sequence of the target. For example, the used sgRNA for *gba1* (LL031, **Figure 2B**) was in close proximity of the exon-intron transition (**Figure 2A**), therefore prediction of the *in silico* mutation using the sequence trace of heterozygous  $F_1$  zebrafish was difficult. The 31 base pair deletion was thought to remove the endogenous splice-site and this hypothesis was confirmed by sequencing cDNA of homozygous samples. Another example (LL038 of *gba2*), resulted in a high ratio of positive samples with the same 6 bp deletion, most likely due to high sequence similarity and microhomology-directed repair using small repeats in the target sequence. Together these findings affirm the importance of part 1 of the described protocol, especially the design and quality of the sgRNA. The possible repair mechanisms, on the other hand, are more difficult to predict, although machine learning is used to predict repair profiles and improve sgRNA design<sup>33</sup>.

As described before, mutant zebrafish are crossed with WT fish for several generations to obtain a heterogeneous outbred stock and thereby segregate unlinked mutation, lower off-target effects and improve general health. Typically, multiple individual zebrafish are crossed with different WT zebrafish, preferably from different WT stocks, in order to prevent selection of genetic variations in individuals.

Whole-genome sequencing was not considered to study off-target effects because of the known high genetic variation in laboratory zebrafish. Instead, the top off-targets of the *gba1* and *gba2* sgRNA sequences were sequenced. These off-targets were predicted using the CRISTA algorithm<sup>34</sup>. No mutations were found at the predicted CRISPR/Cas9 cut site in several individual homozygous mutants of different crossings (**Supplementary Figure 1**). Several indels and SNPs were found in WT and mutant fish, confirming the high genetic variation described above.

### Glycosphingolipid abnormalities in *npc1* and *cln8* knockouts

Knockouts of *gba1*, *gba2*, *asah1a* and *asah1b* are topics of the investigations in chapters 5-7. The *gpnmb*, *npc1* and *cln8* KO larvae have been generated and analysed in this chapter in pilot biochemical experiments. The protein gpNMB is remarkably induced in human Gaucher disease (GD) patients, GD mouse and zebrafish models<sup>35,36</sup>. At present, the physiological function of gpNMB during lysosomal stress is unknown. The ER protein CLN8 has been suggested as candidate modifier of clinical severity of GD. CLN8 is a member of the neuronal ceroid lipofuscinosis (NCL) associated proteins and is thought to be involved in the regulation of ceramide synthesis and glycosphingolipid trafficking<sup>37</sup>. Patients with a defect in CLN8 develop progressive epilepsy with mental retardation (EPMR) and brains displayed reduced levels of glycosphingolipids including ceramide, galactosylceramide and lactosylceramide<sup>38</sup>. In Niemann Pick disease (NPC) the efflux of cholesterol from lysosomes is impaired, due to defects in either NPC1 or NPC2. As a result, secondary (partial) deficiencies in sphingomyelinase (ASMase) and glucocerebrosidase cause accumulation of sphingomyelin, glucosylsphingosine (GlcSph), glucosylceramide (GlcCer) and glucosylcholesterol (GlcChol) in these cholesterol-laden lysosomes<sup>39,40</sup>.

First, glycosphingolipid levels of offspring of *npc1*<sup>-/-</sup> and *cln8*<sup>-/-</sup> inbreds were measured (**Figure 5A**). No significant differences were found for *cln8*<sup>-/-</sup> larvae compared to heterozygous or WT. Surprisingly, no change in GlcSph, GlcCer or GlcChol levels was found in the *npc1*<sup>-/-</sup> larvae as in *Npc1* mouse models<sup>39,40</sup>. The absence of secondary (glyco) sphingolipid abnormalities might be explained by the presence of maternal *Npc1* in the developing offspring, as observed for GCase<sup>41</sup> or the young age of the larvae in general. It suggests that the burden of lysosomal cholesterol is not sufficient enough to develop the proposed secondary deficiencies of ASMase and GCase.

Next, the impact of GCase deficiency in *npc1* or *cln8* genetic backgrounds was determined. Offspring of *npc1* and *cln8* carriers were incubated with a GCase-specific inhibitor for 5 days. Interestingly, *cln8*<sup>-/-</sup> zebrafish larvae showed significantly reduced GlcSph accumulation compared to their *cln8*<sup>+/+</sup> and *cln8*<sup>-/-</sup> siblings, while GlcCer and GlcChol levels in the *Cln8* deficient zebrafish were comparable to their WT and heterozygous counterparts. No apparent differences were found between *npc1*<sup>-/-</sup> zebrafish larvae and



their *npc1*<sup>+/+</sup> siblings, both showing increased GlcSph, GlcCer and GlcChol levels upon GCase inactivation. GlcSph levels appeared lower in the *npc1*<sup>-/-</sup> larvae, however limited biological *npc1* KO samples were evaluated in these pilot lipid analyses.

RT-qPCR analysis revealed a reduction of *npc1* mRNA expression in *npc1*<sup>-/-</sup> larvae compared to WT siblings. This finding indicates that the generated mutation has led to a gene knockout, albeit it is not known if a functional protein knockout is generated. Raising the *Npc1* deficient zebrafish to adulthood would enable analysis of cholesterol and (glyco) sphingolipid abnormalities in older fish in combination with observation of symptoms such as hepatosplenomegaly and neurological abnormalities as reported for other *npc1* KO zebrafish<sup>42</sup>.

No biochemical readout exists to study the endogeneous zebrafish Gpnmb protein and commercially available zebrafish anti-gpnmb antibodies were not reactive (data not shown). Quantification of levels of the *gpnmb* transcript from individual larvae revealed a reduction of mRNA levels in *gpnmb*<sup>-/-</sup> larvae compared to WT siblings (**Figure 5B**). However homozygous *gpnmb* KO adult fish showed no phenotype (data not shown). Upregulation of gpNMB expression has been reported in Gaucher cells of GD patients as well as mouse macrophages with induced lysosomal stress<sup>36,43</sup>. Crossing these *gpnmb* KO fish with animals having a *gba1* mutation could reveal a particular function of Gpnmb during lysosomal stress of macrophages.

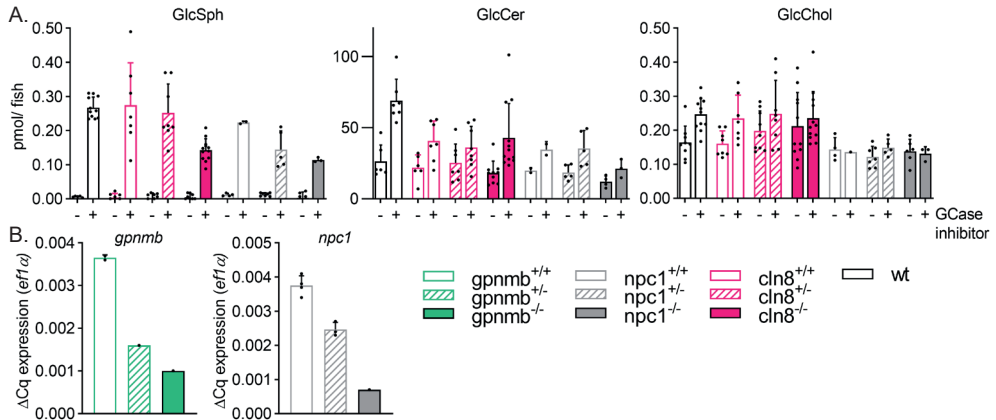


**Figure 5 | Biochemical impact of Cln8, Npc1 and Gpnmb deficiency**

**(A)** GlcSph, GlcCer and GlcChol levels were determined of untreated individual zebrafish larvae (5 dpf, - GCase inhibitor) or embryos treated with the GCase specific inhibitor ME656 (10  $\mu$  M) for 5 days (+ GCase inhibitor) in pmol/fish; WT (n = 9-11); data from<sup>41</sup>, *cln8*<sup>+/+</sup> (n = 7-8), *cln8*<sup>-/-</sup> (n = 8-9), *cln8*<sup>+/-</sup> (n = 12), *npc1*<sup>+/+</sup> (n = 2-4), *npc1*<sup>+/-</sup> (n = 5-7) and *npc1*<sup>-/-</sup> (n = 3-6). Data is depicted as mean  $\pm$  SD. **(B)** mRNA levels of *gpnmb* or *npc1* individual zebrafish larvae (5 dpf) as determined by RT-qPCR using specific primers. *Gpnmb*<sup>+/+</sup> (n = 2), *gpnmb*<sup>+/-</sup> (n = 1), *gpnmb*<sup>-/-</sup> (n = 1), *npc1*<sup>+/+</sup> (n = 4), *npc1*<sup>+/-</sup> (n = 3) and *npc1*<sup>-/-</sup> (n = 1).

### Random integration using the Tol2 transposase technique

As final part of the genome-editing approaches, the Tol2 transposase technique was used to integrate exogenous DNA. Random integration of a donor sequence is mediated by the Tol2 transposon element of the medaka fish (*Oryzias latipes*)<sup>44</sup>. Donor constructs, with the target sequence flanked by the required Tol2 sequences, are integrated by the transposase protein as a single copy with high germline transmission (> 30%)<sup>45,46</sup>. Two targets were chosen for proof-of-concept studies. First, it was appreciated that introduction of human *GBA* in the zebrafish *gba1* KO background could enable evaluating the biological impact of human GCase in the zebrafish GD model. Furthermore, it was rationalized that certain genes would not be suitable for CRISPR/Cas9 mediated genome editing. One such example is the gene encoding the prosaposin precursor protein which is cleaved to four activator lipid-binding proteins: saposin A, -B, -C and -D. Only Saposin C is required for optimal intralysosomal activity of GCase and defects in saposin C cause symptoms similar to Gaucher disease<sup>47-49</sup>. The zebrafish genome appeared to have one prosaposin (*psap*) gene, including annotated sequences for the activator lipid-binding proteins saposin A, -B, -C and -D. It was rationalized that CRISPR/Cas9 genome editing according to the above established protocol would generate a stop codon in the *psap* gene and thereby likely impact the other saposins as well. An alternative approach was considered by introducing a point mutation in the *psap* sequence (T>G, **Supplementary Figure 2**) which would result in a Cys to Gly amino acid substitution and impair one of the predicted disulfide bridges of zebrafish saposin C (predicted Sap C region underlined in **Supplementary Figure 2**)<sup>50</sup>.

Tol2 constructs were generated using the reported three-insert Gateway which combines three entry vectors into a destination vector with the required flanking Tol2 sequences<sup>45</sup>. The generated vectors included a ubiquitin promoter, followed by the target sequence and a polyadenylation signal in a destination vector with a cell-specific reporter cassette ( $\gamma$ -cryst:CFP). The reporter cassette allows easy selection of transgenic carriers because positive zebrafish embryos express the cyan fluorescent protein in their lens. A mixture of 20 pg donor vector and 150 pg SP6-generated capped and polyadenylated transposase mRNA was injected in single- or two-cell stage zebrafish embryos. As for the CRISPR/Cas9 method, the balance between high efficiency, by injecting in the cell cytoplasm with a high concentration of donor vector/Tol2 mRNA, and poor survival of injected zebrafish embryos should be experimentally defined. The concentration of the mixture in these pilot experiments was too high since more than 80% of the injected embryos died before they reached the larval age. However the success rate of Tol2 integration final rate was also high, because 2 out of 6 hGBA injected adult founder fish produced offspring with CFP expression in the lens, 1 of the 2 tested pSAP<sup>WT</sup> zebrafish and 1 of the 3 tested pSAP<sup>mut</sup> injected founder fish produced offspring showing CFP signal. Glycosphingolipid analysis of the generated hGBA:*gba*<sup>-/-</sup> zebrafish larvae revealed a significant lower accumulation of glucosylsphingosine (GlcSph), indicating that human GCase is expressed and functionally active (Chapter 5). The impact of the pSAP<sup>mut</sup>, on the other hand, has not been studied yet. It is necessary to mutate the endogenous zebrafish *psap* gene using the CRISPR/Cas9 protocol before an impact of the pSAP<sup>mut</sup> is expected.

## Discussion

A very practical advantage of zebrafish as research model, as compared to mice, is the speed and convenience of generating gene knockouts. This could allow evaluation of zebrafish with multiple genetic traits in a matter of months. This chapter provides a detailed protocol for generation of gene knockouts in zebrafish by means of CRISPR/Cas9 technology and efficient HRM analysis screening. In addition, established mutations are described, including those in the zebrafish *gba1*, *gba2*, *asah1a*, *asah1b*, *gpnmb*, *cln8* and *npc1* genes.

The protocol includes several notes and considerations for achieving a high mutagenesis efficiency without off-target effects which allows reduction of the amount of necessary injected founders and F<sub>1</sub> animals. To increase the probability of raising founders with a mutation, it is recommended to inject high quality RNA and evaluate the mutagenesis efficiency of multiple different sgRNAs for the same target, prior to baby raising. In general, it is advised to raise about 20 larvae to adulthood, as not all founder fish show germline transmitted mutations. Moreover, mutations do not always lead to frameshifts and some mutations could be small, which complicates the HRM analysis. When a suitable mutation is obtained in the F<sub>2</sub> generation, a reduction of necessary animals in subsequent generations could be achieved by performing mini finclips on larvae of 3-5 dpf<sup>51</sup>. The HRM analysis is a very suitable method as it allows screening in only a few hours.

The Tol2 transposon technique was successfully used to introduce exogenous DNA in the zebrafish genome. A limitation of this approach is the random integration of the target sequence as well as the regulation of expression by a non-endogenous promoter. These limitations can be circumvented by so-called knockin approaches after the generated CRISPR/Cas9 mediated double strand DNA break. This could allow for subsequent introduction of specific point mutations, generation of endogenous target proteins fused to a fluorescent reporter tag or combining an endogenous promoter with a fluorescent protein to express a reporter under the control of that promoter. Small precise modifications of the zebrafish genome have been achieved by directing the homology-directed repair (HDR) pathway to repair the CRISPR/Cas9 mediated double-stranded DNA break with a single-stranded oligodeoxynucleotide (ssODN) with the intended mutation<sup>52</sup>. For larger and more complex modifications, donor plasmids with long homology arms flanking the insert are frequently used to direct HDR with the donor sequence<sup>53</sup>, while another approach uses the dominant NHEJ repair system to insert donor DNA sequences at the target site<sup>54,55</sup>. Both the HDR and NHEJ approach have reported only low efficiency of germline transmission ( $\pm 5-7\%$ )<sup>52,53,55</sup>. At present, we have failed to obtain zebrafish with a precise mutation in *gba1* with the reported protocols, although only limited attempts have been performed and ideally many more embryos should be injected and screened.

In all subsequent chapters, zebrafish gene knockouts are used with stable and known out-of-frame mutations. Using the high efficiency of the CRSIPR/Cas9 system, it is also possible to study the biochemical impact of the knockout directly by evaluating the injected F<sub>0</sub> zebrafish embryos. It has been shown that injection of the sgRNA in complex with a Cas9 ribonucleoprotein can achieve sufficiently high levels of bi-allelic gene disruption in the injected F<sub>0</sub> zebrafish embryos, named crispants<sup>56-58</sup>. For example, 5 dpf crispants of the lysosomal enzyme  $\beta$ -hexosaminidase showed a 95% reduction in enzyme activity and similar phenotypic manifestations as larvae with a stable mutation<sup>58</sup>. Therefore, the crispant approach would be very efficient in combination with the sensitive biochemical analysis by means of activity-based probes (Chapter 3) and LC-MS/MS (Chapter 5). This approach could enable studying the impact of gene disruption in a matter of days, thereby accelerating the research on zebrafish models for lysosomal storage disorders.

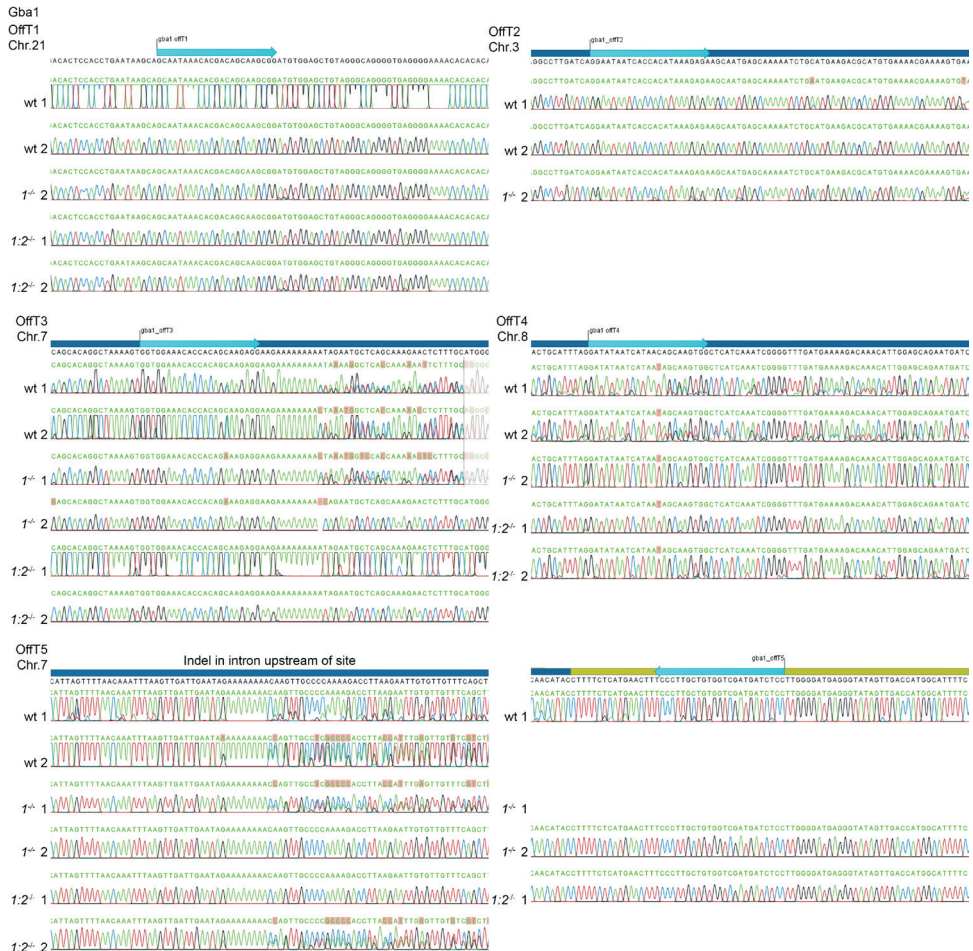
## Acknowledgments

Prof. Annemarie Meijer is kindly acknowledged for providing the pCS2-nCas9n plasmid as well as Dr. Vincenzo Torraca for initial CRISPR/Cas9 protocols. Ralf Boland and Dr. Bjørn Koch are acknowledged for their help with initial injections and Dr. Rolf Boot for generation of the tol2 constructs for human *GBA* as well as WT and mutant *psap*.

# Supplementary data

**Supplementary Table 1** | Available single-, double- and three-double knockouts

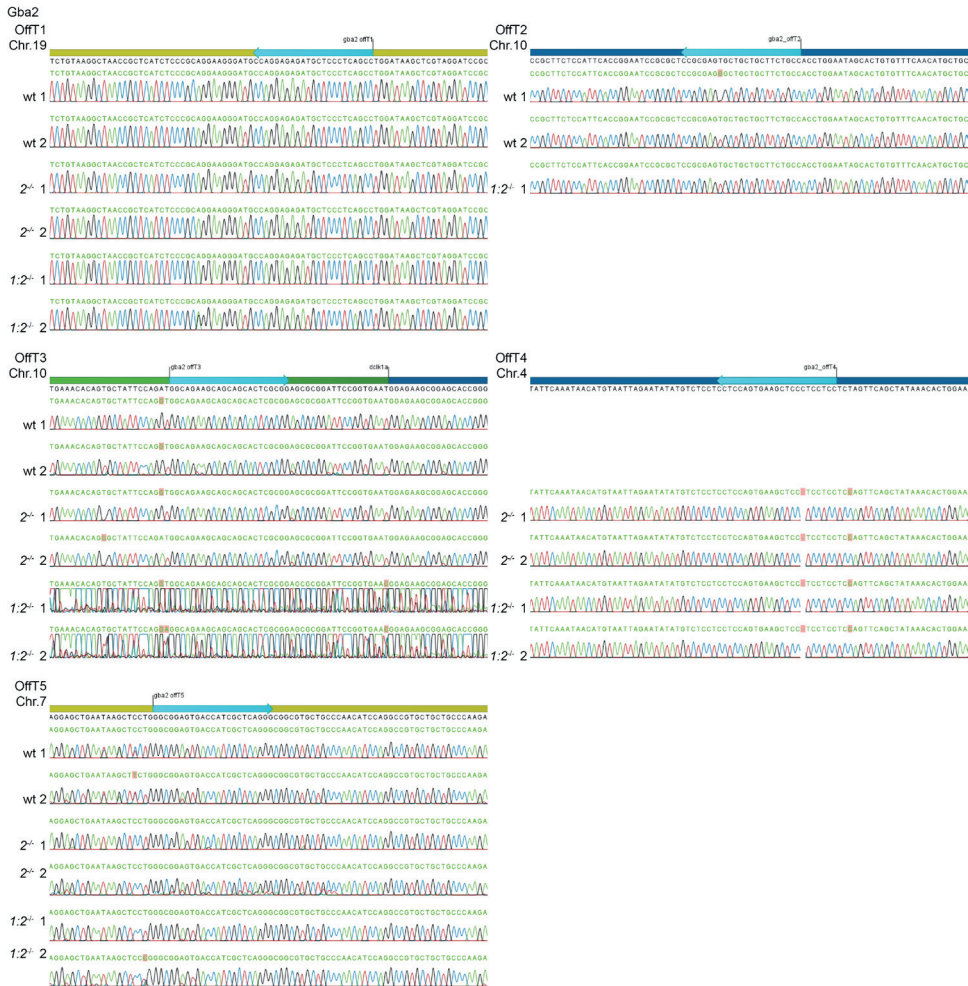
Target	sgRNA	Mutation	Lines
<i>Gba1</i>	LL031	- 31 nt	<i>gba1</i> <sup>-/-</sup> , <i>gba1</i> <sup>-/-</sup> in <i>mpeg:GFP</i> , <i>gba1</i> <sup>-/-</sup> in <i>2CLIP</i> , <i>gba1</i> <sup>-/-</sup> : <i>gba2</i> <sup>-/-</sup> , <i>gpnmb</i> <sup>-/-</sup> : <i>gba1</i> <sup>-/-</sup> , <i>asa</i> <sup>-/-</sup> : <i>h1a</i> <sup>-/-</sup> : <i>gba1</i> <sup>-/-</sup> , <i>asah1b</i> <sup>-/-</sup> : <i>gba1</i> <sup>-/-</sup> , <i>asah1a</i> <sup>-/-</sup> : <i>asah1b</i> <sup>-/-</sup> : <i>gba1</i> <sup>-/-</sup>
<i>Gba2</i>	LL039	- 16 nt	<i>gba2</i> <sup>-/-</sup> , <i>gba2</i> <sup>-/-</sup> , <i>gba1</i> <sup>-/-</sup> : <i>gba2</i> <sup>-/-</sup>
<i>gpnmb</i>	LL100	+ T, -50 bp	<i>gpnmb</i> <sup>-/-</sup>
<i>Asah1a</i>	LL104	- 8 bp	<i>asah1a</i> <sup>-/-</sup> , <i>asah1a</i> <sup>-/-</sup> : <i>asah1b</i> <sup>-/-</sup> , <i>asah1a</i> <sup>-/-</sup> : <i>gba1</i> <sup>-/-</sup> , <i>asah1a</i> <sup>-/-</sup> : <i>asah1b</i> <sup>-/-</sup> : <i>gba1</i> <sup>-/-</sup>
<i>Asah1b</i>	LL178	- 2, +13 bp	<i>asah1b</i> <sup>-/-</sup> , <i>asah1a</i> <sup>-/-</sup> : <i>asah1b</i> <sup>-/-</sup> , <i>asah1b</i> <sup>-/-</sup> : <i>gba1</i> <sup>-/-</sup> , <i>asah1a</i> <sup>-/-</sup> : <i>asah1b</i> <sup>-/-</sup> : <i>gba1</i> <sup>-/-</sup>
<i>Npc1</i>	LL253	- 3, +16 bp	<i>asah1b</i> <sup>-/-</sup> : <i>npc</i> <sup>-/-</sup>
<i>Cln8</i>	LL206	- 23 bp	<i>Cln8</i> <sup>-/-</sup>



**Supplementary Figure 1**

No mutations were found in *gba1*<sup>-/-</sup>, *gba2*<sup>-/-</sup> or *gba1*<sup>-/-</sup>:*gba2*<sup>-/-</sup> samples on the predicted off-targets using the CRISTA algorithm<sup>34</sup> for LL031 (*gba1*) and LL039 (*gba2*; Next page). Predicted off-target sequences are depicted with a light blue box, intron sequence with blue box, mRNA sequence with green box and coding sequence with yellow box.

## Chapter 4



► **Supplementary Figure 2** | Coding sequence of prosapin with the (T/G) point mutation in red, leading to the suspected loss-of-function Cys > Gly mutation of saposin C. The saposin C region of zebrafish prosapin is predicted using a blastp alignment of the reported human saposin C sequence. The predicted saposin C region of the zebrafish is underlined.



ATG ATG CTT CTC ACG CTT CTT TTG GTC ACC ACA GCT GTG GCA AGT CCC CTG TTG GGA ACG  
 M M L L T L L L V T T A V A S P L L G T  
 GAG CAG TGT GCC CGT GGT CCC CCC TAC TGG TGC CAG AAT GTC AAG ACC GCT TCC CTT TGT  
 E Q C A R G P P Y W C Q N V K T A S L C  
 GGT GCT GTC CAG CAC TGC CAA CAG AAT GTG TGG AAC AAG CCT CAG ATG AAA ACT GTG CCA  
 G A V Q H C Q Q N V W N K P Q M K T V P  
 TGT GAT CTG TGC AAA GAG GTG TTG GTG GTA GTG GAG CAG CTG CTG AAG GAC AAT GTA ACC  
 C D L C K E V L V V V E Q L L K D N V T  
 GAG AGC GAA CTC CTC GGG TAT TTG GAG AAG GCA TGT CAG CTG ATC CCT GAT GAG GGC CTG  
 E S E L L G Y L E K A C Q L I P D E G L  
 GCT AAC CAG TGC AAG GAG ATT GTG GAC AAC TAC TTC CCA GTT CTC ATG GGC ATC ATC CAA  
 A N Q C K E I V D N Y F P V L M G I I Q  
 GGA GAG CTG GAT GAC CCT GGT GTA GTG TGT GGC GCT TTG GGT CTG TGC GTA TCC CAG CAG  
 G E L D D P G V V C G A L G L C V S Q Q  
 GCA GCT CTG GCT AAA GCT CAG CTC ACT TCC AAC GAG ATC CCT CAA GTG GAC CTG AAT CAA  
 A A L A K A Q L T S N E I P Q V D L N Q  
 CGC GTC AGC CCC TTC CTG CTG AAC ATC CCA CAG CTG CTC TAT CCT GAA GAG AAA AGA GAG  
 R V S P F L L N I P Q L L Y P E E K R E  
 ACC CCT AAA CAG AAA GGT GAT GTG TGC CAG GAC TGT GGC GTT ATC TTC ACT GAC ACT CAG  
 T P K Q K G D V C Q D C V T F I T D T Q  
 GAT GAA GCC AGA ATC AAT TCT TCC TTT ATC AAC ACT CTG ATT GCA CAG GTG GAG AAC CAG  
 D E A R I N S S F I N T L I A Q V E N Q  
 TGT GAG CTT CTG GGA CCT GGA ATG TCT GAT ATG TGC AAG GAG TAC ATC AGC CAG TAC GGG  
 C E L L G P G M S D M C K E Y I S Q Y G  
 CCT CTG GTC TTC CAG CAG CTC ATG TCT ATG CAA CCC AAG GAC ATC TGT GCT CGC GCT GGC  
 P L V F Q Q L M S M Q P K D I C A R A G  
 TTC CAG CCT ACT AAA CAA AAG TCT GTG CCC ATG GAG AAG CTG CTG GCT GCC AAA TCC ATC  
 F C P T K Q K S V P M E K L L P A K S I  
 CCT GCT GTC AAG ATG TTC CCT GCG GTT AAA GTT GAG AAA CCG GTT GCG ACC ATG CCT GCT  
 P A V K M F P A V K V E K P V A T M P A  
 AAG AAC CTG GTG CGT GTG CGT GAC TCT CCT CAG TGT GCC ATC TGT GAA TAT GTG ATG AAG  
 K N L V R V R D S P Q C A I C E Y V M K  
 GAA ATT GAG AAC ATG ATT CAG GAT CAG ACC TCT GAG GCA GAG ATC GTG CAG GCT GTG GAG  
 E I E N M I Q D Q T S E A E I V Q A V E  
 AAG GTC TGC AAC ATT TTG CCC TCC ACA CTC ACT GCT CAG TGC AAG GAC CTG ATT GAA ACC  
 K V C N I L P S T L T A Q C K D L I E T  
 TAC GGC CAG GCC ATC ATC GAT CTC CTT GTG CAG GAG GCC GAT CCC AAA ACG GTC GGC TCT  
 Y G Q A I I D L L V Q E A D P K T V G(C) S  
 TTC CTT GCA CTC TGC AGT GGG GTC AGC CAT GTC CCT GTG ATG GAT AAG CAG CAT TTC GCA  
 F L A L C S G V S H V P V M D K Q H F A  
 GCA GGT GGT TTC TGT GAT GTG TGC AAG ATG GCT GTG CGC TAT GTG GAC GGG ATC CTG GAG  
 A G G F C D V C K M A V R Y V D G I L E  
 CAG AAC GCC ACT CAG TCT GAG ATC GAG GAG GCC GTG CTG AAA GTC TGC AGC TTC CTG CCT  
 Q N A T Q S E I E E A V L K V C S F L P  
 GAC GCC GTC AAA GAT GAG TGC AAC CAG CTG ATT GAG CAG TAC GAG CCT CTG CTG GTG CAG  
 D A V K D E C N Q L I E Q Y E P L L V Q  
 CTG CTG CTT CAG ACC CTC GAC CCT GAC TTT GTC TGC ATG AAG CTG GGA GCA TGT CCT GAG  
 L L L Q T L D P D F V C M K L G A C P E  
 GCC GTG CAG AGG CTG CTG GGA TTA AAT CAG TGC AGC TGG GGG CCT GCA TAC TGG TGT AAG  
 A V Q R L L G L N Q C S W G P A Y W C K  
 AAC GTG CAG ACC GCC GCT CGC TGT AAC GCC CTG AAC CAC TGC AGG CGT CAC GTT TGG AGC  
 N V Q T A A R C N A L N H C R R H V W S  
 TAA < 1563

\*

## Experimental procedures

**Zebrafish husbandry and lines** - Zebrafish were housed and maintained at Leiden University, the Netherlands, according to standard protocols and described in Chapters 3, 5, 6, 7 and ref 41. Wild-type (WT) zebrafish (ABTL) were a mixed lineage of WT AB and WT TL genetic background. Injections to generate CRISPR/Cas9 mediated knockout (KO) zebrafish were performed in ABTL embryos. Adult zebrafish were outcrossed to ABTL WT zebrafish for several rounds before incrossing. Obtained zebrafish lines were kept as carriers (heterozygous in genotype) and several adult zebrafish of one genetic, mutant line were outcrossed to different WT fish. This type of outcrossing was performed to segregate potential unlinked off-target mutations and to improve a healthy genetic background by preventing sibling mating.

### Reagents and equipment

**Supplementary Table 2** | List of ingredients reagents including supplier and article number

Reagent	Supplier	
Oligonucleotides for sgRNA synthesis	IDT, Newark, USA	Supplementary Table 1
T4 DNA polymerase	Invitrogen, Carlsbad, SA	18005017
dNTPs	Promega, Madison, USA	U1240
Nucleospin PCR and gel clean-up kit	Macherey-Nagel, Duren, Germany	740609250
DEPC treated RNase free H <sub>2</sub> O	In-house	
MEGAscript <sup>TM</sup> T7 Transcription kit	Ambion®, ThermoFisher, Waltham, USA	AM1354
Ethanol (HPLC grade)	VWR, Nederland	1009831000
pCS2-nCas9n	Addgene, Watertown, USA	#47929
NotI	New England Biolabs, Ipswich, USA	R0189L
Zymo DNA clean & concentrator <sup>TM</sup>	Zymo, Irvine, USA	D4004
mMessage mMachine SP6 kit	Ambion®, ThermoFisher	AM1340
RNeasy mini kit	Qiagen, Hilden, Germany	74104
Capillaries		
QuickExtract <sup>TM</sup>	EpiCentre®, Madison, USA	QE09050
IQ SYBR green	Bio-Rad, Hercules, USA	172-5006
Clear 96 PCR plate	Sarstedt, Nümbrecht, Germany	721978202
Phusion high-fidelity DNA polymerase	ThermoFisher	F530 L

**Supplementary Table 3** | List of equipment including supplier

Equipment	Supplier	Notes
PCR machine	Bio-Rad	
DeNovix DS-11	DeNovix, Wilmington, USA	
Bio-Rad CFX96 Touch <sup>TM</sup> Real-Time PCR	Bio-Rad	
P-97 Flaming/Brown micropipette	Sutter instruments	Program 9
puller		
M-33 micromanipulator	Sutter instruments	Injection setup
Eppendorf <sup>TM</sup> Femtojet	ThermoFisher	t= 0.2 s, p= 200-600 Pa Injection setup To obtain 1nL injections
Stereo microscope	Leica M50, Wetzlar, Germany	Injection setup
Dumont <sup>TM</sup> forceps #5	Fine Science tools, Foster city, USA	To break the needle

### Reagent preparation

***In vitro* synthesis of sgRNA:** Adapted from Gagnon and colleagues <sup>26</sup>

Double-stranded DNA (dsDNA) template

- 2 µL Forward oligo (100 µM, **Supplementary Table 4**), 2 µL Reverse oligo (100 µM, LL030) and 16µL MQ
- Anneal: 95°C 5 min, 95°C → 85°C with -2°C/s, 85°C → 25°C with -0,1°C/s, hold at 11°C
- Make premix: 8 µL 5x T4 buffer, 5 µL dNTPs (10 mM), 0.5 µL T4 polymerase and 6 µL Milli-Q for each reaction
- Add 20 µL of T4 DNA mix, incubate for 20 min to 1 h at 12 °
- Add 60 µL Milli-Q and 400 µL MilliQ:NTI (1:1 (v/v)) of the Nucleospin PCR and gel clean-up kit
- Purify according to suppliers instruction

- Elute in 20 µL RNase free H<sub>2</sub>O
- Determine the concentration of the dsDNA template ( ± 200-300 ng/µL)

**Supplementary Table 4** | Single-guide RNA sequences with the T7 promoter underlined, the target specific sequence (20 nucleotides) in bold and single-nucleotide mutations are given as lower case. RNA synthesis starts from the second-to-last 'G' nucleotide of the T7 promoter.

Target	Exon	Code	Sequence 5'→3'
<i>Gba1</i>	1	LL031	GCGTAATACGACTCACTATAG <b>GGATAATCACCACAGCAAG</b> GTTTTAGAGCTAGAAATAGC
<i>Gba2</i>	3	LL038	GCGTAATACGACTCACTATAG <b>gTTCCTCTGGTGGCATT</b> GGGTTTTAGAGCTAGAAATAGC
	3	LL039	GCGTAATACGACTCACTATAG <b>GGCGGAGGGAGCATCACT</b> CGGTTTTAGAGCTAGAAATAGC
<i>gpnmb</i>	2	LL098	GCGTAATACGACTCACTATAG <b>gCAGCTGCGGTTTGAAGGG</b> GTTTTAGAGCTAGAAATAGC
	2	LL099	GCGTAATACGACTCACTATAG <b>GGATACAGAGATT</b> CGTCCCAGTTTTAGAGCTAGAAATAGC
	2	LL100	GCGTAATACGACTCACTATAG <b>GGGAACCGGACACGAACCT</b> GTTTTAGAGCTAGAAATAGC
<i>Asah1a</i>	3	LL104	GCGTAATACGACTCACTATAG <b>gTGTCCTATCTCTCACTAGG</b> GTTTTAGAGCTAGAAATAGC
	3	LL105	GCGTAATACGACTCACTATAG <b>gTATAGAGGAACGTGACC</b> GTTTTAGAGCTAGAAATAGC
<i>Asah1b</i>	4	LL108	GCGTAATACGACTCACTATAG <b>gCAGACGCCTTTGTTCC</b> CAGGTTTTAGAGCTAGAAATAGC
	4	LL109	GCGTAATACGACTCACTATAG <b>GGGAAGCTCATT</b> CAGCTGGGTTTTAGAGCTAGAAATAGC
	4	LL178	GCGTAATACGACTCACTATAG <b>gGCTTCCCGCTGGGAACA</b> AGTTTTAGAGCTAGAAATAGC
	4	LL179	GCGTAATACGACTCACTATAG <b>gATCATGCTCGCCATCTGA</b> GTTTTAGAGCTAGAAATAGC
<i>Ncp1</i>	2	LL253	GCGTAATACGACTCACTATAG <b>GTATCTGGTACGGCGAATGT</b> GTTTTAGAGCTAGAAATAGC
	2	LL254	GCGTAATACGACTCACTATAG <b>GCAGCTCCTGTCCTTCATT</b> GTTTTAGAGCTAGAAATAGC
<i>Cln8</i>	3	LL206	GCGTAATACGACTCACTATAG <b>gGTCTTCGGGCCCTCATGG</b> GTTTTAGAGCTAGAAATAGC
	3	LL207	GCGTAATACGACTCACTATAG <b>gGAACAGATTCCCTCATGA</b> GTTTTAGAGCTAGAAATAGC

#### Transcribe sgRNA using MEGAShortscript™ T7 Transcription kit

!! Use RNase free vials, filter tips, gloves, RNase free H<sub>2</sub>O.

- 0.5 µL 10x buffer, 0.5 µL each of ATP, GTP, UTP and CTP, 0.5-1.5 µL of dsDNA, 0.5 µL of T7 enzyme and add Nuclease-free water to 5 µL.
- Incubate at 37 °C for 3 h to overnight (run 0.5 µL of RNA sample on 1 % agarose gel to evaluate synthesis)
- Add 14 µL RNase free H<sub>2</sub>O + 1 µL Turbo DNase and incubate 15 min at 37 °C
- Add 10 µL 5 M NH<sub>4</sub>OAc (supplied in the kit) and 60 µL 100% ethanol (! Use freshly prepared 75% ethanol)
- Freeze for 30 min to 1 h at -80 °C
- Centrifuge 15 min at 4 °C. Remove supernatant & wash with 1 mL 75 % ethanol
- Centrifuge 10 min at 4 °C, remove all supernatant
- Dry 5 min at RT
- Resuspend in 20 µL RNase free H<sub>2</sub>O. Determine the concentration & run 0.5 µL on 1% agarose gel
- Store 2 µL aliquots at -80 °C to avoid freeze-thaw cycles

#### Cas9 mRNA

- Linearize 1 µg pCS2-nCas9n with NotI for 1 h at 37 °C
- Purify using Zymo DNA clean & concentrator™ and determine the concentration
- Transcribe Cas9 mRNA in 20 µL according to manufacturer's instruction (mMessage mMachinery SP6)
- Clean-up with the RNeasy kit according to the instructions.
- Elute in 20 µL RNase-free water (included in the RNeasy kit), measure the RNA concentration and check the integrity of the Cas9 mRNA on 1% agarose gel.
- Store at -80 °C in 2 µL aliquots to avoid freeze-thaw cycles

## Chapter 4

### Microinjection

- Setup single crossings of WT zebrafish a day prior to injection
- Mix SgRNA, Cas9 mRNA, 0.5 µL phenol red and Milli-Q to a total volume of 5 µL. Final concentration of sgRNA and Cas9 mRNA is dependent on stock concentrations and integrity of the RNA as well as required mutagenic efficiency and mortality rate. Store sgRNA/Cas9 mRNA mix on ice before use.
- Remove the spacer of the single crossings in order to allow mating
- Pull needles with program 9 of the P-97 Flaming/Brown micropipette puller
- Pipet 4 µL in the pulled needle and setup the microinjector setup in order to inject a volume of 1 nL. Change the pressure of the Eppendorf™ Femtojet until a droplet of 1 nL is achieved.
- Place a microscopy slide in a 10 cm plastic petri dish, place the zebrafish embryos along the slide and remove excess water.
- Inject 1 nL in one- or two cell-stage embryos.
- Transfer injected embryos to a petri dish with egg water
- Remove and note the number of unfertilized, dead and deformed embryos
- To test mutagenesis efficiency, mini-finclip embryo at 4-5 dpf or extract genomic DNA from the entire larvae

### Genomic DNA extraction

- Use 10µL QuickExtract per embryo and 15-20µL per finclip of an adult fish in PCR tubes or 96-well plate
- Incubate at 65°C for 10 min followed by 5 min at 98 °C
- Vortex samples to mix, dilute to 100 µL with Milli-Q, spin down quickly to pellet all non-processed particles which could interfere in the PCR reaction. Only use supernatant in PCR reactions.

### HRM analysis (Work in columns: in order to efficiently use the multichannel & excel sheet)

- Master mix: 5 µL IQ SYBR green, 0.3 µL forward primer, 0.3 µL reverse primer (300 µM final concentration of each primer, **Supplementary Table 5**) and 3.4 µL MQ per sample.
- Use dedicated set of multichannel pipettes, to prevent possible contamination
- Add 9 µL HRM mix to each well of a PCR plate → Add 1 µL of gDNA
- Settings for CFX96 Real-Time PCR machine:
  - 95 °C for 3 min; 40x [95°C for 30 sec, 61°C for 30 sec, image plate]; hold at 55 °C for 30 sec; melt program [55-95°C with 0,5°C per step, image plate every step]
- Export melt curve data and process in excel sheet

**Supplementary Table 5 |** Primers for high-resolution melting (HRM) analysis and fragment size

Target	Forward	Sequence 5'->3'	Reverse	Sequence 5'->3'	Fragment
<i>Gba1</i>	LL044	AGTCTCATCGGCAGGATGAG	LL045	CACTTGGACAGAAAGGTAAATC	123 bp
<i>Gba2</i>	LL042	GTATGTGTTGTTTTTTCAGGC	LL043	GCAATAACGGTTTTGTAGTGG	141 bp
<i>Gpnmb</i>	LL101	CAATACATTCTTACCATGCTGTC	LL102	CAGCATATGGTGACATGTTCCC	149 bp
<i>Asah1a</i>	LL106	GTCTAGACTCGAATAAGTTCATG	LL107	TGGGAAACAGTTACCTCTGTG	169 bp
<i>Asah1b</i>	LL110	TGCAAAGAGATGTGTTAGATTG	LL111	TCCTTCAGATGGCGAGCATG	128 bp
<i>Npc1</i>	LL255	GGACCGGTGTAATTGCAGTTCAAC	LL256	GAAGTTGAACTGCAATTACACCG	152 bp
<i>Cln8</i>	LL208	TTCTAGGTTTTCTGGGATTGGC	LL209	AGGACCAGTCTTCTGTCCGAG	133 bp

PCR reaction for sequencing using phusion polymerase

- Master mix for 20 µL PCR reaction: 4 µL 5x HF buffer, 1 µL forward primer, 1 µL reverse primer (10 µM each, **Supplementary Table 6**), 0.4 µL dNTPs (10 mM), 0.2 µL phusion polymerase, 12.4 µL Milli-Q and 1 µL genomic DNA
- Settings of general PCR machine: Den. at 98 °C for 2 min; 35x [98 °C for 10 s, 65 °C for 15 s, 72 °C for 20 s] and a final extension at 72 °C for 5 min.
- Purify PCR product using Zymo DNA Clean & Concentrator™ and elute in 20 µL MQ
- 125-250 ng purified pcr product (size of 300-700 bp), 1 µL of sequence primer (10 µM, either forward or reverse primer, **Supplementary Table 6**) and Milli-Q to a total volume of 10 µL. Sanger sequencing is performed by Macrogen.

**Supplementary Table 6 |** Primers to obtain DNA fragments for Sanger sequencing and fragment size

Target	Forward	Sequence 5'→3'	Reverse	Sequence 5'→3'	Fragment
<i>Gba1</i>	LL023	CATTGCCATTTTCGTTTTTAGG	LL007	GGAAGTGTCTTGACTCTCCAT	439 bp
<i>Gba2</i>	LL036	AATGGTGGTACCGAAAGACC	LL037	AGTACTACAGACTTCATCTGC	322 bp
<i>Gpnmb</i>	LL145	AGCCTAATCGTTGTAATACTCG	LL102	CAGCATATGGTGACATGTTCCC	295 bp
<i>Asah1a</i>	LL146	TGGGATGTATCCACCTAAAGG	LL147	CAGCAAGCAAAAAGATGGACAG	251 bp
<i>Asah1b</i>	LL176	TACGATTTTGGGAGATTATCTC	LL147	CAGCAAGCAAAAAGATGGACAG	451 bp
<i>Npc1</i>	LL321	AGATATTGTCCAACAGAGCATTC	LL258	GTTTCCGATACAAAGCTAACGG	307 bp
<i>Cln8</i>	LL259	TGAATAAGACAGCATTTGAAGCAAC	LL260	CAGTTCACACAACCGCCCTGTC	439 bp

Tol2-mediated transgenesis - The coding sequences of zebrafish prosaposin (NCBI code NM\_001309267) was amplified using generated cDNA of a pool of 5 dpf zebrafish larvae (SuperScript II™ reverse transcriptase, Thermo Fisher Scientific) as template and Phusion high-fidelity DNA polymerase using the primers described in **Supplementary Table 7**. The fragment was subsequently cloned into the pDONR entry vector using GATEWAY™ technology (BP reaction) according to the manufacturer's instruction. The point mutation was introduced in the *psap* pDONR vector using the QuickChange Lightning Site-Directed Mutagenesis Kit (Agilent, Santa Clara, USA) according to the suppliers protocol with the primers given in **Supplementary Table 7**. Generation of the human *GBA* pDONR construct described in chapter 2. The pDONR vectors were sequenced before generating the final destination vector. Destination vectors were obtained by recombining entry vectors of p5E-ubi, pDONR-target and p3E-IRES-GFP-PA with pDEST-Tol2-crystalEye using a LR reaction. The pCS2FA-transposase plasmid was linearized with *NotI* and purified using Zymo DNA clean & concentrator™. Capped and polyadenylated transposase mRNA was generated using the mMessage mMachine SP6 kit and purified using the RNaseasy mini kit as described for Cas9 mRNA. The concentration was determined, the integrity checked on agarose gel and aliquots stored at -80 °C until use.

**Supplementary Table 7 |** Primers to generate pDONR entry vectors (pME)

Target	Sequence 5'→3'	Construct
<i>psap</i> F	GGGGACAAGTTTGTACAAAAAAGCAGGCTTAAACCACCATGATGCTTCTCAGCCTTC	pME-psap WT
<i>psap</i> R	GGGGACCACTTTGTACAAAGAAAGCTGGGTcTTAGCTCCAAACGTGACGC	pME-psap WT
<i>psap</i> -mut F	GCCGATCCCAAAACGGTCggcTCTTTCTTGCACCTCTG	pME-psap mut
<i>psap</i> -mut R	CAGAGTGCAAGGAAAGAgccGACCGTTTGGGATCGGC	pME-psap mut

## References

- Collins F.S., Green E.D., Guttmacher A.E., Guyer M.S. and Institute U.S.N.H.G.R. (2003) A vision for the future of genomics research. *Nature* **422**, 835-847.
- Komor A.C., Badran A.H. and Liu D.R. (2017) CRISPR-Based Technologies for the Manipulation of Eukaryotic Genomes. *Cell* **169**, 559.
- Chen K.Y. and Knöpfel P.S. (2016) To CRISPR and beyond: the evolution of genome editing in stem cells. *Regen Med* **11**, 801-816.
- Bibikova M., Golic M., Golic K.G. and Carroll D. (2002) Targeted chromosomal cleavage and mutagenesis in *Drosophila* using zinc-finger nucleases. *Genetics* **161**, 1169-1175.
- Christian M., Cermak T., Doyle E.L., Schmidt C., Zhang F., Hummel A.,... and Voytas D.F. (2010) Targeting DNA double-strand breaks with TAL effector nucleases. *Genetics* **186**, 757-761.
- Jansen R., Embden J.D., Gaastera W. and Schouls L.M. (2002) Identification of genes that are associated with DNA repeats in prokaryotes. *Mol Microbiol* **43**, 1565-1575.
- Brouns S.J., Jore M.M., Lundgren M., Westra E.R., Slijkhuys R.J., Snijders A.P.,... and van der Oost J. (2008) Small CRISPR RNAs guide antiviral defense in prokaryotes. *Science* **321**, 960-964.
- Deveau H., Barrangou R., Garneau J.E., Labonte J., Fremaux C., Boyaval P.,... and Moineau S. (2008) Phage response to CRISPR-encoded resistance in *Streptococcus thermophilus*. *J Bacteriol* **190**, 1390-1400.
- Garneau J.E., Dupuis M.E., Villion M., Romero D.A., Barrangou R., Boyaval P.,... and Moineau S. (2010) The CRISPR/Cas bacterial immune system cleaves bacteriophage and plasmid DNA. *Nature* **468**, 67-71.
- Jinek M., Chylinski K., Fonfara I., Hauer M., Doudna J.A. and Charpentier E. (2012) A programmable dual-RNA-guided DNA endonuclease in adaptive bacterial immunity. *Science* **337**, 816-821.
- Gasiunas G., Barrangou R., Horvath P. and Siksnys V. (2012) Cas9-crRNA ribonucleoprotein complex mediates specific DNA cleavage for adaptive immunity in bacteria. *Proc Natl Acad Sci U S A* **109**, E2579-2586.
- Jinek M., East A., Cheng A., Lin S., Ma E. and Doudna J. (2013) RNA-programmed genome editing in human cells. *Elife* **2**, e00471.
- Mali P., Yang L., Esvelt K.M., Aach J., Guell M., DiCarlo J.E.,... and Church G.M. (2013) RNA-guided human genome engineering via Cas9. *Science* **339**, 823-826.
- Cong L., Ran F.A., Cox D., Lin S., Barretto R., Habib N.,... and Zhang F. (2013) Multiplex genome engineering using CRISPR/Cas systems. *Science* **339**, 819-823.
- Hwang W.Y., Fu Y., Reyon D., Maeder M.L., Tsai S.Q., Sander J.D.,... and Joung J.K. (2013) Efficient genome editing in zebrafish using a CRISPR-Cas system. *Nat Biotechnol* **31**, 227-229.
- Kuscu C., Arslan S., Singh R., Thorpe J. and Adli M. (2014) Genome-wide analysis reveals characteristics of off-target sites bound by the Cas9 endonuclease. *Nat Biotechnol* **32**, 677-683.
- Wu X., Scott D.A., Kriz A.J., Chiu A.C., Hsu P.D., Dadon D.B.,... and Sharp P.A. (2014) Genome-wide binding of the CRISPR endonuclease Cas9 in mammalian cells. *Nat Biotechnol* **32**, 670-676.
- Pattanayak V., Lin S., Guilinger J.P., Ma E., Doudna J.A. and Liu D.R. (2013) High-throughput profiling of off-target DNA cleavage reveals RNA-programmed Cas9 nuclease specificity. *Nat Biotechnol* **31**, 839-843.
- Howe K., Clark M.D., Torroja C.F., Torrance J., Berthelot C., Muffato M.,... and Stemple D.L. (2013) The zebrafish reference genome sequence and its relationship to the human genome. *Nature* **496**, 498-503.
- Cornet C., Di Donato V. and Terriente J. (2018) Combining Zebrafish and CRISPR/Cas9: Toward a More Efficient Drug Discovery Pipeline. *Frontiers in pharmacology* **9**, 703.
- Postlethwait J., Ruotti V., Carvan M.J. and Tonellato P.J. (2004) Automated analysis of conserved syntenies for the zebrafish genome. *Methods Cell Biol* **77**, 255-271.
- Meyer A. and Schartl M. (1999) Gene and genome duplications in vertebrates: the one-to-four (-to-eight in fish) rule and the evolution of novel gene functions. *Curr Opin Cell Biol* **11**, 699-704.
- Guryev V., Koudijs M.J., Berezikov E., Johnson S.L., Plasterk R.H., van Eeden F.J. and Cuppen E. (2006) Genetic variation in the zebrafish. *Genome Res* **16**, 491-497.
- Montague T.G., Cruz J.M., Gagnon J.A., Church G.M. and Valen E. (2014) CHOPCHOP: a CRISPR/Cas9 and TALEN web tool for genome editing. *Nucleic acids research* **42**, W401-407.
- Labun K., Montague T.G., Gagnon J.A., Thyme S.B. and Valen E. (2016) CHOPCHOP v2: a web tool for the next generation of CRISPR genome engineering. *Nucleic acids research* **44**, W272-276.
- Gagnon J.A., Valen E., Thyme S.B., Huang P., Akhmetova L., Pauli A.,... and Schier A.F. (2014) Efficient mutagenesis by Cas9 protein-mediated oligonucleotide insertion and large-scale assessment of single-guide RNAs. *PLoS one* **9**, e98186.
- Jao L.E., Wente S.R. and Chen W. (2013) Efficient multiplex biallelic zebrafish genome editing using a CRISPR nuclease system. *Proc Natl Acad Sci U S A* **110**, 13904-13909.



28. Varshney G.K., Carrington B., Pei W., Bishop K., Chen Z., Fan C.,... and Burgess S.M. (2016) A high-throughput functional genomics workflow based on CRISPR/Cas9-mediated targeted mutagenesis in zebrafish. *Nat Protoc* **11**, 2357-2375.
29. Talbot J.C. and Amacher S.L. (2014) A streamlined CRISPR pipeline to reliably generate zebrafish frameshifting alleles. *Zebrafish* **11**, 583-585.
30. Pfeffer S.R. (2019) NPC intracellular cholesterol transporter 1 (NPC1)-mediated cholesterol export from lysosomes. *J Biol Chem* **294**, 1706-1709.
31. Tyyne J., Cooper J.D., Khan M.N., Shemilt S.J. and Haltia M. (2004) Hippocampal pathology in the human neuronal ceroid-lipofuscinoses: distinct patterns of storage deposition, neurodegeneration and glial activation. *Brain Pathol* **14**, 349-357.
32. Zhang C.K., Stein P.B., Liu J., Wang Z., Yang R., Cho J.H.,... and Mistry P.K. (2012) Genome-wide association study of N370S homozygous Gaucher disease reveals the candidacy of CLN8 gene as a genetic modifier contributing to extreme phenotypic variation. *Am J Hematol* **87**, 377-383.
33. Shen M.W., Arbab M., Hsu J.Y., Worstell D., Culbertson S.J., Krabbe O.,... and Sherwood R.I. (2018) Predictable and precise template-free CRISPR editing of pathogenic variants. *Nature* **563**, 646-651.
34. Abadi S., Yan W.X., Amar D. and Mayrose I. (2017) A machine learning approach for predicting CRISPR-Cas9 cleavage efficiencies and patterns underlying its mechanism of action. *PLoS Comput Biol* **13**, e1005807.
35. Marques A.R., Gabriel T.L., Aten J., van Roomen C.P., Ottenhoff R., Claessen N.,... and van Eijk M. (2016) Gpnmb Is a Potential Marker for the Visceral Pathology in Niemann-Pick Type C Disease. *PLoS one* **11**, e0147208.
36. Kramer G., Wegdam W., Donker-Koopman W., Ottenhoff R., Gaspar P., Verhoek M.,... and van Eijk M. (2016) Elevation of glycoprotein nonmetastatic melanoma protein B in type 1 Gaucher disease patients and mouse models. *FEBS Open Bio* **6**, 902-913.
37. Carcel-Trullols J., Kovacs A.D. and Pearce D.A. (2015) Cell biology of the NCL proteins: What they do and don't do. *Biochimica et biophysica acta* **1852**, 2242-2255.
38. Hermansson M., Kakela R., Berghall M., Lehesjoki A.E., Somerharju P. and Lahtinen U. (2005) Mass spectrometric analysis reveals changes in phospholipid, neutral sphingolipid and sulfatide molecular species in progressive epilepsy with mental retardation, EPMR, brain: a case study. *J Neurochem* **95**, 609-617.
39. Ferraz M.J., Marques A.R., Gaspar P., Mirzaian M., van Roomen C., Ottenhoff R.,... and Aerts J.M. (2016) Lyso-glycosphingolipid abnormalities in different murine models of lysosomal storage disorders. *Mol Genet Metab* **117**, 186-193.
40. Marques A.R., Mirzaian M., Akiyama H., Wisse P., Ferraz M.J., Gaspar P.,... and Aerts J.M. (2016) Glucosylated cholesterol in mammalian cells and tissues: formation and degradation by multiple cellular beta-glucosidases. *J Lipid Res* **57**, 451-463.
41. Lelieveld L.T., Mirzaian M., Kuo C.L., Artola M., Ferraz M.J., Peter R.E.A.,... and Aerts J. (2019) Role of beta-glucosidase 2 in aberrant glycosphingolipid metabolism: model of glucocerebrosidase deficiency in zebrafish. *J Lipid Res* **60**, 1851-1867.
42. Tseng W.C., Loeb H.E., Pei W., Tsai-Morris C.H., Xu L., Cluzeau C.V.,... and Porter F.D. (2018) Modeling Niemann-Pick disease type C1 in zebrafish: a robust platform for in vivo screening of candidate therapeutic compounds. *Dis Model Mech* **11**.
43. van der Lienden M.J.C., Gaspar P., Boot R., Aerts J. and van Eijk M. (2018) Glycoprotein Non-Metastatic Protein B: An Emerging Biomarker for Lysosomal Dysfunction in Macrophages. *Int J Mol Sci* **20**.
44. Kawakami K. (2005) Transposon tools and methods in zebrafish. *Developmental dynamics : an official publication of the American Association of Anatomists* **234**, 244-254.
45. Kwan K.M., Fujimoto E., Grabher C., Mangum B.D., Hardy M.E., Campbell D.S.,... and Chien C.B. (2007) The Tol2kit: a multisite gateway-based construction kit for Tol2 transposon transgenesis constructs. *Developmental dynamics : an official publication of the American Association of Anatomists* **236**, 3088-3099.
46. Kawakami K., Takeda H., Kawakami N., Kobayashi M., Matsuda N. and Mishina M. (2004) A transposon-mediated gene trap approach identifies developmentally regulated genes in zebrafish. *Dev Cell* **7**, 133-144.
47. Tytki-Szymanska A., Czartoryska B., Vanier M.T., Poorthuis B.J., Groener J.A., Lugowska A.,... and Jurkiewicz E. (2007) Non-neuronopathic Gaucher disease due to saposin C deficiency. *Clin Genet* **72**, 538-542.
48. Tytki-Szymanska A., Groener J.E., Kaminski M.L., Lugowska A., Jurkiewicz E. and Czartoryska B. (2011) Gaucher disease due to saposin C deficiency, previously described as non-neuronopathic form--no positive effects after 2-years of miglustat therapy. *Mol Genet Metab* **104**, 627-630.
49. Vaccaro A.M., Motta M., Tatti M., Scarpa S., Masuelli L., Bhat M.,... and Salvioli R. (2010) Saposin C mutations in Gaucher disease patients resulting in lysosomal lipid accumulation, saposin C deficiency, but normal prosaposin processing and sorting. *Human molecular genetics* **19**, 2987-2997.
50. Vaccaro A.M., Salvioli R., Barca A., Tatti M., Ciaffoni F., Maras B.,... and Pucci P. (1995) Structural analysis of saposin C and B. Complete localization of disulfide bridges. *J Biol Chem* **270**, 9953-9960.
51. Wilkinson R.N., Elworthy S., Ingham P.W. and van Eeden F.J. (2013) A method for high-throughput PCR-based

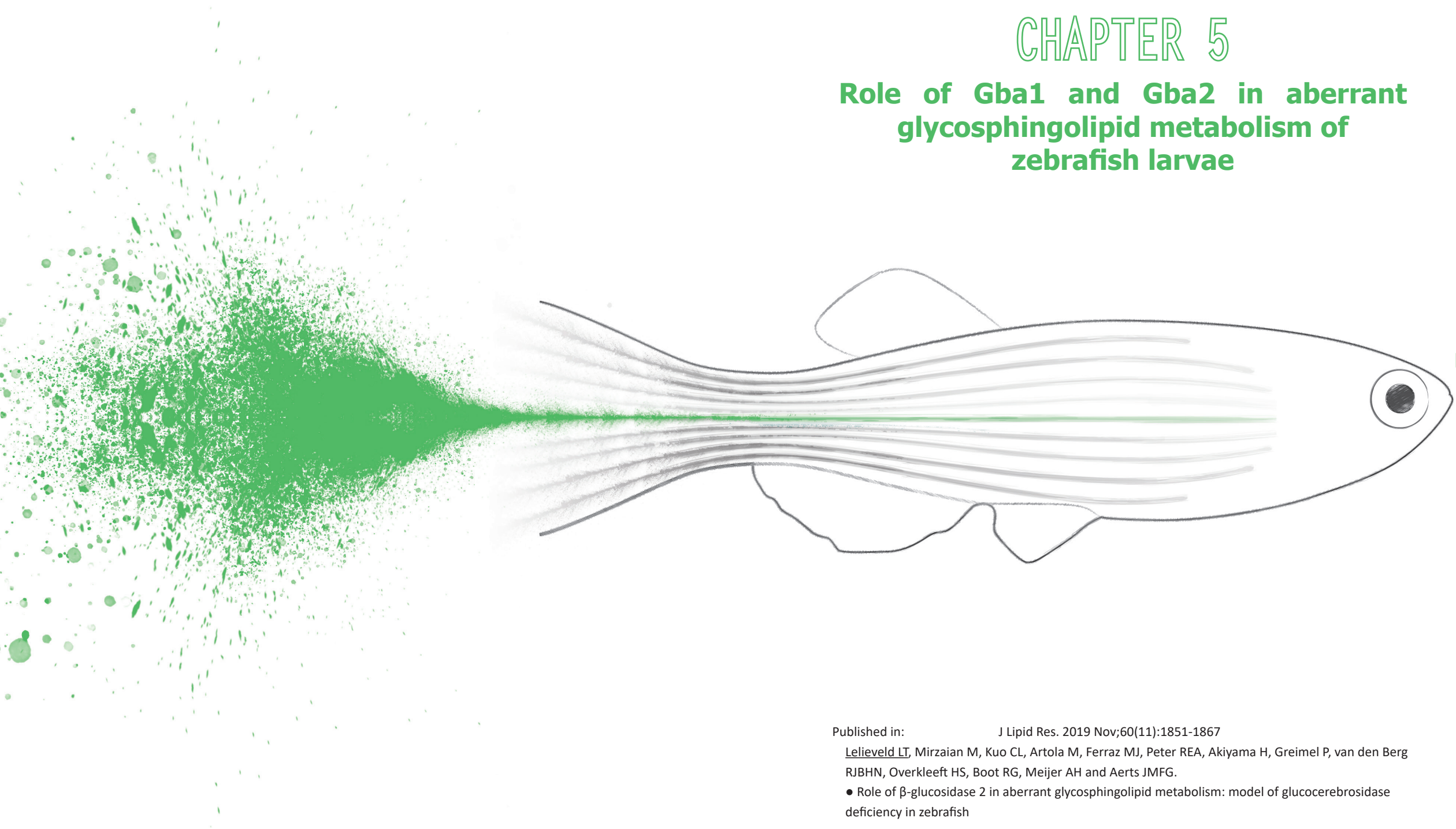
## Chapter 4

- genotyping of larval zebrafish tail biopsies. *Biotechniques* **55**, 314-316.
52. Armstrong G.A., Liao M., You Z., Lissouba A., Chen B.E. and Drapeau P. (2016) Homology Directed Knockin of Point Mutations in the Zebrafish *tardbp* and *fus* Genes in ALS Using the CRISPR/Cas9 System. *PLoS one* **11**, e0150188.
  53. Eschstruth A., Schneider-Maunoury S. and Giudicelli F. (2020) Creation of zebrafish knock-in reporter lines in the *nefma* gene by Cas9-mediated homologous recombination. *Genesis* **58**, e23340.
  54. Auer T.O., Duroure K., De Cian A., Concordet J.P. and Del Bene F. (2014) Highly efficient CRISPR/Cas9-mediated knock-in in zebrafish by homology-independent DNA repair. *Genome Res* **24**, 142-153.
  55. Kesavan G., Chekuru A., Machate A. and Brand M. (2017) CRISPR/Cas9-Mediated Zebrafish Knock-in as a Novel Strategy to Study Midbrain-Hindbrain Boundary Development. *Front Neuroanat* **11**, 52.
  56. Burger A., Lindsay H., Felker A., Hess C., Anders C., Chiavacci E.,... and Mosimann C. (2016) Maximizing mutagenesis with solubilized CRISPR-Cas9 ribonucleoprotein complexes. *Development* **143**, 2025-2037.
  57. Trubiroha A., Gillotay P., Giusti N., Gacquer D., Libert F., Lefort A.,... and Costagliola S. (2018) A Rapid CRISPR/Cas-based Mutagenesis Assay in Zebrafish for Identification of Genes Involved in Thyroid Morphogenesis and Function. *Sci Rep* **8**, 5647.
  58. Kuil L.E., Lopez Marti A., Carreras Mascaro A., van den Bosch J.C., van den Berg P., van der Linde H.C.,... and van Ham T.J. (2019) Hexb enzyme deficiency leads to lysosomal abnormalities in radial glia and microglia in zebrafish brain development. *Glia* **67**, 1705-1718.



# CHAPTER 5

## Role of Gba1 and Gba2 in aberrant glycosphingolipid metabolism of zebrafish larvae



Published in: J Lipid Res. 2019 Nov;60(11):1851-1867

Lelieveld LT, Mirzaian M, Kuo CL, Artola M, Ferraz MJ, Peter REA, Akiyama H, Greimel P, van den Berg RJBHN, Overkleeft HS, Boot RG, Meijer AH and Aerts JMFG.

• Role of  $\beta$ -glucosidase 2 in aberrant glycosphingolipid metabolism: model of glucocerebrosidase deficiency in zebrafish

## Abstract

The  $\beta$ -glucosidases (GBA1 [glucocerebrosidase], GBA2, and GBA3) are ubiquitous, essential enzymes. Lysosomal GBA1 and cytosol-facing GBA2 degrade glucosylceramide (GlcCer); GBA1 deficiency causes Gaucher disease (GD), a lysosomal storage disorder characterized by lysosomal accumulation of GlcCer, which is partly converted to glucosylsphingosine (GlcSph). GBA1 and GBA2 may also transfer glucose from GlcCer to cholesterol, yielding glucosylated cholesterol (GlcChol). Here, we aimed to clarify the role of zebrafish Gba2 in glycosphingolipid metabolism during Gba1 deficiency in zebrafish (*Danio rerio*), which are able to survive total Gba1 deficiency. We developed Gba1 and Gba2 zebrafish knockouts (*gba1*<sup>-/-</sup> and *gba2*<sup>-/-</sup>, respectively) using CRISPR/Cas9, modulated glucosidases genetically and pharmacologically, studied GlcCer metabolism in individual larvae, and explored the feasibility of pharmacologic or genetic interventions. Activity-based probes and quantification of relevant glycolipid metabolites confirmed enzyme deficiency. GlcSph increased in *gba1*<sup>-/-</sup> larvae (0.09 pmol/fish) but did not increase more in *gba1*<sup>-/-</sup>:*gba2*<sup>-/-</sup> larvae. GlcCer was comparable in *gba1*<sup>-/-</sup> and wild-type (WT) larvae but increased in *gba2*<sup>-/-</sup> and *gba1*<sup>-/-</sup>:*gba2*<sup>-/-</sup> larvae. Independent of Gba1 status, GlcChol was low in all *gba2*<sup>-/-</sup> larvae (0.05 vs. 0.18. pmol/fish in WT). Pharmacologic inactivation of zebrafish Gba1 comparably increased GlcSph. Inhibition of glucosylceramide synthase in Gba1-deficient larvae reduced GlcCer and GlcSph, and concomitant inhibition of glucosylceramide synthase and Gba2 with iminosugars also reduced excessive GlcChol. Finally, overexpression of human GBA1 and injection of recombinant GBA1 both decreased GlcSph. We determined that zebrafish larvae offer an attractive model to study glucosidase actions in glycosphingolipid metabolism in vivo, and we identified distinguishing characteristics of zebrafish Gba2 deficiency.

## Introduction

The lysosomal glucocerebrosidase (GBA1) is a retaining  $\beta$ -glucosidase degrading the glycosphingolipid glucosylceramide (GlcCer)<sup>1</sup>. The enzyme receives considerable interest since its deficiency causes Gaucher disease (GD), a recessively inherited lysosomal storage disorder in which GlcCer accumulates in lysosomes, particularly those of tissue macrophages that transform into Gaucher cells<sup>2,3</sup>. GD patients characteristically develop hepatosplenomegaly, leukopenia, especially thrombocytopenia, and abnormalities in coagulation<sup>4</sup>. In more severe cases, neuropathology develops, with oculomotor apraxia as a first sign. In its most severe form, complete lack of GBA1 is associated with an acute failure in skin permeability features, causing the so-called collodion baby with severe ichthyosis<sup>2</sup>. Individuals that have a genetic defect in GBA1, or carriers of such a mutation, have a markedly increased risk for developing Parkinson's disease and Lewy-body dementia<sup>5,6</sup>. The molecular mechanisms underlying the complex pathophysiology of GD and the risk imposed by GBA1 abnormalities for  $\alpha$ -synucleinopathies are presently unknown. The features and functions of GBA1 are presently extensively investigated. Novel research tools in the field are cell-permeable fluorescent activity-based probes (ABPs) that selectively label retaining  $\beta$ -glucosidases in a mechanism-based manner through covalent binding to the catalytic nucleophile. These allow cross-species visualization of active enzyme molecules *in vitro*, *in situ* and *in vivo*<sup>7,8</sup>. Cyclophellitol derivative **1** (**Figure 1A**), carrying the reporter fluorophore at C8 (cyclophellitol number; corresponding to position C6 in glucose), labels selectively GBA1, arguably because the other human retaining  $\beta$ -glucosidases do not accept the presence of a (bulky) fluorophore at this position<sup>7</sup>. Cyclophellitol-aziridine **2** with the fluorophore pointing towards the position occupied by the aglycon of a retaining  $\beta$ -exoglucosidase binds all known cellular human  $\beta$ -glucosidases (GBA1, GBA2 and GBA3) (ABP **2**, **Figure 1A and B**)<sup>8</sup>.

Several corrections for GBA1 deficiency in GD have been developed and novel therapeutic interventions are still being pursued. For almost three decades, non-neuronopathic (type 1) GD can be treated by enzyme replacement therapy (ERT), a treatment based on chronic intravenous administration of GBA1 with mannose-terminal N-glycans ensuring targeting to macrophages, the primary GlcCer storage cells<sup>3,9</sup>. An alternative therapeutic approach is substrate reduction therapy (SRT) that aims to reduce the biosynthesis of GlcCer through inhibition of glucosylceramide synthase (GCS)<sup>10</sup>. The first SRT agent developed for GD is *N*-butyl-deoxynojirimycin (Miglustat) that was registered almost two decades ago for treatment of mild to moderate type 1 GD<sup>11</sup>. More recently, an improved inhibitor for GCS, Eliglustat (**Figure 1C**), has been developed for treatment of type 1 GD patients<sup>12</sup>. At present GCS inhibitors, with improved brain-permeability, have been developed as well as chaperones acting as enzyme stabilizers<sup>3,13,14</sup>. Moreover, augmentation of GBA1 expression by gene therapy approaches is actively studied in animal models<sup>15</sup>.



It has been recently recognized that compensatory mechanisms occur during a GBA1 deficiency<sup>3,16</sup>. For example, in GBA1 deficient lysosomes, accumulating GlcCer is partly converted by lysosomal acid ceramidase to its corresponding sphingoid base, glucosylsphingosine (GlcSph)<sup>17</sup>. As a result, GlcSph is massively increased in tissues and plasma of GD patients and GBA1-deficient mice<sup>17,18</sup>. Roles for GlcSph in pathophysiology of Gaucher disease with respect to organomegaly, osteoporosis, risks for multiple myeloma, Parkinson's disease and reduced cerebral vascularization have been proposed<sup>18-22</sup>.

The cytosol-facing GBA2, which metabolizes cytosolic GlcCer<sup>23-26</sup>, has been recently shown to have transglucosidase activity as well, and is able to produce glucosylated cholesterol (GlcChol) from GlcCer and cholesterol<sup>27</sup>. The role of GBA2 in GD pathophysiology is unclear. Excessive GBA2 activity during deficiency of GBA1 appears detrimental in some aspects. For example, genetically ablating GBA2 in a Gaucher mouse model as well as in Niemann-Pick type C (NPC) mice has been shown to ameliorate symptoms<sup>18,28</sup>. Moreover, pharmacological inhibition of GBA2 by administration of low nanomolar iminosugar derivatives (AMP-DNM and L-ido-AMP-DNM<sup>29,30</sup>, **Figure 1C**) exerts beneficial effects in NPC mice<sup>28</sup>.

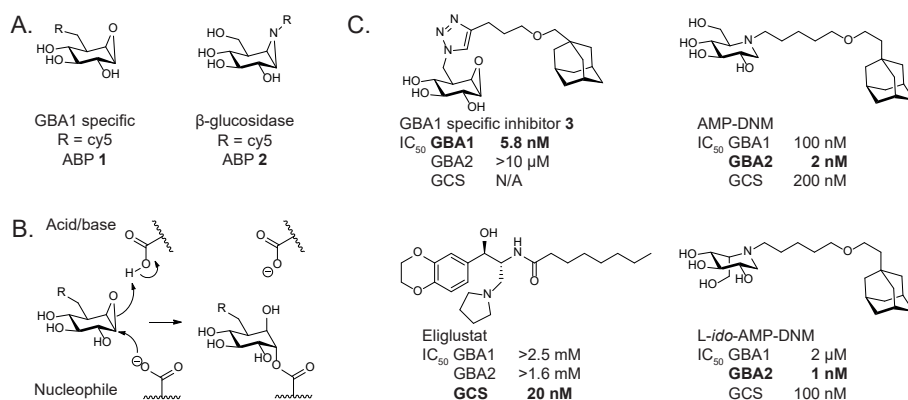


**Figure 1 | Chemical structures of activity-based probes and inhibitors**

**(A)** Chemical structures of activity-based probes (ABPs) used in this study: cyclophellitol-epoxide-based ABP **1** (GBA1 specific) and cyclophellitol-aziridine-based ABP **2** (labelling all retaining  $\beta$ -glucosidases). Both ABPs are equipped with a Cy5 fluorophore as reporter **(B)** Catalytic reaction mechanism of cyclophellitol-based irreversible inhibitors. **(C)** Chemical structures of the GBA1 specific irreversible inhibitor **3** (ME656), iminosugars AMP-DNM and L-ido-AMP-DNM and Eliglustat. IC<sub>50</sub> values are given for GBA1 and GBA2 and GCS<sup>29,31</sup>.

The zebrafish (*Danio rerio*) is a popular vertebrate research model because of low-cost maintenance and the ability to produce large clutches of embryos. Zebrafish larvae develop ex-utero, are transparent and pharmacological modulation can be conveniently performed (in 96-well plates) up to 5 days post-fertilization (5 dpf)<sup>32,33</sup>. Another attractive feature of the zebrafish is the molecular and genetic similarity to mammalian models. For example, the zebrafish genome encodes GlcCer-metabolizing enzymes and their activity can be measured with the same fluorogenic substrates as commonly used for the human and rodent analogues<sup>34</sup>. We have shown recently that zebrafish Gba1 and Gba2 react like their human counterparts with available ABPs<sup>31,34</sup> and exhibit similar inhibitor affinities<sup>34,35</sup>. A complete deficiency of GBA1 causes a fatal skin abnormality in newborn mice and man<sup>36,37</sup>, however the introduction of complete Gba1 deficiency in fish is tolerated<sup>38,39</sup>.

The primary goal of our investigation was to study at organismal level the role of Gba2 in glycosphingolipid metabolism during deficiency of Gba1. For this purpose, we used both genetic and pharmacological approaches to modulate Gba1 and Gba2 and subsequently studied the impact on glycosphingolipid levels in individual zebrafish larvae. In Gba1-deficient fish, either genetic or chemically induced, the most remarkable abnormality is the increase in GlcSph, independent of the Gba2 status. The deficiency of Gba2 in zebrafish larvae leads to reduction of GlcChol, independent of the Gba1 status. As a secondary goal we studied the feasibility of pharmacological and genetic interventions. We demonstrate that inhibition of glucosylceramide synthase prohibits excessive formation of GlcSph and that concomitant inhibition of Gba2 also prevents excessive GlcChol. Overexpression of human GBA1 in Gba1-deficient larvae reduces GlcSph elevation. The same is observed upon infusion of recombinant human GBA1. Altogether, we demonstrate that zebrafish embryos offer an attractive organismal model to study glycosphingolipid abnormalities in genetic and pharmacological models of Gba1 and Gba2 deficiencies and moreover allow the screening of GCS and GBA2 inhibitors regarding corrective effects on lipid abnormalities.



## Results

### Gba1 and Gba2 of zebrafish: detection with fluorescent ABPs.

Zebrafish have one orthologue of human lysosomal GBA1<sup>38</sup> and zebrafish Gba1 (UniProt accession P04062) shows 58% identity and 73% similarity to the human GBA1 enzyme. The zebrafish Gba1 protein consists of 518 amino acids with a predicted mass of 58 kDa. The zebrafish orthologue (UniProt accession E7F5W0) of human non-lysosomal  $\beta$ -glucosidase shows 66% identity and 79% similarity to human GBA2 and a predicted mass of 96 kDa<sup>35</sup>.

We labelled a homogenate of zebrafish embryonic fibroblasts (ZF4 cell line)<sup>40</sup> and a homogenate of pooled WT zebrafish larvae (5 dpf) with ABPs at different pH (**Figure 2A** and **B**). ABP 1, a Cy5 fluorescent cyclophellitol-epoxide targeting specifically Gba1, labelled a protein with an apparent molecular weight around 60 kDa in the zebrafish homogenates, most favourable at pH 4 (**Figure 2A**, top panel). The observed molecular mass coincides with that of the glycosylated zebrafish orthologue of Gba1 and the optimal labelling at acidic pH is consistent with the pH optimum reported for Gba1<sup>7</sup>. Zebrafish material incubated with ABP 2, the fluorescent cyclophellitol-aziridine that labels all retaining  $\beta$ -glucosidases<sup>8</sup>, revealed additionally to Gba1 also a protein with an apparent molecular weight of about 95 kDa (**Figure 2A** and **B**), coinciding with the predicted molecular weight of zebrafish Gba2.

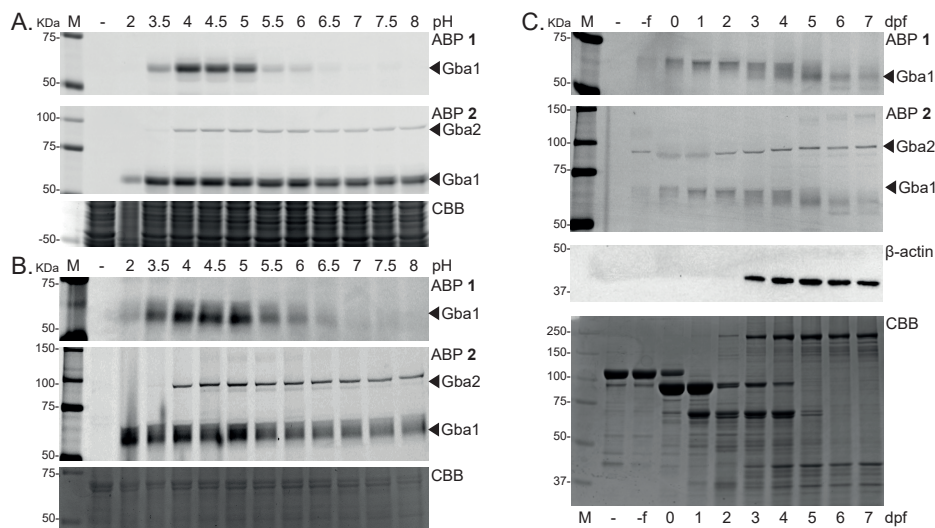


**Figure 2 | Visualization of active Gba1 and Gba2 enzymes in zebrafish**

**(A)** Effect of pH on labelling of ZF4 cell homogenate with ABP 1 (100 nM) and ABP 2 (100 nM). **(B)** Effect of pH on labelling of pooled zebrafish homogenate (5 dpf) with ABP 1 (1  $\mu$ M) and ABP 2 (200 nM). A protein equivalent of one zebrafish was used per condition. **(C)** ABP 1 and ABP 2 labelling of homogenate of oocytes (-f) and developing zebrafish embryos (t = 0-7 dpf). An equivalent of one zebrafish egg or embryo was used per lane. In lane -, sample is denatured prior to ABP addition, Coomassie Brilliant Blue (CBB) staining and  $\beta$ -actin were used as loading controls.

Next, we labelled homogenates of developing zebrafish embryos, from unfertilized oocytes to 7 dpf zebrafish larvae (-f to 7 dpf, **Figure 2C**). Active Gba1 and Gba2 molecules were already detected in both oocytes and fertilized eggs, suggesting the presence of active  $\beta$ -glucosidases in the yolk of the developing embryo deposited by the adult

zebrafish female. The intensity of ABP-labelled Gba2 increased over time (in days), while Gba1 intensity reduced in the developing embryo. Of note, although the presence of very abundant yolk proteins, predominantly isoforms of the phospholipo-glycoprotein vitellogenin<sup>41</sup>, influenced the apparent molecular weight of the ABP-labelled enzyme, it did not influence target engagement of the ABP.

### ***Gba1*<sup>-/-</sup> larvae accumulate GlcSph**

To obtain a *gba1* mutant zebrafish, an appropriate sgRNA sequence was selected in the first exon of *gba1* (Target 1, **Figure 3A** upper and middle panel). Injection of Cas9 mRNA and sgRNA into the one-cell stage of WT embryos, generated a founder fish with a germ-line transmitted deletion of 31 bp in the splice-site region of exon 1 (*gba1*Δ31, **Figure 3A**, lower panel). This founder was subsequently used to generate a heterozygous *gba1*<sup>+/-</sup> zebrafish line without malformations<sup>42</sup>. *Gba1*<sup>-/-</sup> mutant larvae were obtained following crossing of the adult *gba1*<sup>+/-</sup> carriers and characterization of offspring by genotyping.

To validate the *gba1*<sup>-/-</sup> fish (with Δ31 mutation), their Gba1 status was examined by labelling with ABP **1**. Comparison of WT, *gba1*<sup>+/-</sup> and *gba1*<sup>-/-</sup> larvae labelled with ABP **1** revealed a reduction of the ~60 kDa Gba1 in the *gba1*<sup>-/-</sup> 5 dpf larvae (**Figure 2B**). Some residual labelled protein at 60 kDa was observed in the *gba1*<sup>-/-</sup> larvae argued as the deposition of maternal Gba1 enzyme from the heterozygous female<sup>43</sup>.

To establish whether Gba1 is truly impaired in *gba1*<sup>-/-</sup> fish, their glycosphingolipid content was determined. In the 5 dpf *gba1*<sup>-/-</sup> larvae, total hexosylceramide (HexCer), i.e. GlcCer and/or GalCer, and GlcChol was not significantly increased (**Figure 3C**). In the course of the experiments we used HILIC column chromatography to measure sphingolipids with glucose- and galactose moieties in a separate set of zebrafish larvae. This revealed that in the studied 5 dpf larvae more than 70% of HexCer is GlcCer (**Supplementary Figure 1**). This lipid, like total HexCer, did not significantly accumulate in *gba1*<sup>-/-</sup> larvae. Likewise, HILIC separation revealed that solely GlcSph accumulates in the *gba1*<sup>-/-</sup> larvae (**Figure 3C**). No significant difference was detected for other (glyco)sphingolipids such as sphinganine, sphingosine, dihydroceramide, ceramide, GalCer and dihexosylceramide<sup>42</sup>.

Next, 5 dpf larvae were dissected into head and body regions and glycosphingolipid levels were determined (**Supplementary Figure 2**). GlcSph and GlcCer levels were significantly increased in both regions. GlcChol was also detected in the brain region in comparable levels to the body region.

To conclude, the prominent accumulation of GlcSph in the mutant fish resembles the marked increase of GlcSph in Gba1-deficient patients and mice<sup>44</sup>. Thus, we introduced a functional deficiency in lysosomal Gba1 activity in the *gba1*<sup>-/-</sup> fish promoting active conversion of accumulating GlcCer to GlcSph.

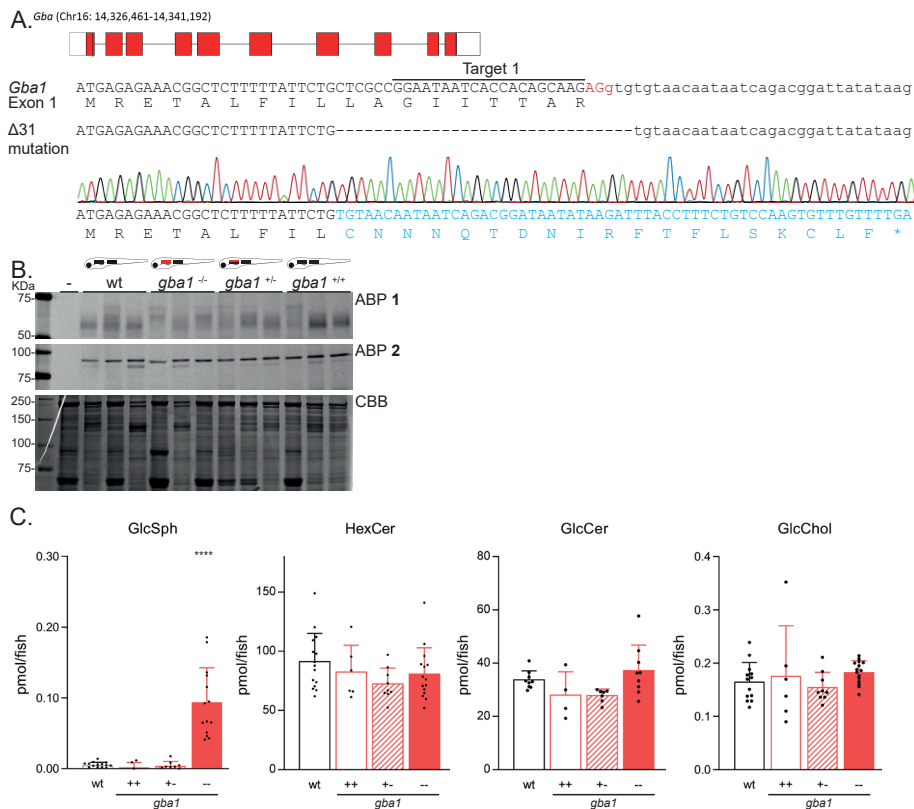


**Figure 3 | CRISPR/Cas9 mediated disruption of *Gba1* in zebrafish**

(A) Top panel: Schematic representation of the *gba1* gene on chromosome 16. Middle panel: DNA sequence of the exon1-intron1 boundary of *gba1* with the exon in upper case and intron in lower case, the sgRNA target sequence underlined, the PAM site in red and the protein sequence shown below. Lower panel: The 31 base pair deletion ( $\Delta 31$ ), obtained from the sequence trace of an homozygous *gba1* $\Delta 31$  larvae, is located in the splice-region with the altered predicted translated protein sequence given in blue and leads to a premature stopcodon (\*). (B) ABP labelling of homogenate of individual zebrafish larvae at 5 dpf (WT, *gba1*<sup>-/-</sup>, *gba1*<sup>+/-</sup> or *gba1*<sup>+/-</sup> from incross, n= 3) with ABP 1 (top panel) or ABP 2 (middle panel). In lane -, sample is denatured prior to ABP addition, CBB staining was used as loading control. (C) GlcSph, HexCer, GlcCer and GlcChol levels were determined of individual zebrafish larvae in pmol/fish; WT (n = 15), *gba1*<sup>+/-</sup> (n = 6), *gba1*<sup>+/-</sup> (n = 9) and *gba1*<sup>-/-</sup> (n = 15) for GlcSph, HexCer and GlcChol and WT (n = 9), *gba1*<sup>+/-</sup> (n = 4), *gba1*<sup>+/-</sup> (n = 7) and *gba1*<sup>-/-</sup> (n = 9) for GlcCer. Data is depicted as mean  $\pm$  SD and analysed using One-Way Anova (Dunnett's test) with WT as control group with \*\*\*\* P < 0.0001.

### Deficiency in *Gba2* results in prominent decrease in GlcChol

Next, we similarly generated a *Gba2* deficient fish. An appropriate sgRNA sequence (Target 2, **Figure 4A**, upper and middle panel) was selected in the third exon of the *gba2* gene and subsequent rounds of screening and crossing resulted in a zebrafish with a 16 bp deletion in exon 3 of *gba2*. This deletion created a premature stop codon (**Figure 4A**, lower panel). Adult homozygous *gba2*<sup>-/-</sup> zebrafish showed no malformations or aberrant behaviour<sup>42</sup>. Moreover, adult homozygous *gba2*<sup>-/-</sup> zebrafish produced regular sized clutches with normally developing larvae until the free-feeding stage of 5 dpf, suggesting that the male *gba2*<sup>-/-</sup> fish are fertile in contrast to some strains of GBA2 KO mice<sup>24,45</sup>.

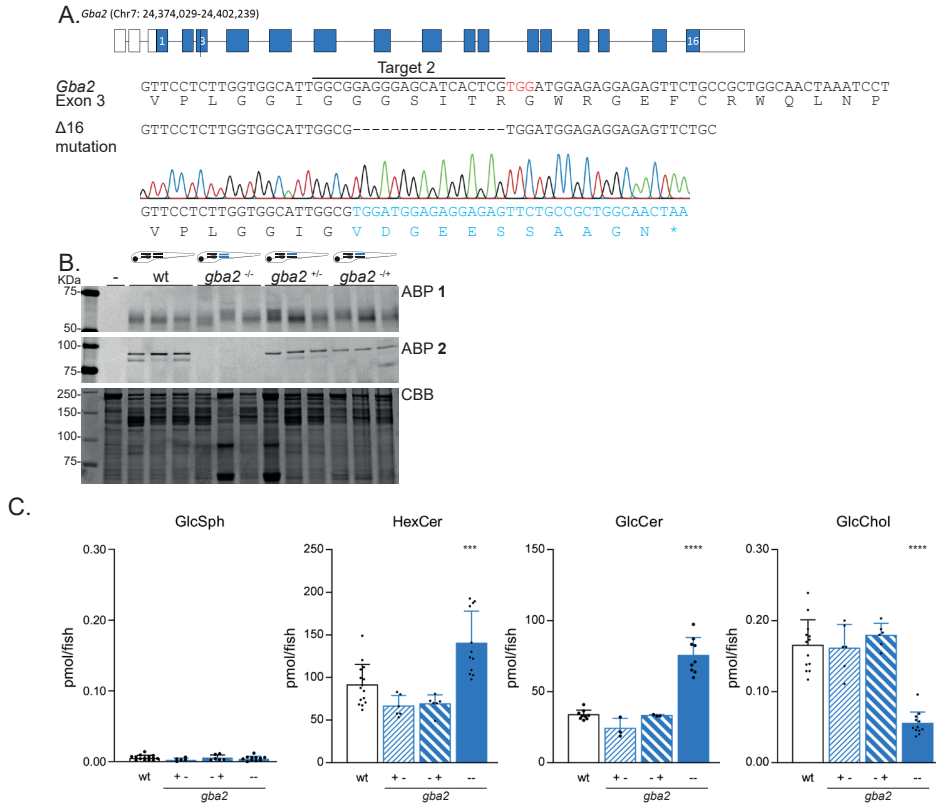


**Figure 4 | CRISPR/Cas9 mediated disruption of *Gba2* in zebrafish**

**(A)** Top panel: Schematic representation of *gba2* gene on chromosome 7. Middle panels: DNA sequence of exon 3 of *gba2* with the sgRNA target sequence underlined, the PAM site in red and the protein sequence shown below. Lower panel: The 16 base pair deletion ( $\Delta 16$ ), as obtained from the sequence trace, introduces a premature stopcodon (\*) in the altered predicted translated protein sequence, given in blue. **(B)** ABP labelling of homogenate of individual zebrafish larvae at 5 dpf (WT, *gba2*<sup>-/-</sup> and both heterozygous *gba2*<sup>+/-</sup> options, n = 3) with ABP 1 (top panel) or ABP 2 (middle panel). In lane -, sample is denatured prior to ABP addition, CBB staining was used as loading control. **(C)** GlcSph, HexCer, GlcCer and GlcChol levels were determined of individual zebrafish larvae in pmol/fish; WT (n = 15), *gba2*<sup>-/-</sup> (n = 6), *gba2*<sup>+/-</sup> (n = 6) and *gba2*<sup>-/-</sup> (n = 12) for GlcSph, HexCer and GlcChol and WT (n = 9), *gba2*<sup>-/-</sup> (n = 3), *gba2*<sup>+/-</sup> (n = 3) and *gba2*<sup>-/-</sup> (n = 9) for GlcCer. Data is depicted as mean  $\pm$  SD and analysed using One-Way Anova (Dunnnett's test) with wt as control group with \*\*\* P < 0.001 and \*\*\*\* P < 0.0001.

To validate GBA2 deficiency in the *gba2*<sup>-/-</sup> fish (with  $\Delta 16$  mutation), enzyme status was examined by ABP 2 labelling. Homogenates of zebrafish larvae of different *gba2* genotypes were incubated with GBA1 specific ABP 1 and broad-spectrum ABP 2. Homozygous *gba2*<sup>-/-</sup> fish showed complete absence of ABP-labelled enzyme at 90 kDa, while heterozygous offspring from two different crossings exhibited residual ABP-labelled Gba2 enzyme (**Figure 4B**). The lipid composition of *gba2*<sup>-/-</sup> larvae (5 dpf) showed an increase in HexCer, predominately GlcCer (**Figure 4C**). Additionally, these larvae exhibited a very prominent decrease of HexChol (**Figure 4C**). As observed for GlcSph, HILIC separation revealed that GlcChol is the predominant form of HexChol (>95%) in 5 dpf zebrafish larvae (**Supplementary Figure 1D-F**). The *gba2*<sup>-/-</sup> fish showed no increase in GlcSph and no significant differences were found for other (glyco)sphingolipids such as sphinganine, sphingosine, dihydroceramide, ceramide,



GalCer and dihexosylceramide (**Figure 4C** and reference 42). The GlcChol reduction was not observed in WT and heterozygous *gba2*<sup>-/-</sup> larvae. The marked reduction in GlcChol in the *gba2*<sup>-/-</sup> zebrafish larvae is similar to that observed in Gba2-deficient mice<sup>27</sup>. This suggests that zebrafish Gba2 also acts as a transglucosylase similar to rodent and human Gba2, generating GlcChol from GlcCer and cholesterol.

#### **Aberrant GlcSph, GlcCer and GlcChol levels in *gba1*<sup>-/-</sup>:*gba2*<sup>-/-</sup> larvae.**

The *gba1*<sup>+/-</sup>:*gba2*<sup>-/-</sup> adult carrier zebrafish, used to produce *gba1*<sup>-/-</sup>:*gba2*<sup>-/-</sup> larvae, did not show malformations and gave regular sized clutches<sup>42</sup>. To examine the *gba1*<sup>-/-</sup>:*gba2*<sup>-/-</sup> double KO zebrafish, we employed the same ABP labelling as described above. As in the respective Gba1 and Gba2 single KO, no Gba2 enzyme was visualized on gel, while a residual ABP-labelled enzyme with a molecular mass comparable to Gba1 was present in the double KO 5 dpf larvae (**Figure 5A**).

(Glyco)sphingolipid analysis of *gba1*<sup>-/-</sup>:*gba2*<sup>-/-</sup> larvae showed increased HexCer levels, predominantly GlcCer, compared to single *gba1*<sup>-/-</sup> larvae but similar to that of single *gba2*<sup>-/-</sup> larvae (**Figure 5B**). Moreover, in the double KO larvae, GlcChol was significantly decreased, similar as observed in *gba2*<sup>-/-</sup> larvae. Compared to WT larvae, a significant accumulation of GlcSph in *gba1*<sup>-/-</sup>:*gba2*<sup>-/-</sup> larvae was detected. GlcSph levels in double KO fish tended to be somewhat higher than in the *gba1*<sup>-/-</sup> larvae (**Figure 5B**), although developing zebrafish showed considerable variation in rapidly accumulating GlcSph.

Next, we analysed the age-dependence of glycosphingolipid changes in developing embryos, from 8 hpf to 5 dpf (**Figure 5C**). The elevation of GlcSph in the *gba1*<sup>-/-</sup> and *gba1*<sup>-/-</sup>:*gba2*<sup>-/-</sup> embryos was detectable from 3 dpf onwards. HexCer (predominantly GlcCer) was found to increase also with age, accumulating more rapidly in *gba2*<sup>-/-</sup> and *gba1*<sup>-/-</sup>:*gba2*<sup>-/-</sup> embryos. GlcChol increased with age in WT and *gba1*<sup>-/-</sup> embryos, but remained low (around 0,05 pmol/fish) in the Gba2-deficient fish. The gradual increase with age of GlcChol suggests that it is formed in the developing embryos. In other words, its origin is unlikely to be entirely the yolk.

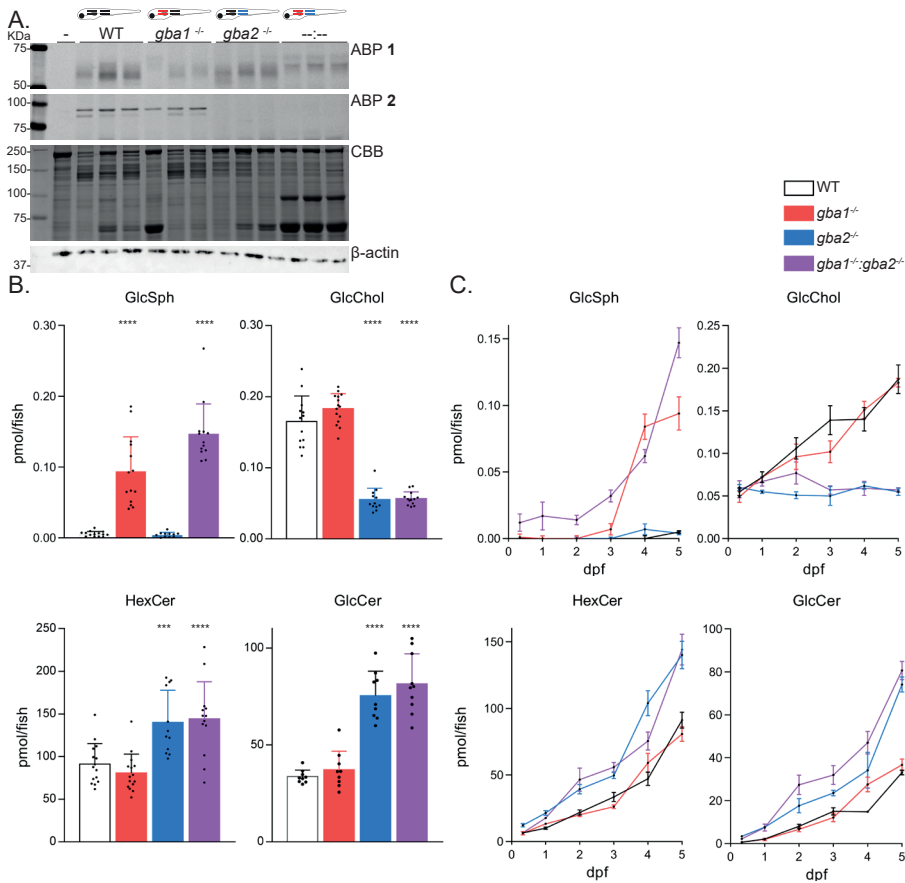


**Figure 5 | Biochemical evaluation of *gba1*, *gba2* and double *gba1:gba2* KO zebrafish larvae**

**(A)** ABP labelling of homogenate of individual zebrafish larvae at 5 dpf (WT, *gba1*<sup>-/-</sup>, *gba2*<sup>-/-</sup> and *gba1*<sup>-/-</sup>:*gba2*<sup>-/-</sup>, n = 3) with ABP 1 (top panel) or ABP 2 (middle panel). In lane -, sample is denatured prior to ABP addition, CBB staining and β-actin were used as loading control (lower panels). **(B)** GlcSph, HexCer, GlcCer and GlcChol levels were determined of individual 5 dpf zebrafish larvae in pmol/fish; WT (n = 15), *gba1*<sup>-/-</sup> (n = 15), *gba2*<sup>-/-</sup> (n = 12) and *gba1*<sup>-/-</sup>:*gba2*<sup>-/-</sup> (n = 13) for GlcSph, HexCer and GlcChol and WT (n = 9), *gba1*<sup>-/-</sup> (n = 9), *gba2*<sup>-/-</sup> (n = 9) and *gba1*<sup>-/-</sup>:*gba2*<sup>-/-</sup> (n = 10) for GlcCer. Data is depicted as mean ± SD and analysed by One-Way Anova (Dunnett's test) with WT as control group. \* P < 0.05, \*\* P < 0.01, \*\*\* P < 0.001 and \*\*\*\* P < 0.0001. **(C)** Developing zebrafish embryos were harvested at different ages and GlcSph, HexCer, GlcCer and GlcChol levels were determined in pmol/fish. 8 hours post fertilization (n = 4-5), 1 dpf (n = 3-5), 2 dpf (n = 3-5), 3 dpf (n = 3-5), 4 dpf (n = 3-6). Data on relevant lipid levels of 5 dpf larvae are obtained from (C). Data is depicted as mean ± SEM

**Additional accumulation of GlcSph in chemical induced Gba1-deficient larvae**

Adamantyl-cyclophellitol **3**, a recently designed highly specific inhibitor of GBA1, was used to investigate the effect of acute pharmacological induction of Gba1 deficiency<sup>31</sup>. Incubation of WT larvae with 10  $\mu$ M of inhibitor **3** for 5 days led to a significant increase in GlcSph in the developing larvae (**Figure 6A**) and also in their surrounding water (**Supplementary Figure 3**). Incubation of *gba2*<sup>-/-</sup> larvae increased GlcSph comparable to WT, which indicates that the increase of GlcSph is independent of the Gba2 status (**Figure 6A**). Incubation of *gba1*<sup>-/-</sup> and *gba1*<sup>-/-</sup>:*gba2*<sup>-/-</sup> larvae with the Gba1 specific inhibitor led to a significant increase in GlcSph compared to vehicle treated *gba1*<sup>-/-</sup> or *gba1*<sup>-/-</sup>:*gba2*<sup>-/-</sup> larvae (**Figure 6A**). GlcChol was only significantly increased in WT treated larvae, while HexCer was increased in all genotypes incubated with **3** (**Figure 6A**). A potential explanation is the additional inhibition of maternal Gba1 by compound **3** immediately after fertilization, thereby generating a completely Gba1 deficient fish larvae. Indeed, ABP-labelling of vehicle treated *gba1*<sup>-/-</sup> backgrounds visualized a 60 kDa protein (**Figure 6B**), while ABP-labelled Gba1 was not visible in any of zebrafish pre-treated with inhibitor **3** (**Figure 6B**). Of note, ABP-labelled Gba1 was present in *Gba1*<sup>-/-</sup> embryos of all ages. (**Figure 6C**). Together, the lipid and ABP data suggest the presence of maternal Gba1 enzyme, which can be inhibited by compound **3**.

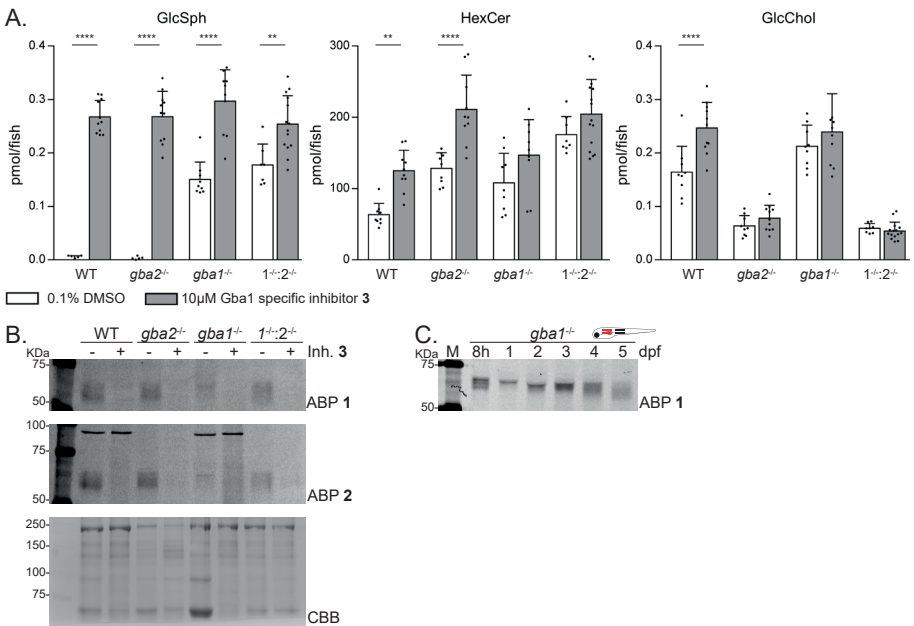


**Figure 6 | Chemical inactivation of Gba1 shows full gba1 deficiency with increased GlcSph levels**

WT, *gba2*<sup>-/-</sup>, *gba1*<sup>-/-</sup> and *gba1*<sup>-/-</sup>:*gba2*<sup>-/-</sup> embryos were treated with vehicle (0.1 % (v/v) DMSO) or inhibitor **3** (10  $\mu$ M) for 5 days and (**A**) relevant lipid levels were determined of individual larvae in pmol/fish (n = 7-15) or (**B**) active  $\beta$ -glucosidase enzyme was visualized with ABP **1** (top panel) or ABP **2** (middle panel); CBB staining was used as loading control (lower panel). (**C**) *Gba1*<sup>-/-</sup> embryos were harvested at different ages and active Gba1 was visualized with ABP **1**. Data of GlcSph, HexCer and GlcChol is depicted as mean  $\pm$  SD and analysed using One-Way Anova (Tukey's test). Ns: not significant, \* P < 0.05, \*\* P < 0.001, \*\*\* P < 0.001 and \*\*\*\* P < 0.0001.

### Lipid corrections by inhibition of glucosylceramide synthase and Gba2

Next, we studied the feasibility of pharmacological intervention and correction of glycosphingolipid abnormalities of Gba1 deficient zebrafish larvae by substrate reduction therapy using treatment with reported GCS inhibitors as well as concomitant GCS and GBA2 inhibitors. WT zebrafish embryos were simultaneously incubated with the Gba1 specific inhibitor **3** and the potent specific GCS inhibitor Eliglustat (**Figure 1C**) to study Gcs inhibition in a Gba1-deficient background. Incubation with 1  $\mu$ M Eliglustat for 5 days led to a decrease in HexCer and the derived lipids GlcSph and GlcChol (**Figure 7A**). As for characterization of the genetic knockout larvae, the reduction in HexCer levels was prominently due to a decrease in GlcCer levels, based on our HILIC method performed on additional larvae<sup>42</sup>.

The iminosugars AMP-DNM and L-ido-AMP-DNM have been reported as low nanomolar GBA2 inhibitors, though they also inhibit GCS and GBA1 at a higher concentration (**Figure 1C**)<sup>29</sup>. Because the reported potencies are *in vitro* and *in situ* IC<sub>50</sub>, we first recapitulated the enzyme specific inhibition of AMP-DNM and L-ido-AMP-DNM in whole WT zebrafish larvae. The embryos were incubated with different concentrations of AMP-DNM (10 nM, 100 nM, 500 nM and 10  $\mu$ M) and L-ido-AMP-DNM (10 nM, 100 nM, 500 nM and 10  $\mu$ M) and GlcSph, HexCer and GlcChol levels were analysed as ratios relative to vehicle treated WT (**Figure 7B**). At the lowest concentration of 10 nM, both iminosugars already caused an increase in HexCer, but no prominent decrease in GlcChol yet. At the higher concentration of 100 nM, both iminosugars caused almost complete *in vivo* inhibition of Gba2 as reflected by decreasing GlcChol and simultaneously increasing HexCer (**Figure 7B**). At very high concentrations of AMP-DNM and L-ido-AMP-DNM (500 nM and 10  $\mu$ M), levels of HexCer, predominantly GlcCer, decreased, indicating that Gcs was inhibited as well (**Figure 7B**). A significant increase in GlcSph was observed at high AMP-DNM concentrations (10  $\mu$ M, **Figure 7B**), but not in case of L-ido-AMP-DNM, which is known to hardly inhibit GBA1.

Next, we analysed the potential of the iminosugars to pharmacologically correct the glycosphingolipid abnormalities in Gba1-deficient zebrafish larvae. WT embryos were simultaneously incubated with **3** and different concentrations of AMP-DNM or L-ido-AMP-DNM, and glycosphingolipid levels were analysed as ratio relative to control Gba1-deficient zebrafish larvae incubated with **3** alone. Incubation with 100 nM of AMP-DNM and L-ido-AMP-DNM resulted in reduction of GlcChol compared to control (**Figure 7C**), indicating Gba2 inhibition. At this concentration, no reduction of GlcSph was found, indicating that pharmacological inhibition of Gba2 in a Gba1-deficient background fails to correct the accumulation of GlcSph at the developmental stage of 5 days post-fertilization. Using high concentrations of AMP-DNM and L-ido-AMP-DNM (10  $\mu$ M, **Figure 7C**), both Gba2 and Gcs were inhibited as indicated by the reduction of GlcChol and HexCer, mainly GlcCer levels (**Figure 7C**). At these high concentrations significant reduction in GlcSph also became apparent.

Thus, both Eliglustat and the iminosugars at higher dose were able to pharmacologically correct glycosphingolipid abnormalities in Gba1 deficient whole zebrafish larvae.

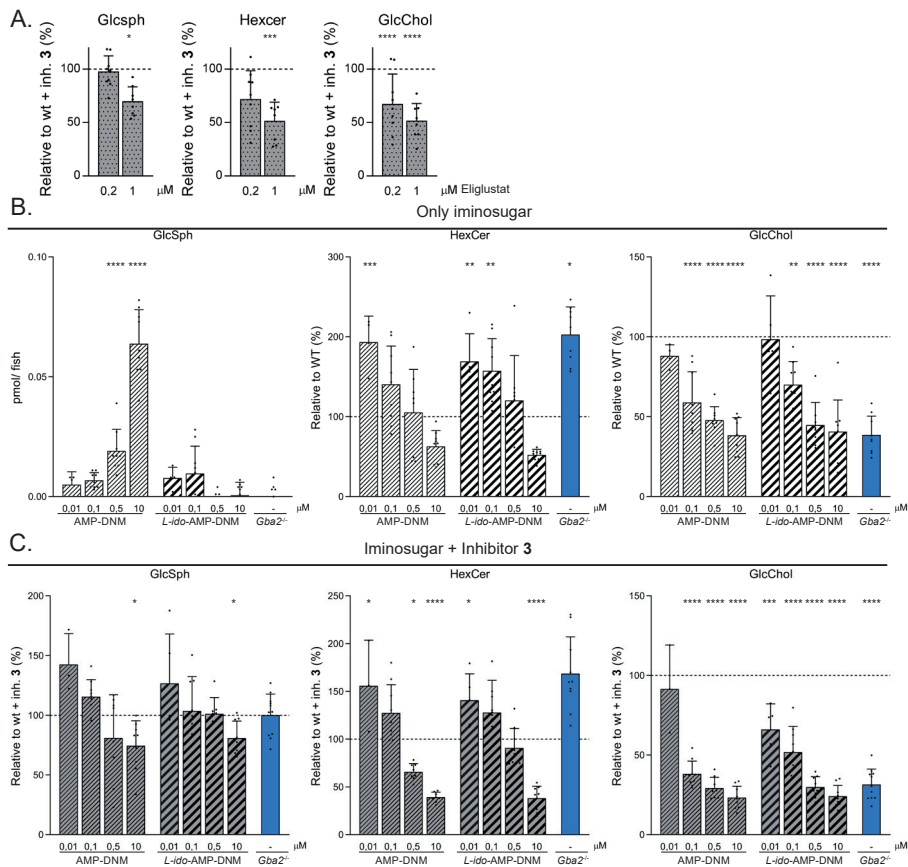


**Figure 7 | Pharmacological inhibition of Gba1, Gba2 and Gcs**  
(A) WT embryos were treated simultaneously with inhibitor 3 and Eliglustat. Lipid levels were determined of individual larvae (n = 8-9). Ratios of GlcSph, HexCer and GlcChol are depicted relative to WT embryos incubated with inhibitor 3 only (100% line). (B) WT embryos were incubated for 5 days with different concentrations of AMP-DNM (striped bars) or L-ido-AMP-DNM (thicker striped bars) and lipid levels were determined of individual larvae (n = 5-9). Data of GlcSph is depicted in pmol/larvae while ratios of HexCer and GlcChol are depicted relative to vehicle treated WT (100% line). (C) WT embryos were treated with inhibitor 3 (10 μM) and different concentrations of AMP-DNM (striped bars) or L-ido-AMP-DNM (thicker striped bars) and lipid levels were determined of individual larvae (n = 5-9). Data of GlcSph, HexCer and GlcChol is depicted relative to inhibitor 3 treated WT (100% line). Inhibitor 3 treated *gba2*<sup>-/-</sup> (blue bar) is used as control for pharmacological Gba1 inhibition in a full genetic Gba2 deficient background. Data is depicted as mean ± SD and analysed by One-Way Anova (Dunnett's test) with WT as control group. \* P < 0.05, \*\* P < 0.01, \*\*\* P < 0.001 and \*\*\*\* P < 0.0001.

### Rescue of Gba1 deficiency by expression or injection of human GBA1

Finally, we studied correction of abnormal glycosphingolipid metabolism by introducing human GBA1 to Gba1-deficient zebrafish embryos. Two approaches were used: overexpression of human GBA1 using the Tol2 transposase method<sup>46</sup> and injection of recombinant GBA1 enzyme (Cerezyme®) in the bloodstream of 2 dpf *gba1*<sup>-/-</sup> zebrafish embryos. The presence of active GBA1 was detected by labelling with ABP 1 (**Figure 8A**). Over-expression in the zebrafish resulted in the presence of human GBA1 with heterogeneous molecular weight, indicating differently glycosylated forms. Infusion of rGBA1 into the embryos led to the presence of one distinct band labelled by the ABP1 (Figure 7A). In the latter experiments variation among individual injected embryos was noted. The significant decrease in GlcSph indicates that both overexpression and infusion of human GBA1 functionally correct the absence of zebrafish Gba1 (**Figure 8B**).

In conclusion, glycosphingolipid abnormalities can be corrected by pharmacological and genetic intervention and corrections can be detected in individual zebrafish samples.

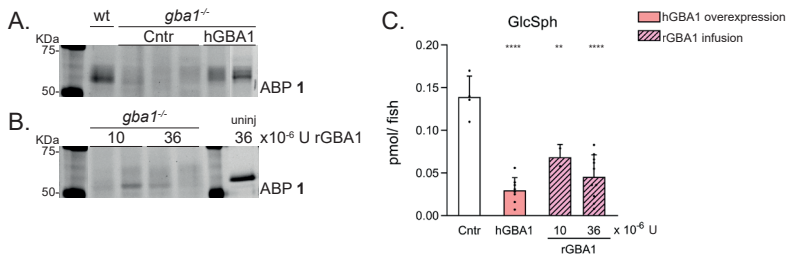


**Figure 8 | Glycosphingolipid correction by introduction of human GBA1**

(A) Human GBA1 was stably overexpressed in the *gba1*<sup>-/-</sup> zebrafish background using the ubiquitin promoter. Zebrafish Gba1 and human GBA1 was visualized with ABP 1. (B) Recombinant GBA1 was introduced by injection in the bloodstream of 2 dpf zebrafish with 10 or 36 x 10<sup>-6</sup> U rGBA1 (Cerezyme®) and visualized with ABP 1. An equivalent of 36 x 10<sup>-6</sup> U rGBA1 was labelled and used as control on gel. (C) GlcSph levels were determined in pmol/fish of uninjected, control *gba1*<sup>-/-</sup> zebrafish (n = 4), *gba1*<sup>-/-</sup> zebrafish stably overexpressing hGBA1 (n = 8) and *gba1*<sup>-/-</sup> zebrafish infused with rGBA1 (n = 2 or 10). Data is depicted as mean ± SD and analysed by One-Way Anova (Dunnnett's test) with WT as control group. \*\* P < 0.01 and \*\*\*\* P < 0.0001.



## Discussion

The primary goal of our investigation was to study GlcCer metabolism during deficiency of the lysosomal Gba1 in a whole organismal model. For this purpose, we selected developing zebrafish larvae until 5 dpf, an attractive model to investigate genetic disorders, related biochemical abnormalities and pharmacological or genetic correction of the disease. We particularly focussed on the potential role of cytosol-facing Gba2 in compensatory GlcCer metabolism during inadequate Gba1 activity. To generate a deficiency of Gba1 and/or Gba2 in zebrafish we used two different approaches: CRISPR/Cas9 mediated knockout of the *gba1* gene (*gba1*<sup>-/-</sup> fish) as well as chemical inactivation using specific inhibitors. A Cy5 fluorescent ABP, labelling active Gba1 enzyme molecules through covalent binding to the catalytic nucleophile<sup>7</sup>, was used to confirm the genetic knockout of Gba1 in *gba1*<sup>-/-</sup> fish as well as its complete inactivation by selective Gba1 inhibitor **3**<sup>31</sup>. Of note, ABP labelling of active Gba1 in *gba1*<sup>-/-</sup> and *gba1*<sup>-/-</sup>*gba2*<sup>-/-</sup> fish in the developing zebrafish embryo pointed to the presence of maternal Gba1. Apparently, maternal Gba1 enzyme is deposited by the heterozygous *gba1*<sup>+/-</sup> mother in the yolk of the embryo, a phenomenon described earlier for other lysosomal enzymes as well<sup>43</sup>.

The viability of *gba1*<sup>-/-</sup> and *gba1*<sup>-/-</sup>*gba2*<sup>-/-</sup> fish deserves notice<sup>38</sup>. In man and mice, a complete deficiency of GBA1 is not compatible with terrestrial life due to altered skin permeability causing trans-epidermal water loss<sup>37,47</sup>. Recently the abundant presence of active GBA1 in the stratum corneum of human skin has been visualized by labelling with a specific fluorescent ABP and zymography<sup>48</sup>. Fortuitously, different properties of fish skin and habitat allow generation of animals with a Gba1 deficiency.

We have earlier developed mass spectrometric methods, using identical <sup>13</sup>C-encoded standards, to sensitively quantify the key lipids of interest during GBA1 deficiency; the primary storage lipid GlcCer and the secondary metabolites GlcSph and GlcChol<sup>27,49</sup>. Mass spectrometry as such does not distinguish between lipids with a glucose or galactose moiety. We used HILIC chromatography to separate glucosyl- and galactosyl-containing lipids of additional larvae and observed that accumulated HexSph is solely GlcSph in 5 dpf larvae, while aberrant HexChol is solely GlcChol. In the case of HexCer about 30 % can be attributed to GalCer in 5 dpf WT zebrafish larvae, whereby GalCer levels do not change upon genetic or pharmacological modulation, and the vast majority being GlcCer, showing aberrant levels upon modulation.

The observed abnormalities in GlcCer and its metabolites GlcSph and GlcChol in 5 dpf Gba1 deficient larvae in the absence or presence of Gba2 warrant discussion. Total HexCer and the HILIC separated GlcCer were found to be not significantly abnormal in the *gba1*<sup>-/-</sup> larvae. Apparently, accumulating GlcCer in *gba1*<sup>-/-</sup> larvae can be alternatively metabolized to GlcSph by acid ceramidase or the presence of maternal enzyme in yolk offers somehow degradative capacity. In contrast, deficiency of Gba2 in the 5 dpf larvae does have a major impact on GlcCer levels. The *gba2*<sup>-/-</sup> larvae showed a clearly elevated HexCer level (two-fold), which is attributed to an increase in GlcCer levels and potentially accumulates at the cytosolic side of membranes. Combined Gba1 and Gba2 deficiency of does not lead to

more prominent HexCer accumulation than deficiency of Gba2 alone.

We assessed the marked elevation of GlcSph, which is from accumulating GlcCer in lysosomes by acid ceramidase<sup>17</sup>. The abnormality is exploited for diagnostic purposes and monitoring of GD patients regarding disease progression and correction by therapy<sup>19,44,50-52</sup>. Prominent accumulation of GlcSph develops in zebrafish with the *gba1*<sup>-/-</sup> background starting around 2-3 dpf, but not in WT or *gba2*<sup>-/-</sup> zebrafish larvae. Elevation of GlcSph is also rapidly induced by exposing larvae to the Gba1 suicide inhibitor **3**, independent of their *gba1* and *gba2* genotype. Thus, our data suggest that Gba2 status does not markedly influence GlcSph levels during Gba1 deficiency. This suggests that either the Gba2 activity towards GlcSph is insufficient to significantly reduce GlcSph accumulation formed in 5 dpf zebrafish or that GlcSph insufficiently reaches Gba2. Of note, Mistry and coworkers observed in mice with induced Gba1 deficiency in the white blood cell lineage an increased GlcSph that was not changed by combined Gba2 deficiency, similar to our findings with zebrafish embryos<sup>18</sup>.

The occurrence of GlcChol abnormalities in zebrafish impaired in Gba1 and/or Gba2 was assessed. The existence of GlcChol has been noted in chicken and mammalian tissues, while the glucosylated sterol was shown to be metabolized by GBA1 as well as GBA2<sup>27,53,54</sup>. Evidence has been presented for mice that GBA1 largely degrades GlcChol to glucose and cholesterol. Contrary, GBA2 forms GlcChol from GlcCer and cholesterol by transglucosylase activity<sup>27</sup>. In case of extreme intralysosomal cholesterol accumulation, as in NPC or chemically induced by U18666A, lysosomal GBA1 actively generates GlcChol via transglucosylation<sup>27</sup>. GlcChol levels tended to be elevated in *gba1*<sup>-/-</sup> and chemically induced Gba1-deficient larvae, in line with Gba1 involvement in GlcChol turnover. While a low level of GlcChol was detected in Gba2 deficient embryos at 8 hpf (0,05 pmol/fish), similar to WT embryos, GlcChol levels did not increase with age in the Gba2 deficient fish, in contrast to WT embryos. This illustrates the contribution of Gba2 to GlcChol biosynthesis in zebrafish, similarly to earlier observations in mice<sup>27</sup>. Taken together, this suggests that sterolglucoside metabolism by Gba1 and Gba2 in the zebrafish is similar to that observed in man and mouse (**Supplementary Table 1**)<sup>27,55</sup>. Given the observed abnormalities in GlcChol during abnormal GlcCer metabolism its physiological significance seems intriguing as well as the role of Gba1 and Gba2 in the molecular function of GlcChol.

The iminosugar Miglustat (*N*-butyl-deoxynojirimycin), a registered oral agent to treat mild type 1 GD, markedly inhibits GBA2 activity at the administered dose (3 times 100 mg daily)<sup>56</sup>. A very large number of type 1 GD patients have been treated with Miglustat for more than a decade without major side effects except for intestinal complaints due to inhibition of intestinal glycosidases<sup>57</sup>. Apparently, in these individuals GBA2 inhibition has no overt detrimental consequences. Moreover, concurrent deficiency of GBA2 in a mouse model with induced deficiency of GBA1 in the white blood cell lineage has been reported to exert positive effects, such as improvements in visceral, hematologic and skeletal symptoms<sup>18</sup>. A beneficial effect of GBA2 deficiency has been also observed for NPC mice, consistent with the use of the GBA2 inhibitor Miglustat in treatment of this disorder<sup>28</sup>. In sharp contrast to all these positive findings regarding reduced GBA2 activity during GBA1 deficiency, loss of function of GBA2 is reported to be associated with hereditary spastic paraplegia and

cerebellar ataxia in man<sup>58-60</sup>. A very recent study reported that some GBA2 KO mice display a strong locomotor defect, while other animals, with the same mutation but in a different background, show only mild alterations of the gait pattern and no signs of cerebellar defects<sup>45</sup>. It thus appears that the outcome of GBA2 deficiency may be subtly influenced by yet poorly understood factors. The recent notion that GBA2 has substrates beyond GlcCer, such as GlcChol, and potentially other glucosylated metabolites, may ultimately lead to an explanation for the presently puzzling heterogeneity in outcome of GBA2 deficiency. In **Supplementary Table 1** an overview is presented of reported glycosphingolipid abnormalities in different GBA1-, GBA2- and GBA1:GBA2 deficient animals (zebrafish, mice and man). Consistently GBA1 deficiency is associated with elevation of GlcSph and GBA2 deficiency with reduced GlcChol levels.

As final part of our investigation, we evaluated the feasibility of reducing GlcCer synthesis by inhibition of glucosylceramide synthase with potent cell-permeable inhibitors. The GCS specific inhibitor Eliglustat, registered for substrate reduction therapy of type 1 GD, led to the expected reduction of HexCer and concomitant decrease of GlcChol in 5 dpf zebrafish. A slight, but significant, decrease in GlcSph was also observed. The iminosugar *L-ido*-AMP-DNM, inhibiting GCS and GBA2 at high doses, also led to reductions of GlcSph and GlcChol in Gba1-deficient larvae. Thus, developing zebrafish embryos offer an organismal model to screen GCS and GBA2 inhibitors and to assess their corrective effect on lipid abnormalities. Also, enzyme replacement therapy was feasible in zebrafish larvae and showed GlcSph correction after injection of recombinant GBA1 with mannos-eterminal N-glycans in the bloodstream of 2 dpf zebrafish embryos.

Finally, genetic overexpression of human GBA1 in the zebrafish Gba1-deficient background ameliorated GlcSph accumulation. This indicates that the zebrafish model is able to synthesize human GBA1 protein, zebrafish Limp2 is able to transport it to the lysosome and the human GBA1 is functionally active in the lysosome shown by the significant reduction of GlcSph, all at the zebrafish optimal temperature of 28.5 °C.

Our present study has focused on the role of Gba2 in glycosphingolipid metabolism during deficiency of Gba1. It will be of great interest to study in the future the possible physiological implications of lipid abnormalities in mutant fish at adult age. It will be of interest to establish whether lipid laden macrophages also play an important role in the pathophysiology in zebrafish with deficient Gba1, as in Gaucher disease. Of interest is also a careful analysis of skin properties of Gba1-deficient zebrafish given the severe abnormalities observed in mice and man completely lacking GBA1<sup>36,37</sup>. Finally, investigation of the male gonads of Gba1-deficient zebrafish is warranted given the reported abnormalities in this tissue of GBA2-deficient rodents<sup>24,61</sup>. Earlier investigations by Zancan et al. and Keatinge et al. reported impaired bone ossification and microglial activation prior to alpha-synuclein-independent neuronal cell death in Gba1-deficient zebrafish, respectively<sup>38,39</sup>. Our mutant zebrafish with combined  $\beta$ -glucosidase deficiencies offer models to obtain further insight in the potential modulating role of Gba2 during Gba1 deficiency, subject of investigations described in chapter 7. This is of great interest, particularly since current treatments of GBA1-deficient Gaucher patients may impact on GBA2. For example, the registered drug Miglustat is a nanomolar GBA2 inhibitor<sup>56</sup>. The recently approved drug Eliglustat, a

potent inhibitor of glucosylceramide synthase, is used for substrate reduction therapy of Gaucher disease<sup>62,63</sup>. This agent, by lowering GlcCer, will likely concomitantly reduce the transglucosylase activity of GBA2 (28). At present it is entirely unclear whether reduction of GBA2 activity during GBA1 deficiency is harmful, beneficial or without consequence.

In conclusion, in zebrafish larvae the inactivation of Gba1 leads to a prominent increase in GlcSph, recently proposed to promote  $\alpha$ -synuclein aggregation characteristic for Parkinson's disease<sup>21</sup>, and a modest increase of GlcChol. Deficiency of Gba2 causes a modest increase in GlcCer levels and a prominent reduction in GlcChol. These findings are reminiscent to findings made in cultured cells as well as mice and humans treated with iminosugars known to inhibit GBA2<sup>28,64</sup>. Gba2 inactivation during Gba1 deficiency in zebrafish embryos exhibited only little impact on GlcSph levels but reduced GlcChol levels. Abnormalities in GlcSph and GlcChol levels in zebrafish can be corrected with iminosugar derivatives with inhibitory activity towards glucosylceramide synthase and Gba2 concomitantly. Regarding pathophysiology of Gaucher disease, models of GBA1 deficiency in the mouse are intrinsically more informative than models in zebrafish. The general physiology of mice is far closer to that of humans. However, the use of zebrafish offers some practical advantages such as the ease with which multiple genetic traits can be modified and the role of genetic modifiers can be subsequently studied. It is planned by us to introduce in fish with a Gba1-deficient background other traits, e.g. acid ceramidase deficiency that should prevent formation of GlcSph and is the subject of investigations described in chapter 6. In conclusion, zebrafish offer an organismal model to assess lipid abnormalities caused by Gba1 deficiency, the impact of Gba2 and the feasibility of pharmacological intervention.

## Acknowledgements

We thank The Netherlands Organization for Scientific Research (NWO–CW, ChemThem grant to J.M.F.G.A. and H.S.O.). Dr. J. Bing is kindly acknowledged for synthesizing ABP 2 used in this study and Arwin Groenewoud for sharing the ZF4 cells and plasmids of the Tol2 kit.

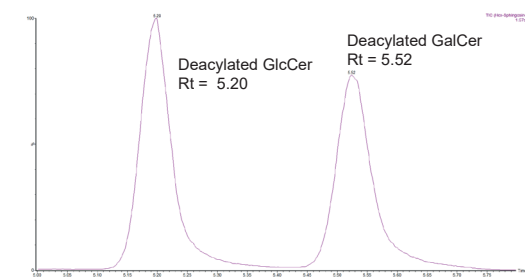
Supplementary Information

**Supplementary Table 1 | Overview of glycosphingolipid abnormalities in different GBA1-, GBA2- and GBA1:GBA2 deficient animal models.** Differences in GlcSph, GlcCer and GlcChol in tissues from human patients (Hu) and published GD models including zebrafish (Zf) and mouse (Ms). *Mx1-Cre<sup>+</sup>*: Gba1 deficiency in the white blood cell lineage, *Limp2*: transporter of GBA1 to lysosomes, *Npc1*: exporter of cholesterol from lysosomes; a defect leads to accumulation of cholesterol and glycosphingolipids. -: no significant increase or reduction, nd: not determined

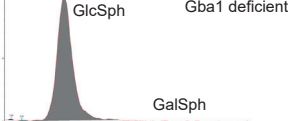
		Animal, organ	GlcSph	GlcCer	GlcChol	Reference
GBA1	Gaucher disease	Hu: plasma	↑↑↑	↑	↑	27,51
	Gba1 deficient (inhibitor 3)	Zf: larvae	↑↑	↑	↑	This chapter ref. 42
	<i>Gba1</i> <sup>-/-</sup> (Full KO)	Zf: larvae	↑↑↑	↑↑	nd	38
		Zf: brain	↑↑↑	↑↑	nd	
	<i>Mx1-Cre<sup>+</sup></i> :GD1	Ms: spleen	↑↑↑	↑	↑	18,27,65
		Ms: liver	↑↑	↑	↑	
GBA2	<i>Limp2</i> <sup>-/-</sup>	Ms: spleen	↑	-	nd	27,65
		Ms: liver	↑	-	↑	
	<i>Npc1</i> <sup>-/-</sup>	Ms: spleen	↑↑	↑	nd	65
GBA1:GBA2	Gba2 KO	Zf: larvae	-	↑	↓	This chapter ref. 42
	<i>Gba2</i> <sup>-/-</sup>	Ms: spleen	-	↑↑	↓	18,27,61,66
		Ms: liver	-	↑↑	↓	
		Ms: testis	nd	↑	nd	
GBA1:GBA2	Gba1:Gba2 KO	Zf: larvae	↑↑	↑	↓	This chapter ref. 42
	<i>Mx1-Cre<sup>+</sup></i> :GD1: <i>Gba2</i> <sup>-/-</sup>	Ms: spleen	↑↑	↑	nd	18
		Ms: liver	nd	↑	nd	
	<i>Npc1</i> <sup>-/-</sup> : <i>Gba2</i> <sup>-/-</sup>	Ms: brain	↑↑	↑	nd	28

HILIC separation - HexSph/ HexCer

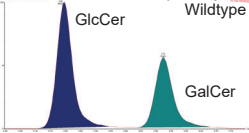
A. Standards (1:1)



B. HexSph

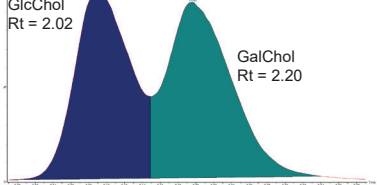


C. Neutral HexCer(deacylated)

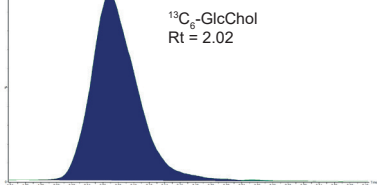


HILIC separation - HexChol

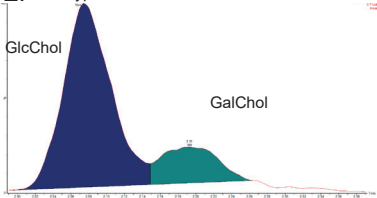
D. Standards (ratio 4:1)



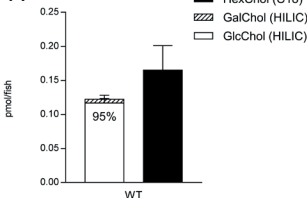
Internal standard (<sup>13</sup>C<sub>6</sub>-GlcChol)



E. Wildtype

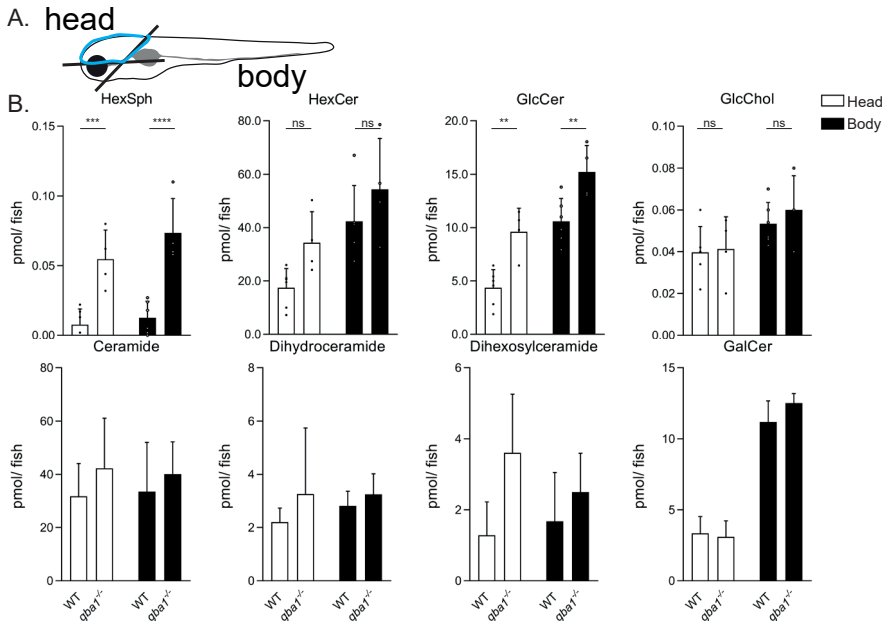


F.



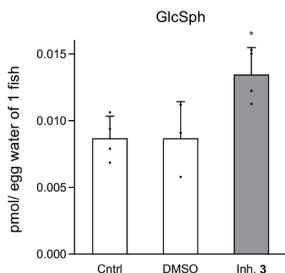
**Supplementary Figure 1 | Elution patterns of HexSph/ deacylated HexCer and HexChol using HILIC separation.**

(A) Elution profile of an equimolar mixture of glucosylceramide and galactosylceramide after microwave-assisted saponification. Deacylated GlcCer (measured as GlcSph) elutes at 5.20 min. and deacylated GalCer (measured as GalSph) elutes at 5.52 min. (B) Elution profile of the upper phase separating GlcSph and GalSph of a Gba1 deficient (inhibitor 3 treated) sample. (C) Elution profile of microwave-assisted deacylation of the lower phase separating deacylated GlcCer and GalCer (measured as GlcSph and GalSph respectively) of a WT sample. (D) Elution profile of a mixture of GlcChol and GalChol (ratio of 4:1) and the  $^{13}\text{C}$ -GlcChol internal standard. (E) Elution profile of a WT sample. (F) Levels of GlcChol and GalChol as determined by HILIC separation (white bar and striped bar respectively,  $n = 3$ ) in pmol/fish compared to HexChol as determined using standard methods (black bar; Figure 4B,  $n = 15$ ) in pmol/fish.



**Supplementary Figure 2 | (Glyco)Sphingolipid analysis in head- and body regions of zebrafish larvae**

(A) Schematic representation of the dissection of a zebrafish larvae into head and body. (B) Glycosphingolipid levels of dissected head and body regions of WT and  $gba1$  KO larvae at 5dpf in pmol/fish. Data is depicted as mean  $\pm$  SD and analysed using One-Way Anova (Dunnett's test) with wt as control group with \*\*\*  $P < 0.001$  and \*\*\*\*  $P < 0.0001$ .



**Supplementary Figure 3 | Excreted GlcSph in egg water: control egg water (no incubation), pooled egg water of DMSO incubated zebrafish individuals (500  $\mu\text{L}$ ,  $n = 5$  individuals) and pooled egg water of inhibitor 3 incubated zebrafish individuals (500  $\mu\text{L}$ ,  $n = 5$  individuals). GlcSph is calculated in pmol/egg water of 1 fish (100  $\mu\text{L}$ ) and depicted as mean  $\pm$  SD.**



## Experimental procedures

**Zebrafish** - Wild-type (WT) zebrafish (ABTL) were a mixed lineage of WT AB and WT TL genetic background. Injections to generate CRISPR/Cas9 mediated knock-out (KO) zebrafish were performed in ABTL embryos and adult zebrafish were outcrossed to ABTL WT zebrafish. *Gba1* mutant zebrafish were maintained as carriers (heterozygous in *gba1* genotype), while *gba2* mutant zebrafish were kept and crossed as KO (homozygous in genotype). *Gba1*<sup>-/-</sup>:*gba2*<sup>-/-</sup> double mutant larvae were continuously generated from adult zebrafish with a *gba1*<sup>+/-</sup>:*gba2*<sup>-/-</sup> background.

Zebrafish were housed and maintained at Leiden University, the Netherlands, according to standard protocols (zfin.org). Adult zebrafish were housed at a density of 40-50 adults per tank, on a cycle of 14 hour light and 10 hour dark and at 28 °C. The breeding of fish lines was approved by the local animal welfare committee (Instantie voor Dierwelzijn) of Leiden University and followed the international guidelines specified by the EU animal Protection Directive 2010/63/EU. Experiments were performed on embryos and larvae before the free-feeding stage, not falling under animal experimentation law according to the EU animal Protection Directive 2010/63/EU. Larvae of 6 and 7 dpf were used according to project licence AVD1060020184725. Embryos and larvae were grown in egg water (60 µg/mL Instant Ocean Sera Marin™ aquarium salts (Sera; Heinsberg, Germany)). During inhibitor incubations, fish were kept in E2 medium (15 mM NaCl, 0.5 mM KCl, 1 mM MgSO<sub>4</sub>, 150 µM KH<sub>2</sub>PO<sub>4</sub>, 50 µM Na<sub>2</sub>HPO<sub>4</sub>, 1 mM CaCl<sub>2</sub>, 0.7 mM NaHCO<sub>3</sub>, 0.5 mg/L methylene blue) at 28 °C.

**Zebrafish cell culture** - Zebrafish embryonic fibroblasts (ZF4 cells<sup>40</sup>) were cultured at 28 °C with 5 % CO<sub>2</sub> in DMEM/F12 (Sigma-Aldrich Chemie GmbH, St Louis, USA) supplemented with 10 % (v/v) Fetal Calf Serum, 1 % (v/v) Glutamax and 0.1 % (v/v) penicillin/streptomycin. Cells were harvested using trypsin (0.25 % (v/v) trypsin in PBS, no EDTA), washed twice with PBS and cell pellets were stored at -80 °C until use.

**Chemicals and reagents** - ABP **1** (ME569)<sup>34</sup>, ABP **2** (JJB367)<sup>8</sup>, compound **3** (ME656)<sup>31</sup>, AMP-DNM and L-ido-AMP-DNM<sup>30</sup>, eliglustat<sup>67</sup>, 13C5-sphinganine, 13C5-sphingosine, 13C5-GlcSph, 13C5-lyso-globotriaosylceramide (LysoGb3), C17-lysosphingomyelin (LysoSM), 13C6-GlcChol and C17-dihydroceramide<sup>27,49</sup> were synthesized as reported. The standards GlcCer (d18:1/16:0), GalCer (d18:1/16:0), β-D-galactosyl cholesterol (GalChol) were obtained from Avanti Polar lipids (Alabaster, USA) and GlcChol from Sigma-Aldrich Chemie GmbH. LC-MS grade methanol, 2-propanol, water, formic acid and HPLC grade chloroform were purchased from Biosolve (Valkenswaard, the Netherlands). LC-MS grade ammonium formate and sodium hydroxide from Sigma-Aldrich, butanol and hydrochloric acid from Merck Millipore (Billerica, USA).

**Genomic DNA extraction and PCR** - Genomic DNA (gDNA) of larvae or fin clips was extracted using QuickExtract™ (EpiCentre®, Madison, USA) by incubation at 65 °C for 10 min, followed by incubation at 98 °C for 5 min. Samples were vortexed, diluted with water and centrifuged quickly to spin down all non-processed particles which interfere in the PCR reaction. For rapid screening of genotypes, a high-resolution melt (HRM) analysis was used as described in Chapter 4 and reference 42.

**Generation of CRISPR/Cas9 mediated knockout zebrafish** - SgRNA targets were designed and sgRNA and Cas9 mRNA were synthesized and purified according to methods described in chapter 4 and <sup>42</sup>. Approximately 1 nL total volume of Cas9 mRNA and sgRNA (200 pg and 150 pg for Cas9 mRNA and sgRNA respectively) were co-injected into the yolk of one-or two-cell stage embryos. Embryos were checked regularly for unfertilized and dead embryos and subsequently raised to adulthood to generate founder fish (F0). Founder fish and F1 zebrafish with germline transmitted mutations were screened using the HRM analysis and Sanger Sequencing of positive samples, according to protocols described in chapter 4 and reference 42. All F1 heterozygous zebrafish were outcrossed to WT fish at least twice (> F3 heterozygous) before incrossing. *Gba1*<sup>+/-</sup>(Δ31 mutation) adult fish were crossed with each other and offspring thereof were used for experiments after genotyping. To generate GBA2-

deficient fish, adult F3 *gba2*<sup>-/-</sup> ( $\Delta 16$  mutation) fish with the desired mutation were crossed with each other and screened. Offspring of the F4 homozygous adult *gba2*<sup>-/-</sup> fish were used for experiments. For heterozygous *gba2* samples, *gba2*<sup>-/-</sup> larvae were obtained by crossing a *gba2*<sup>-/-</sup> female with a WT male while *gba2*<sup>+/-</sup> larvae were obtained by crossing a WT female with *gba2*<sup>-/-</sup> male. To obtain *gba1*<sup>+/-</sup>:*gba2*<sup>-/-</sup> zebrafish, *gba1*<sup>+/-</sup> adult fish were crossed with *gba2*<sup>-/-</sup> adult fish and raised to adulthood. Adult fish were screened for the desired mutations as described above. Double heterozygous *gba1*<sup>+/-</sup>:*gba2*<sup>-/-</sup> fish were crossed with heterozygous *gba2*<sup>+/-</sup> fish, adult fish were screened to obtain fish with the desired genotype (*gba1*<sup>+/-</sup>:*gba2*<sup>-/-</sup>) and the offspring of these fish were used for experiments.

Treatment of fish with inhibitors - Adult fish of WT, *gba1*<sup>+/-</sup>, *gba2*<sup>-/-</sup> or *gba1*<sup>+/-</sup>:*gba2*<sup>-/-</sup> genotype were crossed and developing offspring (8 h post-fertilization) were incubated in 100  $\mu$ L E2 medium immersed with vehicle (0.1-0.2 % (v/v) DMSO) or inhibitor (in 0.1-0.2 % (v/v) DMSO). For embryos of the *gba1*<sup>+/-</sup> and *gba1*<sup>+/-</sup>:*gba2*<sup>-/-</sup> crossings, samples were assigned to their genotype as described above. The Gba1 specific inhibitor **3** (Figure 1A<sup>31</sup>) was used at a final concentration of 10  $\mu$ M in all experiments, the iminosugar inhibitors AMP-DNM<sup>56</sup> and L-ido-AMP-DNM<sup>29</sup> at final concentrations of 10, 100 nM, 500 nM or 10  $\mu$ M and Eliglustat at 200 nM or 1  $\mu$ M final concentration. At 5 dpf, the larvae were washed three times with E2 medium before genotyping and subsequent labelling with ABPs or extraction of lipids as described above.

Generation of Tol2 mediated transgenesis of hGba1 zebrafish - The coding sequence of human GBA1 (NCBI code: NM\_000157) was amplified using Phusion high-fidelity DNA polymerase (primers in reference 42 and **chapter 2**) and subsequently cloned into pDONR using GATEWAY technology (BP reaction, Invitrogen) according to the manufacturer's instruction. The hGba1 Tol2 destination vector was obtained by recombining the pDONR-hGba1 with a p5E-ubi, p3E-polyA and pDEST-Tol2-crystalEye, from the Tol2 kit<sup>46</sup> using a LR reaction. The plasmid containing the Tol2 transposase sequence was linearized using NotI and purified (Nucleospin PCR and gel clean-up kit). Capped and polyadenylated Tol2 mRNA was generated using the mMessage mMachine<sup>®</sup> SP6 kit as described above for Cas9 mRNA. Approximately 1 nL total volume of Tol2 mRNA and pDEST-ubi:hGba1 (100 pg and 20 pg for Tol2 mRNA and plasmid respectively) were co-injected into the yolk of one- or two-cell stage embryos. At 5 dpf, larvae were screened for the expression of Cyan Fluorescent Protein (CFP) in the lens of the eyes and positive larvae were raised to adulthood. Adult zebrafish were crossed with the *gba1*<sup>+/-</sup> carriers, generating ubi:hGba1|*Gba1*<sup>+/-</sup> zebrafish which were crossed and offspring were used for experiments.

Injection of *gba1*<sup>-/-</sup> fish with Cerezyme - *Gba1*<sup>+/-</sup> adults were crossed and offspring (2 dpf) in the bloodstream (i.e. the vein under the yolk sac directed towards the heart) with 16 or 36  $\mu$ U rGba1 (Cerezyme<sup>®</sup>, 1 nL in 25 mM Kpi pH5.2; 1,6- 3.6x10<sup>-5</sup> U/mL; Sanofi Genzyme, Cambridge, USA). No increased lethality was observed after injections in either the yolk or in the bloodstream. At 5dpf, the larvae were collected, genotyped and subsequently labelled with ABPs or lipids were extracted as described above.

Homogenate preparation and protein concentration - ZF4 cell homogenates, oocyte, egg or whole zebrafish embryo homogenates were prepared in potassium phosphate (KPi lysis buffer; 25 mM K<sub>2</sub>HPO<sub>4</sub>-KH<sub>2</sub>PO<sub>4</sub> pH 6.5 + 0.1 % (v/v) Triton-X100 + 25 U/mL Benzonase<sup>®</sup> Nuclease (Merck, Darmstadt, Germany)) by sonication (20 % amplitude, 3 sec on, 3 sec off for 4 cycles) using a Vibra-Cell<sup>™</sup> VCX 130 (Sonics, Newtown, USA) while on ice. Total protein concentration of homogenates was determined using Pierce<sup>™</sup> BCA protein assay kit (Thermo Fisher Scientific, Waltham, USA) and measured using an EMax<sup>®</sup> plus microplate reader (Molecular Devices, Sunnyvale, USA).

Labelling of  $\beta$ -glucosidases with activity-based probes - ABP 1<sup>31</sup> was used for specific labelling of Gba1, whereas for concomitant labelling of the three  $\beta$ -glucosidases Gba1, Gba2 and Gba3, ABP 2 was used<sup>68</sup>. A WT homogenate was denatured prior to ABP labelling (lane -) to account for aspecific adhesion. ZF4 cell homogenate (10  $\mu$ L, 30  $\mu$ g protein) was preincubated with 5  $\mu$ L 300 mM Mcllvaine buffer (pH 2-8) for 5 min on ice before addition of ABP 1 (5  $\mu$ L; 400 nM in MQ with 2 % (v/v) DMSO, final concentration of 100 nM and 0.5 % (v/v) DMSO) or ABP 2 (5  $\mu$ L; 400 nM in MQ, 2 % (v/v) DMSO, final concentration of 100 nM and 0.5 % (v/v) DMSO). Samples were incubated for 30 min at 28 °C before addition of 5x Laemmli sample buffer (5  $\mu$ L; 25 % (v/v) 1.25 M Tris-HCL pH 6.8, 50 % (v/v) 100 % glycerol, 10 % (w/v) sodium dodecyl sulfate (SDS), 8 % (w/v) dithiothreitol (DTT) and 0.1 % (w/v) bromophenol blue) and boiled for 5 min at 98 °C.

Zebrafish homogenate (10  $\mu$ L, 1 zebrafish per incubation) was preincubated with 5  $\mu$ L 300 mM Mcllvaine (pH 2-8) for 5 min on ice before addition of ABP 1 or ABP 2 (5  $\mu$ L ABP 1; 4  $\mu$ M in MQ with 2 % (v/v) DMSO, final concentration of 1  $\mu$ M and 0.5 % (v/v) DMSO or 5  $\mu$ L ABP 2; 800 nM in MQ with 2 % (v/v) DMSO, final concentration of 200 nM and 0.5 % (v/v) DMSO). Samples were incubated for 30 min at 28 °C before addition of 5x Laemmli sample buffer (5  $\mu$ L) and samples were briefly boiled. Homogenates of zebrafish in different developmental stages (10  $\mu$ L, 1 egg or embryo per lane) were incubated with 10  $\mu$ L ABP 1 (2  $\mu$ M in 150 mM Mcllvaine pH 4 with 1 % (v/v) DMSO, final concentration of 1  $\mu$ M with 0.5 % (v/v) DMSO) or ABP 2 (200 nM in 150 mM Mcllvaine pH 6 with 1 % (v/v) DMSO, final concentration of 200 nM and 0.5 % (v/v) DMSO), incubated for 30 min at 28 °C, before addition of 5x Laemmli sample buffer (5  $\mu$ L) and samples were boiled for 5 min at 98 °C.

For characterization of the *gba1*, *gba2* and *gba1:gba2* double knockout, individual zebrafish 5 dpf larvae with different genotypes were homogenized in 30  $\mu$ L KPi buffer using a Dounce homogenizer (10 s; Pellet pestle motor, Kimble® Kontes). Zebrafish homogenate (10  $\mu$ L, 1/3 of a zebrafish) was incubated with ABP 1 and ABP 2 as described for the different developmental stages. In the case of experiments using Gba1 knockout and inhibitor 3 treated WT at different agents as well as larvae overexpressing human GBA1 or injected with Cerezyme were lysed in 20  $\mu$ L KPi buffer. Homogenate (1/3 of a zebrafish) was used to label active Gba1 with ABP 1 as described above, while human GBA1 was labelled using the optimal conditions for human GBA1 (2  $\mu$ M in 150 mM Mcllvaine pH 5.2 with 0.1 % (v/v) Triton-X100 and 0.2 % (w/v) Sodium Taurocholate and 1 % (v/v) DMSO, final concentration of 1  $\mu$ M with 0.5 % (v/v) DMSO)<sup>7</sup>.

Gel electrophoresis and fluorescence scanning - ABP-labelled protein samples were separated by electrophoresis on 8% (w/v) SDS-PAGE gel for 2 h at 90 V, before scanning the fluorescence of the wet-slab gel with a Typhoon FLA 9500 (GE Healthcare, Chicago, USA; Cy5 (635 nm  $\lambda_{ex}$ , 665 nm  $\lambda_{em}$ ), 750 V, pixel size 100  $\mu$ m).

Western blot and total protein staining -  $\beta$ -Actin as loading control was visualized by western blot using primary rabbit anti-actin antibody (ab8227, Abcam, Cambridge, UK) at 1:2000 and donkey anti-rabbit Horseradish Peroxidase (HRP)- linked secondary antibody (Bio-Rad laboratories Inc., Hercules, USA) at 1:5000. Chemiluminescence was visualized using a ChemiDocMP imager (Bio-Rad laboratories Inc.) in chemiluminescence settings with an exposure of 1 min. Total protein loading was visualized using Coomassie brilliant blue G250 and scanned on the ChemiDocMP imager.

(Glyco)sphingolipid analysis - Neutral (glyco)sphingolipids, (glyco)sphingoid bases and glycosylated cholesterol (HexChol) were extracted from the same individual zebrafish using an acidic Bligh and Dyer procedure (1:1:0.9 chloroform: methanol: 100 mM formate buffer pH 3.1) according to methods described before<sup>27,49,69</sup>. To an individual zebrafish was added 20  $\mu$ L of internal standard mixture (0.1 pmol/ $\mu$ L of <sup>13</sup>C<sub>5</sub>-sphinganine, <sup>13</sup>C<sub>5</sub>-sphingosine, <sup>13</sup>C<sub>5</sub>-GlcSph, <sup>13</sup>C<sub>5</sub>-lysoGb3 and C17-lysoSM in methanol), 20  $\mu$ L of C17-dihydroceramide (20 pmol/ $\mu$ L in methanol), 20  $\mu$ L of <sup>13</sup>C<sub>6</sub>-GlcChol (0.1 pmol/ $\mu$ L in methanol) followed by methanol and chloroform (2:1, v/v). After brief mixing, the samples were left at room temperature for 1 h with occasional stirring and 3x 1 min sonication in a bath sonifier (VWR

ultrasonic cleaner usc, Radnor, USA). Samples were centrifuged for 10 min at 13,000 rpm to spin down precipitated proteins. The supernatant was transferred to a clean tube, while excess organic solvent was evaporated and genomic DNA was extracted from the remaining material to validate the genotype. Chloroform and 100mM formate buffer pH 3.1 were added to the supernatant, to a final ratio of 1:1:0.9 methanol: chloroform: formate buffer, to induce separation of phases. The upper phase was used for analysis of lyso(glyco)sphingolipids and the lower phase for analysis of neutral (glyco)sphingolipids and HexChol. After centrifugation, the upper phase was transferred to a clean tube and the lower phase (chloroform phase) was extracted an additional time with methanol and formate buffer. Pooled upper phases were concentrated at 45 °C in an Eppendorf concentrator Plus and a butanol/water (1:1, v/v) extraction was performed. The upper phase (butanol phase) was transferred to a clean tube and concentrated. Lipids were dissolved in 100 µL methanol, stirred, sonicated for 30 sec in a bath sonifier and centrifuged. The supernatant was transferred to a vial for subsequent LC-MS/MS analysis. The remaining lower chloroform phase was transferred to a clean tube and the interphase was washed with chloroform. The pooled lower chloroform phases were split, whereby one part was used to analyse HexChol and the part for analysis of neutral glycosphingolipids was transferred to a pyrex tube and dried at 45 °C under a gentle stream of nitrogen. De-acylation was performed by adding 500 µL sodium hydroxide (0.1 M NaOH in methanol) using a microwave-assisted saponification method<sup>69</sup>. The samples were cooled and neutralized by adding hydrogen chloride (50 µL of 1 M HCl in methanol) and dried, followed by butanol/water extraction and prepared for LC-MS/MS as described above. For determination of HexChol<sup>27</sup>, the other half was concentrated, a butanol/water extraction was performed and samples were prepared for LC-MS/MS analysis as described above. Glycosphingolipid analysis was performed from three independent crossings and incubations, extractions and measurements using biological replicates as described in the results section. For hydrophilic interaction liquid chromatography (HILIC) separation, different individual larvae (n= 3-9) were extracted as described above and lipids were resuspended in acetonitrile:methanol (9:1, v/v) prior to transfer to LC-MS vials.

**LC-MS/MS** - Measurements were performed using a Waters UPLC-Xevo-TQS micro instrument (Waters Corporation, Milford, USA) in positive mode using an electrospray ionization (ESI source). For measurements of (glyco)sphingoid bases, deacylated neutral (glyco)sphingolipids and HexChol, a BEH C18 column (2.1 x 50 mm with 1.7 µm particle size, Waters) was used with eluents and LC-MS/MS programs as described previously for (glyco)sphingoid bases<sup>49</sup> and HexChol<sup>27</sup> respectively. A BEH HILIC column (2.1 x 100 mm with 1.7 µm particle size, Waters) was used at 30 °C for the separation of lipids with glucosyl and galactosyl moiety. In general, eluent A contained 10 mM ammonium formate in acetonitrile/water (97:3, v/v) and 0.01 % (v/v) formic acid and eluent B consisted of 10 mM ammonium formate in acetonitrile/water (75:15, v/v) and 0.01 % (v/v) formic acid. Lyso- and deacylated glycosphingolipids were eluted in 18 min with a flow of 0.4 mL/min using the following program: 85 % A from 0-2 min, 85-70 % A from 2-2.5 min, 70 % A from 2.5-5.5 min, 70-60 % A from 5.5-6 min, 60 % A from 6-8 min, 60-0 % A from 8-8.5 min, 0-85 % A from 8.5-9.5 min and re-equilibration of the column with 85 % A from 10-18 min. HexChol was eluted in 18 min with a flow of 0.25 ml/min using the following program: 100 % A from 0-3 min, 100-0 % A from 3-3.5 min, 0 % A from 3.5-4.5 min, 0-100 % A from 4.5-5 min and re-equilibration with 100 % A from 5-18 min. Data was analysed with MassLynx 4.1 Software (Waters).

**Statistics** - Statistical analysis were performed using GraphPad Prism (v7.00, GraphPadsoftware, CA, USA) and values are presented as mean ± SD. Lipid data were analysed by One-Way Anova using Dunnett's or Tukey's test as described in the results section. Ns=not significant, \*  $P < 0.05$ , \*\*  $P < 0.01$ , \*\*\*  $P < 0.001$  and \*\*\*\*  $P < 0.0001$ .

## References

1. Brady R.O., Kanfer J.N., Bradley R.M. and Shapiro D. (1966) Demonstration of a deficiency of glucocerebrosidase-cleaving enzyme in Gaucher's disease. *The Journal of clinical investigation* **45**, 1112-1115.
2. Beutler E. and Grabowski G.A. (2001) Gaucher disease. In *The Metabolic and Molecular Bases of Inherited disease*, Volume III, 8th Edition, C.R. Scriver, A.L. Beaudet, W.S. Sly and D. Valle, eds. (New York: McGraw-Hill), pp. 3635-3668.
3. Ferraz M.J., Kallemeijn W.W., Mirzaian M., Herrera Moro D., Marques A., Wisse P.,... and Aerts J.M. (2014) Gaucher disease and Fabry disease: new markers and insights in pathophysiology for two distinct glycosphingolipidoses. *Biochimica et biophysica acta* **1841**, 811-825.
4. Hollak C.E., Levi M., Berends F., Aerts J.M. and van Oers M.H. (1997) Coagulation abnormalities in type 1 Gaucher disease are due to low-grade activation and can be partly restored by enzyme supplementation therapy. *Br J Haematol* **96**, 470-476.
5. Sidransky E., Nalls M.A., Aasly J.O., Aharon-Peretz J., Annesi G., Barbosa E.R.,... and Ziegler S.G. (2009) Multicenter analysis of glucocerebrosidase mutations in Parkinson's disease. *New England Journal of Medicine* **361**, 1651-1661.
6. Tsuang D., Leverenz J.B., Lopez O.L., Hamilton R.L., Bennett D.A., Schneider J.A.,... and Zabetian C.P. (2012) GBA mutations increase risk for Lewy body disease with and without Alzheimer disease pathology. *Neurology* **79**, 1944-1950.
7. Witte M.D., Kallemeijn W.W., Aten J., Li K.Y., Strijland A., Donker-Koopman W.E.,... and Aerts J.M. (2010) Ultrasensitive in situ visualization of active glucocerebrosidase molecules. *Nature chemical biology* **6**, 907-913.
8. Kallemeijn W.W., Li K.Y., Witte M.D., Marques A.R., Aten J., Scheij S.,... and Overkleeft H.S. (2012) Novel activity-based probes for broad-spectrum profiling of retaining beta-exoglucosidases in situ and in vivo. *Angewandte Chemie* **51**, 12529-12533.
9. Barton N.W., Furbish F.S., Murray G.J., Garfield M. and Brady R.O. (1990) Therapeutic response to intravenous infusions of glucocerebrosidase in a patient with Gaucher disease. *Proc Natl Acad Sci U S A* **87**, 1913-1916.
10. Platt F.M., Jeyakumar M., Andersson U., Priestman D.A., Dwek R.A., Butters T.D.,... and Zimran A. (2001) Inhibition of substrate synthesis as a strategy for glycolipid lysosomal storage disease therapy. *J Inherit Metab Dis* **24**, 275-290.
11. Cox T., Lachmann R., Hollak C., Aerts J., van Weely S., Hrebicek M.,... and Zimran A. (2000) Novel oral treatment of Gaucher's disease with N-butyldeoxynojirimycin (OGT 918) to decrease substrate biosynthesis. *Lancet* **355**, 1481-1485.
12. Shayman J.A. (2010) ELIGLUSTAT TARTRATE: Glucosylceramide Synthase Inhibitor Treatment of Type 1 Gaucher Disease. *Drugs Future* **35**, 613-620.
13. Jung O., Patnaik S., Marugan J., Sidransky E. and Westbroek W. (2016) Progress and potential of non-inhibitory small molecule chaperones for the treatment of Gaucher disease and its implications for Parkinson disease. *Expert Rev Proteomics* **13**, 471-479.
14. Shayman J.A. (2018) Targeting Glucosylceramide Synthase in the Treatment of Rare and Common Renal Disease. *Semin Nephrol* **38**, 183-192.
15. Dahl M., Doyle A., Olsson K., Mansson J.E., Marques A.R.A., Mirzaian M.,... and Karlsson S. (2015) Lentiviral gene therapy using cellular promoters cures type 1 Gaucher disease in mice. *Mol Ther* **23**, 835-844.
16. Aerts J.M., Ferraz M.J., Mirzaian M., Gaspar P., Oussoren S.V., Wisse P.,... and Marques A.R.A. (2017) Lysosomal Storage Diseases. For Better or Worse: Adapting to Defective Lysosomal Glycosphingolipid Breakdown. In *eLS*. (John Wiley & Sons, Ltd), pp. 1-13.
17. Ferraz M.J., Marques A.R., Appelman M.D., Verhoek M., Strijland A., Mirzaian M.,... and Aerts J.M. (2016) Lysosomal glycosphingolipid catabolism by acid ceramidase: formation of glycosphingoid bases during deficiency of glycosidases. *FEBS Lett* **590**, 716-725.
18. Mistry P.K., Liu J., Sun L., Chuang W.L., Yuen T., Yang R.,... and Zaidi M. (2014) Glucocerebrosidase 2 gene deletion rescues type 1 Gaucher disease. *Proc Natl Acad Sci U S A* **111**, 4934-4939.
19. Lukas J., Cozma C., Yang F., Kramp G., Meyer A., Nesslauer A.M.,... and Rolfs A. (2017) Glucosylsphingosine Causes Hematological and Visceral Changes in Mice-Evidence for a Pathophysiological Role in Gaucher Disease. *Int J Mol Sci* **18**.
20. Nair S., Branagan A.R., Liu J., Boddupalli C.S., Mistry P.K. and Dhodapkar M.V. (2016) Clonal Immunoglobulin against Lysolipids in the Origin of Myeloma. *N Engl J Med* **374**, 555-561.
21. Taguchi Y.V., Liu J., Ruan J., Pacheco J., Zhang X., Abbasi J.,... and Chandra S.S. (2017) Glucosylsphingosine Promotes alpha-Synuclein Pathology in Mutant GBA-Associated Parkinson's Disease. *J Neurosci* **37**, 9617-9631.
22. Smith N.J., Fuller M., Saville J.T. and Cox T.M. (2018) Reduced cerebral vascularization in experimental neuronopathic Gaucher disease. *J Pathol* **244**, 120-128.

23. van Weely S., Brandsma M., Strijland A., Tager J.M. and Aerts J.M. (1993) Demonstration of the existence of a second, non-lysosomal glucocerebrosidase that is not deficient in Gaucher disease. *Biochimica et biophysica acta* **1181**, 55-62.
24. Yildiz Y., Matern H., Thompson B., Allegood J.C., Warren R.L., Ramirez D.M.,... and Russell D.W. (2006) Mutation of beta-glucosidase 2 causes glycolipid storage disease and impaired male fertility. *The Journal of clinical investigation* **116**, 2985-2994.
25. Boot R.G., Verhoeck M., Donker-Koopman W., Strijland A., van Marle J., Overkleeft H.S.,... and Aerts J.M. (2007) Identification of the non-lysosomal glucosylceramidase as beta-glucosidase 2. *J Biol Chem* **282**, 1305-1312.
26. Korschen H.G., Yildiz Y., Raju D.N., Schonauer S., Bonigk W., Jansen V.,... and Wachten D. (2013) The non-lysosomal beta-glucosidase GBA2 is a non-integral membrane-associated protein at the endoplasmic reticulum (ER) and Golgi. *J Biol Chem* **288**, 3381-3393.
27. Marques A.R., Mirzaian M., Akiyama H., Wisse P., Ferraz M.J., Gaspar P.,... and Aerts J.M. (2016) Glucosylated cholesterol in mammalian cells and tissues: formation and degradation by multiple cellular beta-glucosidases. *J Lipid Res* **57**, 451-463.
28. Marques A.R., Aten J., Ottenhoff R., van Roomen C.P., Herrera Moro D., Claessen N.,... and Aerts J.M. (2015) Reducing GBA2 Activity Ameliorates Neuropathology in Niemann-Pick Type C Mice. *PLoS one* **10**, e0135889.
29. Wennekes T., Meijer A.J., Groen A.K., Boot R.G., Groener J.E., van Eijk M.,... and Aerts J.M. (2010) Dual-action lipophilic iminosugar improves glycemic control in obese rodents by reduction of visceral glycosphingolipids and buffering of carbohydrate assimilation. *Journal of medicinal chemistry* **53**, 689-698.
30. Ghisaidoobe A.T., van den Berg R.J., Butt S.S., Strijland A., Donker-Koopman W.E., Scheij S.,... and Overkleeft H.S. (2014) Identification and development of biphenyl substituted iminosugars as improved dual glucosylceramide synthase/neutral glucosylceramidase inhibitors. *Journal of medicinal chemistry* **57**, 9096-9104.
31. Artola M., Kuo C.L., Lelieveld L.T., Rowland R.J., van der Marel G.A., Codee J.D.C.,... and Overkleeft H.S. (2019) Functionalized Cyclophellitols Are Selective Glucocerebrosidase Inhibitors and Induce a Bona Fide Neuropathic Gaucher Model in Zebrafish. *Journal of the American Chemical Society* **141**, 4214-4218.
32. Ordas A., Raterink R.J., Cunningham F., Jansen H.J., Wiweger M.I., Jong-Raadsen S.,... and Spaijk H.P. (2015) Testing tuberculosis drug efficacy in a zebrafish high-throughput translational medicine screen. *Antimicrobial agents and chemotherapy* **59**, 753-762.
33. Rennekamp A.J. and Peterson R.T. (2015) 15 years of zebrafish chemical screening. *Current opinion in chemical biology* **24**, 58-70.
34. Kuo C.L., Kallemeyn W.W., Lelieveld L.T., Mirzaian M., Zoutendijk I., Vardi A.,... and Artola M. (2019) In vivo inactivation of glycosidases by conduritol B epoxide and cyclophellitol as revealed by activity-based protein profiling. *FEBS J* **286**, 584-600.
35. Sultana S., Truong N.Y., Vieira D.B., Wigger J.G., Forrester A.M., Veinotte C.J.,... and van der Spoel A.C. (2016) Characterization of the Zebrafish Homolog of beta-Glucosidase 2: A Target of the Drug Miglustat. *Zebrafish* **13**, 177-187.
36. Sidransky E., Sherer D.M. and Ginns E.I. (1992) Gaucher disease in the neonate: a distinct Gaucher phenotype is analogous to a mouse model created by targeted disruption of the glucocerebrosidase gene. *Pediatr Res* **32**, 494-498.
37. Holleran W.M., Ginns E.I., Menon G.K., Grundmann J.U., Fartasch M., McKinney C.E.,... and Sidransky E. (1994) Consequences of beta-glucocerebrosidase deficiency in epidermis. Ultrastructure and permeability barrier alterations in Gaucher disease. *The Journal of clinical investigation* **93**, 1756-1764.
38. Keatinge M., Bui H., Menke A., Chen Y.C., Sokol A.M., Bai Q.,... and Bandmann O. (2015) Glucocerebrosidase 1 deficient Danio rerio mirror key pathological aspects of human Gaucher disease and provide evidence of early microglial activation preceding alpha-synuclein-independent neuronal cell death. *Human molecular genetics* **24**, 6640-6652.
39. Zancan I., Bellesso S., Costa R., Salvalaio M., Stroppiano M., Hammond C.,... and Moro E. (2015) Glucocerebrosidase deficiency in zebrafish affects primary bone ossification through increased oxidative stress and reduced Wnt/beta-catenin signaling. *Human molecular genetics* **24**, 1280-1294.
40. Driever W. and Rangini Z. (1993) Characterization of a cell line derived from zebrafish (*Brachydanio rerio*) embryos. *In Vitro Cell Dev Biol Anim* **29A**, 749-754.
41. Link V., Shevchenko A. and Heisenberg C.P. (2006) Proteomics of early zebrafish embryos. *BMC Dev Biol* **6**, 1.
42. Lelieveld L.T., Mirzaian M., Kuo C.L., Artola M., Ferraz M.J., Peter R.E.A.,... and Aerts J. (2019) Role of beta-glucosidase 2 in aberrant glycosphingolipid metabolism: model of glucocerebrosidase deficiency in zebrafish. *J Lipid Res* **60**, 1851-1867.
43. Fan X., Klein M., Flanagan-Steet H.R. and Steet R. (2010) Selective yolk deposition and mannose phosphorylation of lysosomal glycosidases in zebrafish. *J Biol Chem* **285**, 32946-32953.



44. Dekker N., van Dussen L., Hollak C.E., Overkleeft H., Scheij S., Ghauharali K.,... and Aerts J.M. (2011) Elevated plasma glucosylsphingosine in Gaucher disease: relation to phenotype, storage cell markers, and therapeutic response. *Blood* **118**, e118-127.
45. Woeste M.A., Stern S., Raju D.N., Grahn E., Dittmann D., Gutbrod K.,... and Wachten D. (2019) Species-specific differences in nonlysosomal glucosylceramidase GBA2 function underlie locomotor dysfunction arising from loss-of-function mutations. *J Biol Chem* **294**, 3853-3871.
46. Kwan K.M., Fujimoto E., Grabher C., Mangum B.D., Hardy M.E., Campbell D.S.,... and Chien C.B. (2007) The Tol2kit: a multisite gateway-based construction kit for Tol2 transposon transgenesis constructs. *Developmental dynamics : an official publication of the American Association of Anatomists* **236**, 3088-3099.
47. Farfel-Becker T., Vitner E.B. and Futerman A.H. (2011) Animal models for Gaucher disease research. *Dis Model Mech* **4**, 746-752.
48. van Smeden J., Dijkhoff I.M., Helder R.W.J., Al-Khakany H., Boer D.E.C., Schreuder A.,... and Bouwstra J.A. (2017) In situ visualization of glucocerebrosidase in human skin tissue: zymography versus activity-based probe labeling. *J Lipid Res* **58**, 2299-2309.
49. Mirzaian M., Wisse P., Ferraz M.J., Marques A.R.A., Gaspar P., Oussoren S.V.,... and Aerts J.M. (2017) Simultaneous quantitation of sphingoid bases by UPLC-ESI-MS/MS with identical (13)C-encoded internal standards. *Clin Chim Acta* **466**, 178-184.
50. Rolfs A., Giese A.K., Grittner U., Mascher D., Elstein D., Zimran A.,... and Mascher H. (2013) Glucosylsphingosine is a highly sensitive and specific biomarker for primary diagnostic and follow-up monitoring in Gaucher disease in a non-Jewish, Caucasian cohort of Gaucher disease patients. *PLoS one* **8**, e79732.
51. Mirzaian M., Wisse P., Ferraz M.J., Gold H., Donker-Koopman W.E., Verhoek M.,... and Aerts J.M. (2015) Mass spectrometric quantification of glucosylsphingosine in plasma and urine of type 1 Gaucher patients using an isotope standard. *Blood Cells Mol Dis* **54**, 307-314.
52. Arkadir D., Dinur T., Revel-Vilk S., Becker Cohen M., Cozma C., Hovakimyan M.,... and Zimran A. (2018) Glucosylsphingosine is a reliable response biomarker in Gaucher disease. *Am J Hematol* **93**, E140-E142.
53. Wertz P.W., Stover P.M., Abraham W. and Downing D.T. (1986) Lipids of chicken epidermis. *J Lipid Res* **27**, 427-435.
54. Akiyama H., Nakajima K., Itoh Y., Sayano T., Ohashi Y., Yamaguchi Y.,... and Hirabayashi Y. (2016) Aglycon diversity of brain sterylglucosides: structure determination of cholesteryl- and sitosterylglucoside. *J Lipid Res* **57**, 2061-2072.
55. Akiyama H. and Hirabayashi Y. (2017) A novel function for glucocerebrosidase as a regulator of sterylglucoside metabolism. *Biochim Biophys Acta Gen Subj* **1861**, 2507-2514.
56. Overkleeft H.S., Renkema G.H., Neele J., Vianello P., Hung I.O., Strijland A.,... and Aerts J.M. (1998) Generation of specific deoxynojirimycin-type inhibitors of the non-lysosomal glucosylceramidase. *J Biol Chem* **273**, 26522-26527.
57. Giraldo P., Andrade-Campos M., Alfonso P., Irun P., Atutxa K., Acedo A.,... and Pocovi M. (2018) Twelve years of experience with miglustat in the treatment of type 1 Gaucher disease: The Spanish ZAGAL project. *Blood Cells Mol Dis* **68**, 173-179.
58. Hammer M.B., Eleuch-Fayache G., Schottlaender L.V., Nehdi H., Gibbs J.R., Arepalli S.K.,... and Singleton A.B. (2013) Mutations in GBA2 cause autosomal-recessive cerebellar ataxia with spasticity. *Am J Hum Genet* **92**, 245-251.
59. Martin E., Schule R., Smets K., Rastetter A., Boukhris A., Loureiro J.L.,... and Stevanin G. (2013) Loss of function of glucocerebrosidase GBA2 is responsible for motor neuron defects in hereditary spastic paraplegia. *Am J Hum Genet* **92**, 238-244.
60. Woeste M.A. and Wachten D. (2017) The Enigmatic Role of GBA2 in Controlling Locomotor Function. *Front Mol Neurosci* **10**, 386.
61. Raju D., Schonauer S., Hamzeh H., Flynn K.C., Bradke F., Vom Dorp K.,... and Wachten D. (2015) Accumulation of glucosylceramide in the absence of the beta-glucosidase GBA2 alters cytoskeletal dynamics. *Plos Genet* **11**, e1005063.
62. Cox T.M., Drelichman G., Cravo R., Balwani M., Burrow T.A., Martins A.M.,... and Peterschmitt M.J. (2017) Eliglustat maintains long-term clinical stability in patients with Gaucher disease type 1 stabilized on enzyme therapy. *Blood* **129**, 2375-2383.
63. Mistry P.K., Lukina E., Ben Turkia H., Shankar S.P., Baris H., Ghosn M.,... and Peterschmitt M.J. (2017) Outcomes after 18 months of eliglustat therapy in treatment-naïve adults with Gaucher disease type 1: The phase 3 ENGAGE trial. *Am J Hematol* **92**, 1170-1176.
64. Ashe K.M., Bangari D., Li L., Cabrera-Salazar M.A., Bercury S.D., Nietupski J.B.,... and Marshall J. (2011) Iminosugar-based inhibitors of glucosylceramide synthase increase brain glycosphingolipids and survival in a mouse model of Sandhoff disease. *PLoS one* **6**, e21758.

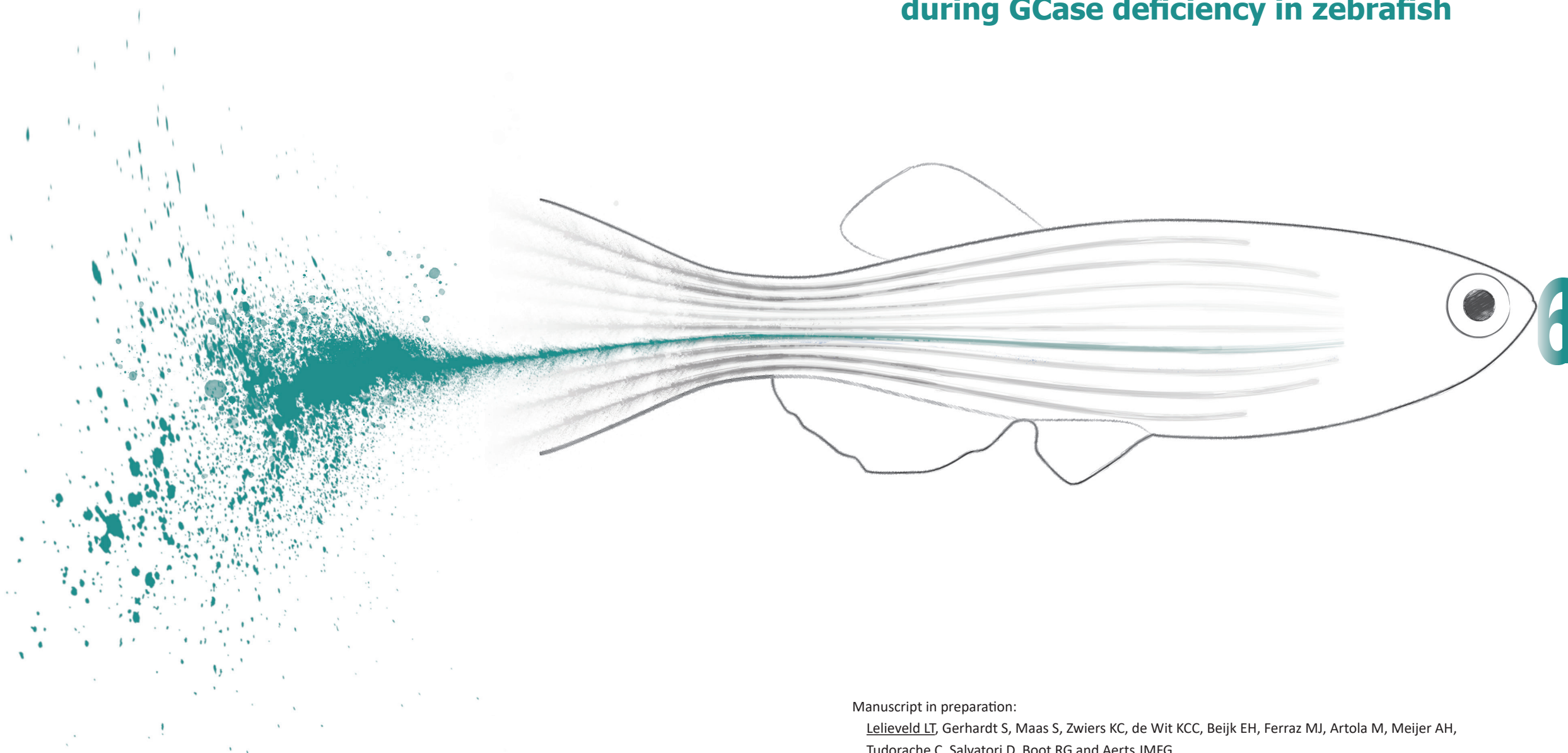


65. Ferraz M.J., Marques A.R., Gaspar P., Mirzaian M., van Roomen C., Ottenhoff R.,... and Aerts J.M. (2016) Lyso-glycosphingolipid abnormalities in different murine models of lysosomal storage disorders. *Mol Genet Metab* **117**, 186-193.
66. Yildiz Y., Hoffmann P., Vom Dahl S., Breiden B., Sandhoff R., Niederau C.,... and Mattheisen M. (2013) Functional and genetic characterization of the non-lysosomal glucosylceramidase 2 as a modifier for Gaucher disease. *Orphanet J Rare Dis* **8**, 151.
67. McEachern K.A., Fung J., Komarnitsky S., Siegel C.S., Chuang W.L., Hutto E.,... and Marshall J. (2007) A specific and potent inhibitor of glucosylceramide synthase for substrate inhibition therapy of Gaucher disease. *Mol Genet Metab* **91**, 259-267.
68. Schroder S.P., van de Sande J.W., Kallemeijn W.W., Kuo C.L., Artola M., van Rooden E.J.,... and Overkleeft H.S. (2017) Towards broad spectrum activity-based glycosidase probes: synthesis and evaluation of deoxygenated cyclophellitol aziridines. *Chemical communications* **53**, 12528-12531.
69. Groener J.E., Poorthuis B.J., Kuiper S., Helmond M.T., Hollak C.E. and Aerts J.M. (2007) HPLC for simultaneous quantification of total ceramide, glucosylceramide, and ceramide trihexoside concentrations in plasma. *Clin Chem* **53**, 742-747.



# CHAPTER 6

## The detrimental role of excessive GlcSph during GCase deficiency in zebrafish



Manuscript in preparation:

Lelieveld LT, Gerhardt S, Maas S, Zwiers KC, de Wit KCC, Beijik EH, Ferraz MJ, Artola M, Meijer AH, Tudorache C, Salvatori D, Boot RG and Aerts JMFG

- The detrimental role of excessive glucosylsphingosine during glucocerebrosidase deficiency

## Abstract

Deficiency of  $\beta$ -glucosidase (GCase) underlies Gaucher disease (GD), a lysosomal storage disorder. GD patients convert part of accumulating glucosylceramide through lysosomal acid ceramidase to the sphingoid base glucosylsphingosine (GlcSph). Chronically elevated GlcSph in blood and tissues of GD patients is thought to contribute to pathology. GCase-deficient *gba1* knockout (KO) zebrafish are viable and develop markedly increased GlcSph. Zebrafish have two orthologues of human acid ceramidase (ACase): *Asah1a* and *Asah1b*. From both single ACase KO fish only the *asah1b* KO fish fail to produce excessive GlcSph during GCase deficiency, while combined deficiency of both *Asah1a* and *Asah1b* is required to accumulate ceramide. Contrary to *gba1* KO fish, double deficient *gba1:asah1b* KO zebrafish show an ameliorated course of disease as reflected by a significant increase in lifespan (30-50%), with delayed development of abnormal locomotor activity and curved back. Both *gba1* and *gba1:asah1b* KO fish showed comparable GlcCer accumulation in tissues and similar induction in expression of storage-cell biomarkers chitinase (*chia.6*) and *gpnmb*. Infiltration of Gaucher-like cells in the periventricular grey zone of the optic tectum also appears comparable. In their brains the two mutant fish showed similar autophagy, indicated by increased protein levels of p62, and inflammation, reflected by increased mRNA levels of *il1- $\beta$* , *tnf $\beta$*  and *apoeb*, as well as indications for similar activation of the complement cascade. In conclusion, the generated mutant zebrafish suggest that excessive GlcSph, generated *in vivo* by ACase, is detrimental. Abolishing *Asah1b*-ACase results in some phenotypic improvements but it does not prevent all abnormalities such as storage cell formation and neuroinflammation.

## Introduction

Glucosylceramide (GlcCer) is a ubiquitous glycosphingolipid in cells and lipoproteins that acts as precursor of more complex glycosphingolipids. The breakdown of glycosphingolipids takes place in lysosomes where the penultimate step is catalysed by the acid  $\beta$ -glucosidase, named glucocerebrosidase (GCase) encoded by the *GBA* gene. Deficient activity of this enzyme causes Gaucher disease in which GlcCer characteristically accumulates in lysosomes of tissue macrophages that transform into storage cells. These 'Gaucher cells' are viable and secrete specific proteins into the circulation such as the enzyme chitotriosidase, the chemokine CCL18 and a soluble fragment of gpNMB<sup>1-3</sup>. The plasma levels of these proteins are clearly increased in symptomatic Gaucher patients and are presently used to assess the body burden of lipid-laden macrophages in patients<sup>4-6</sup>. More recently it has become clear that Gaucher cells are also the main source of the more than hundred-fold elevated glucosylsphingosine (GlcSph) in plasma of Gaucher patients<sup>7</sup>. This striking abnormality is widely employed to monitor Gaucher patients and assist diagnosis<sup>7</sup>. It has been speculated that excessive GlcSph contributes to signs and symptoms of Gaucher disease (see Ferraz *et al.* for a review<sup>8</sup>), including B cell activation and proliferation, aggregation of  $\alpha$ -synuclein in Parkinson's disease, impairment of osteoblast and a harmful role on cerebral microvasculature<sup>9-13</sup>. Moreover, repeated intravenous administration of a relative high dose of GlcSph to mice induces formation of lipid laden storage cells resembling Gaucher cells as well as hepatosplenomegaly and haematological symptoms<sup>14</sup>. Although these findings suggest direct and concentration-dependent roles for GlcSph in the pathological manifestations of Gaucher disease, the translation of findings made with *in vitro* experiments are hampered by the current lack of knowledge of local (sub)cellular concentration of GlcSph during GCase deficiency. Furthermore, it should be taken into account that high concentrations of GlcSph act as inhibitor of GCase and therefore may reduce any catalytic activity of the enzyme<sup>15</sup>. Because of this, the harmful effects observed upon chronic administration of excessive amounts of GlcSph might be partly indirect<sup>14</sup>.

Genetic and pharmacological evidence has been provided for the key role of acid ceramidase (ACase) in the excessive formation of GlcSph during GCase deficiency<sup>16</sup>. It was shown that fibroblasts from Farber patients, with inherited deficiency of ACase, do not form GlcSph upon inactivation of GCase as wildtype (WT) cells do. ACase (*N*-acylsphingosine deacylase; E.C. 3.5.1.23) is encoded by the gene (*ASAH1*) located on chromosome 8. ACase deficiency leads to the lysosomal storage disorder Farber disease (FD), with cells of classic FD patients typically showing less than 10% residual ACase activity. In spinal muscular atrophy with progressive myoclonic epilepsy (SMA-PME), ACase activity is also reduced but residual activity is higher, as much as 32% of controls<sup>17,18</sup>. Classic FD is characterized by deformed joints, subcutaneous nodules and progressive hoarseness, with neurological symptoms in severe patients. ACase hydrolyses ceramide (Cer) with a pH optimum of 4.5–5.0, rendering sphingosine and a free fatty acid as products. The enzyme is known to be able to catalyse the reverse reaction, generating Cer from sphingosine and free fatty acid at a pH optimum of 6.0<sup>19</sup>. ACase is a heterodimer consisting of an  $\alpha$ - (13 kDa) and a  $\beta$ -subunit (40 kDa)<sup>20</sup>. The enzyme is initially synthesized as N-glycated precursor and transported to lysosomes via mannose-6-phosphate mediated sorting. Inside the lysosome, ACase is

processed by autocleavage into the  $\alpha$  and  $\beta$  subunits, thus freeing the catalytic cysteine residue at the novel N-terminus of the  $\beta$ -subunit and triggering a conformational change that opens up the active site for substrate entry<sup>21-23</sup>.

The zebrafish has two orthologues of human ACCase, *Asah1a* and *Asah1b*, and the latter enzyme has been studied best<sup>24,25</sup>. The consequences of *Asah1b* deficiency in zebrafish larvae have been investigated using morpholino knockdown<sup>25</sup>. Morphants showed degeneration of neurons in the spinal cord and less branched motor-neuron axons. The residual acid-ceramidase activity was about 26% and no increase in Cer levels was detected.

Zebrafish lacking lysosomal GCase have been generated using CRISPR/Cas9 technology<sup>26</sup>. The GCase-deficient fish are viable and rapidly develop increased levels of GlcSph, mimicking Gaucher disease<sup>7</sup>. Additionally, small compounds were developed that allow rapid, on-demand inactivation of GCase in zebrafish<sup>27</sup>. In this chapter, gene knockouts of *asah1a* and/or *asah1b* were generated and subsequently studied to evaluate if one or both enzymes are required for formation of GlcSph in zebrafish deficient in GCase. Interestingly, only *Asah1b* is involved in GlcSph formation during GCase deficiency. Raising the double deficient *gba1<sup>-/-</sup>:asah1b<sup>-/-</sup>* fish, lacking excessive GlcSph, to adulthood revealed an improved phenotype compared to *gba1<sup>-/-</sup>* fish, with excessive GlcSph. Comparison of the mutant fish, at the predetermined end stage of 12 weeks post-fertilization (wpf), further indicated that the absence of GlcSph does not prevent inflammation in the brain nor impact on storage cells and increased GlcCer levels in liver and brain during GCase deficiency. The present study also uncovered that *Asah1b* deficiency alone does not cause severe accumulation of Cer. Active *Asah1a* seems to prevent this, given the observed Cer accumulation in *asah1a<sup>-/-</sup>:asah1b<sup>-/-</sup>* zebrafish larvae. In conclusion, a unique *Asah1b* deficient zebrafish model is presented. *Asah1b* deficient zebrafish are unable to deacylate the accumulating primary GlcCer substrate in *gba1<sup>-/-</sup>:asah1b<sup>-/-</sup>* and show an improved phenotype. In future endeavours, these *Asah1b* deficient zebrafish could enable the study of the impact of (toxic) lyso-lipids formed in other lysosomal storage disorders as well.

### Figure 1 | Alignment of the amino acid sequence of human ACCase, zebrafish *Asah1a* and *Asah1b* ►

The amino acid sequences of the pre-mature human ACCase (Uniprot code Q13510), zebrafish *Asah1a* (Uniprot code Q5XJR7) and *Asah1b* (Uniprot code Q6PH71) are aligned using ClustalO(1.2.4)<sup>29</sup>. \* indicates a conserved residue between the three sequences, : a strongly similar residue and . a weakly similar residue. The signal peptide is predicted using SignalP-5.0 and depicted in blue<sup>28</sup>. Important residues in human ACCase are coloured: the catalytic Cys143 is depicted in red, Cys31-Cys340 forming a disulfide bridge in pink, residues important for substrate hydrolysis and autocleavage in orange (Arg159 and Asp162, Glu225, Asn320 and Arg332) and the four assigned glycosylation sites in green<sup>22</sup>.

## Results

### Two acid ceramidase orthologues in zebrafish: asah1a and asah1b

A protein BLAST with human acid ceramidase (UniProt accession Q13510) revealed two zebrafish co-orthologues: Asah1a (Uniprot accession Q5XJR7) and Asah1b (Uniprot accession Q6PH71). To investigate differences between the human protein and both zebrafish orthologs, the protein sequences of human ACCase, Asah1a and Asah1b were aligned (**Figure 1**). The predicted Asah1a protein has 59% identity to the human protein, while Asah1b has 60% identity to the human ACCase, albeit the proteins have 70% identity to each other. The predicted signal peptide showed the most variation (depicted in blue)<sup>28</sup>. The four potential N-glycosylation sites are present in both zebrafish Asah1 proteins (Asn 173, Asn 259, Asn 286 and Asn 342 in yellow)<sup>22</sup>. The catalytic cysteine (Cys 143) in human ACCase, at the free N-terminus of the  $\beta$ -subunit after autocleavage, is present in a highly conserved region of both zebrafish Asah1 proteins (**Figure 1**). The  $\alpha$ - and  $\beta$ -subunit of the mature heterodimeric human ACCase protein are linked by a disulfide bond of Cys 31 and Cys 340, both being conserved in the zebrafish Asah1a and Asah1b proteins. Important residues in the  $\beta$ -subunit of human ACCase, such as Arg 159, Asp 162, Glu 225 and Asn 320, are conserved in both zebrafish proteins (green and orange for Arg/Asp and Glu/Asn respectively). These amino acids are thought to play roles in stabilizing the catalytic N-terminus and/or positioning the ceramide substrate during hydrolysis<sup>22</sup>.

		30		↓1a <sup>-8</sup>	
hACase	MPGRSCVALV-LLAAVSCAVAQHAPPWTE	CRKSTYP	PSGPTYRGAVP	WYTNIN	DLPPY 59
Asah1a	----MKLVFRYNALFISIFIHALYV-QGLE	DCRSGMY	PPKGP	TYRGVNTWY	TNLDLPPS 55
Asah1b	MNNRLNLCCFFI-LSYMCMLSAQYVPPFTE	DCRSGMY	PPNGPT	FKGDVSWY	TVDLDPAS 59
	: :	* :.	*****	***.***:	* * * * : * * * *
		↓1b <sup>+11</sup>			
hACase	KRWHEMLDKAPVLKIVIVNSLKNMINTFV	PSGKIMQV	VEKLPGL	LGNF	GFPEEEMKGI 119
Asah1a	ERWTQIIKDKNTELIEMVQTIKDMAKGF	-HGKLVN	FVDKEL	PFIVDTL	PNPFNEEIKGI 114
Asah1b	KRWTDVIDSKKTEMASMIQAIRDLADAFV	PSGKLIQL	VDKDPL	VMVDTL	PFYPFNEEIRGI 119
	: ** : : : * :	: : : : : . *	: * : : : * : *	: : : . *	: * : * : : * *
		▽			
hACase	AAVTDIPLGEIISFNIFYELFTICTSIVA	EDKKGH	LIHGRN	DFGV	LGNINNDTWVIT 179
Asah1a	AAVSGIPLGEIALFNIFYEVFTVCTSL	VAEDN	NGNIYH	GRNLD	FGLFMGWDRQNKTTWIT 175
Asah1b	ASVSGVPLGEVVLNFNIFYEVFTVCT	SLVAED	VNGLIHA	RNLD	FGLFMGWDLKNSRVVIT 179
	* : : : * * * * :	* * * * * : * * * * :	* : : * * : * * * * :	* : * * : * * * * :	* : * : * :
		200		220	
hACase	EQLKPLTVNLDFQRNNKTVFKASSFAGY	VGMLTG	FKPGLF	SLTLN	ERFSINGGYLGILEW 239
Asah1a	EKLKPLVVNINFERKNQTVFKSTSFAGY	VGMLTG	IRPGL	TLTMN	ERFDFGGYIGILDW 235
Asah1b	EKLKPLVVNIDFTRNGQTVFKSTNFAGY	VGMLTG	IHQNS	FTLTMN	ERFSLDGGYIGILEW 239
	* : * * * * : * *	* : : * * * * : .	: : * : * * * * :	* : * * * * :	* : * * * * :
		260		280	
hACase	ILGKKDVMWIGFLTRTVLENSTSYEEA	KNLLTK	KILAPAY	FILGG	NQSGEGCVITRDRK 299
Asah1a	IFGNRDGMWGTGLTRRVLENSTSYEDA	KDQLS	QTKLLAP	VYFIL	GGNRTGQGCIVITRRI 294
Asah1b	ILGKRDMWMSFLTRSVLENATSYESA	KALLSD	TKLLAPAY	FILGG	NQSGEACIITRSRT 299
	* : : : * * * * :	* * * * * : * * * * :	* : * * * * :	* * * * * :	* : * * * * :
		320		340	
hACase	ESLDVYELDAKQGRWYVVTNYDRWK	HFFLD	DRTPAK	MCNL	RNTSQENISFETMYDVLS 359
Asah1a	NTLDIWELEMLGRWYVLETNVDHWD	KPMFLD	DRTPAM	KCMNQ	TTQANISLASIYNVLS 355
Asah1b	QNISPLELVNKNRGRWYVLETNVDH	WKEFLD	DRTPAM	KCMNQ	TTQTNISVKTVDVLS 359
	: : . * * :	* * * * * : * * * * :	* : * * * * :	* * * * :	* : * * * * :
		380			
hACase	TKPVLNKLTVYTTLIDVTKGQFETYLR	DCPD	PCIGW		395
Asah1a	TKPVLNKLTTYTSLMAVSTGTLESYVR	DCPN	CTFPW		390
Asah1b	TKPVLNKLTTYTTLMEVSKGTLESFIR	DCPN	CPMPW		395
	*****	* : * * :	* : * * :	* : * * :	* * *

Generation of CRISPR/Cas9 mediated knockouts of Asah1a and Asah1b

To study the role of zebrafish ACases *in vivo*, CRISPR/Cas9 mediated knockouts of Asah1a and Asah1b were generated. SgRNA sequences were selected in the third exon of *asah1a*, located on chromosome 14, and the fourth exon of *asah1b* located on chromosome 1 (Figure 2A and B, top and middle panels). Injection of Cas9 mRNA and the appropriate sgRNA in the single-cell stage of wildtype (WT) embryos resulted in founder fish with a germline transmitted deletion of 8 bp for *asah1a* and an insertion of 11 bp for *asah1b* (Figure 2A and B, lower panels). The predicted stop-codons of these mutations are located in exon 3 and exon 4 for *asah1a* and *asah1b* respectively, both in the translated  $\alpha$ -subunit (mutation marked in Figure 1 with an arrow), resulting in no functional  $\beta$ -subunit.

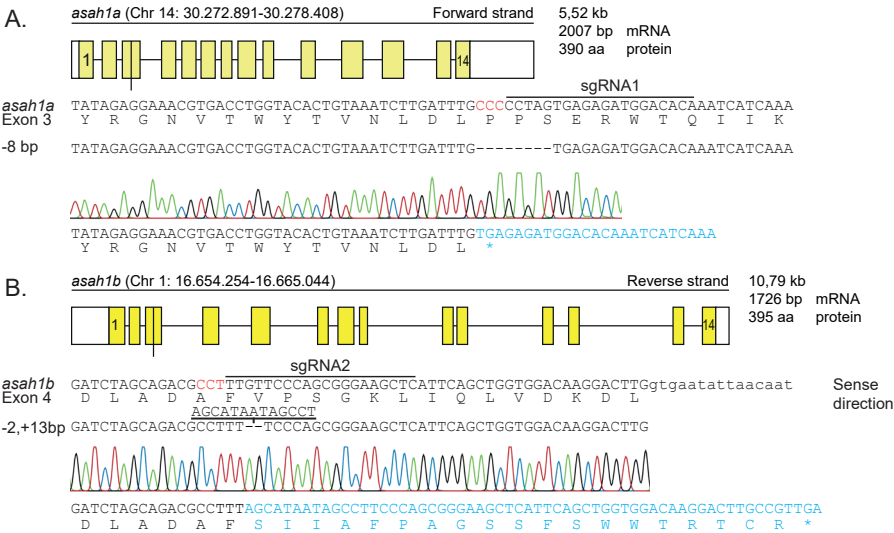


Figure 2| CRISPR/Cas9 mediated disruption of Asah1a and Asah1b in zebrafish

(A) Top panel: Schematic representation of the *asah1a* gene on chromosome 14, encoding the predicted 390 amino acid Asah1a enzyme. Middle panel: DNA sequence of exon 3 of *asah1a* with sgRNA target 1 lined, the PAM site in red and the protein sequence shown below. Lower panel: The 8 base pair deletion, as obtained from the sequence trace, leads to a premature stopcodon (\*). (B) Top panel: Schematic representation of the *asah1b* gene on chromosome 1, encoding the predicted 395 amino acid Asah1b enzyme, with the exon in upper case and intron in lower case. Middle panel: DNA sequence of exon 4 of *asah1b* with sgRNA target 2 lined, the PAM site in red and the protein sequence shown below. Lower panel: The sequence trace showed an insertion of 11 base pairs, which leads to a change amino acid sequence and a premature stopcodon (\*).



### Only the double knockout of *asah1a:asah1b* accumulates primary substrate ceramide

Double heterozygous *asah1a<sup>-/-</sup>:asah1b<sup>-/-</sup>* were crossed and lipid analysis of WT, *asah1a<sup>-/-</sup>*, *asah1b<sup>-/-</sup>* and *asah1a<sup>-/-</sup>:asah1b<sup>-/-</sup>* zebrafish larvae (5 dpf) showed that ceramide was only significantly increased in *asah1a<sup>-/-</sup>:asah1b<sup>-/-</sup>* fish (**Figure 3A**). This finding indicates that Asah1a and Asah1b enzymes are both able to hydrolyse ceramide and that a single enzyme deficiency is not enough to cause ceramide accumulation.

### Only Asah1b generates GlcSph during GCase deficiency

To study the role of either ACase in GCase deficiency we exposed developing zebrafish embryos lacking either Asah1a, Asah1b, or both, to a specific suicide inhibitor of GCase (ME656), known to rapidly inactivate the GCase enzyme<sup>27</sup>. Inhibitor treated WT zebrafish larvae (5 dpf) showed a significant increase in hexosylceramide (HexCer), primarily GlcCer as determined before<sup>26</sup>, GlcChol and GlcSph (**Figure 3B and C**). Contrary to Asah1a-deficient larvae, the inhibitor-treated animals deficient in Asah1b did not show the striking GlcSph elevation, although Asah1b-deficient larvae did accumulate GlcChol and HexCer (**Figure 3C**). In addition, GlcSph levels did not increase in double genetic *gba1<sup>-/-</sup>:asah1b<sup>-/-</sup>* larvae (**Supplementary Figure 1**). Thus, Asah1b in the zebrafish seems responsible for the generation of GlcSph during GCase deficiency.

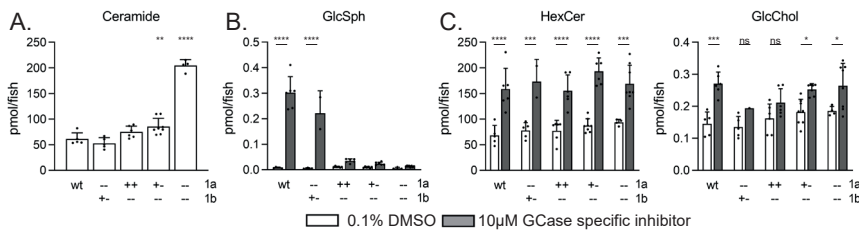


**Figure 3 | (Glyco)sphingolipid abnormalities in Asah1a and/or Asah1b deficient zebrafish larvae**

**(A)** Total ceramide levels were determined of individual zebrafish larvae (5 dpf) of off-spring of *Asah1a<sup>-/-</sup>:asah1b<sup>-/-</sup>* crossings in pmol/fish. Data is depicted as mean  $\pm$  SD and analysed using a Two-Way Anova with Tukey's multiple comparisons Test. **(B)** *Asah1a<sup>-/-</sup>:asah1b<sup>-/-</sup>* adult zebrafish were crossed and off-spring was treated with vehicle (0.1% (v/v) DMSO) or 10  $\mu$ M GCase specific inhibitor (ME656) for 5 days. Relevant lipid levels were determined of individual larvae in pmol/fish. WT (n = 5-6), *asah1a<sup>-/-</sup>:asah1b<sup>-/-</sup>* (n = 1-5), *asah1a<sup>-/-</sup>:asah1b<sup>-/-</sup>* (n = 6), *asah1a<sup>-/-</sup>:asah1b<sup>-/-</sup>* (n = 7-8) and *asah1a<sup>-/-</sup>:asah1b<sup>-/-</sup>* (n = 4-8). Data is depicted as mean  $\pm$  SD and analysed using a Two-Way Anova with Sidak's multiple comparisons test. In general, statistical comparisons are depicted only when a significant difference is apparent and relevant. Ns = not significant, \* P < 0.05, \*\* P < 0.01, \*\*\* P < 0.001 and \*\*\*\* P < 0.0001.

### Biochemical hallmarks in livers and brains of *gba1*<sup>-/-</sup> and *gba1*<sup>-/-</sup>:*asah1b*<sup>-/-</sup> fish

WT, *gba1*<sup>-/-</sup> fish, *asah1b*<sup>-/-</sup> and double deficient *gba1*<sup>-/-</sup>:*asah1b*<sup>-/-</sup> fish were raised to adulthood and (glyco)sphingolipid composition, mRNA expression, protein expression and histopathology of relevant organs were analysed at 12 weeks post-fertilization (wpf).

*Gba1*<sup>-/-</sup> adult zebrafish showed a phenotype as described before<sup>30</sup> and were culled at earlier stages when predetermined end points were observed (t = 10-11 wpf).

### Gaucher-like cells in visceral organs of *gba1*<sup>-/-</sup>:*asah1b*<sup>-/-</sup> fish

Excessive GlcSph was only detected in the livers of *gba1*<sup>-/-</sup> zebrafish (**Figure 4A**). GlcCer was increased comparably in *gba1*<sup>-/-</sup> and *gba1*<sup>-/-</sup>:*asah1b*<sup>-/-</sup> livers (5000 pmol/mg, **Figure 4A**). GlcChol was significantly increased in *gba1*<sup>-/-</sup> fish (10 pmol/mg liver), but not in *gba1*<sup>-/-</sup>:*asah1b*<sup>-/-</sup> fish. The livers of *gba1*<sup>-/-</sup>:*asah1b*<sup>-/-</sup> fish showed minor increases of Cer, GalCer and LacCer (**Figure 4A**). This was not prominent in the tissues of *gba1*<sup>-/-</sup> fish and *asah1b*<sup>-/-</sup> fish.

Next, the expression of mRNAs encoding specific proteins were studied in livers of the different zebrafish (**Figure 4B**). A significant increase in expression of the storage-cell biomarker *gpnmb* was apparent in *gba1*<sup>-/-</sup> and *gba1*<sup>-/-</sup>:*asah1b*<sup>-/-</sup> zebrafish livers. However, no prominent difference in expression of an orthologue of human chitotriosidase (*chia.6*) was detected, while the lysosomal protease Cathepsin D (*catD*) and the inflammatory cytokine *il-1β* showed a slight, but not significant increase and *tnfβ* showed only a significant increase in *gba1*<sup>-/-</sup> livers. To analyse the pathology of multiple different organs and tissues, the whole body of the fish was sectioned sagittally (**Figure 4C-E**).

The liver of zebrafish differs from the mammalian one: the zebrafish liver is not organized in hepatic lobules and Kupffer cells seem absent<sup>31</sup>. In addition, pancreatic cells of the zebrafish are scattered along the intestinal tract<sup>31</sup>. Infiltration of Gaucher-like cells was detected in the liver, spleen and pancreatic cell rich tissue of *gba1*<sup>-/-</sup> and *gba1*<sup>-/-</sup>:*asah1b*<sup>-/-</sup> zebrafish (**Figure 4D** and **E**). Lesions with Gaucher-like cells were apparent in *gba1*<sup>-/-</sup>:*asah1b*<sup>-/-</sup> tissue. No apparent pathological observations were noticed in tissues of *asah1b*<sup>-/-</sup> fish (**Supplementary Figure 2**).

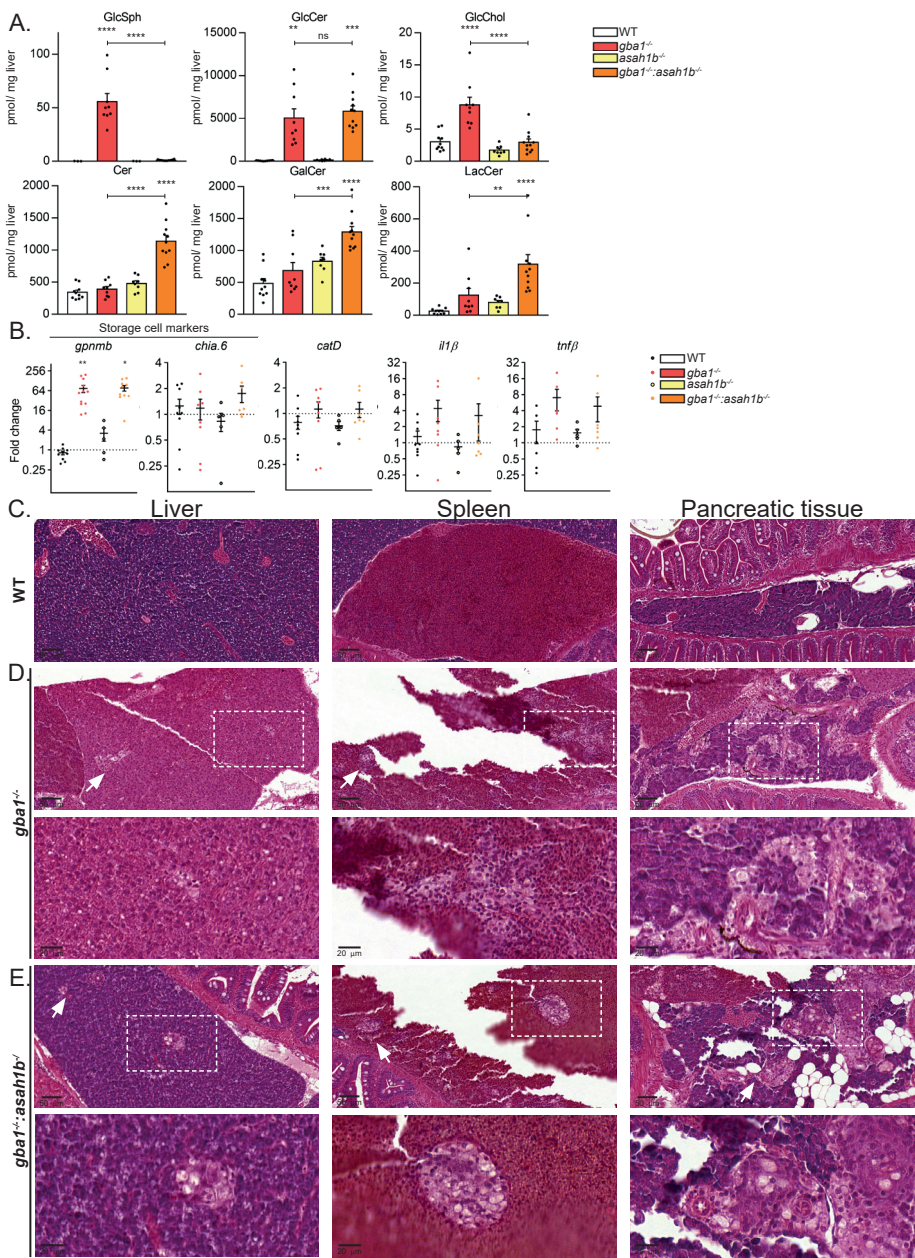


**Figure 4 | Abnormalities in adult zebrafish visceral organs**

(A) Lipid levels were determined in pmol/mg liver tissue. Data is depicted as mean ± SEM; WT (n = 10), *gba1*<sup>-/-</sup> (n = 9), *asah1b*<sup>-/-</sup> (n = 8), *gba1*<sup>-/-</sup>;*asah1b*<sup>-/-</sup> (n = 11). Data is analysed by One-Way Anova (Dunnett's test) with WT as control group. (B) Expression of *gpnmb*, *chia.6*, *il-1β*, *tnfr1*, *apoEb* or *catD* mRNA levels were determined using RT-qPCR analysis; WT (n = 6-9), *gba1*<sup>-/-</sup> (n = 6-8), *asah1b*<sup>-/-</sup> (n = 5), *gba1*<sup>-/-</sup>;*asah1b*<sup>-/-</sup> (n = 7). Data is normalized using two housekeeping genes (*ef1a* and *rpl13*) and analysed by One-Way Anova (Dunnett's test) with WT as control group. H&E staining of liver, spleen and pancreatic tissue of WT (C), *gba1*<sup>-/-</sup> (D) and *gba1*<sup>-/-</sup>;*asah1b*<sup>-/-</sup> (E) zebrafish. Higher magnifications of oxed areas are shown below the respective lower magnifications. \* P < 0.05, \*\* P < 0.01, and \*\*\*\* P < 0.0001.

**Similar lipid abnormalities, autophagy and inflammation in the brain of *gba1<sup>-/-</sup>:asah1b<sup>-/-</sup>***

Analysis of the lipid composition of brains of the mutant zebrafish and that of matched WT animals (**Figure 5A**) showed that the total Cer levels are normal. Accumulation of GlcSph is profound in brains of *gba1<sup>-/-</sup>* zebrafish ( $\pm 0.16$  to 130 pmol/mg for brains of WT and *gba1<sup>-/-</sup>* respectively), while no significant increase in GlcSph levels is detected in brains of *gba1<sup>-/-</sup>:asah1b<sup>-/-</sup>* zebrafish ( $\pm 10$  pmol/mg). The primary substrate of GCase, GlcCer, is comparably elevated in brains of both *gba1<sup>-/-</sup>* and *gba1<sup>-/-</sup>:asah1b<sup>-/-</sup>* ( $\pm 100$ -fold and 120-fold), as well as that of the product glycosphingolipid LacCer ( $\pm 22$ -fold and 33-fold, respectively). GlcChol is elevated in brains of *gba1<sup>-/-</sup>* zebrafish ( $\pm 2.5$ -fold) and slightly in brains of *gba1<sup>-/-</sup>:asah1b<sup>-/-</sup>* fish ( $\pm 1.3$ -fold). The abundant myelin lipid GalCer is only slightly decreased in *gba1<sup>-/-</sup>* brains, however variation among individual fish in this lipid was marked.

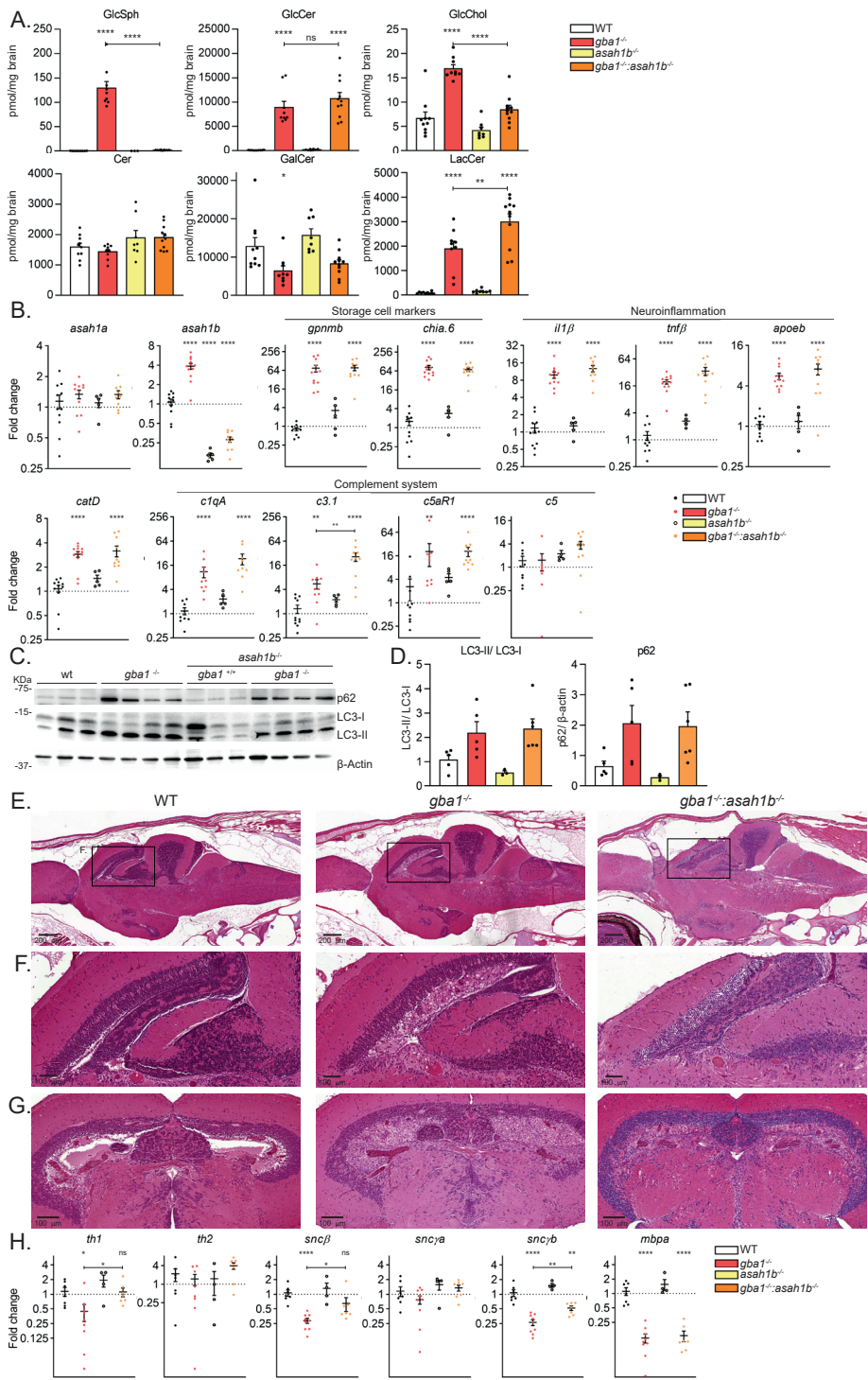
Next, the expression of mRNAs in brains of the different zebrafish were analysed (**Figure 5B**). In both *gba1<sup>-/-</sup>* and *gba1<sup>-/-</sup>:asah1b<sup>-/-</sup>* brains, expression of *gpnmb* and *chia.6* was strikingly increased ( $\pm 70$ -fold for *gpnmb* and *chia.6*). In parallel, we observed increased expression of mRNAs of inflammatory cytokines *il1- $\beta$*  ( $\pm 6.5$ -fold and 8.5-fold for brains of *gba1<sup>-/-</sup>* and *gba1<sup>-/-</sup>:asah1b<sup>-/-</sup>* fish, respectively) and *tnf $\beta$*  ( $\pm 17$ -fold and 30-fold) (**Figure 5B**). In addition, increased mRNA expression was noted in the brains of both *gba1<sup>-/-</sup>* and *gba1<sup>-/-</sup>:asah1b<sup>-/-</sup>* for *catD* (2.5-3-fold), and the microglia marker *apoEb* (5-6-fold)<sup>32,33</sup>. Expression of several genes encoding components of the complement system (*c1qA*, *c3.1*, *c5* and the *c5a* receptor (*c5aR1*)) are significantly increased in both *gba1<sup>-/-</sup>* and *gba1<sup>-/-</sup>:asah1b<sup>-/-</sup>* brains. Western blot analysis revealed that the amount of p62 and the ratio of LC3-II to LC3-I were increased in the brains of both *gba1<sup>-/-</sup>* and *gba1<sup>-/-</sup>:asah1b<sup>-/-</sup>* zebrafish, indicating that autophagy was upregulated (**Figure 5C and D**).

H&E staining showed infiltration of Gaucher-like cells in brains of both *gba1<sup>-/-</sup>* and *gba1<sup>-/-</sup>:asah1b<sup>-/-</sup>* fish, mainly in the periventricular grey zone of the optic tectum (**Figure 5E** with zoom in **Figure 5F**). These abnormal cells were not present in WT or *asah1b<sup>-/-</sup>* zebrafish brain (**Figure 5E and F** for WT, **Supplementary Figure 3** for *asah1b<sup>-/-</sup>*). Transverse sections of the diencephalon, showed infiltration of Gaucher-like cells in both brain halves (**Figure 5G**).

**Figure 5 | Biochemical abnormalities in adult zebrafish brain ►**

(A) Lipid levels were determined of dissected brains in pmol/mg tissue. Data is depicted as mean  $\pm$  SEM; WT (n = 9-10), *gba1<sup>-/-</sup>* (n = 9), *asah1b<sup>-/-</sup>* (n = 8), *gba1<sup>-/-</sup>:asah1b<sup>-/-</sup>* (n = 11). Data is analysed by Two-Way Anova with Dunnett's multiple comparison test and WT as control group. (B) mRNA levels of *asah1a*, *asah1b*, *gpnmb*, *chia.6*, *il-1 $\beta$* , *tnf $\beta$* , *apoEb*, *catD*, *c1qA*, *c3.1*, *c5aR* and *c5* was determined using RT-qPCR analysis; WT (n = 9-11), *gba1<sup>-/-</sup>* (n = 8-11), *asah1b<sup>-/-</sup>* (n = 5), *gba1<sup>-/-</sup>:asah1b<sup>-/-</sup>* (n = 9-10). (C) Representative western blot of p62, LC3-I, LC3-II,  $\beta$ -catenin protein levels in WT, *gba1<sup>-/-</sup>*, *asah1b<sup>-/-</sup>* and *gba1<sup>-/-</sup>:asah1b<sup>-/-</sup>* zebrafish brains, with  $\beta$ -actin as protein loading control. (D) Quantitative analysis of LC3-II/LC3-I levels and p62 protein levels. WT (n = 5), *gba1<sup>-/-</sup>* (n = 5), *asah1b<sup>-/-</sup>* (n = 3), *gba1<sup>-/-</sup>:asah1b<sup>-/-</sup>* (n = 6). (E) H&E staining of brain sagittal sections of WT, *gba1<sup>-/-</sup>* and *gba1<sup>-/-</sup>:asah1b<sup>-/-</sup>*, with infiltration of Gaucher-like in the periventricular grey zone of the optic tectum (F) in *gba1<sup>-/-</sup>* and *gba1<sup>-/-</sup>:asah1b<sup>-/-</sup>* brains. (G) Transversal sectioning with storage cell infiltration in both halves of the periventricular grey zone of the optic tectum. (H) mRNA expression of *th1*, *th2*, *snc $\beta$* , *snc $\gamma$* , *snc $\gamma$ b* and *mbpa* was determined using RT-qPCR analysis; WT (n = 7), *gba1<sup>-/-</sup>* (n = 9), *asah1b<sup>-/-</sup>* (n = 4), *gba1<sup>-/-</sup>:asah1b<sup>-/-</sup>* (n = 7). Data of RT-qPCR is normalized using two housekeeping genes (*ef1a* and *rpl13*), analysed by One-Way Anova with Tukey's multiple comparisons test or Brown-Forsythe and Welch Anova with Dunnett's multiple comparisons test for *gpnmb* and *chia.6* and depicted as scattered dot plot  $\pm$  SEM. In general, statistical comparisons are depicted as WT vs *gba1<sup>-/-</sup>*, WT vs *gba1<sup>-/-</sup>:asah1b<sup>-/-</sup>* or *gba1<sup>-/-</sup>* vs *gba1<sup>-/-</sup>:asah1b<sup>-/-</sup>*, only when a significant difference is apparent and relevant. Ns = not significant, \*\* P < 0.01, \*\*\* P < 0.001 and \*\*\*\* P < 0.0001.





Neurodegeneration was studied by analysis of mRNA levels of the two tyrosine hydroxylase orthologues in the zebrafish brains. A significant decrease in *th1*, but not *th2*, was observed in *gba1*<sup>-/-</sup> zebrafish brains, while no significant reduction was observed in the *gba1*<sup>-/-</sup>:*asah1b*<sup>-/-</sup> brains (**Figure 5H**). In addition, two transcripts of zebrafish orthologues of  $\alpha$ -synuclein, *snc $\beta$*  and *sncyb*, were significantly reduced in *gba1*<sup>-/-</sup> brains compared to WT and *gba1*<sup>-/-</sup>:*asah1b*<sup>-/-</sup> brains. The expression of myelin-basic protein (*mbpa*) was comparably reduced in both *gba1*<sup>-/-</sup> and *gba1*<sup>-/-</sup>:*asah1b*<sup>-/-</sup> brains. These mRNA findings could point to aberrant myelination in both mutants, while dopamine neurons appear to be only abnormal in *gba1*<sup>-/-</sup> fish at this age.

### Phenotypic improvements of adult *Asah1b:Gba1* double knockout zebrafish

In general, experiments were ended at 12 wpf, or earlier for individual *gba1*<sup>-/-</sup> zebrafish when predetermined human end points were observed (t = 10-12 wpf). Up to 8 wpf, no overt phenotype was observed in the WT, *gba1*<sup>-/-</sup>, *asah1b*<sup>-/-</sup> and *gba1*<sup>-/-</sup>:*asah1b*<sup>-/-</sup> fish. From 8 wpf onwards, a drop in the tail of individual *gba1*<sup>-/-</sup> zebrafish was apparent which progressively worsened from 9 to 12 wpf. Differences were noticeable among the different types of mutant fish as well as variation among individual fish within each genotype. All *gba1*<sup>-/-</sup> zebrafish (t= 10-12 wpf) showed phenotypic characteristics such as a curved back and different swimming behaviour (**Figure 7A**). The size of the *gba1*<sup>-/-</sup> zebrafish was significant smaller than WT, while the tortuosity, i.e. the length of the curved back divided by the length from head to tail base, was significantly enlarged (**Figure 7B**). Most of the *gba1*<sup>-/-</sup> fish showed abnormal swimming behaviour, ranging from difficulty with balance, failure to maintain an upright position to the inability to move from the bottom of the tank. Individual zebrafish were tracked to quantify their swimming speed and time spend in the upper part of the tank (**Figure 7C and D**). It was observed that tracking various *gba1*<sup>-/-</sup> fish was more difficult, as they did not move from the bottom of the tank. However, on average, *gba1*<sup>-/-</sup> zebrafish did not show bradykinesia, because the mean speed was not significantly different from WT (**Figure 7D**). A significant difference was observed in the ability of the zebrafish to use the whole tank. In contrast to WT fish, *gba1*<sup>-/-</sup> zebrafish spend significantly less time in the top of the tank (**Figure 7C and D**). These findings suggested that the *gba1*<sup>-/-</sup> zebrafish had abnormal swimming behaviour, predominantly manifested as the inability to use the entire tank, however on average they reach similar velocities as WT.

Contrary to *gba1*<sup>-/-</sup> fish, all *gba1*<sup>-/-</sup>:*asah1b*<sup>-/-</sup> fish at 12 wpf showed no significant difference in length or tortuosity (**Figure 7A and B**). Additionally, *gba1*<sup>-/-</sup>:*asah1b*<sup>-/-</sup> did not show postural imbalance and used the whole tank for swimming as the WT and *asah1b*<sup>-/-</sup> zebrafish (**Figure 7C and D**). Therefore, a pilot longevity study was performed by raising the *gba1*<sup>-/-</sup>:*asah1b*<sup>-/-</sup> zebrafish past 12 wpf until similar phenotypic characteristics were apparent for the *gba1*<sup>-/-</sup> zebrafish at 10 to 12 wpf. Individual double mutant zebrafish showed a curved back (**Figure 7E**), postural imbalance and abnormal swimming behaviour and therefore had to be culled around 15-17 wpf (**Figure 7F and Supplementary Figure 4**).

Thus, there was a marked amelioration of disease course by at least 5 weeks (33%) in the *gba1<sup>-/-</sup>:asah1b<sup>-/-</sup>* zebrafish lacking excessive GlcSph. Importantly, the absence of GlcSph did not prevent, on the longer run, the development of phenotypic abnormalities such as the curved back and differences in swimming behaviour.

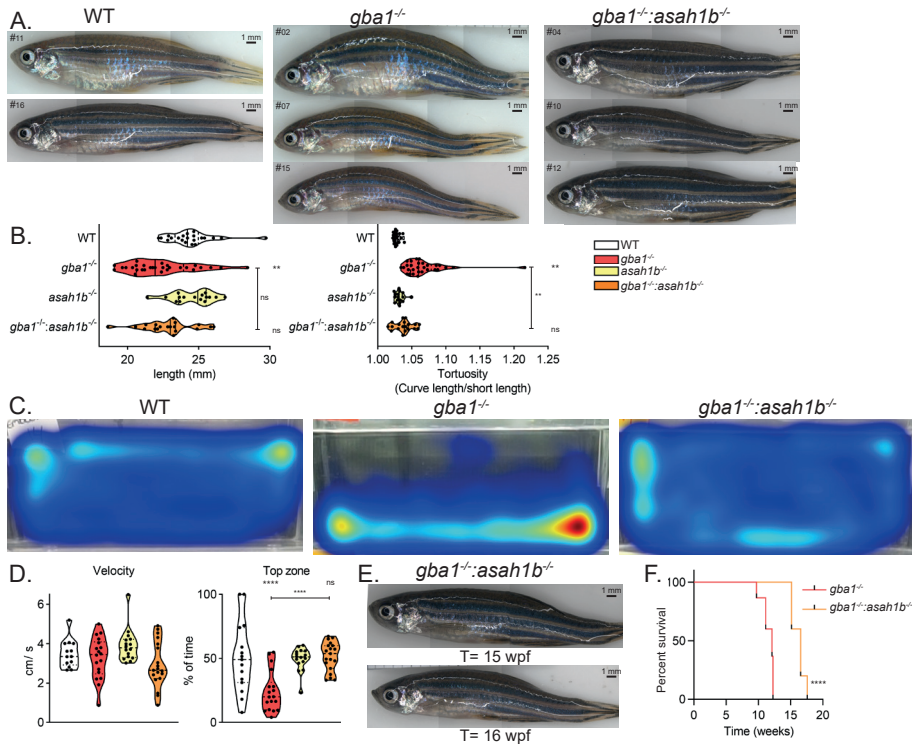


**Figure 7 | Phenotypic improvements of adult Asah1b:Gba1 double deficient zebrafish**

**(A)** Representative photographs of WT, *gba1<sup>-/-</sup>* and *gba1<sup>-/-</sup>:asah1b<sup>-/-</sup>* zebrafish. **(B)** The length of individual zebrafish is determined (head to tail base) as well as the tortuosity, calculated as ratio of the length along the back divided by the length of the fish, as indication for the curved back. Data of individual zebrafish is depicted in a violin plot; WT (n = 21), *gba1<sup>-/-</sup>* (n = 29), *asah1b<sup>-/-</sup>* (n = 16), *gba1<sup>-/-</sup>:asah1b<sup>-/-</sup>* (n = 19), and analysed using a non-parametric Kruskal-Wallis test with Dunn's multiple comparison test. **(C)** Representative movement traces of WT, *gba1<sup>-/-</sup>* and *gba1<sup>-/-</sup>:asah1b<sup>-/-</sup>* zebrafish, all at t = 12 wpf. **(D)** Quantification of individual zebrafish average velocity (in cm/s) and time spend in the top half of the tank. Data of individual zebrafish is depicted in a violin plot; WT (n = 13), *gba1<sup>-/-</sup>* (n = 16), *asah1b<sup>-/-</sup>* (n = 16), *gba1<sup>-/-</sup>:asah1b<sup>-/-</sup>* (n = 19) and analysed using a One-Way Anova with Tukey's multiple comparison test. **(E)** Photograph of individual *gba1<sup>-/-</sup>:asah1b<sup>-/-</sup>* zebrafish at t = 15 and 16 wpf. **(F)** Kaplan-Meier plot indicating the onset of predetermined symptoms, such as the curved back and abnormal swimming resulting in impaired feeding behaviour, of *gba1<sup>-/-</sup>* and *gba1<sup>-/-</sup>:asah1b<sup>-/-</sup>* zebrafish; *gba1<sup>-/-</sup>* (n = 30), *gba1<sup>-/-</sup>:asah1b<sup>-/-</sup>* (n = 5). Curves are analysed using a Log-rank (Mantel-Cos) test. In general, statistical comparisons are depicted as WT vs *gba1<sup>-/-</sup>*, WT vs *gba1<sup>-/-</sup>:asah1b<sup>-/-</sup>* or *gba1<sup>-/-</sup>* vs *gba1<sup>-/-</sup>:asah1b<sup>-/-</sup>*, only when a significant difference is apparent and relevant. Ns = not significant, \*\* P < 0.01 and \*\*\*\* P < 0.0001.



## Discussion

The role of GlcSph in GD pathophysiology is still largely based on circumstantial evidence and therefore tentative. The present study describes the generation of a unique GD zebrafish model that sheds light on the importance of GlcSph in pathology. Zebrafish express two ACase enzymes, Asah1a and Asah1b. Only the combined deficiency of both ACases was found to cause marked accumulation of Cer, as occurs in Farber disease, while only Asah1b was found to be involved in the formation of excessive GlcSph during GCase deficiency in zebrafish. The comparison of adult *gba1*<sup>-/-</sup> fish, with excessive GlcSph, and *gba1*<sup>-/-</sup>:*asah1b*<sup>-/-</sup> fish, without GlcSph, therefore allows delineation of the contribution of this lyso-lipid to different mechanisms underlying GD manifestations, including storage cells, inflammation and autophagy.

Both *gba1*<sup>-/-</sup> and *gba1*<sup>-/-</sup>:*asah1b*<sup>-/-</sup> fish show accumulation of Gaucher-like cells which is accompanied by excessive tissue GlcCer levels. The observation that tissue GlcCer is similar in *gba1*<sup>-/-</sup> fish and *gba1*<sup>-/-</sup>:*asah1b*<sup>-/-</sup> fish indicates that ACase-mediated GlcSph formation reduces marginally GlcCer accumulation during GCase deficiency. Despite the GlcCer accumulation and Gaucher-like cells in brain and liver in both GCase deficient fish, a very marked increase in life span is observed for the *gba1*<sup>-/-</sup>:*asah1b*<sup>-/-</sup> fish. Individual *gba1*<sup>-/-</sup> zebrafish show a drop of the tail around 8-9 wpf, which progresses in subsequent weeks to a characteristic phenotype of a curved back, postural imbalance and more time spent at the bottom of the tank. No curved back nor abnormalities in swimming behaviour develop in *gba1*<sup>-/-</sup>:*asah1b*<sup>-/-</sup> fish at 12 wpf and animals live up to 33% longer until similar manifestations to those of *gba1*<sup>-/-</sup> fish are apparent.

It is tempting to attribute the delayed onset of abnormalities to the absence of GlcSph in GCase-deficient zebrafish lacking ACase-Asah1b. Of note, the absence of GlcSph and improved phenotype was not accompanied by changes in biomarkers of Gaucher cells. The comparably increased expression of mRNAs encoding Gpnmb and Chia.6 in both GCase mutants suggests that similar amounts of lipid-laden macrophages develop in *gba1*<sup>-/-</sup> fish and *gba1*<sup>-/-</sup>:*asah1b*<sup>-/-</sup> zebrafish and that the cells react similarly to lysosomal accumulation of GlcCer by increased production of gpNMB and chitinase proteins. Furthermore, increased autophagy occurs in brains of both types of mutant zebrafish, as well as comparable neuroinflammation, as depicted by increased expression of inflammation markers Il-1 $\beta$ , Tnf- $\beta$  and ApoEb and the lysosomal protease Cathepsin D in brains of both *gba1*<sup>-/-</sup> fish and *gba1*<sup>-/-</sup>:*asah1b*<sup>-/-</sup> fish. Transcript levels of components of the complement system (*c1qA*, *c3.1*, *c5* and the c5a receptor (*c5aR1*)) are comparably increased in *gba1*<sup>-/-</sup> and *gba1*<sup>-/-</sup>:*asah1b*<sup>-/-</sup> brains. In addition, infiltration of Gaucher-like cells in the periventricular grey zone of the optic tectum of the brain is apparent in both *gba1*<sup>-/-</sup> and *gba1*<sup>-/-</sup>:*asah1b*<sup>-/-</sup> fish. It will be of interest to comparatively visualize and quantify more closely microglia in brains of the mutant fish. Altogether, the biochemical findings and pathology examination suggest that the presence of excessive GlcSph is not a prerequisite for inflammation.

The considered activation of the complement cascade as major driver of the inflammatory pathology in GD mice<sup>34</sup> was not apparent in our study. Brains of *gba1<sup>-/-</sup>:asah1b<sup>-/-</sup>* fish without excessive GlcSph and no apparent phenotype at that time-point, showed comparable complement activation, compared to phenotypic *gba1<sup>-/-</sup>* fish of 10-12 wpf. Likewise, impaired autophagy and neuroinflammation did not differ among the GCase-deficient fish with or without excessive GlcSph. Apparently, these processes do not explain the more severe phenotype of GCase-deficient fish with excessive lyso-lipid.

In view of the recently recognized link between mutations in GBA gene and risk for Parkinson disease<sup>35</sup>, the fate of dopaminergic neurons in GCase-deficient fish with or without excessive GlcSph is of interest. The expression of mRNAs encoding tyrosine hydroxylase 1 (*th1*), a marker for dopaminergic neurons, is reduced in *gba1<sup>-/-</sup>* zebrafish brains, but not *gba1<sup>-/-</sup>:asah1b<sup>-/-</sup>* brains. Zebrafish do not encode an orthologue of human  $\alpha$ -synuclein, but instead express  $\beta$ -synuclein (*sncb*) and two  $\gamma$ -synuclein variants (*sncya* and *sncyb*). The  $\beta$ -synuclein and  $\gamma$ 1-synuclein (*sncyb* gene) isoforms are expressed in the cell bodies of TH-positive catecholaminergic cell groups<sup>36</sup>. Two transcripts of zebrafish synucleins, *sncb* and *sncyb*, were significantly reduced in *gba1<sup>-/-</sup>* brains compared to WT and *gba1<sup>-/-</sup>:asah1b<sup>-/-</sup>* brains, while the expression of myelin-basic protein (*mbpa*) is comparably reduced in both *gba1* KO and *gba1:asah1b* KO brains. These findings suggest that the presence of excessive GlcSph might specifically impact dopaminergic neurons. However, visualization and quantification of TH-positive dopamine neurons is required to confirm this. Keatinge and colleagues observed earlier in *gba1<sup>-/-</sup>* zebrafish, a reduction of TH-immunoreactive neurons in the caudal hypothalamus and posterior tuberculum accompanied by abundant Lewy body-like ubiquitinated neuronal cytoplasmic inclusions and neurites in the hindbrain<sup>30</sup>. In addition, a reduction of  $\beta$ - and  $\gamma$ 1-synuclein (*sncgb* gene) protein levels was found. Based on our findings regarding mRNA levels, *gba1<sup>-/-</sup>:asah1b<sup>-/-</sup>* brains lacking excessive GlcSph would likely show a more moderate reduction of TH-immunoreactive neurons. It was earlier observed with GD/PD mouse models that GlcCer levels are not increased in the brain, while GlcSph accumulation already occurs in young mice (8-12 weeks), supposedly triggering  $\alpha$ -synuclein aggregation<sup>11</sup>. Similar observations were made with cultured human neuronal cells<sup>11</sup>. In addition, a recent study with mice heterozygous for GBA deficiency showed development of  $\alpha$ -synucleinopathy concomitantly to overproduction of GlcSph<sup>10</sup>. These observations all point to a detrimental role of excessive GlcSph regarding dopaminergic neurons. Our findings with zebrafish are in line with this. Further research is required to elucidate the exact role of GlcSph in the accelerated neuronal cell death in the  $\alpha$ -synuclein independent zebrafish model. In this connection the proposed harmful effects of complement-activating immune complexes deposited on neuronal cells, oxidative damage and mitochondrial dysfunction<sup>30,37-39</sup> warrant specific attention. Obviously, the absence of  $\alpha$ -synuclein in zebrafish, and the different location of dopaminergic neurons as compared to human brain, could limit their use as genuine models to study Parkinson's disease during GBA deficiency<sup>27,30</sup>. More attractive to some extent are *Oryzias latipes* (medaka) fish expressing endogenous  $\alpha$ -synuclein<sup>32</sup>.

It is important point out that despite delayed disease manifestations and improved life span, *gba1<sup>-/-</sup>:asah1b<sup>-/-</sup>* lacking GlcSph still developed abnormal swimming behaviour at 4 months of age and are culled earlier than WT and *asah1b<sup>-/-</sup>* age-mates. This suggests that GlcSph contributes significantly to the onset of GD symptoms, but is not the only pathogenic factor. In this respect, the impact of accumulating GlcCer and other glucosylated lipids deserves further attention.

The noted differences between the enzymes encoded by *asah1a* and *asah1b* warrant further discussion. Both ACases hydrolyse ceramide and no abnormal phenotype is observed for fish lacking only one of the ACase enzymes, up to the moderately old age of 2 years. Both *asah1a<sup>-/-</sup>:asah1b<sup>+/-</sup>* and *asah1a<sup>+/-</sup>:asah1b<sup>-/-</sup>* adult zebrafish were obtained at predicted Mendelian frequency, however no adult double *asah1a<sup>-/-</sup>:asah1b<sup>-/-</sup>* zebrafish could be raised. This suggests that maternal ACase in the developing larvae is essential during combined Asah1a and Asah1b deficiency. Moreover, after 5 dpf endogenous ACase activity, either Asah1a or Asah1b, is important for viability. The sequence alignment of Asah1a, Asah1b and human ACase shows a high conservation of relevant residues (**Figure 1**). It is known for human ACase that autocleavage of the peptide bond preceding Cys 143 results in activation of the proenzyme and subsequently leads to a conformational change of Tyr 137<sup>22</sup>, a residue also conserved in both Asah1a and Asah1b. Tyr 137 is then stabilized through hydrogen bonding or hydrophobic interactions between the  $\alpha$ -subunit helix (residues 127-140) and  $\beta$ -subunit region (residues 225-250, **Supplementary Figure 5**). The conformational change opens up a hydrophobic pocket hosting the fatty acid of ceramide, as implied by the binding conformation of covalent inhibitor Carmofur<sup>23</sup>. Simple molecular modelling of human and zebrafish enzymes, reveals that Asah1a contains more aromatic residues lining the entrance of the pocket (**Supplementary Figure 6**). However, none of these residues seem to be in close proximity to the proposed catalytic site. Residues Asp 200, Phe 201 and Met 300 located on the loops adjacent to the catalytic site might be close enough to be of significance, assuming that these loops adapt a slightly different orientation towards the catalytic site in solution, in comparison to the crystal structures. Nonetheless, whether these residues provide an explanation for the different substrate specificity of Asah1a and Asah1b remains yet unclear. An alternative explanation for our findings could be that Asah1a is less abundant in lysosomes of macrophages in zebrafish, the most likely source of GlcSph formation. Overall, it will be of interest to elucidate in the future why Asah1a is not able to generate GlcSph in GCCase-deficient fish.

The ACase-mediated formation of deacylated sphingolipid bases from lipids accumulating in lysosomes is not unique to GD. A similar phenomenon is observed with other lysosomal sphingolipidoses: Fabry disease with globotriaosylsphingosine (lysoGb3) formed from accumulating globotriaosylceramide (Gb3); Krabbe disease with galactosylsphingosine (GalSph) formed from galactosylceramide; acid sphingomyelinase deficiency, a.k.a. Niemann-Pick disease types A and B, with phosphocholinesphingosine formed from sphingomyelin<sup>40,41</sup>. As for GlcSph in GD disease, research has been focused on evaluating the neurotoxic actions of lysoGb3 in Fabry disease and galactosylsphingosine in Krabbe disease<sup>42-45</sup>. Recently, ablation of ACase in a mouse model of Krabbe disease, deficient in

galactocerebrosidase (GALC) showed no GalSph accumulation in brain, liver and spleen tissue<sup>42</sup>. As a result, a reduction of activated macrophages/microglia in the cerebellum was observed as well as improved axonal structures, few infiltrating inflammatory cells, little oedema, improved motor activity and increased life span compared to GALC deficient mice. On the other hand, increased levels of ceramide were apparent in liver and spleen of the GALC/ACase deficient mice as well as haematological abnormalities such as vacuoles in the spleen, circulating monocyte and neutrophil populations, as observed in the ACase deficient mice<sup>42</sup>. The established Asah1b deficient zebrafish without ceramide accumulation could offer interesting opportunities to investigate the detrimental role of deacylated sphingolipid bases in the outcome of other lysosomal storage diseases, without the accompanying ceramide accumulation.

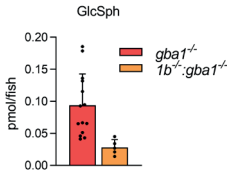
With the improved life span, it is tempting to consider inhibition of ACase as therapeutic avenue in neuronopathic GD with unmet need. Carmofur is a known inhibitor of ACase<sup>46,47</sup>. It has been earlier demonstrated that Carmofur treatment of GCase-deficient cells reduces formation of GlcSph<sup>16</sup>. The compound Carmofur is however not a specific ACase inhibitor, as it also inactivates neutral ceramidases and it is known to inhibit the nucleotide-synthesizing enzyme thymidylate synthetase, an effect underlying its wide-spread use in chemotherapy<sup>46</sup>. More specific ACase inhibitors have been designed by Fabrias and colleagues<sup>48</sup>. Testing such compounds in our zebrafish models of GCase deficiency could be considered as first step to assess clinical applicability. The window for such type of intervention might be very small, or even not exist, given the report that partial ACase deficiency already impairs spinal-cord motor neurons and other areas of the CNS<sup>49</sup>.

In conclusion, the comparison of GCase-deficient zebrafish with or without excessive GlcSph, due to respective presence or absence of Asah1b, reveals that the latter fish show amelioration of swimming abnormalities and increased life span. It is remarkable that this improvement in disease manifestations in the absence of GlcSph is independent of storage cell burden and neuroinflammation.

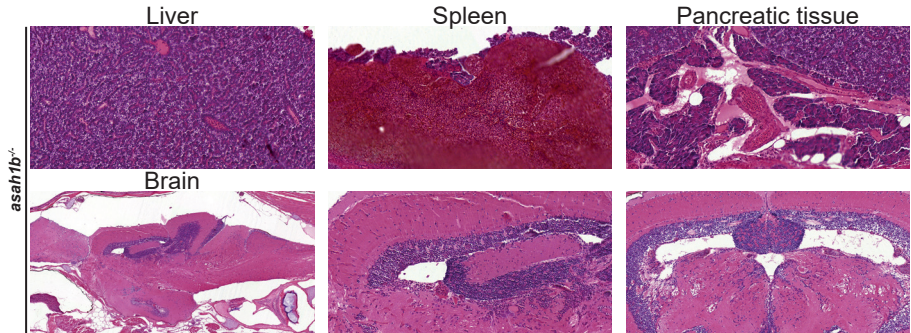
## Acknowledgements

Joost Willemse is kindly acknowledged for the ImageJ plugin to quantify the length and tortuosity of individual zebrafish. Wouter Bax is kindly acknowledged for his work on studying zebrafish Asah1a and Asah1b in vitro and Ulrike Nehrdich, Guus van der Velden and Ruth van Koppen for their overall expertise and particularly for their help in monitoring the mutant zebrafish. The study was supported by the NWO BBOL 2018 (737.016.022) grant.

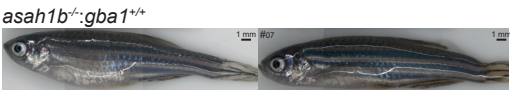
Supplementary Information



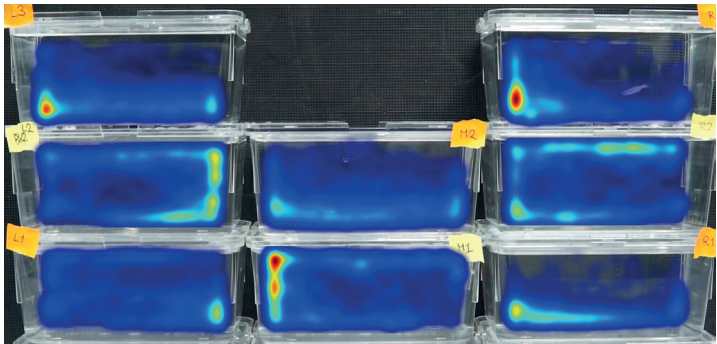
**Supplementary Figure 1** | GlcSph levels of *gba1*<sup>-/-</sup> (n = 14) and *gba1*<sup>-/-</sup>:*asah1b*<sup>-/-</sup> (n = 5) larvae KO at 5dpf in pmol/fish. Data of *gba1*<sup>-/-</sup> is used from chapter 5. Data is depicted as mean ± SD.



**Supplementary Figure 2** | H&E staining of *asah1b*<sup>-/-</sup> zebrafish including liver, spleen and pancreatic tissue as well as sagittal section (left and magnification in the middle panel) and transversal section (right panel) of *asah1b*<sup>-/-</sup> zebrafish brain.



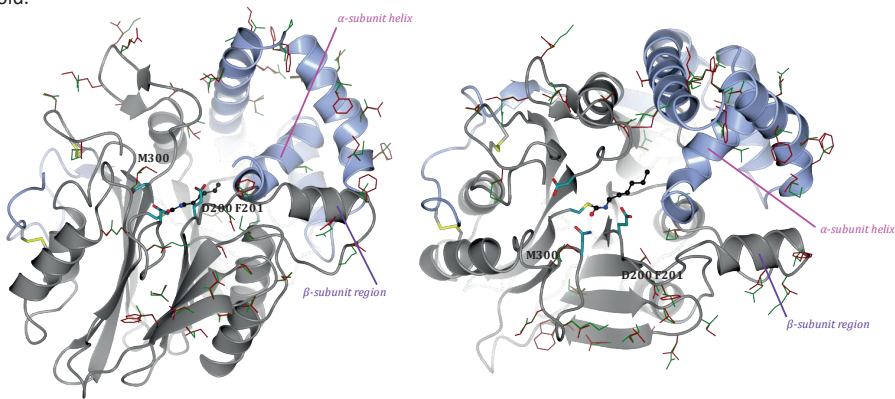
**Supplementary Figure 3** | Photographs of two representative *asah1b*<sup>-/-</sup> zebrafish.



**Supplementary Figure 4** | Heatmaps of individually filmed zebrafish at 15 wpf. Heatmaps of *asah1b*<sup>-/-</sup> (yellow stickers) and *gba1*<sup>-/-</sup>:*asah1b*<sup>-/-</sup> (orange stickers) at 15 wpf, with individual fish starting to show differences in swimming behaviour. Red indicates more time and blue less time spend at that location.

Human ACase	MPGRSCVALV-LLAAVSCAVAQHAPPWTEDCRKSTYPPSGPTYRGAVFWYTNLDDLFPY	59
Asah1a	----MKLVFRYNALFISIFIHALYV-QGLEDCRSGMYPPKGPPTYRGVNTRYTVNLDPSPS	55
Asah1b	MNNRLNLCFFI-LSYMCMLSAQYVPPFTEDCRSGMYPPNGPTEKGDVSWYTVDDLPLPAS	59
	: : * : *	
Human ACase	KRWHELMLDKAPVLKVINSLKNMINTFVPSGKIMQVVDKLPGLLGNNFPGPFEEEMKGI	119
Asah1a	ERWTQIHKDKNTELIEMVQTIKDMAKGF-HGKLVNFVDKELPFIIVDTLPNPFNEEIKGI	114
Asah1b	KRWTDVISEDKTEMASMIQAIKDLADAFVPSGKLIQLVDKDLPLMVDLTPNPFNEEIRGI	119
	: * : : *	
	<u>α-subunit helix</u>	
Human ACase	AAVTDIPLCEIISFNIFYELFTICTSIVAEDKKGHLLHGRNMDFGVFLGWNINNDTWVIT	179
Asah1a	AAVSGIPLGEIALFNIFYEVFTVCTSLVAEDNNGNIYHGRNLDGFLMGWDRONKNTWILT	174
Asah1b	ASVSGVPLGEVVLFNIFYEVFTVCTSLVAEDVNGNLIHARNLDGFLMGWDLKNRSWVIT	179
	: * : : *	
	<u>β-subunit region</u>	
Human ACase	EQLKPLTVNLDIFORNKTVFKASSFAGYVGLMTGFKPGLFSLTLNERFSINGGYLGILEW	239
Asah1a	EKLKPLVVNINFERKNQTVFKSTSFAGYVGLMTGIRPGLTLTMNERFDFDGGYIGILDW	234
Asah1b	EKLKPLVVNIDFTRNGQTVFKSTNFAGYVGLMTGIHONSFTLTMNERFSLDGGYIGILEW	239
	: *	
Human ACase	ILGKDKDVMWIGFLTRTVLENSTSYEEAKNLLTKIKLAPAYFILGGNQSSEGCVITRRK	299
Asah1a	IFGNRDGMWTFGLTRRVLENSTSYEDAKDQLSQTLLAPVYFILGGNRTGGCVITRRRI	294
Asah1b	ILGKRDGMWMSFLTRSVLENATSYESAKALLSDTKLLAPVYFILGGNQSSEACIITRSRT	299
	: * : *	
Human ACase	ESLDVVELDAKQGRWYVVQTNYDRWKHPFLDDRRTPAKMCNLTQSQENISFETMYDVL	359
Asah1a	NTLDIWELEMLGRWYVLETNYDHWKPKPFLDDRRTPAKMCNQTTQANISLASIYNVLS	354
Asah1b	QNISPLELNKNGRWYVLETNYDHWKEPLFLDDRRTPAKMCNQTTQTNISVKTIVDVL	359
	: : : *	
Human ACase	TKPVLNKLTVYTTLIDVTKGQFETYLRDCPDPCIGW 395	
Asah1a	TKPVLNKLTTYTSLMAVSTGTLESYVRDCPNPCTPW 390	
Asah1b	TKPVLNKLTTYTTLMEVSKGTLESFIRDCPNPCMPW 395	
	* *	

**Supplementary Figure 5 |** Sequence alignment of acid ceramidase variants with the predicted signal peptide (depicted in blue), self-cleaved catalytic residue C143 (bold, red) and contrasting residues (highlighted in grey). Modelled residues indicated with black line above while residues D200, F201 and M300 of Asah1a are indicated in bold.



**Supplementary Figure 6 | Structure of human ACCase with modelling of divergent residues of Asah1a and Asah1b**  
Ribbon diagram of the side (left) or top (right) of human ACCase (PDB 6MHM) with α-subunit (light grey), β-subunit (dark grey) and disulfide bonds (yellow) indicated. Inhibitor Carmofur (black, ball and stick) and catalytic residues C143, D162, E225 or N320 (cyan sticks) are also visualized for clarity, as proposed by Dementiev et al.<sup>23</sup>. Divergent residues of Asah1a (red) and Asah11b (green) surrounding the catalytic pocket are superimposed on the human structure.



## Experimental procedures

**Chemicals and reagents** - GCase specific inhibitor (ME656)<sup>27</sup>, <sup>13</sup>C<sub>5</sub>-sphinganine, <sup>13</sup>C<sub>5</sub>-sphingosine, <sup>13</sup>C<sub>5</sub>-GlcSph, <sup>13</sup>C<sub>5</sub>-lyso-globotriaosylceramide (LysoGb3), C17-lysosphingo-myelin (LysoSM), <sup>13</sup>C<sub>6</sub>-GlcChol and C17-dihydroceramide (C17-dhCer)<sup>50,51</sup> were synthesized as reported. All chemicals and reagents were obtained from Sigma-Aldrich Chemie GmbH (St Louis, USA) unless mentioned otherwise. The standards Cer (d18:1/16:0), dhCer (d18:0/16:0), GlcCer (d18:1/16:0), GalCer (d18:1/16:0), LacCer (d18:1/16:0) were obtained from Avanti Polar lipids (Alabaster, USA) and GlcChol from Sigma-Aldrich. LC-MS grade methanol, 2-propanol, water, formic acid, acetonitrile and HPLC grade chloroform were purchased from Biosolve (Valkenswaard, the Netherlands). LC-MS grade ammonium formate, ammonium acetate and sodium hydroxide from Sigma-Aldrich, butanol and hydrochloric acid from Merck Millipore (Billerica, USA).

**Zebrafish** - All zebrafish were housed and maintained at the University of Leiden, the Netherlands, according to standard protocols. Wildtype (WT) zebrafish (ABTL) were a mixed lineage of WT AB and WT TL genetic backgrounds. Zebrafish were kept at constant temperature of 28.5 °C and on a cycle of 14-hour light and 10 hour dark. Experiments with larvae, juvenile and adult zebrafish after the free-feeding stage were approved by the local animal welfare committee (Instantie voor Dierwelzijn) of the University Leiden (Project license AVD1060020184725). Zebrafish from 5 dpf to 2 wpf were fed with both dry food (2x daily; Skretting Gemma micro 75, Zebcare, Nederweert, the Netherlands) and Rotifers (1x daily) and from 3 wpf to the end of the experiment fed with both dry food (2x daily; Skretting Gemma micro 150 until 30 dpf or Gemma Micro 300 mixed with Gemma Diamond for fish from 30 dpf) and hatched Artemia (1x daily).

**Zebrafish sampling, morphology and movement** - In general, zebrafish were sacrificed at 12 wpf or earlier when zebrafish showed symptoms noted as human endpoints in the project license (t = 10-11 wpf for *gba1*<sup>-/-</sup>). Zebrafish (10-12 wpf) were recorded individually from the side for 20 minutes, after 10 minutes of acclimatization in their new tank. Movements of the fish in the individual tank was tracked using Ethiovision software 10.1 (Noldus, Wageningen, the Netherlands). Arenas were setup for each individual tank, with a division for the top and bottom zone, and subsequently data was obtained for 10 minutes. Fish were subsequently sacrificed using an overdose of tricaine methane sulfonate (MS222, 200 mg/L) and photographed using Leica M165C (Wetzlar, Germany). The three or four images of one fish were stitched to obtain one image using Photoshop CC2018 (Adobe, San Jose, USA). The length of the fish from head to tail base (short length) was determined as well as the length of the back from head to tail base (long length) using ImageJ software<sup>52</sup>. The tortuosity was calculated by dividing the long length by the short length. Whole zebrafish were fixed using paraformaldehyde (4% (w/v), Alfa Aesar, Haverhill, USA) or Bouin's solution (5% acetic acid, 9% formaldehyde, 0.9% picric acid, Sigma) for histopathology performed as described below or organs were dissected. Dissected organs were either snap frozen for protein and (glyco)sphingolipid analysis or submerged in RNAlater™ (Invitrogen, Thermo Fisher Scientific, Waltham USA) for RT-PCR analysis (brain or liver) and stored at -80 °C.

**CRISPR/Cas9 mediated knockout of *asah1a* and *asah1b*** - CRISPR/Cas9 mediated *gba1* knockout zebrafish were generated and maintained as previously described<sup>26</sup>. CRISPR/Cas9 mediated zebrafish gene knockouts of *asah1a* and *asah1b* were generated using the protocol previously described (Chapter 4 and<sup>26</sup> with sgRNA1 5'-gGTGTCATCTCTACTAGG and sgRNA2 5'-GgGCTCCCCG CTGGGAACAA for *asah1a* and *asah1b* respectively. Of note, the first or second nucleotide of the sgRNA found by the CHOPCHOP webtool was replaced by a 'g' to improve T7 RNA synthesis. Injected founders were crossed to WT and off-spring screened using an HRM assay with primers described in **Supplementary Table 1**. Fragments for Sanger sequencing were obtained using primers described in **Supplementary Table 1**. Heterozygous adult zebrafish (F2 generation) of both genotypes were crossed to obtain double heterozygous zebrafish (*asah1a*<sup>-/-</sup>:*asah1b*<sup>-/-</sup>). Adult fish were crossed with

each other and off-spring was used for incubations with vehicle (0.1% DMSO) or GCase specific inhibitor (10  $\mu$ M ME656, 0.1% DMSO) for 5 days, followed by (glyco)sphingolipid analysis. The *gba1*<sup>-/-</sup>, *gba1*<sup>+/-</sup>:*asah1b*<sup>-/-</sup> and *gba1*<sup>-/-</sup>:*asah1b*<sup>-/-</sup> zebrafish were generated by appropriate crossings. The status of *gba1* and *asah1b* was determined by fin clipping of 4-5 dpf larvae and subsequent HRM assays.

**Supplementary Table 1** | Forward (F) and reverse (R) primers for HRM analysis and amplification for sequencing

Target	Sequence 5'→3'	Target	Sequence 5'→3'
<i>Asah1a</i> HRM F	GTCTAGACTCGAATAAGTTCATG	<i>Asah1a</i> sequencing F	TGGGATGTATCCACCTAAAGG
<i>Asah1a</i> HRM R	TGGGAAACAGTTACCTCTGTG	<i>Asah1a</i> sequencing R	Same as HRM R
<i>Asah1b</i> HRM F	TGCAAAGAGATGTGTTAGATTG	<i>Asah1b</i> sequencing F	CAGCAAGCAAAAGATGGACAG
<i>Asah1b</i> HRM R	TCCTTCAGATGGCGAGCATG	<i>Asah1b</i> sequencing R	TACGATTTTGGGAGATTATCTC

**Homogenate preparation** - Homogenates of organs were prepared in potassium phosphate lysis buffer (25 mM K<sub>2</sub>HPO<sub>4</sub>-KH<sub>2</sub>PO<sub>4</sub> pH 6.5, 0.1% (v/v) Triton-X100 and EDTA-free protease inhibitor (cOmplete™, EDTA-free Protease Inhibitor Cocktail, Roche, Sigma-Aldrich)). Organs were first homogenized using a Dounce homogenizer (10 strokes) followed by sonication (20% amplitude, 3 sec on, 3 sec off for 4 cycles) using a Vibra-Cell™ VCX 130 (Sonics, Newtown, USA) while on ice. Total protein concentration of homogenates was determined using Pierce™ BCA protein assay kit (Thermo Fisher Scientific, Waltham, USA) and measured using an EMax® plus microplate reader (Molecular Devices, Sunnyvale, USA).

**Western blot** - Proteins of organ homogenates (20  $\mu$ g protein) were denatured using 5x Laemmli sample buffer (25% (v/v) 1.25M Tris-HCL pH 6.8, 50% (v/v) 100% glycerol, 10% (w/v) sodium dodecyl sulphate (SDS), 8% (w/v) dithiothreitol (DTT) and 0.1% (w/v) bromophenol blue), samples were boiled for 5 min at 98 °C and proteins were separated by electrophoresis on a 12% (w/v) SDS-PAGE gel. Proteins were transferred to nitrocellulose membranes (0.2  $\mu$ M, Bio-Rad laboratories Inc., Hercules, USA) using the Trans-Blot® Turbo™ Transfer system (Bio-Rad). Membranes were blocked with 5% (w/v) bovine albumin serum (BSA) and incubated overnight at 4 °C with primary antibodies: rabbit anti-LC3 (1:1000, NB100-2220; Novus Biologicals, Centennial, USA), rabbit anti-p62/SQSTM1 (1:1000, P0067; Sigma) or rabbit anti-actin (1:1000, ab209857; Abcam, Cambridge, UK). Membranes were washed 3 times with TBST and incubated for 1 h at RT with secondary antibody: GARPO goat anti rabbit IgG (H+L) peroxidase (1:5000, Bio-Rad). Chemiluminescence signal is developed using the Clarity Max Western ECL substrate (Bio-Rad), detected using a ChemiDocMP imager (Bio-Rad) and signal quantified by ImageJ software.

**Gene expression analysis** - RNeasy™ was removed and RNA was extracted using a Nucleospin RNA XS column (Machinery-Nagel, Düren, Germany) procedure according to supplier's protocol, without the addition of carrier RNA. Contaminating DNA was degraded on column by a DNase I treatment (supplied in the kit). cDNA was synthesized using SuperScript™ II reverse transcriptase (Invitrogen, ThermoFisher Scientific, Waltham, USA) using oligo(dT) and an input of approximately 200-500 ng total RNA according to the manufacturer's instruction. Generated cDNA was diluted to an approximate concentration of 0.5 ng total RNA input/ $\mu$ L with Milli-Q water. RT-PCR reactions were performed with the IQ SYBR green mastermix (Bio-Rad laboratories Inc., Hercules, USA) in a total volume of 15  $\mu$ L (1x SYBR green, 333  $\mu$ M of forward and reverse primer as given in Supplementary Table 2 and 5  $\mu$ L of the diluted cDNA input) and carried out using a CFX96™ Real-Time PCR Detection system (Bio-Rad laboratories Inc., Hercules, USA) with the following conditions: denaturation at 95 °C for 3 min, followed by 40 cycles of amplification (95 °C for 30 sec and 61 °C for 30 sec), imaging the plate after every extension at 61 °C, followed by a melt program from 55-95 °C with 0.5 °C per step with imaging the plate every step. All biological samples were tested in technical duplicate, differential gene expression was calculated using the  $\Delta\Delta$ Ct method normalized to two house-keeping genes *ef1a* and *rpl13* and depicted as log<sub>2</sub> fold change  $\pm$  SEM, compared to WT.

**Supplementary Table 2 |** Forward and reverse primers for RT-qPCR analysis.

Target	NCBI code	Forward primer sequence (5'→3')	Reverse primer sequence (5'→3')	
<i>Asah1a</i>	NM_001006088	ATTAGGCCCTGGTGAAGTAC	CTGCGAGTAAGAAAACCCGTC	125 bp
<i>Asah1b</i>	NM_200577	TGGACTGTTCATGGGATGGG	CCGGTCAACATCCCCGACATA	150 bp
<i>Gpnmb</i>	XM_009294247	GCAAGGGCGTAGAATTGAAA	TGGCAGGGACATGTCAGTAA	
<i>Chia.6</i>	NM_199603	TCCACGGCTCATGGGAGAGTGTC	AGCGCCCTGATCTCGCCAGT	ref. 53
<i>catD</i>	NM_131710	TGGGTGGAAGGTCTACTCG	CACTCAGGCAGATGTCGTGT	
<i>il18</i>	NM_212844	TGGACTTCGCAGCACAAAATG	GTTCACTTCACGCTCTTGGATG	ref. 54
<i>tnfβ</i>	NM_182873	GCATGTGATGAAGCCAAACG	GATTGTCCTGAAGGGTCACC	ref. 55
<i>apoeb</i>	NM_131098	AAACTGACATGACCGACGCT	TAGGTTGCTACGGTGTTCGC	172 bp
<i>c1qA</i>	NM_001020527	CTCTGTTTCCCTTTTCTCTCTG	CTTTCTCTCCTTTTGGTCCTGG	108 bp
<i>c3a.1</i>	NM_131242	CGGTGCACAAAGTACTTCCAC	GCCAGCTCCATGTCCTTGAC	197 bp
<i>c5aR1</i>	XM_005159274	CCGACAAGCTCGCATCCCTAT	GCGAATGATGGTTATCGCCC	163 bp
<i>c5</i>	XM_001919191	CAAGGCCACGGTTCAATCAG	TCTTCATGCTTTCGGCAGTCA	152 bp
<i>th1</i>	NM_131149	AGCTTTGTGGACGCTACTGA	GTGGGTTGTCCAGCACTTCT	112 bp
<i>th2</i>	NM_001001829	TACAAGCCATTCGACCCAGC	ATGCTGCAAGTGTAGGGGTC	173 bp
<i>sncβ</i>	NM_200969	GGAGTTTGGTCAGGAAGCCA	CCTCGGGCTCATAATCCTGG	107 bp
<i>sncyα</i>	NM_001017567	TGGAGGGGCTGGAGACTATG	AGCATCATGGGACATTCGGTT	123 bp
<i>sncyβ</i>	NM_001020652	ATGGTGAACCCGGGTGACTT	AGGCTTTGGAGCAGAAACGTA	129 bp
<i>mcpa</i>	XM_002665562	TGGTCATCTATCCTCCTCTCCA	CTTTCTCCCAGGCCCAATAGTTCT	150 bp
<i>ef1a</i>		CTGGAGGCCAGCTCAAAACAT	ATCAAGAAGAGTAGTACCGCTAGCATTAC	ref. 56
<i>rpl13α</i>		TCTGGAGGACTGTAAGAGGTATGC	AGACGCACAATCTTGAGAGCAG	ref. 56

**(Glyco)sphingolipid analysis** - Neutral (glyco)lipids, (glyco)sphingoid bases and glycosylated cholesterol were extracted from the same homogenate (10 µL, 20-30 µg total protein in KPi lysis buffer) using an acidic Bligh and Dyer procedure (1/1/0.9 chloroform/methanol/100 mM formate buffer pH 3.1) as described before<sup>26,51</sup>. Lipids were resuspended in methanol for separation by a C18 column or acetonitrile/methanol (9/1, v/v) for separation using a HILIC column and transferred to a vial for LC-MS/MS analysis. LC-MS/MS measurements were performed using a Waters UPLC-Xevo-TQS micro instrument (Waters, Corporation, Milford, USA) in positive mode using an electrospray ionization (ESI) source as described before for separating GlcChol and (glyco)sphingolipids using the C18 column<sup>26,50,51</sup>. To separate lipids by HILIC chromatography, a BEH HILIC column (2.1 x 100 mm with 1.7 µm particle size, Waters) was used at 30 °C as described before<sup>26</sup> with minor modifications in the eluent program allowing a faster run while preserving separation of Glc- and Gal containing lipids. Eluent A contained 10 mM ammonium formate in acetonitrile/water (97:3, v/v) with 0.01% (v/v) formic acid and eluent B consisted of 10 mM ammonium formate in acetonitrile/water (75:15, v/v) with 0.01% (v/v) formic acid. Lyso- and deacylated glycosphingolipids were eluted in 10 min with a flow of 0.6 mL/min using the following program: 85% A from 0-1 min, 85-65% A from 1-2.5 min, 60-0% A from 2.5-4 min, 0% A from 4-4.5, 0-85% A from 4.5-4.6 min and re-equilibration with 85% A from 4.6-10 min. GlcChol was eluted in 18 min with a flow of 0.25 mL/min using the following program: 100% A from 0-3 min, 100-0 % A from 3-3.5 min, 0 % A from 3.5-4.5 min, 0-100 % A from 4.5-5 min and re-equilibration with 100 % A from 5-18 min. Lipid levels were calculated in pmol/mg total protein, sphingoid bases and GlcChol were calculated based on the respective isotopic <sup>13</sup>C internal standard, while deacylated neutral (glyco)sphingolipids were calculated using C17-dhCer as internal standard and normalized using the respective standard.

**Histology** - For H&E staining, zebrafish were fixed in paraformaldehyde (4% PFA (w/v), Alfa Aesar, Haverhill, USA) overnight or Bouin's solution (5% acetic acid, 9% formaldehyde, 0.9% picric acid, Sigma) for 4 days, decalcified for 4 days using formic acid (20% (v/v)) and embedded in paraffin. Subsequently, serial sections of 5 µm thickness were made using a Leica RM2055 microtome. Sections were stained with Haematoxylin and Eosin.

Sequence alignment and modelling - Signal peptides were predicted using the SignalP-5.0 server<sup>28</sup> and sequences aligned with Clustal Omega<sup>29</sup>. Signal peptides were excluded and Asah1a or Asah1b structures were modelled with Swiss-Model<sup>57</sup> using human ACCase, PDB 6MHM<sup>23</sup>, as search model. Structures were superimposed and visualized with CCP4MG<sup>58</sup>.

Statistical analyses - Statistical analyses were performed using GraphPad Prism (v8.1.1, GraphPadsoftware, CA, USA) and data depicted as described in the result section. Data of lipid, protein and mRNA levels was analysed by One-Way Anova using Dunnett's test, with WT as control group, or Tukey's multiple comparison test as described in the result section. Data of length and tortuosity are analysed using a non-parametric Kruskal-Wallis test with Dunn's multiple comparison. In general, statistical comparisons are performed of WT vs *gba1*<sup>-/-</sup>, WT vs *gba1*<sup>-/-</sup>:*asah1b*<sup>-/-</sup> and *gba1*<sup>-/-</sup> vs *gba1*<sup>-/-</sup>:*asah1b*<sup>-/-</sup>, and depicted only when a significant difference is apparent and relevant. Ns = not significant, \*  $P < 0.05$ , \*\*  $P < 0.01$ , \*\*\*  $P < 0.001$  and \*\*\*\*  $P < 0.0001$ .



## References

- Hollak C.E., van Weely S., van Oers M.H. and Aerts J.M. (1994) Marked elevation of plasma chitotriosidase activity. A novel hallmark of Gaucher disease. *The Journal of clinical investigation* **93**, 1288-1292.
- Boot R.G., Verhoek M., de Fost M., Hollak C.E., Maas M., Bleijlevens B.,... and Aerts J.M. (2004) Marked elevation of the chemokine CCL18/PARC in Gaucher disease: a novel surrogate marker for assessing therapeutic intervention. *Blood* **103**, 33-39.
- Kramer G., Wegdam W., Donker-Koopman W., Ottenhoff R., Gaspar P., Verhoek M.,... and van Eijk M. (2016) Elevation of glycoprotein nonmetastatic melanoma protein B in type 1 Gaucher disease patients and mouse models. *FEBS Open Bio* **6**, 902-913.
- van Dussen L., Hendriks E.J., Groener J.E., Boot R.G., Hollak C.E. and Aerts J.M. (2014) Value of plasma chitotriosidase to assess non-neuronopathic Gaucher disease severity and progression in the era of enzyme replacement therapy. *J Inherit Metab Dis* **37**, 991-1001.
- Deegan P.B., Moran M.T., McFarlane I., Schofield J.P., Boot R.G., Aerts J.M. and Cox T.M. (2005) Clinical evaluation of chemokine and enzymatic biomarkers of Gaucher disease. *Blood Cells Mol Dis* **35**, 259-267.
- Murugesan V., Liu J., Yang R., Lin H., Lischuk A., Pastores G.,... and Mistry P.K. (2018) Validating glycoprotein non-metastatic melanoma B (gpNMB, osteoactivin), a new biomarker of Gaucher disease. *Blood Cells Mol Dis* **68**, 47-53.
- Dekker N., van Dussen L., Hollak C.E., Overkleeft H., Scheij S., Ghauharali K.,... and Aerts J.M. (2011) Elevated plasma glucosylsphingosine in Gaucher disease: relation to phenotype, storage cell markers, and therapeutic response. *Blood* **118**, e118-127.
- Ferraz M.J., Kallemeijn W.W., Mirzaian M., Herrera Moro D., Marques A., Wisse P.,... and Aerts J.M. (2014) Gaucher disease and Fabry disease: new markers and insights in pathophysiology for two distinct glycosphingolipidoses. *Biochimica et biophysica acta* **1841**, 811-825.
- Nair S., Boddupalli C.S., Verma R., Liu J., Yang R., Pastores G.M.,... and Dhodapkar M.V. (2015) Type II NKT-TFH cells against Gaucher lipids regulate B-cell immunity and inflammation. *Blood* **125**, 1256-1271.
- Ikuno M., Yamakado H., Akiyama H., Parajuli L.K., Taguchi K., Hara J.,... and Takahashi R. (2019) GBA haploinsufficiency accelerates alpha-synuclein pathology with altered lipid metabolism in a prodromal model of Parkinson's disease. *Human molecular genetics* **28**, 1894-1904.
- Taguchi Y.V., Liu J., Ruan J., Pacheco J., Zhang X., Abbasi J.,... and Chandra S.S. (2017) Glucosylsphingosine Promotes alpha-Synuclein Pathology in Mutant GBA-Associated Parkinson's Disease. *J Neurosci* **37**, 9617-9631.
- Reed M.C., Schiffer C., Heales S., Mehta A.B. and Hughes D.A. (2018) Impact of sphingolipids on osteoblast and osteoclast activity in Gaucher disease. *Mol Genet Metab* **124**, 278-286.
- Smith N.J., Fuller M., Saville J.T. and Cox T.M. (2018) Reduced cerebral vascularization in experimental neuronopathic Gaucher disease. *J Pathol* **244**, 120-128.
- Lukas J., Cozma C., Yang F., Kramp G., Meyer A., Nessler A.M.,... and Rolfs A. (2017) Glucosylsphingosine Causes Hematological and Visceral Changes in Mice-Evidence for a Pathophysiological Role in Gaucher Disease. *Int J Mol Sci* **18**.
- Dekker N., Voorn-Brouwer T., Verhoek M., Wennekes T., Narayan R.S., Speijer D.,... and Aerts J.M. (2011) The cytosolic beta-glucosidase GBA3 does not influence type 1 Gaucher disease manifestation. *Blood Cells Mol Dis* **46**, 19-26.
- Ferraz M.J., Marques A.R., Appelman M.D., Verhoek M., Strijland A., Mirzaian M.,... and Aerts J.M. (2016) Lysosomal glycosphingolipid catabolism by acid ceramidase: formation of glycosphingoid bases during deficiency of glycosidases. *FEBS Lett* **590**, 716-725.
- Park J.H. and Schuchman E.H. (2006) Acid ceramidase and human disease. *Biochimica et biophysica acta* **1758**, 2133-2138.
- Yu F.P.S., Amintas S., Levade T. and Medin J.A. (2018) Acid ceramidase deficiency: Farber disease and SMA-PME. *Orphanet J Rare Dis* **13**, 121.
- Okino N., He X., Gatt S., Sandhoff K., Ito M. and Schuchman E.H. (2003) The reverse activity of human acid ceramidase. *J Biol Chem* **278**, 29948-29953.
- Bernardo K., Hurwitz R., Zenk T., Desnick R.J., Ferlinz K., Schuchman E.H. and Sandhoff K. (1995) Purification, characterization, and biosynthesis of human acid ceramidase. *J Biol Chem* **270**, 11098-11102.
- Ferlinz K., Kopal G., Bernardo K., Linke T., Bar J., Breiden B.,... and Sandhoff K. (2001) Human acid ceramidase: processing, glycosylation, and lysosomal targeting. *J Biol Chem* **276**, 35352-35360.
- Gebai A., Gorelik A., Li Z., Illes K. and Nagar B. (2018) Structural basis for the activation of acid ceramidase. *Nature communications* **9**, 1621.
- Dementiev A., Joachimiak A., Nguyen H., Gorelik A., Illes K., Shabani S.,... and Doan N. (2019) Molecular Mechanism of Inhibition of Acid Ceramidase by Carmofur. *Journal of medicinal chemistry* **62**, 987-992.

24. Rajput V.B., Karthikeyan M. and Ramasamy S. (2019) Zebrafish acid ceramidase: Expression in *Pichia pastoris* GS115 and biochemical characterization. *Int J Biol Macromol* **122**, 587-593.
25. Zhou J., Tawk M., Tiziano F.D., Veillet J., Bayes M., Nolent F.,... and Melki J. (2012) Spinal muscular atrophy associated with progressive myoclonic epilepsy is caused by mutations in *ASA1*. *Am J Hum Genet* **91**, 5-14.
26. Lelieveld L.T., Mirzaian M., Kuo C.L., Artola M., Ferraz M.J., Peter R.E.A.,... and Aerts J. (2019) Role of beta-glucosidase 2 in aberrant glycosphingolipid metabolism: model of glucocerebrosidase deficiency in zebrafish. *J Lipid Res* **60**, 1851-1867.
27. Artola M., Kuo C.L., Lelieveld L.T., Rowland R.J., van der Marel G.A., Codee J.D.C.,... and Overkleeft H.S. (2019) Functionalized Cyclophellitols Are Selective Glucocerebrosidase Inhibitors and Induce a Bona Fide Neuropathic Gaucher Model in Zebrafish. *Journal of the American Chemical Society* **141**, 4214-4218.
28. Almagro Armenteros J.J., Tsirigos K.D., Sonderby C.K., Petersen T.N., Winther O., Brunak S.,... and Nielsen H. (2019) SignalP 5.0 improves signal peptide predictions using deep neural networks. *Nat Biotechnol* **37**, 420-423.
29. Madeira F., Park Y.M., Lee J., Buso N., Gur T., Madhusoodanan N.,... and Lopez R. (2019) The EMBL-EBI search and sequence analysis tools APIs in 2019. *Nucleic acids research* **47**, W636-W641.
30. Keatinge M., Bui H., Menke A., Chen Y.C., Sokol A.M., Bai Q.,... and Bandmann O. (2015) Glucocerebrosidase 1 deficient Danio rerio mirror key pathological aspects of human Gaucher disease and provide evidence of early microglial activation preceding alpha-synuclein-independent neuronal cell death. *Human molecular genetics* **24**, 6640-6652.
31. Menke A.L., Spitsbergen J.M., Wolterbeek A.P. and Woutersen R.A. (2011) Normal anatomy and histology of the adult zebrafish. *Toxicol Pathol* **39**, 759-775.
32. Uemura N., Koike M., Ansai S., Kinoshita M., Ishikawa-Fujiwara T., Matsui H.,... and Takahashi R. (2015) Viable neuronopathic Gaucher disease model in Medaka (*Oryzias latipes*) displays axonal accumulation of alpha-synuclein. *Plos Genet* **11**, e1005065.
33. Peri F. and Nusslein-Volhard C. (2008) Live imaging of neuronal degradation by microglia reveals a role for v0-ATPase a1 in phagosomal fusion in vivo. *Cell* **133**, 916-927.
34. Pandey M.K., Grabowski G.A. and Kohl J. (2018) An unexpected player in Gaucher disease: The multiple roles of complement in disease development. *Semin Immunol* **37**, 30-42.
35. Sidransky E., Nalls M.A., Aasly J.O., Aharon-Peretz J., Annesi G., Barbosa E.R.,... and Ziegler S.G. (2009) Multicenter analysis of glucocerebrosidase mutations in Parkinson's disease. *N Engl J Med* **361**, 1651-1661.
36. Milanese C., Sager J.J., Bai Q., Farrell T.C., Cannon J.R., Greenamyre J.T. and Burton E.A. (2012) Hypokinesia and reduced dopamine levels in zebrafish lacking beta- and gamma1-synucleins. *J Biol Chem* **287**, 2971-2983.
37. Vitner E.B., Farfel-Becker T., Eilam R., Biton I. and Futerman A.H. (2012) Contribution of brain inflammation to neuronal cell death in neuronopathic forms of Gaucher's disease. *Brain* **135**, 1724-1735.
38. Blesa J., Trigo-Damas I., Quiroga-Varela A. and Jackson-Lewis V.R. (2015) Oxidative stress and Parkinson's disease. *Front Neuroanat* **9**, 91.
39. Pandey M.K., Burrow T.A., Rani R., Martin L.J., Witte D., Setchell K.D.,... and Grabowski G.A. (2017) Complement drives glucosylceramide accumulation and tissue inflammation in Gaucher disease. *Nature* **543**, 108-112.
40. Ferraz M.J., Marques A.R., Gaspar P., Mirzaian M., van Roomen C., Ottenhoff R.,... and Aerts J.M. (2016) Lyso-glycosphingolipid abnormalities in different murine models of lysosomal storage disorders. *Mol Genet Metab* **117**, 186-193.
41. Welford R.W., Garzotti M., Marques Lourenco C., Mengel E., Marquardt T., Reunert J.,... and Groenen P. (2014) Plasma lysosphingomyelin demonstrates great potential as a diagnostic biomarker for Niemann-Pick disease type C in a retrospective study. *Plos one* **9**, e114669.
42. Li Y., Xu Y., Benitez B.A., Nagree M.S., Dearborn J.T., Jiang X.,... and Sands M.S. (2019) Genetic ablation of acid ceramidase in Krabbe disease confirms the psychosine hypothesis and identifies a new therapeutic target. *Proc Natl Acad Sci U S A* **116**, 20097-20103.
43. Jeon Y.J., Jung N., Park J.W., Park H.Y. and Jung S.C. (2015) Epithelial-Mesenchymal Transition in Kidney Tubular Epithelial Cells Induced by Globotriaosylsphingosine and Globotriaosylceramide. *Plos one* **10**, e0136442.
44. Rombach S.M., van den Bogaard B., de Groot E., Groener J.E., Poorthuis B.J., Linthorst G.E.,... and Aerts J.M. (2012) Vascular aspects of Fabry disease in relation to clinical manifestations and elevations in plasma globotriaosylsphingosine. *Hypertension* **60**, 998-1005.
45. Sanchez-Nino M.D., Sanz A.B., Carrasco S., Saleem M.A., Mathieson P.W., Valdivielso J.M.,... and Ortiz A. (2011) Globotriaosylsphingosine actions on human glomerular podocytes: implications for Fabry nephropathy. *Nephrol Dial Transplant* **26**, 1797-1802.
46. Realini N., Solorzano C., Pagliuca C., Pizzirani D., Armirotti A., Luciani R.,... and Piomelli D. (2013) Discovery of highly potent acid ceramidase inhibitors with in vitro tumor chemosensitizing activity. *Sci Rep* **3**, 1035.



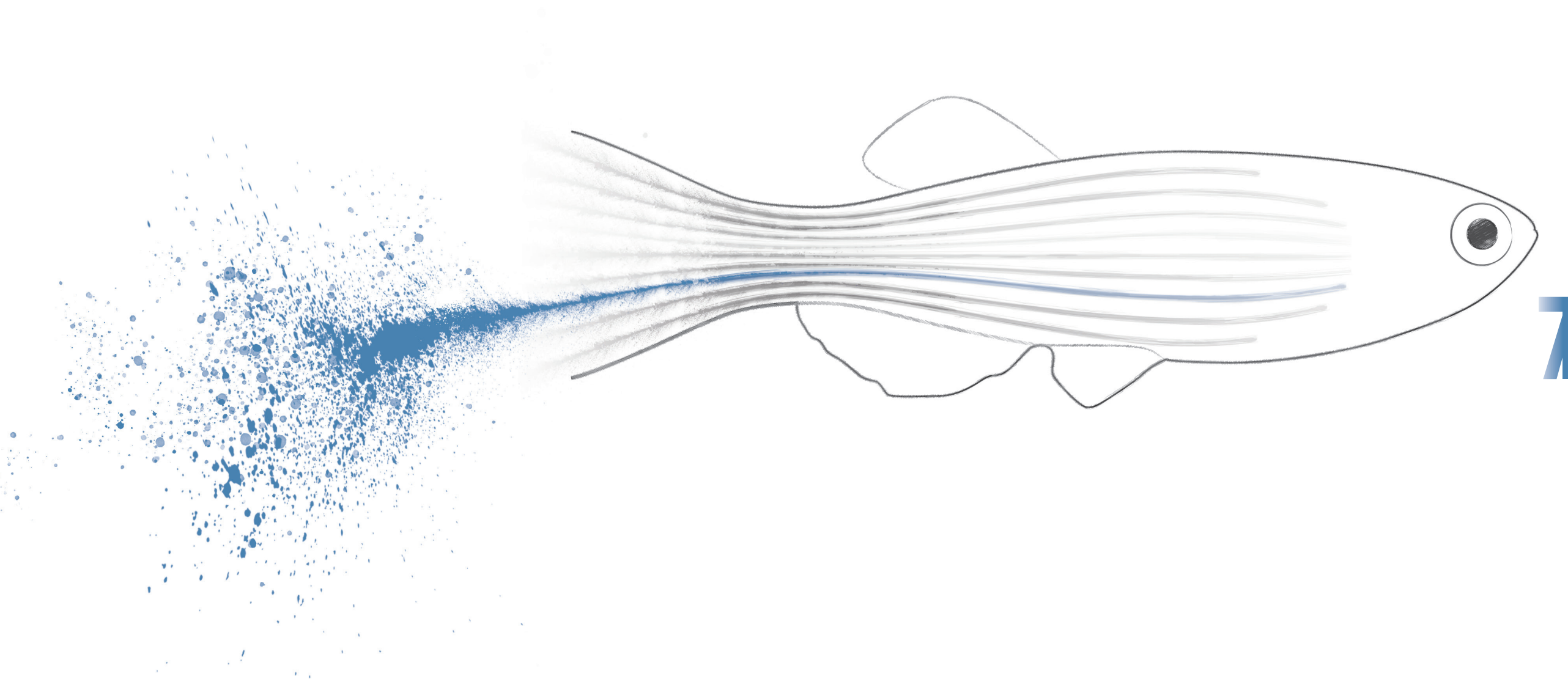
## Chapter 6

47. Ouairy C.M., Ferraz M.J., Boot R.G., Baggelaar M.P., van der Stelt M., Appelman M.,... and Overkleeft H.S. (2015) Development of an acid ceramidase activity-based probe. *Chemical communications* **51**, 6161-6163.
48. Ordonez Y.F., Abad J.L., Aseeri M., Casas J., Garcia V., Casasampere M.,... and Fabrias G. (2019) Activity-Based Imaging of Acid Ceramidase in Living Cells. *Journal of the American Chemical Society* **141**, 7736-7742.
49. Rubboli G., Veggiotti P., Pini A., Berardinelli A., Cantalupo G., Bertini E.,... and Michelucci R. (2015) Spinal muscular atrophy associated with progressive myoclonic epilepsy: A rare condition caused by mutations in *ASAH1*. *Epilepsia* **56**, 692-698.
50. Marques A.R., Mirzaian M., Akiyama H., Wisse P., Ferraz M.J., Gaspar P.,... and Aerts J.M. (2016) Glucosylated cholesterol in mammalian cells and tissues: formation and degradation by multiple cellular beta-glucosidases. *J Lipid Res* **57**, 451-463.
51. Mirzaian M., Wisse P., Ferraz M.J., Marques A.R.A., Gaspar P., Oussoren S.V.,... and Aerts J.M. (2017) Simultaneous quantitation of sphingoid bases by UPLC-ESI-MS/MS with identical (13)C-encoded internal standards. *Clin Chim Acta* **466**, 178-184.
52. Schneider C.A., Rasband W.S. and Eliceiri K.W. (2012) NIH Image to ImageJ: 25 years of image analysis. *Nat Methods* **9**, 671-675.
53. Koch B.E., Stougaard J. and Spaink H.P. (2014) Spatial and temporal expression patterns of chitinase genes in developing zebrafish embryos. *Gene Expr Patterns* **14**, 69-77.
54. Nguyen-Chi M., Laplace-Builhe B., Travnickova J., Luz-Crawford P., Tejedor G., Lutfalla G.,... and Djouad F. (2017) TNF signaling and macrophages govern fin regeneration in zebrafish larvae. *Cell Death Dis* **8**, e2979.
55. Harjula S.E., Ojanen M.J.T., Taavitsainen S., Nykter M. and Ramet M. (2018) Interleukin 10 mutant zebrafish have an enhanced interferon gamma response and improved survival against a *Mycobacterium marinum* infection. *Sci Rep* **8**, 10360.
56. Tang R., Dodd A., Lai D., McNabb W.C. and Love D.R. (2007) Validation of zebrafish (*Danio rerio*) reference genes for quantitative real-time RT-PCR normalization. *Acta Biochim Biophys Sin (Shanghai)* **39**, 384-390.
57. Waterhouse A., Bertoni M., Bienert S., Studer G., Tauriello G., Gumienny R.,... and Schwede T. (2018) SWISS-MODEL: homology modelling of protein structures and complexes. *Nucleic acids research* **46**, W296-W303.
58. McNicholas S., Potterton E., Wilson K.S. and Noble M.E. (2011) Presenting your structures: the CCP4mg molecular-graphics software. *Acta Crystallogr D Biol Crystallogr* **67**, 386-394.



## CHAPTER 7

### Progression of pathology in zebrafish with GCase deficiency



## Abstract

The penultimate step in the degradation of glycosphingolipids is the hydrolysis of glucosylceramide into glucose and ceramide. GlcCer is degraded in lysosomes by the acid  $\beta$ -glucosidase glucocerebrosidase (GCase). Mutations in the gene encoding GCase (gene name: *GBA*) lead to the common lysosomal storage disorder Gaucher disease (GD), characterized by lysosomal accumulation of GlcCer which partly is metabolized by acid ceramidase (ACase) into neurotoxic glucosylsphingosine (GlcSph). GlcCer can also be hydrolysed in the cytosol by the membrane-associated GBA2. Defective GBA2 has been found in association with autosomal-recessive cerebellar ataxia (ARCA) and hereditary spastic paraplegia (HSP). In the present study, zebrafish with complete knockouts (KOs) of the genes encoding GCase (*gba1*), Gba2 (*gba2*), ACase (*asah1b*) and combinations thereof, were raised to adulthood (12 weeks post-fertilization (wpf)) and characterized. Their phenotype as well as biochemical and pathological parameters are described. Carrier *gba1*<sup>+/-</sup> fish show no apparent phenotype nor any biochemical abnormalities, while the Gba2 knockout fish only develop a significant increase in specific GlcCer species in the brain. No clear abnormal phenotype is observed for any of the GCase deficient fish at 8 wpf, even though increases in GlcCer, neuroinflammation and autophagy are already demonstrable. Phenotypic abnormalities of the single *gba1* knockout zebrafish have an early onset ( $\pm$  9 wpf), starting with a drop of the tail and progressing into a change in swimming behaviour. In contrast, the double *gba1:gba2* knockout do not show the preceding characteristics such as the drop of the tail, but many develop a severe phenotypical abnormalities in a matter of days and have a significantly shorter lifespan than single *gba1* knockouts. Pilot experiments indicate a related earlier onset of dopaminergic neuron degradation in the *gba1:gba2* knockout fish, however the precise underlying pathophysiological mechanism is still elusive.

## Introduction

Glucosylceramide (GlcCer) is the precursor of more complex glycosphingolipids. Hydrolysis of GlcCer into glucose and ceramide is catalysed by different  $\beta$ -glucosidases with different subcellular locations (**Figure 1**). Acid  $\beta$ -glucosidase, or glucocerebrosidase (GCase), is a lysosomal  $\beta$ -glucosidase, hydrolysing GlcCer in lysosomes, while the membrane-associated GBA2 and cytosolic GBA3 hydrolyse GlcCer in the cytosol. Mutations in the gene encoding GCase lead to Gaucher disease, characterized by lysosomal accumulation of GlcCer primarily in tissue macrophages<sup>1</sup>. Clinical symptoms range from hepatosplenomegaly, anaemia, thrombocytopenia to bone deterioration in type 1 GD patients and, additionally, neuropathological symptoms in type 2 and 3 GD patients. Lysosomal acid ceramidase (ACase) is able to hydrolyse the fatty acid of the accumulating GlcCer, forming glucosylsphingosine (GlcSph). GlcSph is thought to be neurotoxic and to contribute to B-cell activation,  $\alpha$ -synuclein aggregation and reduced cerebral microvasculature<sup>2-5</sup>. Carriers of a mutation in GCase, have a markedly increased risk for developing Parkinson's disease and Lewy-body dementia<sup>6,7</sup>. However, to date, the underlying molecular mechanisms, imposed by GCase abnormalities, are not fully elucidated. Little is known about the physiological role of the non-lysosomal GBA2 and the impact of its deficiency. On one hand, mutations in the gene encoding GBA2 have been associated with autosomal-recessive cerebellar ataxia (ARCA) and hereditary spastic paraplegia (HSP)<sup>8-11</sup>. On the other hand, mildly affected type 1 GD patients are treated for more than a decade with the iminosugar Miglustat (*N*-butyl-deoxynojirimycin) and develop no major complications, even though this compound markedly inhibits GBA2 activity at the administered dose (3 times 100 mg daily)<sup>12,13</sup>.

In the past years, several research models have been generated in order to study the impact of defective GCase or GBA2 and evaluate treatments of GD<sup>14</sup>. Complete GCase-deficient mouse models die prematurely due to trans-epidermal water loss<sup>15,16</sup>. For that reason, GD has been studied by pharmacological induction of GCase deficiency<sup>17</sup> or using conditional knockouts of *GBA1* where GCase deficiency is limited to specific cell lineages. Examples are the GD mouse models with a defective GCase in the hematopoietic stem cell lineage<sup>18</sup>, neuronal cells<sup>19</sup> or all tissues except skin<sup>19</sup>. GBA2 knockout mice are viable and develop a moderately increased GlcCer in testis, brain and liver (Marques and Ferraz; unpublished data and ref. 20). Male KO mice are found to display impaired fertility<sup>20-22</sup>. Remarkable interindividual differences were recently noted among GBA2 deficient mice with some animals developing marked neurological abnormalities and others not<sup>21</sup>. Interestingly, concomitant GBA2 deficiency in a conditional GCase deficient mouse model, limited to the haematopoietic stem cell lineage, revealed a correction of the visceral, hematologic and bone phenotype. In addition, a partial correction of increased cytokines was observed, even though persistent Gaucher cells were observed as well as increased GlcCer and GlcSph levels in liver and spleen of double mutant mice<sup>23</sup>. Amelioration of phenotypic manifestations of Niemann-Pick type C (NPC) mice, including behaviour and neuropathology, were apparent in mice with a concomitant genetic- or pharmacological GBA2 deficiency upon treatment with GBA2-specific iminosugars<sup>24</sup>. At present the impact of defective GBA2 in GD mice regarding neurological symptoms remains elusive.

Recent research has revealed that both GCase and GBA2 have substrates beyond GlcCer. Both enzymes may act as transglucosidase, catalysing the (reversible) transfer of the glucose from GlcCer to an acceptor moiety such as cholesterol and thereby forming glucosylated cholesterol (GlcChol, **Figure 1**)<sup>25,26</sup>. GD patients and GD mouse models show an increase in GlcChol levels, while GBA2 deficient mice show a decrease<sup>25</sup>. Although GCase can perform transglucosylation *in vitro*, increased levels of GlcChol during GCase deficiency suggest a primary role of the enzyme in hydrolysis of lysosomal GlcChol<sup>25</sup>. It is presently unclear whether elevated GlcChol during GCase deficiency contributes to pathology. Previously, CRISPR/Cas9 technology was successfully used to generate mutations in the zebrafish orthologues of GCase and GBA2. The developing zebrafish off-spring of 5 days post-fertilization (5 dpf) were studied regarding aberrant glucosylceramide metabolism of *gba1*, *gba2* and double *gba1:gba2* knockout (KO) individuals. At 5dpf, single *gba1*<sup>-/-</sup> zebrafish larvae show accumulation of GlcSph, but no GlcCer accumulation, while single *gba2*<sup>-/-</sup> zebrafish larvae show accumulation of GlcCer and a decrease in GlcChol<sup>27</sup>.

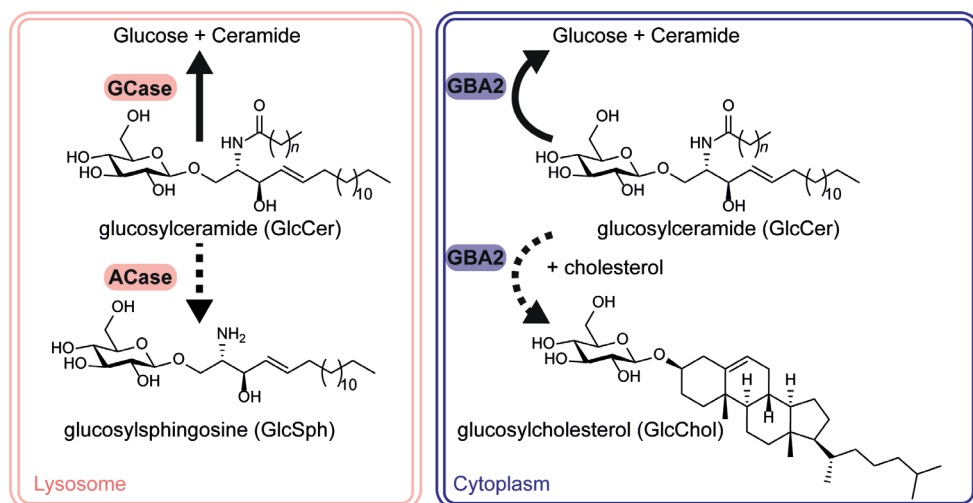


**Figure 1 | Schematic representation of GlcCer hydrolysis by lysosomal GCase and membrane-associated GBA2.** Secondary pathways of GlcCer catabolism are described. ACCase is able to hydrolyse accumulating lysosomal GlcCer to GlcSph during GCase deficiency. Next to hydrolysis of GlcCer, GBA2 is also able to transfer the glucose of GlcCer to a cholesterol acceptor, generating GlcChol.

The primary goal of the present study was to evaluate adult *Gba2* KO zebrafish and to study the impact of the absence of *Gba2* during GCase deficiency. For this purpose, zebrafish were raised to adulthood and several morphological, histopathological and biochemical features were assessed and compared between the different mutants. This study also included *gba1*<sup>+/-</sup> (carriers), *asah1b*<sup>-/-</sup> and *gba1*<sup>-/-</sup>:*asah1b*<sup>-/-</sup> fish. Given the significant difference in occurrence of symptoms and accompanying lifespan of *gba1*<sup>-/-</sup>, *gba1*<sup>-/-</sup>:*gba2*<sup>-/-</sup> and *gba1*<sup>-/-</sup>:*asah1b*<sup>-/-</sup> fish, attention was paid to the progression of pathology in the various mutant zebrafish. Zebrafish with *gba1*, *gba2*, *gba1:gba2* and *asah1b:gba1* mutations were examined at different developmental ages with respect to neuroinflammation that likely precedes neurodegeneration.



## Results

**Lipid abnormalities of *gba1:gba2* KO zebrafish as compared to *gba1* and *gba1:asah1b* KO**

Glycosphingolipids in brains and livers of 12 wpf zebrafish with a KO of *gba1*, *gba2* and *asah1b* and combinations thereof were quantified. Recently, Hisako Akiyama at the RIKEN discovered the existence of galactosylcholesterol (GalChol) in tissues, particularly the brain<sup>28</sup>. GalChol is synthesized by GBA2. With the initial LC-MS/MS method GlcChol and GalChol were not separated. This prompted the use of a different LC chromatography in order to individually measure GlcChol and GalChol. With this method in place, brains of mutant zebrafish were investigated. Brains and livers of *gba1*<sup>-/-</sup> zebrafish presented significantly increased GlcSph, total GlcCer, lactosylceramide (LacCer) and GlcChol levels but no significantly elevated GalChol, ceramide and sphingosine levels (brain) (**Figure 2A and B** for liver and brain respectively). A reduction in galactosylceramide (GalCer) levels was apparent in *gba1*<sup>-/-</sup> but this was not significantly different.

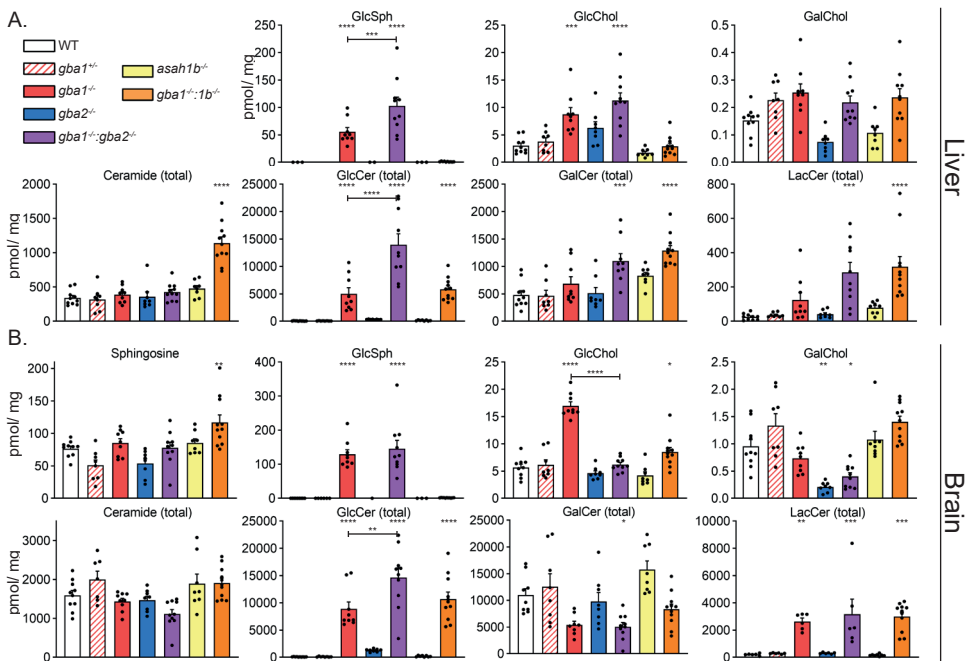


**Figure 2 | Relevant (glyco)sphingolipids in livers and brains of end stage zebrafish (t = 9-12 wpf)**

Relevant glycosphingolipids, GlcSph, GlcChol, GalChol as well as total ceramide, total GlcCer, total GalCer and total LacCer, were determined of zebrafish livers and brains in pmol/mg tissue. Livers and brains were dissected of zebrafish at t = 12 wpf or at the end stage, following pre-determined human end points for *gba1*<sup>-/-</sup> (t = 10-12 wpf) and *gba1*<sup>-/-</sup>:*gba2*<sup>-/-</sup> zebrafish (t = 9-12 wpf). Data is depicted as mean ± SEM; end stage; (n = 8-11). Data is analysed by One-Way Anova with Tukey's multiple comparison test. Ns = not significant, \*\* P < 0.01, \*\*\* P < 0.001 and \*\*\*\* P < 0.0001.

*Gba1*<sup>-/-</sup>:*asah1b*<sup>-/-</sup> brains and livers displayed no excessive GlcSph, while total GlcCer and LacCer levels were increased (see also chapter 6). No significant accumulation of GlcChol was observed in the *gba1*<sup>-/-</sup>:*asah1b*<sup>-/-</sup> brains in contrast to the *gba1*<sup>-/-</sup> brains.

No significant differences were apparent in any of the lipids quantified in brains and livers of *gba1*<sup>-/-</sup> (carrier) zebrafish compared to wildtype (WT) (striped bars, **Figure 2A and B**). GlcSph, total GlcCer and LacCer levels were significantly elevated in the *gba1*<sup>-/-</sup>:*gba2*<sup>-/-</sup> livers and brains compared to WT (purple bars, **Figure 2A and B**). Statistical analysis revealed that GlcCer levels of *gba1*<sup>-/-</sup>:*gba2*<sup>-/-</sup> livers and brains were significantly higher compared to single *gba1*<sup>-/-</sup> and *gba1*<sup>-/-</sup>:*asah1b*<sup>-/-</sup> samples, while only significant higher GlcSph levels were detected in livers of *gba1*<sup>-/-</sup>:*gba2*<sup>-/-</sup>, compared to those of *gba1*<sup>-/-</sup> fish. GalCer levels were significantly reduced in the double *gba1*<sup>-/-</sup>:*gba2*<sup>-/-</sup> deficient fish brains compared to WT. GlcCer tended to be increased in livers and brains of *gba2*<sup>-/-</sup> zebrafish, while no significant reduction of GlcChol was measured in either *gba2*<sup>-/-</sup> or *gba1*<sup>-/-</sup>:*gba2*<sup>-/-</sup> samples (**Figure 2A and B**). The latter was unexpected, as zebrafish larvae (5 dpf) presented increased GlcCer levels and a reduction of GlcChol<sup>27</sup>. Moreover, GBA2 deficient mice accumulate GlcCer in their livers and show a decrease in GlcChol levels<sup>20,21,23,25</sup>. The chromatographic separation of GlcChol and GalChol revealed that the latter is significantly decreased in brains of *gba2*<sup>-/-</sup> and *gba1*<sup>-/-</sup>:*gba2*<sup>-/-</sup> fish compared to WT but not in *gba1*<sup>-/-</sup> or *gba1*<sup>-/-</sup>:*asah1b*<sup>-/-</sup> brains.

### Fatty acid composition of GSLs and SM

Neutral (glyco)sphingolipids consist of a sphingosine backbone linked to a fatty acid, which can differ in carbon chain length and presence of double bonds. Our routine LC-MS/MS method for sphingolipids contains a microwave-assisted deacylation step<sup>29,30</sup> and consequently renders no information on fatty acyl composition of measured sphingolipids. Another type of modified ceramide is sphingomyelin (SM), which has a phosphocholine headgroup and is the most predominant sphingolipid in cell membranes. However, phosphatidylcholine (PC) has similar m/z transitions as the SM species, including an identical daughter of 184.1 Da which is the phosphocholine headgroup of either SM or PC.

In order to study aberrant (glyco)sphingolipids with specific fatty acids, a LC-MS/MS procedure was developed using hydrophilic interaction liquid chromatography (HILIC) which enabled separation of sphingolipids with glucosyl- and galactosyl moieties as well as separation of SM and PC species. The ceramide species and the internal standard dihydroceramide eluted in the first 2 min, followed by GlcCer and GalCer lipids (2.5 to 3 min), LacCer (± 5 min), PC (± 8 min) and finally the more polar SM (± 9 min) (**Figure 3A**). First, the fatty acyl composition of ceramide, GlcCer, GalCer and SM species in WT brain was determined (**Figure 3B**). Ceramide species mainly had fatty acyls 16:0 (9.4%); 18:0 (24.6%); 24:0 (25.1%) and 24:1 (30.7%). In the brain, the main monohexosylceramide is GalCer (± 97%) (**Figure 2B**). The major fatty acyl species of GlcCer were 16:0 (61.2%) and 18:0 (13.8%), while GalCer mainly had the longer fatty acyls 22:0 (17.9%), 24:2 (10.1%), 24:1 (39.4%) and 24:0 (15.8%). SM mainly showed 16:0 (702.6 m/z, 30.7%), 18:0 (730.6 m/z, 16.5%) and 24:1 (812.7 m/z, 32.4%) fatty acyls.

However, in theory the composition of the double bonds on the sphingosine backbone and fatty acid of SM could be different due to the used phosphocholine headgroup as daughter in the LC-MS/MS method instead of the sphingosine backbone (264.4 m/z) for the other (glyco)sphingolipids. The fatty acyl composition of ceramide, GlcCer, GalCer and SM species in the liver was different from that of the brain (**Figure 3C**).

The majority of ceramide species in the liver had 16:0 (46.8 %) and 24:1 (21.8 %) fatty acyls, GlcCer predominantly contained 18:0 (81.1 %), while GalCer had comparable levels of 16:0 (23.7 %), 22:0 (27.3 %), 24:1 (23.7 %) and 24:0 (18.6 %) fatty acyls and SM predominantly 16:0 (48.9 %) fatty acyls with smaller fractions of 22:0, 22:1 and 24:1 (11.8%, 10.7% and 17.1 % respectively).

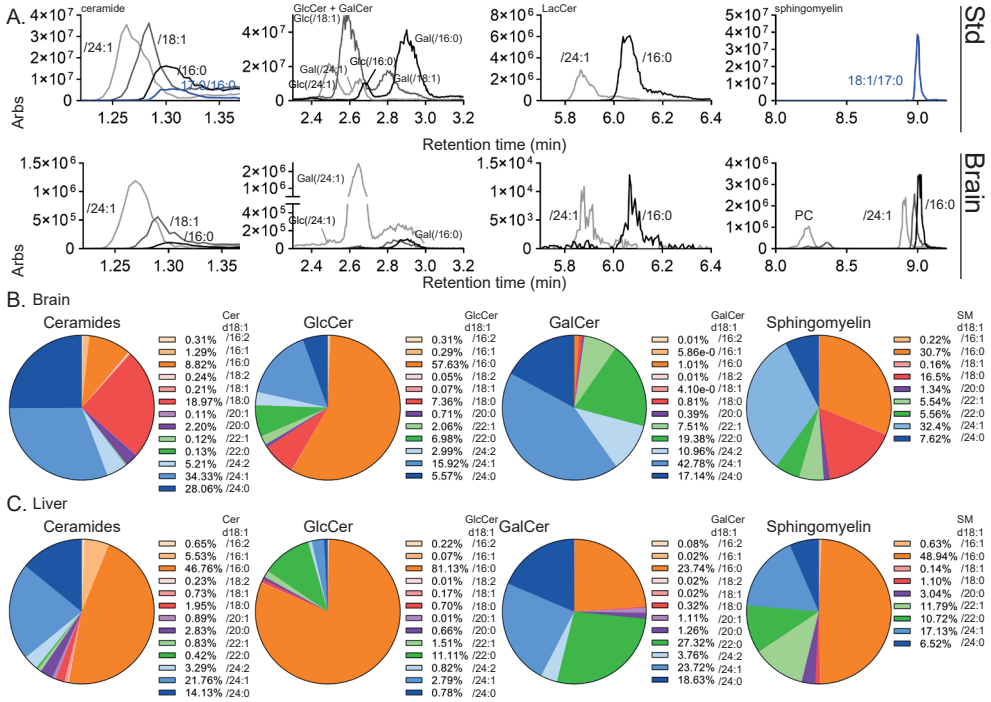


**Figure 3 | LC-MS/MS method for analysis of neutral (glyco) sphingolipids with fatty acyl**

(A) Combined chromatograms showing elution of different ceramides, GlcCer, GalCer, LacCer and sphingomyelin species from a sample with different standards (top panel) or a WT brain (bottom panel). The internal standards (dhCer d17:0/16:0 and SM d18:1/17:0) are shown in blue, lipids with 16:0 fatty acyl in black, 18:0 or 18:1 in grey and 24:1 fatty acyl in light grey. (Glyco) sphingolipids with different fatty acyl compositions were measured of WT brains (B) and livers (C) and depicted as ratio of the total of respective lipid species. WT, 12 wpf: n = 4

The same method was used to determine specific fatty acyl composition of sphingolipids in brain and liver of knockout zebrafish. A trend with regard to ceramide species was observed in brains of the *gba1*<sup>-/-</sup> and *gba1:asah1b* KO fish. Ceramide species with 16:0 and 18:0 fatty acyls appeared increased in *gba1*<sup>-/-</sup> and *gba1:asah1b*<sup>-/-</sup> brains, but only a significant increase of 16:0 was apparent in *gba1:asah1b*<sup>-/-</sup> brain ( $\pm$  6-fold, **Figure 4A**). In the liver, ceramide species with 16:0 and 18:0 ceramides were only significantly increased in *gba1:asah1b* KO fish (**Figure 4B**). Ceramides levels with longer fatty acyls (24:1, 24:0, 26:1 and 26:0) showed a slight, but not significant reduction in brains of *gba1*<sup>-/-</sup>, *gba1:asah1b*<sup>-/-</sup> and *gba1:asah1b:gba2*<sup>-/-</sup> zebrafish. SM showed a similar trend of increased 16:0 fatty acyls and decreased levels of longer fatty acyls, but none of the differences were significant (**Supplementary Figure 1A**).

All GlcCer species were increased in brain and liver of the three *gba1* mutant zebrafish. GlcCer with 18:0 and 20:0 fatty acyls showed the highest increase, while GlcCer species with 22:0 and 24:0 fatty acyls showed only small increases. Total GlcCer levels were not increased in *gba2*<sup>-/-</sup> brain and liver, however the GlcCer species with 18:0 and 20:0 fatty acids were significantly increased in brain of *gba2*<sup>-/-</sup> zebrafish. Brains of *gba1*<sup>-/-</sup>:*gba2*<sup>-/-</sup> double mutant fish showed significant higher levels of GlcCer with 18:0 and 20:0 fatty acyls compared to single *gba1*<sup>-/-</sup> and *gba1*<sup>-/-</sup>:*asah1b*<sup>-/-</sup> fish. LacCer, a product of GlcCer, also showed higher levels of species with 16:0 and 18:0 fatty acyls in the three *gba1* mutant zebrafish brains, consistent with increases of specific GlcCer species (**Supplementary Figure 1B**).

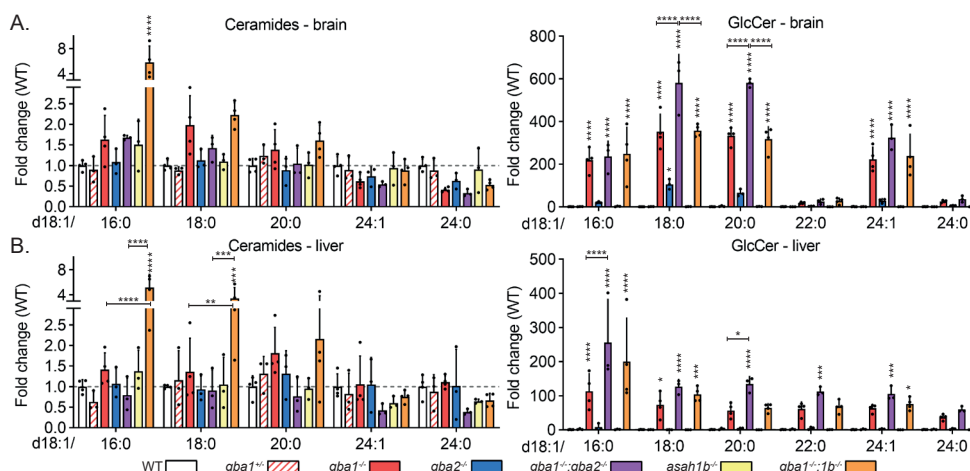


**Figure 4 | Changes in levels of ceramide and GlcCer with specific fatty acyls**

Levels of ceramide and GlcCer species with different fatty acyls in brains (**A**) and livers (**B**) of WT (n = 4), *gba1*<sup>+/-</sup> (n = 3), *gba1*<sup>-/-</sup> (n = 4), *gba2*<sup>-/-</sup> (n = 3), *gba1*<sup>-/-</sup>:*gba2*<sup>-/-</sup> (n = 3), *asah1b*<sup>-/-</sup> (n = 3) and *gba1*<sup>-/-</sup>:*asah1b*<sup>-/-</sup> (n = 4). Ceramide and GlcCer species were measured and calculated as relative abundance in the target sample compared to the mean of the WT sample. Data is depicted as mean ± SEM. Data is analysed by Two-Way Anova with Tukey's multiple comparison test. In general, statistical comparisons are depicted of WT vs respective mutant, *gba1*<sup>-/-</sup> vs *gba1*<sup>-/-</sup>:*gba2*<sup>-/-</sup>, *gba1*<sup>-/-</sup> vs *gba1*<sup>-/-</sup>:*asah1b*<sup>-/-</sup> or *gba1*<sup>-/-</sup>:*gba2*<sup>-/-</sup> vs *gba1*<sup>-/-</sup>:*asah1b*<sup>-/-</sup>, only when a significant difference is apparent and relevant. Ns = not significant, \* P < 0.05, \*\* P < 0.01, \*\*\* P < 0.001 and \*\*\*\* P < 0.0001.

### Infiltration of Gaucher-like cells in visceral tissues during GCase deficiency

Zebrafish were sectioned along the sagittal plane and stained using haematoxylin and eosin (H&E) (**Figure 5** and **Supplementary Figure 2**). Infiltration of Gaucher-like cells was observed in liver (**5A**), spleen (**5B**) and pancreas (**5C**) of *gba1*<sup>-/-</sup> zebrafish (panels left down). The same was observed for tissues of *gba1*<sup>-/-</sup>:*gba2*<sup>-/-</sup> and *gba1*<sup>-/-</sup>:*asah1b*<sup>-/-</sup> fish, while no storage cells were observed in the tissues of *gba2*<sup>-/-</sup> zebrafish. No apparent abnormalities were observed in other tissues such as kidney, testis and skin (**Supplementary Figure 2**). One zebrafish with a *gba1*<sup>-/-</sup>:*gba2*<sup>-/-</sup> background showed exceptionally very persistent infiltration of storage cells in liver, spleen, pancreas, kidney and testis (**Supplementary Figure 3**).



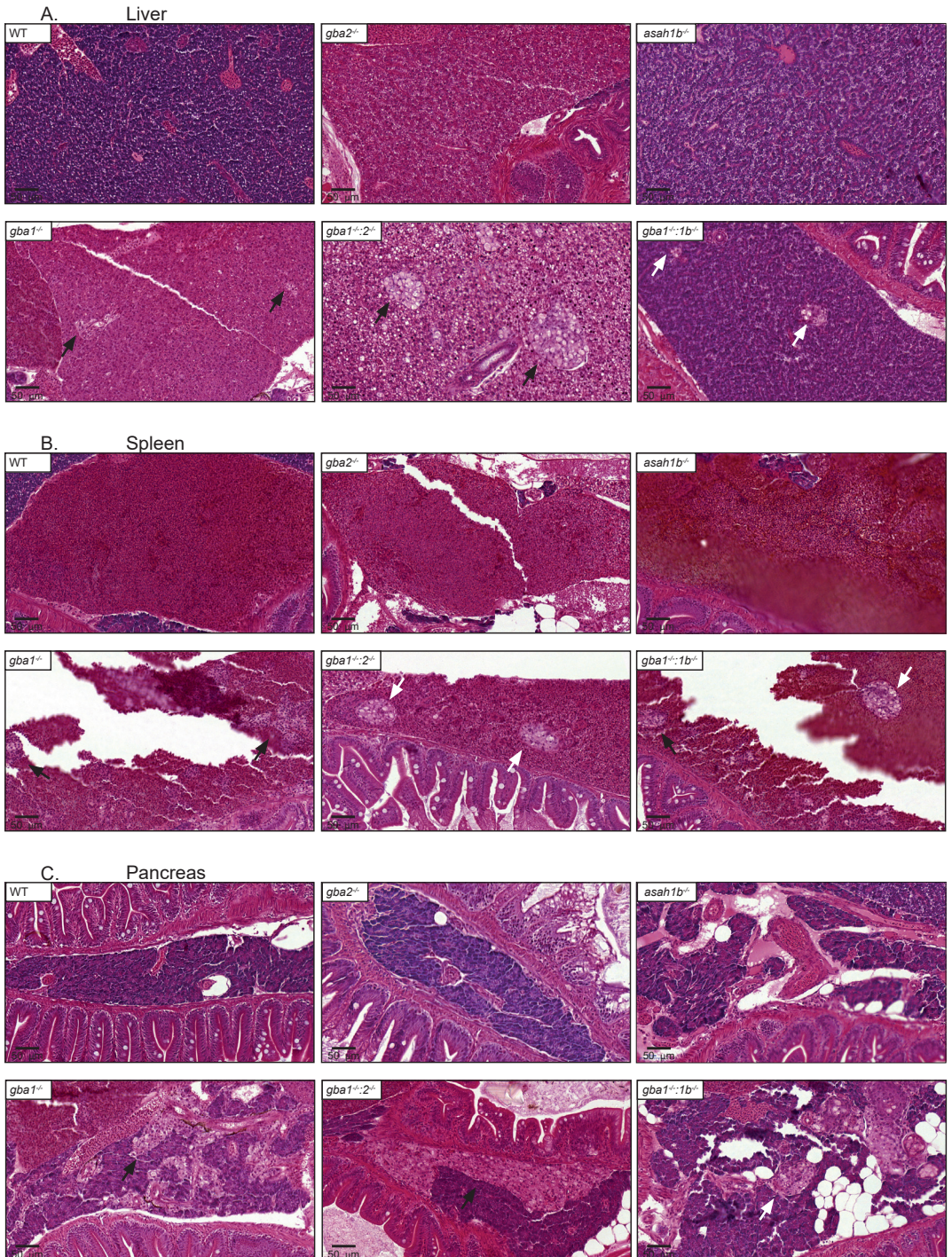


**Figure 5 | Histopathology of visceral tissues**

Haematoxylin and eosin (H&E) staining of liver (A), spleen (B) and pancreas (C) of WT and mutant zebrafish. Gaucher-like cells are indicated with arrows.



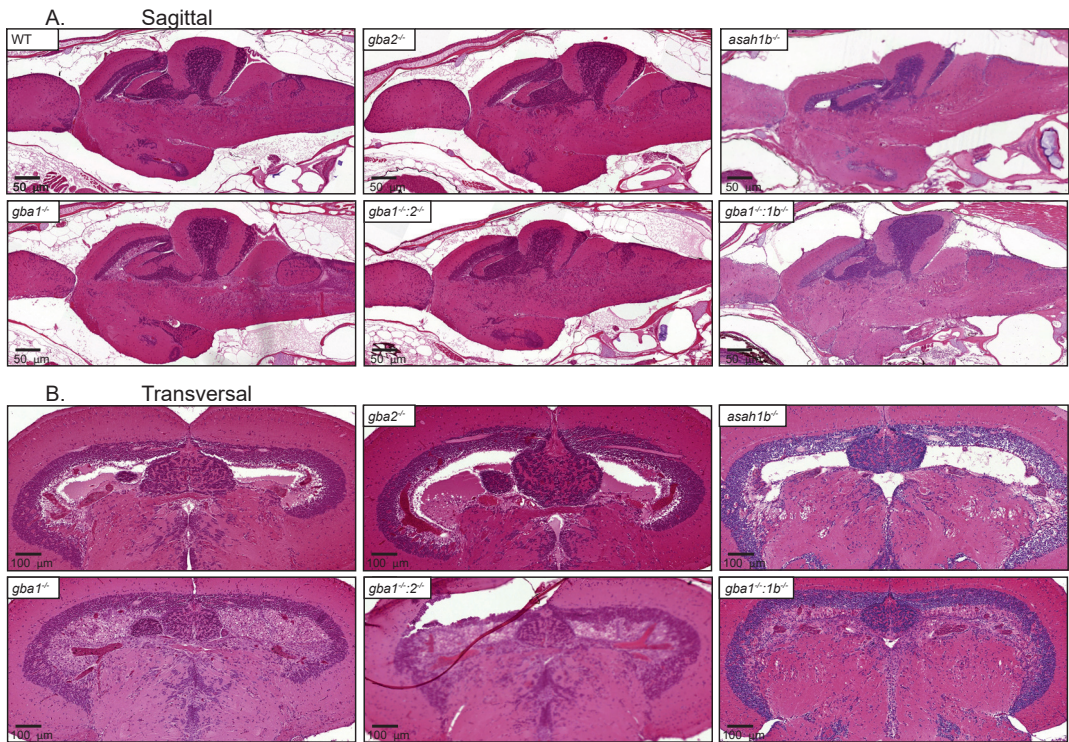


**Figure 6 | Histopathology of brain.**

H&E staining of brain sagittal (A) and transversal sections (B) of WT and mutant zebrafish

### Infiltration of Gaucher-like cells in brain during GCase deficiency

Next, brains were analysed for the presence of storage cells. No overt pathology was apparent in *gba1*<sup>+/-</sup> (carrier) brains and *gba2*<sup>-/-</sup> brains, while marked infiltration of Gaucher-like cells was observed in *gba1*<sup>-/-</sup>:*gba2*<sup>-/-</sup> and *gba1*<sup>-/-</sup> and *gba1*<sup>-/-</sup>:*asah1b* brains (Figure 6). This infiltration was remarkably high in the periventricular grey zone of the optic tectum.

### Neuroinflammation and neurodegeneration in *gba1:gba2* KO zebrafish

Brains were analysed for abnormal autophagy, storage cell presence, induction of lysosomes, inflammation, complement activation and neurodegeneration by analysis of the expression of relevant proteins and mRNAs. Upregulation of autophagy was evaluated by immunoblotting of p62, a ubiquitin-binding protein targeting other proteins for selective autophagy, and the two forms of LC-3, cytosolic LC3-I and lipid conjugate LC3-II which is recruited to autophagosomal membranes. *Gba1*<sup>-/-</sup>, *gba1*<sup>-/-</sup>:*gba2*<sup>-/-</sup> and *gba1*<sup>-/-</sup>:*asah1b*<sup>-/-</sup> brains showed increased levels of LC3-II and p62, indicating increased autophagy (Figure 7A and B). Consistent with upregulation of the lysosomal-autophagy pathway, increased expression of the lysosomal protease *catd* was observed in all of the *gba1*<sup>-/-</sup> brains. In analogy to the histopathology examination (Figure 6), mRNA levels of storage cell biomarkers *gpnmb* and *chia.6* were increased in all of the *gba1*<sup>-/-</sup> brains (Figure 7C).



The same was observed for genes involved in neuroinflammation, such as *il-1b*, *tnfβ*, the gene for the microglia marker *apoeb* and genes involved in the complement system *c1qA*, *c3.1* and *c5aR* (**Figure 7C**). Of note, no significant difference was found between *gba1<sup>-/-</sup>* and *gba1<sup>-/-</sup>:gba2<sup>-/-</sup>* for any of the studied proteins or genes.

The study described in chapter 6 suggested a potential harmful role for GlcSph in accelerating dopaminergic neuronal loss. Indeed, *gba1<sup>-/-</sup>:asah1b<sup>-/-</sup>* fish lacking excessive GlcSph as compared to *gba1<sup>-/-</sup>* fish show a significantly improved expression of mRNAs encoding the tyrosine hydroxylase (*th1*), indicative for dopaminergic neurons, as well as improved expression the two zebrafish synuclein orthologues, *sncβ* and *sncγb* (**Figure 7C**). Brains of *gba1<sup>-/-</sup>:gba2<sup>-/-</sup>* zebrafish with excessive GlcSph showed a significant reduction of *th1*, *sncβ* and *sncγb* mRNAs like *gba1<sup>-/-</sup>* fish (**Figure 7C**). In all three *gba1* mutant brain a reduction of the transcript encoding myelin-binding protein (*mbpa*) was observed. Thus, no protective effect by the combined GBa2 deficiency in this respect was observed.

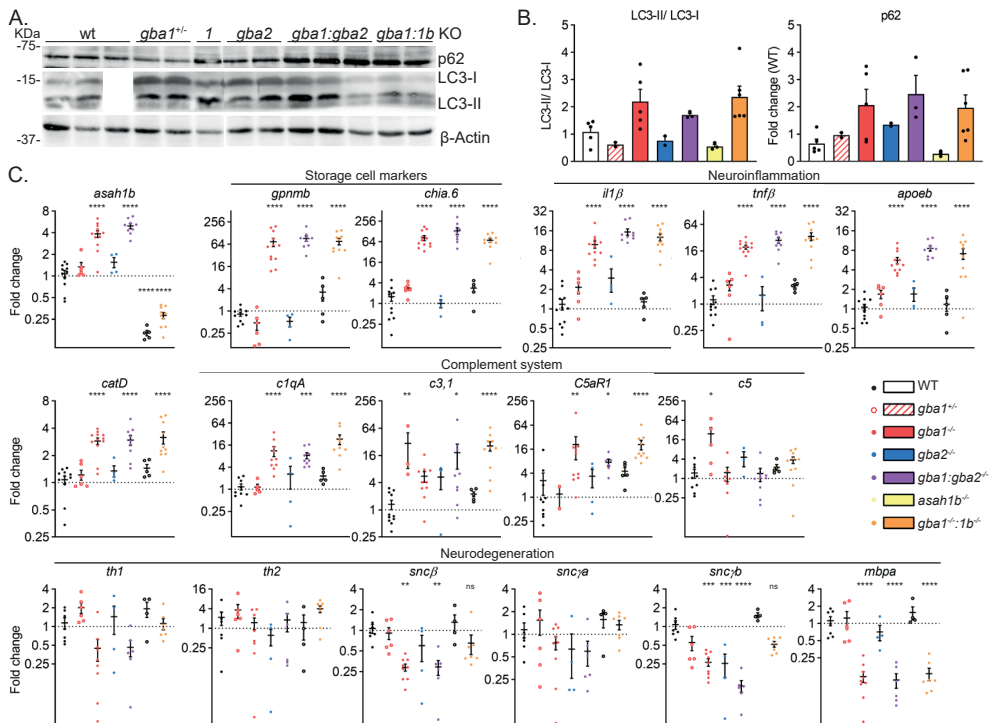


**Figure 7 | Protein and RNA abnormalities in WT and knockout zebrafish**

**(A)** Representative western blots of p62, LC-3 and β-actin as loading control. **(B)** Quantification of protein abnormalities with the ratio of LC-3II/LC-3I and ratio of p62/WT (n = 2-5). **(C)** mRNA levels of *asah1a*, *asah1b*, *gpnmb*, *chia.6*, *il-1b*, *tnfβ*, *apoEb*, *catD*, *c1qA*, *c3.1*, *c5aR*, *c5*, *th1*, *th2*, *sncβ*, *sncγa*, *sncγb* and *mbpa* were determined using RT-qPCR analysis of n = 5-11 fish. Data is normalized using two housekeeping genes (*ef1α* and *rpl13*), analysed by One-Way Anova with Tukey's multiple comparison test or Brown-Forsythe and Welch Anova with Dunnett's multiple comparisons test for *gpnmb* and *chia.6* and depicted as scattered dot plot ± SEM. \* P < 0.05, \*\* P < 0.01, \*\*\* P < 0.001 and \*\*\*\* P < 0.0001.

### Unpredictable disease progression of *gba1:gba2* deficient zebrafish

The *gba1*<sup>-/-</sup> zebrafish develop a progressive phenotype and it was necessary to cull individual fish before the experimental end point of 12 wpf (see chapter 6). In contrast, *gba1*<sup>-/-</sup>:*asah1b*<sup>-/-</sup> fish lacking excessive GlcSph developed similar phenotypic symptoms at later age, around 15-17 wpf (**Figure 8A**). Most *gba1*<sup>-/-</sup> zebrafish developed a characteristic drop of the tail prior to the change in swimming behaviour. In this respect, *gba1*<sup>-/-</sup>:*gba2*<sup>-/-</sup> zebrafish showed a very unpredictable course of disease manifestations. The change in swimming behaviour could occur in only a matter of days and was not preceded by a drop in the tail. Many *gba1*<sup>-/-</sup>:*gba2*<sup>-/-</sup> fish had to be sacrificed earlier than their *gba1*<sup>-/-</sup> counterparts, at approximately 10-11 weeks (**Figure 8A**). No abnormal morphology was observed for the *gba1*<sup>+/-</sup> (carrier), *gba2*<sup>-/-</sup>, *asah1b*<sup>-/-</sup> and *gba1*<sup>-/-</sup>:*asah1b*<sup>-/-</sup> fish at 12 wpf (**Figure 8B and C**). Both *gba1*<sup>-/-</sup> and *gba1*<sup>-/-</sup>:*gba2*<sup>-/-</sup> fish were significantly smaller and more curved than WT or *gba1*<sup>-/-</sup>:*asah1b*<sup>-/-</sup> fish (**Figure 8B and C**), while *gba1*<sup>-/-</sup> and *gba1*<sup>-/-</sup>:*gba2*<sup>-/-</sup> age-matched fish appeared comparable (t= 10, 11 and 12 wpf; **Supplementary Figure 4**).

### Swimming patterns

All zebrafish were individually filmed at 12 wpf, or at the end stage of their lives, to quantify their swimming pattern (**Figure 8D and E**). Most *gba1*<sup>-/-</sup> zebrafish and *gba1*<sup>-/-</sup>:*gba2*<sup>-/-</sup> zebrafish failed to maintain an upright position, while some severe *gba1*<sup>-/-</sup>:*gba2*<sup>-/-</sup> individuals were swimming upside down complicating their tracking (**Figure 8D**). A significant reduction in velocity was observed for *gba1*<sup>-/-</sup>:*gba2*<sup>-/-</sup> zebrafish compared to WT and *gba1*<sup>-/-</sup> zebrafish (**Figure 8D and E**). Noteworthy, the tracked *Gba1:Gba2* double mutant zebrafish showed movement throughout the tank, in contrast to the significant increase of time spent at the bottom of the tank by *gba1*<sup>-/-</sup> zebrafish (**Figure 8D and E**).

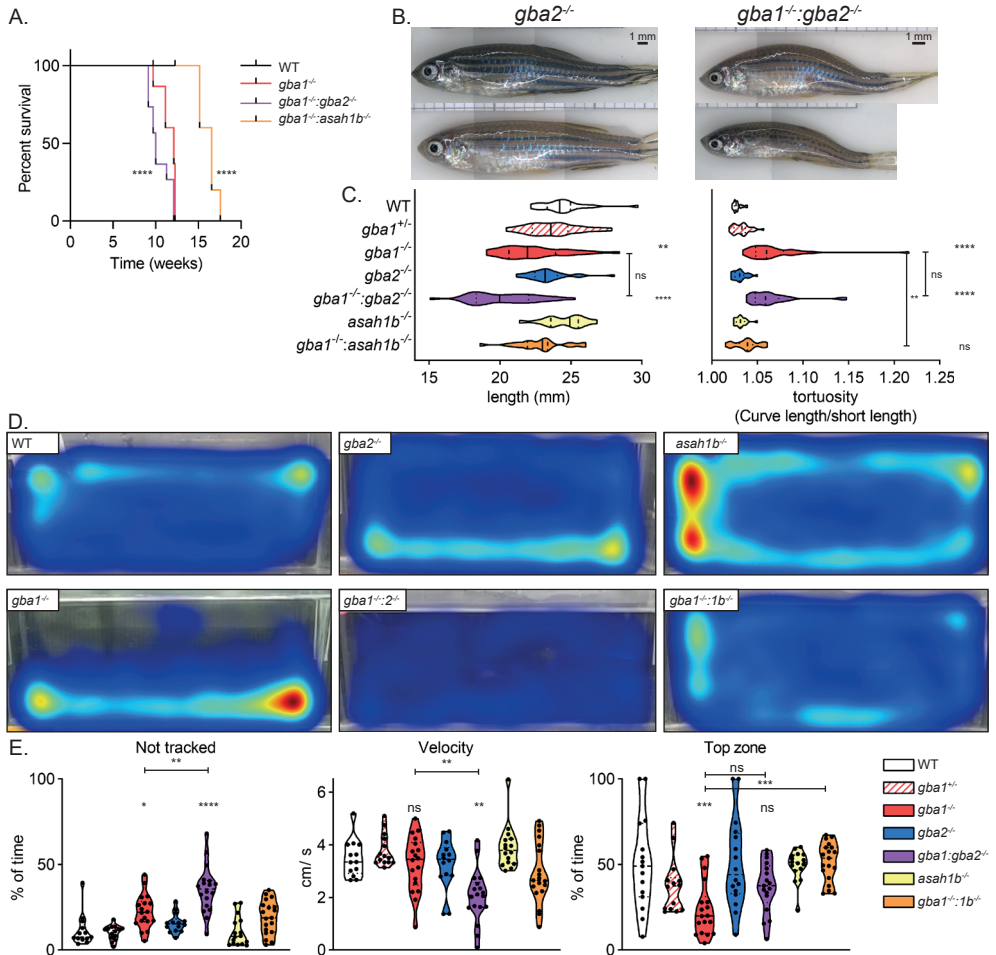


**Figure 8 | Morphology phenotype and change in behaviour of *gba1*<sup>-/-</sup> and *gba1*<sup>-/-</sup>:*gba2*<sup>-/-</sup> zebrafish**

(A) Kaplan-Meier plot for the onset of predetermined symptoms; *gba1*<sup>-/-</sup> (n = 29), *gba1*<sup>-/-</sup>:*gba2*<sup>-/-</sup> (n = 30) and *gba1*<sup>-/-</sup>:*asah1b*<sup>-/-</sup> (n = 5). Curves of *gba1*<sup>-/-</sup>:*gba2*<sup>-/-</sup> and *gba1*<sup>-/-</sup>:*asah1b*<sup>-/-</sup> were compared to the curve of *gba1*<sup>-/-</sup> and analysed using a Log-rank (Mantel-Cox) test. (B) Representative photographs of *gba2*<sup>-/-</sup> and *gba1*<sup>-/-</sup>:*gba2*<sup>-/-</sup> zebrafish. (C) The length of individual zebrafish, head to tail base, is determined as well as the tortuosity, calculated as ratio of the length along the back divided by the length of the fish. Data of individual zebrafish is depicted in a violin plot; WT (n = 21), *gba1*<sup>+/-</sup> (n = 28), *gba1*<sup>-/-</sup> (n = 29), *gba2*<sup>-/-</sup> (n = 23), *gba1*<sup>-/-</sup>:*gba2*<sup>-/-</sup> (n = 30), *asah1b*<sup>-/-</sup> (n = 16), *gba1*<sup>-/-</sup>:*asah1b*<sup>-/-</sup> (n = 19) and analysed using a non-parametric Kruskal-Wallis test with Dunn's multiple comparison's test. (D) Representative movement traces recorded at 12 wpf, except for the 10 wpf *gba1*<sup>-/-</sup>:*gba2*<sup>-/-</sup>. Red indicates more time and blue less time spend at that location. (E) Quantification of the movement traces of individual zebrafish, including the time (%) unable to track individual zebrafish, the average velocity (in cm/s) and time spend in the top half of the tank (%). Data of individual zebrafish is depicted in a violin plot; WT (n = 13), *gba1*<sup>-/-</sup> (n = 14), *gba1*<sup>-/-</sup> (n = 16), *gba2*<sup>-/-</sup> (n = 14), *gba1*<sup>-/-</sup>:*gba2*<sup>-/-</sup> (n = 18), *asah1b*<sup>-/-</sup> (n = 16), *gba1*<sup>-/-</sup>:*asah1b*<sup>-/-</sup> (n = 19) and analysed using One-Way Anova with Tukey's multiple comparison's test. In general, statistical comparisons are depicted of WT vs respective mutant, *gba1*<sup>-/-</sup> vs *gba1*<sup>-/-</sup>:*gba2*<sup>-/-</sup> or *gba1*<sup>-/-</sup> vs *gba1*<sup>-/-</sup>:*asah1b*<sup>-/-</sup> only when a significant difference is apparent and relevant. Ns = not significant, \* P < 0.05, \*\* P < 0.01, \*\*\* P < 0.001 and \*\*\*\* P < 0.0001.

### GCase deficient juveniles accumulate GSLs, but show no obvious phenotype

Overall, a more severe and unpredictable phenotype was observed for the *gba1<sup>-/-</sup>:gba2<sup>-/-</sup>* zebrafish compared to the *gba1<sup>-/-</sup>* zebrafish, even though at the end stage no significant biochemical differences were observed in lipid abnormalities or physiological processes such as autophagy and neuroinflammation. Therefore, fish were also examined at earlier developmental stages, when the phenotype was not apparent yet. Up to 8 wpf no significant difference in size (**Figure 9A**, 4 and 8 wpf) or curvature of the back (tortuosity in **Figure 9B**, 4 and 8 wpf) was apparent and no abnormal swimming behaviours were observed in any of the groups. Only at the end of the experiment (12 wpf maximal), *gba1<sup>-/-</sup>* and *gba1<sup>-/-</sup>:gba2<sup>-/-</sup>* zebrafish were significantly smaller and more curved than WT (**Figure 9**, end stage).

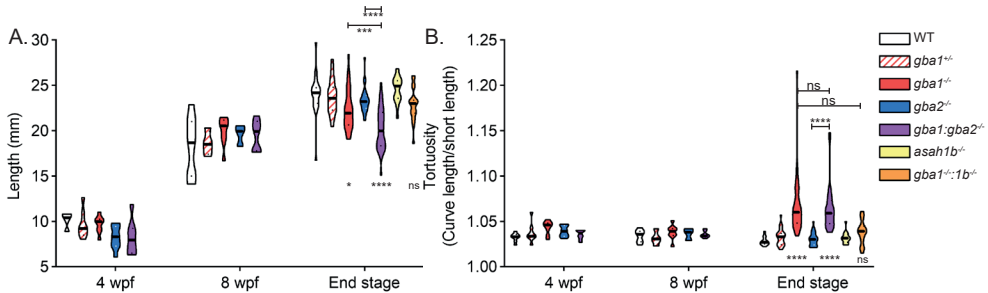


**Figure 9 | Morphology of juvenile zebrafish at different ages**

**(A) Length (B) Tortuosity** WT (white bars: 4 wpf, n = 9; 8 wpf, n = 8; end stage, n = 23), *Gba1<sup>-/-</sup>* (red, striped bars: 4 wpf, n = 9; 8 wpf, n = 4; end stage, n = 28), *gba1<sup>-/-</sup>* (red bars: 4 wpf, n = 8; 8 wpf, n = 8; end stage, n = 29), *gba2<sup>-/-</sup>* (blue bars: 4 wpf, n = 9; 8 wpf, n = 3; end stage, n = 26), *gba1<sup>-/-</sup>:gba2<sup>-/-</sup>* (purple bars: 4 wpf, n = 8; 8 wpf, n = 7; end stage, n = 30). Data is depicted as violin plot, with the mean as black line and quartiles as dashed lines and analysed using a two-way ANOVA with Tukey's multiple comparison test. Ns = not significant, \* < 0.05, \*\*\* P < 0.001 and \*\*\*\* P < 0.0001.

### Abnormalities in head and body region in developing fish.

Head and body regions of zebrafish of different age were separated to analyse glycosphingolipid, protein and RNA changes. At 2 and 4 wpf the juvenile fish were too small to dissect distinct organs, while, at 8 and 12 wpf, homogenates of distinct organs could be prepared. Lipid analysis revealed that GlcSph had accumulated in head and body samples of *gba1<sup>-/-</sup>* and *gba1<sup>-/-</sup>:gba2<sup>-/-</sup>* fish of all developmental ages, as observed for 5 dpf larvae and adult organs (**Figure 10A**). As in the 5 dpf zebrafish larvae, GlcSph levels in the *gba1:gba2* KO fish appeared somewhat higher than in *gba1* KO counterparts but no significant and progressive trend was observed. Total GlcCer was slightly, but not significantly, increased in *gba1<sup>-/-</sup>* zebrafish of 2 wpf and significantly increased in 2 wpf *gba2<sup>-/-</sup>* and the *gba1:gba2* double mutant zebrafish (**Figure 10B**). The lack of significant GlcCer accumulation was also described for the 5 dpf *gba1<sup>-/-</sup>* larvae, which was attributed to the deposition of maternal RNA and protein in the yolk (Chapter 6). However, at the age of 2 wpf it is not likely that maternally derived GCase is still highly present.

GlcCer levels of *gba1<sup>-/-</sup>* and *gba1<sup>-/-</sup>:gba2<sup>-/-</sup>* zebrafish showed a progressive increase at 4 wpf and 8 wpf, while GlcCer levels of *gba2<sup>-/-</sup>* zebrafish did not increase further. GlcCer accumulation was more profound in the head region of 4 wpf and 8 wpf *gba1<sup>-/-</sup>* and *gba1<sup>-/-</sup>:gba2<sup>-/-</sup>* zebrafish compared to the body region.

GlcChol levels of *gba1*<sup>-/-</sup> zebrafish became significantly increased in the brain at 8 wpf and 12 wpf (**Figure 9C**), indicating that GCase is important for the lysosomal hydrolysis of GlcChol. A reduction in GlcChol levels was reported in the 5 dpf larvae with a *Gba2* deficient background, consistent with the ability of *Gba2* to synthesize GlcChol as transglucosidase<sup>27</sup>. Surprisingly, none of the older *gba2*<sup>-/-</sup> or *gba1*<sup>-/-</sup>:*gba2*<sup>-/-</sup> zebrafish showed a prominent difference in GlcChol levels compared to WT (**Figure 10C**). A possible explanation for this discrepancy might involve the presence of glucosylated sterols in the provided plant-based food starting from the 5 dpf timepoint reported before. The detected GlcChol in the zebrafish might, therefore, stem largely from the exogenous source.

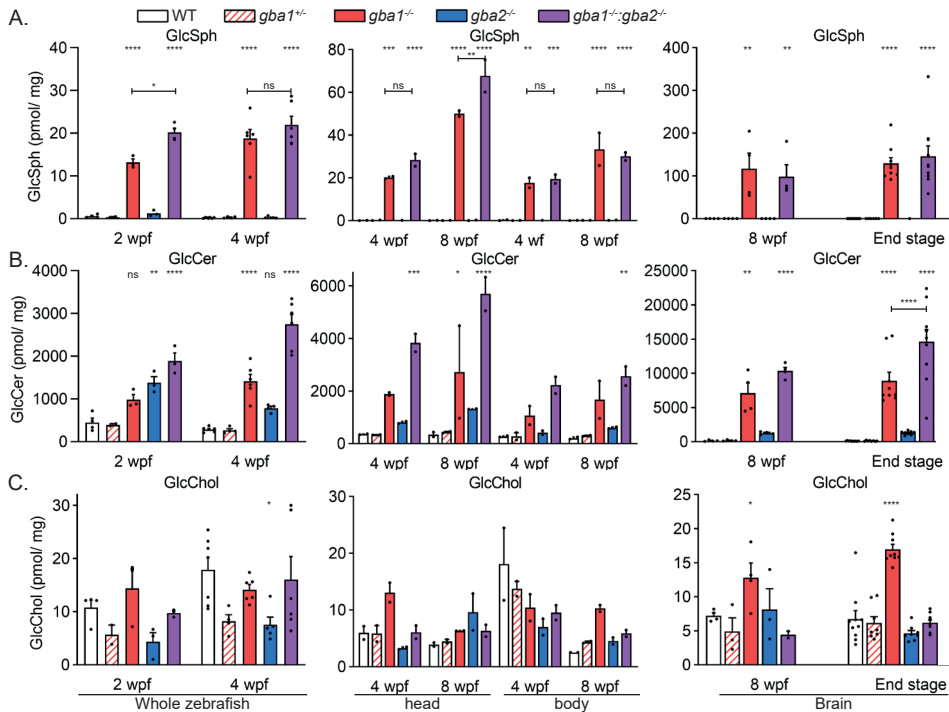


**Figure 10 | Relevant glycosphingolipids of juvenile zebrafish at different ages**

GlcSph (A), GlcCer (B) and GlcChol (C) were measured of whole zebrafish at 2 and 4 wpf (left), head and body regions at 4 and 8 wpf (middle) and brains of 8 wpf and end stage fish (right). Whole fish: 2 wpf (n = 2-4); 4 wpf (n = 4-7), Head/body: 4 wpf (n = 2); 8 wpf (n = 2) and brains: 8 wpf (n = 3-4); end stage (n = 8-12). Data is depicted as mean ± SEM and analysed using a two-way ANOVA with Tukey's multiple comparison test.

### Development of neuropathology.

Glycosphingolipid abnormalities are already detectable in GCase-deficient zebrafish at a few dpf and increase progressively, while phenotypic manifestations become detectable only at much older age. The progression of neuroinflammation was therefore analysed in developing zebrafish by measurement of protein and RNA abnormalities in head (4 and 8 wpf) and brain (8wpf) region. The p62 marker of autophagy was found to be low in WT, *gba1*<sup>-/-</sup> and *gba2*<sup>-/-</sup> samples at 4 and 8 wpf, but increased in samples of all fish with a GCase deficiency (**Figure 11A** and **B**). The storage-cell biomarker *chia.6* was already significantly increased at 8 wpf in brains of GCase-deficient fish, with *gpnmb* levels showing a similar

trend (**Figure 11C**). Transcript levels of the lysosomal protease *catD* and microglia marker *apoeb* were also significantly increased in 8 wpf brain, as well as the inflammation markers *il1b* and *tnfb* (data not shown). Expression of complement components *c1qa* and *c3.1* was slightly, but not significantly increased at 8 wpf. At the same age, a reduction of mRNA levels of *th1*, *sncb* and *snycb* was apparent, however only the reduction of *sncb* and *snycb* levels in *gba1<sup>-/-</sup>:gba2<sup>-/-</sup>* brains reached significance. Overall, the protein and mRNA analyses indicate that neuroinflammation and autophagy already becomes abnormal at 8 wpf, clearly before the onset of morphological and behaviour disease manifestation, while genes related to neurodegeneration were not significantly reduced yet at this age.

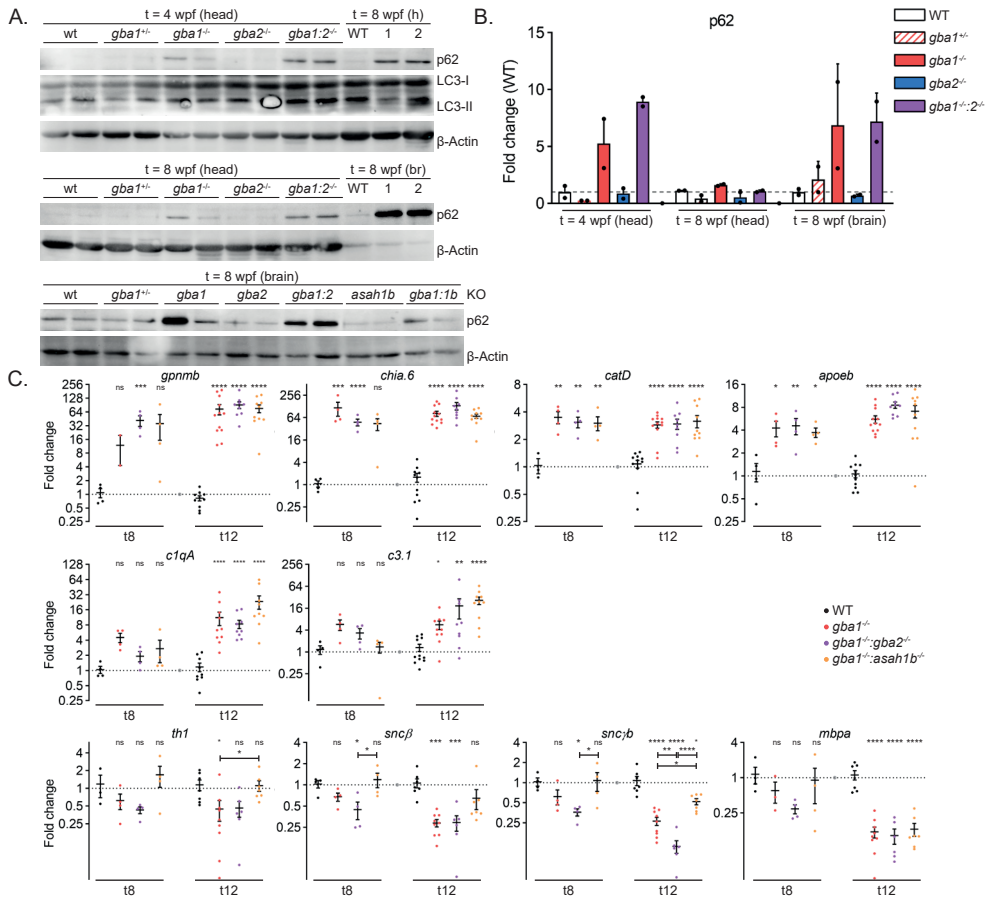


**Figure 11 | Protein and RNA abnormalities in WT and knockout zebrafish**

**(A)** Representative western blots of p62, LC-3 and β-actin as loading control of head regions (h) at 4 wpf and 8 wpf or dissected brains (br) at 8 wpf. **(B)** Quantification of protein abnormalities with the ratio of p62/WT (n = 2-4). **(C)** mRNA levels of *asah1a*, *asah1b*, *gpnmb*, *chia.6*, *il-1b*, *tnfb*, *apoEb*, *catD*, *c1qa*, *c3.1*, *c5aR*, *c5*, *th1*, *th2*, *sncb*, *snycb* and *mbpa* in brains of 8 wpf or 11 wpf zebrafish were determined using RT-qPCR analysis of n = 2 for *gpnmb*, *gba1<sup>-/-</sup>* and n = 4-11 fish for others. Data is normalized using two housekeeping genes (*ef1a* and *rpl13a*), analysed by One-Way Anova with Tukey's multiple comparison test or Brown-Forsythe and Welch Anova with Dunnett's multiple comparisons test for *gpnmb* and *chia.6* and depicted as scattered dot plot ± SEM. In general, statistical comparisons are depicted of WT vs respective mutant, *gba1<sup>-/-</sup>* vs *gba1<sup>-/-</sup>:gba2<sup>-/-</sup>*, *gba1<sup>-/-</sup>* vs *gba1<sup>-/-</sup>:asah1b<sup>-/-</sup>* or *gba1<sup>-/-</sup>:gba2<sup>-/-</sup>* vs *gba1<sup>-/-</sup>:asah1b<sup>-/-</sup>*, only when a significant difference is apparent and relevant. Ns = not significant, \* P < 0.05, \*\* P < 0.01, \*\*\* P < 0.001 and \*\*\*\* P < 0.0001.



## Discussion

The ubiquitous glycosphingolipid GlcCer is degraded by cells in their lysosomes by the acid  $\beta$ -glucosidase GCase or in the cytosolic membrane leaflet by the membrane-associated GBA2. Deficiency of GCase in humans leads to the lysosomal storage disorder GD. Little is presently known about the impact of GBA2 during impaired lysosomal degradation of GlcCer. GCase deficiency in humans is not only accompanied by accumulation of GlcCer, but also the formation of excessive GlcSph by lysosomal acid ceramidase (ACase). In addition, accumulation of glucosylated cholesterol (GlcChol) during GCase deficiency is reported<sup>25</sup>. GlcChol is typically synthesized by GBA2 via a transglucosylation reaction using GlcCer as sugar donor and normally degraded by GCase to cholesterol and glucose<sup>25</sup>. The potential contribution of the excessive GlcCer, GlcSph and GlcChol during GCase deficiency to specific symptoms is poorly understood at present. To generate new insights, mutant zebrafish were generated by CRISPR/Cas9 with a knockout (KO) of the *gba1*, *gba2* and *asah1b* genes encoding respectively GCase, GBA2 and the ACase responsible for formation of GlcSph. The present study primarily focussed on a comparison of *gba1*<sup>-/-</sup>, *gba1*<sup>-/-</sup>:*gba2*<sup>-/-</sup> and *gba1*<sup>-/-</sup>:*asah1b*<sup>-/-</sup> fish up to the adult age of 12 weeks. In addition, adult carrier *gba1*<sup>+/-</sup>, *gba2*<sup>+/-</sup> and *asah1b*<sup>+/-</sup> zebrafish were studied. An overview of findings of the different zebrafish is given in **Supplementary Table 1**.

First of all, attention was paid to lipid abnormalities in the various mutant zebrafish. GlcCer accumulated in *gba1*<sup>-/-</sup> fish relatively late. The fish showed at young age (up to 2 wpf) little accumulation of GlcCer. The lipid levels of GlcCer became significantly increased at 4 wpf. The *gba1*<sup>+/-</sup> carrier fish showed no GlcCer abnormalities whatsoever up to 12 wpf. The *gba2* KO fish developed an increase of GlcCer in the brain, specifically the species with a 18:0 fatty acyl, but total GlcCer increase was statistically not significant. An increase of HexCer 18:0 was also reported for cerebellum of GBA2-deficient mice, where again the increase of total HexCer did not reach significance<sup>21</sup>. Interestingly, total GlcCer levels were only significantly increased in young *Gba2* deficient zebrafish (0-2 wpf) and decreased thereafter, in contrast to the GCase-deficient fish. This finding might indicate that the GlcCer catabolism by *Gba2* is relatively higher in young zebrafish. The mutant *gba1:gba2* fish was striking with respect to the increase in GlcCer. In brain there was a prominent increase of GlcCer with 18:0 and 20:0 fatty acyls was observed, exceeding that observed in *gba1*<sup>-/-</sup> brains. Increased levels of these specific GlcCer species were also observed in brains of *gba2* KO fish, therefore it is likely that these species of GlcCer accumulate in the cytosol due to the concurrent *Gba2* deficiency. In the liver, GlcCer 16:0 was markedly increased, again exceeding the abnormality in the same lipid in *gba1*<sup>-/-</sup> fish. The total GlcCer increase in *gba1:gba2* double KO fish already was significant at the age of 1 wpf<sup>27</sup> and GlcCer levels tended to be at all ages the highest among all genotypes. Finally, *gba1*<sup>-/-</sup>:*asah1b*<sup>-/-</sup> fish were quite comparable to *gba1*<sup>-/-</sup> fish in their GlcCer abnormalities in brain and liver.

GlcSph started to accumulate in *gba1*<sup>-/-</sup> fish and *gba1*<sup>-/-</sup>:*gba2*<sup>-/-</sup> fish at very young age (before 5 dpf as described in chapter 5<sup>27</sup>) and these levels increased over time. GlcSph levels tended to be higher in *gba1*<sup>-/-</sup>:*gba2*<sup>-/-</sup> fish than *gba1*<sup>-/-</sup> fish at various ages, however these differences never reached significance. Slightly elevated GlcSph levels were earlier also detected in spleens of mice with GCase deficiency in hematopoietic cells with or without a GBA2 deficiency<sup>23</sup>. The *gba1*<sup>+/-</sup> (carrier) fish and *gba2*<sup>-/-</sup> fish showed no accumulation of GlcSph, while brains and livers of *gba1*<sup>-/-</sup>:*asah1b*<sup>-/-</sup> fish showed no GlcSph at 12 wpf because of their Asah1b deficiency as described in chapter 6.

GlcChol levels increased from 4 wpf in *gba1*<sup>-/-</sup> fish and were significantly increased in the brains of 8 and 12 wpf fish. An unexpected finding was the similar GlcChol level in *Gba2* deficient fish compared to WT. In mice and larvae different observations in this respect have been made. Adult GBA2 deficient mouse livers and *Gba2* deficient larvae (up to 5 dpf) were found to show a reduced GlcChol<sup>25,27</sup>, consistent with the role of *Gba2* in synthesis of GlcChol. Reduced GlcChol levels were detected in developing *Gba2* deficient zebrafish until the age of 4 wpf, but levels became quite comparable to WT at 8 and 12 wpf. A possible explanation for these findings might be offered by the zebrafish diet and its lipid composition. Glucosylated sterols are present in various plants<sup>31</sup>, although campesterol, sitosterol and stigmasterol are the main types of sterols found in plants<sup>32</sup>. Next to the manufactured, plant-based food, zebrafish also receive food of animal origin starting at the age of 5 dpf life. This to provide optimal and consistent rates of survival and growth during larval rearing and promote natural active feeding behaviour<sup>33,34</sup>. The larvae are fed with *Brachionus plicatilis* (rotifers), an aquatic invertebrate species, from 5 dpf to 2 weeks of age, while juveniles and adults receive *Artemia*, a genus of small aquatic crustaceans. At present, no lipid measurements of these food sources have been performed, however it is conceivable that the animal food could contain glucosylated sterols which are taken up by the developing zebrafish.

The absence of a clear phenotype of the adult *Gba2*-deficient fish is remarkable in view of the findings made with rodents regarding male infertility associated with *Gba2* deficiency<sup>20-22</sup> and the observed association of GBA2 defects with neurological complications in some individuals<sup>21</sup>. The *Gba2*-deficient fish did not show abnormal fertility: a regular sized tank of *gba2* KO adults produced average clutches with normally developing larvae, comparable to WT fish. Of note, in the present study lipid levels in the testis and sperm morphology were not analysed. The *gba2* KO fish were maintained for many months without symptoms. The fish only showed aging features after 2 years, comparable to the WT strains. In sharp contrast, HSP and ARCA patients with mutations in *GBA2* develop a progressive neurological phenotype, including muscle weakness and spasticity, with an early onset in infancy or childhood<sup>8,10</sup>. GBA2-knockout mice develop mild defects in the gait pattern, but strong locomotor defects were only observed in a few individuals<sup>21</sup>. Overall, *Gba2*-deficient zebrafish appear to have similar biochemical results to the reported GBA2 knockout mice, including an increase in specifically GlcCer d18:1/18:0, while the lifespan and lack of a clear phenotype contrasts with patients carrying mutations in *GBA2* and with GBA2-deficient mice showing male infertility.

The impact of the enzyme Gba2 during deficiency of GCase in zebrafish warrants discussion. Two studies with mice with a reduced GCase activity (conditional GCase deficiency in hematopoietic cells and secondary GCase deficiency in NPC1 mutants) reported amelioration of some symptoms in animals by concomitant GBA2 deficiency<sup>23,24</sup>. Comparison of the findings made with *gba1*<sup>-/-</sup> and *gba1*<sup>-/-</sup>;*gba2*<sup>-/-</sup> zebrafish is therefore of interest. The *gba1* KO zebrafish showed a clear onset and progression of symptoms, starting with a drop in the tail, followed by postural imbalance and a change in swimming behaviour. In contrast, *gba1:gba2* double KO fish showed an unpredictable course of disease manifestation and no clear characteristic drop of the tail was observed as onset. Severe postural imbalance and abnormal swimming behaviour could be observed in only a matter of days, with some individual fish starting to swim upside down overnight. *Gba1:gba2* KO fish were culled earlier than single *gba1* KO fish and the decreased lifespan and quality of life of most *gba1:gba2* KO fish was unexpected. It should be taken in mind the studied fish are complete knockouts in both enzymes, contrary to the mouse models mentioned above. In the type 1 GD mice, GCase was functional in the neuronal lineage. In the NPC1 model, GCase deficiency is only partial and the animals have a far less severe disease progression than neuronopathic GD mice lacking GCase in neuronal cells (life spans of 85 vs 21 days for NPC1 knockout<sup>24</sup> and nestin:Cre:GD mice respectively<sup>19</sup>). Consistently, GlcCer and GlcSph levels in brain of 85 day old NPC1 mice are lower than in 21 day old neuronopathic GD mice (GlcCer: 311 pmol/mg wet weight vs 338 pmol/mg tissue and GlcSph: 1.4 pmol/mg wet weight vs 28 pmol/mg tissue<sup>17,24</sup>).

The mechanisms underlying the onset, progression and severity of symptoms in GCase-deficient zebrafish are puzzling. The present study indicates that the presence of storage cells, neuroinflammation, and impairment of autophagy is comparable in the brains of *gba1*<sup>-</sup>, *gba1:gba2*<sup>-</sup> and *gba1:asah1b* KO fish while the latter animals have a much milder phenotype. Storage cells, neuroinflammation and impaired autophagy were already apparent in brains of all GCase-deficient zebrafish at 8 wpf, clearly prior to the onset of phenotypic symptoms. Dopaminergic neuronal cell loss likely underlies some of the observed neurological complications in the mutant zebrafish. The expression of mRNAs coding for tyrosine hydroxylase (*th1*), a protein required for formation of dopamine, and two synuclein genes (*sncβ* and *sncγb*) was found to be significantly reduced in brains of *gba1* KO and *gba1:gba2* KO fish at 10-12 wpf, but not in those of *gba1:asah1b* KO fish. These important findings need confirmation at protein level by immunohistochemistry. In addition, it will be important to study more closely (activated) microglia in the mutant zebrafish. A prominent role for microglia activation and astrogliosis in neuronal loss occurring in neuropathic Gaucher mice has been proposed by Futerman and co-workers<sup>35,36</sup>. This process would be driven by GlcCer accumulation according to these investigators<sup>35,37</sup>. It has recently been reported that *Gpnmb* is a marker for activated microglia in neuronopathic GD mice and is also elevated in cerebral spine fluid from type 3 GD patients<sup>38</sup>. *Gpnmb* mRNA levels are also increased in mutant zebrafish but this does not correlate with the course of neurodegeneration or phenotypic manifestations.

To conclude, at present it remains unclear whether exposure to excessive GlcSph in zebrafish drives dopaminergic neuronal loss after some time or whether microglia activation, driven by GlcCer accumulation, is a driving force for neurodegeneration. It is *a priori* conceivable that both processes occur hand in hand and that the sequence and importance of pathology events differs among species. In fact, it is known that the consequences of pharmacologically induced GCase deficiency in different mice strains with conduritol B-epoxide (CBE) may differ dramatically<sup>39</sup>. It was observed that the age of survival following CBE administration varied from 40 to 200 days. It can be argued that toxic activated microglia will likely promote loss of dopaminergic neurons and subsequent symptomatology and excessive GlcSph may speed up such events.

Likewise, spatio-temporal assessment of GlcSph and specific GlcCer species in brain regions may be of value. Various mass spectrometry-based imaging techniques for this purpose are presently developed and applied. A recent study reported a correlation of GlcCer d18:1/18:0 accumulation with microglia activation in brain of neuronopathic GD mice<sup>40</sup>. Of particular interest will be correlation of lipids with complement-activating immune complexes deposited on neuronal cells, oxidative stress and mitochondrial dysfunction<sup>37,41-43</sup>.

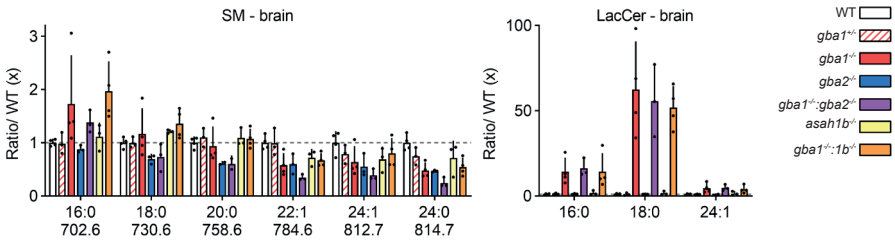
In conclusion, the comparative investigation of *gba1*-, *gba1:gba2*- and *gba1:asah1b* KO fish provided new insights as well as questions regarding pathology induced during GCase deficiency. It is apparent that excessive GlcSph is associated with more severe disease manifestation but the role of microglia activation and neuroinflammation warrants further investigation. The role of excessive GlcChol could not be elucidated since adult *gba1:gba2* KO fish did unexpectedly not show reduced levels of GlcChol in their brains.

## Acknowledgements

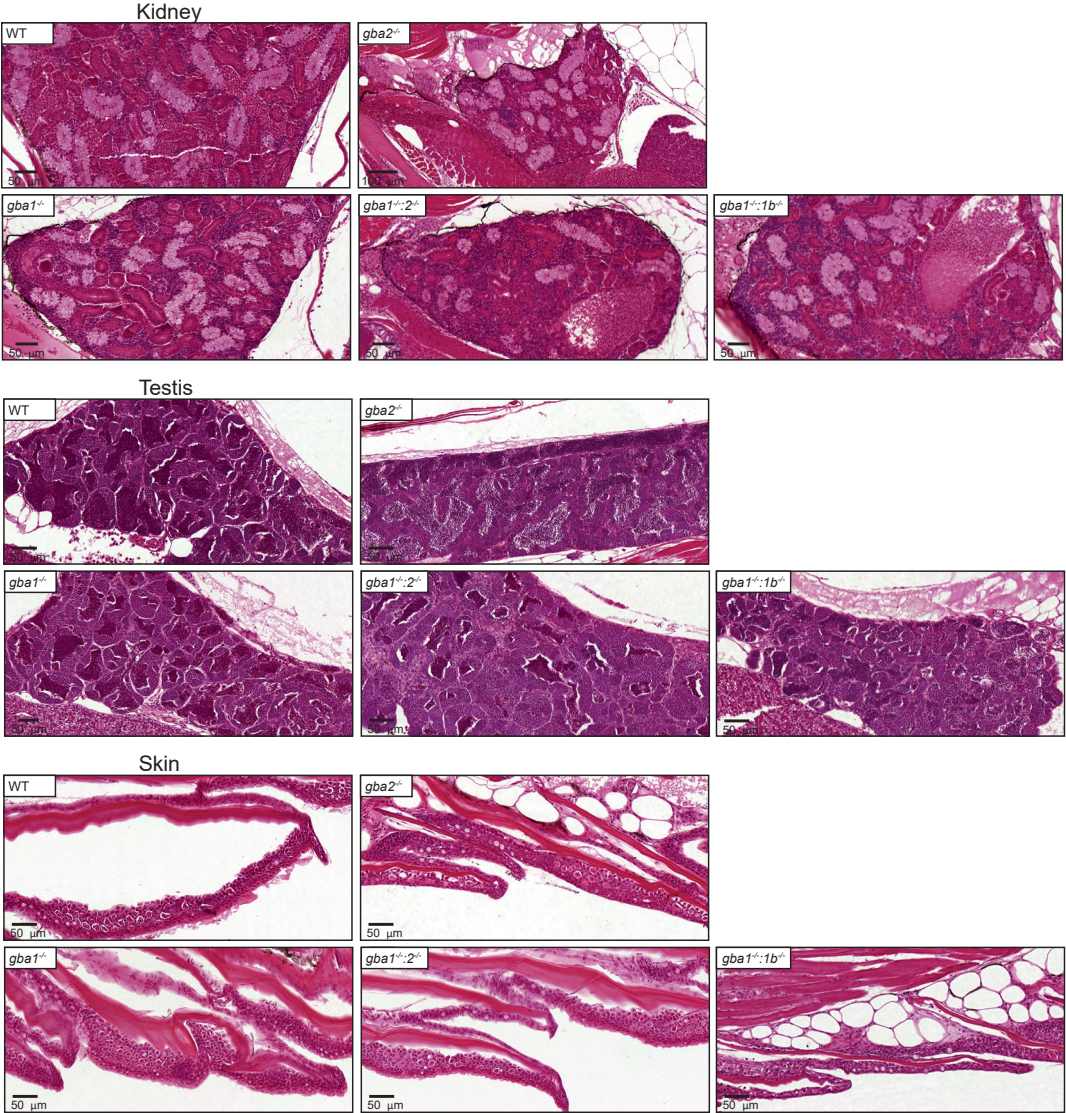
Joost Willemse is kindly acknowledged for the ImageJ plugin to quantify the length and tortuosity of individual zebrafish. Sophie Gerhardt and Saskia Maas are acknowledged for the histology procedures and Daniela Salvatori for the pathological examination. Ernst Bijk, Claire de Wit and Christian Tudorache are kindly acknowledged for their work on tracking and quantifying zebrafish movements. The study was supported by the NWO BBOL 2018 (737.016.022) grant.



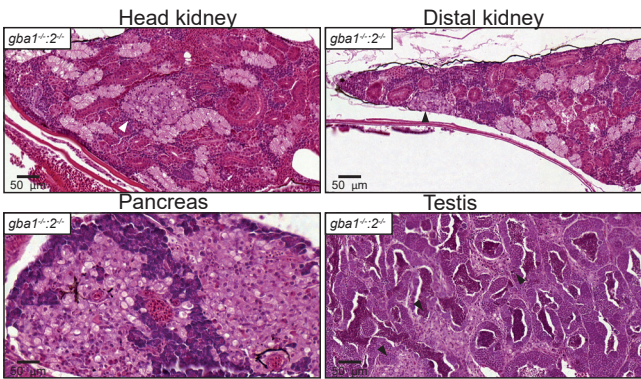
Supplementary Information



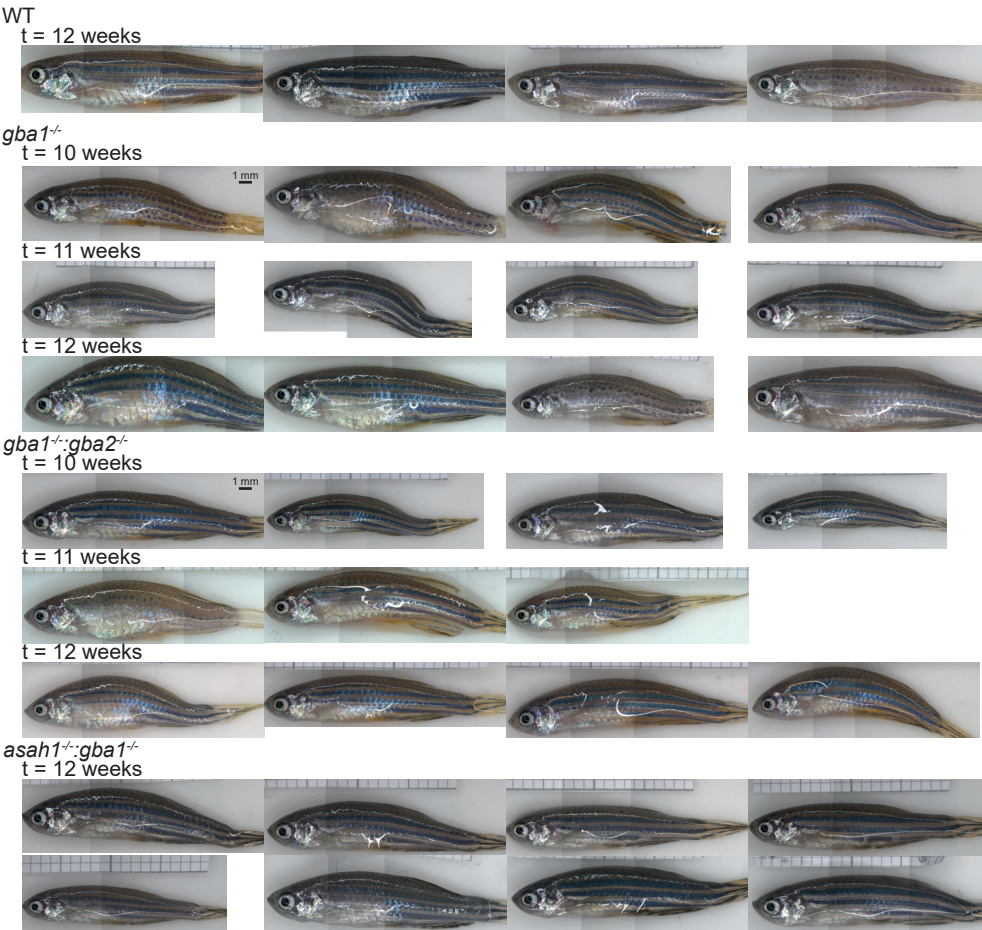
**Supplementary Figure 1** | Levels of SM and LacCer with different fatty acids in brains of WT (n = 4), *gba1<sup>-/-</sup>* (n = 3), *gba1<sup>-/-</sup>; gba2<sup>-/-</sup>* (n = 3), *gba1<sup>-/-</sup>; asa1b<sup>-/-</sup>* (n = 3) and *gba1<sup>-/-</sup>; 1b<sup>-/-</sup>* (n = 4). Lipid species were measured, calculated and analysed as described in the experimental procedures. \* P < 0.05



**Supplementary Figure 2** | H&E staining of kidney, testis and skin of WT and mutant zebrafish.



**Supplementary Figure 3** | H&E staining of one individual, severe *gba1<sup>-/-</sup>;gba2<sup>-/-</sup>* zebrafish head kidney, distal kidney and testis. Patches with Gaucher-like cells are marked with arrows.



**Supplementary Figure 4** | Different *gba1<sup>-/-</sup>* and *gba1<sup>-/-</sup>;gba2<sup>-/-</sup>* zebrafish at 10, 11 and 12 wpf as well as WT and *gba1<sup>-/-</sup>;asah1b<sup>-/-</sup>* individuals at 12 wpf.



**Supplementary Table 1** | Overview of findings in brains of WT, *gba1*<sup>+/-</sup> carriers, *gba1*, *gba2*, *gba1:gba2*, *asah1b* and *gba1:asah1b* KO fish.

Enzyme	Lipids			mRNA expression				Pathology
	GlcSph	GlcCer	GlcChol	Storage cells	Inflammation	Complement activation	th & synucleins	Infiltration of Gaucher-like cells
WT	-	-	-	-	-	-	-	-
<i>gba1</i> <sup>+/-</sup>	-	-	-	-	-	-	-	-
<i>gba1</i> KO	↑↑	↑↑ Only 18:0	↑	↑↑	↑	↑	↓	↑
<i>gba2</i> KO	-	-	-	-	-	-	-	-
<i>gba1:gba2</i> KO	↑↑	↑↑↑	-	↑↑	↑	↑	↓	↑
<i>asah1b</i> KO	-	-	-	-	-	-	-	-
<i>asah1b:gba1</i> KO	-	↑↑	-	↑↑	↑	↑	-	↑

## Experimental procedures

**Chemicals and reagents** - GCase specific inhibitor (ME656)<sup>44</sup>, <sup>13</sup>C<sub>5</sub>-sphinganine, <sup>13</sup>C<sub>5</sub>-sphingosine, <sup>13</sup>C<sub>5</sub>-GlcSph, <sup>13</sup>C<sub>5</sub>-lyso-globotriaosylceramide (LysoGb3), C17-lysosphingo-myelin (LysoSM), <sup>13</sup>C<sub>6</sub>-GlcChol and C17-dihydroceramide (dhCer)<sup>25,30</sup> were synthesized as reported. All chemicals and reagents were obtained from Sigma-Aldrich Chemie GmbH (St Louis, USA) unless mentioned otherwise. The standards Cer (d18:1/16:0), dhCer (d18:0/16:0), GlcCer (d18:1/16:0), GalCer (d18:1/16:0), LacCer (d18:1/16:0) were obtained from Avanti Polar lipids (Alabaster, USA) and GlcChol from Sigma-Aldrich. LC-MS grade methanol, 2-propanol, water, formic acid, acetonitrile and HPLC grade chloroform were purchased from Biosolve (Valkenswaard, the Netherlands). LC-MS grade ammonium formate, ammonium acetate and sodium hydroxide from Sigma-Aldrich, butanol and hydrochloric acid from Merck Millipore (Billerica, USA).

**Zebrafish** - All zebrafish were housed and maintained at the University of Leiden, the Netherlands, according to standard protocols. Wildtype (WT) zebrafish (ABTL) were a mixed lineage of WT AB and WT TL genetic backgrounds. Zebrafish were kept at constant temperature of 28.5 °C and on a cycle of 14-hour light and 10 hour dark. CRISPR/Cas9 mediated knockout zebrafish of *gba1*, *gba2* and *asah1b* were generated and maintained as described in chapters 4, 5 and 6. Heterozygous (*gba1* background) or homozygous (*gba2* or *asah1b* background) adults were in-crossed and raised to adulthood (*gba2*<sup>-/-</sup>) or genotyped at 4-5 dpf before raising to adulthood (*gba1*<sup>+/-</sup>, *gba1*<sup>-/-</sup>, *gba1*<sup>-/-</sup>:*gba2*<sup>-/-</sup>, *asah1b*<sup>-/-</sup> and *gba1*<sup>-/-</sup>:*asah1b*<sup>-/-</sup>). Experiments with larvae, juvenile and adult zebrafish after the free-feeding stage were approved by the local animal welfare committee (Instantie voor Dierwelzijn) of the University Leiden (Project license AVD1060020184725). Zebrafish from 5 dpf to 2 wpf were fed with both dry food (2x daily; Skretting Gemma micro 75, Zebcare, Nederweert, the Netherlands) and Rotifers (1x daily) and from 3 wpf to the end of the experiment fed with both dry food (2x daily; Skretting Gemma micro 150 until 30 dpf or Gemma Micro 300 mixed with Gemma Diamond for fish from 30 dpf) and hatched Artemia (1x daily).

**Zebrafish sampling** – Zebrafish were sacrificed at 12 wpf or earlier when zebrafish showed symptoms noted as human endpoints. From 8 wpf, zebrafish were monitored extensively for phenotypic and morphological symptoms such as curvature of the back and abnormal swimming behaviour. Human endpoints were defined as follows: 1) fish having a moderate to extreme curvature of the spine independent of the feeding consumption, 2) fish with a slight curvature but clear abnormal swimming behaviour or 3) fish with a slight curvature which are unable to reach and consume the provided food. *Gba1*<sup>-/-</sup> zebrafish were sacrificed between 10 and 12 wpf, while no symptoms were observed for WT, *asah1b*<sup>-/-</sup> and *gba1*<sup>-/-</sup>:*asah1b*<sup>-/-</sup>. The same human endpoints were used for the longevity study of the *gba1*<sup>-/-</sup>:*asah1b*<sup>-/-</sup>. Individual zebrafish were transferred to single tanks (1 L external breeding tank with lid, Techniplast, West Chester, USA) acclimatized for 10 minutes and recorded as described below. Afterwards, fish were sacrificed using an overdose of tricaine methane sulfonate (MS222, 200 mg/L) and photographed using a Leica M165C microscope (Wetzlar, Germany). Whole zebrafish were fixed for histopathology or organs were dissected. Dissected organs were either snap frozen in liquid nitrogen for protein and (glyco)sphingolipid analysis or submerged in RNAlater (Invitrogen, Thermo Fisher Scientific, Waltham USA) for RT-PCR analysis (brain or liver) and stored at -80 °C.

**Movement analysis** – The individual tanks were randomly placed in a 3x4 or 4x4 setup and the camera was placed at a distance dependent on the setup to include all tanks. Zebrafish were left for at least 10 min to acclimatize and recorded for 20 min using a Sony A6000 camera (Tokyo, Japan) with a 30 mm objective. Movements of the fish in the individual tank were tracked using Ethiovision software 10.1 (Noldus, Wageningen, the Netherlands). Arenas were setup for each individual tank by drawing a rectangular shape in the tank, thereby not including any reflections at the top, bottom and sides. The arenas without reflection accompanied approximately 46 ± 5% of the total area of the individual tank (± 17 cm length x 8 cm width). A horizontal and vertical line were used to calibrate the area

to the measurements of the tank and each arena was divided in two equal zones: a top and bottom zone. The detection settings were set as follows: model-based and differencing settings for Nose-tail detection; the subject colour was brighter than background, sensitivity of 45; subject size with a minimum of 80 and maximum of 2042 pixels and video sample rate of 6.25 per sec. Data was acquired every 0.16 sec for a total of 10 minutes after a 5 min delay. The data was exported and the velocity was calculated by averaging the velocity of all datapoints, while the time spend in the bottom zone was obtained by dividing the amount time spend in the bottom zone by the total time.

Zebrafish morphology – The three or four images of one fish, obtained with the Leica microscope, were stitched to obtain one image using Photoshop CC2018 (Adobe, San Jose, USA) The length of the fish from head to tail base (body length) was determined as well as the length of the back from head to tail base (long length) using ImageJ software. The tortuosity was calculated by dividing the long length by the body length.

Homogenate preparation - Homogenates of organs were prepared in potassium phosphate (KPi lysis buffer; 25 mM  $K_2HPO_4$ - $KH_2PO_4$  pH 6.5, 0.1% (v/v) Triton-X100 and EDTA-free protease inhibitor (cOmplete™, EDTA-free Protease Inhibitor Cocktail, Roche, Sigma-Aldrich). Organs were first homogenized using a Dounce homogenizer (10 strokes) followed by sonication (20% amplitude, 3 sec on, 3 sec off for 4 cycles) using a Vibra-Cell VCX 130 (Sonics, Newtown, USA) while on ice. Total protein concentration of homogenates was determined using Pierce BCA protein assay kit (Thermo Fisher Scientific, Waltham, USA) and measured using an EMax® plus microplate reader (Molecular Devices, Sunnyvale, USA).

Western blot - Proteins of organ homogenates (20 µg protein) were denatured using 5x Laemmli sample buffer (25% (v/v) 1.25M Tris-HCL pH 6.8, 50% (v/v) 100% glycerol, 10% (w/v) sodium dodecyl sulphate (SDS), 8% (w/v) dithiothreitol (DTT) and 0.1% (w/v) bromophenol blue), samples were boiled for 5 min at 98 °C and proteins were separated by electrophoresis on a 12% (w/v) SDS-PAGE gel. Proteins were transferred to nitrocellulose membranes (0.2 µM, Bio-Rad laboratories Inc., Hercules, USA) using the Trans-Blot® Turbo™ Transfer system (Bio-Rad). Membranes were blocked with 5% (w/v) bovine albumin serum (BSA) and incubated overnight at 4 °C with primary antibodies: rabbit anti-LC3 (1:1000, NB100-2220; Novus Biologicals, Centennial, USA), rabbit anti-p62/SQSTM1 (1:1000, P0067; Sigma) or rabbit anti-actin (1:1000, ab209857; Abcam, Cambridge, UK). Membranes were washed 3 times with TBST and incubated for 1 h at RT with secondary antibody: GARPO goat anti rabbit IgG (H+L) peroxidase (1:5000, Bio-Rad). Chemiluminescence signal is developed using the Clarity Max Western ECL substrate (Bio-Rad), detected using a ChemiDocMP imager (Bio-Rad) and signal quantified by ImageJ software.

**Gene expression analysis** - RNAlater was removed and RNA was extracted using a Nucleospin RNA XS column (Machinery-Nagel, Düren, Germany) procedure according to suppliers protocol, without the addition of carrier RNA. Contaminating DNA was degraded on column by a DNase I treatment (supplied in the kit). cDNA was synthesized using SuperScript II reverse transcriptase (Invitrogen, ThermoFisher Scientific, Waltham, USA) using oligo(dT) and an input of approximately 200-500 ng total RNA according to the manufacturer's instruction. Generated cDNA was diluted to an approximate concentration of 0.5 ng total RNA input/ $\mu$ L with Milli-Q water. QPCR reactions were performed with the IQ SYBR green mastermix (Bio-Rad laboratories Inc., Hercules, USA) in a total volume of 15  $\mu$ L (1x SYBR green, 333  $\mu$ M of forward and reverse primer as given in Supplementary Table 2 and 5  $\mu$ L of the diluted cDNA input) and carried out using a CFX96™ Real-Time PCR Detection system (Bio-Rad laboratories Inc., Hercules, USA) with the following conditions: denaturation at 95 °C for 3 min, followed by 40 cycles of amplification (95 °C for 30 sec and 61 °C for 30 sec), imaging the plate after every extension at 61 °C, followed by a melt program from 55-95 °C with 0.5 °C per step with imaging the plate every step. All biological samples were tested in technical duplicate, differential gene expression was calculated using the  $\Delta\Delta C_t$  method normalized to two house-keeping genes *ef1a* and *rpl13* and depicted as  $\log_2$  fold change  $\pm$  SEM, compared to WT.

**Supplementary Table 2 |** Forward and reverse primers for RT-qPCR analysis.

Target	NCBI code	Forward primer sequence (5'->3')	Reverse primer sequence (5'->3')	
<i>Asah1a</i>	NM_001006088	ATTAGGCCCTGGTGAACCTGAC	CTGCGAGTAAGAAAACCCGTC	125 bp
<i>Asah1b</i>	NM_200577	TGGACTGTTTCATGGGATGGG	CCGGTCAACATCCCGACATA	150 bp
<i>Gpnmb</i>	XM_009294247	GCAAGGGCGTAGAATTGAAA	TGGCAGGGACATGTCAGTAA	
<i>Chia.6</i>	NM_199603	TCCACGGCTCATGGGAGAGTGTC	AGCGCCCTGATCTCGCCAGT	ref. 45
<i>catD</i>	NM_131710	TGGGTGGAAGGTCTACTCG	CACTCAGGCAGATGTCGTGT	
<i>il18</i>	NM_212844	TGGACTTCGCAGCACAAAATG	GTTCACTTCACGCTCTTGGATG	ref. 46
<i>tnf8</i>	NM_182873	GCATGTGATGAAGCCAAACG	GATTGTCTTGAAGGGTCACC	ref. 47
<i>apoeb</i>	NM_131098	AAACTGACATGACCGACGCT	TAGGTTGCTACGGTGTTCGCG	172 bp
<i>c1qa</i>	NM_001020527	CTCTGTTTCCCTTTTCTCTCTG	CTTCTCTCTCTTTGGTCCTGG	108 bp
<i>c3a.1</i>	NM_131242	CGCTGCACAAAGTACTTCCAC	GCCAGCTCCATGTCTCTTGAC	197 bp
<i>c5aR1</i>	XM_005159274	CCGACAAGCTCGCATCCTAT	GCGAATGATGGTTATCGCCC	163 bp
<i>c5</i>	XM_001919191	CAAGGCCACGGTTCAATCAG	TCTTCATGCTTTTCGGCAGTCA	152 bp
<i>th1</i>	NM_131149	AGCTTTGTGGACGCTACTGA	GTGGGTTGTCCAGCACTTCT	112 bp
<i>th2</i>	NM_001001829	TACAAGCCATTTCGACCCAGC	ATGCTGCAAGTGTAGGGGTC	173 bp
<i>snc8</i>	NM_200969	GGAGTTTGGTCAGGAAGCCA	CCTCGGGCTCATAATCCTGG	107 bp
<i>sncyA</i>	NM_001017567	TGGAGGGGCTGGAGACTATG	AGCATCATGGGACATTCGGTT	123 bp
<i>sncyb</i>	NM_001020652	ATGGTGAACCCGGGTGACTT	AGGCTTTGGAGCAGAAACGTA	129 bp
<i>mcpa</i>	XM_002665562	TGGTCATCTATCCTCTCTCCA	CTTCTCCAGGCCCAATAGTTCT	150 bp
<i>ef1a</i>		CTGGAGGCCAGCTCAAACAT	ATCAAGAAGAGTAGTACCGCTAGCATTAC	ref. 48
<i>rpl13a</i>		TCTGGAGGACTGTAAGAGGTATGC	AGACGCACAATCTTGAGAGCAG	ref. 48

**(Glyco)sphingolipid (GSL) analysis** - Neutral (glyco)lipids, (glyco)sphingoid bases and glycosylated cholesterol were extracted from the same homogenate (10  $\mu$ L, 20-30  $\mu$ g total protein in KPi lysis buffer) using an acidic Bligh and Dyer procedure (1/1/0.9 chloroform/methanol/100 mM formate buffer pH 3.1) as described before<sup>27,30</sup>. Lipids were resuspended in acetonitrile/methanol (9/1, v/v) for separation using a HILIC column and transferred to a vial for LC-MS/MS analysis. LC-MS/MS measurements were performed using a Waters UPLC-Xevo-TQ5 micro instrument (Waters, Corporation, Milford, USA) in positive mode using an electrospray ionization (ESI) with a BEH HILIC column (2.1 x 100 mm with 1.7  $\mu$ m particle size, Waters) was used at 30 °C as described before<sup>27</sup> with minor modifications in the eluent program allowing a faster run while preserving separation of Glc- and Gal containing lipids. Eluent A contained 10 mM ammonium formate in acetonitrile/water (97:3, v/v) with 0.01% (v/v) formic acid and eluent B consisted of 10 mM ammonium formate in acetonitrile/water (75:15, v/v) with 0.01% (v/v) formic acid. Lyso- and deacylated glycosphingolipids were eluted in 10 min with a flow of 0.6 mL/min using the following program: 85% A from 0-1 min, 85-65% A from 1-2.5 min, 60-0% A from 2.5-4 min, 0% A from 4-4.5, 0-85% A from 4.5-4.6 min and re-equilibration with 85% A from 4.6-10 min. GlcChol was eluted in 18 min with a flow of 0.25 ml/min using the following program: 100% A from 0-3 min, 100-0 % A from 3-3.5 min, 0 % A from 3.5-4.5 min, 0-100

% A from 4.5-5 min and re-equilibration with 100 % A from 5-18 min. Lipid levels were calculated in pmol/mg total protein, sphingoid bases and GlcChol were calculated based on the respective isotopic <sup>13</sup>C internal standard, while deacylated neutral (glyco)sphingolipids were calculated using C17-dhCer as internal standard and normalized using the respective standard.

For the analysis of neutral glycosphingolipids with fatty acyls, 20 µL of the internal standard dhCer d17:0/16:0 (20 pmol/µL in methanol) and 20 µL of SM d18:1/17:0 (20 pmol/µL in methanol) was added to homogenates (10 µL, ± 10 µg total protein in KPi lysis buffer) and lipids were extracted using an acidic Bligh and Dyer procedure (1/1/0.9 chloroform/methanol/100 mM formate buffer pH 3.1), the lower phase was collected, dried and a butanol/water extraction was performed. Lipids were resuspended in acetonitrile/methanol (9/1, v/v) for separation using a HILIC column and transferred to a vial for LC-MS/MS analysis. The same eluent composition was used as described above and neutral glycosphingolipids were eluted in 23 min with a flow of 0.25 mL/min using the following program: 100% A from 0-3 min, 100-70% A from 3-3.5 min, 70% A from 3.5-6 min, 70-0% A from 6-9.5 min, 0% A from 9.5-10.5 min and re-equilibration with 100% A from 10.6-23 min. Lipid levels were calculated based on SM d18:1/16:0 for SM lipids or dhCer d17:0/16:0 for the other glycosphingolipids, normalized using the protein concentration and depicted as ratio compared WT.

**Supplementary Table 3 |** Transitions, cone voltage and collision energy of neutral GSLs with different fatty acyls.

Lipid	Transition	Cone	Collision	Lipid	Transition	Cone	Collision
dhCer d17:0/16:0 (IS)	526.7>264.4	10	20				
Cer d18:1/16:1	536.6>264.4	10	20	HexCer d18:1/16:1	698.6>264.4	10	44
Cer d18:1/16:0	538.6>264.4	10	20	HexCer d18:1/16:0	700.6>264.4	10	44
Cer d18:1/18:1	564.6>264.4	10	20	HexCer d18:1/18:1	726.6>264.4	10	44
Cer d18:1/18:0	566.6>264.4	10	20	HexCer d18:1/18:0	728.6>264.4	10	44
Cer d18:1/20:1	592.6>264.4	10	20	HexCer d18:1/20:1	754.6>264.4	10	46
Cer d18:1/20:0	594.6>264.4	10	20	HexCer d18:1/20:0	756.6>264.4	10	46
Cer d18:1/22:1	620.6>264.4	10	20	HexCer d18:1/22:1	782.6>264.4	10	48
Cer d18:1/22:0	622.6>264.4	10	20	HexCer d18:1/22:0	784.6>264.4	10	48
Cer d18:1/24:1	648.6>264.4	10	20	HexCer d18:1/24:1	810.6>264.4	10	52
Cer d18:1/24:0	650.6>264.4	10	20	HexCer d18:1/24:0	812.6>264.4	10	52
SM d18:1/17:0 (IS)	717.6>264.4	30	30				
SM d18:1/16:1	701.6>184.1	30	30				
SM d18:1/16:0	703.6>184.1	30	30	LacCer d18:1/16:0	862.7>264.4	30	48
SM d18:1/18:1	729.6>184.1	30	30				
SM d18:1/18:0	731.6>184.1	30	30	LacCer d18:1/18:0	890.7>264.4	30	48
SM d18:1/20:1	757.6>184.1	30	30				
SM d18:1/20:0	759.6>184.1	30	30				
SM d18:1/22:1	785.7>184.1	30	30				
SM d18:1/22:0	787.7>184.1	30	30				
SM d18:1/24:1	813.7>184.1	30	40	LacCer d18:1/24:1	972.8>264.4	30	50
SM d18:1/24:0	815.7>184.1	30	40	LacCer d18:1/24:0	974.8>264.4	30	50

**Histology** - For H&E staining, zebrafish were fixed in paraformaldehyde (4% PFA (w/v), Alfa Aesar, Haverhill, USA) overnight or Bouin's solution (5% acetic acid, 9% formaldehyde, 0.9% picric acid, Sigma) for 4 days, decalcified for 4 days using formic acid (20% (v/v)) and embedded in paraffin. Subsequently, serial sections of 5 µm thickness were made using a Leica RM2055 microtome. Sections were stained with Haematoxylin and Eosin.

**Statistical analyses** - Statistical analyses were performed using GraphPad Prism (v8.1.1, GraphPadsoftware, CA, USA) and data depicted as described in the result section. Data of lipid, protein and mRNA levels was analysed by One-Way Anova using Dunnett's test, with WT as control group, or Tukey's multiple comparison test as described in the result section. Data of length and tortuosity are analysed using a non-parametric Kruskal-Wallis test with Dunn's multiple comparison. In general, statistical comparisons are performed of WT vs *gba1*<sup>-/-</sup>, WT vs *gba1*<sup>-/-</sup>:*asah1b*<sup>-/-</sup> and *gba1*<sup>-/-</sup> vs *gba1*<sup>-/-</sup>:*asah1b*<sup>-/-</sup>, and depicted only when a significant difference is apparent and relevant. Ns = not significant, \* *P* < 0.05, \*\* *P* < 0.01, \*\*\* *P* < 0.001 and \*\*\*\* *P* < 0.0001.

## References

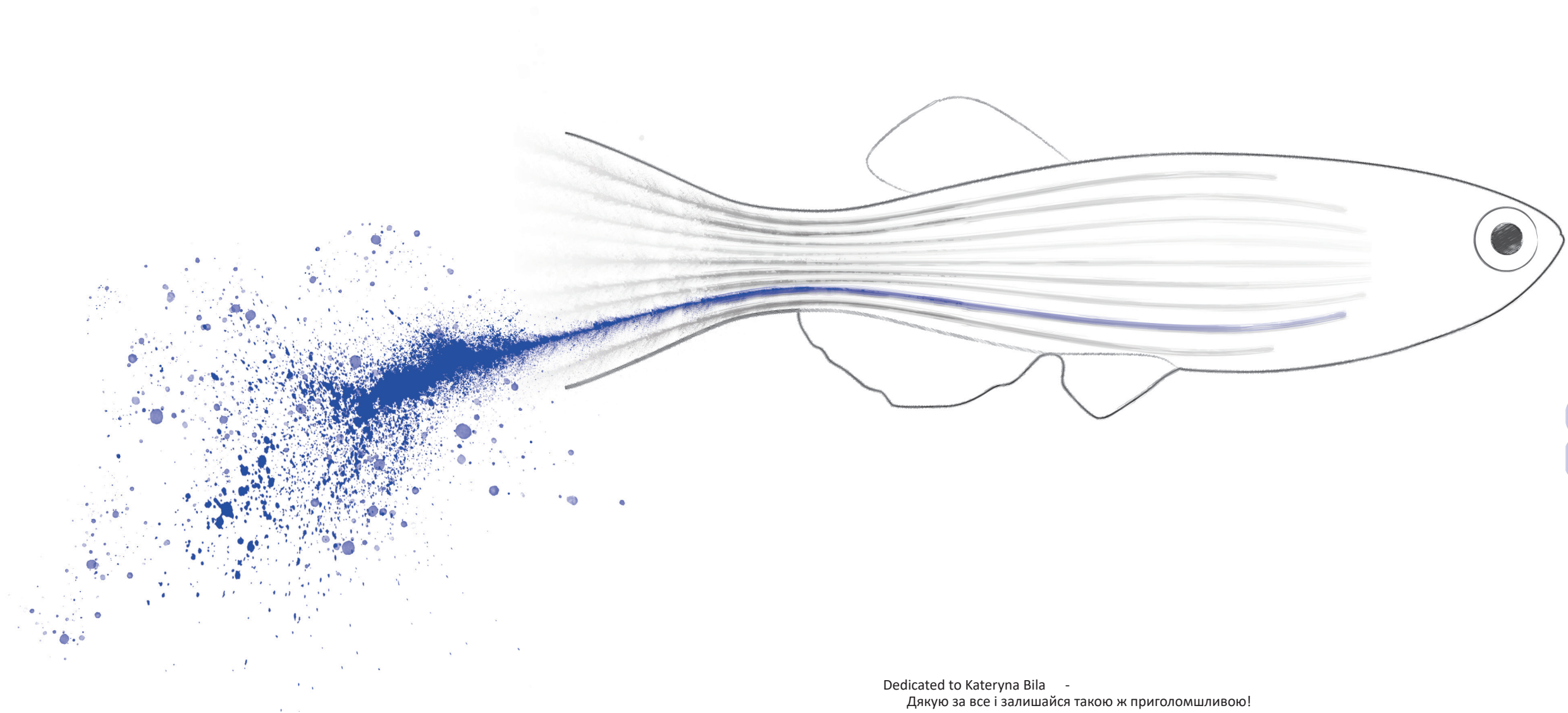
1. Brady R.O., Kanfer J.N., Bradley R.M. and Shapiro D. (1966) Demonstration of a deficiency of glucocerebrosidase-cleaving enzyme in Gaucher's disease. *The Journal of clinical investigation* **45**, 1112-1115.
2. Nair S., Boddupalli C.S., Verma R., Liu J., Yang R., Pastores G.M.,... and Dhodapkar M.V. (2015) Type II NKT-TFH cells against Gaucher lipids regulate B-cell immunity and inflammation. *Blood* **125**, 1256-1271.
3. Ikuno M., Yamakado H., Akiyama H., Parajuli L.K., Taguchi K., Hara J.,... and Takahashi R. (2019) GBA haploinsufficiency accelerates alpha-synuclein pathology with altered lipid metabolism in a prodromal model of Parkinson's disease. *Human molecular genetics* **28**, 1894-1904.
4. Taguchi Y.V., Liu J., Ruan J., Pacheco J., Zhang X.,... and Chandra S.S. (2017) Glucosylsphingosine Promotes alpha-Synuclein Pathology in Mutant GBA-Associated Parkinson's Disease. *J Neurosci* **37**, 9617-9631.
5. Smith N.J., Fuller M., Saville J.T. and Cox T.M. (2018) Reduced cerebral vascularization in experimental neuronopathic Gaucher disease. *J Pathol* **244**, 120-128.
6. Sidransky E., Nalls M.A., Aasly J.O., Aharon-Peretz J., Annesi G., Barbosa E.R.,... and Ziegler S.G. (2009) Multicenter analysis of glucocerebrosidase mutations in Parkinson's disease. *New England Journal of Medicine* **361**, 1651-1661.
7. Tsuang D., Leverenz J.B., Lopez O.L., Hamilton R.L., Bennett D.A., Schneider J.A.,... and Zabetian C.P. (2012) GBA mutations increase risk for Lewy body disease with and without Alzheimer disease pathology. *Neurology* **79**, 1944-1950.
8. Hammer M.B., Eleuch-Fayache G., Schottlaender L.V., Nehdi H., Gibbs J.R., ... and Singleton A.B. (2013) Mutations in GBA2 cause autosomal-recessive cerebellar ataxia with spasticity. *Am J Hum Genet* **92**, 245-251.
9. Woeste M.A. and Wachten D. (2017) The Enigmatic Role of GBA2 in Controlling Locomotor Function. *Front Mol Neurosci* **10**, 386.
10. Martin E., Schule R., Smets K., Rastetter A., Boukhris A., Loureiro J.L.,... and Stevanin G. (2013) Loss of function of glucocerebrosidase GBA2 is responsible for motor neuron defects in hereditary spastic paraplegia. *Am J Hum Genet* **92**, 238-244.
11. Votsi C., Zamba-Papanicolaou E., Middleton L.T., Pantzaris M. and Christodoulou K. (2014) A novel GBA2 gene missense mutation in spastic ataxia. *Ann Hum Genet* **78**, 13-22.
12. Overkleeft H.S., Renkema G.H., Neele J., Vianello P., Hung I.O.,... and Aerts J.M. (1998) Generation of specific deoxynojirimycin-type inhibitors of the non-lysosomal glucosylceramidase. *J Biol Chem* **273**, 26522-26527.
13. Giraldo P., Andrade-Campos M., Alfonso P., Irun P., Atutxa K., Acedo A.,... and Pocovi M. (2018) Twelve years of experience with miglustat in the treatment of type 1 Gaucher disease: The Spanish ZAGAL project. *Blood Cells Mol Dis* **68**, 173-179.
14. Farfel-Becker T., Vitner E.B. and Futerman A.H. (2011) Animal models for Gaucher disease research. *Dis Model Mech* **4**, 746-752.
15. Sidransky E., Sherer D.M. and Ginns E.I. (1992) Gaucher disease in the neonate: a distinct Gaucher phenotype is analogous to a mouse model created by targeted disruption of the glucocerebrosidase gene. *Pediatr Res* **32**, 494-498.
16. Tybulewicz V.L., Tremblay M.L., LaMarca M.E., Willemsen R., Stubblefield B.K., Winfield S.,... and et al. (1992) Animal model of Gaucher's disease from targeted disruption of the mouse glucocerebrosidase gene. *Nature* **357**, 407-410.
17. Vardi A., Zigdon H., Meshcheriakova A., Klein A.D., Yaacobi C., Eilam R.,... and Futerman A.H. (2016) Delineating pathological pathways in a chemically induced mouse model of Gaucher disease. *J Pathol* **239**, 496-509.
18. Mistry P.K., Liu J., Yang M., Nottoli T., McGrath J., Jain D.,... and Zaidi M. (2010) Glucocerebrosidase gene-deficient mouse recapitulates Gaucher disease displaying cellular and molecular dysregulation beyond the macrophage. *Proc Natl Acad Sci U S A* **107**, 19473-19478.
19. Enquist I.B., Lo Bianco C., Ooka A., Nilsson E., Mansson J.E., Ehinger M.,... and Karlsson S. (2007) Murine models of acute neuronopathic Gaucher disease. *Proc Natl Acad Sci U S A* **104**, 17483-17488.
20. Yildiz Y., Matern H., Thompson B., Allegood J.C., Warren R.L., Ramirez D.M.,... and Russell D.W. (2006) Mutation of beta-glucosidase 2 causes glycolipid storage disease and impaired male fertility. *The Journal of clinical investigation* **116**, 2985-2994.
21. Woeste M.A., Stern S., Raju D.N., Grahn E., Dittmann D., Gutbrod K.,... and Wachten D. (2019) Species-specific differences in nonlysosomal glucosylceramidase GBA2 function underlie locomotor dysfunction arising from loss-of-function mutations. *J Biol Chem* **294**, 3853-3871.
22. Raju D., Schonauer S., Hamzeh H., Flynn K.C., Bradke F.,... and Wachten D. (2015) Accumulation of glucosylceramide in the absence of the beta-glucosidase GBA2 alters cytoskeletal dynamics. *Plos Genet* **11**, e1005063.
23. Mistry P.K., Liu J., Sun L., Chuang W.L., Yuen T., Yang R.,... and Zaidi M. (2014) Glucocerebrosidase 2 gene deletion rescues type 1 Gaucher disease. *Proc Natl Acad Sci U S A* **111**, 4934-4939.
24. Marques A.R., Aten J., Ottenhoff R., van Roomen C.P., Herrera Moro D., Claessen N.,... and Aerts J.M. (2015)



- Reducing GBA2 Activity Ameliorates Neuropathology in Niemann-Pick Type C Mice. *PLoS one* **10**, e0135889.
25. Marques A.R., Mirzaian M., Akiyama H., Wisse P., Ferraz M.J., Gaspar P.,... and Aerts J.M. (2016) Glucosylated cholesterol in mammalian cells and tissues: formation and degradation by multiple cellular beta-glucosidases. *J Lipid Res* **57**, 451-463.
  26. Akiyama H. and Hirabayashi Y. (2017) A novel function for glucocerebrosidase as a regulator of sterylglucoside metabolism. *Biochim Biophys Acta Gen Subj* **1861**, 2507-2514.
  27. Lelieveld L.T., Mirzaian M., Kuo C.L., Artola M., Ferraz M.J., Peter R.E.A.,... and Aerts J. (2019) Role of beta-glucosidase 2 in aberrant glycosphingolipid metabolism: model of glucocerebrosidase deficiency in zebrafish. *J Lipid Res* **60**, 1851-1867.
  28. Akiyama H., Ide M., Nagatsuka Y., Sayano T., Nakanishi E., Uemura N.,... and Hirabayashi Y. (2020) Glucocerebrosidases catalyze a transgalactosylation reaction that yields a newly-identified brain sterol metabolite, galactosylated cholesterol. *J Biol Chem* **295**, 5257-5277.
  29. Groener J.E., Poorthuis B.J., Kuiper S., Helmond M.T., Hollak C.E. and Aerts J.M. (2007) HPLC for simultaneous quantification of total ceramide, glucosylceramide, and ceramide trihexoside concentrations in plasma. *Clin Chem* **53**, 742-747.
  30. Mirzaian M., Wisse P., Ferraz M.J., Marques A.R.A., Gaspar P., Oussoren S.V.,... and Aerts J.M. (2017) Simultaneous quantitation of sphingoid bases by UPLC-ESI-MS/MS with identical (13)C-encoded internal standards. *Clin Chim Acta* **466**, 178-184.
  31. Sugawara T. and Miyazawa T. (1999) Separation and determination of glycolipids from edible plant sources by high-performance liquid chromatography and evaporative light-scattering detection. *Lipids* **34**, 1231-1237.
  32. Nystrom L., Schar A. and Lampi A.M. (2012) Steryl glycosides and acylated steryl glycosides in plant foods reflect unique sterol patterns. *Eur J Lipid Sci Tech* **114**, 656-669.
  33. Lawrence C. (2011) Advances in zebrafish husbandry and management. *Methods Cell Biol* **104**, 429-451.
  34. Spence R., Gerlach G., Lawrence C. and Smith C. (2008) The behaviour and ecology of the zebrafish, *Danio rerio*. *Biological reviews of the Cambridge Philosophical Society* **83**, 13-34.
  35. Farfel-Becker T., Vitner E.B., Kelly S.L., Bame J.R., Duan J., Shinder V.,... and Futerman A.H. (2014) Neuronal accumulation of glucosylceramide in a mouse model of neuronopathic Gaucher disease leads to neurodegeneration. *Human molecular genetics* **23**, 843-854.
  36. Farfel-Becker T., Vitner E.B., Pressey S.N., Eilam R., Cooper J.D. and Futerman A.H. (2011) Spatial and temporal correlation between neuron loss and neuroinflammation in a mouse model of neuronopathic Gaucher disease. *Human molecular genetics* **20**, 1375-1386.
  37. Vitner E.B., Farfel-Becker T., Eilam R., Biton I. and Futerman A.H. (2012) Contribution of brain inflammation to neuronal cell death in neuronopathic forms of Gaucher's disease. *Brain* **135**, 1724-1735.
  38. Zigdon H., Savidor A., Levin Y., Meshcheriakova A., Schiffmann R. and Futerman A.H. (2015) Identification of a biomarker in cerebrospinal fluid for neuronopathic forms of Gaucher disease. *PLoS one* **10**, e0120194.
  39. Klein A.D., Ferreira N.S., Ben-Dor S., Duan J., Hardy J., Cox T.M.,... and Futerman A.H. (2016) Identification of Modifier Genes in a Mouse Model of Gaucher Disease. *Cell Rep* **16**, 2546-2553.
  40. Jones E.E., Zhang W., Zhao X., Quason C., Dale S., Shahidi-Latham S.,... and Sun Y. (2017) Tissue Localization of Glycosphingolipid Accumulation in a Gaucher Disease Mouse Brain by LC-ESI-MS/MS and High-Resolution MALDI Imaging Mass Spectrometry. *SLAS Discov* **22**, 1218-1228.
  41. Keatinge M., Bui H., Menke A., Chen Y.C.,... and Bandmann O. (2015) Glucocerebrosidase 1 deficient *Danio rerio* mirror key pathological aspects of human Gaucher disease and provide evidence of early microglial activation preceding alpha-synuclein-independent neuronal cell death. *Human molecular genetics* **24**, 6640-6652.
  42. Blesa J., Trigo-Damas I., Quiroga-Varela A. and Jackson-Lewis V.R. (2015) Oxidative stress and Parkinson's disease. *Front Neuroanat* **9**, 91.
  43. Pandey M.K., Burrow T.A., Rani R., Martin L.J., Witte D., Setchell K.D.,... and Grabowski G.A. (2017) Complement drives glucosylceramide accumulation and tissue inflammation in Gaucher disease. *Nature* **543**, 108-112.
  44. Artola M., Kuo C.L., Lelieveld L.T., Rowland R.J., van der Marel G.A., Codee J.D.C.,... and Overkleeft H.S. (2019) Functionalized Cyclophellitols Are Selective Glucocerebrosidase Inhibitors and Induce a Bona Fide Neuropathic Gaucher Model in Zebrafish. *Journal of the American Chemical Society* **141**, 4214-4218.
  45. Koch B.E., Stougaard J. and Spaik H.P. (2014) Spatial and temporal expression patterns of chitinase genes in developing zebrafish embryos. *Gene Expr Patterns* **14**, 69-77.
  46. Nguyen-Chi M., Laplace-Builhe B., Travnickova J., Luz-Crawford P., Tejedor G., Lutfalla G.,... and Djouad F. (2017) TNF signaling and macrophages govern fin regeneration in zebrafish larvae. *Cell Death Dis* **8**, e2979.
  47. Harjula S.E., Ojanen M.J.T., Taavitsainen S., Nykter M. and Ramet M. (2018) Interleukin 10 mutant zebrafish have an enhanced interferon gamma response and improved survival against a *Mycobacterium marinum* infection. *Sci Rep* **8**, 10360.
  48. Tang R., Dodd A., Lai D., McNabb W.C. and Love D.R. (2007) Validation of zebrafish (*Danio rerio*) reference genes for quantitative real-time RT-PCR normalization. *Acta Biochim Biophys Sin (Shanghai)* **39**, 384-390

# CHAPTER 8

## $\alpha$ -Galactosidases in zebrafish



Dedicated to Kateryna Bila -  
Дякую за все і залишайся такою ж приголомшливою!

## Abstract

Human  $\alpha$ -galactosidase A ( $\alpha$ -GAL A) is responsible for the hydrolysis of terminal  $\alpha$ -galactosyl moieties from glycosphingolipids in lysosomes. Mutations in the X-linked *GLA* gene resulting in deficient  $\alpha$ -GAL A cause the lysosomal storage disorder Fabry disease. The highly homologous enzyme,  $\alpha$ -N-acetylgalactosaminidase ( $\alpha$ -NAGAL), primarily cleaves terminal N-acetylgalactosamine moieties from glycoconjugates, but it is *in vitro* also active towards  $\alpha$ -galactosides. This chapter investigates the presence of  $\alpha$ -galactosidase enzymes in zebrafish embryonic fibroblast cells, zebrafish larvae (5 days post-fertilization) and organs of adult fish. The zebrafish genome annotates one  $\alpha$ -Gal A and one  $\alpha$ -Nagal orthologue. The presence of  $\alpha$ -Gal A and  $\alpha$ -Nagal proteins in zebrafish cells and larvae was confirmed by chemical proteomics using an  $\alpha$ -Gal configured activity-based probe (ABP). Both enzymes have N-linked glycans and a comparable molecular weight of 45 kDa as determined by SDS-PAGE. Fluorogenic  $\alpha$ -galactoside and  $\alpha$ -N-acetylgalactosaminide substrates reveal considerable  $\alpha$ -Nagal activity in zebrafish larvae and adult organs.  $\alpha$ -Gal A activity is lower than  $\alpha$ -Nagal activity, but higher in fertilized eggs, reproductive organs, liver and kidney. Interestingly, no Gb3 could be detected using sensitive LC-MS/MS methods in any of the studied zebrafish materials such as cells, larvae, brain, liver, kidney and testis. The absence of the lipid Gb3 is consistent with the absence of a gene encoding lactosylceramide 4- $\alpha$ -galactosyltransferase (A4gGALT; Gb3 synthase) in zebrafish or any other teleost species. HEK293T cells lacking endogenous  $\alpha$ -GAL A were generated using CRISPR/Cas9 technology. The increase in endogenous Gb3 levels in these cells could be comparably corrected by over-expression of either human  $\alpha$ -GAL A or zebrafish  $\alpha$ -Gal A. These findings indicate that zebrafish  $\alpha$ -Gal A can hydrolyse the endogenous substrate Gb3 in the cellular setting, however it seems that it is not able to hydrolyse the artificial substrate NBD-Gb3 *in vitro*. The role of the conserved  $\alpha$ -galactosidase encoded by the *gla* gene in the zebrafish remains elusive. It is envisioned that *gla*<sup>-/-</sup> zebrafish expressing human A4GALT might render a useful Fabry disease model. The comparison of such fish with those with a concomitant *asha1b* KO might assist the investigation of the specific impact of excessive lysoGb3 in Fabry disease pathology.

## Introduction

Human  $\alpha$ -galactosidase A ( $\alpha$ -Gal A; E.C.3.2.1.22, Uniprot accession P06280) is encoded by the *GLA* gene at locus Xq22 and responsible for the hydrolysis of terminal  $\alpha$ -linked galactosyl moieties of primarily the  $\alpha$ -1,4-linked glycosphingolipids globotriaosylceramide (Gb3) and galabiosaolceramide (diGalCer) in lysosomes<sup>1,2</sup>. In addition, ABO blood group antigens are determined by terminal  $\alpha$ -1,3-Gal and/or  $\alpha$ -1,3-linked N-acetylgalactosamine (GalNAc) of glycolipids and glycoconjugates and antibodies against the opposite blood group antigens are of clinical importance in transfusion and transplantation<sup>3</sup>.

Deficiency of  $\alpha$ -Gal A leads to Fabry disease, an X-linked lysosomal storage disorder which is characterized by lysosomal accumulation of the globoside Gb3, the deacylated globotriaosylsphingosine (lysoGb3), diGalCer and blood group B GSLs in tissues as well as increased levels in body fluids<sup>4-6</sup>. Heart and kidney tissues are often affected in Fabry male patients who may develop clinical symptoms such as angiokeratoma, anhidrosis, acroparesthesias, gastrointestinal complaints, cardiomyopathy, cerebrovascular disease, renal insufficiency and spontaneous or triggered pain episodes<sup>2</sup>.

In the last decade, several cyclophellitol-configured activity-based probes (ABPs) have been developed as chemical tools to study corresponding retaining glycosidase enzymes and assist the diagnosis of lysosomal storage disorders stemming from enzyme deficiencies including, but not limited to, Gaucher disease, Fabry disease and Krabbe disease<sup>7-9</sup>. These ABPs bind in a mechanism-based irreversible manner to the catalytic nucleophile of the retaining glycosidase, while the attached fluorophore or biotin allows detection of the target enzymes<sup>10</sup>. The fluorescent  $\alpha$ -Gal configured cyclophellitol aziridine ABP has been shown to label  $\alpha$ -Gal A in human, mouse and plant material<sup>8,11</sup>. The  $\alpha$ -Gal configured ABP also labels the homologous N-acetyl-galactosaminidase ( $\alpha$ -NAGAL), which has arisen by a gene duplication<sup>11,12</sup>. The  $\alpha$ -NAGAL enzyme specifically hydrolyses terminal  $\alpha$ -galactose moieties with a N-acetyl substituent on the 2-position of the galactose sugar ( $\alpha$ -GalNAc) and mutations in the *NAGA* gene lead to the very rare Schindler disease<sup>13,14</sup>. However due to structural differences,  $\alpha$ -NAGAL can also accommodate and hydrolyse  $\alpha$ -galactose configured lipids *in vitro*, while  $\alpha$ -GAL A can only hydrolyse  $\alpha$ -galactose moieties<sup>15,16</sup>. Modified  $\alpha$ -NAGAL enzymes have been developed as possible enzyme replacement therapy for Fabry disease enabling Gb3 and lyso-Gb3 corrections without the immunological cross-reactivity that can occur with recombinant  $\alpha$ -Gal A treatment<sup>16-18</sup>.

The aim of the present study was to characterize  $\alpha$ -galactosidase enzymes in zebrafish materials including embryonic cells, larvae of 5 days post-fertilization (5 dpf) and organs of adult fish. The presence of both  $\alpha$ -Gal A and  $\alpha$ -Nagal was confirmed using a combination of mRNA analysis, activities towards artificial  $\alpha$ -Gal substrates as well as labelling and identification of the corresponding glycosidases using  $\alpha$ -Gal configured ABPs. The physiological role of  $\alpha$ -Gal A in the zebrafish remains elusive since no Gb3 has been found in any of the tested zebrafish materials.

## Results

### Presence of $\alpha$ -galactosidase enzymes in zebrafish cells and larvae

Firstly, artificial fluorogenic substrates 4-methylumbelliferyl  $\alpha$ -D-galactopyranoside (4MU- $\alpha$ -Gal) and 4-MU  $\alpha$ -D-N-acetylgalactosaminide (4MU- $\alpha$ -GalNAc) were used to study the occurrence of corresponding hydrolytic activities in homogenates of cultured zebrafish embryonic fibroblasts (ZF4 cells) and a pool of 5 dpf zebrafish larvae. Activity towards both substrates was observed with an optimum around pH 4.0-4.5 (**Figure 1**). The activity towards 4MU- $\alpha$ -Gal in lysates of zebrafish cells was much higher than activity towards 4MU- $\alpha$ -GalNAc (**Figure 1A**; black and grey circles for 4MU- $\alpha$ -Gal and 4MU- $\alpha$ -GalNAc respectively). Only a small amount of activity towards 4MU- $\alpha$ -Gal was lost upon inhibition of the suspected  $\alpha$ -Nagal enzyme with a high concentration of the  $\alpha$ -GalNAc (NAGA) sugar (**Figure 1A**; open circles, incubation with 200 mM final concentration of  $\alpha$ -GalNAc).

In lysates of zebrafish larvae, the activity towards 4MU- $\alpha$ -GalNAc was higher than that towards 4MU- $\alpha$ -Gal (**Figure 1B**; black and grey circles for 4MU- $\alpha$ -Gal and 4MU- $\alpha$ -GalNAc respectively). About 50% of hydrolysis of 4MU- $\alpha$ -Gal could be inhibited by the presence of 200 mM  $\alpha$ -GalNAc (**Figure 1A**; open circles, incubation with  $\alpha$ -GalNAc). An apparent IC<sub>50</sub> of 11 mM was noted for  $\alpha$ -GalNAc regarding 4MU- $\alpha$ -GalNAc activity (**Supplementary Figure 1**). In the presence of 200 mM of  $\alpha$ -GalNAc the residual  $\alpha$ -Nagal activity was only 5%. Thus, activity towards 4MU- $\alpha$ -Gal can be differentiated in two components: activity inhibitable by  $\alpha$ -GalNAc (zebrafish  $\alpha$ -Nagal), and activity that is not inhibitable with the sugar, (zebrafish  $\alpha$ -Gal A), analogous to the situation in mammalian cells in tissues.

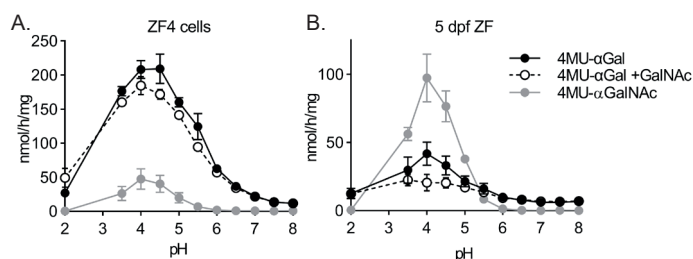


**Figure 1 | Hydrolytic activity of zebrafish cells and larvae towards 4MU- $\alpha$ -Gal and 4MU- $\alpha$ -GalNAc**

Activity towards 4MU- $\alpha$ -Gal (black) and 4MU- $\alpha$ -GalNAc (grey) at a range of pH values (pH 2-8) in homogenates of zebrafish embryonic cells (**A**) and zebrafish larvae of 5 dpf (**B**). Specific activity of  $\alpha$ -Gal A was measured by blocking  $\alpha$ -Nagal activity using 200 mM GalNAc sugar (black, open circles). Activity is measured from three independent homogenate preparations. Data is depicted as mean  $\pm$  SD.

Next, the effect of different α-galactose configured cyclophellitol aziridines was tested in cell and larvae lysates by measuring residual enzymatic activity towards 4MU-α-Gal and 4MU-α-GalNAc. Tested were ME737 and ME539 extended with an alkyl moiety at the nitrogen and TB474 conjugated further with a Cy5 fluorophore (see **Supplementary Figure 2** for structures of the inhibitors). The three compounds inhibited both α-Gal A and α-Nagal activities, with low micromolar apparent IC<sub>50</sub> values (**Figure 2A and B, Table 1**). The Cy5 configured ABP (TB474) was more potent in inactivating α-galactosidase activity in the ZF4 cell and zebrafish larvae lysates than the compounds without the bulky fluorescent group (ME737 and ME739).

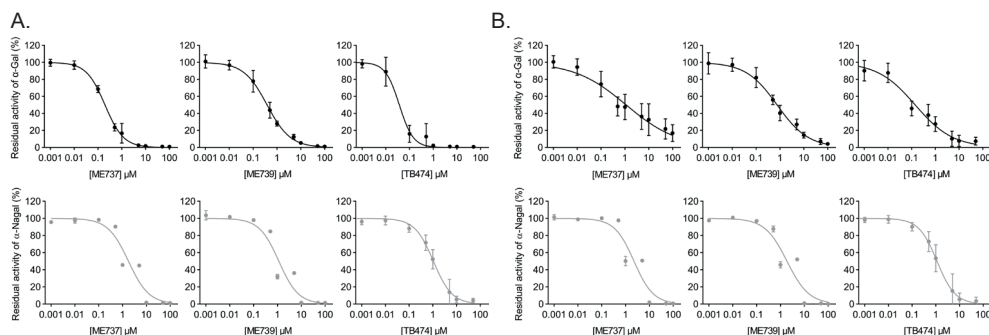


**Figure 2 | Potency of α-Gal configured cyclophellitol aziridine inhibitors for α-Gal and α-Nagal**

Residual activity towards 4MU-α-Gal (black) and 4MU-α-GalNAc (grey) for α-Gal A and α-Nagal respectively, in cell homogenates of ZF4 cells (**A**) and 5 dpf zebrafish larvae (**B**) treated *in vitro* with the α-Gal configured inhibitors ME737, ME739 and ABP TB474. Residual activity is measured from three independent incubations using different homogenates. Data is depicted as mean ± SD.

**Table 1 |** Apparent IC<sub>50</sub> values of α-Gal configured ME737, ME739 and ABP TB474 for *in vitro* inhibition of α-Gal A and α-Nagal enzymes in homogenates of ZF4 cells and 5 dpf zebrafish larvae (ZF).

Compound	α-Gal A		α-Nagal	
	ZF4 cells	ZF (5 dpf)	ZF4 cells	ZF (5 dpf)
ME737 (μM)	0.197 ± 0.044	1.129 ± 1.152	1.770 ± 1.107	2.264 ± 1.56
ME739 (μM)	0.385 ± 0.113	0.755 ± 0.321	1.144 ± 0.742	1.878 ± 1.353
TB474 (ABP) (μM)	0.037 ± 0.019	0.141 ± 0.098	1.058 ± 0.334	1.123 ± 0.436

In order to visualize the α-Gal enzymes, homogenates were incubated with the α-Gal configured ABP (TB474) for 30 min, proteins were separated using SDS-PAGE and labelled proteins were detected by in-gel fluorescence scanning. An ABP-enzyme complex with an apparent molecular weight of 45 kDa was detected in both cell and larvae lysate (**Figure 3A; +ABP (TB474)**). The intensity of this enzyme-ABP complex was significantly less, when the homogenates were pre-incubated with non-fluorescent α-Gal configured cyclophellitol aziridine inhibitor ME739 (**Figure 3A**). The intensity of the other labelled bands was not competed with ME739, indicating aspecific labelling of abundant proteins in the zebrafish material.



After translation,  $\alpha$ -Gal enzymes are modified with high-mannose N-linked glycans acquiring terminal mannose 6-phosphate moieties that mediate transport of correctly folded enzyme to lysosomes<sup>19</sup>. Removal of all N-linked glycans with PNGase F digestion led to a reduction of the molecular weight of ABP-labelled enzyme from to 40 kDa, both for enzyme in homogenates of ZF4 cells and zebrafish larvae (**Figure 3B**). Fabrazyme, the recombinant human  $\alpha$ -Gal A used to treat Fabry patients, also showed a quite comparable reduction of molecular weight following PNGase F digestion. Next, the binding to concanavalin A (ConA)-Sephrose beads was examined for the zebrafish proteins that are labelled with ABP. The lectin beads bind to the N-linked glycans in glycoproteins without interference of the active site and therefore allow subsequent activity assays. The  $\pm$  45 kDa protein labelled with ABP bound to the ConA beads, both for homogenates of ZF4 cells and 5 dpf larvae (**Figure 3C**). Hydrolysis of 4-MU- $\alpha$ -Gal A and 4MU- $\alpha$ -NAGA was nearly absent in the unbound fraction, indicating binding of the majority of active enzymes to the lectin beads (**Supplementary Figure 3**).

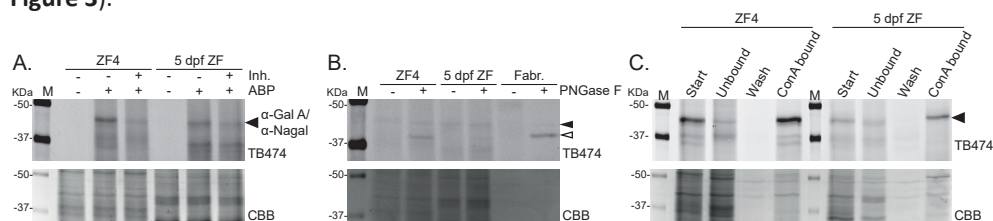


**Figure 3 | In vitro labelling of  $\alpha$ -Gal A and  $\alpha$ -Nagal with  $\alpha$ -Gal configured ABP**

**(A)** Labelling of homogenates of ZF4 cells and a pool of 5 dpf zebrafish larvae with  $\alpha$ -Gal configured ABP (TB474, 1 $\mu$ M) in the absence or presence of inhibitor ME739 (50  $\mu$ M). **(B)** Homogenates and recombinant  $\alpha$ -Gal A (Fabrazyme) were labelled with ABP TB474, before deglycosylation using PNGase F. Apparent deglycosylated protein was depicted with the open triangle. **(C)** Glycoproteins were enriched using Concanavalin A (ConA)-Sephrose beads. Start material, supernatant (unbound), wash and ConA bound material were collected and  $\alpha$ -Gal A and  $\alpha$ -Nagal was visualized using ABP TB474 in equal volumes relative to the starting material. Coomassie Brilliant Blue (CBB) was used as protein loading control in A-C.

### Prediction of $\alpha$ -galactosidase and N-acetylgalactosaminidase in zebrafish genome

The zebrafish genome was evaluated for orthologues of human  $\alpha$ -galactosidase A (Uniprot code P06280) using a protein blast. Two zebrafish orthologues were found (F1Q5G5 and F1QR55). Only F1Q5G5 showed a corresponding *gla* gene (ncbi code NM\_001006103), located on chromosome 14. The genomic location of F1QR55 is allocated to chromosome 14 as well, however annotated as alternative chromosome. The two predicted proteins have 95% identity, whereby F1QR55 misses part of the N-terminal sequence of F1Q5G5. The *in silico* data suggest that only one annotated  $\alpha$ -Gal A is expressed, while the other likely arises from genetic variation among fish. The zebrafish  $\alpha$ -Gal A F1Q5G5 precursor protein shows 67% identity with its human  $\alpha$ -Gal A counterpart. The predicted mature zebrafish  $\alpha$ -Gal A contains 389 amino acids, slightly less compared to the 398 polypeptide of human  $\alpha$ -Gal A. The zebrafish genome also shows one orthologue of human  $\alpha$ -N-acetylgalactosaminidase (Uniprot code P17050). The zebrafish *naga* gene is located on chromosome 4 and two encoding transcripts are annotated, A0A2R8QPJ2 of 415 residues and A0A0R4IJL2 of 437 residues. Only the longer  $\alpha$ -Nagal enzyme has a predicted signal peptide (A0A0R4IJL2). The predicted mature zebrafish  $\alpha$ -Nagal polypeptide has 420 amino acids, compared to 394 amino acids of the human  $\alpha$ -NAGAL.

### Identification of $\alpha$ -galactosidase enzymes in zebrafish

ABP ME741, containing a biotin tag (see **Supplementary Figure 1**), was used to isolate ABP-reactive proteins from both the zebrafish cell and larvae homogenate and to subsequently establish their identity by proteomics with a similar streptavidin pull down based procedure as used earlier<sup>11</sup>. Peak lists were searched against the UniProt database of *Danio rerio*. In this manner, among the ABP-reactive proteins in the zebrafish cell homogenate the two zebrafish  $\alpha$ -Gal A enzymes and two annotated enzymes of  $\alpha$ -Nagal were detected. Both  $\alpha$ -Gal A and  $\alpha$ -Nagal were detected in two of the three independent experiments (**Table 2**). Among the ABP-reactive proteins in the homogenate of pools of 5 dpf zebrafish larvae, only the two annotated  $\alpha$ -Gal A enzymes were detected, even though activity towards 4MU- $\alpha$ -Nagal was measured in this material. Likely, the enzymes are not abundant enough to be always detected with the used chemical proteomics method.

The detected peptide sequences (**Supplementary Table 1**) were compared to the predicted amino acid sequences of  $\alpha$ -Gal A and  $\alpha$ -Nagal (underlined in **Supplementary Figure 4**). All detected peptide sequences were judged to be specific for one of the two enzymes. In conclusion, the ABP-based chemical proteomics method confirmed the presence of both  $\alpha$ -Gal A and  $\alpha$ -Nagal proteins in the zebrafish materials investigated.

**Table 2 |** Overview of chemical proteomics experiments using  $\alpha$ -Gal ABP (ME741) in homogenate of ZF4 cell (performed 3 independent times) and 5 dpf zebrafish larvae (performed 2 independent times). ND = not detected, - = experiment not performed

			Experiment 1 (25-10-2018)			Experiment 2 (09-11-2018)			Experiment 3 (10-01-2019)		
	Found	Mass (kDa)	Score	Matched peptides	Coverage (%)	Score	Matched peptides	Coverage (%)	Score	Matched peptides	Coverage (%)
ZF4 cells	$\alpha$ -Gal A: F1Q5G5	2/3 46.8	6555	13	31	1787	14	37	ND		
	$\alpha$ -Gal A: F1QR55	2/3 37.5	6090	10	31	1704	10	34	ND		
	$\alpha$ -Nagal: A0A0R4IJL2	2/3 49.8	218.4	4	8.5	ND			1311	6	14
	$\alpha$ -Nagal: A0A2R8QPI2	2/3 47.4	218.4	4	8.9	ND			1311	6	15
5 dpf ZF	$\alpha$ -Gal A: F1Q5G5	2/2 46.8	-			145	5	12.5	289	9	25
	$\alpha$ -Gal A: F1QR55	2/2 37.5				141	4	15.5	280	8	28
	$\alpha$ -Nagal: A0A0R4IJL2	0/2				ND			ND		
	$\alpha$ -Nagal: A0A2R8QPI2	0/2				ND			ND		

### Alignment and evaluation of zebrafish $\alpha$ -Gal A compared to human

The structure of human  $\alpha$ -Gal A has been solved by X-ray crystallography and revealed that  $\alpha$ -Gal A is a homodimeric glycoprotein<sup>15</sup>. Alignment of human  $\alpha$ -Gal A with zebrafish  $\alpha$ -Gal A (isoform F1Q5G5) indicates conservation of large stretches of amino acids. Moreover, several important features and residues are conserved in the zebrafish  $\alpha$ -Gal A protein sequence. The cysteine residues forming five disulfide bonds are conserved, however only one N-linked glycan site is conserved in the zebrafish  $\alpha$ -Gal A (**Figure 4**, orange for cysteine residues and green for N-glycosylation sites respectively). Importantly, the catalytic nucleophile and acid/base residues are conserved in zebrafish  $\alpha$ -Gal A (**Figure 4**, red; human catalytic nucleophile D170 and acid/base D231) as well as residues with side chains thought to have primary interactions with the  $\alpha$ -galactose moiety<sup>15</sup> (**Figure 4**; W47, D92, D93, Y134, K168, E203, L206, Y207, R227 and M267 in blue and C142 and C172 in orange).



**Figure 4 | Alignment of human  $\alpha$ -GAL A with zebrafish  $\alpha$ -Gal A.**

The amino acid sequences of the pro-protein of human  $\alpha$ -GAL A (Uniprot P06280) and zebrafish  $\alpha$ -Gal A (Uniprot F1Q5G5) were aligned using Clustal Omega<sup>20</sup>. \* indicates a conserved residue, : a strongly similar residue and . a weakly similar residue. The signal peptide is predicted using SingalP-5.0<sup>21</sup> and depicted in purple. The catalytic Asp residues are depicted in red, Asn residues with reported N-linked in green, the cysteine residues forming five disulfide bridges in orange and residues interacting and stabilizing the  $\alpha$ -galactose in blue. The Glu and Leu residues which form specificity of the  $\alpha$ -galactose moiety are emphasized with #.

The protein sequence and structure of  $\alpha$ -GAL A and  $\alpha$ -NAGAL enzymes are quite similar<sup>15</sup>. The substrate specificity for either a hydroxyl or a N-acetyl substituent on the 2-position of the  $\alpha$ -galactose moiety is thought to arise from the side chains of two amino acids in the  $\beta 5$ - $\alpha 5$  loop. The side chains of E203 and L206 of human  $\alpha$ -GAL A sterically block the larger N-acetyl substituent. The residues of  $\alpha$ -NAGAL at the two positions are serine and alanine and these side chains do not block the N-acetyl group and tolerate a

hydroxyl group. Alignment of zebrafish  $\alpha$ -Gal with  $\alpha$ -Nagal (isoform A0A0R4IJL2) indicates conservation of the residues involved in the reported interactions with the  $\alpha$ -galactose or N-acetylgalactosamine moiety (depicted in blue in **Supplementary Figure 4**). Moreover, the Glu and Leu residues are present in zebrafish  $\alpha$ -Gal A, while Ser and Ala residues are present in zebrafish  $\alpha$ -Nagal (**Figure 4**; # for human and zebrafish  $\alpha$ -Gal A and **Supplementary Figure 4**; # for zebrafish  $\alpha$ -Gal A and  $\alpha$ -Nagal).

### *In vivo* inhibition of $\alpha$ -Gal A does not show lipid abnormalities

Next, it was attempted to examine the physiological role of the zebrafish  $\alpha$ -galactosidase enzymes *in vivo*. First it was established which concentration of the  $\alpha$ -Gal inhibitors ME737 and ME739 led to complete inhibition of  $\alpha$ -galactosidase activities in cultured cells and developing zebrafish larvae. A concentration of 1  $\mu$ M ME737 and 24 hours of incubation was enough to block most of the  $\alpha$ -Gal activity in cultured ZF4 cells, which showed residual  $\alpha$ -Nagal activity (**Figure 5A**). Incubation of developing zebrafish larvae from fertilization up to 5 dpf with 100  $\mu$ M ME737 or ME739 led to a reduction in  $\alpha$ -Gal and  $\alpha$ -Nagal activity (**Figure 5B**). High concentrations of ME737 and ME739 were used to study the glycosphingolipid changes in developing zebrafish larvae by earlier established LC-MS/MS methods<sup>22</sup>. No significant change was found in neutral glycosphingolipids such as lactosylceramide, glucosylceramide or ceramide (**Figure 5C**). No Gb3 was detected in samples of zebrafish larvae, neither in those of  $\alpha$ -Gal inhibitor treated fish (**Supplementary Figure 5A**).

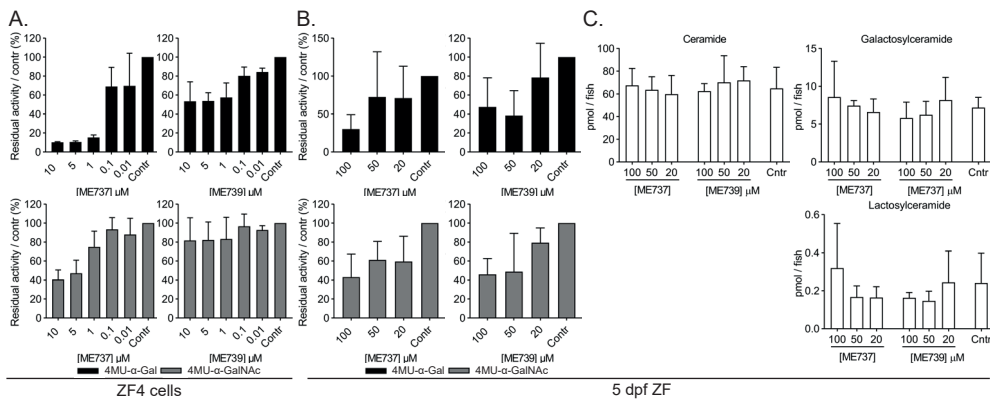


**Figure 5 | *in vivo* inhibition of  $\alpha$ -Gal A and  $\alpha$ -Nagal**

**(A)** ZF4 cells were treated with different concentrations of ME737 or ME739 (0.1-10  $\mu$ M) for 24 hours and residual activity towards 4MU- $\alpha$ -Gal (black bars) and 4MU- $\alpha$ -GalNAc (grey bars) was measured. Data is obtained from three individual incubations and depicted as mean  $\pm$  SD. **(B)** Developing zebrafish embryos were treated with ME737 or ME739 (20-100  $\mu$ M) for 5 days. Residual activity towards 4MU- $\alpha$ -Gal (black bars) and 4MU- $\alpha$ -GalNAc (grey bars) was measured in homogenates of a pool of 3 zebrafish. Data is obtained from three individual incubations and depicted as mean  $\pm$  SD. **(C)** Ceramide, galactosylceramide and lactosylceramide levels were measured of individual zebrafish larvae (5 dpf) treated with 100, 50 or 20  $\mu$ M ( $n = 4$ ) and DMSO treated controls ( $n = 7$ ) in pmol/fish. Data is obtained from two independent incubations and depicted as mean  $\pm$  SD.

**Gla expression and  $\alpha$ -Gal A activity in adult organs, but no Gb3**

Next, experiments were performed to analyse the specific mRNA expression,  $\alpha$ -galactosidase activity and the glycosphingolipid composition of developing zebrafish embryos ( $t = 0 - 5$  dpf) as well as different organs. Evaluation of specific mRNA expression using RT-qPCR showed highest *gla* expression in fertilized eggs, brain and testis, while expression of *naga* appeared highest in fertilized eggs, brain, fin and spleen (**Figure 6A**). The expression of *naga* mRNA was relatively higher than *gla* mRNA, likely corresponding to the relatively higher activity towards 4MU- $\alpha$ -GalNAc in the measured materials (**Figure 6A** and **6C**). High specific  $\alpha$ -Gal A activity was found in the liver, kidney, reproductive organs and fertilized zebrafish eggs (0 dpf) (**Figure 6B** and **Supplementary Figure 6**). Interestingly, the lipid Gb3 was not detected in brain, liver, kidney, testis or ovary tissues either (**Supplementary Figure 5A**).

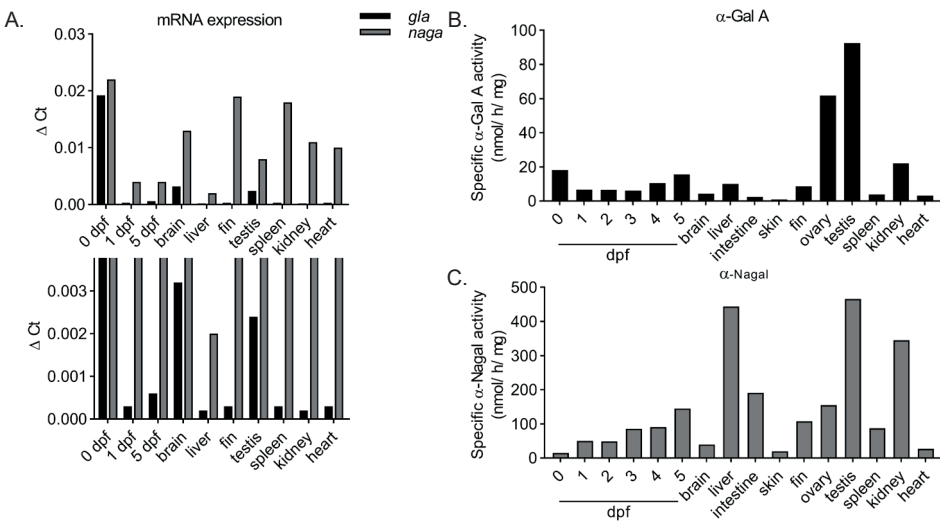


**Figure 6 | mRNA expression and activity in developing zebrafish and adult organs**

**(A)** mRNA levels of *gla* and *naga* in developing zebrafish embryos (0, 1 and 5 dpf) and adult fish organs and tissue (brain, liver, fin, testis, spleen, kidney and heart) analysed using RT-qPCR. Data is normalized using *Ef1 $\alpha$*  and *rp13 $\alpha$* , in technical duplicate and depicted as relative expression compared to the housekeeping genes. An inset zooming on *gla* mRNA levels is depicted below. **(B)** Specific  $\alpha$ -Gal A activity in homogenates of developing zebrafish embryos and adult fish organs and tissue, determined as the residual activity towards 4MU- $\alpha$ -Gal after inactivation of  $\alpha$ -Nagal activity using 200 mM GalNAc sugar. **(C)** Specific  $\alpha$ -Nagal activity determined as activity towards 4MU- $\alpha$ -GalNAc. Activity is measured in technical duplicate of a single biological sample.

### Zebrafish α-Gal A can hydrolyse Gb3 *in situ*, but not NBD-Gb3 *in vitro*

In order to study the catalytic features of zebrafish α-Gal A and compare the enzyme to human enzyme, cells without endogenous α-Gal A were generated. Human embryonic kidney (HEK293T) cells were mutated in the human *GLA* gene using CRISPR/Cas9 technology and deficient cells were grown from single cell cultures. Two cell populations showed no endogenous human α-Gal A protein upon ABP labelling and subsequent immunoblotting with a specific human α-Gal A antibody (**Figure 7A**). Next, human α-Gal A and zebrafish α-Gal A enzymes were expressed in the established *GLA* knockout (KO) cells under the CMV promoter and at 37 °C. Expression of both α-Gal A enzymes restored activity towards the artificial substrate 4MU-α-Gal (**Figure 7B**). No hydrolysis of the fluorescent NBD-Gb3 lipid was detected in lysates of untransfected cells (#4 in **Figure 7C**), while expression of human α-Gal A restored hydrolysis of NBD-Gb3 into NBD-LacCer (**Figure 7C**). Interestingly, cell lysates containing zebrafish α-Gal A showed no formation of NBD-LacCer from NBD-Gb3, indicating that the fish enzyme is not able to hydrolyse the fluorescent Gb3 substrate, while at the same time its activity towards 4MU-α-Gal is high.

As final part of this study, corrections of the endogenous glycosphingolipids were studied in unmodified HEK293T (wildtype, WT), *GLA* KO cells and *GLA* KO cells transiently expressing human α-Gal A or zebrafish α-Gal A. Levels of Gb3 were increased in the *GLA* KO cells and Gb3 levels were corrected to WT levels in both the human α-Gal A expressing cells as well as the zebrafish α-Gal A expressing cells (**Figure 7D**). These pilot findings indicate that the zebrafish α-Gal A is able to hydrolyse the natural substrate Gb3 in the cellular conditions.

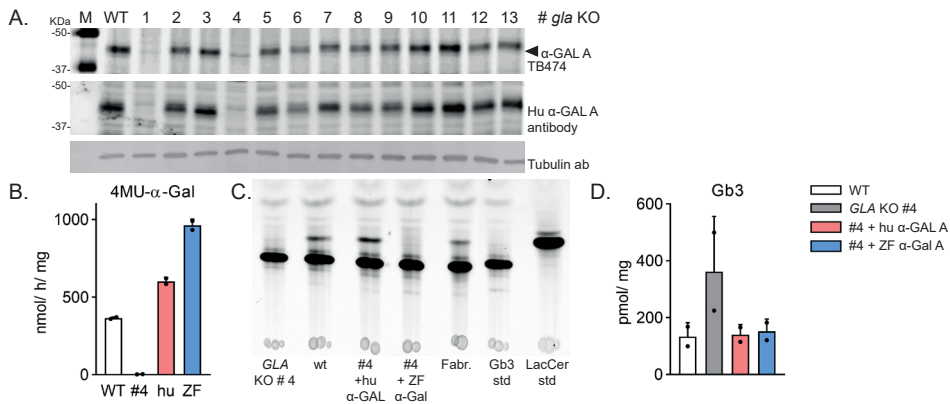


**Figure 7 | Catalytic features of human and zebrafish α-Gal A in *GLA* KO cells**

**(A)** Homogenates of unmodified HEK293T cells and various single cell populations after CRISPR/ Cas9 mediated mutagenesis in the *GLA* gene, were labelled with α-Gal configured ABP (top panel, TB474, 1μM) to visualize active enzyme, while all human α-Gal A protein was subsequently detected using an antibody (middle panel). α-tubulin was used as protein loading control (bottom panel). Cell populations # 1-2 were obtained using px335-sgRNA1+sgRNA2, #3-6 using px330-sgRNA1 and #7-13 using px330-sgRNA2. **(B)** Activity towards 4MU-α-Gal in homogenates of unmodified HEK293T cells and *GLA* KO cells as well as *GLA* KO cells expressing human α-Gal A or zebrafish α-Gal A. **(C)** Hydrolysis of NBD-Gb3 by the different cell homogenates and subsequent separation of NBD-lipids by HPTLC using CHCl<sub>3</sub>/MeOH/15 mM CaCl<sub>2</sub> (60/35/8 (v/v/v)). NBD-Gb3 and NBD-LacCer are used as standards. **(D)** Endogenous Gb3 levels in WT cells, *GLA* KO cells and *GLA* KO cells expressing human α-Gal A or zebrafish α-Gal A in pmol/mg. Lipids are measured from two independent transfections in technical duplicate.



## Discussion

The zebrafish is a popular research model to study genetic disorders such as lysosomal storage diseases. The CRISPR/Cas9 technology described in this thesis enables efficient generation of zebrafish disease models and is used in previous chapters to evaluate the impact of GBA2 or acid ceramidase defects in the zebrafish Gaucher disease model. A present challenge is to generate a zebrafish model of Fabry disease that is caused by deficiency of  $\alpha$ -galactosidase activity. The present study focused on evaluating the presence of endogenous GLA-like  $\alpha$ -galactosidase in zebrafish in order to establish whether a Fabry disease zebrafish model is feasible. One orthologue of human  $\alpha$ -GAL A and one orthologue of human  $\alpha$ -NAGAL was found using an *in silico* BLAST. The presence of zebrafish  $\alpha$ -Gal A and  $\alpha$ -Nagal was experimentally confirmed in zebrafish materials using  $\alpha$ -Gal configured ABPs. The two enzymes contain N-linked glycans and a very similar molecular weight using SDS-PAGE. Next, chemical proteomics was used to detect specific peptides of  $\alpha$ -Gal A and  $\alpha$ -Nagal to confirmed the presence of both proteins. In this manner both enzymes were detected at protein level in the zebrafish cells, while only  $\alpha$ -Gal A could be identified in the fish larvae. Specific mRNA transcripts of *gla* and *naga* were detected in developing zebrafish and various adult tissues as well as activity towards the artificial substrates 4MU- $\alpha$ -Gal and 4MU- $\alpha$ -GalNAc in these materials.

Although  $\alpha$ -Gal configured cyclophellitol aziridine inhibitors blocked the activities of  $\alpha$ -galactosidase enzymes in zebrafish cells and developing larvae, no accumulation of relevant glycosphingolipids, such as Gb3, was observed. In fact, Gb3 was not detectable in any of the measured zebrafish materials, including those with relatively high *gla* expression and activity towards 4MU- $\alpha$ -Gal. The apparent absence of the glycosphingolipid Gb3 in zebrafish materials, including larvae, brain, liver, kidney, testis and ovary, warrants discussion. Lactosylceramide 4- $\alpha$ -galactosyltransferase (A4GALT) is a member of the glucosyltransferase 32 (GT32) family and the enzyme mediating transfer of an  $\alpha$ -galactose moiety from UDP- $\alpha$ -D-galactose to  $\beta$ -D-galactosylceramide,  $\beta$ -D-galactosyl-1,4- $\beta$ -D-glucosylceramide (lactosylceramide)<sup>23,24</sup>. No protein orthologue of human A4GALT was found using a protein BLAST and no *a4galt* gene is annotated in the zebrafish genome. An orthologue of human A4GALT is also absent in other ray-finned fish species, such as *Oryzias latipes* (medaka) and salmon. Orthologues are present in *Drosophila melanogaster* and *Xenopus tropicalis* (**Supplementary Figure 7**). The only fish species with a known A4GALT orthologue is the coelacanth, the oldest living lineage of Sarcopterygii. The coelacanth is a translational species between fish and tetrapods being more related to lungfish and tetrapods than to ray-finned fish<sup>25</sup>.

A number of possible explanations can be considered for the presence of an  $\alpha$ -Gal A-like enzyme in zebrafish that apparently lack endogenous Gb3. Firstly, it may mediate intestinal degradation of exogenous oligosaccharides and glycosphingolipids from incoming food. Glycosphingolipid analysis of various food sources was inconclusive about the presence of Gb3. A lipid with similar LC-MS/MS parameters as Gb3 was detected, however the retention time was quite different (**Supplementary Figure 5B**).

Secondly, the enzyme might play a role in turnover of other types of molecules with an  $\alpha$ -galactosyl moiety such as polysaccharides composed of one or more  $\alpha$ -1,6-linked galactose moieties including plant-derived melibiose, raffinose and stachyose<sup>26</sup>. Nonetheless, these oligosaccharides are not hydrolysed by the intraluminal or intestinal enzymes of humans or other monogastric animal. Instead they are hydrolysed by  $\alpha$ -galactosidases of bacteria in the lower small intestine and colon, which produce gas and short-chain fatty acids, such as acetic, propionic and butyric acids<sup>27</sup>. Several publications report on the expression and characterization of  $\alpha$ -galactosidases from different sources, including bacteria<sup>28</sup>, microspora<sup>29</sup>, mushroom<sup>30</sup> and plants<sup>11</sup>, not only to treat Fabry disease but also for applications in the food and feed industry<sup>26</sup>. Limited information is available about the intraluminal and intestinal enzymes of digestive tract of zebrafish, only that their intestine consists of one long tube without a distinct stomach, small intestine or large intestine<sup>31</sup>. Finally, specific *gla* mRNA expression and  $\alpha$ -Gal A activity was high in the reproductive organs, liver and kidney of the zebrafish, corresponding to high RNA and protein expression in the same tissues of humans<sup>32</sup>. In contrast, the zebrafish intestine showed relatively low  $\alpha$ -Gal A activity.

Investigated were also other glycosyltransferase families able to transfer galactose using another glycosidic linkage besides the described  $\alpha$ -1,4-linkage mediated by A4GALT (GT32) and the  $\alpha$ -1,6-linkage of the raffinose family. In the GT6 family, several globoside  $\alpha$ -1,3-N-acetylgalactosaminyltransferases (Forssman synthase-like) are annotated in the zebrafish genome (Gbgt1l1 (Uniprot accession Q7ZTV7), Gbgt1l2 (B0ROW5), Gbgt1l3 (A2CED1), Gbgt1l4 (Q7SXD8)), and one possible  $\alpha$ -1,3-galactosyltransferase<sup>33</sup>. However, at present it is unknown whether this annotated ABO blood group transferase (transferase A,  $\alpha$ -1,3-N-acetylgalactosaminyltransferase; transferase B,  $\alpha$ -1,3-galactosyltransferase; Uniprot code B0S7I1) encodes a functional enzyme and whether active enzymes could have both A ( $\alpha$ -1,3-GalNAc) or B ( $\alpha$ -1,3-Gal) activity, depending on the sequence, as in humans<sup>3</sup>. Another member of the GT6 family is isogloboside 3 synthase (iGb3S, also called A3GALT), which is reported to transfer an  $\alpha$ -1,3-galactosyl moiety to LacCer, generating iGb3<sup>34</sup>. Even though orthologues of iGb3S are annotated in other fish, such as *Oryzias latipes*, no orthologue is documented in the zebrafish genome<sup>33</sup>.

Thus, the presence and role of  $\alpha$ -Gal A in zebrafish larvae and adult organs remains elusive. No Gb3 is detected using LC-MS/MS techniques nor an orthologue of A4GALT or iGb3S is found in the zebrafish. However, the presence and activity of  $\alpha$ -Gal A in zebrafish larvae and distinct adult organs could indicate towards an additional role of  $\alpha$ -Gal A besides the hydrolysis of Gb3,  $\alpha$ -1,4-galactosyl or  $\alpha$ -1,3-galactosyl modified glycoconjugates mediated by A4Galt or iGb3S respectively. On the other hand, the  $\alpha$ -Gal A enzyme could have been evolutionary pressured to be present and functional in order to hydrolyse  $\alpha$ -Gal containing lipids and proteins of non-endogenous invaders such as bacteria and viruses.

For future endeavours, a zebrafish knockout of *gla* might be useful to study clinical manifestation in the absence of the well-known substrate Gb3 and thereby investigate potentially unknown roles of  $\alpha$ -Gal A. Only a few animal disease models for Fabry disease have been developed which are all limited to rodents. Male Fabry mice show a modest to large increase in Gb3 in different tissues, but display no renal complications, only mild myocardial alterations, no spontaneous vascular manifestation and decreased sensitivity to painful stimuli<sup>35-37</sup>. Fabry rats showed accumulation of  $\alpha$ -galactosyl glycosphingolipids in serum, dorsal root ganglia, kidney and heart tissue as well as renal tubule dysfunction, mitral valve thickening and neuropathic pain<sup>38,39</sup>.

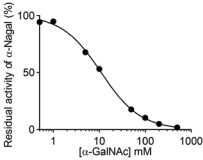
In addition, it would be of great interest to introduce the ability to synthesize the lipid Gb3 in zebrafish. This would allow investigation of the impact of Gb3 by itself as well as Gb3 accumulation during  $\alpha$ -Gal A deficiency. In view of this consideration, it was essential to confirm the ability of zebrafish  $\alpha$ -Gal A to hydrolyse the substrate Gb3. For this purpose, *GLA* KO HEK293T cells were generated using CRISPR/Cas9 technology and subsequent expression of zebrafish  $\alpha$ -Gal A in these cells enabled the study of its catalytic features. Interestingly, expression of zebrafish  $\alpha$ -Gal A in the established *GLA* KO cells showed a high *in vitro* activity towards 4MU- $\alpha$ -Gal, but no hydrolysis of the fluorescent NBD-Gb3 lipid was observed. When sensitive LC-MS/MS methods were used to quantify the endogenous Gb3 levels in the different cells, it became apparent that zebrafish  $\alpha$ -Gal A was able to correct the increased Gb3 levels of the *GLA* KO cells to WT levels similar to human  $\alpha$ -GAL A. These findings indicate that zebrafish  $\alpha$ -Gal A is able to hydrolyse endogenous Gb3 *in vivo*. Apparently, the NBD tagged Gb3 does not fit the active site of the zebrafish enzyme or the enzyme requires specific additives in order to be active towards lipid substrates *in vitro*.

In principle, it should be feasible to insert the human *A4GALT* gene in the zebrafish genome using the Tol2 transposon technique, as performed in chapter 4 for human *GBA*. It could be evaluated whether such transgenic fish produce Gb3 and whether their endogenous  $\alpha$ -Gal A is able to hydrolyse this *in vivo*. If successful, Gb3-producing Fabry zebrafish (*huA4GALT:gla* KO) could be generated and crossed with *asha1b* KO fish. In this manner Fabry fish could be generated that are unable to form lysoGb3 during  $\alpha$ -Gal A deficiency. In analogy to the study on GlcSph in chapter 6, meticulous comparison of Fabry zebrafish with excessive lysoGb3 and those without lysoGb3 will further clarify the postulated toxic action of lysoGb3 in Fabry disease.

## Acknowledgements

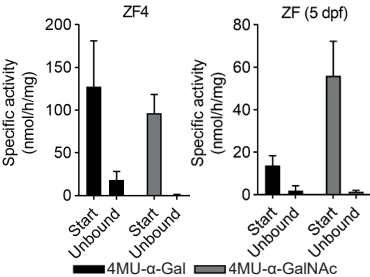
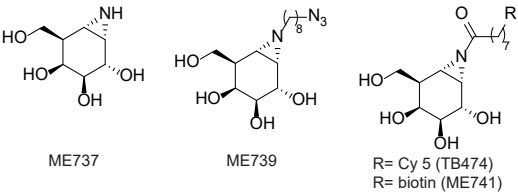
Kateryna Bila is kindly acknowledged for major contributions to the experimental data in this chapter. Kimberley Zwiers is acknowledged for her contribution on the alignments of zebrafish and human enzymes, Kassiani Kytidou for her input on generating the *GLA* KO cells by CRISPR/Cas9, Rolf Boot for the design of sgRNA sequences and Claire de Wit for her contribution on the characterization of the *GLA* KO HEK293T cells and transient expression of  $\alpha$ -GAL A.

Supplementary Figures



◀ **Supplementary Figure 1 | IC<sub>50</sub> curve of GalNAc (NAGA)**  
Homogenate of zebrafish larvae was incubated with a range of α-GalNAc concentrations (1-500 mM final concentration) and residual activity of α-Nagal was measured using the fluorogenic substrate 4MU-α-GalNAc in technical duplicate.

**Supplementary Figure 2 | Structures of used α-Gal configured inhibitors and ABP ▶**



◀ **Supplementary Figure 3 | Activity before and after ConA binding.**  
Activity towards 4MU-α-Gal and 4MU-α-GalNAc was measured of homogenate of zebrafish cells (ZF4) and 5 dpf zebrafish larvae (ZF) before Concanavalin A enrichment (Start) and of the unbound fraction. Activity was measured in technical duplicate.

**Supplementary Table 1 |** Detected peptide sequences with a score higher than 5.0 (PLGS software) or 25 (Mascot software). The “ ” indicates the position of trypsin digestion and the peptide sequence within the two “ ” is found. ND = not detected

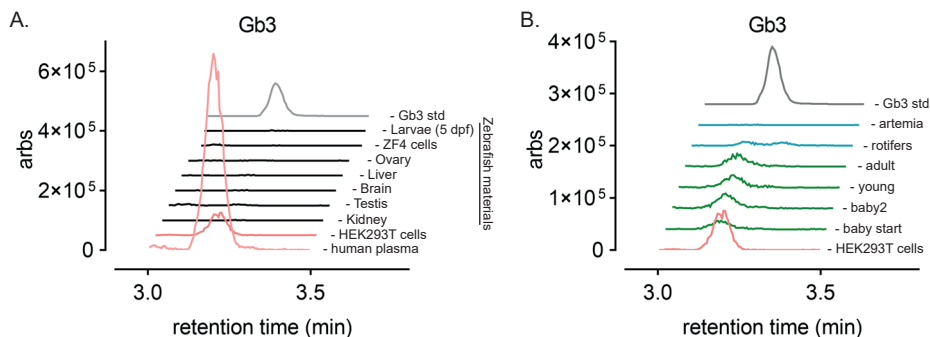
		Peptide sequence			Peptide sequence
ZF4 cells	α-Gal A: F1Q5G5	R.LAVAVMNR.Q	ZF4 cells	A-Nagal A: A0A0R4IJL2	R.LSEDGWK.E
		K.LADYVHSK.G			K.GASALVFFSR.R
		K.LGIYADVGTK.T			K.AVISNQDPLGIQGR.R
		K.KLADYVHSK.G			R.GIPHLAQYVHDR.G
		K.TFADWGVDLLK.F			
		K.QIIAINQDPLGK.Q			
		R.NYGDVYDQWTSVK.S			
		K.TCAGYPGSLGYDIDAK.T			
5 dpf ZF	α-Gal A: F1Q5G5	K.SILDWTAEK.Q	5 dpf ZF	A-Nagal A: A0A0R4IJL2	ND
		R.NYGDVYDQWTSVK.S			
		R.LAVAVMNR.Q			
		K.QIIAINQDPLGK.Q			
		K.SILDWTAEK.Q			
		K.LGIYADVGTK.T			

## Chapter 8

[illegible]

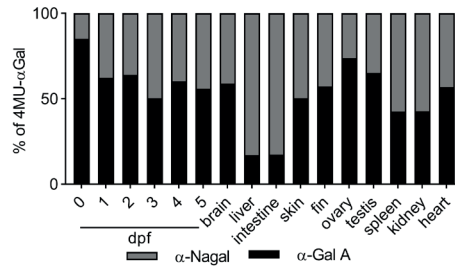
Supplementary Figure 4 | Alignment of zebrafish  $\alpha$ -Gal A with zebrafish  $\alpha$ -Nagal.

The amino acid sequences of the pro-protein of zebrafish  $\alpha$ -Gal A (Uniprot F1Q5G5) and zebrafish  $\alpha$ -Nagal (Uniprot A0A0R4JLJ2) were aligned using Clustal Omega<sup>20</sup>. \* indicates a conserved residue, ; a similar residue. The signal peptide is predicted using SignalP-5.0<sup>21</sup> and depicted in purple. The catalytic Asp residues are depicted in red, the cysteine residues forming disulfide bridges in orange and residues interacting and stabilizing the  $\alpha$ -galactose in blue. The Glu and Leu residues of  $\alpha$ -Gal A and Ser and Ala residues of  $\alpha$ -Nagal, which form specificity of the  $\alpha$ -galactose of N-acetylgalactosamine moiety are emphasized with #. Specific peptides sequences, obtained from PLGS or Mascot analysis after chemical proteomic, as described in the result section, are underlined in black for  $\alpha$ -Gal A and in red for  $\alpha$ -Nagal respectively.



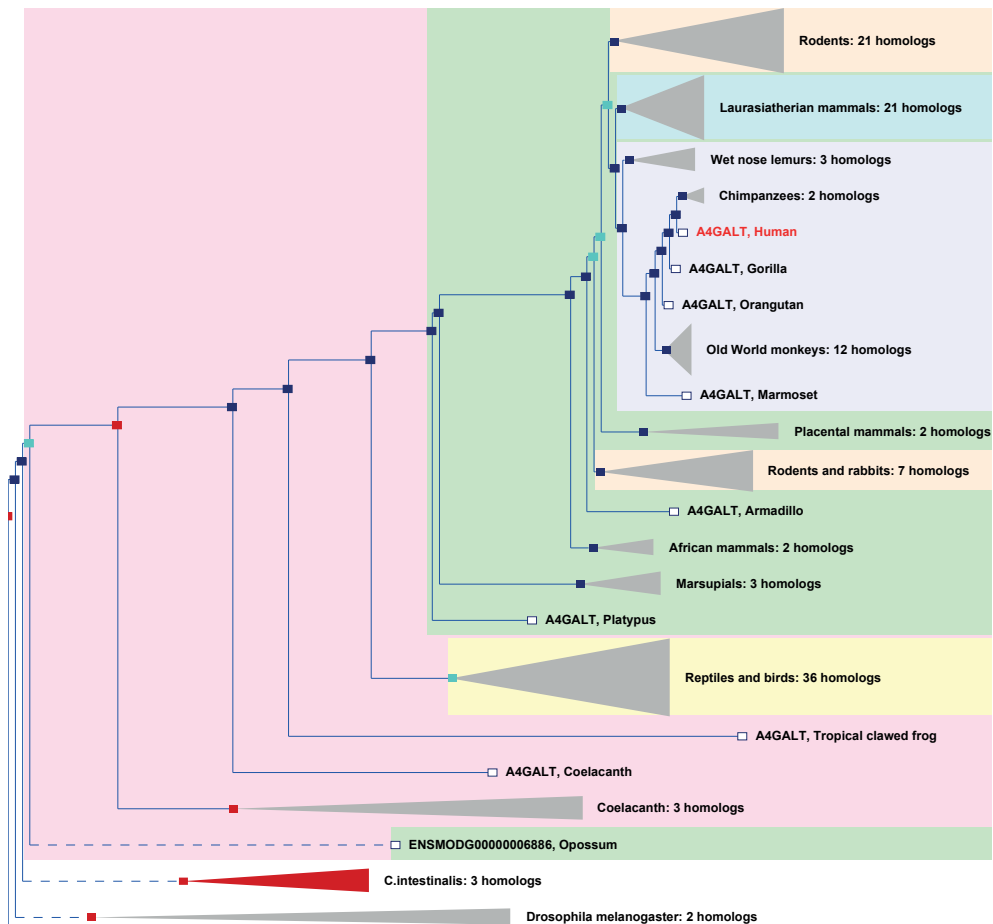
Supplementary Figure 5 | Detection of Gb3 in various samples using LC-MS/MS

**(A)** Glycosphingolipids were extracted of different human and zebrafish materials and the presence of deacylated Gb3 (784.4→282.3, parent→ daughter) was detected and visualized. Two human sources were used as controls (pink lines): 25  $\mu$ L human plasma and 20  $\mu$ g of HEK293T WT cell homogenate. Zebrafish homogenates were used of various samples (15  $\mu$ g protein): kidney, testis, brain, liver, ovary, zebrafish embryonic cells (ZF4) and 5 dpf zebrafish larvae (black lines). **(B)** Lipids of various food sources were also extracted and a peak with the correct parent/daughter was observed in manufactured, plant-based food (green lines), however it is unclear if this signal is actually Gb3. The signal of an extracted equivalent of Gb3 (4 pmol) was used as standard in both figures (grey line).



#### Supplementary Figure 6 | Specific activity of $\alpha$ -Gal A

The activity towards 4MU- $\alpha$ -Gal was measured of homogenates of zebrafish of different ages ( $t = 0$ -5 dpf) and various adult organ tissues with and without the presence of 500 mM  $\alpha$ -GalNac to inhibit the endogenous  $\alpha$ -Nagal enzyme. The hydrolytic activity of  $\alpha$ -Nagal towards 4MU- $\alpha$ -Gal was determined and depicted as ratio of the total activity towards 4MU- $\alpha$ -Gal. The specific  $\alpha$ -Gal A activity was determined as the residual activity towards 4MU- $\alpha$ -Gal with 500 mM  $\alpha$ -GalNac inhibitor and subsequently used in Figure 6B.



#### Supplementary Figure 7 | Gene tree of A4GALT

Phylogenetic (gene) tree displaying annotated orthologues of human A4GALT. No ray-finned fish species are depicted in this gene tree. Figure is obtained and exported from Ensembl.



## Experimental procedures

**Chemicals and reagents** - The  $\alpha$ -Gal specific inhibitors (ME737 and ME739), ABPs (TB474 and ME741) and C17-dihydroceramide were synthesized at Leiden University (the Netherlands) as reported<sup>16,40</sup>. Chemicals were obtained from Sigma-Aldrich (St. Louis, MO, USA) if not otherwise indicated. LC-MS grade methanol, 2-propanol, water, formic acid and HPLC grade chloroform were purchased from Biosolve (Valkenswaard, the Netherlands). Butanol and hydrochloric acid were obtained from Merck Millipore (Billerica, USA). 4-Methylumbelliferyl 2-acetamido-2-deoxy- $\alpha$ -D-galactopyranoside (4MU- $\alpha$ -GalNAc) was purchased from Carbosynth (Compton, UK), N-Dodecanoyl-NBD-ceramide trihexoside (NBD-C12-Gb3) from Matreya (State college, USA) and C12-NBD Lactosyl Ceramide from Avanti. Primers were ordered from Integrated DNA technologies (IDT; Coralville, USA) without additional purification.

**Zebrafish husbandry and samples** - Wild-type (WT) zebrafish (ABTL) were a mixed lineage of WT AB and WT TL genetic background. Zebrafish were housed and maintained at Leiden University (the Netherlands) according to standard protocols. The breeding of fish lines was approved by the local animal welfare committee (Instantie voor Dierwelzijn) of Leiden University and followed the international guidelines specified by the EU animal Protection Directive 2010/63/EU. Experiments using embryos and larvae were performed before the free-feeding stage, not falling under animal experimentation law according the EU animal Protection Directive 2010/63/EU. Embryos and larvae were grown in egg water (60  $\mu$ g/mL Instant Ocean Sera Marin<sup>TM</sup> aquarium salts (Sera; Heinsberg, Germany)). No adult zebrafish were used for experimentation and organs used in experiments were only obtained from defined old and excess WT zebrafish (> 1.5 years). Animal caretakers killed the WT zebrafish according to in-house protocols, after which organs were dissected from the dead zebrafish. Organs were snap frozen for protein analysis or stored in RNAlater (Invitrogen, ThermoFisher Scientific, Waltham USA) for RT-qPCR analysis and stored at -80 °C.

**Cloning** - Design of cloning primers and single-guide RNA sequences (sgRNA) were based on NCBI sequences NM\_000169 for human *GLA* and NM\_001006103 for zebrafish *gla*. The coding regions were amplified using Phusion HighFidelity PCR mastermix (Thermo Fisher Scientific, Waltham, USA) with cDNA as template (in-house human cDNA library or cDNA from extracted 5 dpf zebrafish larvae) using the primers given in **Supplementary Table 2**. Fragments of human and zebrafish *GLA* were cloned into the pDONR vector using GATEWAY<sup>TM</sup> recombination cloning technology (BP reaction, Thermo Fisher) according to the manufacturer's protocol and sequenced before shuttling the *GLA* fragments to the pDEST-zeo expression vector (derived by replacing the neomycin selection marker in the pDEST vector with a zeomycin selection marker) using the LR reaction. Several pDONR constructs were sequenced with the zebrafish *gla* insert and the insert with the least amount of mutations compared to NM\_001006103 was used (**Supplementary Figure 8**). For CRISPR/Cas9 mediated *GLA* targeting in HEK293T cells, sgRNA sequences, given in **Supplementary Table 2**, were cloned into the BbsI restriction site of the px330-U6-chimeric\_BB-CB-hSpCas9 vector (Addgene plasmid #42230) or the px335-U6-Chimeric\_BB-CBh-hSpCas9n vector (Addgene #42335) for SpCas9 nickase expression. All plasmids were isolated from transformed DH5 $\alpha$  cells using a plasmid isolation kit (Qiaprep spin Miniprep kit; Qiagen, Hilden, Germany) and sequenced using Sanger sequencing (Macrogen, Leiden, The Netherlands).

**Supplementary Table 2 |** List of oligonucleotide sequences.

Primer	Sequence (5' -3')	Purpose
Hu <i>GLA</i> sgRNA1 F	caccgTTGTCCAGTGTCTAGCCCC	sgRNA: px330/335
Hu <i>GLA</i> sgRNA1 R	aaacGGGGCTAGAGCACTGGACAAC	sgRNA: px330/335
Hu <i>GLA</i> sgRNA2 F	caccgTTGGCAAGGACGCTACCAT	sgRNA: px330/335
Hu <i>GLA</i> sgRNA2 R	aaacATGGTAGGCGTCCTTGCCAAc	sgRNA: px330/335
Human <i>GLA</i> F	GGGGACAAGTTTGTACAAAAAGCAGGCTACCACCATGCAGCTGAGGAACCCAGA	Gateway cloning
Human <i>GLA</i> R	GGGGACCACTTTGTACAGAAAGCTGGGTCTTAAAGTAAGTCTTTTAAATGACATC	Gateway cloning
Zebrafish <i>gla</i> F	ggggacaagtttgtacaaaaagcaggcttcaccaccATGCGTGCCTCAATTATAGTC	Gateway cloning
Zebrafish <i>gla</i> R	ggggaccacttttgtacaagaaagctgggtcCAGTGGGTGACGGTGAGTAG	Gateway cloning

**Cell culture and transfection** - Zebrafish embryonic fibroblasts (ZF4 cells<sup>41</sup>) were cultured at 28 °C and 5% CO<sub>2</sub> in DMEM/F12 medium, supplied with 10% (v/v) Fetal Calf Serum, 0.1% (w/v) penicillin/streptomycin, and 1% (v/v) Glutamax. HEK293T cells were cultured at 37 °C and 5% CO<sub>2</sub> in DMEM medium, supplied with 10% (v/v) FCS, 0.1% (w/v) penicillin/streptomycin and 1% (v/v) Glutamax. HEK293T *GLA* KO Cells were obtained by transfecting HEK293T cells seed in 6-well plates with the px330-*GLA* construct (px330-*GLA*-sgRNA1 or px330-*GLA*-sgRNA2) or both px335-*GLA* constructs (sgRNA1+sgRNA2) in combination with PEI (PEI/DNA, 3/1 (w/w)). After 72 hours, cells were diluted to approximately 0.5 cell/ well, seeded in 96-well plates and individual clones were cultured over the next weeks. Activity towards 4MU-α-Gal was determined as well as ABP labelling as described in the result section and the two clones (#1 and #4) without residual activity and ABP-labelled protein were maintained. *GLA* KO clone 4 was used for subsequent experiments and further mentioned as *GLA* KO cells. *GLA* KO cells were transfected using PEI and the pDEST-zeo-*GLA* construct (PEI/DNA, 3/1 (w/w)) and incubated for 72 hours before harvesting. In general, HEK293T cells were harvested by pipetting in PBS, while ZF4 cells were harvested using trypsin (0.25% (v/v) trypsin in PBS, no EDTA). Cell pellets were washed twice with PBS and stored at -80 °C until use.

**Homogenate preparation** - Cell homogenates were prepared in potassium phosphate (Kpi lysis buffer, supplemented with Triton-X100 and benzonase (25 mM K<sub>2</sub>HPO<sub>4</sub>-KH<sub>2</sub>PO<sub>4</sub>, pH 6.5, 0.1% (v/v) Triton-X100 and 25 U/mL benzonase) and lysed using sonication (20% amplitude, 3s on, 3s off for 4cycles) while on ice. Whole zebrafish embryos or larvae or zebrafish organs were resuspended in Kpi lysis buffer (12.5 µL/embryo, 100 µL for small organs (spleen, kidney, heart, fin) or 200-400 µL for larger organs (brain, liver, intestine, skin), supplemented with 0.1% Triton-X100 and EDTA-free protease inhibitor (25 mM K<sub>2</sub>HPO<sub>4</sub>-KH<sub>2</sub>PO<sub>4</sub>, pH 6.5, 0.1% (v/v) Triton-X100 an 1x cComplete™, EDTA-free Protease Inhibitor Cocktail, Roche, Basel, Switzerland). Embryos and organs were first homogenized using a Dounce homogenizer (10 strokes), followed by sonication as described. Total protein concentration of homogenates was determined using Pierce™ BCA protein assay kit (ThermoFisher Scientific) and measured using an EMax® plus microplate reader (Molecular Devices, Sunnyvale, USA). Homogenates of organs were stored at -80 °C, homogenates with a protein concentration higher than 5 mg/mL were diluted with KPi lysis buffer and stored in aliquots.

### Enzyme activity assay

**General assay procedures** - Generally assays were performed using homogenate in KPi (12.5 uL, 12.5-50 µg total protein) by addition of McIlvaine (citric acid – Na<sub>2</sub>HPO<sub>4</sub>) buffer of the appropriate pH (12.5 uL; 150 mM McIlvaine pH4) and supplemented with a covalent inhibitor if mentioned, before addition of 4-methylumbelliferone (4MU-aglycone) mixes; 100 µL of 3.75 mM 4-MU α-D-galactopyranoside (4MU-α-Gal) substrate with 0.1% (w/v) Bovine Albumin Serum (BSA) or 100 µL of 1 mM 4-MU α-D-N-acetylgalactoside (4MU-α-GalNAc) substrate. Incubation was performed at 37 °C for 30 min for ZF4 cells and 60 min for zebrafish embryos or organs unless indicated otherwise and stopped by addition of glycine-NaOH STOP buffer (200 µL; 1 M Glycine-NaOH, pH 10.3). All activity assays were measured using a LS-55 (PerkinElmer, Waltham, USA; λ<sub>ex</sub> of 366 nm, λ<sub>em</sub> of 445nm) and calculated using a standard of 1 nmol 4MU.

## Chapter 8

$\alpha$ -Nagal activity was blocked by addition of the sugar  $\alpha$ -N-acetyl-galactosaminide ( $\alpha$ -GalNAc; NAGA), with a final concentration of 200 mM in the assay (concentration in substrate mix: 250 mM NAGA). For the zebrafish embryo and larvae samples, a homogenate without substrate mix was included and used as blank to account for background fluorescent signal originating from the sample. All activities were measured using 3 independent homogenates measured in technical duplo unless indicated otherwise in the result section.

**pH curves** - PH curves were obtained by incubating homogenate (12.5  $\mu$ L,  $\pm$  12.5  $\mu$ g total protein) with Mcllvaine of the appropriate pH (62.5  $\mu$ L; 300 mM Mcllvaine, pH 2-8) on ice for 5 minutes before addition of two-times concentrated 4MU- $\alpha$ -Gal or 4MU- $\alpha$ -GalNAc substrate mix (50  $\mu$ L; 7,5 mM 4MU- $\alpha$ -Gal or 2 mM 4MU- $\alpha$ -GalNAc, 0.2% (w/v) BSA in MilliQ).

**IC<sub>50</sub> measurements** - For the covalent  $\alpha$ -Gal configured inhibitors, homogenate (12.5  $\mu$ L,  $\pm$  12.5  $\mu$ g total protein) was pre-incubated with the inhibitor (2x concentrated in 300mM Mcllvaine pH 4 with 1% (v/v) DMSO; final concentration of 0.5% (v/v) DMSO and 0.001- 100  $\mu$ M for ME737 and ME739, 0.0001- 50  $\mu$ M for TB474) for 1 h at 37 °C, before addition of 100  $\mu$ L 4MU- $\alpha$ -Gal or 4MU- $\alpha$ -GalNAc substrate mix and incubation as described in the general assay procedures. IC<sub>50</sub> values were calculated using Graphpad Prism (v8.1.1, GraphPadsoftware, CA, USA).

### Activity-based probe (ABP) labelling and chemical proteomics

**General ABP labelling procedure** - Zebrafish cell, embryo or organ homogenate (10  $\mu$ L, xxx  $\mu$ g total protein) was labelled with the  $\alpha$ -Gal configured ABP TB474 (2  $\mu$ M TB474 in 10  $\mu$ L 300 mM Mcllvaine buffer pH 4, 1% (v/v) DMSO; final concentration of 1  $\mu$ M TB474 and 0.5% (v/v) DMSO) for 30 min at 37 °C. For the inhibitor experiment, zebrafish  $\alpha$ -Gal and Nagal were preblocked by incubating homogenate (10  $\mu$ L) with  $\alpha$ -Gal configured inhibitor ME737 (100  $\mu$ M in 10  $\mu$ L 300 mM Mcllvaine buffer pH 4, 1% (v/v) DMSO; final concentration of 50  $\mu$ M and 0.5% (v/v) DMSO) for 30 min at 37 °C before the addition of TB474 (3  $\mu$ M TB474 in 10  $\mu$ L 300 mM Mcllvaine buffer pH 4, 1% DMSO; final concentration of 1  $\mu$ M TB474 and 0.5% (v/v) DMSO). Proteins were denatured with 5x Laemmli sample buffer (25% (v/v) 1.25 M Tris-HCl pH 6.8, 50% (v/v) 100% glycerol, 10% (w/v) sodium dodecyl sulfate (SDS), 8% (w/v) dithiothreitol (DTT); and 0.1% (w/v) bromophenol blue) and boiled for 5 min at 98 °C. ABP-labelled protein samples were separated by electrophoreses on 10% (w/v) SDS-PAGE gels, before scanning the fluorescence of the wet-slab gel with a Typhoon FLA 9500 (GE Healthcare, Chicago, USA; Cy5 ( $\lambda_{ex}$  of 635 nm,  $\lambda_{em}$  of 665 nm), 750 V, pixel size 100  $\mu$ m). Gels were stained with Coomassie Brilliant Blue staining (CBB-G250) and scanned on a ChemiDoc™ MP imager (Bio-Rad; Hercules, USA). For western blotting, proteins were transferred to a nitrocellulose membrane (0.2  $\mu$ M, Bio-Rad) using the Trans-blot® Turbo™ Transfer system (Bio-Rad). Membranes were blocked with 5% (w/v) bovine albumin serum (BSA) and incubated overnight at 4 °C with primary antibodies: mouse anti-human  $\alpha$ -tubulin (1:10.000; clone DM1A) or rabbit anti- $\alpha$ -Gal A (1:1000; Abnova, Taipei, Taiwan). Membranes were washed 3 times with TBST and incubated with 1 h at RT with complementary secondary antibodies: donkey anti-mouse Alexa 488 (1:10.000; Invitrogen) or GARPO goat anti rabbit IgG (H+L) peroxidase (1:5000, Bio-Rad). Fluorescent signal was detected using a Typhoon, while chemiluminescence signal was detected using a ChemiDoc MP imager.

**Deglycosylation using PNGase F** - Glycoproteins were deglycosylated using PNGase F (New England Biolabs, Ipswich, USA) according to the manufacturer's instructions. Briefly, zebrafish cell and larvae homogenate was labelled with TB474, as described above, in 2x volumes (40  $\mu$ L final volume). After incubation for 30 min at 37 °C, the mixture was denatured using Glycoprotein buffer (supplied) and boiled for 10 min at 98 °C. The sample was divided, NP-40 (supplied) and MQ was added to both samples NP-40 and one 20  $\mu$ L sample was incubated with PNGase F, while the other 20  $\mu$ L sample was incubated with MQ for 1 h at 37 °C. Laemmli sample buffer (5x) was added after incubation and the samples were separated on a 10% (w/v) SDS-PAGE gel and scanned as described above.

**Chemical proteomics** - ZF4 cell and zebrafish 5 dpf embryos homogenate (125  $\mu$ L; 125  $\mu$ g total protein) was incubated with biotin-ABP ME741 (5  $\mu$ M ME741 in 150 mM Mcllvaine buffer pH 4; final DMSO concentration of 0.5% and final volume 250  $\mu$ L) for 2 h at 37 °C. The labelling was stopped by addition of 20  $\mu$ L 20% (w/v) SDS and subsequent boiling of the sample at 95 °C for 5 min. Proteins were precipitated by chloroform/methanol, proteins were rehydrated in 2% (w/v) SDS in PBS followed by reduction using DTT (final concentration of 5 mM DTT in MQ) for 30 min at 45 °C and alkylation using iodacetamide (final concentration of 15 mM in MQ) for 30 min at RT in dark. Another chloroform/methanol precipitation was performed, proteins were rehydrated in 2% (w/v) in PBS buffer and ABP-bound proteins were enriched by incubation with paramagnetic avidin beads (Dynabeads™ MyOne™ Strptavidin T1, Thermo Fisher Scientific) at 4 °C overnight. Beads were washed with 0.1% (w/v) SDS in PBS, 2x with PBS, 1x with 4 M urea in 50 mM  $\text{NH}_4\text{HCO}_3$  followed by a wash with PBS and 2x MQ. On-bead tryptic digestion was performed by incubating the beads in trypsin digestion buffer (100  $\mu$ L, 2.5 ng/ $\mu$ L trypsin in 50 mM  $\text{NH}_4\text{NO}_3$ , pH 8 with 2% (v/v) CAN and 1 mM  $\text{CaCl}_2$ ) overnight at 37 °C with shaking. Prior to LC-MS analysis, peptides were desalted by StageTips prepared using Empore™ C18 47-mm extraction discs<sup>42</sup>. Samples were analysed on a Synapt G2Si mass spectrometer (Waters, Milford, USA) operating with Masslynx for acquisition as previously described<sup>43</sup>, proteins were identified using the *Danio rerio* proteome (Uniprot code UP000000437) and either Mascot software or ProteinLynx Global Server (PLGS) was used for peptide identification.

**Concanavalin A lectin binding** - Concanavalin A-Sepharose 4B beads (ConA beads; Sigma) were first washed three times in 0.1 M sodium acetate, 0.1 M NaCl, 1 mM  $\text{MgCl}_2$ , 1 mM  $\text{CaCl}_2$ , 1 mM  $\text{MnCl}_2$ , pH 6.0, washing buffer using brief centrifugation at 2000 rpm for 2 min. Next, 100  $\mu$ L of beads were mixed with 100  $\mu$ L of 4 mg/ml zebrafish or cells lysate. The samples were incubated overnight at 4 °C while rotating. Afterwards, the mixture was centrifuged at 13000 rpm at 4 °C for 10 min. The supernatant was collected, the beads were washed three times with washing buffer and the beads were stored in 100  $\mu$ L wash buffer. Four fractions were collected: sample prior to ConA beads incubation ('start'), supernatant after incubation with the beads ('unbound'), supernatant after the third wash ('wash') and beads pellet ('ConA bound'). Afterwards, the fractions were labelled with ABP TB474 and enzyme activity towards 4MU- $\alpha$ -GAL and 4MU- $\alpha$ -GalNAc was measured as described in the general assay procedures. The protein concentrations of the unbound, wash and ConA bound fraction were determined. Instead, the amount of sample for ABP labelling and enzyme activity was the same for the 4 fractions and the specific activity was calculated as nmol/mL sample or depicted as ratio of the start material.

**Treatment of cells or embryos with inhibitors** - ZF4 cells were transferred to 6-well plates and grown to 70-80% confluency before addition of 1mL fresh culture medium supplemented with vehicle (0.5% (v/v) DMSO) or inhibitor (0.001, 0.01, 1, 5 or 10  $\mu$ M of ME737 or ME739). Cells were incubated for 24 hours, washed three times with PBS before harvesting the well content on ice by addition of 100  $\mu$ L ice-cold KPi lysis buffer (25 mM KPi buffer pH 6.5, 0.1% (v/v) Triton X-100 and protease inhibitor) and scraping. The sample is collected, sonicated to obtain a homogenate sample and the total protein was determined using the BCA assay as described before. Using this procedure, the protein concentration of these *in situ* treated cell homogenates was between 1 and 2 mg/mL. Enzyme activity towards 4MU- $\alpha$ -Gal and 4MU- $\alpha$ -GalNAc was measured in technical replicate as described in the general assay procedures. Adult WT zebrafish were crossed and developing off-spring (8 h post-fertilization) was incubated in 100  $\mu$ L egg water immersed with vehicle (0.5% (v/v) DMSO) or inhibitor (20, 50 or 100  $\mu$ M ME737 or ME739 with 0.5% (v/v) DMSO) for 5 days at 28 °C. Larvae (5 dpf) were washed with egg water and stored in pools of 3 larvae for enzyme activity measurements and single larvae in 2 mL Safe-Lock Eppendorf tubes for glycosphingolipid analysis. Homogenate was prepared by addition of 60  $\mu$ L KPi lysis buffer, sonication and protein determination was performed as described before. Enzyme activity towards 4MU- $\alpha$ -Gal and 4MU- $\alpha$ -GalNAc was measured in technical replicate as described in the general assay procedures.

## Chapter 8

**Glycosphingolipid analysis** – The internal standard C17-dihydroceramide (20  $\mu$ L, 20 pmol/  $\mu$ L in MeOH) was added to homogenate (10  $\mu$ L, 20-50  $\mu$ g total protein in KPi lysis buffer) and neutral (glyco) sphingolipids were extracted using an acidic Bligh and Dyer procedure (1/1/0.9 chloroform/ methanol/ 100 mM formate buffer pH 3.1) as described before<sup>22,40</sup>. The lower phase was concentrated and lipids were deacylated using sodium hydroxide (0.5 M NaOH in MeOH) in combination with a microwave protocol described before<sup>44</sup>. Samples were neutralized, a butanol/water clean-up was performed and lipids were resuspended in methanol for separation as described before<sup>40</sup>.

**Hydrolytic activity towards NBD-Gb3** – NBD-C12-Gb3 was concentrated and resuspended in McIlvaine buffer (150 mM McIlvaine buffer pH 4.5, 0.05% (v/v) Triton X-100 and 0.05% (w/v) sodium taurocholate and MQ to a total volume of 60  $\mu$ L; 5  $\mu$ M NBD-C12-Gb3 final concentration) before addition of cell homogenate (40  $\mu$ L, 80  $\mu$ g total protein) or Fabrazyme (0.18 pmol in 40  $\mu$ L McIlvaine buffer pH 4.5 with 0.05% (v/v) Triton-X100 and 0.2% (w/v) sodium taurocholate). Samples were incubated for 3 h at 37°C and stopped by addition of MeOH,  $\text{CHCl}_3$  and MQ to a final ratio of 1/1/0.9 with subsequent Bligh and Dyer extraction. The lower phase was concentrated and lipids reconstituted in  $\text{CHCl}_3$ /MeOH (2/1) and separated by thin layer chromatography on a HPTLC silica gel 60 plate (VWR) using  $\text{CHCl}_3$ /MeOH/  $\text{CaCl}_2$  (60/35/8 (v/v) of  $\text{CHCl}_3$ /MeOH/15 mM  $\text{CaCl}_2$ ) as eluent. The HPTLC plate with NBD-lipids was scanned using a Typhoon imaging system (cy2 settings ( $\lambda_{\text{ex}}$  of 488 nm,  $\lambda_{\text{em}}$  of 515-535 nm), 250 V, pixel size 100  $\mu$ M).

**Gene expression analysis** - RNA of organs and zebrafish eggs or larvae (10 eggs or larvae per sample) was extracted using a Nucleospin RNA XS column (Machinery-Nagel, Düren, Germany) according to supplier's protocol, without the addition of carrier RNA. Contaminating DNA was degraded on column by a DNase I treatment (supplied in the kit). cDNA was synthesized using SuperScript™ II reverse transcriptase (Invitrogen, ThermoFisher Scientific, Waltham, USA) using oligo(dT) and an input of approximately 1000 ng total RNA according to the manufacturer's instruction. Generated cDNA was diluted to an approximate concentration of 0.5 ng total RNA input/ $\mu$ L with Milli-Q water. RT-qPCR reactions were performed with the IQ SYBR green mastermix (Bio-Rad) in a total volume of 15  $\mu$ L (1x SYBR green, 333  $\mu$ M of forward and reverse primer as given in **Supplementary Table 3** and 5  $\mu$ L of the diluted cDNA input) and carried out using a CFX96™ Real-Time PCR Detection system (Bio-Rad) with the following conditions: denaturation at 95 °C for 3 min, followed by 40 cycles of amplification (95 °C for 30 sec and 61 °C for 30 sec), imaging the plate after every extension at 61 °C, followed by a melt program from 55-95 °C with 0.5 °C per step with imaging the plate every step. All biological samples were tested in technical duplicate and gene expression was normalized to two house-keeping genes *ef1a* and *rpl13a* and depicted as  $\Delta\text{Ct}$  value.

**Supplementary Table 3 |** Forward and reverse primers for RT-qPCR analysis.

Target	Forward primer sequence (5'->3')	Reverse primer sequence (5'->3')	
<i>gla</i>	TCTGGGCAAACAGGGCTAT	GGGTTACGTTGCATTTTCGGG	188 bp
<i>naga</i>	TCGCTCCGTCTCCAGAATA	ATGGCATATCAGACCTGCGG	167 bp
<i>ef1a</i>	CTGGAGGCCAGCTCAAACAT	ATCAAGAAGAGTAGTACCGCTAGCATTAC	Ref. 45
<i>rpl13a</i>	TCTGGAGGACTGTAAGAGGTATGC	AGACGCACAATCTTGAGAGCAG	Ref. 45

```

ATG CGT GCC TCA ATT ATA GTC GTT ATC GGA CTT GTA TGT TTA TTA GTC CCA GCC
M  R  A  S  I  I  V  V  I  G  L  V  C  L  L  V  P  A
GCG GCG CTA GAC AAC GGC CTG GCT TTA ACT CCC ACC ATG GGC TGG CTG CAC TGG
A  A  L  D  N  G  L  A  L  T  P  T  M  G  W  L  H  W
GAG AGA TTC ATG TGC AAC ACA GAC TGT GAT GCG GAT CCT CAA AAC TGC ATT AGA
E  R  F  M  C  N  T  D  C  D  A  D  P  Q  N  C  I  R
GAG GAG CTC TTC ATG CAG ATG GCA GAT GTG ATG GTG AAG GAG GGA TGG AAG GAT
E  E  L  F  M  Q  M  A  D  V  M  V  K  E  G  W  K  D
GCT GGA TAT GAG TTT GTG TGC ATT GAT GAT TGC TGG CCT TCG CAA CAA AGG GAC
A  G  Y  E  F  V  C  I  D  D  C  W  P  S  Q  Q  R  D
GCA CAG GGG CGC CTG CAG GCA GAC CCC AAA AGG TTT CCC AGT GGC ATC AAA AAA
A  Q  G  R  L  Q  A  D  P  K  R  F  P  S  G  I  K  K
CTG GCA GAT TAT GTC CAT TCT AAA GGA CTG AAG CTG GGA ATA TAT GCA GAT GTG
L  A  D  Y  V  H  S  K  G  L  K  L  G  I  Y  A  D  V
GGC ACA AAA ACT TGT GCA GGT TAC CCT GGG AGT TTG GGC TAT TAT GAC ATC GAT
G  T  K  T  C  A  G  Y  P  G  S  L  G  Y  Y  D  I  D
GCA AAA ACC TTT GCG GAC TGG GGT GTG GAT CTG TTA AAA TTT GAG GGG TGT TTC
A  K  T  F  A  D  W  G  V  D  L  L  K  F  D  G  C  F
ATG CCT GAC TGG CAT CAG CTG GGA GAA GGT TAT ATA AAT ATG TCA AGT GCA CTA
M  P  D  W  H  Q  L  G  E  G  Y  I  N  M  S  S  A  L
AAC CAG ACT GGC AGA AGT ATT GTT TAC TCT TGT GAA TGG CCG TTA TAT GAG TGG
N  Q  T  G  R  S  I  V  Y  S  C  E  W  P  L  Y  E  W
CAG CAC CAA CAG CCT GAC TAT GAG GCA ATT CGC AAG ACC TGT AAC CAC TGG CGT
Q  H  Q  Q  P  D  Y  E  A  I  R  K  T  C  N  H  W  R
AAT TAT GGA GAT GTG TAT GAC CAG TGG ACC AGT GTG AAG AGC ATC CTG GAC TGG
N  Y  G  D  V  Y  D  Q  W  T  S  V  K  S  I  L  D  W
ACA GCA GAA AAG CAG AAG ATC GTC CCA GTG GCA GGA CCA GGA GGA TGG AAT
T  A  E  K  Q  K  I  V  P  P  V  A  G  P  G  G  W  N
GAC CCT GAC ATG CTG ATC ATT GGA AAC TTC GGC TTG AGT CGC GAT CAG CAG CAG
D  P  D  M  L  I  I  G  N  F  G  L  S  R  D  Q  Q  Q
ACT CAG ATG GCA TTG TGG GCA ATC ATG GCG GCT CCA CTT CTA ATG TCT AAC GAC
T  Q  M  A  L  W  A  I  M  A  A  P  L  L  M  S  N  D
CTG CGA GAC ATC TGT CCC AAA GAA GAA CTA CTG CAG AAC AAC CAG ATC ATC
L  R  D  I  C  P  K  A  K  E  L  L  Q  N  K  Q  I  I
GCC ATC AAC CAG GAC CCT CTG GGC AAA CAG GGC TAT CGG ATA TTG AAG GCT GAC
A  I  N  Q  D  P  L  G  K  Q  G  Y  R  I  L  K  A  D
AGT TTT GAG CTG TGG GAA AGG CCC TTG TCA GGC AAC AGG CTG GCC GTG GCA GTG
S  F  E  L  W  E  R  P  L  S  G  N  R  L  A  V  A  V
ATG AAC AGA CAG GAG ATT GGA GGT CCG CGC AGA TTT ACT ATT TCG GTG GCA ATA
M  N  R  Q  E  I  G  G  P  R  R  F  T  I  S  V  A  I
ATG CCT AGC TGG AAG CTT TGT AAC CCG AAA TGC AAC GTA ACC CAG ATC CTG CCC
M  P  S  W  K  L  C  N  P  K  C  N  V  T  Q  I  L/M P
ACT TAC AAG GAA ATG GGTTGTC CAA AAT CTC TTG TCA GAG GTG ATG GTC CAA GTC
T  Y  K  E  M  G  V  Q  N  L  L  S  E  V  M/v V  Q  V
AAC CCT ACA GGC ACA ACA CTA CTC ACC GTC AAC CCA CTG TGA < 1230
N  P  T  G  T  T  L  L  T  V  N  P  L  *

```

### Supplementary Figure 8 | zebrafish *gla* sequence

The zebrafish *gla* coding sequence is amplified using zebrafish cDNA as template and cloned into the pDONR vector as described in the experimental procedures. This sequence is obtained from Sanger sequencing of the resulting pDONR-*gla*. The obtained sequence showed genetic variations resulting in the same amino acid (depicted in orange) compared to the annotated gene (NCBI code NM\_001006103), but only one polymorphism resulting in an amino acid substitution (depicted in red, with the NCBI annotated amino acid given after the /).



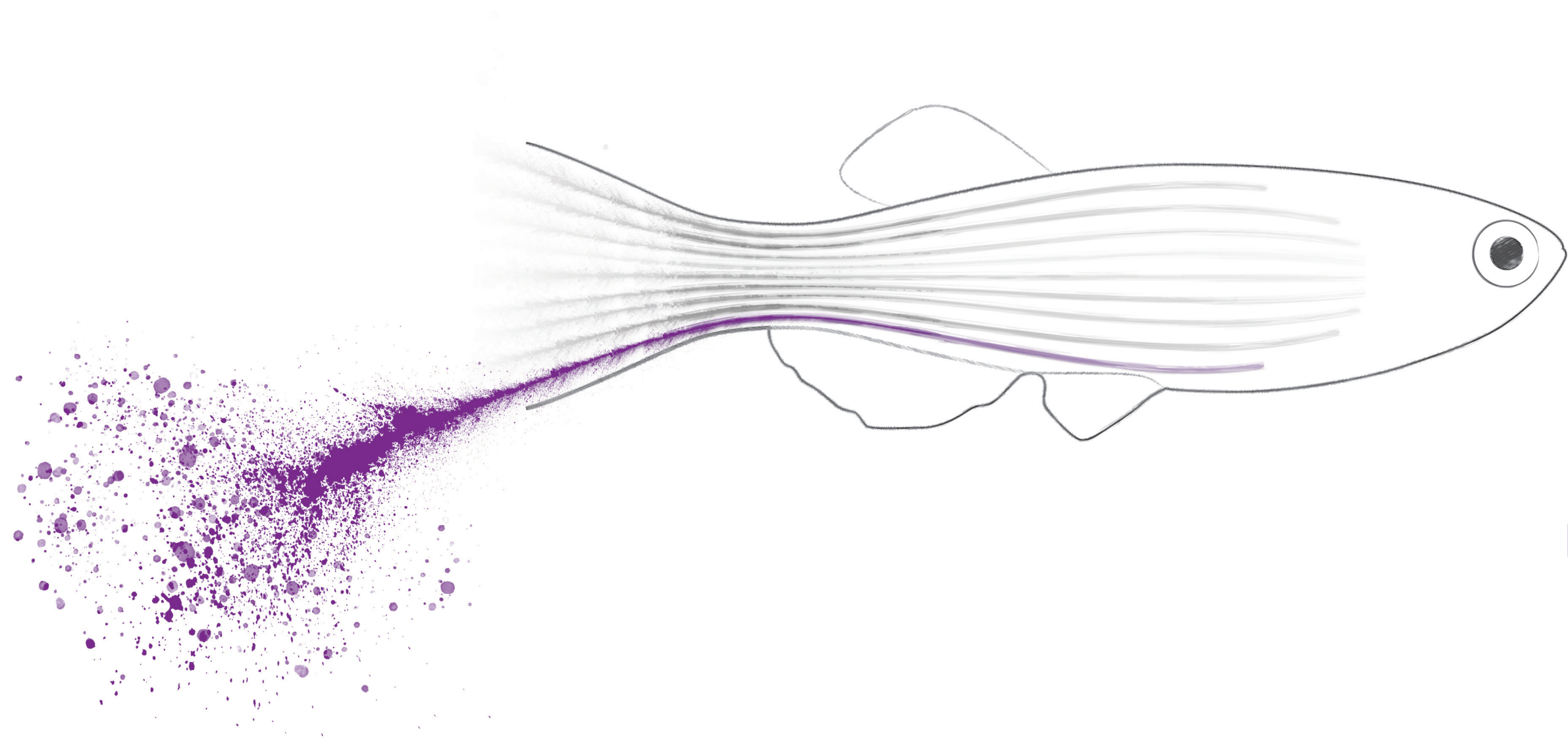
## References

1. Sweeley C.C. and Klionsky B. (1963) Fabry's Disease: Classification as a Sphingolipidosis and Partial Characterization of a Novel Glycolipid. *J Biol Chem* **238**, 3148-3150.
2. Desnick R.J., Ioannou Y. and Eng C.M. (2001)  $\alpha$ -Galactosidase A deficiency: Fabry disease. In *The metabolic and Molecular Bases of Inherited Disease*, C.R. Scriver, A.L. Beaudet, W.S. Sly and D. Valle, eds. (New York: McGraw-Hill), pp. 3733-3744.
3. Yamamoto F. (2004) Review: ABO blood group system--ABH oligosaccharide antigens, anti-A and anti-B, A and B glycosyltransferases, and ABO genes. *Immunohematology* **20**, 3-22.
4. Gold H., Mirzaian M., Dekker N., Joao Ferraz M., Lugtenburg J., Codee J.D.,... and Poorthuis B.J. (2013) Quantification of globotriaosylsphingosine in plasma and urine of fabry patients by stable isotope ultraperformance liquid chromatography-tandem mass spectrometry. *Clin Chem* **59**, 547-556.
5. Aerts J.M., Ferraz M.J., Mirzaian M., Gaspar P., Oussoren S.V., Wisse P.,... and Marques A.R.A. (2017) Lysosomal Storage Diseases. For Better or Worse: Adapting to Defective Lysosomal Glycosphingolipid Breakdown. In *eLS*. (John Wiley & Sons, Ltd), pp. 1-13.
6. Ledvinova J., Poupetova H., Hanackova A., Pisacka M. and Elleder M. (1997) Blood group B glycosphingolipids in alpha-galactosidase deficiency (Fabry disease): influence of secretor status. *Biochimica et biophysica acta* **1345**, 180-187.
7. Witte M.D., Kallemeijn W.W., Aten J., Li K.Y., Strijland A., Donker-Koopman W.E.,... and Aerts J.M. (2010) Ultrasensitive in situ visualization of active glucocerebrosidase molecules. *Nature chemical biology* **6**, 907-913.
8. Willems L.I., Beenakker T.J., Murray B., Scheij S., Kallemeijn W.W., Boot R.G.,... and Overkleeft H.S. (2014) Potent and selective activity-based probes for GH27 human retaining alpha-galactosidases. *Journal of the American Chemical Society* **136**, 11622-11625.
9. Marques A.R., Willems L.I., Herrera Moro D., Florea B.I., Scheij S., Ottenhoff R.,... and Aerts J.M. (2017) A Specific Activity-Based Probe to Monitor Family GH59 Galactosylceramidase, the Enzyme Deficient in Krabbe Disease. *Chembiochem* **18**, 402-412.
10. Kuo C.L., van Meel E., Kytidou K., Kallemeijn W.W., Witte M., Overkleeft H.S.,... and Aerts J.M. (2018) Activity-Based Probes for Glycosidases: Profiling and Other Applications. *Methods Enzymol* **598**, 217-235.
11. Kytidou K., Beekwilder J., Artola M., van Meel E., Wilbers R.H.P., Moolenaar G.F.,... and Aerts J. (2018) Nicotiana benthamiana alpha-galactosidase A1.1 can functionally complement human alpha-galactosidase A deficiency associated with Fabry disease. *J Biol Chem* **293**, 10042-10058.
12. Wang A.M. and Desnick R.J. (1991) Structural organization and complete sequence of the human alpha-N-acetylgalactosaminidase gene: homology with the alpha-galactosidase A gene provides evidence for evolution from a common ancestral gene. *Genomics* **10**, 133-142.
13. Schindler D., Bishop D.F., Wolfe D.E., Wang A.M., Egge H., Lemieux R.U. and Desnick R.J. (1989) Neuroaxonal dystrophy due to lysosomal alpha-N-acetylgalactosaminidase deficiency. *N Engl J Med* **320**, 1735-1740.
14. Vandiggelen O.P., Schindler D., Kleijer W.J., Huijman J.M.G., Galjaard H., Linden H.U.,... and Cantz M. (1987) Lysosomal Alpha-N-Acetylgalactosaminidase Deficiency-a New Inherited Metabolic Disease. *Lancet* **2**, 804-804.
15. Garman S.C. and Garboczi D.N. (2004) The molecular defect leading to Fabry disease: structure of human alpha-galactosidase. *J Mol Biol* **337**, 319-335.
16. Kytidou K., Beenakker T.J.M., Westerhof L.B., Hokke C.H., Moolenaar G.F., Goosen N.,... and Aerts J. (2017) Human Alpha Galactosidases Transiently Produced in Nicotiana benthamiana Leaves: New Insights in Substrate Specificities with Relevance for Fabry Disease. *Front Plant Sci* **8**, 1026.
17. Tajima Y., Kawashima I., Tsukimura T., Sugawara K., Kuroda M., Suzuki T.,... and Sakuraba H. (2009) Use of a modified alpha-N-acetylgalactosaminidase in the development of enzyme replacement therapy for Fabry disease. *Am J Hum Genet* **85**, 569-580.
18. Tamasic I.B., Metcalf M.C., Guce A.I., Clark N.E. and Garman S.C. (2010) Interconversion of the specificities of human lysosomal enzymes associated with Fabry and Schindler diseases. *J Biol Chem* **285**, 21560-21566.
19. Eng C.M., Guffon N., Wilcox W.R., Germain D.P., Lee P., Waldek S.,... and International Collaborative Fabry Disease Study G. (2001) Safety and efficacy of recombinant human alpha-galactosidase A replacement therapy in Fabry's disease. *N Engl J Med* **345**, 9-16.
20. Madeira F., Park Y.M., Lee J., Buso N., Gur T., Madhusoodanan N.,... and Lopez R. (2019) The EMBL-EBI search and sequence analysis tools APIs in 2019. *Nucleic acids research* **47**, W636-W641.
21. Almagro Armenteros J.J., Tsirigos K.D., Sonderby C.K., Petersen T.N., Winther O., Brunak S.,... and Nielsen H. (2019) SignalP 5.0 improves signal peptide predictions using deep neural networks. *Nat Biotechnol* **37**, 420-423.
22. Lelieveld L.T., Mirzaian M., Kuo C.L., Artola M., Ferraz M.J., Peter R.E.A.,... and Aerts J. (2019) Role of beta-glucosidase 2 in aberrant glycosphingolipid metabolism: model of glucocerebrosidase deficiency in zebrafish. *J Lipid Res* **60**, 1851-1867.

23. Kojima Y., Fukumoto S., Furukawa K., Okajima T., Wiels J., Yokoyama K.,... and Furukawa K. (2000) Molecular cloning of globotriaosylceramide/CD77 synthase, a glycosyltransferase that initiates the synthesis of globo series glycosphingolipids. *J Biol Chem* **275**, 15152-15156.
24. Keusch J.J., Manzella S.M., Nyame K.A., Cummings R.D. and Baenziger J.U. (2000) Cloning of Gb3 synthase, the key enzyme in globo-series glycosphingolipid synthesis, predicts a family of alpha 1, 4-glycosyltransferases conserved in plants, insects, and mammals. *J Biol Chem* **275**, 25315-25321.
25. Meyer A. and Scharl M. (1999) Gene and genome duplications in vertebrates: the one-to-four (-to-eight in fish) rule and the evolution of novel gene functions. *Curr Opin Cell Biol* **11**, 699-704.
26. Bhatia S., Singh A., Batra N. and Singh J. (2019) Microbial production and biotechnological applications of alpha-galactosidase. *Int J Biol Macromol*.
27. Gray G.M. (1975) Carbohydrate digestion and absorption. Role of the small intestine. *N Engl J Med* **292**, 1225-1230.
28. Huang Y., Zhang H., Ben P., Duan Y., Lu M., Li Z. and Cui Z. (2018) Characterization of a novel GH36 alpha-galactosidase from *Bacillus megaterium* and its application in degradation of raffinose family oligosaccharides. *Int J Biol Macromol* **108**, 98-104.
29. Yang D., Tian G., Du F., Zhao Y., Zhao L., Wang H. and Ng T.B. (2015) A Fungal Alpha-Galactosidase from *Pseudobalsamia microspora* Capable of Degrading Raffinose Family Oligosaccharides. *Appl Biochem Biotechnol* **176**, 2157-2169.
30. Xu L., Chen B., Geng X., Feng C., Meng J. and Chang M. (2019) A protease-resistant alpha-galactosidase characterized by relatively acid pH tolerance from the Shitake Mushroom *Lentinula edodes*. *Int J Biol Macromol* **128**, 324-330.
31. Menke A.L., Spitsbergen J.M., Wolterbeek A.P. and Woutersen R.A. (2011) Normal anatomy and histology of the adult zebrafish. *Toxicol Pathol* **39**, 759-775.
32. Uhlen M., Fagerberg L., Hallstrom B.M., Lindskog C., Oksvold P., Mardinoglu A.,... and Ponten F. (2015) Proteomics. Tissue-based map of the human proteome. *Science* **347**, 1260419.
33. Turcot-Dubois A.L., Le Moullac-Vaidye B., Despiau S., Roubinet F., Bovin N., Le Pendu J. and Blancher A. (2007) Long-term evolution of the CAZY glycosyltransferase 6 (ABO) gene family from fishes to mammals—a birth-and-death evolution model. *Glycobiology* **17**, 516-528.
34. Keusch J.J., Manzella S.M., Nyame K.A., Cummings R.D. and Baenziger J.U. (2000) Expression cloning of a new member of the ABO blood group glycosyltransferases, iGb3 synthase, that directs the synthesis of isoglybo-glycosphingolipids. *J Biol Chem* **275**, 25308-25314.
35. Ohshima T., Murray G.J., Swaim W.D., Longenecker G., Quirk J.M., Cardarelli C.O.,... and Kulkarni A.B. (1997) alpha-Galactosidase A deficient mice: a model of Fabry disease. *Proc Natl Acad Sci U S A* **94**, 2540-2544.
36. Nguyen Dinh Cat A., Escoubet B., Agrapart V., Griol-Charhbili V., Schoeb T., Feng W.,... and Jaisser F. (2012) Cardiomyopathy and response to enzyme replacement therapy in a male mouse model for Fabry disease. *PLoS one* **7**, e33743.
37. Rodrigues L.G., Ferraz M.J., Rodrigues D., Pais-Vieira M., Lima D., Brady R.O.,... and Sa-Miranda M.C. (2009) Neurophysiological, behavioral and morphological abnormalities in the Fabry knockout mice. *Neurobiol Dis* **33**, 48-56.
38. Miller J.J., Aoki K., Mascari C.A., Beltrame A.K., Sokumbi O., North P.E.,... and Dahms N.M. (2019) alpha-Galactosidase A-deficient rats accumulate glycosphingolipids and develop cardiorenal phenotypes of Fabry disease. *FASEB J* **33**, 418-429.
39. Miller J.J., Aoki K., Moehring F., Murphy C.A., O'Hara C.L., Tiemeyer M.,... and Dahms N.M. (2018) Neuropathic pain in a Fabry disease rat model. *JCI Insight* **3**.
40. Mirzaian M., Wisse P., Ferraz M.J., Marques A.R.A., Gaspar P., Oussoren S.V.,... and Aerts J.M. (2017) Simultaneous quantitation of sphingoid bases by UPLC-ESI-MS/MS with identical (13)C-encoded internal standards. *Clin Chim Acta* **466**, 178-184.
41. Driever W. and Rangini Z. (1993) Characterization of a cell line derived from zebrafish (*Brachydanio rerio*) embryos. *In Vitro Cell Dev Biol Anim* **29A**, 749-754.
42. Rappsilber J., Ishihama Y. and Mann M. (2003) Stop and go extraction tips for matrix-assisted laser desorption/ionization, nanoelectrospray, and LC/MS sample pretreatment in proteomics. *Anal Chem* **75**, 663-670.
43. van Rooden E.J., Florea B.I., Deng H., Baggelaar M.P., van Esbroeck A.C.M., Zhou J.,... and van der Stelt M. (2018) Mapping in vivo target interaction profiles of covalent inhibitors using chemical proteomics with label-free quantification. *Nat Protoc* **13**, 752-767.
44. Groener J.E., Poorthuis B.J., Kuiper S., Helmond M.T., Hollak C.E. and Aerts J.M. (2007) HPLC for simultaneous quantification of total ceramide, glucosylceramide, and ceramide trihexoside concentrations in plasma. *Clin Chem* **53**, 742-747.
45. Tang R., Dodd A., Lai D., McNabb W.C. and Love D.R. (2007) Validation of zebrafish (*Danio rerio*) reference genes for quantitative real-time RT-PCR normalization. *Acta Biochim Biophys Sin (Shanghai)* **39**, 384-390.

CHAPTER 9

General discussion  
&  
Future prospects



In this thesis, zebrafish are used as vertebrate model to study the lysosomal storage disorder Gaucher disease (GD). GD is characterized by mutations in the gene encoding glucocerebrosidase (GCase). Lysosomal GCase hydrolyses the glucosylceramide (GlcCer) as penultimate step in the catabolism of glycosphingolipids. Zebrafish are at first glance an appealing model organism to study GD disease since they produce the lipid GlcCer, their genome contains an orthologue of the human *GBA* gene and an active acid  $\beta$ -glucosidase is expressed. Zebrafish also express candidate modifier proteins, such as non-lysosomal Gba2 and lysosomal acid ceramidase (ACase).

**Zebrafish GCase** –To establish whether the highly homologous zebrafish GCase enzyme has similar enzymatic properties to its human counterpart, a detailed comparison of GCase enzymes was performed (chapter 2). For this purpose, GCase of zebrafish and humans was comparatively expressed in GCase-deficient HEK293T cells and examined regarding catalytic features. Both enzymes showed an acid pH optimum and a similar sensitivity for inhibitors. In addition, over-expression of both GCase enzymes corrected the increased levels of GlcCer and its deacylated sphingoid base, glucosylsphingosine (GlcSph), in the GCase-deficient HEK293T cells. Differences between the human and zebrafish GCase were also noted. Firstly, the human GCase enzyme required additives for optimal *in vitro* hydrolysis while no additives were necessary for zebrafish GCase activity. Secondly, the fish enzyme was equally active at 10 and 37 °C, whereas the human enzyme showed about three-fold higher activity at 37 °C. Lastly, the zebrafish enzyme was unable to transglucosylate, i.e. form glucosylated cholesterol (GlcChol) from GlcCer as sugar donor and with cholesterol as acceptor. A modest transglucosylation activity of zebrafish GCase was noted with ceramide as acceptor that is more flexible than the rigid cholesterol. Of note, zebrafish GCase, like human enzyme, is able to hydrolyse GlcChol, both *in vitro* (chapter 2) and *in vivo* (chapters 5 and 7).

**Evolutionary aspects and protein dynamics** – In the same investigation, GCase of turtle and frog were studied as well to reveal an evolutionary trend. Subtle differences in characteristics were noted for each of the enzymes when compared to human GCase. The ability to transglucosylate cholesterol was demonstrable for frog and turtle enzyme. Thus, the zebrafish is unique in its incapacity to position cholesterol as acceptor for transglucosylation. Taken together, it may be speculated that the fish GCase, over-expressed in mammalian cells, is more permanently present in an active status as compared to the other enzymes studied. Such more ‘rigid’ conformation of zebrafish GCase may as downside limit the enzyme’s ability to transfer glucose to structurally rigid acceptors like cholesterol. For human GCase, it has been proposed that specific side-chain conformations favour a more ordered region near the catalytic pocket and reduce unfolding at neutral pH<sup>1</sup>. In an acidic environment, GCase shows an increased half-life, higher melting temperature and lower sensitivity to tryptic digestion<sup>2</sup>. Binding of (semi-)covalent inhibitors increases the structural stability of recombinant GCase further<sup>2</sup>. *In silico* comparison of modelled structures of zebrafish and human GCases revealed divergent residues in the three loops surrounding the catalytic pocket. Site-directed mutagenesis of specific residues in loops of the zebrafish GCase did not change hydrolytic activity or ability to transglucosylate.

Swapping of loops among the GCases of different species might be more helpful in future experiments. Of interest will be future meticulous comparative investigations of GCases of various species regarding protein dynamics by means of measuring melting curves and performing deuterium exchange mass spectrometry<sup>2</sup>.

**Generation of double knockout zebrafish** – An enormous practical advantage of the zebrafish, compared to mice, is the speed and convenience with which new gene knockouts (KOs) can be generated and these KOs crossed with fish with other genetic traits. Chapter 4 provides a detailed protocol for the generation of gene KOs in zebrafish by means of CRISPR/Cas9 technology. Knockouts of *gba1*, *gba2*, *asah1a*, and *asah1b* have already been successfully established and are topics of the investigations described in chapters 5-7 of which the results are discussed below. Chapter 4 also describes generated mutations in the zebrafish *gpnmb*, *cln8* and *npc1* genes. Follow-up investigations with fish of these gene KOs are of interest as well as the combined KO with GCase deficiency.

**gpNMB** – The protein gpNMB is remarkably induced in plasma and Gaucher cells of GD patients as well as in GlcCer-laden macrophages of GD and NPC mice<sup>3,4</sup>. Exposing cultured RAW cells to stressors of lysosomes, e.g. HEPES, chloroquine or sucrose, leads to prominent increases in gpNMB<sup>5</sup>. Zebrafish with a GCase deficiency show a remarkable increase in the expression of *gpnmb* mRNA (chapter 6). The question remains whether the marked overexpression of this protein during lysosomal stress of macrophages serves a particular function. Crossing *gpnmb* KO fish, with or without a concurrent GCase deficiency, with fish expressing a fluorescent reporter in macrophages, under regulation of the *mpeg* promoter<sup>6</sup>, will allow an assessment of the impact of Gpnmb on macrophages. Moreover, careful examination of *gpnmb* KO fish regarding their sensitivity for infections should be considered.

**CLN8** – Appealing is a follow-up investigation on the role of CLN8 during GCase deficiency in zebrafish. CLN8 is an ER protein that is considered as modifier of clinical severity of GD. Its possible impact on disease severity was first indicated by a GWAS study involving more than a hundred type 1 GD patients homozygous for N370S mutation<sup>7</sup>. Several SNPs in the locus of the *CLN8* gene were associated with a more severe outcome of type 1 GD. Moreover, a higher expression of *CLN8* mRNA was observed in fibroblasts of mild GD patients compared to severe GD patients. Independently, the *Cln8* gene locus was linked to the variation in plasma GlcCer levels in inbred mouse sub-strains (Argmann, Aerts unpublished observations). More recently, it was reported that the CLN8 protein is involved in the ER-to-Golgi transfer of many newly formed soluble lysosomal enzymes, such as cathepsins<sup>8,9</sup>. Upon CLN8 deficiency, maturation of lysosomal enzymes was delayed and a reduction of several enzymes in the lysosome observed<sup>8</sup>. In chapter 4, *cln8* KO zebrafish larvae with concurrent GCase deficiency show a significant reduction in the accumulating GlcSph, warranting further investigation. Possibly, acid ceramidase is reduced but other explanations for the observation can't be excluded yet. It will of great interest to examine whether CLN8 modulates the clinical course of *gba1*<sup>-/-</sup> fish.



**NPC1** – Finally, the viability of *npc1* mutant fish opens possibilities for exciting novel research. There are indications for an intricate interplay between cholesterol and GSL metabolism. In Niemann Pick disease (NPC), the efflux of cholesterol from lysosomes is impaired, due to defects in either NPC1 or NPC2. In cholesterol-laden lysosomes of cells of NPC patients and NPC mouse models, secondary partial deficiencies in activities of sphingomyelinase (ASMase) and GCase cause accumulation of SM and GlcCer<sup>4,10</sup>. In NPC lysosomes, GlcChol is actively formed by GCase. Normally, GlcChol is synthesized in cells by the cytosol-faced enzyme GBA2 and degraded by GCase<sup>11</sup>. It has been reported that *npc1* KO zebrafish develop prominent accumulation of lysosomal cholesterol similar to NPC patients<sup>12,13</sup>. In the presented study, no glycosphingolipid abnormalities were detected in the generated *npc1* KO larvae up to 5 days post-fertilization (dpf) (chapter 4). In young larvae, compensatory maternal *Npc1* might be available or the burden of lysosomal cholesterol might yet not be high enough to induce secondary deficiencies of ASMase and GCase. Raising the *npc1* KO fish to adulthood will enable analysis of cholesterol and glycosphingolipid levels at adult age as well as close monitoring of the expected symptoms, such as hepatosplenomegaly, neuropathology and uncoordinated swimming<sup>12,13</sup>. In addition, analysis of *Npc1*-deficient, with and without concurrent GCase deficiency, will indicate whether they also start to accumulate GlcChol as occurs in NPC mice and patients<sup>11</sup>. If so, it could be attempted to prohibit formation of excessive GlcChol with potent iminosugar inhibitors of GBA2 and GlcCer synthase (GCS)<sup>14</sup>. Inhibition of GBA2 in NPC mice, either by pharmacological or genetic ablation, was earlier found to ameliorate disease manifestations and increase life span of the animals<sup>15,16</sup>. Likewise, the available *Gba2* KO fish could be used to test whether NPC disease can also be ameliorated by *Gba2* modulation in zebrafish. For this, the clinical course of *npc1*<sup>-/-</sup>:*gba2*<sup>+/+</sup>, *npc1*<sup>-/-</sup>:*gba2*<sup>-/-</sup> and *npc1*<sup>-/-</sup>:*gba2*<sup>-/-</sup> fish could be compared.

**ACase-deficient zebrafish** – The generated GCase deficient zebrafish have already been combined with deficiencies of two other enzymes (*Asah1b* and *Gba2*) and the outcome of these double KO has been investigated. Given the role of acid ceramidase (ACase) in formation of the presumed toxic GlcSph lyso-lipid in mouse and man<sup>17</sup>, it was decided to generate zebrafish lacking such enzyme and consequently being unable to generate GlcSph during GCase deficiency. In zebrafish the genes *asah1a* and *asah1b* encode two orthologues of human ACase. Only the enzyme encoded by the *asah1b* gene was found to be able to generate GlcSph during GCase deficiency, while *Asah1a* and *Asah1b* seem complementary regarding degradation of ceramide (chapter 6). Combined deficiency of the two enzymes is not viable, likely as the result of massive ceramide accumulation mimicking Farber disease, a devastating disorder in humans. It will be of interest to study the cause for the differences in substrate specificity of the two fish ACases, *Asah1a* and *Asah1b*, that is presently not understood. Substrate specificity might be caused by subtle difference in amino acid composition of *Asah1a* and *Asah1b*. On the other hand, expression of the two enzymes in cells accumulating GlcCer during GCase deficiency could differ, with *Asah1b* being present far more prominently in lysosomes of macrophages. Recently, highly specific ABPs for ACase were developed by Fabrias and colleagues<sup>18</sup>. These probes could assist studies on the cellular and subcellular distribution of *Asah1a* and *Asah1b*. The available *asha1a* and *asah1b* KO zebrafish will be helpful in such investigations.



**GCcase-deficient fish unable to produce excessive GlcSph** – *Gba1*<sup>-/-</sup>:*asah1b*<sup>-/-</sup> fish were successfully generated as a model of GCcase deficiency without concomitant GlcSph excess. The comparison of adult *gba1* KO fish, with excessive GlcSph, and adult *asah1b:gba1* KO zebrafish, without GlcSph, excites several topics for further discussion. Importantly, the *gba1:asah1b* KO fish developed a milder course of disease than *gba1* KO animals. This finding suggests that excessive GlcSph during GCcase deficiency is indeed toxic. Secondly, *gba1*- and *asah1b:gba1* KO zebrafish accumulate comparably GlcCer in tissues and develop similarly Gaucher-like storage cells. In their brains, the two mutant fish showed similar abnormal autophagy, indicated by increased protein levels of p62, similar inflammation, reflected by comparably increased mRNA levels of *il1-β*, *tnfβ* and *apoeb*, and indications for similar activation of the complement cascade. The infiltration of Gaucher-like storage cells, likely microglia, in the periventricular grey zone of the optic tectum also appeared comparable. Keatinge and colleagues earlier reported a reduction in dopaminergic neurons of *gba1* KO fish in the presence of ubiquitin-positive, intra-neuronal inclusions<sup>19</sup>. Own findings with *gba1*- and *gba1:asah1b* KO fish suggest that the presence of excessive GlcSph might accelerate dopaminergic neuron loss, by a presently unknown mechanism. It is noteworthy that the observed amelioration of disease in *asah1b:gba1* KO fish, lacking GlcSph, appears to be independent of storage cell burden, neuroinflammation and complement activation, commonly assumed major drivers of GD pathology<sup>20-24</sup>. In GD/PD mouse models and human neuronal cells, GlcSph has been found to trigger α-synuclein aggregation<sup>24,25</sup>. The zebrafish has no orthologue of human α-synuclein and only express a β-synuclein and two γ-synuclein orthologues<sup>26,27</sup>. In this respect zebrafish offer no simple copy of PD. Nevertheless, the available zebrafish that are able or unable to form GlcSph during GCcase deficiency can be exploited to investigate GlcSph driven neuropathology independent of α-synuclein. It should be noted that the *asah1b:gba1* KO fish lacking excessive GlcSph do develop symptoms at 4 months. Thus, it seems that GlcSph indeed contributes to the onset of neuropathology but is not the only toxic factor during GCcase deficiency and other pathological mechanisms are involved. In this respect, the impact of accumulating GlcCer and other glucosylated lipids deserves further attention.

It is tempting to consider inhibition of ACCase as therapeutic avenue for neuronopathic GD with present unmet need. The more specific ACCase inhibitors recently designed by Fabrias and colleagues could be tested in the now available zebrafish models of GCcase-deficiency<sup>18</sup>. The window for such intervention is likely narrow given the fact that a partial ACCase deficiency impairs spinal-cord motor neurons<sup>28</sup>.

Regarding toxicity of GlcSph, it has to be taken into consideration that present investigations only quantified GlcSph with a regular C18-sphingosine moiety. Several species of GlcSph with distinct sphingosine moieties do however occur<sup>29</sup>. For example, the regular C18-sphingosine containing GlcSph is the most prominent species in plasma of GD patients, while in their urine it is only a very minor species and hydroxylated sphingoid bases are common<sup>29</sup>. It will be of interest to study more closely specific GlcSph isoforms in brain of GCcase deficient zebrafish and to establish whether these contribute to severity of symptoms.

**Other glycosphingolipidoses** – The ACCase-mediated deacylation of accumulating glycosphingolipids in lysosomes to sphingolipid bases is not unique to GD<sup>30</sup>. ACCase also converts accumulating globotriaosylceramide (Gb3) in lysosomes of Fabry disease (FD) patients, having a defective  $\alpha$ -galactosidase A ( $\alpha$ -GAL A), into globotriaosylsphingosine (lysoGb3)<sup>17</sup>. At present many symptoms of FD patients are attributed to excessive lysoGb3, but caution is warranted since solid proof for the physiological relevance in patients is largely lacking<sup>31-34</sup>. In analogy to chapter 6, *asah1b* KO fish could be exploited to increase insight in the toxicity of lysoGb3. Chapter 8 reports the presence of an acid  $\alpha$ -galactosidase ( $\alpha$ -Gal A) and acid  $\alpha$ -N-acetylgalactosaminidase ( $\alpha$ -Nagal) in zebrafish cells, larvae and adult tissues. Zebrafish  $\alpha$ -Gal A, despite prominent homology with the human enzyme, seems unable to degrade fluorescent NBD-Gb3 *in vitro*, but shows correction of Gb3 accumulation *in situ*. Noteworthy, fish lack the enzyme responsible for the synthesis of Gb3 from lactosylceramide, Gb3 synthase (a.k.a. A4GALT). Consequently, the globo-series glycosphingolipids could not be detected in the investigated zebrafish materials. Introducing A4GALT should allow generation of the non-endogenous Gb3 in fish. Next, accumulation of lysoGb3 should be induced by  $\alpha$ -Gal A inactivation in fish expressing A4GALT and it should be prohibited in *asah1* KO fish expressing A4GALT. In this way, organismal models could be obtained allowing investigation of the toxicity of endogenous lysoGb3 *in vivo*.

The same approach as described above could be considered for other diseases in which ACCase generates sphingoid bases from accumulating sphingolipids in lysosomes<sup>30</sup>. Recently, Li and colleagues describe the amelioration of disease manifestations in a Krabbe mouse model by introducing ACCase deficiency, thereby lacking the ability to from galactosylsphingosine (GalSph) from accumulating galactosylceramide<sup>35</sup>. In contrast to the described AC deficient mice, *asah1b* KO zebrafish show no features of Farber disease until the relatively old age of 2 years. Other interesting LSDs in this respect are Sandhoff disease where lysoGM2 is formed from the ganglioside GM2<sup>36</sup> and acid sphingomyelinase deficiency, a.k.a. Niemann-Pick disease type A/B type (NP A/B), where lyso-sphingomyelin is formed from sphingomyelin<sup>37</sup>. Orthologues of the defective lysosomal hydrolases involved in these LSD are present in the zebrafish genome (**Table 1**), as well as most of the enzymes of glycosphingolipid synthesis (**Supplementary Table 1**).

**Table 1 |** Zebrafish orthologues of human lysosomal hydrolases defective in LSDs. The zebrafish gene is given, as well as the genomic location and Uniprot code of the encoded proteins.

	gene		Protein		gene		Protein
Gaucher disease	<i>gba</i>	Chr 16	E7EZM1	Tay-sachs disease/ Sandhoff disease	<i>hexa</i>	Chr 25	F1RDQ5
Krabbe disease	<i>galca</i>	Chr 20	Q5SNX7	Sandhoff disease	<i>hexb</i>	Chr 5	A2BHD8/ F1QUU0
	<i>galcb</i>	Chr 17	F1QYH2	NP type A/B	<i>smgd1</i>	Chr 10	F8W546
Fabry disease	<i>gla</i>	Chr 14	F1Q5G5	MLD	<i>arsa</i>	Chr 18	A5WV48
Schindler disease	<i>naga</i>	Chr 4	A0A0R4IIL2	GM1-gangliosidosis	<i>glb1</i>	chr 1	A2BG54
Farber disease	<i>asah1a</i>	Chr 14	Q5XJR7	Sialidosis	<i>neu1</i>	Chr 19	Q1LWP9
	<i>asah1b</i>	Chr 1	Q6PH71	Pompe disease	<i>gaa</i>	Chr 3	E7FGC0/ F1R7G7

**Combined GCase and Gba2 deficiency in zebrafish** – GBA2 is a  $\beta$ -glucosidase tightly associated with membranes that catalyzes metabolism of GlcCer in the cytosolic membrane-leaflet. It has been demonstrated that GBA2 is able to act as transglucosylase and generates GlcChol using GlcCer as sugar donor and cholesterol as acceptor, both in zebrafish (chapter 5) and in mammals<sup>11</sup>. Lack of Gba2 in the zebrafish is therefore predicted to reduce GlcChol and to increase GlcCer in cytosolic membrane leaflets. Double *gba1:gba2* KO zebrafish were generated to examine the impact of the proposed reduction of GlcChol on disease manifestations. Investigations in chapter 7 reveal that *gba2* KO fish lack a clear phenotype, while *gba1:gba2* KO individuals do not show apparent phenotypic improvements when compared to *gba1* KO fish.

A prominent increase of GlcCer lipids with specific fatty acyls is observed in brains of *gba2* KO fish, as also reported for cerebellum of GBA2-deficient mice<sup>38</sup>. Moreover, levels of these particular GlcCer lipid species in brains of *gba1:gba2* KO fish exceed those observed in *gba1* KO brains. It is likely that these additional 18:0 and 20:0 fatty acyl GlcCer lipids accumulate at the cytosolic membrane leaflets in *gba1:gba2* KO fish, instead of intra-lysosomal. The findings regarding GlcChol warrant discussion. GlcChol is increased in GCase-deficient fish and it is reduced in young *gba2* KO fish, consistent with the role of Gba2 in synthesis of GlcChol and the role of GCase in hydrolysis of GlcChol (chapter 5 and 7<sup>11</sup>). Unexpectedly, GlcChol levels in older Gba2 deficient fish were found to be quite comparable to those in WT fish. The presence of GlcChol in the diet of the zebrafish, receiving both plant- and animal-based food, possibly explains this discrepancy. Supporting this hypothesis is the finding by Akiyama and co-workers that brain of chicken contains GlcChol, but also plant sterols and glucosylated plant sterols<sup>39</sup>. This suggests that food-derived glucosylated sterols indeed are taken up and even reach the brain. Therefore, it is of interest to raise the *gba1:gba2* KO zebrafish without the supplementary animal food, likely high in GlcChol, to examine disease manifestations in fish receiving different diets.

**Macrophage storage cells** – GCase-deficient zebrafish develop lipid-laden cells, reminiscent to Gaucher cells in GD patients. Besides *gpnmb*, GCase-deficient fish show increased expression of the chitinase, *chia.6*. The most extreme biomarker of human Gaucher cells is also a chitinase called chitotriosidase<sup>40,41</sup>. Similarly, GD fruit flies deficient in GCase over-express a chitinase<sup>42</sup>. While the zebrafish genome encodes six homologous *chia* genes, *chia.1-chia.6*, with different tissue distributions<sup>43</sup> only *chia.5* and *chia.6* mRNA levels are increased in brains of GCase-deficient fish. Of interest for future experiments is examining the spatial location of *gpnmb* and *chia.6* expression in the GCase-deficient zebrafish by for example *in situ* hybridization. It will also be of interest to study more closely what drives lipid-laden macrophages to massively overexpress proteins with unknown functions in GD, such as gpNMB and a chitinase with apparent antifungal and possible anti-microbial activity. For this purpose, the promoters of *chia.6* and *gpnmb* could be combined with a reporter to visualize the induction of lipid-laden macrophages in transparent larvae. Such visualization could be of particular use to study different disease conditions resulting in lipid-laden macrophages and microglia in developing larvae.

**Genome-editing approaches** – In this thesis, CRISPR/Cas9 technology has been used in zebrafish to generate gene knockouts, while Tol2 transposase technique introduced exogenous DNA in the zebrafish genome (chapter 4). Random integration of the target sequence and its expressional regulation by ubiquitous and reported cell-specific promoters are two limitations of the Tol2 transposase technique. Of particular interest for future research is optimization of so-called knockin approaches after CRISPR/Cas9 mediated DNA cleavage. Several applications can be envisioned including a study on the impact of human GD-causing mutations in zebrafish, generation of the described *gpnmb* or *chia.6* reporter fish or combining an endogenous gene sequence with a reporter tag. For example, the subcellular localization of the membrane-associated Gba2 is still poorly understood and a fluorescently tagged Gba2 may assist detailed analysis of subcellular localization of this enzyme in the transparent larvae.

**Small compound interventions** – Zebrafish offer a convenient organismal model to study small compound inhibitors. The investigation described in chapter 3 reveals comparable selectivity of GCase inhibitors, as cultured human cells. GCase was specifically inactivated when intact zebrafish larvae were exposed to ME656, a cyclophellitol modified at C8 with a bulky adamantyl moiety, in the swimming water. Moreover, it could be demonstrated with adult fish that ME656 cyclophellitol passes the blood brain barrier and inactivates GCase in the brain. Given the specificity of ME656, not targeting other retaining  $\beta$ -glucosidases<sup>44,45</sup> it appears feasible to generate pharmacologically a *bona fide* organismal model of neuronopathic Gaucher disease. Likewise, addition of small compound iminosugars inhibitors of GCS and GBA2 to the medium of GCase-deficient larvae resulted in expected corrections in lipid abnormalities as detected with sensitive LC-MS/MS allowing analysis of individual fish (chapter 5).

The studies in this thesis illustrate that in essence similar fluorogenic substrates, ABPs and LC-MS/MS techniques can be used to evaluate enzyme characteristics and relevant lipids, as those used for human and mouse materials.

### Opportunities and limitations of zebrafish as disease model

GCase deficiency in zebrafish results in a number of similar biochemical abnormalities that are similar to those in GD patients and GD mice models. GlcSph and GlcCer massively increase and storage cells accumulate in tissues, likely being the source of increased *gpnmb* and *chia.6* expression. The focus of investigations in this thesis has been primarily the brain. The zebrafish models might equally be exploited to study other common GD manifestations, such as splenomegaly, hepatomegaly, focal lesions, blood abnormalities and bone involvements, such as bone crises and osteoporosis. In view of the common symptoms of GD patients, key organ systems are discussed regarding anatomical and physiological similarities and differences between fish and mammals. The impact of GCase deficiency in these organ systems in fish and humans is discussed.

**Spleen and haematopoiesis** – In mammals, haematopoiesis takes largely place in bone marrow and the spleen is involved in the removal of senescent blood cells from the circulation. The infiltration of viable Gaucher cells in bone marrow, spleen and liver of GD patients are thought to underlie cytopenia, hepatosplenomegaly and bone defects<sup>46</sup>. The zebrafish spleen, as in nearly all vertebrates, is a non-vital organ and similar in structure to a large lymph node located inside the serosal lining of the intestine<sup>47</sup>. It acts primarily as a blood filter and plays important roles regarding red blood cells and the immune system. As in GD patients, GCase-deficient fish accumulate Gaucher-like cells in their spleen, which are more apparent in the *gba1:gba2* and *gba1:asah1b* KO fish.

Zebrafish fundamentally differ from mammals in the site of haematopoiesis. In adult fish, the kidney marrow acts as the main site for haematopoiesis, analogous to specialized bone marrow in mammals<sup>48</sup>. Development of the haematopoiesis system is regulated by similar molecular mechanisms as the mammalian system<sup>48,49</sup>. Fish have similar blood cells as mammals: erythrocytes, however nucleated, neutrophils, eosinophils, lymphocytes and macrophages<sup>48,49</sup>.

The kidneys of the *gba1*-, *gba1:gba2*- and *gba1:asah1b* KO fish appeared normal with standard haematoxylin and eosin staining. It will be of interest to study the haematological abnormalities and/or disturbed haematopoiesis in the three *gba1* mutants. Blood sampling is feasible from an adult zebrafish, although limited to only a few microliter<sup>50</sup>. Zancan and colleagues reported that in 3-10 dpf larvae hepatomegaly, thrombocytopenia, anaemia were already demonstrable<sup>51</sup>. In this respect, transgenic zebrafish lines can be used to investigate hepatocytes (*fabp10a* gene element), thrombocytes (*oitga2b*), erythrocytes (*gata1*) and blood vessel architecture (*krdl*)<sup>51</sup>. It will be particularly interesting to study blood abnormalities in *gba1:gba2* zebrafish as it has been described that ablation of GBA2 in mice with GCase deficiency in the haematopoietic lineage improves the observed cytopenia, amongst other symptoms<sup>52</sup>.

**Bone** – Common among GD patients is the occurrence of bone defects, characterized by a reduction in bone mineral density, reduction of bone mass and a decrease in the trabecular volume of long bones. This results in brittle bones that are more prone to fracture. Osteoporosis is caused by a dysregulation of bone homeostasis with decreased bone metabolism, by reduced activity of osteoblasts and osteocytes, and increased catabolism, by enhanced osteoclast activity. Several studies have indicated that osteoblastic bone formation is particularly impaired in GD patients<sup>52,53</sup>.

The skeletal physiology of the zebrafish shows strong similarities to mammals<sup>54,55</sup>. In zebrafish, as in mammals, bone is formed *de novo* by osteoblasts and remodelled by the coupled action of osteoclasts. Terrestrial vertebrates have thicker bones compared to zebrafish, however the relevant skeletal cell types and modes of regulation, including osteoblast and osteoclast coupling and bone remodelling, are conserved between zebrafish and higher vertebrates<sup>54,56</sup>. The first cartilaginous structures, chondrocytes and osteoblasts are formed in the few days of development, however osteoclasts are not formed until 10-12 dpf<sup>54</sup>. Therefore, true remodelling through combined activity of osteoblasts and osteoclasts starts in the second week of development. Previously discussed research, using transgenic zebrafish, also reveals reduced bone mineralization, impaired osteoblast differentiation and a defect in canonical Wnt signalling in the GCase deficient larvae<sup>51</sup>. Increased reactive oxygen species production was found to precede the Wnt signalling impairment. Reduced Wnt signalling activity was also observed in GD fibroblasts resulting from increased  $\beta$ -catenin degradation<sup>51</sup>. The three GCase-deficient zebrafish models have not been examined yet for skeletal abnormalities. Of note, the mutants do show a curvature of the back but it is presently unknown whether this abnormality has not a neurological nature. In view of the hypothesized interference of excessive GlcSph in normal osteoblast bone formation<sup>57</sup>, it will be particularly interesting to study the bone in *gba1:asah1b* fish lacking excessive GlcSph. Examining bone defects in the *gba1:gba2* KO zebrafish is also of interest, given the reported improvement of bone in GD mice with concomitant GBA2 deficiency<sup>52</sup>.

In order to study bone defects in developing zebrafish larvae, reported transgenic zebrafish lines can be used, studying for example osteoblasts (*Ola.Sp7* gene element), osteoclasts (*ctsk*), chondrocytes (*col2a1*) or neural crest derived-skeleton (*sox10*)<sup>51,56</sup>. The skeletal phenotype of larvae and adult zebrafish can also be studied using histological stains, that bind calcium and calcium-containing materials, or X-ray based imaging of live animals<sup>58</sup>. Micro-computed tomography analysis has, for example, been used to evaluate developmental skeletal defects in a zebrafish model for mucopolysaccharidosis type II (MPSII)<sup>59</sup>. Underlying molecular mechanisms can be studied by means of protein or RNA analysis of different skeletal structures. For example, the tail fin of adult zebrafish is easily accessible, contains several separated vertebrae and has been extensively used as model for regenerating bone<sup>54,60</sup>.



**Liver** – Mildly affected GD patients develop a moderate hepatosplenomegaly due to infiltration of Gaucher cells<sup>61</sup>. In severely affected GD patients, chronic liver injury and inflammation lead to collagen deposition and fibrosis which may lead to loss of metabolic and synthetic functions, also called hepatic cirrhosis<sup>61,62</sup>. The zebrafish liver differs in important aspects from the mammalian one. It encompasses three lobes, containing hepatocytes, endothelial cells and bile duct epithelial cells, but specialized macrophages, called Kupffer cells, seem absent<sup>47</sup>. Hepatocytes form plates and are lined with sinusoids and biliary ducts, but are not clearly organized in cords or lobules with portal triads as in the mammalian liver<sup>47,63</sup>. Hepatocytes of females are basophilic due to production of vitellogenin, which results in a slightly different staining of the female and male livers using standard haematoxylin and eosin staining<sup>47</sup>.

Gaucher-like cells are apparent in liver of GCase-deficient fish, while hepatocytes in these livers appear relatively normal. No enlarged spleen or liver was observed during dissections of GCase-deficient zebrafish and their histopathological examination. Further characterization of the observed Gaucher-like cells by immunostaining for macrophage markers, and *in situ* hybridization of *gpnmb* or *chia.6* should be undertaken.

**Brain** – GD patients with very low residual GCase activity display neurological impairments, which are either severe and manifest at very young age (type 2 GD) or more mild and variable of nature (type 3 GD)<sup>46</sup>. Mutations in the *GBA* gene encoding GCase are a prominent risk factor for Parkinson's disease<sup>64</sup>.

The zebrafish brain resembles the mammalian brain in many aspects, however there are differences to point out. The zebrafish brain is also anatomically divided into fore-, mid- and hindbrain with defined regions such as the diencephalon, telencephalon, cerebellum and spinal cord<sup>55,65</sup>. The telencephalon, or forebrain, is responsible for aspects of memory, colour vision as well as reproductive- and feeding behaviours<sup>66</sup>. The midbrain, or mesencephalon, is relatively large and anatomically subdivided in the tectum and optic tectum<sup>47</sup>. The optic tectum in fish appears to have a high degree of complexity and is suggested to perform vision-related functions performed by the neocortex of mammals<sup>67</sup>. The blood-brain barrier (BBB) develops fast in zebrafish and has a similar structure and function compared to that of higher vertebrates<sup>68,69</sup>.

The zebrafish brain uses the same neurotransmitters as mammals such as dopamine, noradrenaline, serotonin, histamine and acetylcholine<sup>68,70</sup>. The adjustment of movement is regulated predominantly by the monoaminergic system that is highly conserved in vertebrates<sup>68,70</sup>. Tyrosine hydroxylase (TH) mediates the first step of catecholamine biosynthesis and is therefore an important marker of catecholaminergic neurons. Two orthologues of the mammalian *TH* gene exist in the zebrafish genome and the encoding Th1 and Th2 proteins are highly similar to mammalian TH. Th1 expressing dopaminergic neurons are found in the olfactory bulb, telencephalon, diencephalon and locus coeruleus, while Th2 expressing neurons are found in the diencephalon, ventral proptic region and hypothalamus. Th1 and Th2 neuron populations are intermingled in the diencephalon, however neurons mostly express either one of the enzymes. Importantly, only Th1 reacts with the available antibodies, therefore catecholaminergic populations visualized by immunohistochemistry are Th1-positive populations<sup>70,71</sup>.

## Chapter 9

Several reported hallmarks of neuronopathic GD in mouse models are also observed in GCase-deficient zebrafish, such as infiltration of Gaucher-like cells, likely expressing *gpnmb* and *chia.6*, increased neuroinflammation, abnormal autophagy, complement system activation and neurodegeneration<sup>72-74</sup>. The various available mutant fish with GCase deficiency discussed above will allow follow-up investigations on the role of specific lipid abnormalities in neuropathology.

Given the interest in the relationship between GCase and Parkinson's disease (PD), it is of interest to point out that zebrafish lack the dopaminergic neuronal populations in the midbrain that are involved in PD<sup>75</sup>. In PD, selective degeneration of dopaminergic neurons occurs in the pars compacta of the substantia nigra, a basal ganglia structure located in the midbrain, which is thought to be responsible for its motor symptoms. In the zebrafish, the telencephalon contains a significant population of dopaminergic neurons that is not present in mammalian brain. Diencephalic dopaminergic cell populations in the posterior tuberculum of the zebrafish brain are considered as functional homolog of the mammalian dopaminergic neurons in the substantia nigra<sup>75</sup>. In PD, cytoplasmic inclusion bodies termed Lewy bodies, mainly composed of  $\alpha$ -synuclein, are a histopathological hallmark. As mentioned, above an orthologue of the human  $\alpha$ -synuclein is not to be present in the zebrafish genome. Zebrafish express three synuclein isoform:  $\beta$ -,  $\gamma$ 1- and  $\gamma$ 2-synuclein, the first two showing involvement in normal dopaminergic neuron development<sup>26,27</sup>. Over-expression of  $\gamma$ 1-synuclein in zebrafish results in formation of neuronal aggregates and neurotoxicity, similar to that observed for human  $\alpha$ -synuclein in PD<sup>76</sup>.

Levels of  $\beta$ - and  $\gamma$ 1-synucleins were found to be reduced in brains of GCase-deficient zebrafish, both at mRNA (chapter 7) and protein level<sup>19</sup>. This reduction is likely attributed to loss of neurons<sup>19</sup>. This investigation by Keatinge and coworkers with *gba1* KO fish also revealed intra-neuronal inclusions, resembling Lewy bodies in PD patients<sup>19</sup>. It is difficult to judge at present whether *gba1* KO zebrafish provide a useful model for studying PD or only offer a model for neuronopathic GD<sup>68,77</sup>.

Endogenous  $\alpha$ -synuclein is expressed by another type of teleost fish, *Oryzias latipes* (medaka). *Gba1* KO medaka fish show infiltration of Gaucher-like cells in the brain, progressive neuronal loss and microgliosis<sup>78</sup>. Accumulation of  $\alpha$ -synuclein in axonal swellings is observed, however disruption of the gene encoding  $\alpha$ -synuclein does not improve lifespan, formation of axonal swellings, neuronal loss or neuroinflammation<sup>78</sup>. Medaka fish might intrinsically offer more attractive PD models than zebrafish.

**Skin** – Skin of collodion GD patients and null-allele GD mice show severe barrier abnormalities, incompatible with terrestrial life, with increased GlcCer levels and decreased ceramide levels in the stratum corneum<sup>79,80</sup>. The extracellular outer skin layer of mammals prevents against water loss and protects the epidermis and dermis<sup>81</sup>. The stratum corneum consists of terminally differentiated keratinocytes, called corneocytes, embedded in lipid lamellae that consist largely of ceramide, cholesterol and free fatty acids<sup>81</sup>. Keratinocytes extrude GlcCer and sphingomyelin, via lamellar bodies, into the interface with the stratum corneum as well as GCase and ASMase. These enzymes generate locally the ceramides from the lipid precursors, an essential process for formation of desired barrier properties of the skin<sup>82</sup>.

Fish are, in sharp contrast to mammals, ectotherm (rely on environmental heat sources), poikilotherm (body temperature varies with the ambient temperature) and their skin is adapted to the aqueous environment<sup>83,84</sup>. The teleost skin consists of an epidermis and dermis and contains no keratin or water barrier<sup>84</sup>. The protective outer cuticle contains a mix of glycoproteins and immune component containing mucus, which is the mechanical and biochemical barrier against pathogens<sup>83,84</sup>. Fish lack a similar structure to the stratum corneum of mammals. The presence of sphingolipids in teleost skin is poorly studied. Only limited data is available for total skin, indicating the presence of quite similar GlcCer, SM and ceramide levels to those in other tissues<sup>85,86</sup>. The absence of a specialized, ceramide-enriched stratum corneum in fish might explain the observed viability of GCase deficient zebrafish (chapters 5, 6 and 7).

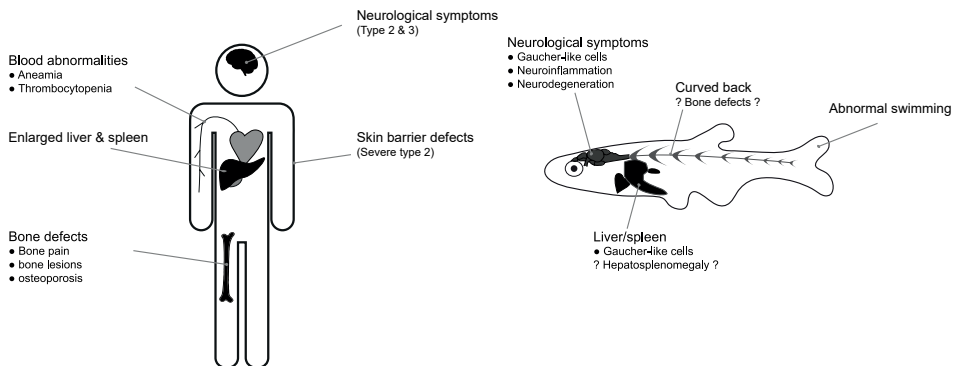


**Figure 1 | GD disease manifestations in human patients and zebrafish model**

Schematic representation of common disease manifestations of human GD patients and the observed symptoms of the established GCase-deficient zebrafish.

## Concluding remarks

The studies in this thesis illustrate the great potential of the zebrafish as vertebrate model to study Gaucher disease. The practical advantages of zebrafish have enabled generation of various gene knockouts and screening of small molecule inhibitors. Similar techniques can be applied in zebrafish larvae and adult tissues as earlier established for human and mouse materials. Glycosphingolipid metabolism can be evaluated using fluorogenic substrates, ABPs and LC-MS/MS techniques, while standard pathology, protein and RNA analysis offer opportunities to study underlying molecular mechanisms.

Obviously, fish are no phenocopy of humans due to differences in anatomy and physiology. However, zebrafish prove to be an attractive model to study molecular mechanism of disease manifestation at an organismal level. Moreover, GD zebrafish allow convenient screening for drugs and the evaluation of their efficacy in correcting aberrant metabolism at organismal level. Insights that are obtained in this manner complement information obtained by studying cultured human cells and mouse models. In particular, the unique *asah1b* KO fish, not able to generate the presumed toxic lyso-lipid, could give valuable insights into the role of GlcSph, GalSph, lyso-Gb3 or other lyso-lipids in accelerating disease manifestations.

## Supplementary information

**Supplementary table 1 |** Zebrafish (ZF) orthologues of human proteins responsible for GSL metabolism. Limited information is available on the cell-specific expression, localization and substrate specificity of these zebrafish enzymes as compared to their human orthologue.

	ZF gene	Uniprot		ZF gene	Uniprot
<b>Serine palmitoyl transferase</b>	<i>sptlc1</i>	Chr 10 Q502G6/F1QEL4	<b>GSL</b>	<i>ugt8</i>	Chr 1 E7FDZ0
	<i>sptlc2a</i>	Chr 17 F1QCX4		<i>gal3st1a</i>	Chr 5 A2BGH3
	<i>sptlc2b</i>	Chr 20 F1Q992		<i>gal3st1b</i>	Chr 10 E9QCM2
	<i>sptlc3</i>	Chr 13 F1QQP7		<i>ugcg</i>	Chr 10 F1QNT4
<b>Desaturase</b>	<i>segs1</i>	Chr 13 B8A4A2	<b>LacCer</b>	<i>b4galt5</i>	Chr 23 Q3YL68
	<i>degs2</i>	Chr17 F1QW74		<i>a4galt/</i>	N o t found
				<i>a3galt2</i>	found
<b>Ceramide synthase</b>	<i>cers1</i>	Chr 22 F1Q5B1	<b>Lacto- series</b>	<i>b3gnt5a</i>	Chr 11 Q7T3S5
	<i>cers2a</i>	Chr 19 Q90YY7		<i>b3gnt5b</i>	Chr 2 A5WVT9
	<i>cers2b</i>	Chr 16 E7F9X7		<i>b4galnt1a</i>	Chr 23 A1L229
	<i>cers3a</i>	Chr 7 E7F1Q9	<b>Ganglio- series</b>	<i>b4galnt1b</i>	Chr 6 X1WFC5
	<i>cers3b</i>	Chr 18 F1QVG1		<i>st3gal5</i>	Chr 14 F1RCA6
	<i>cers4a</i>	Chr 22 Q1L8N1		<i>st8sia1</i>	Chr 4 Q6KC13/A1A5W4
	<i>cers4b</i>	Chr 2 E7FCM3	<b>LacCer</b>	<i>st3gal2</i>	Chr 18 Q6EV31
	<i>cers5</i>	Chr 22 A7E7D4		<i>b4galt5</i>	Chr 23 Q3YL68
	<i>cers6</i>	Chr 9 F1QPF3		<i>a4galt/</i>	N o t found
<b>Cer1P SM</b>	<i>cerk</i>	Chr 4 AWWZ0	<b>Lacto- series</b>	<i>a3galt2</i>	found
	<i>sgms1</i>	Chr 12 A0JMN0		<i>b3gnt5a</i>	Chr 11 Q7T3S5
	<i>sgms2a</i>	Chr 1 B8A5Q0	<b>Lysosomal protein</b>	<i>Npc1</i>	Chr 2 F1QNG7
	<i>sgms2b</i>	Chr 23 Q6DEI3		<i>Npc2</i>	Chr 17 Q9DGJ3
			<b>Activator protein</b>	<i>Psap</i>	Chr 13 B8JI17

## References

- Do H.V. (2016) Variant, recombinant beta-glucocerebrosidase proteins with increased stability and increased retained catalytic activity **Volume US9254313B2**. (United States: Amicus Therapeutics Inc ).
- Ben Bdira F., Kallemeijn W.W., Oussoren S.V., Scheij S., Bleijlevens B., Florea B.I.,... and Aerts J. (2017) Stabilization of Glucocerebrosidase by Active Site Occupancy. *ACS Chem Biol* **12**, 1830-1841.
- Kramer G., Wegdam W., Donker-Koopman W., Ottenhoff R., Gaspar P., Verhoek M.,... and van Eijk M. (2016) Elevation of glycoprotein nonmetastatic melanoma protein B in type 1 Gaucher disease patients and mouse models. *FEBS Open Bio* **6**, 902-913.
- Marques A.R., Gabriel T.L., Aten J., van Roomen C.P., Ottenhoff R., Claessen N.,... and van Eijk M. (2016) Gpnmb Is a Potential Marker for the Visceral Pathology in Niemann-Pick Type C Disease. *PLoS one* **11**, e0147208.
- van der Lienden M.J.C., Gaspar P., Boot R., Aerts J. and van Eijk M. (2018) Glycoprotein Non-Metastatic Protein B: An Emerging Biomarker for Lysosomal Dysfunction in Macrophages. *Int J Mol Sci* **20**.
- Ellett F., Pase L., Hayman J.W., Andrianopoulos A. and Lieschke G.J. (2011) mpeg1 promoter transgenes direct macrophage-lineage expression in zebrafish. *Blood* **117**, e49-56.
- Zhang C.K., Stein P.B., Liu J., Wang Z., Yang R., Cho J.H.,... and Mistry P.K. (2012) Genome-wide association study of N370S homozygous Gaucher disease reveals the candidacy of CLN8 gene as a genetic modifier contributing to extreme phenotypic variation. *Am J Hematol* **87**, 377-383.
- di Ronza A., Bajaj L., Sharma J., Sanagasetti D., Lotfi P., Adamski C.J.,... and Sardiello M. (2018) CLN8 is an endoplasmic reticulum cargo receptor that regulates lysosome biogenesis. *Nat Cell Biol* **20**, 1370-1377.
- Luzio J.P. (2018) CLN8 safeguards lysosome biogenesis. *Nat Cell Biol* **20**, 1333-1335.
- Newton J., Milstien S. and Spiegel S. (2018) Niemann-Pick type C disease: The atypical sphingolipidosis. *Adv Biol Regul* **70**, 82-88.
- Marques A.R., Mirzaian M., Akiyama H., Wisse P., Ferraz M.J., Gaspar P.,... and Aerts J.M. (2016) Glucosylated cholesterol in mammalian cells and tissues: formation and degradation by multiple cellular beta-glucosidases. *J Lipid Res* **57**, 451-463.
- Lin Y., Cai X., Wang G., Ouyang G. and Cao H. (2018) Model construction of Niemann-Pick type C disease in zebrafish. *Biol Chem* **399**, 903-910.
- Tseng W.C., Loeb H.E., Pei W., Tsai-Morris C.H., Xu L., Cluzeau C.V.,... and Porter F.D. (2018) Modeling Niemann-Pick disease type C1 in zebrafish: a robust platform for in vivo screening of candidate therapeutic compounds. *Dis Model Mech* **11**.
- Ghisaidoobe A.T., van den Berg R.J., Butt S.S., Strijland A., Donker-Koopman W.E., Scheij S.,... and Overkleeft H.S. (2014) Identification and development of biphenyl substituted iminosugars as improved dual glucosylceramide synthase/neutral glucosylceramidase inhibitors. *Journal of medicinal chemistry* **57**, 9096-9104.
- Marques A.R., Aten J., Ottenhoff R., van Roomen C.P., Herrera Moro D., Claessen N.,... and Aerts J.M. (2015) Reducing GBA2 Activity Ameliorates Neuropathology in Niemann-Pick Type C Mice. *PLoS one* **10**, e0135889.
- Aerts J., Kuo C.L., Lelieveld L.T., Boer D.E.C., van der Lienden M.J.C., Overkleeft H.S. and Artola M. (2019) Glycosphingolipids and lysosomal storage disorders as illustrated by gaucher disease. *Current opinion in chemical biology* **53**, 204-215.
- Ferraz M.J., Marques A.R., Appelman M.D., Verhoek M., Strijland A., Mirzaian M.,... and Aerts J.M. (2016) Lysosomal glycosphingolipid catabolism by acid ceramidase: formation of glycosphingoid bases during deficiency of glycosidases. *FEBS Lett* **590**, 716-725.
- Ordóñez Y.F., Abad J.L., Aseeri M., Casas J., García V., Casasampere M.,... and Fabrias G. (2019) Activity-Based Imaging of Acid Ceramidase in Living Cells. *Journal of the American Chemical Society* **141**, 7736-7742.
- Keatinge M., Bui H., Menke A., Chen Y.C., Sokol A.M., Bai Q.,... and Bandmann O. (2015) Glucocerebrosidase 1 deficient Danio rerio mirror key pathological aspects of human Gaucher disease and provide evidence of early microglial activation preceding alpha-synuclein-independent neuronal cell death. *Human molecular genetics* **24**, 6640-6652.
- Lukas J., Cozma C., Yang F., Kramp G., Meyer A., Nessler A.M.,... and Rolfs A. (2017) Glucosylsphingosine Causes Hematological and Visceral Changes in Mice-Evidence for a Pathophysiological Role in Gaucher Disease. *Int J Mol Sci* **18**.
- Nair S., Boddupalli C.S., Verma R., Liu J., Yang R., Pastores G.M.,... and Dhodapkar M.V. (2015) Type II NKT-TFH cells against Gaucher lipids regulate B-cell immunity and inflammation. *Blood* **125**, 1256-1271.
- Pavlova E.V., Wang S.Z., Archer J., Dekker N., Aerts J.M., Karlsson S. and Cox T.M. (2013) B cell lymphoma and myeloma in murine Gaucher's disease. *J Pathol* **231**, 88-97.
- Smith N.J., Fuller M., Saville J.T. and Cox T.M. (2018) Reduced cerebral vascularization in experimental neuronopathic Gaucher disease. *J Pathol* **244**, 120-128.
- Taguchi Y.V., Liu J., Ruan J., Pacheco J., Zhang X., Abbasi J.,... and Chandra S.S. (2017) Glucosylsphingosine



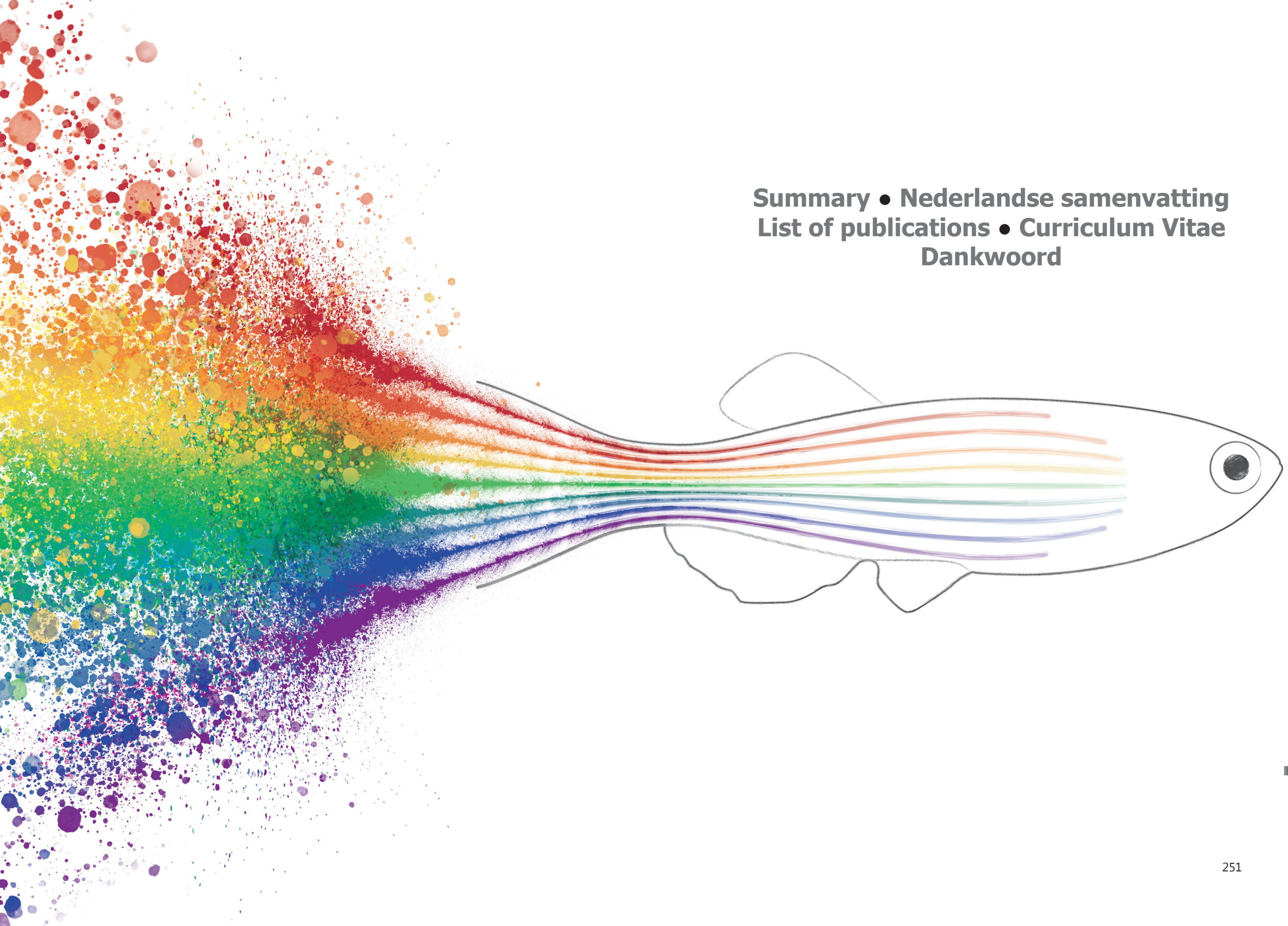
- Promotes alpha-Synuclein Pathology in Mutant GBA-Associated Parkinson's Disease. *J Neurosci* **37**, 9617-9631.
25. Ikuno M., Yamakado H., Akiyama H., Parajuli L.K., Taguchi K., Hara J.,... and Takahashi R. (2019) GBA haploinsufficiency accelerates alpha-synuclein pathology with altered lipid metabolism in a prodromal model of Parkinson's disease. *Human molecular genetics* **28**, 1894-1904.
  26. Milanese C., Sager J.J., Bai Q., Farrell T.C., Cannon J.R., Greenamyre J.T. and Burton E.A. (2012) Hypokinesia and reduced dopamine levels in zebrafish lacking beta- and gamma1-synucleins. *J Biol Chem* **287**, 2971-2983.
  27. Sun Z. and Gitler A.D. (2008) Discovery and characterization of three novel synuclein genes in zebrafish. *Developmental dynamics : an official publication of the American Association of Anatomists* **237**, 2490-2495.
  28. Schuchman E.H. (2016) Acid ceramidase and the treatment of ceramide diseases: The expanding role of enzyme replacement therapy. *Biochimica et biophysica acta* **1862**, 1459-1471.
  29. Mirzaian M., Wisse P., Ferraz M.J., Gold H., Donker-Koopman W.E., Verhoeke M.,... and Aerts J.M. (2015) Mass spectrometric quantification of glucosylsphingosine in plasma and urine of type 1 Gaucher patients using an isotope standard. *Blood Cells Mol Dis* **54**, 307-314.
  30. Ferraz M.J., Marques A.R., Gaspar P., Mirzaian M., van Roomen C., Ottenhoff R.,... and Aerts J.M. (2016) Lyso-glycosphingolipid abnormalities in different murine models of lysosomal storage disorders. *Mol Genet Metab* **117**, 186-193.
  31. Choi L., Vernon J., Kopach O., Minett M.S., Mills K., Clayton P.T.,... and Wood J.N. (2015) The Fabry disease-associated lipid Lyso-Gb3 enhances voltage-gated calcium currents in sensory neurons and causes pain. *Neurosci Lett* **594**, 163-168.
  32. Jeon Y.J., Jung N., Park J.W., Park H.Y. and Jung S.C. (2015) Epithelial-Mesenchymal Transition in Kidney Tubular Epithelial Cells Induced by Globotriaosylsphingosine and Globotriaosylceramide. *PLoS one* **10**, e0136442.
  33. Sanchez-Nino M.D., Carpio D., Sanz A.B., Ruiz-Ortega M., Mezzano S. and Ortiz A. (2015) Lyso-Gb3 activates Notch1 in human podocytes. *Human molecular genetics* **24**, 5720-5732.
  34. Sanchez-Nino M.D., Sanz A.B., Carrasco S., Saleem M.A., Mathieson P.W., Valdivielso J.M.,... and Ortiz A. (2011) Globotriaosylsphingosine actions on human glomerular podocytes: implications for Fabry nephropathy. *Nephrol Dial Transplant* **26**, 1797-1802.
  35. Li Y., Xu Y., Benitez B.A., Nagree M.S., Dearborn J.T., Jiang X.,... and Sands M.S. (2019) Genetic ablation of acid ceramidase in Krabbe disease confirms the psychosine hypothesis and identifies a new therapeutic target. *Proc Natl Acad Sci U S A* **116**, 20097-20103.
  36. Kodama T., Togawa T., Tsukimura T., Kawashima I., Matsuoka K., Kitakaze K.,... and Sakuraba H. (2011) Lyso-GM2 ganglioside: a possible biomarker of Tay-Sachs disease and Sandhoff disease. *PLoS one* **6**, e29074.
  37. Kuchar L., Sikora J., Gulinello M.E., Poupetova H., Lugowska A., Malinova V.,... and Ledvinova J. (2017) Quantitation of plasmatic lysosphingomyelin and lysosphingomyelin-509 for differential screening of Niemann-Pick A/B and C diseases. *Anal Biochem* **525**, 73-77.
  38. Woeste M.A., Stern S., Raju D.N., Grahn E., Dittmann D., Gutbrod K.,... and Wachten D. (2019) Species-specific differences in nonlysosomal glucosylceramidase GBA2 function underlie locomotor dysfunction arising from loss-of-function mutations. *J Biol Chem* **294**, 3853-3871.
  39. Akiyama H., Nakajima K., Itoh Y., Sayano T., Ohashi Y., Yamaguchi Y.,... and Hirabayashi Y. (2016) Aglycon diversity of brain sterylglucosides: structure determination of cholesteryl- and sitosterylglucoside. *J Lipid Res* **57**, 2061-2072.
  40. Ferraz M.J., Kallemijn W.W., Mirzaian M., Herrera Moro D., Marques A., Wisse P.,... and Aerts J.M. (2014) Gaucher disease and Fabry disease: new markers and insights in pathophysiology for two distinct glycosphingolipidoses. *Biochimica et biophysica acta* **1841**, 811-825.
  41. van Dussen L., Hendriks E.J., Groener J.E., Boot R.G., Hollak C.E. and Aerts J.M. (2014) Value of plasma chitotriosidase to assess non-neuronopathic Gaucher disease severity and progression in the era of enzyme replacement therapy. *J Inheret Metab Dis* **37**, 991-1001.
  42. Cabasso O., Paul S., Dorot O., Maor G., Krivoruk O., Pasmanik-Chor M.,... and Horowitz M. (2019) Drosophila melanogaster Mutated in its GBA1b Ortholog Recapitulates Neuronopathic Gaucher Disease. *J Clin Med* **8**.
  43. Koch B.E., Stougaard J. and Spink H.P. (2014) Spatial and temporal expression patterns of chitinase genes in developing zebrafish embryos. *Gene Expr Patterns* **14**, 69-77.
  44. Artola M., Kuo C.L., Lelieveld L.T., Rowland R.J., van der Marel G.A., Codee J.D.C.,... and Overkleeft H.S. (2019) Functionalized Cyclophellitols Are Selective Glucocerebrosidase Inhibitors and Induce a Bona Fide Neuropathic Gaucher Model in Zebrafish. *Journal of the American Chemical Society* **141**, 4214-4218.
  45. Kuo C.L., Kallemijn W.W., Lelieveld L.T., Mirzaian M., Zoutendijk I., Vardi A.,... and Artola M. (2019) In vivo inactivation of glycosidases by conduritol B epoxide and cyclophellitol as revealed by activity-based protein profiling. *FEBS J* **286**, 584-600.
  46. Stirnemann J., Belmatoug N., Camou F., Serratrice C., Froissart R., Caillaud C.,... and Berger M.G. (2017) A Review of Gaucher Disease Pathophysiology, Clinical Presentation and Treatments. *Int J Mol Sci* **18**.

47. Menke A.L., Spitsbergen J.M., Wolterbeek A.P. and Woutersen R.A. (2011) Normal anatomy and histology of the adult zebrafish. *Toxicol Pathol* **39**, 759-775.
48. Jagannathan-Bogdan M. and Zon L.I. (2013) Hematopoiesis. *Development* **140**, 2463-2467.
49. Ellett F. and Lieschke G.J. (2010) Zebrafish as a model for vertebrate hematopoiesis. *Curr Opin Pharmacol* **10**, 563-570.
50. Zang L., Shimada Y., Nishimura Y., Tanaka T. and Nishimura N. (2015) Repeated Blood Collection for Blood Tests in Adult Zebrafish. *Journal of visualized experiments : JoVE*, e53272.
51. Zancan I., Bellesso S., Costa R., Salvalaio M., Stroppiano M., Hammond C.,... and Moro E. (2015) Glucocerebrosidase deficiency in zebrafish affects primary bone ossification through increased oxidative stress and reduced Wnt/beta-catenin signaling. *Human molecular genetics* **24**, 1280-1294.
52. Mistry P.K., Liu J., Sun L., Chuang W.L., Yuen T., Yang R.,... and Zaidi M. (2014) Glucocerebrosidase 2 gene deletion rescues type 1 Gaucher disease. *Proc Natl Acad Sci U S A* **111**, 4934-4939.
53. van Dussen L., Lips P., Everts V.E., Bravenboer N., Jansen I.D., Groener J.E.,... and Hollak C.E. (2011) Markers of bone turnover in Gaucher disease: modeling the evolution of bone disease. *J Clin Endocrinol Metab* **96**, 2194-2205.
54. Bergen D.J.M., Kague E. and Hammond C.L. (2019) Zebrafish as an Emerging Model for Osteoporosis: A Primary Testing Platform for Screening New Osteo-Active Compounds. *Front Endocrinol (Lausanne)* **10**, 6.
55. Lieschke G.J. and Currie P.D. (2007) Animal models of human disease: zebrafish swim into view. *Nat Rev Genet* **8**, 353-367.
56. Hammond C.L. and Moro E. (2012) Using transgenic reporters to visualize bone and cartilage signaling during development in vivo. *Front Endocrinol (Lausanne)* **3**, 91.
57. Mistry P.K., Liu J., Yang M., Nottoli T., McGrath J., Jain D.,... and Zaidi M. (2010) Glucocerebrosidase gene-deficient mouse recapitulates Gaucher disease displaying cellular and molecular dysregulation beyond the macrophage. *Proc Natl Acad Sci U S A* **107**, 19473-19478.
58. Silvent J., Akiva A., Brumfeld V., Reznikov N., Rechav K., Yaniv K.,... and Weiner S. (2017) Zebrafish skeleton development: High resolution micro-CT and FIB-SEM block surface serial imaging for phenotype identification. *PLoS one* **12**, e0177731.
59. Bellesso S., Salvalaio M., Lualdi S., Tognon E., Costa R., Braghetta P.,... and Moro E. (2018) FGF signaling deregulation is associated with early developmental skeletal defects in animal models for mucopolysaccharidosis type II (MPSII). *Human molecular genetics* **27**, 2407.
60. Knopf F., Hammond C., Chekuru A., Kurth T., Hans S., Weber C.W.,... and Weidinger G. (2011) Bone regenerates via dedifferentiation of osteoblasts in the zebrafish fin. *Dev Cell* **20**, 713-724.
61. James S.P., Stromeyer F.W., Chang C. and Barranger J.A. (1981) Liver abnormalities in patients with Gaucher's disease. *Gastroenterology* **80**, 126-133.
62. Adar T., Ilan Y., Elstein D. and Zimran A. (2018) Liver involvement in Gaucher disease - Review and clinical approach. *Blood Cells Mol Dis* **68**, 66-73.
63. Cheng D., Shami G.J., Morsch M., Chung R.S. and Braet F. (2016) Ultrastructural Mapping of the Zebrafish Gastrointestinal System as a Basis for Experimental Drug Studies. *Biomed Res Int* **2016**, 8758460.
64. Sidransky E. and Lopez G. (2012) The link between the GBA gene and parkinsonism. *Lancet Neurol* **11**, 986-998.
65. Kalueff A.V., Stewart A.M. and Gerlai R. (2014) Zebrafish as an emerging model for studying complex brain disorders. *Trends Pharmacol Sci* **35**, 63-75.
66. Roberts R.J. and Ellis A.E. (2012) Fish pathology. In *Fish pathology*, R.J. Roberts, ed. (Blackwell Publishing), pp. 17-61.
67. Friedrich R.W., Jacobson G.A. and Zhu P. (2010) Circuit neuroscience in zebrafish. *Curr Biol* **20**, R371-381.
68. Vaz R.L., Outeiro T.F. and Ferreira J.J. (2018) Zebrafish as an Animal Model for Drug Discovery in Parkinson's Disease and Other Movement Disorders: A Systematic Review. *Front Neurol* **9**, 347.
69. Jeong J.Y., Kwon H.B., Ahn J.C., Kang D., Kwon S.H., Park J.A. and Kim K.W. (2008) Functional and developmental analysis of the blood-brain barrier in zebrafish. *Brain Res Bull* **75**, 619-628.
70. Panula P., Chen Y.C., Priyadarshini M., Kudo H., Semenova S., Sundvik M. and Sallinen V. (2010) The comparative neuroanatomy and neurochemistry of zebrafish CNS systems of relevance to human neuropsychiatric diseases. *Neurobiol Dis* **40**, 46-57.
71. Filippi A., Mahler J., Schweitzer J. and Driever W. (2010) Expression of the paralogous tyrosine hydroxylase encoding genes th1 and th2 reveals the full complement of dopaminergic and noradrenergic neurons in zebrafish larval and juvenile brain. *J Comp Neurol* **518**, 423-438.
72. Enquist I.B., Lo Bianco C., Ooka A., Nilsson E., Mansson J.E., Ehinger M.,... and Karlsson S. (2007) Murine models of acute neuronopathic Gaucher disease. *Proc Natl Acad Sci U S A* **104**, 17483-17488.
73. Vardi A., Zigdon H., Meshcheriakova A., Klein A.D., Yaacobi C., Eilam R.,... and Futerman A.H. (2016) Delineating pathological pathways in a chemically induced mouse model of Gaucher disease. *J Pathol* **239**, 496-509.

74. Pandey M.K., Burrow T.A., Rani R., Martin L.J., Witte D., Setchell K.D.,... and Grabowski G.A. (2017) Complement drives glucosylceramide accumulation and tissue inflammation in Gaucher disease. *Nature* **543**, 108-112.
75. Rink E. and Wullimann M.F. (2001) The teleostean (zebrafish) dopaminergic system ascending to the subpallium (striatum) is located in the basal diencephalon (posterior tuberculum). *Brain Res* **889**, 316-330.
76. Lulla A., Barnhill L., Bitan G., Ivanova M.I., Nguyen B., O'Donnell K.,... and Bronstein J.M. (2016) Neurotoxicity of the Parkinson Disease-Associated Pesticide Ziram Is Synuclein-Dependent in Zebrafish Embryos. *Environ Health Perspect* **124**, 1766-1775.
77. Flinn L., Bretaude S., Lo C., Ingham P.W. and Bandmann O. (2008) Zebrafish as a new animal model for movement disorders. *J Neurochem* **106**, 1991-1997.
78. Uemura N., Koike M., Ansai S., Kinoshita M., Ishikawa-Fujiwara T., Matsui H.,... and Takahashi R. (2015) Viable neuronopathic Gaucher disease model in Medaka (*Oryzias latipes*) displays axonal accumulation of alpha-synuclein. *Plos Genet* **11**, e1005065.
79. Holleran W.M., Ginns E.I., Menon G.K., Grundmann J.U., Fartasch M., McKinney C.E.,... and Sidransky E. (1994) Consequences of beta-glucocerebrosidase deficiency in epidermis. Ultrastructure and permeability barrier alterations in Gaucher disease. *The Journal of clinical investigation* **93**, 1756-1764.
80. Sidransky E., Sherer D.M. and Ginns E.I. (1992) Gaucher disease in the neonate: a distinct Gaucher phenotype is analogous to a mouse model created by targeted disruption of the glucocerebrosidase gene. *Pediatr Res* **32**, 494-498.
81. van Smeden J. and Bouwstra J.A. (2016) Stratum Corneum Lipids: Their Role for the Skin Barrier Function in Healthy Subjects and Atopic Dermatitis Patients. *Curr Probl Dermatol* **49**, 8-26.
82. van Smeden J., Dijkhoff I.M., Helder R.W.J., Al-Khakany H., Boer D.E.C., Schreuder A.,... and Bouwstra J.A. (2017) In situ visualization of glucocerebrosidase in human skin tissue: zymography versus activity-based probe labeling. *J Lipid Res* **58**, 2299-2309.
83. Dash S., Das S.K., Samal J. and Thatoi H.N. (2018) Epidermal mucus, a major determinant in fish health: a review. *Iran J Vet Res* **19**, 72-81.
84. Holden J., Layfield L. and Matthews J. (2012) Integument (skin). In *The Zebrafish: Atlas of Macroscopic and Microscopic Anatomy*, J. Schwendinger-Schreck, ed. (Cambridge, UK: Cambridge University Press).
85. Cheng K., Bou M., Ruyter B., Pickova J., Ehteshami E., Du L.,... and Moazzami A.A. (2018) Impact of Reduced Dietary Levels of Eicosapentaenoic Acid and Docosahexaenoic Acid on the Composition of Skin Membrane Lipids in Atlantic Salmon (*Salmo salar* L.). *J Agric Food Chem* **66**, 8876-8884.
86. Duan J., Sugawara T. and Hirata T. (2010) Rapid quantitative analysis of sphingolipids in seafood using HPLC with evaporative light-scattering detection: its application in tissue distribution of sphingolipids in fish. *J Oleo Sci* **59**, 509-513.



**Summary • Nederlandse samenvatting  
List of publications • Curriculum Vitae  
Dankwoord**



## Summary

The primary goal of this thesis has been to evaluate zebrafish as vertebrate animal model for the investigation of lysosomal storage disorders, in particular Gaucher disease (GD). Deficiency of glucocerebrosidase (GCase) degrading glucosylceramide (GlcCer) in lysosomes constitutes the molecular basis of GD. Zebrafish are an appealing model organism to study genetic disorders due to their facile maintenance, their ability to generate hundreds of off-spring which rapidly develop, are transparent and fit in a 96-wells plate. Zebrafish appear to be particularly interesting to study GD since they produce the lipid GlcCer, their genome contains an orthologue of the human *GBA* gene and an active acid  $\beta$ -glucosidase is expressed. Zebrafish also express many of the candidate modifier proteins, such as non-lysosomal Gba2 and lysosomal acid ceramidase (ACase). Research described in this thesis primarily focused on optimizing and using several biochemical and genetic techniques to study the catalytic features of zebrafish GCase and the consequences of its defect in zebrafish larvae and adults. In addition, the impact of two other enzymes, non-lysosomal GBA2 and lysosomal acid ceramidase, on GCase-deficient zebrafish received attention.

**Chapter 1** provides an overview of the biological function, synthesis and catabolism of (glyco)sphingolipids (GSLs). Defects in one of the enzymes responsible for degradation of these lipids lead to a group of orphan diseases called lysosomal storage disorders (LSDs). Three LSDs are of particular importance in this thesis: Gaucher disease caused by deficiency of lysosomal GCase, Fabry disease caused by deficiency of lysosomal  $\alpha$ -galactosidase A ( $\alpha$ -GAL A) and Farber disease caused by deficiency of acid ceramidase (ACase). Zebrafish are introduced as attractive vertebrate research model, for LSDs. The chapter concludes with an overview of tools used to study lysosomal glycosidases in zebrafish larvae and adults, including fluorogenic substrates, activity-based probes (ABPs) and sensitive LC-MS/MS techniques to measure (glyco)sphingolipids.

In **chapter 2**, a combination of biochemical assays and molecular modelling is used to study and compare features of GCase enzymes from different species, including man, zebrafish, frog and turtle. All GCase enzymes showed hydrolysis of the artificial substrate 4-methylumbelliferyl  $\beta$ -glucoside (4MU- $\beta$ -Glc) at an acidic pH optimum. Although human GCase required either saposin C or sodium taurocholate at pH of 5.2 for optimal activity, zebrafish and frog GCase showed high hydrolysis rates at pH 4.0 without additives. Increased levels of endogenous GlcCer and the deacylated sphingoid base, glucosylsphingosine (GlcSph), in the *GBA*-depleted HEK293T cells were corrected by over-expression of any of the GCase enzymes. In sharp contrast to human and frog GCase, the zebrafish enzyme was unable to perform an *in vitro* transglucosylation reaction with cholesterol as acceptor. It was suggested that cholesterol might not fit as acceptor in the catalytic pocket of zebrafish GCase. *In silico* comparison of modelled structures of the various GCase enzymes, based on the established 3D-structure of the human enzyme, revealed that residues of the catalytic pocket were highly conserved, while divergent residues were observed in the three flexible loops surrounding the catalytic pocket of GCase. Attention was drawn to three residues

with hydrophobic chains positioned close to the catalytic pocket of zebrafish GCase. Site-directed mutagenesis revealed that zebrafish GCase with substitutions of these amino acids did not show improvement in transglucosylation. To further test the hypothesis it should be considered to swap entire loops among enzymes of different species.

**Chapter 3** describes the use of zebrafish as convenient organismal model to study *in vivo* target engagement of the mechanism-based irreversible GCase inhibitors. The potency and selectivity of conduritol B epoxide (CBE) and cyclophellitol (CP) were evaluated in developing zebrafish larvae and compared with findings in cultured human cells. Only at high CBE concentrations, non-lysosomal glucosylceramidase (GBA2) and lysosomal  $\alpha$ -glucosidase were identified as major off-targets in cells and zebrafish larvae. CP was found to inactivate GCase and GBA2 with equal affinity and is therefore not suitable to generate genuine GD-like models. New CP derivatives, functionalized with a bulky hydrophobic moiety at C8, were validated as potent and selective GCase inhibitors in cultured cells and developing zebrafish larvae. Moreover, these CP analogues selectively inhibit GCase in the brain of adult fish. Overall, **chapter 3** demonstrates the suitability of the zebrafish model to evaluate drug potency, specificity and biodistribution, in particular brain permeability. The investigations in **chapter 2** and **3** illustrate that similar fluorogenic substrates, ABPs and LC-MS/MS techniques can be used to evaluate enzyme characteristics and relevant lipids as those used for human and mouse materials.

A practical advantage of the zebrafish, compared to mice, is the speed and convenience with which new gene knockouts (KOs) can be generated. **Chapter 4** provides a detailed protocol for the generation of gene KOs in zebrafish by means of CRISPR/Cas9 technology. It also describes the already generated mutations in the zebrafish *gba1*, *gba2*, *asah1a*, *asah1b*, *gpnmb*, *cln8* and *npc1* genes. RNA expression and lipid analysis of mutant larvae of *Gpnmb*, *Npc1* and *Cln8* confirmed that functional gene knockout have been generated. The impact of defective *Gba1*, *Gba2*, *Asah1a* and/or *Asah1b* is described in detail in **chapters 5-7**. Pilot experiments using the Tol2 transposase technique were undertaken to introduce an exogenous target DNA sequence in the zebrafish genome. The coding sequence of human *GBA* was introduced in the zebrafish *gba1*<sup>-/-</sup> genetic background, as well as the coding sequence of zebrafish prosaposin with a point mutation in the saposin C region thought to impair a disulfide bridge.

**Chapters 5-7** report on GCase deficient “Gaucher” zebrafish, which are viable in contrast to mouse models, and describe the impact of concurrent GBA2 deficiency (**chapters 5 and 7**) and the impact of excessive GlcSph (**chapter 6**).

**Chapter 5** focused on the role of zebrafish *Gba2* in glycosphingolipid metabolism during GCase deficiency. Genetic and pharmacological modulation has been used to study GCase- and/or *Gba2* deficiency in individual zebrafish larvae of 5 days post-fertilization (dpf) by evaluating their enzyme status using specific ABPs and their GlcCer metabolism using sensitive LC-MS/MS methods. Prominent formation of GlcSph was apparent in *gba1* KO and *gba1:gba2* KO larvae as well as during pharmacologic inactivation of zebrafish GCase. Accumulation of GlcCer in GCase-deficient fish is relatively limited, likely due to the



alternative metabolism of the lipid to its sphingoid base and the presence of active GCase derived from the heterozygous mother. Significantly higher levels of GlcCer and lower levels of GlcChol were measured in Gba2 deficient zebrafish larvae, underlining the importance of Gba2 for generation of GlcChol. Iminosugar inhibitors for GlcCer synthase and Gba2 were used to assess and correct abnormalities of GlcCer metabolism during GCase deficiency. In addition, overexpression of human GCase and injection of recombinant GCase both corrected the increased GlcSph levels.

In **chapter 6** the potential toxicity of excessive GlcSph during GCase deficiency is examined. Zebrafish have two orthologues of human acid ceramidase (ACase): Asah1a and Asah1b. From both single ACase KO fish only the *asah1b* KO fish fail to produce excessive GlcSph during GCase deficiency, while combined deficiency of both Asah1a and Asah1b is required to accumulate ceramide. A detailed comparison of *gba1* KO fish with excessive GlcSph and *gba1:asah1b* KO zebrafish without GlcSph revealed several differences but also interesting similarities. A significant amelioration of phenotype was observed in the *gba1:asah1b* KO fish. These fish did not show the same abnormalities in posture and swimming behaviour as *gba1* KO fish at 12 weeks post-fertilization (wpf). Double deficient *gba1:asah1b* KO fish showed an increased lifespan, however at 15-17 wpf abnormal swimming was apparent. Both *gba1* and *gba1:asah1b* KO fish showed comparable GlcCer accumulation in tissues and increased expression of the storage-cell biomarkers chitinase (*chia.6*) and *gpnmb*. The infiltration of microglia and storage cells in the periventricular grey zone of the optic tectum also appeared comparable. In their brains the two mutant fish showed similar autophagy, indicated by increased protein levels of p62, and inflammation, reflected by increased mRNA levels of *il1- $\beta$* , *tnf $\beta$*  and *apoeb*, as well as indications for similar activation of the complement cascade. Thus, abolishing Asah1b-ACase results in some phenotypic improvements but it does not prevent all abnormalities such as storage cell formation, neuroinflammation and complement activation.

**Chapter 7** gives an overview of findings using zebrafish with complete KOs of the genes encoding GCase (*gba1*), Gba2 (*gba2*), ACase (*asah1b*) and combinations thereof. These fish are raised to 12 wpf and their phenotype as well as biochemical and pathological parameters are described. Carrier *gba1*<sup>+/-</sup> fish show no apparent phenotype nor any biochemical abnormalities, while brain of Gba2 KO fish only reveal significant increased levels of specific GlcCer species. No clear abnormal phenotype is observed for any of the GCase deficient fish at 8 wpf, even though increases in GlcCer, neuroinflammation and autophagy are already demonstrable. Phenotypic abnormalities of the single *gba1* KO zebrafish have an early onset ( $\pm$  9 wpf), starting with a drop of the tail and progressing into a change in swimming behaviour. In contrast, many of the double *gba1:gba2* KO develop severe phenotypical abnormalities in a matter of days, without the preceding characteristics such as the drop of the tail. Additionally, they have a significantly shorter lifespan than single *gba1* KO fish. Pilot experiments indicate a related earlier onset of dopaminergic neuronal loss in the *gba1:gba2* KO fish, however the underlying pathophysiological mechanism remains elusive.

ACase-mediated deacylation of accumulating glycosphingolipids to its sphingolipid bases is not unique to GD. **Chapter 8** evaluates the potential of using zebrafish to study another common lysosomal storage disorder Fabry disease (FD). Deficiency of  $\alpha$ -GAL A constitutes the molecular basis of FD, characterized by accumulating globotriaosylceramide substrate in lysosomes which is partly converted by ACase into globotriaosylsphingosine (lysoGb3). **Chapter 8** shows that the zebrafish genome annotates one  $\alpha$ -Gal A and one orthologue of the highly homologous  $\alpha$ -N-acetylgalactosaminidase ( $\alpha$ -Nagal). The presence of  $\alpha$ -Gal A and  $\alpha$ -Nagal proteins in zebrafish cells and larvae was confirmed by chemical proteomics using an  $\alpha$ -Gal configured ABP. Fluorogenic  $\alpha$ -galactoside and  $\alpha$ -N-acetylgalactosaminide substrates reveal considerable  $\alpha$ -Nagal activity in zebrafish larvae and adult organs.  $\alpha$ -Gal A activity is typically lower than  $\alpha$ -Nagal activity, but relatively high in fertilized eggs, reproductive organs, liver and kidney, compared to other tissues. Interestingly, no Gb3 could be detected using sensitive LC-MS/MS methods in any of the studied zebrafish materials such as cells, larvae, brain, liver, kidney and testis. The absence of the lipid Gb3 is consistent with the absence of a gene encoding lactosylceramide 4- $\alpha$ -galactosyltransferase (A4galt; Gb3 synthase) in zebrafish or any other teleost species. HEK293T cells lacking endogenous  $\alpha$ -GAL A were generated using CRISPR/Cas9 technology. The increase in endogenous Gb3 levels in these cells could be comparably corrected by over-expression of either human  $\alpha$ -GAL A or zebrafish  $\alpha$ -Gal A. These findings indicate that zebrafish  $\alpha$ -Gal A can hydrolyse the endogenous substrate Gb3 in the cellular setting, however it showed no *in vitro* hydrolysis of the artificial substrate NBD-Gb3. The role of the conserved  $\alpha$ -galactosidase encoded by the *gla* gene in the zebrafish remains unknown. It is envisioned that *gla* knockout zebrafish expressing human A4GALT might render a useful Fabry disease model. The comparison of such fish with those with a concomitant *asha1b* KO might assist the investigation of the specific impact of excessive lyso-Gb3 in Fabry disease pathology.

**Chapter 9** discusses the obtained results of the undertaken investigations and describes future prospects of research. In addition, established and novel techniques are highlighted which could be useful to study other common clinical manifestations of GD patients, such as bone defects and blood abnormalities. Comparison of the different *gba1* KO zebrafish models might reveal underlying molecular mechanisms of common clinical manifestations upon concomitant GBA2 or ACase deficiency. Anatomical and physiological similarities and differences of the zebrafish compared to mammals are also discussed, in order to put the use of the zebrafish GD model in perspective.

In conclusion, investigations described in this thesis show that zebrafish offer exciting new possibilities to study molecular mechanisms underlying pathological processes during lysosomal hydrolase deficiencies. Due to differences, information obtained from *gba1* KO fish might not directly be translated to GD patients, however important mechanistic insights may be revealed by studying these teleost models. In particular, the unique *asha1b* KO fish, not able to generate the presumed toxic lyso-lipid, could give valuable insights into the role of GlcSph, psychosine, lyso-Gb3 or other lyso-lipids in accelerating disease manifestations.

## Nederlandse samenvatting

Het voornaamste doel van het onderzoek, beschreven in dit proefschrift, is het maken en karakteriseren van zebravis modellen om lysosomale stapelingsziekten te bestuderen, met in het bijzonder de ziekte van Gaucher. De ziekte van Gaucher wordt gekenmerkt door een defect in glucocerebrosidase (GCase), een enzym dat het lipide glucosylceramide (GlcCer) afbreekt in lysosomen. De zebravis is een aantrekkelijk model organisme voor onderzoeksdoelstellingen vanwege de kostenbesparende huisvesting en het vermogen om honderden nakomelingen te genereren. De nakomelingen, ook wel larven genoemd, zijn klein, transparent en hebben een snelle embryonale ontwikkeling ondergaan.

Zebravissen hebben een aantal specifieke kenmerken waardoor ze potentieel erg geschikt zijn om de ziekte van Gaucher te bestuderen: Ze produceren het lipide GlcCer, hun genoom heeft een ortholoog van het menselijke GBA gen en synthetiseert een actief  $\beta$ -glucosidase. Daarnaast komen ook twee interessante eiwitten tot expressie die de uitkomst van de ziekte mogelijk beïnvloeden: Het niet-lysosomale GBA2 en lysosomaal acid ceramidase (ACase).

Het onderzoek in dit proefschrift is voornamelijk gericht op het genereren van zebravissen met een deficiëntie van deze interessante (lysosomale) eiwitten, alsmede het optimaliseren en gebruiken van verschillende biochemische en genetische technieken om de katalytische kenmerken van GCase in de zebravis te bestuderen. Hiermee kunnen de gevolgen van deze deficiënties (of dubbel deficiënties) onderzocht worden bij jonge vissen (larven) en volwassenen. Ook is onderzocht wat de impact is van de GBA2 en ACase op het ziektebeeld van de GCase-deficiënte zebravissen.

**Hoofdstuk 1** geeft een overzicht van de biologische functie, synthese en katabolisme van (glyco)sfingolipiden. Een defect in een van de enzymen die verantwoordelijk zijn voor de afbraak van deze lipiden leidt tot een groep erfelijke ziekten die lysosomale sfingolipide stapelingsziekten genoemd worden.

Drie van dergelijke stapelingsziekten staan centraal in dit proefschrift: De ziekte van Gaucher veroorzaakt door een deficiëntie in lysosomaal GCase, de ziekte van Fabry veroorzaakt door een deficiëntie in lysosomaal  $\alpha$ -galactosidase A ( $\alpha$ -GAL A) en de ziekte van Farber veroorzaakt door een deficiëntie in acid ceramidase (ACase). Vervolgens worden de aantrekkelijke kenmerken van de zebravis voor onderzoek naar genetische aandoeningen geïntroduceerd, gevolgd door reeds beschreven zebravis modellen voor verschillende lysosomale stapelingsziekten.

Het hoofdstuk eindigt met een overzicht van instrumenten en technieken, die thans veelal worden gebruikt om zebravis larven en volwassenen te bestuderen. Ook zijn er specifieke technieken beschikbaar om lysosomale glycosidases te bestuderen, zoals fluorogene substraten, activity-based probes (ABPs) en gevoelige LC-MS/MS technieken om afwijkende (glyco)sfingolipide hoeveelheden te meten.

In **hoofdstuk 2** wordt een combinatie van biochemische assays en moleculaire modellen gebruikt voor de bestudering en vergelijking van GCase enzymen van verschillende diersoorten, waaronder de mens, de zebravis, de kikker en de schildpad. Alle GCase enzymen vertoonden hydrolyse van het kunstmatige substraat 4-methylumbelliferyl  $\beta$ -glucoside (4MU- $\beta$ -Glc) bij een zuur pH-optimum. Menselijk GCase vereiste saposine C of natriumtaurocholaat bij een pH van 5,2 voor optimale activiteit, terwijl GCase van de zebravis en kikker een optimale hydrolyse vertoonde bij pH 4,0 zonder deze toevoegingen. Verhoogde niveaus van endogeen GlcCer en het gedeacyleerde lipide, glucosylsingosine (GlcSph) werden gemeten in de GBA-deficiënte HEK293T-cellen en deze levels werden gecorrigeerd door expressie van elk van de GCase enzymen. Het enzym van de zebravis bleek, in schril contrast met de GCase van mens en kikker, niet in staat te zijn om de glucose van een 4MU- $\beta$ -Glc of GlcCer donor over te dragen naar een cholesterol acceptor. Mogelijk past een cholesterol molecuul niet in de katalytische pocket van het zebravis GCase.

Vervolgens zijn *in silico* vergelijkingen uitgevoerd van de gepubliceerde 3D-structuur van het menselijke GCase met gemodelleerde structuren van de zebravis, kikker en schildpad enzymen. Hier kwam een hoge mate van algemene conservering naar voren inclusief conservering van de twee katalytische glutaminezuur residuen en andere residuen die deel uitmaken van de katalytische pocket. In deze *in silico* vergelijkingen bevinden zich afwijkende residuen in de drie flexibele loops van GCase die de katalytische pocket omringen. Drie specifieke residuen in het zebravis GCase leken potentieel interessant omdat hun hydrofobe zijgroepen mogelijk impact kunnen hebben op katalyse. Zebravis GCase enzymen met deze aminozuur veranderingen zijn vervolgens gemaakt en getest, maar deze enzymen vertoonden geen verbetering in transglucosylering. Om de hypothese verder te testen wordt overwogen om volledige loops te wisselen tussen de enzymen van verschillende diersoorten.

**Hoofdstuk 3** beschrijft het gebruik van zebravissen als handig orgaanmodel om *in vivo* de doelgerichtheid van irreversibele GCase-remmers te bestuderen. De effectiviteit en selectiviteit van conduritol B-epoxide (CBE) en cyclophellitol (CP) werd geëvalueerd in ontwikkelende zebravislarven en vergeleken met bevindingen in gekweekte menselijke cellen. Alleen bij hoge CBE-concentraties werden niet-lysosomaal GBA2 en lysosomaal  $\alpha$ -glucosidase geïdentificeerd als belangrijke off-targets, zowel in cellen als in zebravislarven. CP bleek GCase en GBA2 met dezelfde affiniteit te inactiveren en is daarom niet geschikt om modellen voor de ziekte van Gaucher te genereren. Nieuwe CP-derivaten, gefunctionaliseerd met een omvangrijke hydrofobe groep op de C8 positie, werden gevalideerd als krachtige en selectieve GCase remmers in gekweekte cellen en zebravislarven.

Hoofdstuk 3 toont bovendien dat het zebravis diermodel aantrekkelijke eigenschappen heeft voor het evalueren van de effectiviteit, specificiteit en biologische verspreiding van geneesmiddelen, in het bijzonder de permeabiliteit van de hersenen. De onderzoeken in hoofdstuk 2 en 3 demonstreren dat vergelijkbare fluorogene substraten, ABPs en LC-MS/MS technieken gebruikt kunnen worden in de zebravis om enzymkenmerken en relevante lipiden te evalueren als die voor menselijke- en muismaterialen.

Een praktisch voordeel van de zebravis, in vergelijking met de muis, is de snelheid en het gemak waarmee nieuwe genetische knockouts gegenereerd kunnen worden. **Hoofdstuk 4** biedt een gedetailleerd protocol voor het genereren van genetische knockouts in zebravissen door middel van CRISPR/Cas9 technologie. Het beschrijft ook de reeds gemaakte mutaties in de zebravis genen voor *Gba1*, *Gba2*, *Asah1a*, *Asah1b*, *Gpnmb*, *cln8* en *Npc1*. Analyses van RNA-expressie en (glyco)sfingolipide waarden van mutante larven van *Gpnmb*, *Cln8* en *Npc1*, bevestigen dat een functionele genetische knockout is gegenereerd. De impact van defecten in *Gba1*, *gba2*, *Asah1a* en/of *Asah1b* wordt in hoofdstuk 5-7 in detail beschreven.

Ook wordt in hoofdstuk 4 de Tol2-transposase techniek toegepast om een exogene DNA sequentie in het genoom van de zebravis te introduceren. Op die manier werd de coderende sequentie van menselijk *GBA* geïntroduceerd in de genetische achtergrond van de zebravis *gba1*<sup>-/-</sup>. Dit menselijke GCCase was functioneel en leidde tot verlaging van GlcSph, beschreven in hoofdstuk 5. In een ander project werd de coderende sequentie van de zebravis prosaposine geïntroduceerd met een puntmutatie in het saposine C gebied, waarvan wordt gedacht dat het een disulfidebrug aantast.

De hoofdstukken 5 tot en met 7 rapporteren over GCCase-deficiënte “Gaucher” zebravissen. Het focust ook op de impact van een gelijktijdig defect in *GBA2* (hoofdstukken 5 en 7) of de impact van overmatig GlcSph (hoofdstuk 6).

**Hoofdstuk 5** is gericht op de rol van zebravis *Gba2* in het glycosfingolipide metabolisme tijdens GCCase-deficiëntie. Zebravislarven met een GCCase- en/of *Gba2*-deficiëntie zijn gegenereerd door middel van genetische- of farmacologische inactivering. Vervolgens zijn de enzymstatus en de glycosfingolipide levels geëvalueerd van zebravislarven van 5 dagen oud (5 dagen na bevruchting, 5 dpf). De afwezigheid of inactivering van GCCase of *Gba2* is gevisualiseerd met behulp van specifieke ABPs, terwijl het GlcCer-metabolisme geanalyseerd is met behulp van gevoelige LC-MS/MS methoden.

Prominente vorming van GlcSph werd geconstateerd bij zowel de *gba1* en *gba1:gba2* genetische knockout larven als tijdens farmacologische inactivatie van GCCase in de zebravislarven. De accumulatie van GlcCer bij de GCCase-deficiënte vissen is relatief beperkt, waarschijnlijk vanwege het alternatieve metabolisme van het lipide tot GlcSph en de aanwezigheid van actief GCCase afkomstig van de heterozygote moeder. Significant hogere GlcCer- en lagere GlcChol waarden werden gemeten bij *Gba2*-deficiënte zebravis larven, wat het belang van *Gba2* voor de vorming van GlcChol weergeeft. Ook zijn iminosuikermers gebruikt om GlcCer-synthase en *Gba2* te remmen om zo de afwijkingen van het GlcCer metabolisme tijdens GCCase-deficiëntie te corrigeren. Over-expressie van humaan GCCase en injectie van recombinant GCCase zorgden beiden voor een correctie van de GlcSph waarden.

In **hoofdstuk 6** wordt de mogelijke toxiciteit van overmatig GlcSph tijdens GCase-deficiëntie onderzocht. Zebravissen hebben twee orthologen van humaan acid ceramidase (ACase): Asah1a en Asah1b. Een belangrijke observatie was de afwezigheid van GlcSph wanneer specifiek een Asah1b-deficiëntie werd geïntroduceerd, gelijktijdig met de GCase-deficiëntie. Ceramide accumulatie, zoals voorkomend bij de ziekte van Farber, werd alleen gedetecteerd wanneer zebravissen een gelijktijdige Asah1a- en Asah1b-deficiëntie hadden.

Een gedetailleerde vergelijking van *gba1* genetische knockout vissen, met overmatig GlcSph, en *gba1:asah1b* knockout zebravissen, zonder GlcSph, onthulde enkele morfologische en biochemische verschillen maar ook interessante overeenkomsten. Een significante verbetering van het fenotype werd waargenomen in de *gba1:asah1b* knockout vissen. Deze vissen vertoonden rond 12 weken na bevruchting niet dezelfde afwijkingen in houding en zwemgedrag als de *gba1* knockout vissen. De *gba1:asah1b* knockout vissen vertoonden een ongeveer 1,5x langere levensduur dan *gba1* knockout vissen. Toch vertoonden de dubbel deficiënte vissen ook abnormaal zwemgedrag rond 15-17 weken na bevruchting.

Zowel *gba1* als *gba1:asah1b* knockout vissen vertoonden vergelijkbare GlcCer accumulatie in weefsels en verhoogde expressie van de biomarkers chitinase (*chia.6*) en *gpnmb*. De infiltratie van microglia en stapelingscellen in de periventriculaire grijze zone van het optisch tectum leek ook vergelijkbaar. In het brein vertoonden de twee GCase-deficiënte vissen vergelijkbare autofagie, weerspiegeld door verhoogde eiwitniveaus van p62, en inflammatie, door verhoogde mRNA-levels van *il1-β*, *tnfβ* en *apoeb*, evenals indicaties voor een vergelijkbare activering van de complement cascade. Het ontbreken van Asah1b-ACase resulteert dus in enkele fenotypische verbeteringen, maar voorkomt niet alle afwijkingen, zoals stapelingscellen, neuroinflammatie en complement activering.

**Hoofdstuk 7** geeft een overzicht van de bevindingen van zebravissen met een mutatie in genen die coderen voor GCase (*gba1*), Gba2 (*gba2*), ACase (*asah1b*) en combinaties van deze mutaties. Deze vissen zijn opgegroeid tot maximaal 12 weken oud en zowel hun fenotype als biochemische en pathologische kenmerken worden beschreven.

Vissen die drager zijn van de mutatie in *gba1* (*gba1<sup>+/−</sup>*) vertoonden geen duidelijk fenotype noch biochemische afwijkingen, terwijl bij *gba2* knockout vissen alleen significante toenames werden gedetecteerd van specifieke GlcCer soorten in de hersenen.

Er werd geen duidelijk abnormaal fenotype waargenomen voor een van de GCase-deficiënte vissen tot 8 weken na bevruchting, hoewel toenames in GlcCer, neuroinflammatie en autofagie wel aantoonbaar waren. Fenotypische afwijkingen van de *gba1* knockout zebravis start rond 9 weken met een neergang van de staart en deze neergang verslechtert met de tijd, waardoor de balans en het zwemgedrag van de vis is verstoord. In tegenstelling tot de enkele *gba1* knockout vissen, ontwikkelden veel van de dubbele *gba1:gba2* knockout vissen binnen enkele dagen de ernstigere afwijkingen in het zwemgedrag, zonder de voorafgaande kenmerken zoals de progressieve daling van de staart. Deze dubbele knockout vissen hebben daarom ook een aanzienlijke kortere levensduur.

Pilot experimenten wezen op een mogelijke vroegtijdige afbraak van dopamine neuronen in de *gba1:gba2* knockout vis, maar de precieze onderliggende pathofysiologische mechanismen zijn nog onbekend.



ACase-gemedieerde deacylering van ophopende glycosfingolipiden tot de sfingolipide-basen is niet uniek voor de ziekte van Gaucher. **Hoofdstuk 8** evalueert de mogelijkheid om zebravissen te gebruiken om de ziekte van Fabry te bestuderen, een andere veel voorkomende lysosomale stapelingsziekte. Een mutatie in het gen coderend voor  $\alpha$ -galactosidase A ( $\alpha$ -GAL A) vormt de moleculaire basis van de ziekte van Fabry. Deze ziekte wordt gekenmerkt door lysosomale accumulatie van globotriaosylceramide (Gb3), dat gedeeltelijk door ACase wordt omgezet in globotriaosylsphingosine (lyso-Gb3).

Hoofdstuk 8 toonde aan dat het genoom van de zebravis één ortholoog van humaan  $\alpha$ -GAL A annoteert en één ortholoog van het zeer homologe  $\alpha$ -N-acetylgalactosaminidase ( $\alpha$ -NAGAL). De aanwezigheid van  $\alpha$ -Gal A en  $\alpha$ -Nagal eiwitten in zebravis cellen en larven werd bevestigd door proteomics met behulp van een op  $\alpha$ -Gal geconfigureerde ABP. Zebravis larven en volwassen organen vertoonden een aanzienlijke  $\alpha$ -Nagal activiteit, gemeten door hydrolyse van fluorogene  $\alpha$ -galactoside- en  $\alpha$ -N-acetylgalactosamine substraten. De  $\alpha$ -Gal A activiteit is doorgaans lager dan  $\alpha$ -Nagal activiteit, maar relatief hoog in bevruchte eieren, voortplantingsorganen, lever en nier, in vergelijking met andere weefsels. Ondanks de aanwezigheid van het  $\alpha$ -Gal A enzym, kon het primaire substraat van  $\alpha$ -Gal A, Gb3, gedetecteerd worden in de bestudeerde zebravis materialen zoals zebravis cellen, larven, brein, lever, nier en testis. De afwezigheid van Gb3 komt overeen met de afwezigheid van een gen dat codeert voor lactosylceramide 4- $\alpha$ -galactosyltransferase (A4GALT of Gb3 synthase) in zebravissen of andere vissoorten.

Om recombinant humaan en zebravis  $\alpha$ -GAL A te bestuderen en vergelijken werden humane HEK293T cellen zonder endogeen  $\alpha$ -GAL A gegenereerd door middel van CRISPR/Cas9 technologie. De accumulatie van endogene Gb3 waarden in deze  $\alpha$ -GAL A deficiënte cellen werd vergelijkbaar gecorrigeerd door over-expressie van ofwel humaan  $\alpha$ -GAL A of zebravis  $\alpha$ -Gal A. Deze bevindingen toonden aan dat zebravis  $\alpha$ -Gal A het endogene substraat Gb3 in de cellulaire setting kon hydrolyseren. Interessant genoeg leek het zebravis  $\alpha$ -Gal A niet in staat om het kunstmatige substraat NBD-Gb3 te hydrolyseren bij dezelfde *in vitro* condities als humaan  $\alpha$ -GAL A.

De rol van het geconserveerde  $\alpha$ -galactosidase dat gecodeerd wordt door het *gla* gen in de zebravis blijft onbekend. Een toekomstig doel is om humaan A4GALT tot expressie te brengen in de zebravissen in combinatie met *gla* knockout zebravissen. Indien deze zebravissen een accumulatie van Gb3 en lyso-Gb3 vertonen, zouden ze mogelijk een model kunnen zijn om de ziekte van Fabry te kunnen bestuderen. De vergelijking van dergelijke vissen met zebravissen met een gelijktijdige *asah1b* knockout zou nuttig kunnen zijn om de specifieke impact van overmatig lyso-Gb3 in de ziekte van Fabry, zoals uitgevoerd voor GlcSph in de ziekte van Gaucher.

Hoofdstuk 9 bediscussieert de verkregen resultaten van de uitgevoerde onderzoeken en beschrijft vooruitzichten van toekomstig onderzoek. Daarnaast worden gevestigde en nieuwe technieken uitgelicht, die nuttig zouden kunnen zijn om andere veelvoorkomende klinische manifestaties van patiënten met de ziekte van Gaucher, zoals botdefecten en bloedafwijkingen, in meer detail te bestuderen in de gegenereerde GCase-deficiënte zebravis modellen. Ook worden zowel anatomische en fysiologische overeenkomsten als verschillen uiteengezet van de zebravis en zoogdieren, om zo het gebruik van het zebravis model van de ziekte van Gaucher in perspectief te plaatsen.

Tezamen tonen de onderzoeken beschreven in dit proefschrift, aan dat zebravissen aantrekkelijke nieuwe mogelijkheden bieden om mechanismen te bestuderen die ten grondslag liggen aan pathologische processen tijdens lysosomale sfingolipidoses. Vanwege anatomische en fysiologische verschillen is aannemelijk dat informatie verkregen met *gba1* knockout vissen niet rechtstreeks vertaald kunnen worden naar patiënten met de ziekte van Gaucher. Daarentegen zouden belangrijke mechanistische inzichten kunnen worden onthuld door het bestuderen van deze vis modellen. Met name de unieke *asah1b* knockout vis, die niet in staat is het veronderstelde toxische lyso-lipide te genereren, zou waardevolle inzichten kunnen geven in de rol van GlcSph, psychosine, lyso-Gb3 of andere lyso-lipiden bij het versnellen van ziekteverschijnselen.



## List of publications

### **The detrimental role of excessive glucosylsphingosine during glucocerebrosidase deficiency. New insights from zebrafish models**

Lelieveld LT, Gerhardt S, Maas S, Zwiers K, de Wit KCC, Beijk EH, Ferraz MJ, Artola M, Meijer AH, Tudorache C, Salvatori D, Boot RG and Aerts JMFG - Manuscript in preparation

### **Glycosphingolipids and lysosomal storage disorders as illustrated by gaucher disease**

Aerts JMFG, Kuo CL, [Lelieveld LT](#), Boer DEC, van der Lienden MJC, Overkleeft HS and Artola M. (2019) *Curr Opin Chem Biol*. **53**, 204-215. doi: 10.1016/j.cbpa.2019.10.006

### **Role of $\beta$ -glucosidase 2 in aberrant glycosphingolipid metabolism: model of glucocerebrosidase deficiency in zebrafish**

[Lelieveld LT](#), Mirzaian M, Kuo CL, Artola M, Ferraz MJ, Peter REA, Akiyama H, Greimel P, van den Berg RJBHN, Overkleeft HS, Boot RG, Meijer AH and Aerts JMFG (2019) *J Lipid Res*. **60**, 11, 1851-1867. doi: 10.1194/jlr.RA119000154.

### **Functionalized Cyclophellitols Are Selective Glucocerebrosidase Inhibitors and Induce a Bona Fide Neuropathic Gaucher Model in Zebrafish**

Artola M, Kuo CL, [Lelieveld LT](#), Rowland RJ, van der Marel GA, Codée JDC, Boot RG, Davies GJ, Aerts JMFG and Overkleeft HS. (2019) *J Am Chem Soc*. **141**, 10, 4214-4218. doi:10.1021/jacs.9b00056.

### **In vivo inactivation of glycosidases by conduritol B epoxide and cyclophellitol as revealed by activity-based protein profiling**

Kuo CL, Kallemeijn WW, [Lelieveld LT](#), Mirzaian M, Zoutendijk I, Vardi A, Futerman AH, Meijer AH, Spaink HP, Overkleeft HS, Aerts JMFG and Artola M. (2019) *FEBS J*. **286**, 3, 584-600. doi: 10.1111/febs.14744.

## Publications not related to this thesis

### **Activity-based proteomics and lipidomics of zebrafish larvae as tools in early drug discovery**

Kantae V, van Esbroeck ACM, Stevens AF, [Lelieveld LT](#), van Rooden EJ, Florea BI, van Wijk RC, Harms AC, van der Graaf PH, Overkleeft HS, Aerts JMFG, Hankemeier T and van der Stelt M - Manuscript in preparation

### **Total Chemical Synthesis of SUMO and SUMO-Based Probes for Profiling the Activity of SUMO-Specific Proteases**

Mulder MPC, Merx R, Witting KF, Hameed DS, El Atmioui D, [Lelieveld L](#), Liebelt F, Neefjes J, Berlin I, Vertegaal ACO and Ovaa H. (2018) *Angew Chem Int Ed Engl*. **57**, 29, 8958-8962. doi: 10.1002/anie.201803483.

## About the author

Lindsey Theresia Lelieveld was born on July 28, 1990 in Monster, the Netherlands. In 2008 she obtained her high school diploma (VWO) at the Interconfessionele Scholengroep Westland Gasthuislaan (ISW Gasthuislaan) in 's-Gravenzande. The same year she started the Bachelor program of Molecular Life Sciences at the Radboud University of Nijmegen. In 2012 she studied for four months at the Washington & Jefferson College in Washington, Pennsylvania (USA) and followed courses in psychology, immunology, chemistry seminar and advanced organic synthesis as part of an exchange program. First contact with fundamental research occurred during a bachelor internship in the department of Bio-Organic Chemistry at the Radboud University in Nijmegen under the supervision of Anika Jonker and Dr. Dennis Löwik.

After obtaining her bachelor's degree from the Radboud University of Nijmegen, she started in 2012 the research Master of Life Science & Technology at Leiden University. A master internship was performed in 2013 in the BioSyn group under supervision of Prof. Mario van der Stelt and daily supervision of Marc Baggelaar focusing on optimization of *in vitro* and *in situ* target engagement, using activity-based probes in combination with bio-orthogonal chemistry. In 2014, a second master internship was performed in the group of Prof. Huib Ovaa of the Chemical Biology group at the Netherlands Cancer Institute (NKI), under supervision of Dr. Remco Merks focusing on the synthesis of functionalized SUMO activity-based probes and subsequent target evaluation of these probes. In 2015, she obtained her Master of Science degree with honours (*cum laude*).

In March 2015 she started her PhD research in the newly established department, Medical Biochemistry at Leiden University, under supervision of Prof. Hans Aerts. This project focused on zebrafish as animal model for the investigation of lysosomal storage disorders, in particular Gaucher disease (GD). For this purpose, she learned various research techniques ranging from CRISPR/Cas9 technology, throughput genetic screenings and zebrafish dissections to biochemical assays and quantitative mass spectrometry. During her PhD, she was involved in teaching of several academic courses and practicals, and the supervision of two bachelor interns, three master interns and one Erasmus Exchange Student. Part of the research has been presented at (inter)national conferences: ESGLD, Pozzuoli (2015); Reedijk symposium, Leiden (2017); ABPP meeting, Gent (2019) and the EWGGD, Clermont-Ferrand (2019).

In 2020 she will continue as a post-doctoral researcher in the department of Medical Biochemistry. She will pursue additional investigations using the described zebrafish in an effort to gain more insights into molecular mechanisms of lysosomal storage disorders. In addition she started the expression and purification of various mammalian and non-mammalian (lysosomal) enzymes in order to evaluate their biochemical properties and opportunities.

## Dankwoord

Zo kleurrijk en veelzijdig als dit proefschrift, zo divers zijn ook de mensen die mijn promotie traject kleur hebben gegeven. In deze vijf jaar heb ik enorm veel geleerd, gelachen, gestrest, gefeest, mooie momenten meegemaakt en misschien ook een aantal mensen een klein beetje doof gemaakt. Daarvoor wil ik een iedereen enorm bedanken, hoewel het onmogelijk is om op deze twee pagina's iedereen de welgemeende dank en waardering te geven die ze verdienen

Allereerst wil ik mijn promotor professor *Hans Aerts* bedanken voor de kans om op een project te werken wat ver buiten mijn toenmalige comfort zone lag. Jouw enthousiasme, werkkraft, ideeën en zowel kritische als motiverende woorden hebben ervoor gezorgd dat ik een betere wetenschapper ben geworden. Het eerste jaar moesten we wel erg aan elkaar wennen en waren we het vaker oneens dan eens (helaas had jij vaak gelijk). Tegenwoordig zitten we gelukkig vaak op "hetzelfde spoor" en hebben we nog tal van mooie projecten bedacht, waar ik mij het komende jaar nog in mag vastbijten.

Als tweede wil ik mijn co-promotor *Rolf* bedanken. Wij hadden weinig tijd nodig om aan elkaar te wennen. Bedankt voor de motiverende woorden, de praktische tips en uiteraard de PCR-reacties, die ik na X pogingen aan jou gaf. Dat je altijd tijd vrij maakte (lees: moest maken) als ik het kantoor in kwam denderen en dat je altijd weer een extra idee had als ik even vastliep. Ook voor de biertjes die ik kreeg als ik wel gelijk had, de vele koffies en nog zo veel meer. Je hebt zoveel invloed gehad op mijn promotie traject dat je uitspraak: "Je kan het ene doen en het andere niet laten" het zelfs geschopt heeft tot stelling. Maar we hebben ook geleerd dat "je soms het ene niet moet doen en het andere juist moet laten".

Dan alle collega's van de afdeling Medische Biochemie in Leiden, waar ik jaren zowel wetenschap als kletspraat, successen als frustraties, koffiemomentjes als biertjes en zo veel meer mee heb gedeeld. *Kim, Daphne, Maria, Rebecca, Kassiani, Martijn, Ethan, Rianne, Remco, Bas, Qin, Marta, Marco, Laura, Rene, Astrid en Patrick* - en zeker ook oud-collega's - *Wouter, Marri, Eline, Per, Mina, Judith, Saskia en Marc* - hartelijk dank hiervoor. Ik heb meer geleerd van eenieder van jullie dan in dit dankwoord onder woorden is te brengen. Speciaal bedankje voor *Wouter*: jouw initiële enthousiasme en bekwaamheid met de inhibitors en ABPs hebben ervoor gezorgd dat het zebravis project vanaf het eerste moment razendsnel ging.

Ook wil ik mijn paranimfje en kamergenootje - *Kim* - bedanken voor haar matchende enthousiasme, gekwebbel en luisterend oor. Mijn gekwetter in de ochtend leverde me soms een moeilijk gezicht op, maar ik zou met niemand anders willen twinnen op 'old McDonald'. Komend jaar knallen we er nog een paar gram eiwit, een paar hoofdstukken en nog meer dove oren uit :)

Ook bedankt aan alle studenten die ik de afgelopen jaren heb mogen begeleiden - *Remco, Wouter, Daniël, Kate, Claire* en *Lisanne*. Jullie gezelligheid, enthousiasme en harde werk hebben een onmiskenbare bijdrage geleverd aan dit proefschrift. Special thanks to *Kate Bila* - your enthusiasm and drive matched perfectly with mine and you were the driving force behind the  $\alpha$ -galactosidase project.

Natuurlijk wil ik ook alle (oud-)collega's van zowel Molecular Physiology en BioSyn bedanken voor hun gezelligheid tijdens de werkuren (of erna) en de hulp bij het vinden van dat ene protocol of compound. Twee mensen wil ik speciaal bedanken: *Tom* - die muur heeft toch weinig invloed gehad, want we blijven toch nog even samen plakken in Leiden, en *Annelot* - bedankt voor de gezelligheid, kletspraat en steun de afgelopen jaren.

Ook een speciaal bedankje naar *Bobby* en de party-crew van mijn stage en eerste jaren PhD - *Nora, Daphne, Joanna, Sander, Sybrin, Hans* en *Anne-Geert*. Zonder Bobby's datingshow tijdens de Wooping in mijn stage-jaar had ik waarschijnlijk heel wat feestjes, ADE moshpits, Texel weekendjes en Hello Kitty slaapfeestjes moeten missen.

Dan wil ik ook graag alle collega's van het Instituut van Biologie bedanken. *Annemarie Meijer* voor de prettige samenwerking en de tips & tricks, vooral de tip om morpholino's over te slaan. *Ralf* en *Bjørn* voor hun hulp om me wegwijs te maken in de zebrafishfaciliteit, waardoor ik snel mijn eerste injecties kon uitvoeren. *Christian Tudorache* voor de gedragsexperimenten en *Gerda Lamers* en *Joost Willemse* voor de microscopie training en expertise. Ook wil ik de diervverzorgers bedanken voor de uitstekende verzorging en gezelligheid in de faciliteit: *Ulrike* (ik weet bij voorbaat dat het een uur van mijn tijd gaat kosten als er Duitse schlager door de speakers klinkt), *Guus*, *Natasha* en oud-dierverzorgers *Ruth*, *Corinna* en *Michelle*. Of the LUMC, I would like to thank *Daniela Salvatori* for her expertise and guidance regarding the pathology parts of this thesis. Ook wil ik *Sophie Gerhardt* en *Saskia Maas* bedanken voor de prettige samenwerking en het verwerken van mijn visjes.

Daarnaast ben ik ook heel dankbaar voor alle mensen buiten mijn wetenschappelijke regenboog. Voor jullie is de grote vraag wat ik nou eigenlijk precies doe in Leiden en daar zal met dit proefschrift waarschijnlijk geen verandering in komen.

Lieve Aruniantjes - *Chantal*, *Esther*, *Imke*, *Jade*, *Jasmijn*, *Jonneke* en *Maud*. Aangezien een groot gedeelte ook promoveert of een bèta opleiding heeft gedaan (of ons er zo vaak over hebben gehoord :), begrijpen jullie mijn geklaag en gestress nog het meest. Het blijft helemaal goud dat ik jullie in mijn eerste studiejaar heb leren kennen en we elkaar nog steeds vaak opzoeken. We verspreiden ons wel steeds verder over Nederland, maar rood en roze zal de mooiste kleurencombinatie blijven.

Ook wil ik *Bianca*, *Joram*, *Jantine* en *Karen* bedanken voor al jaren vriendschap en ik hoop hier nog vele jaren aan vast te plakken.

Voetbalhartjes van dames 1 & 2. Door mijn werk en reistijd was ik zelden op tijd voor een training, maar ik ben heel blij dat ik iedere week weer afleiding had in de vorm van een bal, een bak enthousiasme, mijn eigen uitschuifkuiten en een Jillze (of twee). Ook alle lunches, terras-middagjes, weekendjes weg, 3e helften en andere feestjes (op de voetbal of daarbuiten) zijn me erg dierbaar.

Speciale dank aan de Sportgeitenkaasjes en blijde eieren - *Chantalle*, *Estella*, *Ilse*, *Sacha*, *Britt*, *Marieke* en *Carlissa* - ooit leren kennen via voetbal, tennis en via-via, maar jullie hebben me afgelopen jaren door lief en leed geholpen met sport, festivals, wintersport, stranddagen, EK/WK festiviteiten (BELGIEEEEE), terrasjes, etentjes, drankjes en een hele hoop grappen en grollen. Dat er in de toekomst maar veel +1s bij mogen komen.

Ook wil ik mijn familie bedanken voor hun support, gezelligheid en betrokkenheid - *Maurice*, *Antoinette*, *John*, *Petra*, *Jelle*, *Thijme*, *Hidde*, *Ruud*, *Deborah*, *Dionne*, *Lorraine*, *Leo*, *Esmeralda*, *Tim*, *Bram*, oma *Aly*, *Linda* & *Sammy*. Speciale dank voor mijn lieve, 'kleine' broertje - *Mitchel*. Qua karakter kan ik nog heel veel van je leren en ik hoop dat ik jouw rust en stress-vrije eigenschappen de komende jaren ook zelf mag ontdekken.

Lieve *papa* en *mama*. Een regenboog wordt veroorzaakt door zonlicht en waterdruppels en ik ben dus ook zeer dankbaar voor alle kansen, steun en liefde die jullie me hebben gegeven, zowel tijdens mijn periodes van zonneschijn als regen. Er is weer een hoofdstuk afgerond, maar ik hoop jullie in de toekomst nog trotser te kunnen maken.

Als laatste wil ik 'mijn wijffie' bedanken. Volgens lers bijgeloof staat aan het einde van de regenboog een pot met goud, zo ook aan het einde van mijn regenboog. *Marco* - je hebt er een paar jaar onder gestaan, maar ik ben erg blij dat ik mijn gouden 'wijffie' heb gevonden. **Samen** pas een paar jaartjes gehad met hopelijk nog veel avonturen te gaan: voor altijd en altijd en altijd...

Liefs  
Lindsey

Monster - 30 augustus 2020



